Application of Transketolase from *Geobacillus stearothermophilus* for Broad Synthesis of *N*-Arylhydroxamates and Development of a Novel High-Throughput Reactivity Assay

TECHNISCHE UNIVERSITÄT DARMSTADT

Vom Fachbereich Chemie

der Technischen Universität Darmstadt

zur Erlangung des Grades

Doctor rerum naturalium

(Dr. rer. nat)

Dissertation

Inés Fúster Fernández

geboren in Madrid, Spanien

Erstgutachter: Prof. Dr. Wolf-Dieter Fessner

Zweigutachter: Prof. Dr. Harald Kolmar

Darmstadt, 2022

Tag der Einreichung: 16.08.2022

Tag der mündlichen Prüfung: 24.10.2022

Fúster Fernández, Inés: Application of Transketolase from *Geobacillus stearothermophilus* for Broad Synthesis of N-Arylhydroxamates and Development of a Novel High-Throughput Reactivity Assay
Darmstadt, Technische Universität Darmstadt,
Jahr der Veröffentlichung der Dissertation auf TUprints: 2022
URN: urn:nbn:de:tuda-tuprints-228452
Tag der mündlichen Prüfung: 24.10.2022

Die experimentellen Arbeiten für die vorliegende Dissertation wurden unter der Leitung von Prof. Dr. Wolf-Dieter Fessner am Clemens-Schöpf-Institut für Organische Chemie und Biochemie der TU-Darmstadt im Zeitraum von April 2016 bis Juli 2021 durchgeführt.

Erklärungen

§8 Abs. 1 lit. c der Promotionsordnung der TU Darmstadt

Ich versichere hiermit, dass die elektronische Version meiner Dissertation mit der schriftlichen Version übereinstimmt und für die Durchführung des Promotionsverfahrens vorliegt.

§8 Abs. 1 lit. d der Promotionsordnung der TU Darmstadt

Ich versichere hiermit, dass zu einem vorherigen Zeitpunkt noch keine Promotion versucht wurde und zu keinem früheren Zeitpunkt an einer in- oder ausländischen Hochschule eingereicht wurde. In diesem Fall sind nähere Angaben über Zeitpunkt, Hochschule, Dissertationsthema und Ergebnis dieses Versuchs mitzuteilen.

§9 Abs. 1 der Promotionsordnung der TU Darmstadt

Ich versichere hiermit, dass die vorliegende Dissertation selbstständig und nur unter Verwendung der angegebenen Quellen verfasst wurde.

§9 Abs. 2 der Promotionsordnung der TU Darmstadt

Die Arbeit hat bisher noch nicht zu Prüfungszwecken gedient.

Darmstadt, den 16.08.2022

Inés Fúster Fernández

Teile dieser Arbeit sind bereits publiziert.

Zeitschriftenartikel:

Inés Fúster Fernández, Laurence Hecquet, Wolf-Dieter Fessner, "Transketolase catalyzed synthesis of *N*-aryl hydroxamic acids", Advanced Synthesis & Catalysis, **2022**, *364*, 612-621, DOI: 10.1002/adsc.20210110

Konferenzbeiträge:

Titel: *A novel colorimetric assay for transketolase activity via generation of N-aryl hydroxamic acids*

- Poster: Biotrans 2021, Graz, Austria (Online-Konferenz)

Titel: *Generating a novel colorimetric assay for transketolase activity measurement*

- Poster: Biotrans 2019, Groningen, Niederlande.
- Poster und Kurzvortrag: Doktorandentag, FB Chemie TU Darmstadt 2019, Darmstadt,
- Deutschland.

Titel: *Exploring the conversion of nitrosobenzene by transketolase for the development of a novel reactivity assay*

- Poster: Novel Enzymes 2018, Darmstadt, Deutschland.

Titel: *Exploring the biotransformation of nitrosobenzene with* TK_{gst}

- Poster und Kurzvortrag: Summer School „Biocatalysis as a Key Enabling Technology" 2017, Siena, Italien.
- Poster: Biotrans 2017, Budapest, Ungarn.

“The only way to discover the limits of the possible is to venture a little way past them into the impossible.”

Arthur C. Clarke

Acknowledgements

I would like to commence by expressing my utmost gratitude to my supervisor Prof. Wolf-Dieter Fessner for his constant support and encouragement. I thank him whole-heartedly for always uplifting me whenever I needed guidance, which helped me overcome the obstacles in the way. I am also grateful for his patience and genuine empathy. All this truly contributed to the success of this work and my personal growth. Vielen lieben Dank!

I am very grateful to the other members of the examination board: Prof. H. Kolmar, Prof. G. Buntkowsky and Prof. K. Schmitz. I also thank our cooperative partner Prof. L. Hecquet for giving me the opportunity to do a short internship at her laboratory in Clermont-Ferrand within the transketolase project, which was very enriching for the progress of my further work in Germany. I sincerely thank Karin Schmidtkunz (group of Prof. M. Jung) for performing the inhibition tests with the potential anticancer hydroxamic acids I synthesized. Moreover, I want to thank all the members of the NMR and mass department. In particular, Prof. R. Meusinger, Mrs. C. Rudolph, and Dr. A. Schießer, whose contribution has been a great help.

I would like to thank all my new and old colleagues for the good working environment and the fun shared, which made the exhausting working days much more bearable. My special thanks go to: Dr. Sebastian Junker, for becoming a true friend to me since the start, always assisting and encouraging me, and for sharing with me a thousand memorable times; Dr. Yen Chi Thai for her never-ending empathy, for always having a listening ear for me, for her support and willingness to help in the personal and professional area, and for the joy we shared; Hans-Michael Orfgen for his availability and readiness to help in all professional and personal matters. He made everything a little bit easier for me; Dr. Yuriy Sheludko, my lab "uncle", for his patience and kindness whenever I asked him for advice, for the inspiring and interesting conversations, for his positive spirit and repertoire of nice words, and above all, for always bringing me chocolate from his travels; Alexander Santana for our entertaining chats and his good suggestions; Michael Hofmeister for sharing his positive, fair and team-oriented character; Serbet Pinar-Safi for the administrative work; Michael Kickstein for his competent biochemical support and patience; and Bettina Harnischfeger for ordering and organizing all the material needed, and for sharing with me her amazing "Kochkäse".

Furthermore, I would like to thank (Dr.) Estefi from the bottom of my heart, who has been there with me through thick and thin, being my right-hand woman for all personal and professional decisions. Despite the distance, our friendship only keeps growing. I am also beyond grateful to all the rest of my friends and family anywhere in the globe for their valuable moral support and for the much-needed moments of fun and disconnection, which helped me enormously throughout the tough times. I cannot mention them all but I am sure they know who they are!

Last but not least, I cannot thank enough my unconditionally loving parents, Ana and Oscar, and my sister Marta, for encouraging me to always be better, aim higher, and to never surrender because I am capable of whatever I set my mind into. Thank you for your patience and comprehension. This would not have been possible without your continuous support and faith in me throughout all my life decisions. Hence, part of this belongs to you. Os quiero.

Table of contents

Zusammenfassung in deutscher Sprache

Die Transketolase (TK, EC 2.2.1.1) katalysiert in Natur die reversible und stereospezifische Übertragung einer C2-Ketoleinheit auf das Carbonylende einer Vielzahl von Aldehyden. Die Verwendung der TK zur Bildung von Kohlenstoff-Kohlenstoff-Bindungen ist vorteilhaft, da die hoch stereoselektive Bildung eines (*S*)-konfigurierten Chiralitätszentrums Zugang zu phosphorylierten Ketosen mit D-*threo* (3*S*, 4*R*)-Konfiguration bietet.[1-3] Die TK ist ein sehr vielseitiges Enzym, da es bei synthetischer Anwendung die Möglichkeit bietet, sowohl die Akzeptor- als auch die Donorsubstrate der von ihr katalysierten Reaktionen zu variieren, was zu vielen verschiedenen Synthesemöglichkeiten und einer großen Vielfalt an natürlichen und synthetischen Produkten führt. Beispielsweise werden die TK-Reaktionen durch die Verwendung von Kohlendioxid freisetzenden Donorsubstraten wie β-Hydroxypyruvat (HPA) praktisch irreversibel.[4]

Während einer kürzlich durchgeführten Zusammenarbeit zwischen den Gruppen von Hecquet und Fessner, wurde die erste thermophile TK aus *Geobacillus stearothermophilus* (TK_{gst}) als thermostabiler Katalysator mit vielversprechenden möglichen Anwendungsmöglichkeiten identifiziert.[5] Kürzlich wurde die TK_{gst} vom Arbeitskreis Fessner dahingehend modifiziert, dass sie Benzaldehyd als nichtnatürliches Akzeptorsubstrat akzeptiert.[6] Aufgrund der hohen elektronischen und strukturellen Ähnlichkeit zwischen Nitrosobenzol (**5a**) und Benzaldehyd (**7**) wurden TK_{gst}-Varianten erfolgreich entwickelt und verwendet, um Nitrosoarene als alternative elektrophile Substrate in die entsprechenden *N*-Arylhydroxamsäuren (HA) umzuwandeln (Schema 1).

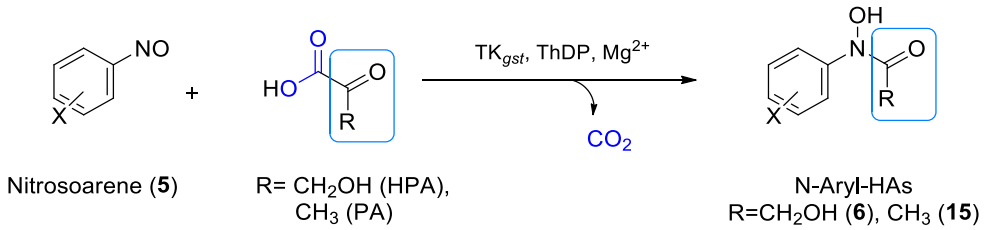

Schema 1. Allgemeines Reaktionsschema der durch TK_{gst}-katalysierten Bildung von *N*-Aryl-HA durch Ketol-Addition an Nitrosoarenen.

HA bilden eine Klasse von Verbindungen mit außergewöhnlicher pharmazeutischer, biochemischer und industrieller Bedeutung; unter Anderem besitzen manche HA Antitumor-Eigenschaften.[7-9] Sie verdanken diese pharmazeutische Vielseitigkeit der Fähigkeit ihrer HA-Funktionalität RC(=O)N(-OH)R', als zweizähniger Ligand zu wirken und starke Chelatkomplexe mit vielen verschiedenen Übergangsmetallen, wie Eisen(III) oder Zink(II) zu bilden.

Im ersten Kapitel wurde eine Reihe unterschiedlich *para*-, *meta*- und *ortho*-mono- und disubstituierter Nitrosoarene (**5a-p**) unter Verwendung der TK_{gst} L382N/D470S-Variante getestet, die für eine verbesserte Akzeptanz von Benzaldehyd mit HPA als Donorsubstrat entwickelt worden war. Hinsichtlich der Reaktionsgeschwindigkeiten und Reaktionsausbeuten schien die elektronenziehende Substitution die Reaktivität zu beschleunigen, während stark

elektronenschiebende Gruppen die Reaktionsgeschwindigkeit signifikant verzögerten. Beispielsweise wurde aus der TK_{gst}-katalysierten Reaktion mit *N*,*N*-Dimethyl-4-nitrosoanilin (**5p**) kein HA erzeugt. Darüber hinaus wurden durch die Verwendung von Pyruvat (PA) als Ketosäure-Donorkomponente strukturelle Modifikationen in der HA-Struktur eingeführt. Die Akzeptanz von Pyruvat (PA) als Donor durch die konstruierte TK_{gst} H102L/H474S-Variante erweitert den Anwendungsbereich dieses Enzyms um die Kombination aus nicht-hydroxylierten 2-Oxosäuren und aromatischen Elektrophilen, jedoch auf Kosten reduzierter Reaktionsraten und Produktausbeuten. Um die Substrattoleranz auf die gleichzeitige Verwendung von zwei nicht-nativen Komponenten zu erhöhen, sind jedoch neue gentechnisch veränderte TK-Varianten erforderlich. Dennoch konnten mit dieser Methode sechzehn verschiedene *N*-Aryl-HA-Verbindungen hergestellt werden, von denen zwölf isoliert werden konnten (Tabelle 1).

Tabelle 1. Isolierte HA erhalten durch TK_{gst}-katalysierte Synthese von HA aus **5** und HPA oder PA.

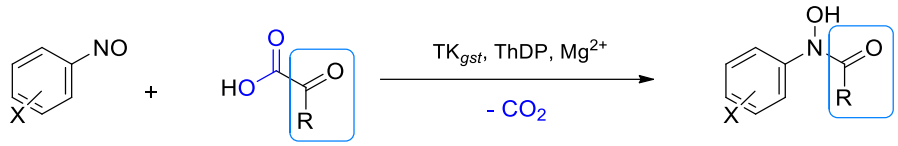

Nitrosoarene	Aryl substitution (X)*	Acyl residue (R)	HA product
5a	H	CH_2OH	**6a**
5b	4-Br	CH_2OH	**6b**
5c	4-Cl	CH_2OH	**6c**
5d	3-Cl	CH_2OH	**6d**
5f	3,4-Cl_2	CH_2OH	**6f**
5g	4-CH_3	CH_2OH	**6g**
5h	3-CH_3	CH_2OH	**6h**
5i	4-Cl, 3-CH_3	CH_2OH	**6i**
5j	3-Cl, 4-CH_3	CH_2OH	**6j**
5k	4-CF_3	CH_2OH	**6k**
5l	3-CF_3	CH_2OH	**6l**
5a	H	CH_3	**15a**

* Substituent positions relative to the nitroso group

Aus einem Co-Solvens-Screening während der Reaktionsoptimierung erwies sich Aceton als besonders vorteilhaft hinsichtlich der deutlich vereinfachten Aufarbeitung und den höheren Produktausbeuten. Auch durch die Bildung des tief gefärbten Eisen(III)-HA-Komplexes (Schema 2) konnte der eindeutige und sensitive Nachweis der HA-Bildung durchgeführt werden. Darüber hinaus scheint die chemo-katalytische Bildung der entsprechenden HA stark von der Struktur des eingesetzten Nitrosoarens und der Ketosäure-komponente abzuhängen.

Beispielsweise wurde festgestellt, dass Eisen(III) die Reaktion mit PA zur Bildung der entsprechenden HA katalysiert, während mit HPA keine durch Eisen(III)-Katalyse vermittelte Bildung von HA beobachtet werden konnte.

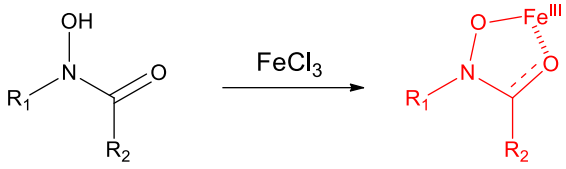

Schema 2. Eisen(III)-Komplexierung durch eine allgemeine HA.

Im zweiten Kapitel wurde ein neuartiger kolorimetrischer Endpunkt-Assay für das Screening der TK_{gst} entwickelt, der auf der Grundlage der Fähigkeit von HA, Metalle wie Eisen(III) zu chelatieren, im Hochdurchsatz anwendbar ist und die Bestimmung des während der enzymatischen Katalyse erzeugten HA-Produkts ermöglicht. Daraus kann eine qualitative und sogar halbquantitative Bewertung der Enzymaktivität erfolgen. In Schema 3 sind die Schritte des Eisen(III)-Assays gezeigt. Zunächst erfolgt die durch TK_{gst}-vermittelte Katalyse mit Nitrosobenzolderivaten (**5**) als Substratakzeptoren und HPA als Substratdonor, in Gegenwart der TK-Cofaktoren ThDP und Mg^{2+}. Dann wird $FeCl_3$ *in situ* hinzugefügt, um den entsprechenden Eisen(III)-HA-Komplex zu erzeugen. Dieses Chelat nimmt bei niedrigem pH-Wert ein 3:1-Verhältnis an und erhält eine rotviolette Farbe, die mit bloßem Auge sichtbar ist und bei 500 nm mit einem Mikrotiterplatten-Photometer gemessen werden kann.

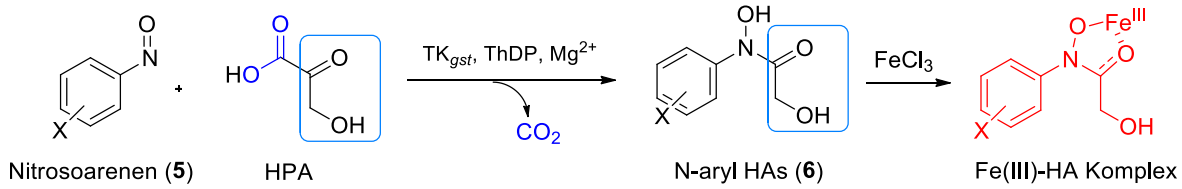

Schema 3. Prinzip des diskontinuierlichen Eisen(III)-Assays zur Bestimmung der TK-Aktivität mit Nitrosoarenen durch anschließende *in situ*-Bildung des Eisen(III)-HA-Komplexes zur Detektion.

Der Assay wurde zunächst entwickelt, optimiert und erfolgreich im Flüssigphasen-Screening eingesetzt, wobei eine 96-Well-Platte aus der von D. Yi erstellten L382X/D470X-Bibliothek verwendet wurde, um seine breite Anwendungsmöglichkeit zu beweisen. Anschließend wurde die Methode für ein Festphasen-Screening modifiziert, um aktive TK_{gst}-Kolonien mit verschiedenen Nitrosoarenen direkt mit bloßem Auge zu erkennen. Ein schematischer Vergleich zwischen Flüssig- und Festphasenassay ist in Abbildung 1 dargestellt.

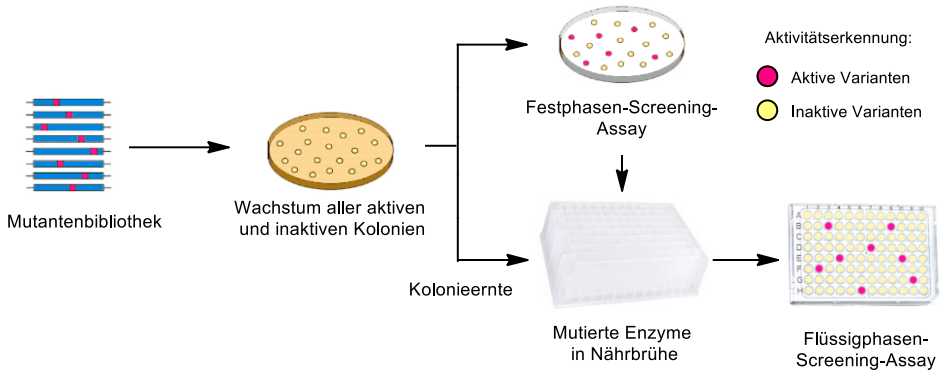

Abbildung 1. Allgemeine Darstellung des kolorimetrischen Eisen(III)-Assays auf fester Oberfläche im Vergleich zu einer in flüssiger Phase durchgeführtem Assay ausgehend von derselben Agarplatte nach Mutagenese.

Zur Visualisierung der schnellen Auswertungsmöglichkeit des Eisen-chlorid-Prinzips beim Screening der TK$_{gst}$ L382X/D470X-Bibliothek sind in Abbildung 2 sowohl Bilder eines Festphasen- als auch eines Flüssigphasen-Screenings zu sehen.

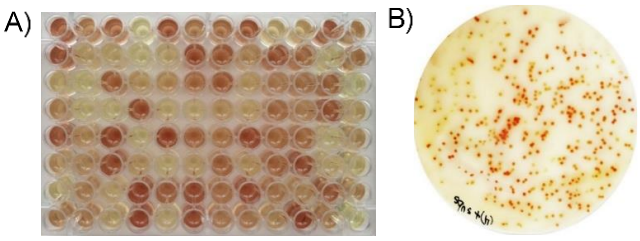

Abbildung 2. Anwendung des Eisenchlorid-Prinzips in Flüssigphase (A) und Festphase (B) mit der L382X/D470X TK$_{gst}$-Bibliothek.

Die mit beiden Assay-Formaten erzielten Ergebnisse waren vergleichbar, da die positiven Treffer im Festphasen-Assay bei allen Substraten auch Aktivität im Flüssigphasen-Screening-Verfahren gezeigt hatten, während die inaktiven Kolonien im Ersteren auch keine nachweisbare Aktivität im Letzteren aufwiesen. Diese empfindlichen Screening-Methoden sollten sich als geeignet erweisen, um die Substrattoleranz von TKs aus verschiedenen Quellen mit einer breiten Sammlung von nitrosohaltigen Verbindungen abzuschätzen. Da diese kolorimetrischen Screening-Methoden unkompliziert sind, sollten sie sich auch als relevant für das zuverlässige Screening breiter TK-Bibliotheken erweisen, die für die gerichtete Evolution neuer Enzyme unverzichtbar sind.

Im dritten Kapitel wurde die Hypothese aufgestellt, dass *N*-Aryl-HA (**2**), auch „Retro-HA“ genannt, vermutlich ähnliche pharmakologische Eigenschaften wie die wohlbekannte *C*-Aryl-HA (**3**) besitzen, weil beide Konstitutionsisomere die Fähigkeit haben, Metallionen wie Eisen(III) und Zink(II) in ähnlicher Weise zu chelatieren. (Schema 4).

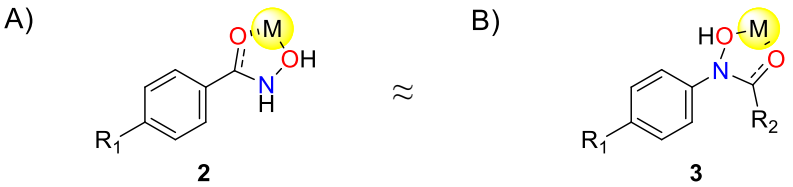

Schema 4. Metallchelation durch C-arylierte HA vs. isomere N-arylierte HA. M= Metallion, R_2= H, CH_3, CH_2OH.

Um diese Hypothese zu testen, wurden das leicht zugängliche potente HDAC*i* *N*-hydroxy-4-(4-phenylbutyrylamino)benzamid (HTPB)[10] und verwandte *N*-Aryl-HA chemisch synthetisiert. Anschließend wurden *In-vitro*-HDAC-Hemmungstests in der Gruppe von Jung durch K. Schmidtkunz durchgeführt. Die Ergebnisse der HDAC-Assays bestätigten die vorgeschlagene Prämisse, da alle getesteten Retro-HA eine akzeptable bis gute HDAC-Hemmung bei der höchsten analysierten Konzentration (100 µM) für humanes hHDAC8 aufwiesen. Zusätzlich bot das direkte HTPB-Analogon HA **28** eine akzeptable inhibitorische Aktivität bei 100 µM für alle getesteten humanen HDACs, einschließlich HDAC1, HDAC6 und hHDAC8, und sogar von *Schisosoma mansoni*, wie smHDAC8. Nur das HDAC von *Trypanosoma cruci*, tcDAC2, wurde durch die Retro-HA nicht beeinflusst.

Obwohl die wirksamste Konzentration (100 µM) weit über der wünschenswerten nanomolaren Skala lag, kamen wir zu dem Schluss, ist dies keine abschließende Bewertung für seine biologische Wirkung, gerade wenn Therapeutika zur Bekämpfung von Krebs eingesetzt werden.[11] Es ist denkbar, dass die Modifikation der Struktur der Retro-HA mittels molekularer Docking-Studien Substanzen mit größerer HDAC-Hemmfähigkeit hervorbringen könnte. Unseres Wissens nach scheinen Retro-HA bisher nicht für biomedizinische Anwendungen getestet worden zu sein. Daher könnten diese Informationen bei der Suche nach neuartigen Arzneimitteln gegen Krebs wertvoll werden.

Außerdem wurde in einem Proof-of-Concept Verfahren gezeigt, dass **30**, das bei einer Konzentration von 100 µM hHDAC8 um 60 % hemmt, mittels TK_{gst}-vermittelter Katalyse hergestellt werden kann. Da Enzyme eine Vielzahl von Vorteilen bieten,[12] eröffnet dies die aufregende Anwendung von Biokatalysatoren für die Erzeugung von Retro-HA mit biomedizinischen Eigenschaften.

1. General introduction

1.1. Biocatalysis

The process in which a substance is able to increase the rate of a reaction by lowering its activation energy without being altered is known as catalysis. The substance involved in this operation is called catalyst.[13] Traditionally, chemical catalysts have been employed for a vast number of chemical processes.[14-16] However, a range of issues connected to chemical catalysts have been described, such as use of toxic transition metals, or employment of harsh reaction conditions. Also low enantiomeric excess and therefore tedious separation of enantiomers from racemic mixtures can have a detrimental effect on the environment when used in large industrial processes.[17] In a racemic mixture, both enantiomers are present in an equal ratio and display identical physical and chemical properties, yet have very different biological properties, differing in the pharmacokinetic and pharmacodynamic behaviors, which leads to different efficacies and toxicities for the enantiomers. One enantiomer could have the desired beneficial effect whereas the other one could interact with a different target causing undesired side effects, which at worst can lead to harmful effects for the individual.[18]

Thus, applying enantiopure substances is of outmost importance. The chiral drug thalidomide (α-phthalimidoglutarimide) offers an egregious example of this phenomenon.[19] During the 1960s, it was prescribed to pregnant women for the treatment of morning sickness. It was administered as a racemic mixture (1:1 ratio) of (*R*)-(+)-thalidomide and (*S*)-(-)-thalidomide (Scheme 1.1). Unfortunately, while the *(R)*-(+)-enantiomer gave the desired sedative properties to the women, the (*S*)-(-)-enantiomer caused teratogenic effects to the embryos.[20] The total number of affected embryos is estimated at 10.000, with a survival rate between 40 and 70%.[21]

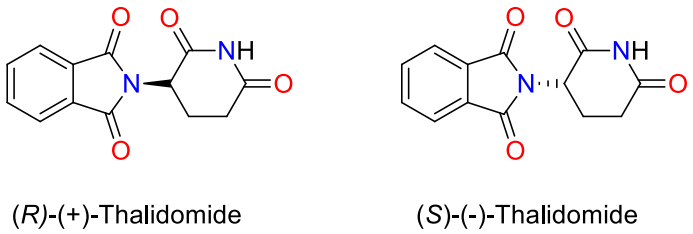

Scheme 1.1. Chiral drug thalidomide in its two enantiomeric forms.

After that tragic example, it became clear that racemic mixtures of agrochemicals and pharmaceuticals had to be treated with extreme caution. Throughout time, major efforts have been invested in solving these problems and directly accessing enantiomerically pure compounds, such as through the application of chiral transition metal complexes and organocatalysts, among others.[22] However, although high enantiomeric excess can be achieved by these techniques, these methods are still expensive and may be detrimental for the environment. In the recent past, chemists have admitted the urgency to consider both economic and environmental metrics when establishing new methodologies towards application in the production of chemicals and pharmaceuticals.[23]

For these reasons, the concept of "green chemistry" has gained impact. The purpose of green chemistry is to reduce the use or the complete avoidance of hazardous substances in the chemical process, such as reagents, solvents, feedstock, products, and byproducts. Green chemistry regards sustainability, suggesting that economic growth and industrialization should be achievable without environmental damage, and that it is essential to develop new processes to manufacture chemical products in a more resource-saving, energy-efficient and environment-friendly manner.[24-25]

With all that in mind, the interest in biological catalysts, also called biocatalysts, has raised significantly over the years. Biocatalysts can refer to an enzyme, an enzyme complex, a cell organelle or a whole cell.[26] Enzymes are the subset of proteins with catalytic activity that catalyze reactions occurring in all living organisms. Therefore, it can be said that enzymes enable the chemistry of life by catalyzing all the reactions in the living nature.[27] In addition to the natural reactions that they catalyze, these biological molecules are also able to perform biotransformations for the synthesis or degradation of chemicals.[28] The concept of applying nature's toolbox for the production of chemicals is known as biocatalysis. Moreover, biocatalysts are primarily produced from microorganisms grown from renewable resources; and they are environmentally friendly, as they are biodegradable, nontoxic and non-hazardous. This makes biocatalysis both a sustainable and green science complying with the twelve principles of green chemistry established by *Anastas and Warner* in 1998 (Fig. 1.1.).[23, 29]

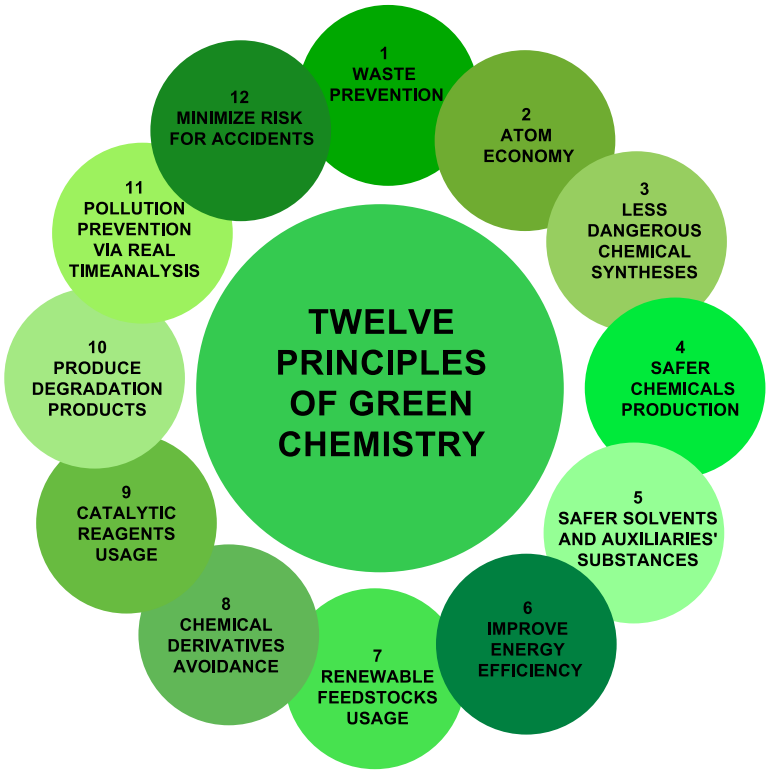

Figure 1.1. Green chemistry principles proposed by *Anastas and Warne*r.

In comparison to chemical catalysts, biocatalysts offer many advantages which are difficult to achieve by conventional organic catalysis: enzymes are very efficient catalysts; the enzyme-mediated reaction rates are typically far above the values which the chemically-catalyzed reactions are capable of reaching; enzyme reactions are usually performed under relatively mild conditions in means of temperature, pressure, pH and solvent usage. Additionally, enzymes are compatible with each other and hence, can be coupled in a cascade-like fashion in a single system; they are not restricted to their natural role, being catalytically promiscuous as they can catalyze a broad range of reactions.[12]

Also, contrary to most organic syntheses, enzyme-meditated reactions do not require functional-group protection, deprotection, nor activation, which simplifies the processes significantly. Enzymes are extremely chemoselective, regioselective, diastereoselective, and enantioselective. Their intrinsic chirality allows them to be used in asymmetric syntheses to produce enantiomerically pure compounds in an economical and environment-friendly way.[12, 30] Along with the ability of enzymes to catalyze asymmetric synthesis, they can also resolve racemic mixtures to obtain enantiopure compounds. This allows for a reduction of the price of the starting materials and the number of synthetic steps considerably.[31]

Because of all the aforementioned advantages, green biotechnological processes and products are more and more involved in industrial applications in numerous sectors, such as the synthesis of active pharmaceutical ingredients, chemicals, detergents, food production and processing, pulp and paper treatment, textile fibers treatment and their bleaching, agriculture, and many other applications (Fig. 1.2).[32]

The global market size for industrial enzymes was valued at ca. $5.6 billion in 2019 and it is expected to develop at a compound annual growth rate (CAGR) of approximately 6.4% from 2020 to 2027, reaching $9.14 billion by that year.[33] In 2019, the food and beverage segment dominated the industrial enzymes market with a total share of more than 36%, being the fastest growing application segment. Enzymes assist the food processing segment in increasing the quality of the final products, augmenting the yield of the reactions, optimizing resources, lowering environmental contamination and reducing wastage, all that leading to decreased costs.[34] North America led the market and assumed over 35% share of the global income in 2019, followed by Asia Pacific and Europe as the second-largest enzymes consumers in the world, with Europe being one of the major manufacturers of pharmaceutical, medicinal and cosmetic products.[33-34]

In recent years, the application of biocatalysts, such as transaminases, lipases, hydrolases, transferases, polymerases, esterases, phosphatases, alcohol dehydrogenases and proteases, for valuable building block syntheses in chemical and pharmaceutical industries, has earned high interest. The global healthcare specialty enzymes market segment is expected to augment at a CAGR of 6.2% from 2020 to 2027.[30, 34] Moreover, due to the COVID-19 pandemic and the measures taken by the governments to combat it, some of the enzyme application fields, such as the pharmaceutical and detergent sector, are expected to grow exponentially in demand. Accordingly, COVID-19 has to be taken as a key market contributor.[33, 35]

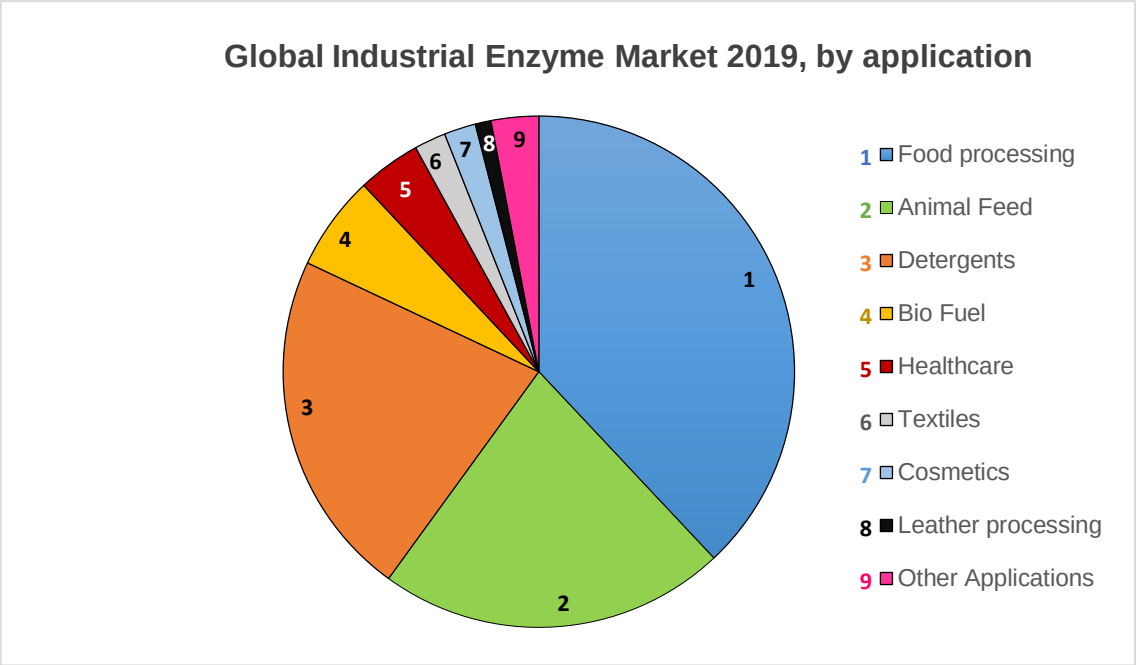

Fig. 1.2. Global industrial enzymes market in 2019, sorted by application. Graphic based on Mordor Intelligence report.[34]

However, biocatalysts also have some disadvantages which should be taken into account for industrial purposes: natural enzymes are provided in only one enantiomeric form; they cannot function under harsh operating conditions, such as extreme pH (below 7 or above 8 in most cases) elevated pressures, high temperatures for non-thermostable enzymes; non-aqueous solutions due to their low tolerance towards organic solvents, where most of the organic compounds are best soluble; and oxidative conditions. Moreover, natural enzymes are normally easily inhibited.[12, 36]

To overcome these drawbacks and broaden the applicability of biocatalysis, many technologies have been applied, such as the employment of thermophilic enzymes and enzyme immobilization, leading to a better stabilization of the biocatalysts;[37-38] use of whole cell catalysis and coenzyme regeneration methodologies, ensuring the sustainability and decreasing the cost of the biocatalytic reactions;[39] performance of biological reactions in organic media, modifying the behavior of the biocatalysts and thus extending their application scope;[39-42] use of multiphase reaction systems and construction of micro reactors to enhance catalytic efficiency and facilitate product obtainment;[43-44] among others. Thanks to the aforementioned technologies, biocatalysis is no longer limited to the natural molecule diversity; rather it is also applicable to various non-natural target compounds, which can serve as pharmaceutical intermediates and interesting fine chemicals.[45]

1.2. Protein engineering

Natural enzymes, which are extraordinarily versatile and very competent catalysts, have been procured and optimized by nature through millions of years of evolution. Traditionally, in order

to find suitable biocatalysts with improved properties, tens of thousands of microorganisms from the environment would be screened. This is still a very important and fundamental method. Nonetheless, industry cannot always apply native enzymes to solve the impediments caused due to the differences between the native function of the enzyme and the human-designed industrial demands. In those cases, the enzyme activity and/or properties may be improved applying protein engineering methodologies.[46]

Targeted protein design enables the development of tailored enzymes for the catalysis of specific reactions;[47] protein engineering serves essentially to modify the amino acid sequence of an existing enzyme to improve enzyme characteristics like extension of the substrate scope, increase of the temperature or solvent stability, and improvement of enzymatic activity.[48-49] Many protein engineering methods are available currently, and have been thoroughly reviewed in the literature.[50] The two main approaches are directed evolution and rational protein design, and are very often used in combination.

1.2.1. Directed evolution

Among all the methods, directed protein evolution *in vitro* is probably the most successful strategy when *a priori* little or no knowledge of the structure of the target enzyme is available, as it is sufficient to know the function and DNA sequence coding for the enzyme. Directed evolution began with the pioneering contributions of W. "Pim" Stemmer and F. Arnold in the mid and late 1990s.[51-54] This technique combines the increased knowledge of evolution, the advanced techniques of molecular biology and the different screening methods available to mimic the process of natural selection for the *in vitro* evolution of enzymes towards a tailored aim.

This technology involves iterative rounds of random amino acid changes in a protein by altering its corresponding genes. While there are several approaches for the random replacement of amino acids in the protein sequence, the best-known method is error prone PCR (epPCR), which generates point mutations during PCR amplification.[55] Other techniques used in directed evolution are oligonucleotide-directed mutagenesis, which introduces mutations at intended specific locations in the DNA sequence; and DNA shuffling, which produces changes in the DNA sequence by exchanging whole blocks of sequences among two or more DNA strands.[56-57] After the random mutageneses, the generated enzyme libraries must be screened and selected by high-throughput screening (HTS) methods to identify variants with enhanced properties, such as substrate specificity, specific activity, enantioselectivity, organic solvent tolerance, enzyme stability, and even novel catalytic capabilities. The selected enzymes are usually subjected to the same process repeatedly to obtain further improved variants (Fig. 1.3).[58-59]

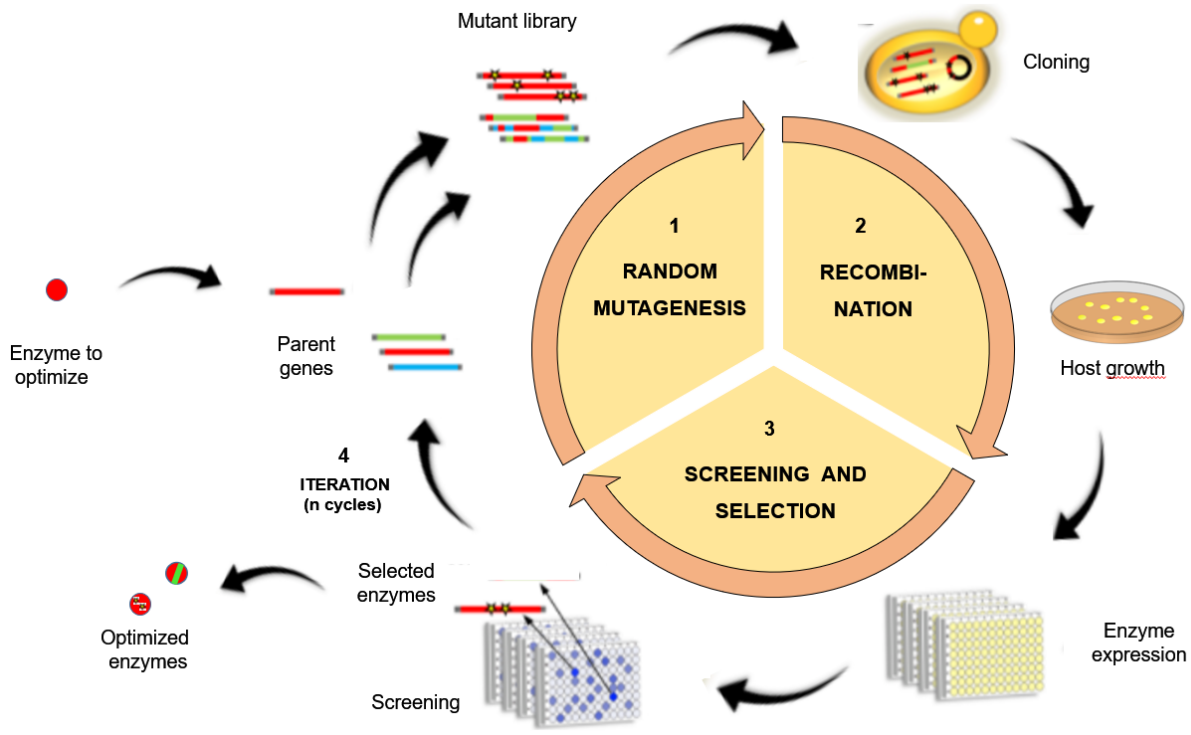

Figure 1.3. Principle of directed evolution. Representation modified from EvoEnzyme.[60]

Over the years, protein engineering technologies have been further developed and there has been significant progress in the improvement of existing biocatalysts by creating novel features even including novel activities.[45-46] However, there are still a few challenges associated to these technologies. In spite of the various methods that are available to construct libraries, the frequency of random mutations to a gene of interest is still small, in comparison to the vastly large sequence space.[45, 61] In addition, efficient identification of desirable variants from the large generic libraries is the most challenging step of directed evolution, thus, the design of appropriate screening methods is critical when using this technique.[62] Yet, not all enzymes are susceptible for development of HTS methods. Therefore, further work on protein engineering technology is still required to solve these limitations. A summary of the most common screening methods is presented in the introduction to Chapter II of this doctoral thesis (Section 6.2).

1.2.2. Rational protein design

Rational design relies on the computer-assisted identification of amino acids that are suitable for targeted mutations in order to achieve the desired protein properties. This approach requires information about the 3D structure of the protein, such as a protein model or crystal structure to provide a fundamental understanding of the structure and function relationship, since these are not always available and can't be easily obtained, the general application of rational design is limited. Thus, the greatest challenge of rational design lies in the identification of critical amino acids.[63] Yet, its greatest advantage lies in the fact that rather small libraries are created, which reduces time and costs for the screening process.

1.3. Thiamine diphosphate-dependent enzymes

After years of technological development of biocatalysts, an extensive diversity of enzyme classes have been successfully employed for organic synthesis, including hydrolases, oxidoreductases, lyases, transferases, isomerases and ligases.[64-68] Among them, enzymatic carboligation has become a very important reaction for the synthesis of chiral building blocks for the pharmaceutical industry. Several enzymes are capable of catalyzing enzymatic carboligation reactions by forming new carbon-carbon bonds under mild reaction conditions with uncompromised stereochemical fidelity and high chemical efficiency, avoiding the demand for protecting sensitive or reactive functional groups.[1] Especially, the class of thiamine diphosphate-dependent enzymes offers several examples of enzymes able to perform synthetic carboligation reactions.

Thiamine or vitamin B_1 was the first vitamin to be isolated in pure form. Its discovery and isolation are the result of the extensive work of numerous researchers driven by the identification of the impact of thiamine deficiency in humans. It was first discovered in 1897 by C. Eijkman during his studies on the beriberi disease in Java,[69] and crystals were first isolated in 1926 by B. Jansen and W. F. Donath*[70]. However, it was not until 1936 that R. R. Williams elucidated its structure and synthesized this very important vitamin for the first time.[71] Thiamine is only biologically produced in microorganisms, plants, and fungi, yet it is a crucial nutrient for animals and humans. Therefore, we rely on external sources, such as vegetables, grains, or dietary complements to obtain it. The term "vitamin" was proposed in 1912 by the scientist C. Funk (vita=life, and amine= nitrogen-containing compound) after his investigations led him to realize that even traces of these elements were extremely necessary for life. In fact, deficiency of elements from the vitamin B-complex are the cause of various diseases, such as beriberi, polyneuritis and pellagra.[72]

Thiamine diphosphate (ThDP) is the biologically active form of vitamin B_1. Its synthesis is catalyzed by the enzyme thiamine diphosphokinase (ThDPK), which transfers two phosphorous-containing groups to thiamine.[73] The structure of ThDP consists of three principal elements: an aromatic 2'-methyl-4'-aminopyrimidine (MAP) ring, which is joined via a methylene bond to a 4-methyl-thiazolium (MT) ring, which is likewise linked to a diphosphate (PP) moiety through a hydroxyethyl side chain (scheme 1.2).[1]

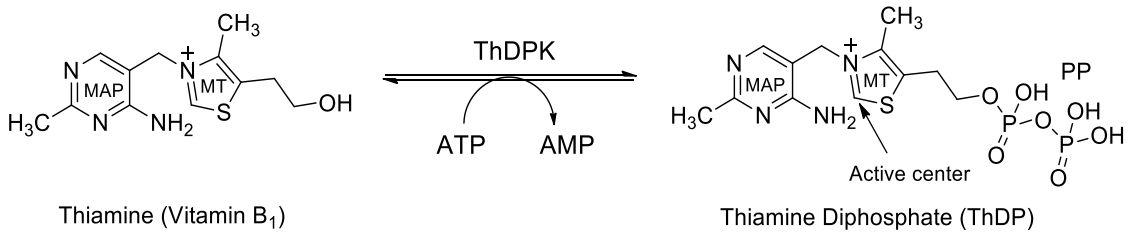

Scheme 1.2. Simplified ThDP generation reaction catalyzed by the ThDPK enzyme.

There exists an extensive family of biocatalysts in nature that uses ThDP as an essential cofactor for the reactions they catalyze. This class of enzymes is made up of the so-called ThDP-dependent enzymes, which are involved in a large number of metabolic pathways in all living systems, being able to catalyze the formation and cleavage of carbon-nitrogen, carbon-oxygen,

carbon-sulfur and, most importantly for organocatalysis and bioorganic synthesis, carbon-carbon bonds. The mechanism of action of these type of enzymes has been extensively studied.[74-76] Due to their competence for asymmetric bond production, and because of their high tolerance towards a broad substrate spectrum, they have been widely utilized to catalyze a collection of biotransformations (Scheme 1.3).[1, 77-79]

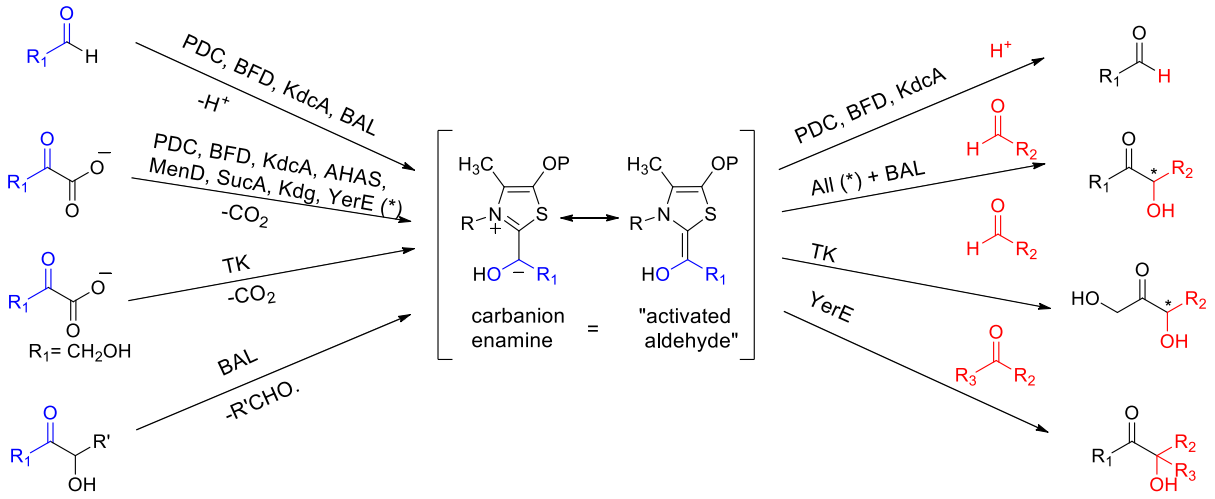

Scheme 1.3. Reactions catalyzed by the ThDP-dependent enzymes. The generation of the 2-α-carbanion intermediate is common to all reactions catalyzed by this class of enzymes. KdcA (ketoacid decarboxylase from *Lactococcus lactis*), BAL (benzaldehyde lyase), AHAS (acetohydroxy acid synthase), MenD (2-succinyl-5-enolpyruvyl-6-hydroxy-3-cyclohexene-1-carboxylate synthase), SucA (α-ketoglutarate decarboxylase subunit of the α-ketoglutarate dehydrogenase from *E. coli*), Kdg (α-ketoglutarate decarboxylase from *Mycobacterium tuberculosis*), YerE (ThDP enzyme from *Yersinia pseudotuberculosis*). Representation adapted from Hailes *et al.*[80]

Considering the wide range of reactions they catalyze, ThDP-dependent enzymes exhibit great diversity in their sequence and structural organization. In order to store all the information and establish a consistent and in-depth comparison of protein sequences and structures of this enzyme family, a data base named "The Thiamine diphosphate dependent Enzyme Engineering Database" (TEED) was created. The enzymes can be classified into 8 superfamilies, according to their structural arrangement and their domains: decarboxylases (DC), oxidoreductases (OR), sulfopyruvate decarboxylases (SPDC), phosphopyruvate decarboxylases (PPDC), α-ketoglutarate dehydrogenases (KDH) subfamily K1 and KDH subfamily K2, and transketolases (TK).[81]

1.4. Transketolase

One very important ThDP-dependent catalyst is the enzyme transketolase (EC 2.2.1.1, TK) which belongs to the enzyme class of transferases. TK catalyzes the formation and cleavage of C-C bonds reversibly extending the carbon chain length by 2-carbon units.[1] This enzyme was first isolated in 1953 from baker's yeast by Racker *et al.*[82]. TK is a key enzyme for the carbohydrate metabolism; together with the enzyme transaldolase, TK provides a reversible bridge between the glycolysis and the pentose phosphate pathway (PPP) (Scheme 1.4). It is also involved in the Calvin cycle in plants.

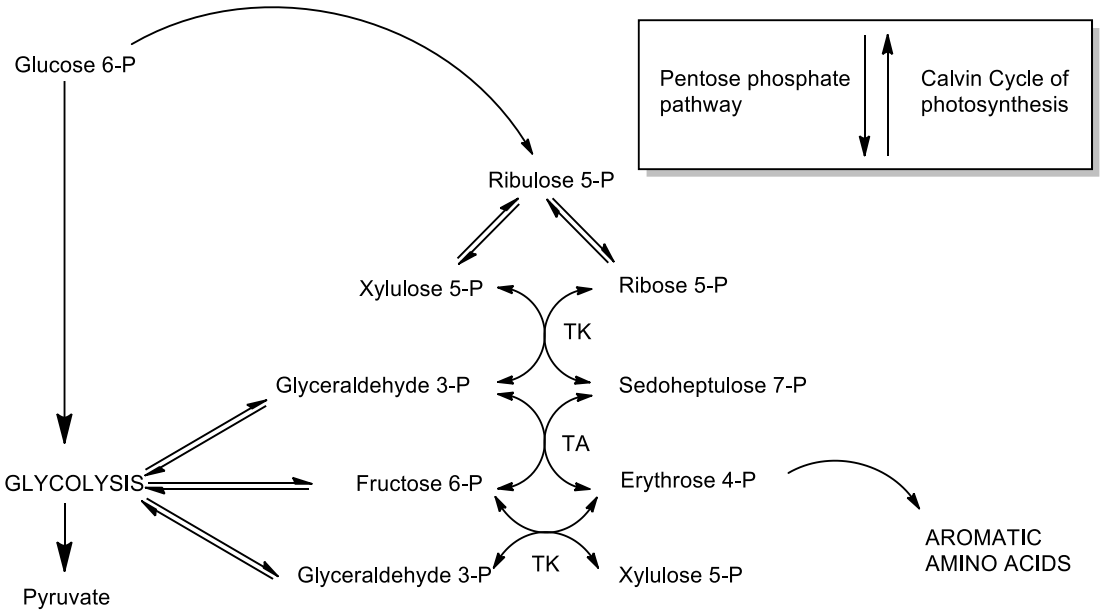

Scheme 1.4. Simplified illustration of the reactions catalyzed by transketolase (TK) and transaldolase (TA) that serve as a link between the glycolysis and the penthose phosphate pathway (PPP). The Calvin cycle of photosynthesis operates in the opposite direction. Representation based on Kochetov *et al.*[83]

In vivo, TK catalyzes the reversible transfer of a two-carbon unit, a hydroxyacetyl group or "ketol", between phosphorylated ketoses, as donors, and phosphorylated aldoses, as acceptors, both originating from sugar phosphates. This catalysis occurs in the presence of its two cofactors, ThDP and a divalent metal cation, such as Ca^{2+}, Mn^{2+} or Mg^{2+}. [1-2] In the pentose phosphate pathway, TK catalyzes the relocation of a two-carbon hydroxyacetyl moiety from D-xylulose 5-phosphate (X5P, 5 carbon atoms ketose) to D-ribose 5-phosphate (R5P, 5 carbon atoms aldose) to produce D-sedoheptulose 7-phosphate (S7P, 7 carbon atoms ketose); and from X5P to D-erythrose 4-phosphate (E4P, 4 carbon atoms aldose), to produce D-fructose 6-phosphate (F6P, 6 carbon atoms ketose). In both reactions D-glyceraldehyde 3-phosphate (GA3P) is produced as the secondary product (Scheme 1.5).[1] The phosphorylated monosaccharides that are produced in this pathway allow the synthesis of essential biomolecules, such as aromatic amino acids, nucleic acids, vitamins, and cell wall constituents.[84] In the Calvin cycle of the photosynthesis this synthetic path is reversed. The reactions catalyzed by native TKs are stereospecific and form new chiral centers with (*S*)-configuration, providing access to phosphorylated ketoses of D-*threo* (*3S*, *4R*) configuration, because the enzyme only consumes α-hydroxyaldehyde substrates with (*R*)-configuration at the second carbon (Scheme 1.5).[3]

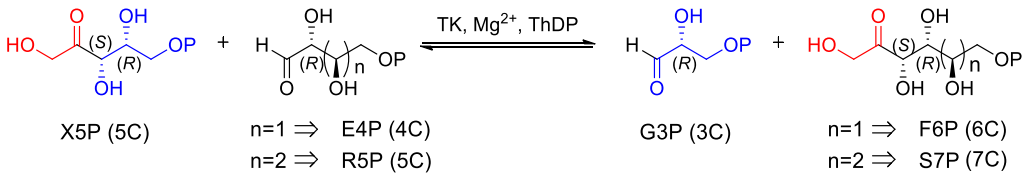

Scheme 1.5. Reactions catalyzed by TK *in vivo*.

TK is also able to resolve racemic aldehyde starting materials, and consequently less priced racemic mixtures could be employed as substrates for the synthesis of enantiomerically pure

products.[85-86] Moreover, TK is present in every photosynthetic organism and in every living creature able to use the pentose phosphate pathway, as it is involved in the non-oxidative branch of this route. Therefore, it has been found in both prokaryotes and eukaryotes, such as bacteria, yeast, plants and animals.

1.4.1. Transketolase structure and function

The structure of TK of *Saccharomyces cerevisiae* (TK_{yst}) was first elucidated in 1992 and then was refined to 2 Å in 1994 (TK_{yst}, PDB code 1TRK) (Fig. 1.4, A).[87-88] From then on, the TK crystal structures from a vast diversity of TK sources have been elucidated, for example: *Escherichia coli* (TK_{eco}, PDB code 2R8O, 2R8P, 1QGD)[89-91]; *Bacillus anthracis* (TK_{ban}, PDB code 3M49 and 3HYL); *Leishmania Mexicana* (PDB code 1R9J)[92]; and *Chamydomonas reinhardtii* (PDB code 5ND)[93]; to name a few.

Within all TK sources known up to date, the enzymes bear a conserved structure of homodimers consisting of two subunits with a molecular weight of approximately 74 kDa. Accordingly, TKs have two active sites of equal catalytic activity, each containing a ThDP molecule and a bivalent metal cation. The presence of the latter has been found to be a requirement for the efficient binding of the coenzyme ThDP; in the absence of it the affinity of the active site towards the ThDP molecule remarkably decreases.[94] Normally, Ca^{2+} can act as the cofactor, yet Mg^{2+}, Mn^{2+} and Co^{2+} may also substitute for it. However, the affinity of the apo-TK (apoenzyme: inactive enzyme) towards the ThDP molecule seems to be higher in the presence of a Ca^{2+} ion.[94-95] Each TK subunit consists of three domains: a diphosphate (PP), a pyrimidine (Pyr), and a C-terminal domain. The dimeric structure of TK is maintained principally by the diphosphate and pyrimidine domains (Fig.1.4, A).[87] The C-terminal domain, which is located further from the active site, is not involved in the cofactor binding. In fact, its presence does not appear to be essential for TK activity since studies with TK_{eco} have shown retention of the enzymatic activity after suppression of this domain.[96]

TK from different sources, although having different sequences, share a common characteristic: The coenzyme is buried deeply in the active site at the interface of both adjacent TK subunits between the PP and Pyr domains (Fig. 1.4, B). In fact, these domains are common to all ThDP-dependent enzymes.[96-98] The diphosphate group of the ThDP molecule is connected to the diphosphate domain of one subunit and the aminopyrimidine ring is linked to the pyrimidine domain of the second subunit. These crucial interactions between the two subunits build two deep and equivalent active site clefts, where the cofactors are located.

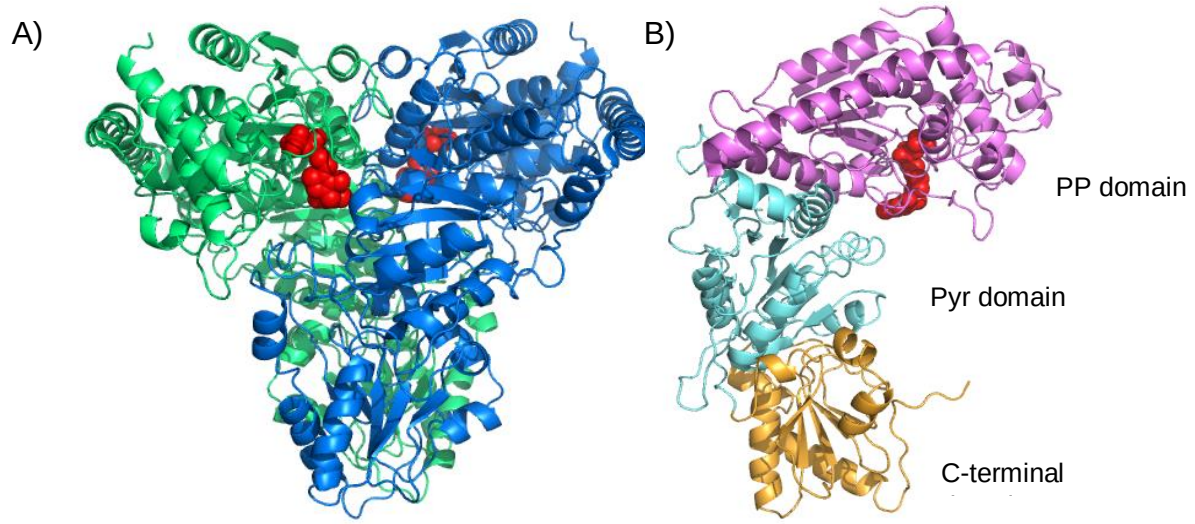

Figure 1.4. Structure of *Saccharomyces cerevisiae* TK (TK_{yst}). A) Structure of the TK homodimer. The two chains are shown in different colors (green and blue). B) The three domains of a TK monomer are displayed, PP domain (purple), Pyr domain (cyan) and C-terminal domain (yellow). The α-helices are shown as helices, the β-sheets as ribbons, and ThDP is represented as red spheres. Figure produced in PYMOL (PDB code 1TRK).

Since TK_{yst} has been the most extensively studied TK, it will be used as model to explain the interactions within the active site of the enzyme. The residues His69, His263, and Gly158 form hydrogen bonds with the diphosphate group of the coenzyme, binding the ThDP to the protein directly (Fig. 1.5).

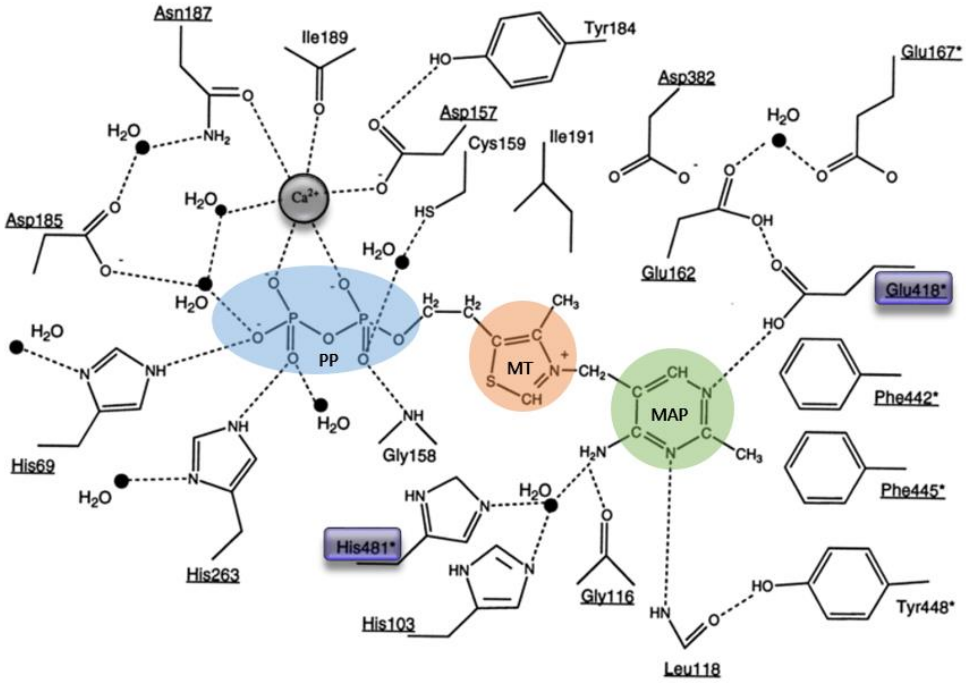

Figure 1.5. Interactions between the cofactors and the active site residues of TK_{yst}. The conserved residues are underlined and the residues belonging to the second subunit are followed by an asterisk. The residues Glu418 and His481 from the second subunit are displayed inside a blue square. Illustration adapted from Schneider *et al.*[99]

The diphosphate group is also indirectly stabilized by interactions with the divalent metal ion (Ca^{2+} in TK_{yst}), which, at the same time, is anchored to the active site of the protein via interactions with Asn187 and Ile191. The thiazolium ring of the ThDP is bound to the active site of the protein mainly via hydrophobic interactions with the residues of both subunits, since it is located between the diphosphate domain from one subunit and the pyrimidine domain from the other subunit. The conserved hydrophilic aspartic acid residue, Asp382, located in the vicinity of the thiazolium ring, is essential for the binding of the cofactor ThDP to the enzyme and, in addition, it is probably involved in compensating the positive charge of the thiazolium ring. The aminopyrimidine ring is connected to a hydrophobic pocket consisted mainly by residues of the pyrimidine domain of the other subunit, Phe442 and Phe445, and Tyr448. Because both subunits are involved in the active site arrangement, the dimer shall be considered as a catalytically competent entity.[99-100]

The most important residues for TK catalysis are glutamic acid 418 and histidine 481. The former one establishes a hydrogen bond to the N1' of the aminopyrimidine ring of the ThDP molecule, which has been found to be present in all ThDP-dependent enzymes, whereas the latter is located to dissociate the proton of the active imino group.[1] This is essential for the catalytic activity of the enzyme as it is critical for the reaction mechanism,[99] which is indicated to be consistent with a Ping Pong Bi Bi mechanism. There, the ketol donor substrate and the aldehyde acceptor bind to the enzyme sequentially, with subsequent release of the product.[101] The detailed catalytic mechanism of the ketol transfer reaction has been thoroughly explained in the literature.[88, 90, 102-103]

When ThDP is bound to the enzyme, it adopts a V-conformation, which is less energetically favorable but more active. The V-conformation, because it brings the amino group of the pyrimidine ring closer to the C2 carbon of the thiazolium ring, grants the intramolecular activation of the catalytically important C2 atom. The reaction therefore starts with the intramolecular deprotonation of the C2 atom. In this step a carbanion named "ThDP ylide" is formed (Scheme 1.6). It has been proven that the abstraction of this proton is necessary for catalysis, since it leads to the generation of a carbon nucleophile for attack to the carbonyl group of the donor substrate.[1, 74, 104]

The attack of the negatively charged C2 atom to the carbonyl of the ketose donor substrate (*e.g.* X5P) is followed by the cleavage of the C2-C3 bond of the substrate and subsequent release of the donor fragment, an aldose. This yields the ThDP molecule covalently bound to the keto unit as an α,β-dihydroxyethyl-ThDP (DHE-ThDP) enamine. Then, the acceptor molecule (*e.g.* R5P) enters the active site and a nucleophilic attack by the DHE-ThDP on the acceptor substrate takes place. In this way, the dihydroxyethyl group is ligated to the acceptor substrate and a ketose product with an elongated carbon skeleton is finally released from the active site (*e.g.* S7P). Because the product also bears a ketol group, it can act as a ketol donor, making the reaction absolutely reversible.

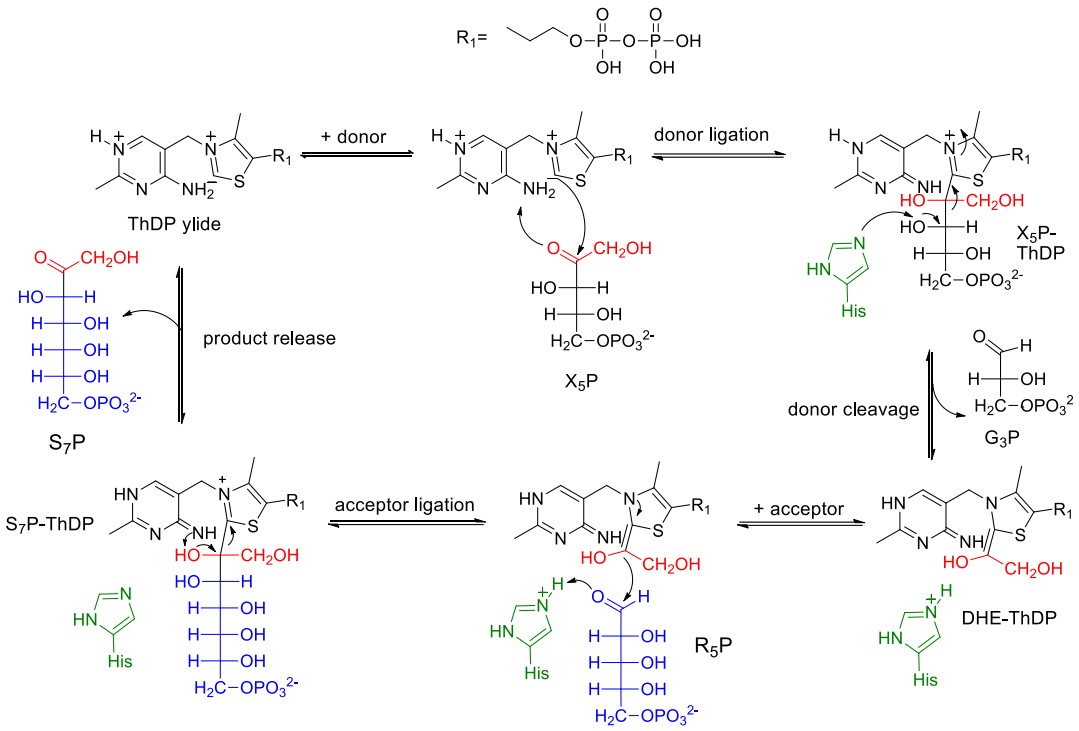

Scheme 1.6. Catalytic mechanism of TK with X5P as donor and R5P as acceptor substrate to form S7P.[105]

Comparing the crystal structures of TK$_{yst}$, TK$_{eco}$ and TK$_{ban}$, it is noticeable that they all have a comparable active site arrangement (Fig. 1.6). This fact suggests that these three bacterial TKs have an analogous mechanism for their carbon-carbon bond forming reactions, due to the highly conserved residues that build the active site of each protein, as related above.

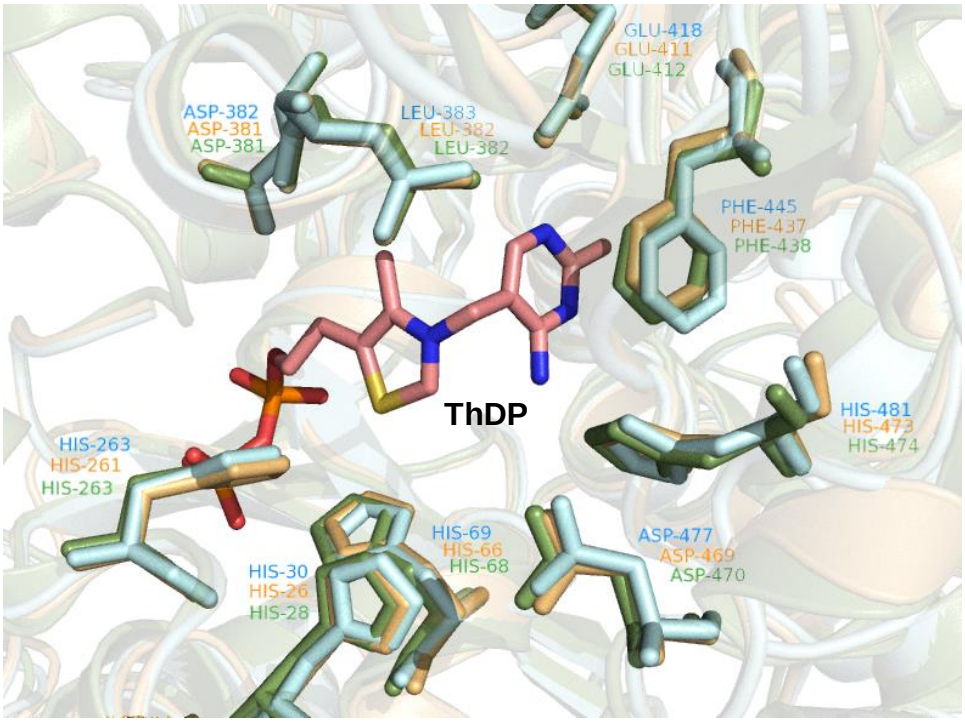

Figure 1.6. Active site alignment of TK$_{yst}$ (blue, PDB code 1TRK), TK$_{eco}$ (orange, PDB code 1GQD) and TK$_{ban}$ (green, PDB code 3M49) for ThDP cofactor binding.

1.4.2. Natural substrate specificity

Transketolase is a very versatile enzyme; it offers the opportunity to vary both the acceptor and donor substrates, leading to many distinct synthesis possibilities and a wide variety of products.[106] To take advantage of this fact, several scientists have carried out numerous studies with the aim of finding new suitable substrates to extend the substrate scope of this enzyme. Bacterial TK and yeast TK (TK_{yst}) are among the most utilized TK for synthetic purposes, because they possess high soluble expression in prokaryotic systems, rather high stability, and an extensive substrate range.[1] [107]

1.4.2.1. Natural donor substrates

Although the wild-type TK (WT-TK) is able to accept a broad diversity of acceptor substrates, particularly those carrying an α-hydroxy group, it shows rather narrow tolerance towards the donor substrates with regards to synthetic aims.[108] Natural phosphorylated ketose donors are expensive and they can be replaced for non-phosphorylated ketoses, such as dihydroxyacetone[108], L-erythrulose[109], 1-deoxy-D,L-erythrulose,[109] 1-deoxy-L-erythrulose,[109] L-sorbose,[110] D-fructose,[110] and D-sedoheptulose.[110] However, the TK-catalyzed reaction with all these donors is fully reversible as there exists an equilibrium between substrates and products, which reduces the maximum product yields significantly. For application in practical synthesis, a strategy to shift the equilibrium towards the desired product is necessary.

A common approach to accomplish this is by using carbon dioxide-releasing donor substrates, which render the TK-reactions practically irreversible. Accordingly, β-hydroxypyruvic acid (HPA) can be utilized as a suitable donor substrate.[82] The reaction proceeds with concomitant release of carbon dioxide from the reaction mixture as by-product, together with a two-carbon fragment transfer. Thus, the application of HPA as the non-phosphorylated ketol donor shifts the equilibrium of the enzymatic reaction entirely towards the product formation, leading to a practically non-reversible product generation (Scheme 1.7).[4, 111]

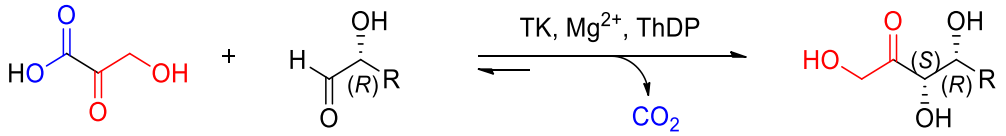

Scheme 1.7. General reaction catalyzed by TK *in vitro*, in the presence of HPA as the donor substrate.

Due to the high cost of commercial HPA, its lithium salt (Li-HPA) is generally used for preparative scale purposes. The Li-HPA synthesis that is most commonly employed follows the protocol established by *Dickens and Williamson* in 1958.[112-113] As a result of this discovery, it has been feasible to exploit the synthetic potential of TK for the synthesis of ketoses and analogs. This renders TK catalysis more generally useful and widely applicable, making TK a very promising and potent biocatalyst for the industry.[3]

Because WT-TK is able to readily accept HPA as donor substrate of the reaction, the eagerness to find analogs of HPA also accepted by the enzyme led various research groups to work towards this goal. A wide variety of α-ketoacids have been considered to replace the keto donor role of HPA in the TK catalyzed reactions. The prerequisite for the use of these substrates as TK donors for preparative synthesis purposes is that the decarboxylation principle remains intact so that the reaction continues to be quasi-irreversible.

With this in mind, the group of L. Hecquet has tested pyruvate (PA), mercaptopyruvate, chloropyruvate and glyoxylate for this purpose.[114] From that study, it appeared that pyruvate, mercaptopyruvate and chloropyruvate were not suitable as substrates for the TK reaction. However, the TK-mediated syntheses with glyoxylate as formyl group transfer successfully furnished the desired products: D-threose was obtained from D-glyceraldehyde, D-altrose from D-ribose, and L-glucose from L-arabinose. Furthermore, analytical studies with other halogenated analogs of HPA were performed by the group of Kochetov.[108] In this case, chloropyruvate, dichloropyruvate, fluoropyruvate, dibromopyruvate, and bromopyruvate were investigated in comparison to HPA as positive control for TK_{yst} reactions. The authors reported that the latter was the most active donor, giving even higher activity than HPA. Additionally, TK reactions with the dihalogenated PA derivatives gave an activity comparable to the one obtained for HPA. Moreover, other α-ketoacids, such as PA again, oxaloacetic acid and ketogluconic acid have also been tested by the group of U. Hanefeld as potential donor substrates for the TK reaction.[106] Unfortunately, no activity was detected for any tested substrate on an analytical scale in the presence of glycolaldehyde as an excellent acceptor.

1.4.2.2. Natural acceptor substrates

Both TK_{eco} and TK_{yst} have shown *in vitro* tolerance towards a wide range of non-phosphorylated α-hydroxylated aliphatics and aldose sugars as acceptor substrates.[115-119]

In the presence of polyhydroxylated aldehydes the rate of the TK reaction decreases as the carbon chain lengthens, a property shared with fructose-bisphosphate aldolase. For instance, the TK activity towards D-glucose (6 C atoms) is lower than towards D-erythrose (4 C atoms), itself lower than that of D-glyceraldehyde (3 C atoms). Moreover, TK has shown very strict kinetic preference for α-hydroxylated aldehyde acceptors bearing a hydroxyl group in *2R*-configuration. Therefore, deoxyaldehydes or L-α-hydroxylated aldehydes, such as L-glycer-aldehyde or propanal, are not suitable substrates for the natural TK reaction. This has been demonstrated by the relative reaction rates of D-glyceraldehyde (78%) and L-glyceraldehyde (ca. 0%) compared to glycolaldehyde (100%) as reference substrate. Thus, (*2R*)-α-hydroxylated aldehydes yield exclusively ketoses of D-*threo* (*3S*, *4R*) configuration.[115, 117-118, 120] Comparable results were obtained with the TK of spinach leaves in the presence of α-hydroxylated aldehydes. The reaction of (*2R*)-configurated aldoses, such as L-arabinose, L-lyxose, D-xylose and D-ribose, in the presence of HPA as donor, led to the production of the corresponding products, L-*gluco*-heptulose, L-*galacto*-heptulose, D-*ido*-heptulose and D-sedoheptulose, while the (*2S*)-configurated aldoses were not accepted by the TK.[110] This

feature has been profitable in order to produce (*2S*)-α-hydroxylated aldehydes from racemic mixtures.[121]

Furthermore, a study revealed that the activity of TK is also influenced by the configuration of the 3C of the polyhydroxylated aldehyde substrates. For instance, spinach TK was at least 2-fold more active against D-erythrose (*2R, 3R*) than against L-threose (*2R, 3S*). That indicates that, as well as the (*2R*)-configuration, the (*3R*)-configuration is preferred by the TK. This trend has been validated by the determination of the K_M of the TK from spinach leaves towards erythroses, such as L-lyxose (*2R, 3R, 4S*) and D-ribose (*2R, 3R, 4R*); versus towards threoses, such as L-arabinose (*2R, 3S, 4S*) and D-xylose (*2R, 3S, 4R*). For the former two compounds the K_M is significantly lower than for the two latter ones.[110]

TK has also been shown to accept non-α-hydroxylated aldehydes, yet with significantly lower activity compared to the corresponding α-hydroxylated aldehydes. For example, when employing acetaldehyde the reaction rate of TK_{yst} is only ca. 25% compared to that with glycolaldehyde (100%).[117] Noticeable is that for these non-α-hydroxylated aldehydes, the 3C-configuration no longer appears to be essential for TK activity, however, the (*3R*)-configuration still seems to be slightly favored by TK. This argument was verified by determining the kinetic constants K_M and V_{max} of TK_{yst} against a panel of β-hydroxylated and non-α-hydroxylated aldehydes.[122]

Finally, more peculiar α-hydroxylated aldehydes have also been accepted by WT-TK, particularly those bearing an alkene, alkyne, azide, cyano, and even 1,3-dithiane groups, yet with rather low activities.[79, 85]

1.4.2.3. One substrate reaction

Interestingly, the group of Kochetov has discovered that in addition of the TK-mediated keto transfer reaction between the ketose donor and the aldose acceptor, WT-TK is also able to catalyze the so-called one-substrate reaction by utilizing only a single substrate at a time as either donor or acceptor. First, the application of TK_{yst} for the reaction with a ketose phosphate (X5P) acting both as donor and acceptor was achieved (Scheme 1.8).[123-124]

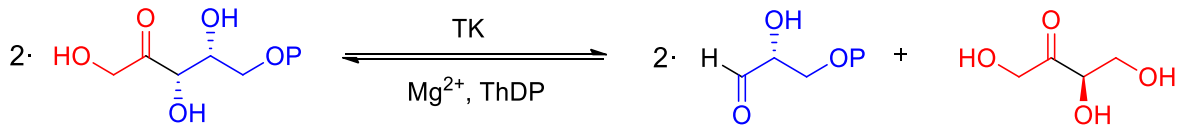

Scheme 1.8. One substrate TK reaction with X5P as donor and acceptor to yield G3P and erythrulose.

The mechanism of this type of single substrate reactions was unknown until new mechanistic studies were reported in 2020.[125-126] During these studies, HPA was utilized as both the donor and acceptor substrate for the one-substrate reaction, and the subsequent erythrulose formation was analyzed. As in the two-substrate reaction, the use of HPA renders the one-substrate reaction quasi-irreversible by release of carbon dioxide. The first half of the mechanism is common to the two-substrate reaction, as it consists on the deprotonation of the C2 atom of the

thiazole ring and the stabilization of the formed carbanion by the aminopyridine group. According to mass spectrometry (MS) and 3D modelling studies, the first glycol aldehyde residue bound to the C2 atom of the thiazole ring should be transferred to another binding site during the second half of the catalysis, the aminopyrimidine ring. Then, the second keto substrate molecule should subsequently bind to the C2 atom, producing the second glycolaldehyde moiety. Afterwards, the two glycolaldehyde molecules would condensate and form erythrulose in the thiazole ring of ThDP, which would be released from the active site (Scheme 1.9). The function of the ThDP amino group as the covalent binding site for the transferred moiety of the substrate was proved by the independent obtention of three fragments of different forms of the main intermediate (MI) (164.082, 180.076, and 182.092) in MS.

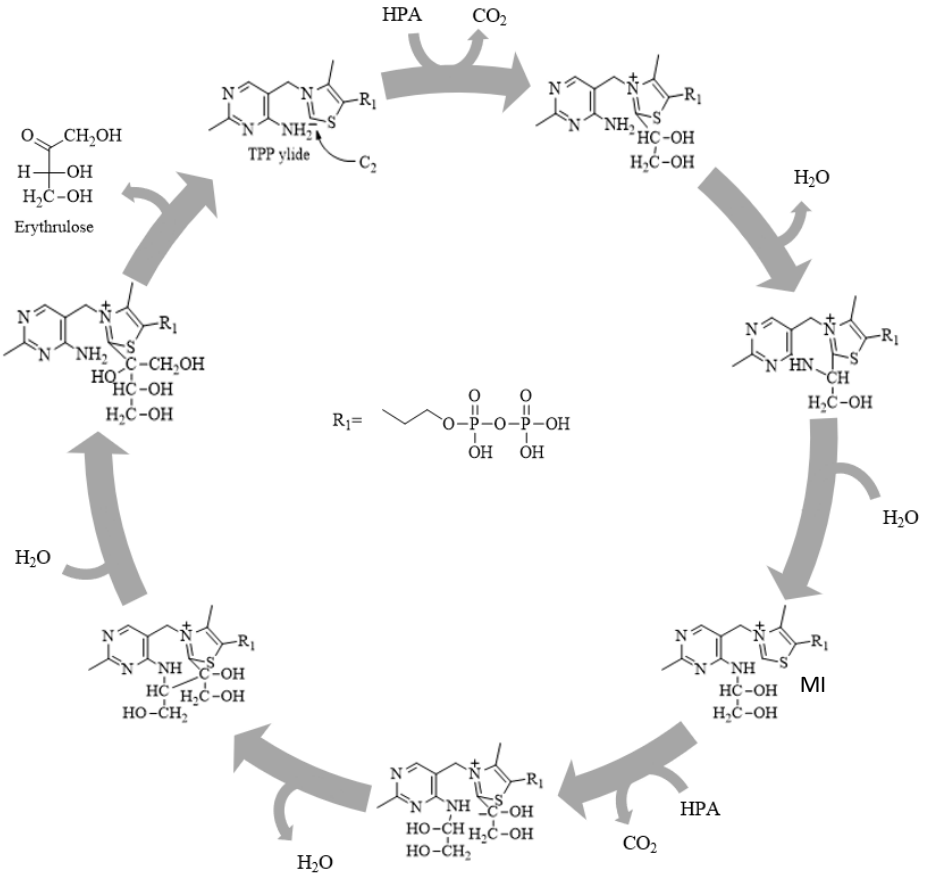

Scheme 1.9. Proposed mechanism for the one-substrate TK reaction with HPA as donor and acceptor. The formation of erythrulose could eventually happen at the C2 atom of the thiazole ring or at the N atom of the aminopyrimidine ring. Representation adapted from Solovjeva *et al.*[126]

Moreover, the possibility of utilizing only an aldose as both donor and acceptor substrate for the TK*yst* reaction was investigated. The use of glycolaldehyde as both donor and acceptor yielded erythrulose as the only product (Scheme 1.10).[127]

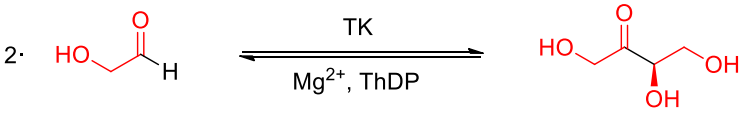

Scheme 1.10. One substrate TK reaction with glycolaldehyde as donor and acceptor to yield erythrulose as the only product.

In this case, the mechanism is very similar to that of a two-substrate reaction, since the coenzyme can interact with glycolaldehyde directly to form the DHE-ThDP intermediate. Then the glycol aldehyde residue is transferred to a free glycolaldehyde molecule and erythrulose is produced as the only reaction product. However, the rate of the one-substrate reaction is significantly lower than that of the two-substrate reaction, being the rates 0.23 and 18 U/mg, respectively. [127]

1.4.3. Directed evolution of TK

1.4.3.1. Engineering the acceptor and donor substrate scope of TK

As previously mentioned, the *in vivo* acceptor substrates of TK are phosphorylated sugars. Although TK has also shown tolerance towards various acceptor substrates, structurally very distant from its natural substrates, its activity is greatly reduced leading to low relative reaction rates; as for example, with non-phosphorylated aldehydes, non-phosphorylated long-chain polyhydroxylated aldehydes, aliphatics, aromatic aldehydes and heteroaromatics. For a successful application of TK on a preparative scale, this limitation must be overcome. For that reason, TK has been engineered by applying diverse directed evolution strategies to accept a large number of novel donor and acceptor substrates.[128]

The first protein engineering studies were carried out with TK_{eco} by the groups of Dalby and Hailes.[129] The goal was to expand the tolerance of TK towards non-phosphorylated polar acceptor substrates. This was achieved by constructing saturation mutagenesis libraries on the active site of TK_{eco} with the chosen acceptor substrate glycolaldehyde. Twenty amino acid residues neighboring the ThDP molecule and the acceptor were selected as candidates for mutation. The best variant H461S was able to improve the activity of TK_{eco} 4.8-fold when using HPA as donor.[129] Considering the strict enantioselectivity of WT-TK towards acceptors with a hydroxyl group in α position, the desire to find suitable non-polar acceptors led the researchers to the re-screening of the constructed libraries towards a non-hydroxylated non-phosphorylated aliphatic aldehyde substrate, the non-natural propionaldehyde. Thirteen mutants with enhanced activity were identified in this case and the most outstanding variant D469T gave an improvement of 4.9-fold in activity relative to WT-TK. This mutant also displayed 8.5-fold specificity towards propionaldehyde compared to glycolaldehyde, which supposes a considerable augment. This confirms that the lack of phosphorylation and hydroxylation on an acceptor substrate was not detrimental in any way for TK activity.[130] Additional TK development was accomplished by screening for TK mutants with enhanced activity towards lengthy aliphatic[131], cyclic[131], aromatic[132-134] and heteroaromatic[132] aldehyde acceptor substrates. It is worth mentioning, that the acceptance of aromatic benzaldehyde derivatives by TK opens potential roads to chiral aromatic amino-alcohols such as nor-ephedrine and chloramphenicol antibiotics, among others.[133-134]

Then, the group of Hanefeld investigated the improvement of TK_{yst} towards long chain polyhydroxylated acceptor substrates, such as D-ribose (5 C atoms) and D-glucose (6 C atoms), by directed evolution.[106] Five libraries were created and screened by site saturation mutagenesis. The best single variant R528Q showed a 1.7-fold activity improvement towards

D-ribose and 1.9-fold towards D-glucose in comparison with the WT-TK. A second generation of double mutants was subsequently created combining the prior best variants. The mutant R528Q/S527T displayed the best result, as it was able to enhance the activity of TK_{yst} by a factor of 2.6 and 2.1 relative to the WT-TK for D-ribose and D-glucose, respectively.[98] In this work it was possible to observe the synergistic effect of simultaneous mutations by following the "group-mutation" strategy proposed by Reetz *et al*.[135]

Lately, there has been increased interest in researching the use of waste biomass sugar beet pulp to generate valuable chemicals. The acceptance by TK towards L-arabinose, one of the major components of this waste, results in L-*gluco*-heptulose, a rare natural heptose with potential therapeutic uses in cancer and hypoglycemia.[136-137] For that reason, the activity of TK_{eco} towards L-arabinose, which is a long chain polyhydroxylated aldehyde, has been recently enhanced by the teams of Dalby and[137] Three libraries, each containing 90 randomly selected variants, were created by saturation mutagenesis of the conserved residues R358, H461 and R520. The screening of the reaction plates was implemented by using a high throughput colorimetric assay, and the result was afterwards corroborated *via* both HPLC and GC-MS. The two best mutants, R520Y and R520P, showed the greatest improvements towards L-arabinose with a 2.1-fold activity enhancement for R520Y and 1.5-fold for R520P relative to WT-TK. The variant H461Y and the variant R520Y were additionally selected because of the higher conversion rates and good enzyme stability in comparison to the other mutants. In preparative scale syntheses, L-*gluco*-heptulose was successfully generated with a 45% isolated yield for the first mutant and 45% for the second one.[137]

Very recently, TK_{eco} was again engineered to tolerate unnatural acceptor aliphatic aldehydes, such as propanal, pentanal and hexanal, the aromatic acceptor aldehyde 3-formylbenzoic acid (3-FBA), and also the non-hydroxylated PA donor simultaneously.[138] The authors reasoned that in order to stabilize novel donor substrates lacking the donor C1-hydroxyl group, exchange of the hydrogen bonds that build the interaction between the donor C1-hydroxyl group and the residues His100 and His473 in the active site of the enzyme might be necessary, and thus, the creation of new hydrophobic interactions between the methyl group in PA and other local residues might be beneficial instead to achieve that purpose. With that in mind, the authors identified nine residues (His26, His66, His100, Leu116, Ile198, His261, Ser385, Asp469 and His473) as promising mutation sites, based on structural alignment with PA decarboxylase (PDC) and prior knowledge of TK_{eco} and TK from *Geobacillus stearothermophilus* (TK_{gst}) (see Section 3.1) variants. Twenty single-variants were first created and then a small library with the favorable ones was combined. The library was screened for the two reactions separately, first between PA as donor using propanal as acceptor, and afterwards with 3-FBA as acceptor. Out of the first library screening, H192P/A282P/I365L/G506A/H100L/D469E/R520Q was identified as the best variant showing considerably enhanced efficiency relative to WT-TK. It displayed a 9.2-fold improvement in the reaction yield towards PA and propanal. Out of the second library screening, H192P/A282P/I365L/G506A/H100L/D469T was pointed out as the best mutant, as it showed 47% 3-FBA substrate conversion with PA within 24h, while no conversion was detected with WT-TK. For enzymes using two substrates for their catalysis, concurrent optimization of the affinities of both substrates is sought. Mutations that are

responsible for the simultaneous donor and acceptor tolerance appeared to have a cooperative effect, as suggested by docking studies. Therefore, this work presented a model for the future research in engineering more than one substrate specificities concurrently.[138]

A summary of the acceptor substrates that have been tolerated by engineered TKs up to date is presented in Scheme 1.11.

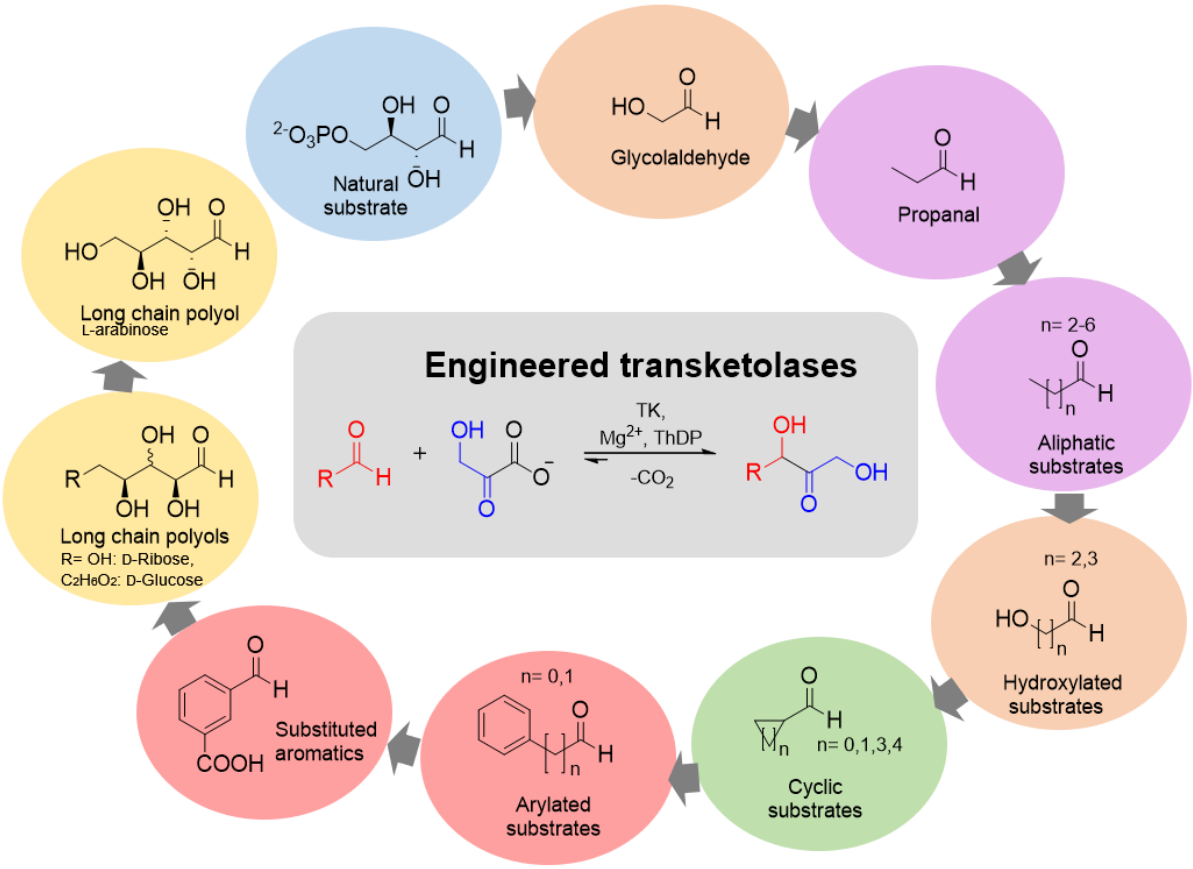

Scheme 1.11. Scope of acceptor substrates accepted by engineered TKs in the presence of their cofactors, using HPA as donor substrate to render the reaction practically irreversible by release of carbon dioxide. Representation adapted and actualized from Hailes *et al.*[80]

1.4.3.2. Engineering the stereoselectivity of TK

Because for synthetic uses biocatalysts should possess good substrate tolerance and high stereoselectivities, directed evolution has also been applied to enhance and even reverse the enantioselectivity of TK. After screening saturation mutagenesis libraries, several single variants were found able to both increase and reverse the stereoselectivity of TK$_{eco}$ towards propionaldehyde, leading to a product with (*3R*)-configuration.[139] Then, the variants D469E and H26Y were employed in reactions with lipophilic longer chain aldehydes, and cyclic compounds, such as cyclopropane-, cyclopentane- and cyclohexanecarbaldehyde. Results showed that for butanal, pentanal, and hexanal the TK provided high stereoselectivities (>97 % *ee*), and notably, the highest stereoselectivity was achieved when using aldehydes of a similar size as for the typical *in vivo* TK substrates. Also, the mutant D469E enhanced the enantioselectivity (*S*-configurated) of the cyclic aldehydes to >99% *ee* in the case of

cyclopropane and cyclopentane, and 97% *ee* for cyclohexane, being significantly higher than that of WT-TK.[131] Further, mutations at D469, that led to improvements on the TK catalytic activity, were combined with other variants from the same coevolved network, and were screened against propionaldehyde. Remarkable fascinating variants that showed increased enantioselectivities relative to the single-point variants were D469T/R520Q [68% *ee* (*S*)], D469Y/R520V [85% *ee* (*R*)] and D469Y/ R520Q [65% *ee* (*R*)], all having a more than 6-fold improvement in specific activity compared to WT-TK.[80]

1.4.3.3. Engineering the thermostability of TK

Thermostability is a powerful and valuable characteristic for an enzyme. The stability of an enzyme biocatalyst is affected by various factors, such as pH, oxidation, temperature, binding or dissociation of cofactors, solvents, and substrate and product inhibition.[140] Among all these potential protein denaturing factors, temperature is the best studied. At high temperatures many enzymes become totally or partially unfolded or inactivated, and thus, the enzymes cannot longer execute the corresponding tasks.[141] Thermostable enzymes allow reactions at elevated temperatures, providing usually higher reaction rates than at lower temperatures. In addition, at these temperatures the solubility of the acceptors, such as hydrophobic aldehyde substrates, is normally increased. Therefore, elevated thermostability makes it possible to improve the enzyme tolerance towards unconventional hydrophobic organic acceptors.[5] From an industrial point of view, thermostable enzymes are of significant biotechnological interest, as their improved thermal stability could provide opportunities to expand the TK biocatalytic applications for preparative synthetic uses and for improvement of future biocatalysts.[141]

Despite the great improvements that have been achieved in modifying the substrate range of TK_{eco}, its rather limited thermostability is still a challenge for industrial applications, since elevated temperatures are often used to increase reaction rates, enhance substrate solubility in aqueous solutions, and reduce the risk of microbial pollution. Optimum TK_{eco} activity is reached between 20-40 ºC and drops very fast when temperatures rise above 55 ºC. For that reason, the thermotolerance of TK_{eco} has been engineered by the group of Dalby and Hailes by progressively mutating the cofactor-binding loops of the enzyme (residues 185-192 in sequence 1 and 382-392 in sequence 2) towards the analogous amino acid sequence located in *Thermus thermophilus*.[142] The mutation of residues belonging to sequence 2 showed a detrimental effect on the TK activity at high temperatures, while the mutations in sequence 1 seemed to be fruitful. The best variant found, H192P, was able to improve the enzyme thermostability by a factor of 2 relative to WT-TK, and its specific activity was also enhanced 3-fold when incubated at 60 ºC and 19-fold when subjected at 65 ºC. Additionally, the activity was improved 2.7-fold and 4-fold after one hour incubation time at 55 ºC and 60 ºC respectively. To be noted is that the thermotolerance of TK_{eco} was not examined during periods longer than one hour.

Although the optimal temperature of TK_{eco} could be raised from 55 ºC to 60 ºC,[142] significant improvement in both thermostability and specific activity was still sought in order to accomplish the preparative scale reactions with good yields. In 2017, the team of Dalby discovered a strategy to engineer TK_{eco} for enhanced thermostability by mutating the flexible loops of the protein, which have already been found to play a significant role in modulating the

enzyme stability.[143-144] In this case, several specific mutation sites were targeted in a low-throughput approach, while traditional directed evolution consists of repetitive cycles of library creation employing random mutagenesis techniques and high-throughput screening. Forty single-variants in five flexible loops were created. From those, three single-variants were identified to have more thermostability than the WT-TK (I189H, A282P and D143K), and in particular, the combination of A282P with H192 from the previous library[142] provided the best results. The mutant H192P/A282P was able to improve 3-fold the half-life of the enzyme at 60 ºC and 5-fold its specific activity at 65 ºC relative to that of the WT-TK.[143] However, when compared to TK_{gst} (see Section 3.1), the latter is still more thermostable than the best engineered variant of TK_{eco}.

1.4.4. Role of TK in industrial applications

TK executes the transfer of a two-carbon ketol fragment with carbon-carbon bond formation and introduction of an asymmetric hydroxyl methylene group to the C3 position of the product. This validates TK as a powerful biocatalyst for asymmetric synthesis, particularly for the synthesis of chiral α–hydroxyketone products, which afford a valuable backbone as a precursor to chiral aminodiols, ketosugars, and other relevant molecules that could serve as building blocks for pharmaceutical compounds synthesis. This feature is extremely interesting since this category of molecules are difficult to obtain by chemical methods.[79, 145]

TK could be valuable for implementing in a large number of industrial applications. Its utility has already been demonstrated in the synthesis of pharmaceuticals;[146-148] chemicals for the food industry;[149] fine chemicals;[150-151] and agrochemicals, such as in the production of (+)-*exo*-brevicomin, a naturally occurring beetle pheromone.[152] In addition, E4P, which is generated by TA and TK during the pentose phosphate pathway, allows the biosynthesis of amino acids, such as L-phenylalanine, L-tyrosine, and L-tryptophan. This is of outmost importance since these aromatic amino acids complement a human and animal diet. Moreover, the compounds that can be chemically produced from these amino acids are considered as high-value products; *e.g.* L-phenylalanine can be converted into the artificial sweetener aspartame, whereas L-tyrosine and L-tryptophan can be transformed into eumelanin and indigo respectively.[153] The investigations of TK for industrial purposes continue to increase, making TK a very attractive biocatalyst for the industry.

1.5. Hydroxamic acids

1.5.1. Structure and function

In 1869, during the treatment of hydroxylamine with diethyl oxalate, Heinrich Lossen accidentally synthesized oxalohydroxamic acid. This fortuitous discovery led to a whole new class of compounds, the hydroxamic acids (HAs).[154] However, there was considerable lack of knowledge concerning these molecules until the 1980s, when their biomedical applications started becoming attractive for different industries, such as the pharmaceutical and agricultural

industries, among others. Since then, there has been extensive research respecting their synthesis and properties because of their applicability in various areas of modern medicine.[7]

This type of chemical molecules bears the general structure R-CO-NR'-OH, where the R and R' moieties correspond to organic residues, which can be a hydrogen, an alkyl or an aryl group. Accordingly, a large number of HA derivatives are known.[155] Their HA functionality makes them perform as weaker acids than their structurally related carboxylic acids, yet they have relatively high acidity compared to the corresponding amides. For instance, the ionization constant of aceto-HA is 2.8 x 10^{-8}.[156] The acidity of the NH or OH protons of the HA molecule are somewhat affected by the nature of the substituents.[157] The remarkable ability of the oxygen atoms in the HA to bind metals such as iron, zinc, magnesium and calcium, among others, makes them extremely interesting as organic bioligands.[156]

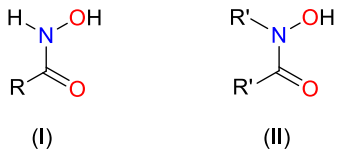

Scheme 1.12. HA classification as primary (I) or secondary hydroxamic acids (II).

HA can be regarded as derivatives of both carboxylic acids and hydroxylamines, and they can be classified as primary (I) or secondary (II) HA if the R' group is a hydrogen or an organic rest, respectively (Scheme 1.12).[158] NMR spectroscopic data revealed that HA present two diastereoisomers, *Z* (*zusammen*, together) and *E* (*entgegen*, opposite).[159] The isomerization from the *s-trans* to the *s-cys*-configuration in *N*-methylaceto-HA is much slower than expected for the rotation around a single bond, with a rate constant value of 3 s^{-1}. This can be explained considering a partial double bond character for the C-N bond, which indicates that these molecules should have two resonance structures. This hypothesis was further confirmed, as HA have been proved to exist in either of two tautomeric forms (Scheme 1.13).[156, 160]

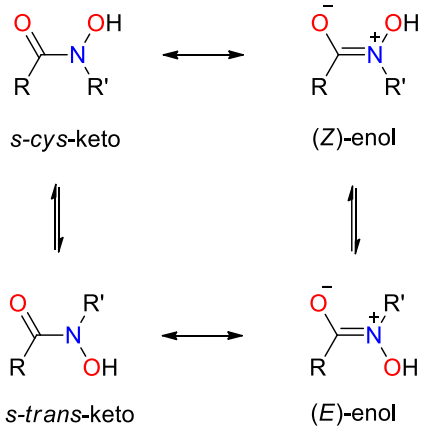

Scheme 1.13. Keto and enol resonance structures of HA.

Infrared spectroscopic studies have been employed in the literature to confirm the keto form as the predominant form.[161] Noteworthy is to remark the role of the solvent in promoting the *s-trans* to *s-cys* conformational shift. Indeed, the *s-cys*-configuration is stabilized by protic solvents by forming intermolecular hydrogen bonds (Scheme 1.14, A). However, intramolecular hydrogen bonds not involving the solvent can also stabilize the *s-cys*-configuration (Scheme 1.14, B).[159]

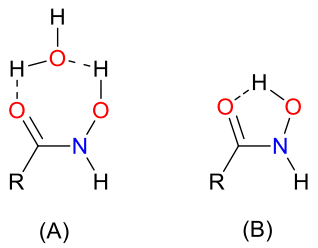

Scheme 1.14. HA in its *s-cys*-configuration with intermolecular (A) or intramolecular (B) hydrogen bonds.

The ability of these organic molecules to form hydrogen bonds plays an important role in their biomedical applications. They can form hydrogen bonds through their OH group, NH group and through the carbonyl oxygen. The OH and NH groups may act as hydrogen bond donor and acceptor, and the carbonyl oxygen as a hydrogen bond acceptor only. Therefore, depending upon the number of locations available in the receptor, hydroxamates can form 3 to 5 hydrogen bonds. This characteristic aids on strengthening the drug-receptor interactions.[156]

There is not yet consensus about which configuration is predominant in solution and as whether these molecules undergo nitrogen- or oxygen-deprotonation.[162] However, independently of the preferred structure and of the deprotonation, for a mononuclear complex formation, HA should adopt the *s-cys*- or *E*-configuration, and the chelation process should involve O-deprotonation.[163]

The dissociation of these organic molecules has been the object of a long-standing debate. Whereas the structure of the acid in favor of the keto tautomer is established, the structure of the anion formed by deprotonation is still object of research. Primary HA carry two potentially acidic protons bound to the nitrogen and to the oxygen atom of the hydroxamate group, respectively. Nonetheless, they behave only as monoprotic acids and can dissociate to form an anionic species. The double deprotonation of HA has hitherto never been observed even when investigated at the highest concentration of OH^- ions.[164] Three possible structures of the HA anion produced from oxygen or nitrogen deprotonation are reported in Scheme 1.15.

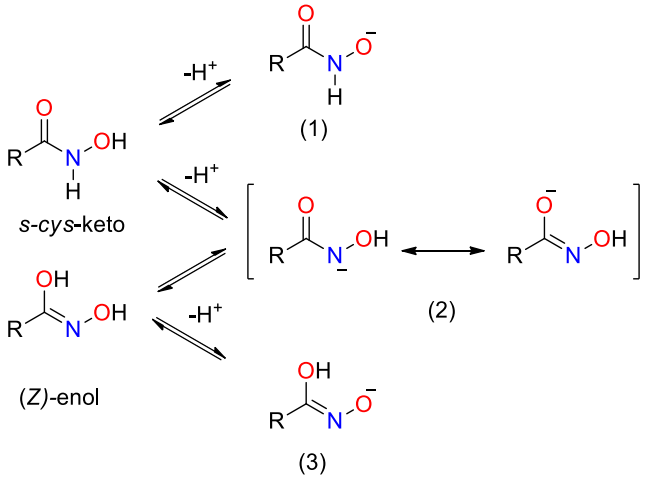

Scheme 1.15. Possible dissociation structures for HAs.

A strong controversy about the actual ionization sites for HA still remains, both N-ionization and OH-deprotonation have been proposed for primary (unsubstituted) HA, depending upon the solvent contribution. For instance, in the presence of DMSO and in the gas phase the deprotonation of the acids occurs at the nitrogen, thus acting as *N*-acids, whereas in aqueous solutions, an OH-deprotonation is favored leading to *O*-acids.[165]

Additionally, in the presence of mineral acids at least at a 1M concentration, HA may assume base character in that they are able to bind a proton at the carbonylic site, the nitrogen site or the OH site (Scheme 1.16).

Experimental results indicate that in solution and in the gas phase the former one is the preferred protonation center (Scheme 1.16, 4).[165]

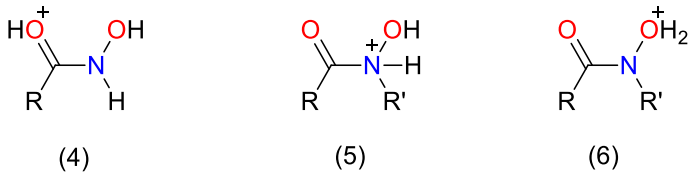

(4) (5) (6)

Scheme 1.16. Possible protonation locations for primary HA.

1.5.2. Synthesis

HA can be prepared by different methods, the majority of them having hydroxylamine as the common component of the reaction. The most frequent methods are the reaction between acid chlorides and hydroxylamine, and the reaction between esters and hydroxylamine. The most straightforward road to HA is the direct *N*-acylation of hydroxylamine. The *N*-acylation of hydroxylamine can be obtained by reaction with acid chlorides, which are readily produced from the corresponding carboxylic acids (Scheme 1.17).[166]

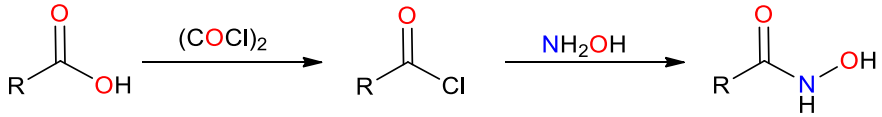

Scheme 1.17. Preparation of HA by reaction of an acid chloride with hydroxylamine.

This reaction can also be performed in the presence of coupling reagents, including ethyl-(*N',N*'-dimethylamino)propylcarbodiimide hydrochloride (EDC), benzotriazol-1-yloxytris(dimethyl-amino)phosphonium hexafluorophosphate **(**BOP), and *N,N'*-diisopropylcarbodiimide (DIC). This strategy has been employed for the synthesis of numerous biologically significant molecules, such as inhibitors of matrix metalloproteinases (MMP),[167] and of the Tumor Necrosis Factor-α-converting enzyme (TACE).[168] The *N*-acylation can take place with free or *O*-protected hydroxylamines with common protective groups, such as benzyl, allyl, and silyl groups, among others.[166, 169] This may be done to prevent potential *O*-acylation or other undesirable side reactions involveing the acidic OH or NH groups. In addition, the preparation of *O*-protected or *O,N-bis*-protected HA has been also reported.[170] After the *N*-acylation of the protected hydroxylamine the protecting group has to be removed.[166]

Additionally, carboxylic acids may be activated using appropriate chloroformates, such as ethyl chloroformate, followed by reaction with hydroxylamine in a one-pot reaction, leading to the corresponding HA. Cyanuric chloride has also been used for the activation of carboxylic acid derivatives followed by treatment with hydroxylamine, yielding HA.[171] HA can also be generated from carboxylic acid esters by reaction with hydroxylamine under basic conditions.

The free acid is obtained by acidification of the cold solution. This method has been widely used in the preparation of bioactive HA (Scheme 1.18).[172-173]

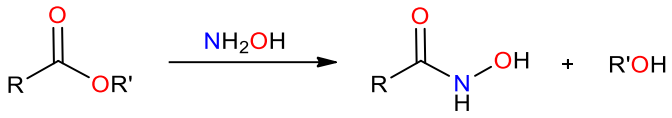

Scheme 1.18. Preparation of HA by reaction of hydroxylamine with a carboxylic acid ester.

Hydroxylamine may also be generated *in situ* by using strong bases, such as NaOH, KOH or CH_3ONa in methanol from hydroxylamine hydrochloride.[171]

Other less common methods have also been utilized for the preparation of HA: the reaction between acid anhydride and amides with hydroxylamine;[174] the oxidation of aldoximes, amines, aldehydes, amides, nitriles and ammonia by Caro's reagent (H_2SO_5);[175] solid phase synthesis of HA,[176] conversion of *N*-acyloxazolidinones using samarium triflate as a Lewis acid;[177] and using a modified Angeli-Rimini reaction between an aldehyde and solid-supported *N*-hydroxybenzenesulfonamide,[178] among other chemical methods.[166, 171, 179] Recently, an efficient photoorganocatalytic synthesis of HA has been achieved from the aldehyde precursor directly, where first the hydroacylation of dialkylazodicarboxylate is accomplished and subsequently hydroxylamine hydrochloride is added.[180]

Enzyme-mediated production of HAs has also been implemented by enzymes which are able of transferring an acyl group, such as nitrilase, lipase, amidase.[181]

In addition to the usual type of HA, there exists the constitutional isomeric reverse or retro-HA. This class of HA are *N*-alkyl/arylated derivatives of *N*-formylhydroxylamine. For example, the retro-HA of acetohydroxamic acid (AHA) is *N*-methyl-*N*-formylhydroxylamine (Scheme 1.19).

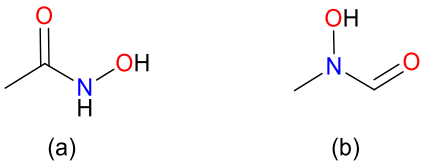

Scheme 1.19. AHA (a) vs retro-HA *N*-methyl-*N*-formylhydroxylamine (b).

The *O*-benzylation of the *N*-formyl- or *N*-acetylhydroxylamine group is frequent in synthesis of retro-HA in solution.[182] This type of retro-HAs have also been prepared *via* solid-phase synthesis.[8, 183]

1.5.3. Metal complexation

HA form stable coordination complexes with a large variety of metals or metalloids building metal-hydroxamate complexes with a wide structural diversity. Because hydroxamates have two oxygen atoms and one nitrogen, they can act as monodentate ligands through one oxygen or nitrogen atom, as well as bidentate ligands in various possible combinations, such as (*N*,*O*)-coordination, (*N*,*N*')-coordination or (*O*,*O*)-coordination.[156, 184] When amino-HA form metal

complexes, their (*N*,*O*)-coordination gives a four-membered ring (a), whereas (*O*,*O*)-coordination yields a five-membered ring (b) and the (*N*,*N*')-coordination a six-membered ring (c) (Scheme 1.20).[185-189]

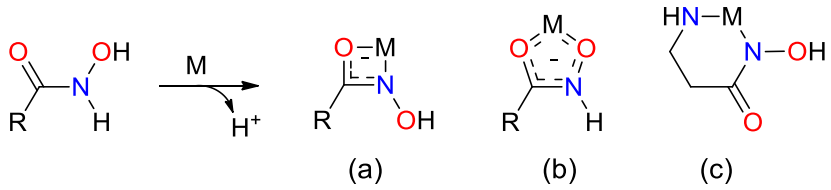

Scheme 1.20. General HA (*O*,*N*) (a), (*O*,*O*) (b), and (*N*,*N*') (c)-coordination of a metal cation (M).

However, most of the experimental data favor the bidentate mode through the two oxygen atoms. X-ray crystallographic studies showed that the most common coordination of a metal ion in HA occurs via deprotonation of the OH group and the subsequent (*O*,*O*)-bidentate metal coordination through the carbonyl oxygen and the deprotonated OH (Scheme 1.20, b).[156, 159] Because of the relevance of iron(III) complexation for biological applications, this metal was the first one to be studied. An study about the X-ray diffraction of this metal complex confirmed that the iron(III) chelation involves the carbonyl oxygen and the deprotonated hydroxamate oxygen.[190]

Studies on the metal complex formation with primary HA acid ligands in aqueous solutions demonstrated that, depending on the metal ion, the pH of the medium, and the presence of substituents on the nitrogen atom, two (*O*,*O*)-binding modes of the ligands are available to metal ions like Cu(II) and V(IV): namely the hydroxamato anion (1) and the hydroximato dianion (2) (Scheme 1.21). [191-193]

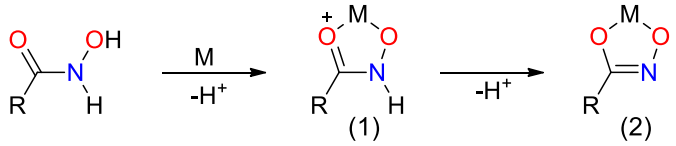

Scheme 1.21. HA complexes depending of the pH conditions: hydroxamato (1) or hydroximato (2) complex. M= Metal cation. Adapted from Adiguzel *et al*.[193]

The hydroxamato anion type (1) is the most common structure and arises from the first deprotonation step, involving the coordination of the NHO^- moiety. At high pH, the hydroximato ligand type (2) is produced by further metal-induced deprotonation of the NHO^- group.[156] Both of the forms are able to build a stable five-membered *O*,*O*-chelated ring.

Mononuclear homoleptic complexes with bidentate (*O*,*O*)-coordination have been identified and characterized with Fe(III), In(III), Cr(III), Ga(III), Co(III), Si(IV) and Ge(IV), B(III), Cu(II), Th(IB) and Hf(IV). Mononuclear heteroleptic complexes also with bidentate (*O*,*O*)-coordination have been described for Si(IV), Co(II), Co(III), V(V), Ni(II), Mo(VI), Zn(II), Ru(III), Sn(IV), W(VI), Rh(III), Os(III), U(IV) and Pt(II). Dinuclear, trinuclear and heptanuclear complexes have also been characterized.[8]

For the (*O*,*O*)-coordination to take place, it is essential that the HA groups of the siderophore are prearranged in the *cis* (*Z*)-configuration in order to chelate the metal ion (M) effectively.

Yet, X-ray crystallographic studies show that most of the secondary HA occur in the trans (E)-configuration. This fact implies that the solvent of the metal complexation reaction must play a key role in facilitating the required conformation adjustments for the (*O,O*) coordination. In chloroform both *Z*- and *E*-isomers may exist, while in DMSO the *s-cys* generally predominates, as corroborated by IR and NMR solution studies.[159]

Additionally, after being bound to the metal, the HA moiety still possesses multiple sites for potential hydrogen bond interaction with a protein backbone. These are key structural elements that make HAs even more potent drugs (Scheme 1.22).[166]

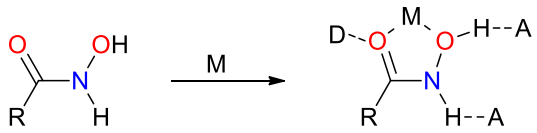

Scheme 1.22. HA-metal complexation with hydrogen bond stabilization. A: Hydrogen bond acceptor, D: Hydrogen bond donor. M= Metal cation

1.5.4. Applications in biomedical science

HA are a well-studied and important class of compounds because of their significance in many different areas of life sciences. As aforementioned, their HA functionality RC(=O)N(-OH)R' may act as a bidentate ligand, which tends to form strong chelate complexes with many different transition metals, mostly iron(III) and zinc(II) cofactors.[7]

The outstanding chemical feature of HA for sequestering iron(III) from the environment has been already used by nature millions of years before the accidental synthesis of the first HA. The hydroxamate functional group is located in diverse natural products: in various antibiotics, such as aspergillic acid (Scheme 1.23, a) and 2,4-dihydroxy-7-methoxy-1,4-benzoxazin-3-one (DIMBOA) (Scheme 1.23, b), the latter serving as anti-fungal agent as well; and in siderophores, as for example, in ferrichrome, among others.[194]

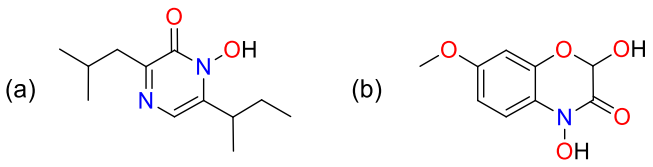

Scheme 1.23. Structure of aspergillic acid (a) and DIMBOA (b) containing the HA functionality.

The siderophores are rather small compounds that are produced by microorganisms, such as bacteria, yeast and fungi, which grow in iron-limited media, for scavenging the trivalent iron from the environment and therefore making this metal available to the microbes.[195-196] The use of HA as siderophores to selectively bind trivalent iron over other metals was one of the first reported pharmacological applications.[197] The uptake of iron and the removal of metals from the body to combat, for example, iron deficiency, iron overload or accidental metal poisoning are phenomenal properties of these type of molecules; the lack or excess of Fe (III) in the body may lead to organ failure and even death in some severe cases.

However, the properties of these compounds are not limited to their siderophore ability, and an extraordinary effort has been made into finding other therapeutic applications.[8] In fact, their metal chelating ability confers them with high pharmacological versatility; including anti-cancer, anti-inflammatory, anti-fungal, anti-bacterial, anti-malarial, antidiabetic, anti-fibrotic, antiviral, and anti-tubercular properties. They are, thus, used in the design of therapeutics to treat cardiovascular diseases, malaria, Alzheimer, human immunodeficiency virus (HIV), and allergic diseases, among others. Additionally, HA have also been employed as anti-microbials, plant growth regulators and insecticides. Moreover, they are also employed in the industry as antioxidants, inhibitors of corrosion, as redox switches for electronic devices, and even for the extraction of toxic elements.[7-8, 198-199] Among other reasons, these properties are due to the ability of HA to inhibit the activity of numerous enzymes, including ureases, peroxidases, matrix metalloproteinases (MMPs) and histone deacetylases (HDACs).[7, 200]

Furthermore, HA could serve to develop a variety of enzyme assays starting from chromogenic or fluorogenic substrates. For instance, it could serve as metal chelator to efficiently compete with the fluorescent sensor obtained from quinacridone for Cu(II) coordination and induce a fluorescence increase (Scheme 1.24). Such an effect should allow the monitoring of an enzyme-catalyzed synthesis of a noncoordinating fluorescent substrate (fluorophore) into a weakly chelating nonfluorescent product.[201-202]

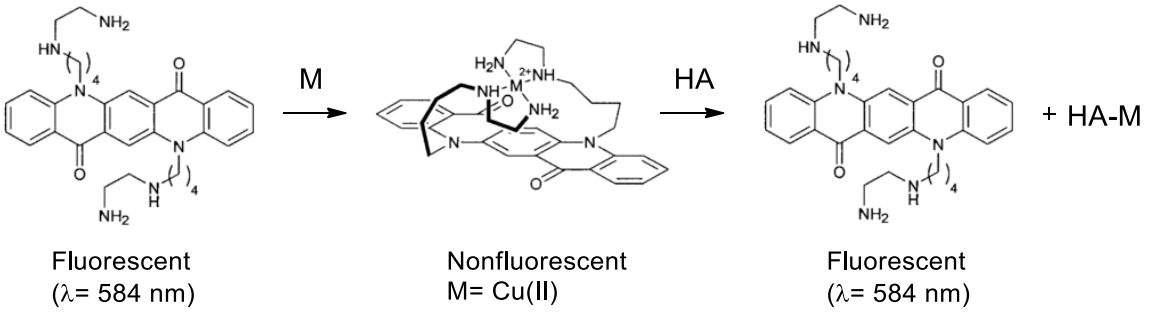

Scheme 1.24. Fluorescence assay principle coupled with a HA as metal chelator. Scheme extracted and adapted from the literature.[201]

2. Objectives

Although HA are widely used in the industry for various of applications,[7] retro-HA, which are formed by coupling an *N*-alkylated/arylated hydroxylamine with formic acid, or akin acyl units, are less frequent even though they can be expected to present very similar metal binding capability. Because of their lack of application to date, it was interesting to investigate this class of compounds. With that in mind, it was hypothesized that TK from *Geobacillus stearothermophilus* (TK_{gst}) should be able to accept nitrosoarenes as potential substrates, with the subsequent generation of *N*-aryl HAs. In order to investigate this hypothesis, nitrosobezene will be used as alternative acceptor substrate for TK_{gst}. If this premise turns out to be true, it is desirable to have a broad variety of potential substrates of different nature to expand the application scope of TK_{gst}. In addition, for finding suitable TK_{gst} variants for the conversion of nitrosoarenes, a high-throughput screening method specific for the identification of HA needs to be established. Furthermore, to the best of our knowledge, retro-HAs don't seem to have been investigated yet for biomedical applications. Hence, it is rather relevant to synthesize retro-HA analogous to traditional HA with proven medicinal properties in order to test their biological activity.

Specific objectives

Chapter I

2.1. TK reaction with nitrosobenzene

In order to investigate the hypothesis and expand the scope of TK_{gst} towards nitrosoarenes as potential TK substrates, nitrosobezene will be used as alternative acceptor substrate. This operation would lead to the generation of retro-HAs having complementary structures to the conventional HA type (Scheme 2.1).

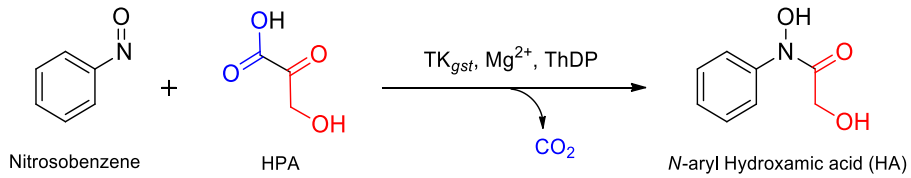

Scheme 2.1. TK reaction with nitrosobenzene as acceptor substrate and HPA as donor.

2.2. Synthesis of TK substrates

Once the hypothesis that TK_{gst} should be able to accept nitrosobenzene is proved, it is sought to have a wide range of potential substrates of different nature in order to further investigate the enzyme scope. Most of the nitrosoarene substrates for TK catalysis cannot be purchased, hence they need to be synthesized chemically from commercially available reagents. Amines are a known precursor of nitrosoarenes and, because of their commercial availability and reduced costs, the make an appropriate starting material for synthetic purposes. By using standard

laboratory protocols and adapting them for each specific compound, a wide library of nitrosoarenes as starting materials for the TK$_{gst}$ reaction will be produced (Scheme 2.2).[203]

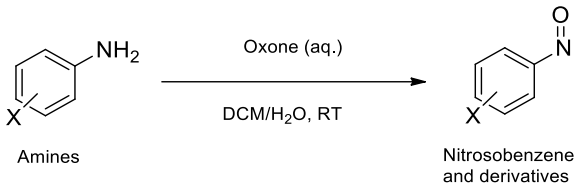

Scheme 2.2. Method for preparation of nitrosoarenes from amines according to Priewisch and Braun.[203]

2.3. TK reaction engineering and enlargement of acceptor substrate range

With the array of nitrosoarenes at hand, the acceptor scope of TK$_{gst}$ will be further investigated. Different arylated nitroso compounds will be tested employing TK$_{gst}$ as biocatalyst with HPA as donor substrate, in the presence of Mg^{2+} and ThDP as cofactors (Scheme 2.3).

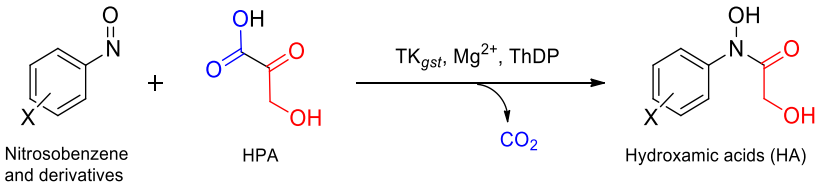

Scheme 2.3. General scheme of TK reaction with nitrosoarenes as acceptor substrates and HPA as donor.

In order to optimize the reaction efficiency and conditions, including time, quantity of enzyme, reaction handling, product purification, and yield, reaction engineering will be carried out.

2.4. Expanding the substrate tolerance of TK

To also investigate the donor substrate scope of TK$_{gst}$ towards other α-oxoacids, PA will be employed for TK$_{gst}$ catalysis as an alternative decarboxylating agent in the presence of cofactors Mg^{2+} and ThDP (Scheme 2.4).

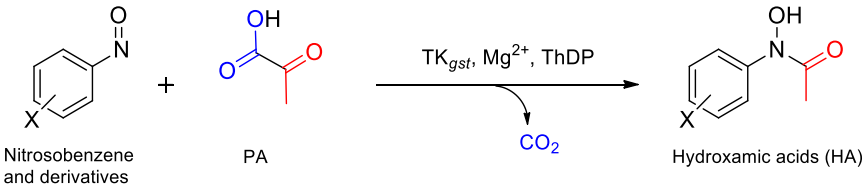

Scheme 2.4. General scheme of TK reaction with nitrosoarenes as acceptor substrates and PA as donor.

Chapter II

2.5. Identification of suitable TK variants

Since nitrosoarenes are usually highly volatile and air sensitive, high-throughput screening methods based on spectrophotometric monitoring, such as measurement of NADH consumption,[204] or pH-based assays[205] are potentially less suitable to unambiguously and reproducibly identify TK best variants. Monitoring of reactions via HPLC analysis is possible, however, this method is not applicable to large enzyme libraries as it is high effort demanding and very time consuming. Thus, it is of interest to design a specific method for the fast measurement of TK activity towards nitrosoarenes to yield diverse retro-HA, and for the identification of suitable TK variants for preparative scale synthesis.

Taking advantage of the metal chelating properties of HA (Scheme 2.5), this work aims for the development and optimization of a high-throughput colorimetric screening method with TK based on the strategy of measuring the quantity of product generated as the iron(III)-HA complex, and ensure its applicability for agar plates, as well as for microtiter plates.

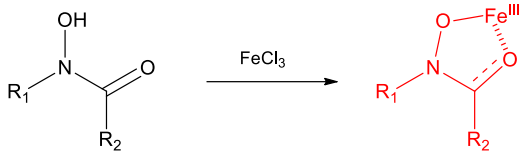

Scheme 2.5. Iron (III) entrapment by a general HA, leading to red colored iron(III)-HA complexes.

Chapter III

2.6. Inhibition tests for biological activity of retro-hydroxamic acids

Because the biological properties of HA are closely linked to their ability to chelate metals, such as iron(III) and Zn(II) among others, it is alluring to determine if reverse HA, having an inverse constitution yet the same metal chelation capacity, also bear the same biological properties. Accordingly, the chemical synthesis of more complex retro-HA with potential anti-cancer activity is pursued together with the applicability of TK for synthesizing this type of compounds via enzyme catalysis. *N*-Hydroxy-4-(4-phenylbutyrylamino)benzamide HTPB[10] (Scheme 2.6) is a molecule that has been patented for the inhibition of HDAC activity in nanomolar range to treat diverse types of tumors.[206] Due to its relatively simple structure, fairly easy synthesis and biological feasibility, it is an adequate molecule to be used as reference for the biological tests to investigate the similarity in their biological properties, and thus, the medicinal properties of reverse HA.

Scheme 2.6. Structural comparison between HTPB and the targeted retro-HA compounds. M=metal cation

Chapter I

Synthesis of *N*-Aryl Hydroxamic Acids Catalyzed by Transketolase

3. Theoretical background

3.1. Transketolase from *Geobacillus stearothermophilus*

Geobacillus stearothermophilus is a Gram-positive bacterium that habits in various environments, such as soil, hot-springs, artic waters, ocean sediments and desert sand, among others. The minimum growth temperature of this microorganism is 40 ºC with a maximum growth temperature of 65-75 ºC. Since the microbe is thermostable, it generates a wide range of thermostable enzymes, many of which are of industrial importance.[207-208]

In 2013, during a collaboration between the groups of Hecquet and Fessner, the first thermophilic TK from this bacterium (TK_{gst}) was identified as a thermostable catalyst with promising applications.[5] This heat-resistant enzyme grants numerous advantages compared to non-thermostable TKs: it has shown enhanced resistance towards non-conventional media; extended catalyst life-time in reactions operated under elevated temperature, with an extraordinary high activity and stability under these conditions; and significant robustness against protein damaging factors introduced by mutagenesis during the engineering of a protein to improve its properties and broaden the enzyme scope.[5]

Studies have shown that this enzyme has an optimum temperature interval of around 60-70 ºC and is able to retain nearly 100% of activity for one full week at 50 ºC, and when rising the temperature up to 65 ºC, it still maintains its full activity for three entire days. To evaluate the scope of this feature, several experiments have been performed comparing the conduct of TK_{gst} at different temperatures. When examining its behavior for glycolaldehyde in particular, the reaction rate of the enzyme showed a four-fold higher activity at 50ºC in comparison to 20 ºC, and an 8 to 14-fold raise at 70 ºC under the same conditions. Moreover, for other aldehyde acceptors, the TK_{gst} activity was roughly three times higher at 50 ºC than at 20 ºC.[5] Taking into account that TK from non-thermostable sources, such as WT-TK_{eco}, have shown a total loss of activity if incubated at 60 ºC for one hour or even faster if subjected to 65 ºC, the thermostability is a very functional and exceptional property of TK_{gst}.[209] Furthermore, the outstanding enzyme stability under intense heat allows for an easy and fast purification of the catalyst by a straightforward heat shock treatment of the crude cell extracts at 70 ºC.

The thermostable TK_{gst} has also been engineered for upgraded properties, extended substrate tolerance and higher specific activity.

3.1.1. Engineering the acceptor scope of TK_{gst}

Based on sequence alignment with TK_{eco}, TK_{gst} was engineered to tolerate short-chain aliphatic aldehydes with improved or reversed stereoselectivity,[210-212] and aromatic aldehyde acceptors.[6] Because the specific activity of TK towards acceptor substrates lacking a 2-hydroxylation is ca. 40-fold lower than for the related hydroxylated substrates, TK_{gst} was engineered to accept substrates without a hydroxyl group in the second position. The library was created by D. Yi (former Ph.D. student in Fessner group) towards propanal as acceptor substrate.[210] As mentioned in the introduction, TK_{gst} has high protein sequence similarity to

TK_{ban} and TK_{yst}, for which protein crystal structures have been determined with bound substrates.[102, 213] Nine amino acid residues, including H462, R521, D470, H28, G264, H263, L191, L382 and S385, create a channel for substrate entrance to the catalytic core of the enzyme (Figure 3.1). They bind the acceptor molecule and arrange its electrophilic carbonyl group towards a nucleophilic attack. Consequently, these nine residues are presumptive candidates for alteration of the TK substrate specificity. From computer studies with PyMOL, D470 seemed to control the enantioselective binding of 2-hydroxyaldehydes in the catalytic pocket of the enzyme by creating a specific hydrogen bond to the OH group of 2-hydroxylated molecules. Therefore, it was reasoned that replacing this amino acid residue by others with larger side chains should narrow the acceptor access tunnel and thus, improve the binding of aliphatic aldehyde acceptors like propanal. This would in consequence increase the acceptance of TK towards these type of non-2-hydroxylated acceptor molecules. Moreover, L382 is situated at almost opposite position to D470, what probably proffers a hydrophobic contribution to the substrate binding. Hence, in an attempt to complement consequences from D470 mutagenesis, this position was also targeted. Two single libraries (L382 and D470) and one double library (L382/D470) combining both selected residues were constructed by site-specific saturation mutagenesis (SSM).[210]

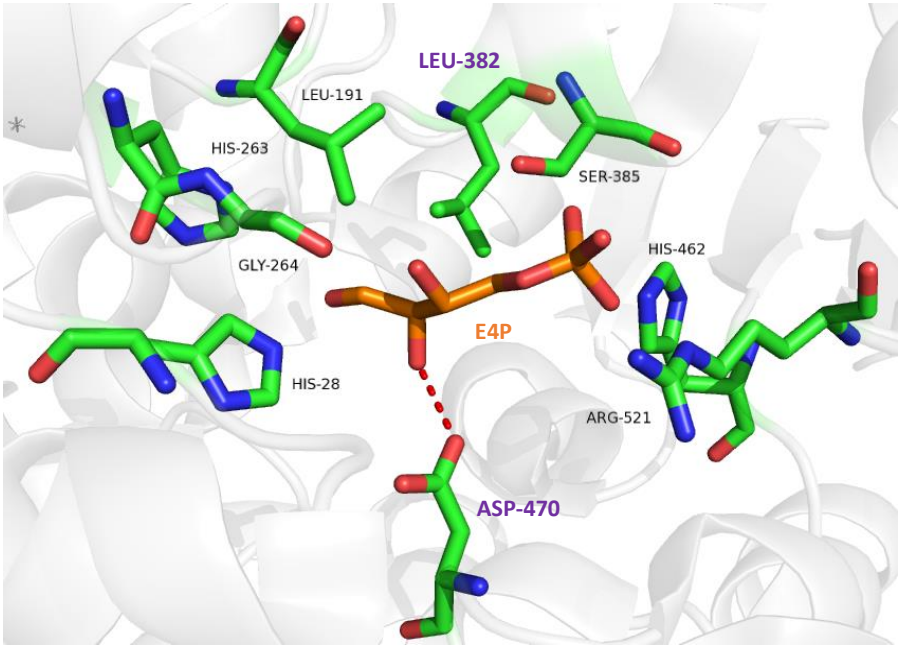

Figure 3.1. Model of the acceptor binding pocket employing the ThDP liganded X-ray crystal structure of TK_{ban} (PDB entry 3M49) with conformation of natural substrate E4P from the TK crystal structure (PDB entry 1NGS). The dotted red lines correspond to the hydrogen bond formed between the 2-OH group of E4P and D470. Residue numbering corresponds to TK_{gst}, being L382 and D470 colored purple. Image was generated by PyMOL.[214]

This L382X/D470X library was created to permit the cooperative adaptation of the TK_{gst} active site towards generic alkanals with diverse modifications in the electrophilic substrate, including stereochemical inversion,[211] increased steric bulk, and enhanced hydrophobic contact zone.[210] Because benzaldehyde and related aromatics are aryl-containing analogs which also lack the 2-hydroxylation, the same L382X/D470X library was screened towards arylated acceptor substrates by T. Saravanan (former postdoc in Fessner group).[6] From the results of

these screenings, it became apparent that an exchange of the native negatively charged D470 with a polar but uncharged serine or threonine residue improved the binding of benzaldehyde for the carboligation step. Thus, at least one hydrogen bond donating residue at position 470 seems to be crucial to maintain high activity with substrates lacking the 2-hydroxylation. Moreover, an exchange of the hydrophobic L382 by a polar or even anionic amino acid residue lead to the highest activities. This was surprising as by its placement it should be in direct contact with the hydrophobic aromatic ring system. New hydrogen bonding contacts to neighboring residues, as well as π bonding in an appropriate substrate orientation, could partially explain this finding. However, in the absence of a reliable computational model for the hits found or an experimental structure, a more detailed interpretation could not be extracted.

In 2019, an eco-friendly stereoselective protocol for the synthesis of rare ketoses was developed by employing HPA as donor substrate and TK_{gst} as catalyst.[215] Rare sugar ketoses offer tremendous potential for applications in pharmaceutical, medicinal, food, and synthetic chemistry.[216-219] However, the chemical way to synthesize such class of compounds involves tedious protection/deprotection steps, and the use of enzymes *in vitro* usually requires multi-enzymatic procedures together with protein engineering. Thus, the improvement of TK activity towards non-phosphorylated long chain aldehydes to prepare non-phosphorylated ketoses with extended carbon-chains still remained an issue to be solved.[215] A few related studies have already been described in the literature,[106, 137] but in the majority of the cases there was no isolation and characterization of the ketose products. In this study, two variant libraries were constructed by simultaneous site saturation mutagenesis (SSM) targeting two or three key positions in the enzyme active site. Three TK_{gst} variants showed improved activities relative to WT-TK towards the tested aldoses. The first variant, L382F/F435Y, showed an activity improvement of ca. 4-fold towards two tetroses (D-threose, L-erythrose); the second one, R521Y/S325/H462N, showed ca. 3.5-fold activity increase towards two pentoses (D-xylose, D-ribose); and the third variant, R521V/385D/H462S, showed some activity towards two hexoses (D-allose, D-glucose) even though the specific activities were low (0.15 $U \cdot mg^{-1}$), while for the WT-TK no activity was detected. Then the three variants were used in a one-pot preparative reaction with the six aldoses at 60 ºC at near-neutral pH. All the ketose products were synthesized and isolated with excellent diastereoselectivities (>95% *ee*) and reasonable yields, with the exception of D-glucose whose enantiomeric excess and yield were not determined.[215]

3.1.2. Engineering the donor scope of TK_{gst}

In 2017, directed evolution was employed to modify the donor promiscuity of TK_{gst} towards PA, 2-oxobutyrate and 3-methyl-2-oxobutyrate.[220] The double variant H102L/H474S outstood all the other variants including the WT-TK, as it showed 10-fold activity improvement relative to WT-TK towards PA when utilizing glycol as acceptor substrate. Also, the same double mutant displayed the best catalytic rate with 2-oxobutyrate, very similar to that of PA. The single mutant H102T showed the highest activity towards 3-methyl-2-oxobutyrate.

Recently in 2020, TK_{gst} was again engineered to widen its donor scope towards aliphatic PA homologues in the presence of aliphatic aldehydes as acceptors.[221] Utilizing the double mutant

from the former library (H102L/H474S), which was previously found to improve TK_{gst} activity toward PA homologues,[220] and combining it with a F435I exchange, which was identified among other residue exchanges for providing a hydrophobic contribution to substrate binding, the novel triple variant H102L/H474S/F435I was designed. This triple mutant was able to synthesize long-chain aliphatic acyloins (5-10 carbon atoms) from 2-oxobutyrate and 2-oxovalerate in the presence of aliphatic aldehydes as acceptors with significantly enhanced activity. Particularly for the reaction of 2-oxobutyrate with propanal, butanal, and pentanal as acceptors, the specific activity reached was quasi equivalent to that obtained with HPA. Also, another triple mutant (H102L/D474S/L191I) showed similar activity to the previous triple variant with 2-oxobutyrate, yet only for propanal and octanal as acceptors. For the bulkier 2-oxovalerate, the double variant H102L/H474S was able to restore considerable activity for smaller acceptors, such as propanal, butanal and pentanal. Also, H102L/H474S/F435I was the best candidate toward butanal as acceptor. No variant was able to accept more sterically demanding substrates, such as hexanal and heptanal. Additionally, the preparative scale synthesis of the hydroxyketones was performed, using the single mutant L382F for the generation of 1,3-hydroxyketones with HPA and the triple mutant H102L/H474S/F435I for the synthesis of 4-hydroxyketones with 2-oxobutyrate and 2-oxovalerate. The corresponding 4-hydroxyketones were never reported before as TK products.[221]

3.2. TK_{gst}-catalyzed synthesis of *N*-aryl hydroxamic acids

HA are a very relevant class of compounds for many different areas of life sciences because of their high pharmacological versatility.[7, 198] Despite the various methods that have been reported to synthesize HAs (**2**), they are commonly generated from an activated carboxylic acid derivative (**1**). Curiously, HA bearing an inverse constitution (**3**), are substantially less common although a very similar metal binding capacity can be anticipated. A comparison between the two types of HA is depicted in Scheme 3.1.

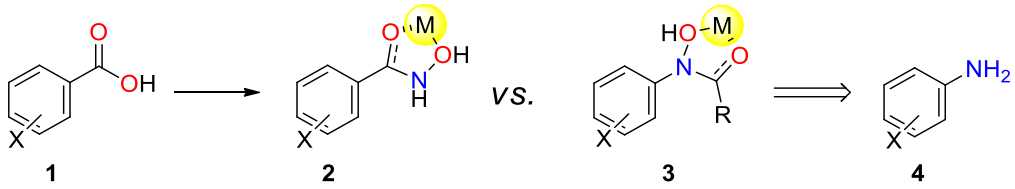

Scheme 3.1. General synthesis of isomeric HA and retro-HA starting from benzoic acids or anilines respectively. M= metal ion; R= H, CH_3, CH_2OH.

To our knowledge, this sort of retro-HA (**3**) appear not to have been submitted yet to biological testing for pharmacological applications. In this chapter, an enzymatic approach to the latter type based on the nucleophilic acyl transfer from an α-oxoacid to nitrosoarene electrophiles catalyzed by transketolase is presented.

4. Results and discussion

4.1. Nitrosobenzene as a transketolase acceptor substrate

Recently, TK_{gst} has been engineered by our group to accept benzaldehyde as a non-natural acceptor substrate.[6] Because of the high structural similarity between nitrosobenzene (**5a**) and benzaldehyde (**7**), we presumed that variants from the TK_{gst} L382X/D470X library should also be able to convert the former (**5a**) and other nitrosoarenes as alternative electrophilic substrates. To investigate this hypothesis, benzaldehyde (yellow) and nitrosobenzene (light pink) were superimposed over natural TK substrate E4P (orange) in the PyMOL graphic of the model of the acceptor binding pocket of TK_{gst} (Figure 4.1).

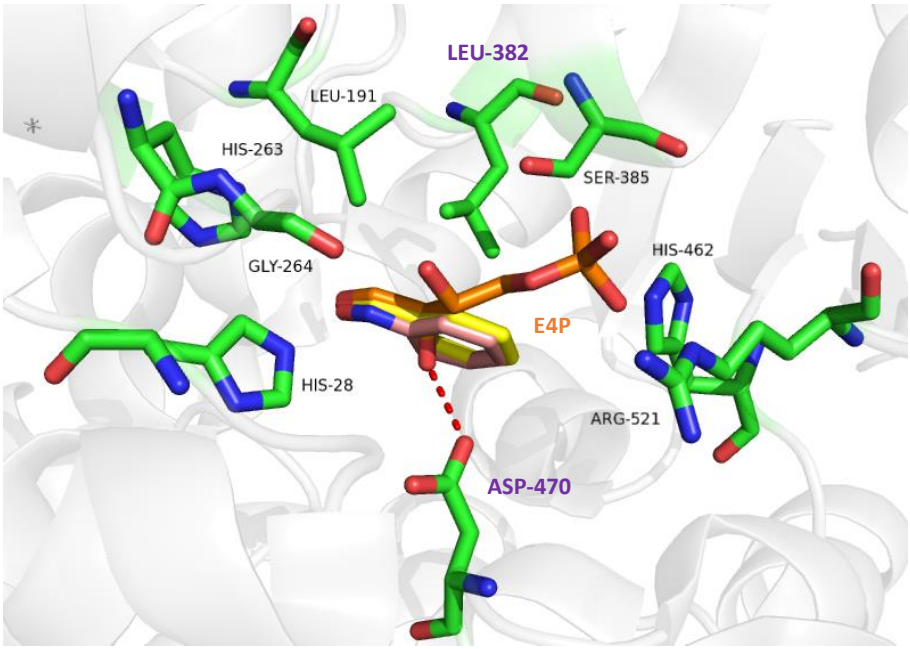

Figure 4.1. Model of the acceptor binding pocket employing the X-ray crystal structure of TK_{ban} (PDB entry 3M49) with substrate conformation of E4P from the TK_{yst} crystal structure (PDB entry 1NGS). The dotted red lines correspond to the hydrogen bond formed between the 2-OH group of E4P and D470. Benzaldehyde (**7**, yellow) and nitrosobenzene (**5a**, light pink) are superimposed over the 2-hydroxylated E4P (orange). Residue numbering corresponds to TK_{gst}, being L382 and D470 colored purple. Image was generated using PyMOL.[214]

As previously mentioned in Section 3.1.1, when exchanging the natural TK substrate E4P for the original substrate of the L382X/D470X library (propanal), the interaction from the 2-hydroxylated compounds vanished. Accordingly, when employing hydrophobic substrates also lacking the 2-hydroxylation and containing hydrophobic aromatic ring systems, such as nitrosobenzene and benzaldehyde, the same phenomenon was observed. This confirmed that D470 was an appropriate mutation for aromatics as well. Furthermore, because L382 is located opposite to D470, this position also seemed constructive for nitrosoarene acceptance. Therefore, it was reasoned that the same L382/D470 library should also result beneficial for increasing the tolerance of TK_{gst} towards nitrosoarenes. Apart from the high structural analogy between nitrosobenzene (**5a**) and benzaldehyde (**7**), both compounds have also high electronic

similarity. This further supports the premise that TK_{gst} variants should also be able to accept nitrosoarenes as alternative acceptor substrates. Such an action would lead to the generation of *N*-aryl HA *via* creation of a new carbon-nitrogen bond instead of the usual stereospecific carboligation, leading to structures complementary to the conventional HA type (Scheme 4.1).

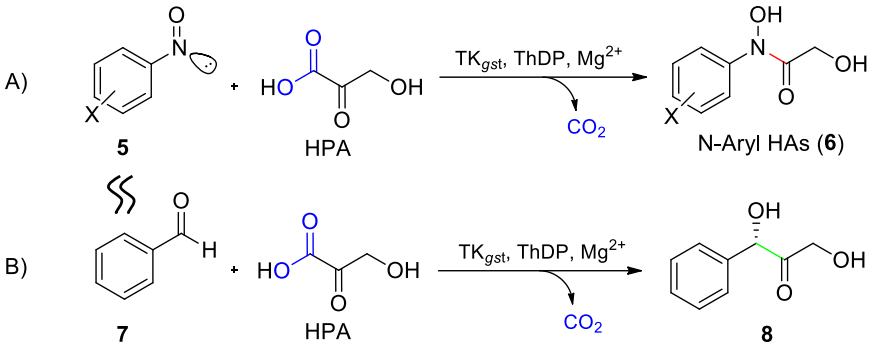

Scheme 4.1. Comparison of the TK_{gst} reaction of benzaldehyde (**7**, A) versus nitrosobenzene (**5a**, B) in the presence of TK_{gst} cofactors and HPA as donor. New C-C bond is shown in green and new C-N bond in red.

For a better understanding of the enzymatic reaction with nitrosoarenes, the mechanism of the TK-catalyzed reaction adapted to nitrosobenzene is depicted in Scheme 4.2.

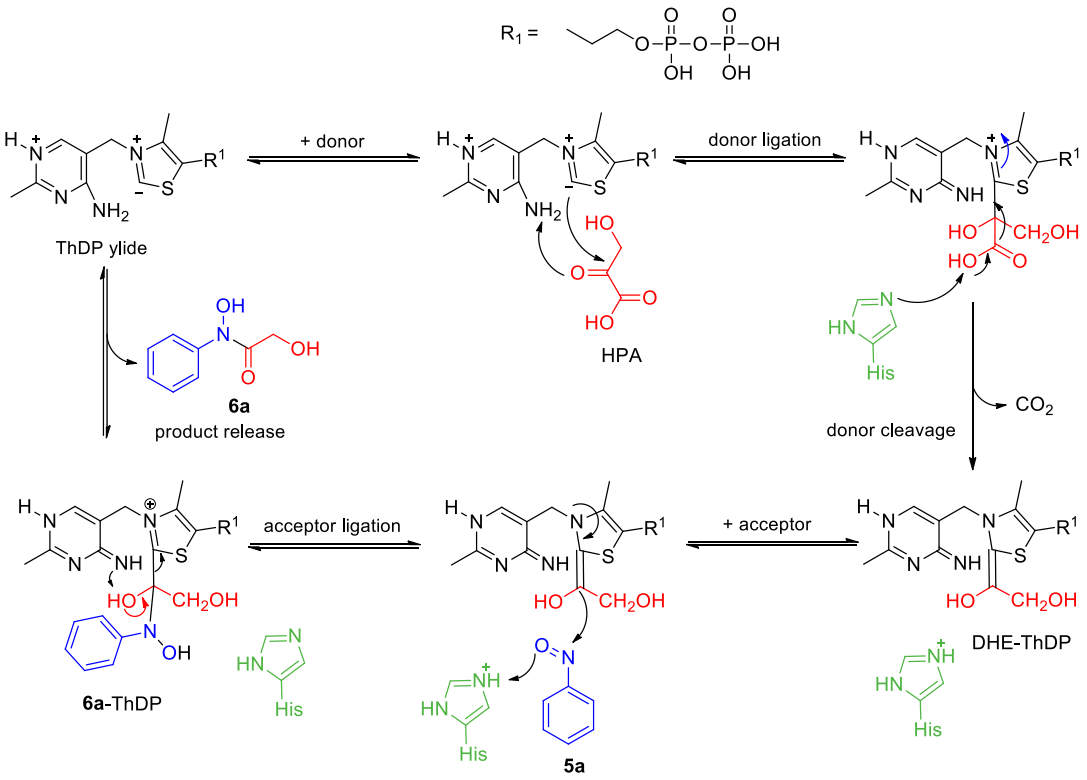

Scheme 4.2. Presumed catalytic mechanism of TK with HPA as donor and **5a** as acceptor to yield the corresponding *N*-aryl HA **6a**. Adapted from the literature.[105]

The reactive carbanion in the ThDP ylide attacks the partial positive carbonyl group of the HPA and the O from the keto group takes a proton from the nearby amino group. The nucleophile nitrogen atom of the histidine residue from the active site removes a proton from the acid and

carbon dioxide is released. Then the enol from the intermediate DHE-ThDP attacks the electrophilic nitrogen atom of **5a** and a C-N bond is generated. Finally, the target molecule **6a** is released and the ThDP ylide is regenerated, which can be used in the next cycle of the biocatalysis.

The TK_{gst} variant that offered the best tolerance for ketol addition to benzaldehyde was the L382N/D470S variant (short: N/S). For that reason, this variant was also tested to convert nitrosoarenes to *N*-aryl HA. By means of the nanoDSF method, the stability of TK_{gst} N/S against thermal unfolding was measured according to the literature.[222] Fortunately, the melting temperature of this variant appeared to be only slightly lower than that of the WT-TK_{gst} enzyme, being the melting temperatures 73.9 °C and 75.5 °C, respectively.

Firstly, analytical scale reactions (500 µL) were tested with commercial **5a** at RT. Because of the low aqueous solubility of nitrosobenzene owing to its hydrophobic nature, DMSO (20%) was added as co-solvent of the reaction as successfully done for the preparative synthesis using benzaldehyde.[6] Control reactions each in the absence of acceptor, donor, or the TK_{gst} variant were incubated in parallel. This confirmed that only reactions containing all the reagents successfully yielded the desired HA product (visualized by TLC) and no product formation was detected in the absence of enzyme. Secondly, a preparative-scale reaction was performed in order to isolate **6a** and confirm its identity. Only 8% of DMSO was employed on the preparative scale to avoid tedious purification. Reactions were stirred at 50 ºC. Because of the known limited stability of HPA solutions,[223] the substrates were added in portions and the reaction progress was monitored by HPLC. Fortunately, the reaction proved to be extremely fast even with low enzyme quantities, and identical results were achieved when adding all reagents at once. After the reaction appeared finished, the reaction mixture was subjected to an acid/base extractive work-up followed by column chromatography over silica. After removal of the solvent, *N*-phenyl-*N*,2-dihydroxyacetamide (**6a**) was isolated and identified *via* NMR. The product **5a** was also prepared by chemical synthesis adapting a literature procedure,[224] and used as an authentic sample for comparison of both HA by TLC, HPLC and NMR. This further confirmed the success of the enzymatic method.

4.2. Expanding the substrate scope of TK_{gst}

4.2.1. Generation of a nitrosoarene library

To investigate the reaction scope, a wide library of variously mono- and disubstituted nitrosoarene starting materials (SM) was procured. A few oxidation methods for the synthesis of nitrosoarenes from anilines have been described in the literature,[225] *e.g.* utilizing the oxidizing agents Caro's acid (peroxomonosulfuric acid), 3-chloroperoxybenzoic acid, peracetic acid, potassium permanganate, or hydrogen peroxide in the presence of a heterogeneous catalysts, such as compounds containing tungsten, rhenium, or molybdenum. However, a much more simple and efficient approach has been reported by *Priewisch and Rück-Braun*[203] for the use of commercial oxone ($2KHSO_5 \cdot KHSO_4 \cdot K_2SO_4$) to oxidize anilines to nitrosoarenes. oBecause this triple salt is inexpensive, safe, and environmentally benign,[226] it was preferred

for this synthetic step to other more aggressive oxidants. The corresponding reaction is depicted in Scheme 4.3.

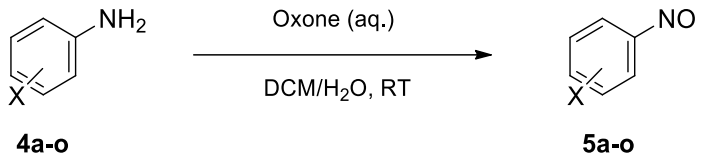

Scheme 4.3. Synthesis of nitrosoarenes (**5**) by oxone oxidation of anilines (**4**).

During the oxidation of anilines (**4**), side reactions may occur, such as the formation of nitro compounds (**10**) from the further oxidation of nitrosoarenes (**5**); condensation reactions leading to azobenzenes (**12**) from the reaction between nitrosoarenes (**5**) and anilines (**4**); or azoxybenzenes (**11**) from the reaction between *N*-arylhydroxylamine intermediate (**9**) and aniline (**4**).[203, 227] The oxidation products mentioned are represented in Scheme 4.4.

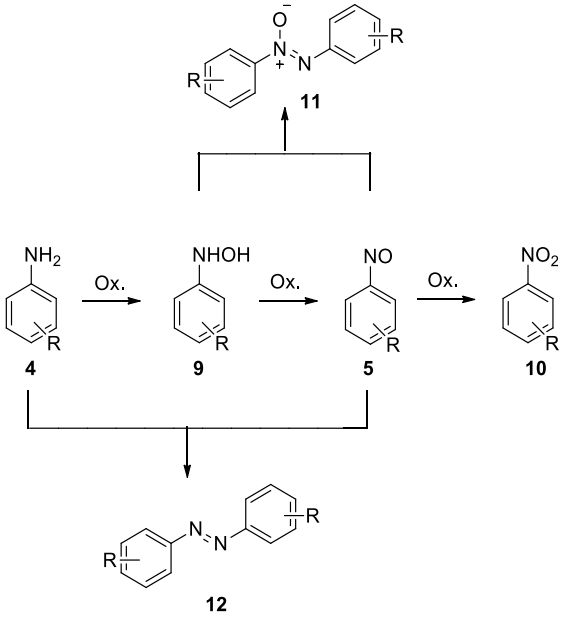

Scheme 4.4. Representation of all typical oxidation products starting from the amino compound **4**. Scheme adapted from the literature.[203]

The oxone approach enables high conversion to the nitroso compounds employing a two-phase heterogeneous system composed by oxone solved in an aqueous solution and the aniline solved in DCM. A biphasic system such as this one is supposed to help in the separation of the less water-soluble nitrosoarenes **5** from the *N*-arylhydroxylamine intermediate and the aniline precursors **4**, and prevent in this way both type of condensation reactions.[203] To perform this oxidation reaction, the amine **4** was solved in DCM under inert atmosphere. Then, an aqueous solution of oxone previously purged with argon was added dropwise into the aniline solution at RT to avoid the excess of oxone and/or the high temperatures causing further undesired oxidations. After TLC and HPLC confirmed the total conversion of starting material, the reactions were quenched and worked-up following the standard protocol. Due to the high volatily and reactivity of most nitrosoarenes (**5**), the solvent was removed under reduced pressure at RT. Analysis of the products *via* HPLC (λ=320 nm), NMR, and MS confirmed the

obtention of the desired nitrosoarenes. A set of diverse mono- and disubstituted nitrosoarenes (**5a-o**) was produced from commercial anilines (**4a-o**) by oxone oxidation. (Table 4.1).

Table 4.1. Synthesis of nitrosoarenes (**5a-o**) by oxone oxidation from the corresponding anilines **4**.

Aniline	Aryl substitution	Nitrosoarene	Yield (%)[a)]
4b	4-Br	**5b**	96
4c	4-Cl	**5c**	94
4d	3-Cl	**5d**	80
4e	2-Cl	**5e**	89
4f	3,4-Cl_2	**5f**	91
4g	4-CH_3	**5g**	78
4h	3-CH_3	**5h**	98
4i	4-Cl, 3-CH_3	**5i**	91
4j	3-Cl, 4-CH_3	**5j**	quant.[b)]
4k	4-CF_3	**5k**	74
4l	3-CF_3	**5l**	70
4m	4-NO_2	**5m**	70
4n	4-COOH	**5n**	87
4o	3-COOH	**5o**	84

[a] Isolated yields with approximately 80-90% purity, [b] quantitative yield.

Even though the selectivity towards the nitrosoarenes was enhanced by using a biphasic system, side products were still concomitantly produced to some extent, including nitro- (**10**), azo- (**12**), and azoxybenzenes (**11**) in different compositions. Attempts to purify **5c** by column chromatography (CH/EA 50:1) resulted in partial decomposition. Moreover, purification of **5l** by sublimation was also attempted. The crude product (1.20 g) was placed inside a cooling finger located inside an oil bath at 60 ºC. A crystal blue substance was sublimated on the cooled glass (450 mg) while a brown one remained on the bottom. Both fractions were isolated and analyzed by NMR (Figure 4.2).

Because nitroso compounds are very reactive and easily decomposed, their purification is difficult and leads to poor yields. In view of the difficulty of purification of nitrosoarenes (**5**), the compounds were employed in the enzymatic step without further purification. This posed no complications because the side products apparently were interfering with the enzymatic conversion of nitrosoarenes due to their higher chemical stability.

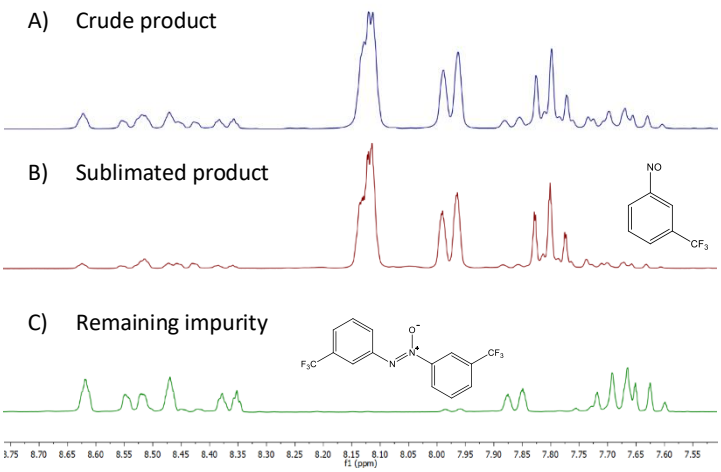

Figure 4.2. Comparison of ^{1}H-NMR spectra of a) crude product (**5l**), b) sublimated **5l**, and c) remaining impurity.

From the NMR comparison it is apparent that the sublimation did purify the compound to some extent, however, the impurity was not removed completely. From NMR calculation, the sublimated product **5l** was obtained with a purity of ca. 90%, while the crude product had a purity of ca. 82% before purification. The purification yield was only ca. 46%, indicating a big loss of material with a minor increase in impurity. Thus, sublimation as a method por purification of nitrosoarenes was also not further contemplated.

4.2.2. Enzymatic reaction with hydroxypyruvate as donor substrate

Once the set of nitroso compounds was at hand, it was proceeded to the enzymatic synthesis of the corresponding *N*-aryl HA. The general synthesis of HA is shown in Scheme 4.5.

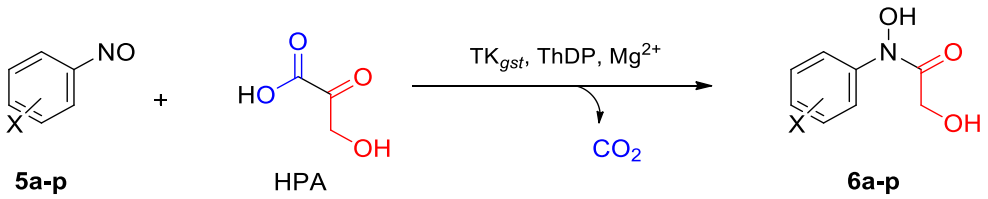

Scheme 4.5. General TK$_{gst}$-catalyzed synthesis of *N*-aryl HA by ketol addition to nitrosoarenes.

The reactions with the synthesized SM (**5a-o**), together with commercially available *p*-nitroso-*N*,*N*-dimethylaniline (**5p**), were first tested on analytical scale (500 µL) under the same conditions as for the unsubstituted nitrosobenzene (**5a**). Monitoring of the conversions by HPLC analysis indicated that all nitroso substrates prepared were converted to some degree, yet no HA product was detected for **5p** at an analytical scale. Considering this, preparative-scale (25 mL) reactions at 50 ºC with all substrates dissolved in DMSO (8%) were carried out. Most of the HA products were isolated by means of column chromatography for spectroscopic characterization. The yields of the HA array produced is shown in Table 4.2.

Table 4.2. TK_{gst}-catalyzed synthesis of HA from nitrosoarenes **5a-p** and HPA.

Nitrosoarene	Aryl substitution[a)]	HA product	Yield (%)[b)]
5a	H	**6a**	41
5b	4-Br	**6b**	28
5c	4-Cl	**6c**	41
5d	3-Cl	**6d**	20
5e	2-Cl	**6e**	n.i.
5f	3,4-Cl_2	**6f**	10
5g	4-CH_3	**6g**	49
5h	3-CH_3	**6h**	29
5i	4-Cl, 3-CH_3	**6i**	37
5j	3-Cl, 4-CH_3	**6j**	32
5k	4-CF_3	**6k**	9
5l	3-CF_3	**6l**	17
5m	4-NO_2	**6m**	n.i.
5n	4-COOH	**6n**	n.i.
5o	3-COOH	**6o**	n.i.
5p	4-$N(Me)_2$	**6p**	0

[a] Substituent position relative to the nitroso group, [b] Isolated yields, n.i.: product formation confirmed but compound not isolated.

In order to examine the effects of the diverse substituents on the reaction rates and yields, the empirical studies of L. P. Hammett are shortly introduced and discussed. Hammett proposed an empirical correlation between the structure of the organic compounds and their chemical reactivity. This was based on the quantitative relation between the nature (electron donating or withdrawing) and position of the substituent R (*meta*- or *para*-) on a benzene ring and the reactivity of the side chain Y (Figure 4.3).

For *ortho*-substituted aromatics the adjacent substituent R might impose steric impediments on the reaction, and therefore their reactivity was expected to be much lower than for the corresponding *para*- and *meta*-substituted compounds. Thus, the *ortho*-position was not considered in his studies.

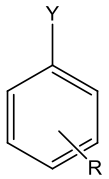

Figure 4.3. General structure of benzene ring with different substituents.

Indeed, the reactivity of nitroso compounds in the enzymatic ketol addition appeared to be regulated by both electronic and steric factors. The electrophilicity of the π-conjugated nitroso moiety raises when electron withdrawing substituents are attached to the benzene ring, increasing both reaction rates and product yields with a Hammett-like trend.[228] Substitution in *para*- position of the benzene ring

is well accepted, whereas *ortho*- and *meta*- substitution increase the steric hindrance of the molecule and thus, complicate the fitting of the nitroso compound on the substrate channel of the enzyme active site. This observation was verified with the nitroso compounds, being the yield of the *p*-substituted double as of the *m*-substituted, and this one much higher than that of the *o*-substituted. For instance, the yield of **6c** is higher than that of **6d**, which is at the same time much higher than for **6e**, which could not be isolated due to the low product quantities formed under the same reaction conditions.

Moreover, electrophilic nitrosoarenes are more vulnerable to chemical redox processes in aqueous solution. This favors the generation of side products, such as hydroxylamine (**9**), nitro- (**10**), azo- (**12**) and azoxybenzenes (**11**), decreasing HA yields and complicating their isolation. For instance, HPLC analysis of the reaction with **5e** showed conversion of SM forming two new peaks in the absence of enzyme; after TK was added an additional peak was detected. Analysis of the reactions by TLC revealed the additional spot to turn red upon contact with the $FeCl_3$ staining reagent (*vide infra*), corroborating the peak to be the corresponding HA (**6e**), yet produced in much lower concentration than the *para*- and *meta*-substituted nitrosoarenes. Furthermore, the yields with two-fold substituted nitrosoarenes in *para*- and *meta*-position (*e.g.* **6f**) were lower than with the corresponding single substituted nitrosoarenes.

The strongest electron withdrawing *p*-NO_2 group (**5m**) was also unfavored in the enzymatic reaction, yielding mainly side products. However, TLC and HPLC analysis indicated generation of small quantities of HA (**6m**) that were not isolated. Plausibly, by optimizing the reaction conditions for both **6e** and **6m** the quantity produced could also be enhanced and thus, the isolation would be facilitated. In accordance to the problematic chemical reactivity of *p*-nitro-substituted **6m**, the electron poor *p*-trifluoromethyl-nitrosoarene (**6k**) produced the corresponding HA with a lower yield than **6l**, being the latter favored despite increased steric effects. All this indicated that too strong electron withdrawal substituents in the benzene ring have a negative impact on the enzymatic compared to chemical reaction selectivity.

Carboxylic acid groups are only moderately resonance active groups; however, they are able to raise the substrate solubility, favoring the enzymatic reaction. Both *para*- and *meta*-substituted nitrosobenzoic acids (**5n** and **5o**) were well accepted by the enzyme and led to the corresponding HAs (**6n** and **6o**). Unfortunately, the purification of these highly polar HA products by silica gel column chromatography led to large loss of material while small amounts of side products remained. Therefore, the compounds could not be fully isolated. See Appendix for NMR of **6n** (page 218) and HPLC/TLC proof of HA formation for **6o** (page 225).

Conversely, strong electron donating groups decelerate the reaction rate. For example, the strongest electron donating *p*-dimethylamino group (**5p**) led to a great number of byproducts while not producing any detectable HA product. This result is in accordance with early kinetic studies performed by Corbett *et al*,[224] which employed yeast TK as catalyst and fructose 6-phosphate as substrate donor. However, both substrates containing electronically different *p*-CH_3 (**5g**) or *p*-Cl (**5c**) substitution afforded comparable results with TK_{gst}, as verified by HPLC analysis and by comparing isolated product yields. Additionally, reactions with both regioisomeric, *meta*- and *para*-substituted chloro-nitrosotoluenes (**5i** and **5j**) resulted in very

similar yields. In contrast, in spite of its similar steric hindrance, the dichloro-substituted nitrosoarene **5f** gave the corresponding HA with a significantly lower yield, indicating that deactivating substituents induce lower reaction selectivity, being this particularly important for molecules having a double deactivating effect. For instance, the yield for **6f** was much lower than for the compounds **6c** and **6d**.

4.2.3. Activity comparison of TK$_{gst}$ L382N/D470S variant *vs* wild-type TK$_{gst}$

It was observed that WT-TK$_{gst}$ is able to accept nitrosoarenes to some extent. Therefore, the relative rate advantage of employing the TK$_{gst}$ N/S variant instead of the WT-TK was determined for **6b**. Experiments were performed at RT for 30 minutes employing acetone (20%) as co-solvent, and in the presence of either the WT-TK$_{gst}$ or the TK$_{gst}$ N/S at varying concentrations (0.1-0.2 mg/mL). Control reactions in the absence of enzyme were simultaneously incubated. Both the product generation and the consumption of SM were monitored by HPLC analysis at 254 nm and 320 nm, respectively. The reactions with the highest enzyme quantity (0.2 mg/mL) gave the best results. In Figure 4.4, a comparison of the HPLC profiles for the product formation with after 5 minutes is shown (A), together with a comparison of the HPLC profiles showing the leftover SM after 30 min incubation time (B).

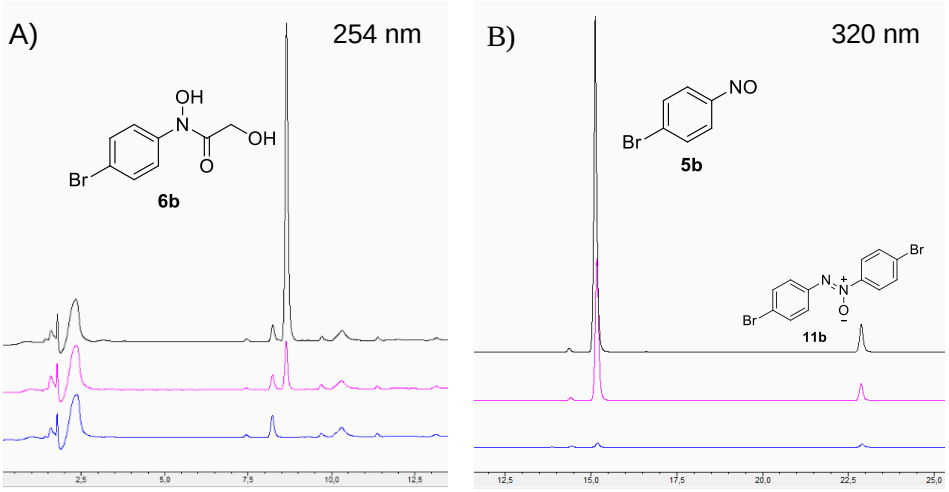

Figure 4.4. A) Comparison of HPLC profiles after 5 minutes showing the formation of HA product **6b** in the absence of enzyme (blue), with the WT-TK$_{gst}$ (pink), and with the TK$_{gst}$ N/S variant (black), visualized at λ= 254 nm. B) HPLC profiles after 30 minutes comparing the amount of SM **5b** left in the absence of enzyme (black), with the WT-TK (pink) and with the TK$_{gst}$ N/S variant (blue), visualized at λ= 320 nm.

In the control reaction without enzyme, no HA formation was detected. When adding the highest quantity of TK (0.2 mg/mL), the variant proved to be nearly 7-fold faster in generating the desired HA than the WT-TK$_{gst}$ after already 5 minutes of incubation, which implies less decomposition of SM as well. Also, when halving the quantity of the TK to a concentration so low as 0.1 mg/mL, the reaction rate with the variant was still 5.5 times that of the WT-TK within the first 5 minutes. Moreover, after 30 min incubation time with the highest enzyme quantity (0.2 mg/mL) the variant had reached practically complete conversion (ca. 98%) whereas the WT had only converted roughly half of the substrate (ca. 57%). These results verify

that using the engineered variant offers a significant advantage in regard to the WT even when applying very low enzyme concentrations.

4.2.4. Chemical synthesis of *N*-phenyl-*N*-hydroxyacetamide

N-Phenyl-*N*-hydroxyacetamide (**13**) was synthesized chemically in order to have a structurally related *N*-aryl HA regarding the HA functionality for comparison with the HA library synthesized with HPA (see below in Section 4.2.5.). This reaction was performed in acidic aqueous medium according to a literature protocol.[229]

Nitrosobenzene (**5a**) is known to play an a electrophile role in many of its reactions,[230] including the TK reaction, however, it also bears nucleophilic character, being able to act both as nucleophile and electrophile. Indeed, this acid-catalyzed reaction appears to be initiated by a nucleophilic attack by the nitroso nitrogen on the carbon atom of the keto group of the α-oxoacid (PA) and followed by protonation of the intermediate. The resulting transient adduct **13a** is then converted to the corresponding HA **15a** through decarboxylation and loss of a proton (Scheme 4.6). The decarboxylation is presumably the driving force for the forward reaction.

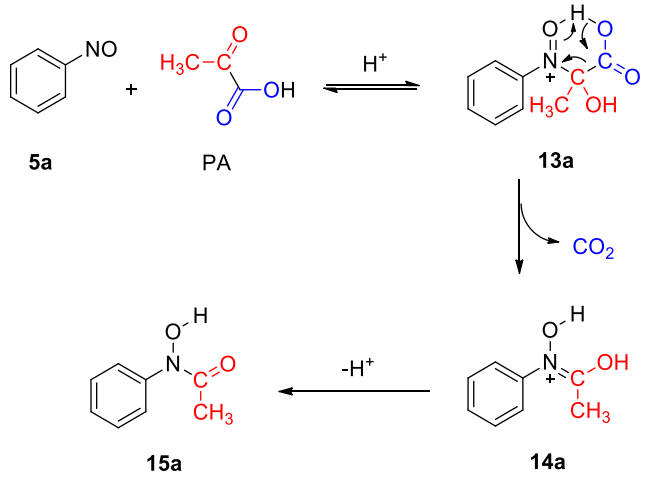

Scheme 4.6. Proposed mechanism of the chemical synthesis of **14a** in aqueous acidic medium.

4.2.5. Chelate complex formation with iron (III) ions

The most outstanding property of HA is their capacity to chelate iron (III) ions (Scheme 4.7). In alkaline media the complex favors a stable fully hexacoordinate 3:1 structure, whereas at acidic pH the 1:1 complex is preferred. The 1:1 structure is characterized by a deep red-purple color. [194]

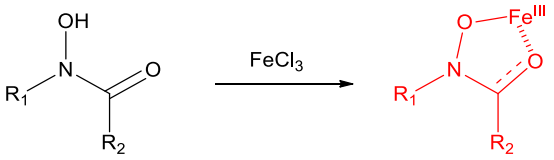

Scheme 4.7. Iron (III) entrapment by a general HA, leading to red-colored iron(III)-HA chelated structures.

Hence, the iron complex formation can be used as a method for unequivocal identification of the HA formed by TLC staining with the ferric chloride staining reagent and for following the HA synthesis reactions in liquid-phase. This discontinuous monitoring method was performed by mixing equal quantities of the reaction mixture or the pure product solutions in MeOH with aqueous $FeCl_3$ (0.5% w/v). Upon mixing both solutions, an intense red-violet color was immediately developed. The usefulness of this iron(III) method was validated (in duplicates) by detecting the fully isolated HA array in liquid phase (A) and upon TLC analysis after development with CH/EA (1:4) and spraying with methanolic $FeCl_3$ solution (B) (Figure 4.5).

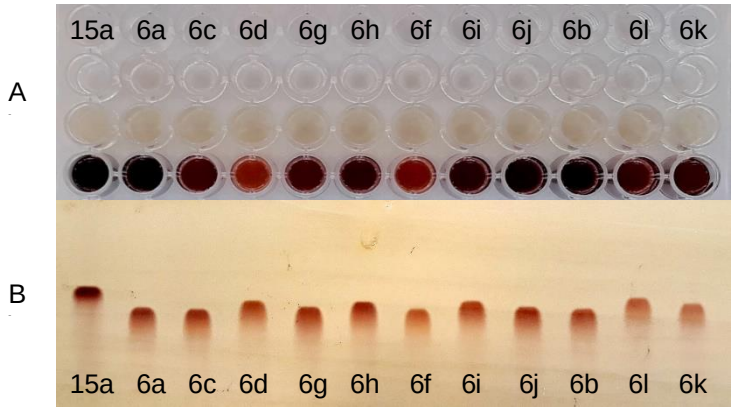

Figure 4.5. A) 96-Well microtiter plate for analysis of chelate complex formation. Top: purified HA array (**6a-p**) solved in MeOH compared to **15a** from chemical synthesis; center: 0.5% aqueous $FeCl_3$; bottom: both solutions equally mixed. B) TLC plate spotted with the HA array after development with CH/EA (1:4) and staining with $FeCl_3$ solution.

The authentic standard *N*-phenyl-*N*-hydroxyacetamide **15a**, prepared previously *via* chemical was used to compare the R_f of the HA set produced with HPA as donor in the TLC plate, and to verify the ferric chloride principle also with a slightly different HA structure. Indeed, mixing the solutions with $FeCl_3$ immediately gave an intense red-violet color for all HA samples in the product array.

4.2.6. Enzymatic reaction with pyruvate as donor substrate

Although the mammalian PA dehydrogenase complex has been shown to be able to generate the corresponding *N*-hydroxy-*N*-arylacetamides,[231] TK was stated to be very specific for the ketol transfer reaction.[106, 114, 232] In order to challenge this, TK_{gst} was recently engineered by the *Fessner* group by directed *in vitro* evolution to be able to accept PA as a resembling non-hydroxylated donor substrate.[220] So far, this reaction type was only demonstrated for the conversion of 2-hydroxylated aliphatic aldehydes as the preferred native substrate type of TK enzymes. Regarding the apparent high kinetic reactivity of nitrosoarenes (**5**), the ability of those engineered variants to convert these arylated substrates as alternative acceptor substrates was probed (Scheme 4.8).

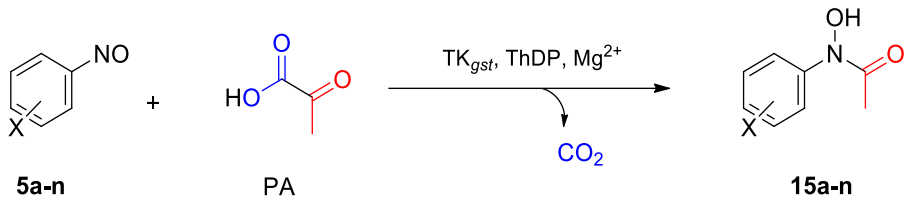

5a-n PA **15a-n**

Scheme 4.8. General TK$_{gst}$-catalyzed synthesis of *N*-aryl HA (**15a-p**) with PA as donor substrate. X: H (**5a**/**15a**), 4-Br (**5b**/**15b**), 4-Cl (**5c**/**15c**), 3-Cl (**5d**/**15d**), 3,4 -Cl (**5f**/**15f**), 4-CH3 (**5g**/**15g**), 3-CH3 (**5h**/**15h**), 4-Cl, 3-CH3 (**5i**/**15i**), 3-Cl, 4-CH3 (**5j**/**15j**), 4-CF3 (**5k**/**15k**), 3-CF3 (**5l**/**15l**), 4-COOH (**5n**/**15n**).

To evaluate this, commercial **5a** and the TK$_{gst}$ H102L/H474S (short: L/S) variant, which had offered the best overall properties with PA,[220] were used. In the first place, the stability of TK$_{gst}$ L/S against thermal unfolding was measured with the nanoDSF method in order to confirm that this engineered variant had maintained its thermostable properties. Delightfully, the melting temperature of this variant appeared to be equal to that of the WT-TK$_{gst}$, the respective melting temperatures being 75.5 °C and 75.6 °C, which is in correlation with co-solvent tolerance studies.[222]

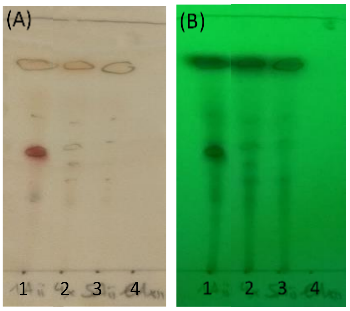

Figure 4.6. TLC of the reaction with PA and **5a** stained with $FeCl_3$ (A) or visualized under UV-light (B)

The first tests were conducted on a semi-preparative scale (1 mL) at RT for 24 h. From these initial tests, formation of **15a** was detected and confirmed by staining the reaction TLC sheet with the ferric chloride staining reagent (Figure 4.6). Control reactions in the absence of enzyme (2) or of either the donor (3) or acceptor (4) did not produce any red-colored spot upon contact with $FeCl_3$. When performing the synthesis on a preparative scale, the TK$_{gst}$ L/S quantity had to be significantly incremented, compared to the reactions with TK$_{gst}$ N/S and HPA as donor substrate. At least 5-fold amounts of TK$_{gst}$ L/S (2 mg/mL) were necessary to be able to isolate **14a**, although the yield was rather low (5%). This was due to a substantial increase of consumptive byproducts, particularly azoxybenzene. In Figure 4.7, HPLC monitoring of the reactions after 5 min, 1 h, 2h, 3h and 4h is shown. After 4h the reaction was stopped.

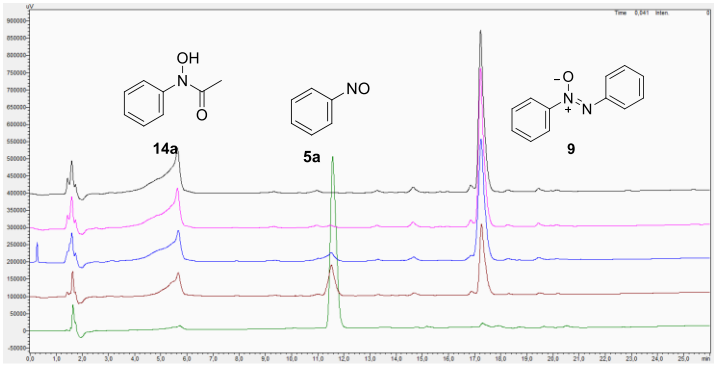

Figure 4.7. HPLC monitoring of TK$_{gst}$-catalyzed reactions between **5a** and PA to generate **15** after 5 min (green), 1 h (brown), 2h (blue), 3 h (pink) and 4 h (black).

The identity of the enzymatically produced **15a** was further verified against the authentic standard prepared by chemical synthesis (Section 4.2.4). TLC and HPLC analysis as well as comparison of NMR spectra of both isolated materials proved that the engineered TK_{gst} L/S variant is able to convert PA as donor substrate.

Additionally, because in principle carboxylic acid groups are capable of raising the substrate solubility favoring the enzymatic reaction, the conversion of the *p*-substituted carboxylic acid **5n** to **15n** was also probed by adding TK_{gst} L/S (2.8 mg/mL) to the reaction with PA as donor substrate. It was demonstrated that **5n** is well tolerated by the engineered enzyme leading to the corresponding HA **15n**. Unfortunately, NMR analysis showed that the purification of this highly polar HA product **15n** by silica gel column chromatography was not very successful, considering that side products were still present while a large loss of material occurred, as it had happened for **6n** and **6o**. Therefore, the compound could also not be fully isolated. See Appendix for NMR (page 226) and TLC proof of HA **15n** formation (page 226).

To further broaden the application scope of the enzymatic acyl transfer from PA, the rest of the nitroso substrate set was examined for conversion by the engineered TK_{gst} L/S variant employing PA as donor substrate. For this, only the nitrosoarenes (**5b-l**) were tested that before had led to HA **6**, which could be isolated and characterized. The product generation was monitored *via* HPLC during 24h and confirmed by ferric chloride staining on TLC plates as previously done. The TLC plate of the reactions performed with the 5 first substrates that were tested (**15c**, **15d**, **15g**, **15h**, and **15f**) are shown in Figure 4.8 in or der to prove that the corresponding HA were enzymatically generated from PA and also to prove that by means of the ferric chloride principle nitrosoarene conversions can be distinguished. The reaction mixtures were spotted multiple times onto the TLC plates.

Figure 4.8. TLC of the TK reaction mixtures to yield **15c**, **15d**, **15g**, **15h** and **15f** stained with $FeCl_3$ reagent.

Because these conversions were found to be not very efficient, the generated HA products **15b-l** were not isolated for characterization. However, the relative R_f migration pattern in RP-HPLC of the HA array synthesized with PA can be directly compared to that of the HA library generated from HPA reaction (Figure 4.9). Although the highly polar HA functionality dominates the physicochemical properties of both product sets, the R_f values in TLC and HPLC spread considerably relative to the reference compounds **6a**/**15a** as a consequence of the aryl substitution pattern. To be noted is that the lack of one hydroxyl group slightly lowers the polarity of the HA, and therefore, the compounds appear slightly shifted to the right side relative to the products from the HPA reactions. Overall, this primary screening with PA verified that the TK_{gst} L/S variant is not only able to accept nitrosoarenes as electrophilic substrates yet also PA as alternative donor substrate. Probably, upon further optimization of the reaction conditions the yields of the PA reactions could be further enhanced. Howbeit, in order to truly widen the reaction scope of TK_{gst} towards two non-native substrates in combination, *i.e.* for both aromatic electrophiles as acceptors and PA or other 2-oxoacids not yet studied as donors, exhaustive further screening towards novel engineered TK_{gst} variants is required.

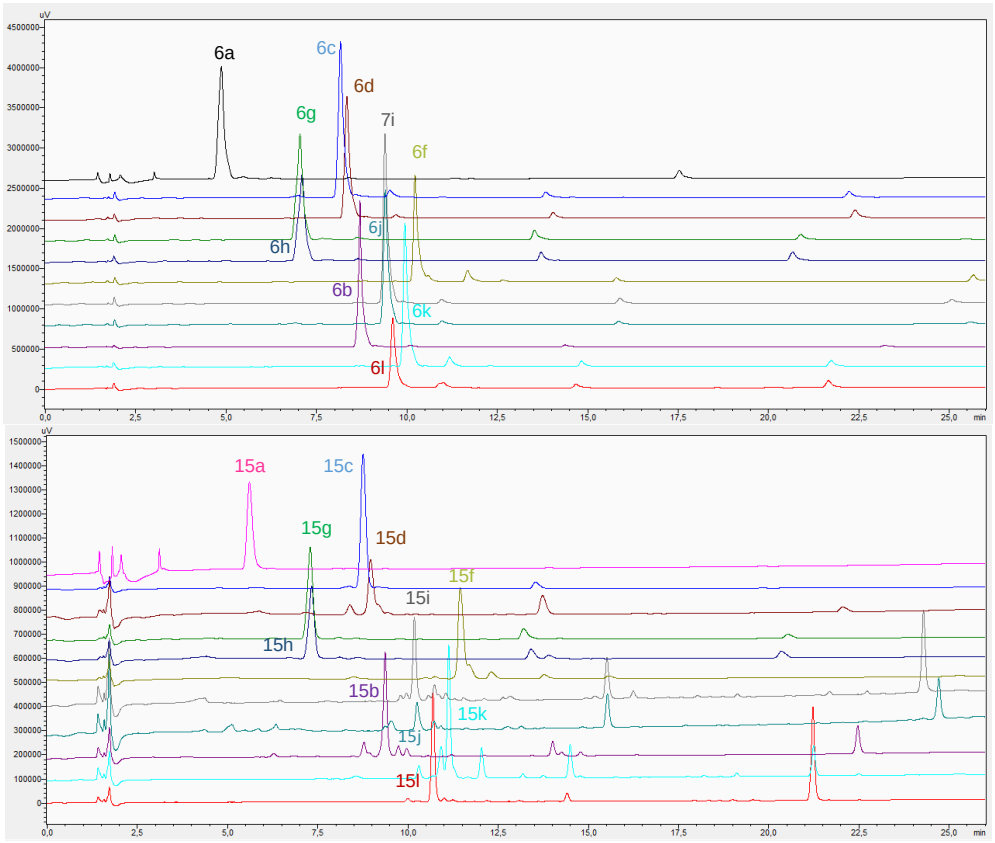

Figure 4.9. A) HPLC profile of the HA array (**6a-l**) synthesized using HPA as donor. B) HPLC profile of the HA array (**15a-l**) synthesized using PA as donor. Both reactions were analyzed after 24h.

Intriguingly, HPLC analysis of the control experiments in the absence of enzyme revealed a small chemical background formation of HA **15**, albeit much smaller with respect to the reaction with the enzyme variant TK$_{gst}$ L/S. Probably for that reason it had not been detected during the TLC analysis staining with ferric chloride. This phenomenon was most significant for the reaction with unsubstituted nitrosobenzene (**15a**), however, it was also observed in smaller quantities for other nitrosoarenes (Figure 4.10). Hence, PA is not suitable as donor substrate for the TK reaction with nitrosoarenes for screening purposes of TK libraries.

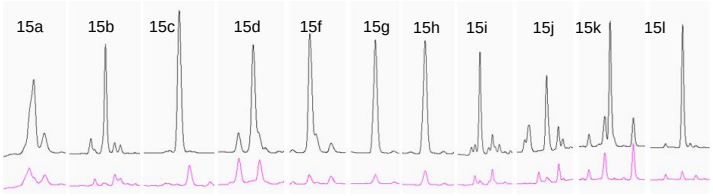

Figure 4.10. Formation of the corresponding HA (**15**) after 4h incubation visualized by HPLC from enzyme reactions with PA in the presence of TK$_{gst}$ L/S (black) and in its absence (pink). A small chemical background generation of HA **15** is observed when no enzyme was present.

This may be initiated by a redox reaction involving PA, as no HA 6 generation in the absence of enzyme was detected by HPLC when employing HPA as donor substrate (Figure 4.11).

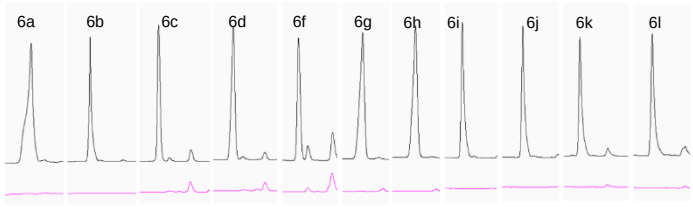

Figure 4.11. Formation of the corresponding HA (**6**) after 4h incubation visualized by HPLC from enzyme reactions with HPA in the presence of TK_{gst} N/S (black) and in its absence (pink). No HA generation is observed when no enzyme was present.

4.2.7. Iron(III) catalysis of *N*-aryl HA formation with pyruvate

Furthermore, HPLC analysis showed that iron(III) was able to react with PA in the TK_{gst}-catalyzed reaction with nitrosoarenes (**5**) to form the corresponding HAs (**15**), which was also confirmed by means of TLC analysis with ferric chloride staining reagent. In Figure 4.12. the reactions with PA in the absence of iron but presence of enzyme (black) and in the presence of iron but absence of enzyme (pink) are shown.

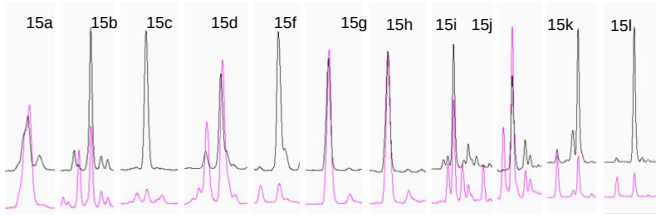

Figure 4.12. Formation of the corresponding HA (**15**) visualized by HPLC from enzyme reactions with PA in the presence of TK_{gst} L/S (black) and in the presence of $FeCl_3$ (1% w/v) yet absence of enzyme (pink).

Interestingly, the HA generation by iron(III) seemed to be more favored when the substrates bore electron donating groups, such as for **15g** and **15h**, **15i** and **15j**. Whereas for compounds carrying strong electron withdrawing groups, including **15k** and **15l**, the generation of HA was much reduced. Moreover, the Cl substitution in *para*-position appears to be less favored for the reaction with iron(III), as, for instance, **15c** and **15f** are formed in the smallest amount. This can be explained considering the catalytic mechanism.

The catalysis of the reaction between formaldehyde[233] or glyoxylate[234] and nitrosoarenes (5) by ferric ions to generate the corresponding HA had been previously observed in the literature. The presumed mechanism from the reaction of **5a** with α-oxoacids promoted by iron(III) ions is shown in Scheme 4.9.

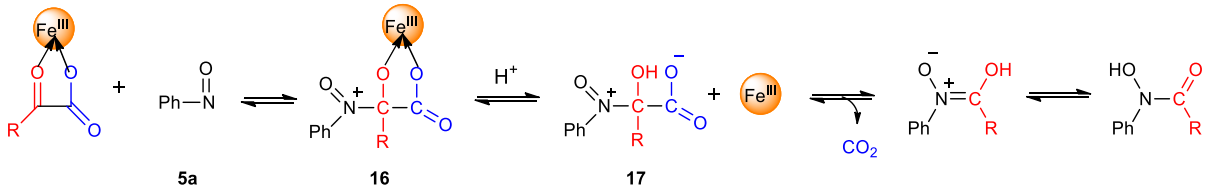

Scheme 4.9. Proposed mechanism for the reaction between nitrosobenzene and a general α-oxoacid mediated by iron(III). Scheme adapted from Radivoj *et al.*[234]

The formation of *N*-phenyl substituted HA in this type of reactions with nitrosoarenes is strongly catalyzed by ferric ions. Apparently, first the α-oxo group coordinates with the iron(III) ion and forms a complex. Then, a nucleophilic attack by the nitroso nitrogen on the carbonyl carbon of the α-oxoacid coordinated to iron(III) leads to C-N bond formation, generating the intermediate **16**. Subsequently, protonation of **16** promotes the release of iron(III), forming the second intermediate **17**. After decarboxylation of the latter, the corresponding *N*-aryl HA is formed. Regarding the mechanism proposed, it is obvious that electron donating groups should favor the iron(III) catalysis of HA, because they supply electron density to the nitroso nitrogen for the nucleophilic attack. Whereas for electron withdrawing groups it should be disfavored as they remove electron density from the ring and thus, make the nitroso nitrogen more electrophilic.

Nevertheless, this feature does not apply to all α-oxoacids. In Figure 4.13. the reactions with HPA in the absence of iron but presence of enzyme (black) and in the presence of iron but absence of enzyme (pink) are shown. For the reactions with HPA, basically no HA was formed in the absence of enzyme by iron(III) catalysis. Hence, the application of TK_{gst} for the reaction between nitrosoarenes and HPA, coupled with a novel colorimetric screening method based on the generation of the corresponding iron(III)-HA chelate complex presents a promising outlook and will be presented in Chapter II.

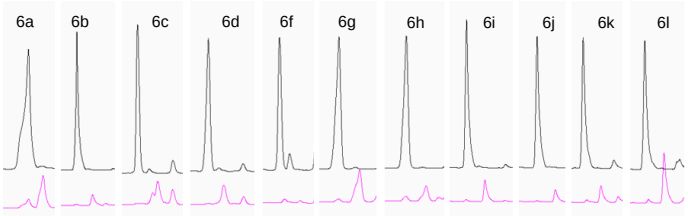

Figure 4.13. Formation of the corresponding HA (**6**) visualized by HPLC from enzyme reactions with HPA in the presence of TK_{gst} N/S (black) and in the presence of $FeCl_3$ (1% w/v) yet absence of enzyme (pink).

4.2.8. Optimization of the reaction conditions: Reaction engineering

Considering the low yields obtained with both HPA and PA, the initially developed reaction conditions demanded improvement. In order to upgrade the product yields while minimizing byproducts from the reaction, and also to avoid tedious purification steps, reaction engineering was attempted. Because nitrosobenzene (**5a**) is highly volatile, the experiments to optimize the reaction conditions were conducted with *p*-bromonitrosobenzene (**5b**). Both offered very similar reactivity but the latter is much less volatile, reducing material loss from evaporation of nitrosobenzene (**5a**). Because HPA is better tolerated by TK_{gst}, it was utilized for the optimization of the reaction conditions.

Continuous feeding of acceptor substrate with syringe pump

To avoid substrate evaporation and decomposition, attempts for a continuous feeding strategy were carried out. The compound **5b** (50 mM) was dissolved in DMSO (2 mL) and was added to the enzyme reaction by means of a syringe pump over 5 hours at a rate of 0.4 mL/h, which is equal to 20% of the total concentration of **5b** per hour. The final volume was adjusted to 25 mL. Unfortunately, continuous feeding of the nitroso compound during the reaction led to a significant increase of side products compared to desired HA, which resulted in a decrease of HA formation so significant that its isolation was not possible. A new side product was isolated never reported before in this type of enzymatic reactions. This will be discussed further below in Section 4.2.9. However, this could be due to instability of HPA over the prolonged reaction time. Hence, an alternative to this method could be to simultaneously pump both the acceptor and the donor substrate to the enzyme reaction separately.

Increasing DMSO concentration

To aid the miscibility of the nitrosoarenes in aqueous solution and thus the yield, experiments with a larger DMSO concentration (10%), which should still be tolerated by the enzyme,[222] were attempted. However, not only did **6b** conversion not improve, but also the product purification was made more laborious due to the need for DMSO removal by column chromatography.

Using ethanol as co-solvent

In another effort to improve the solubility of the SM, ethanol was contemplated as possible co-solvent for the TK reaction, and the reaction was incubated at 50 ºC. Ethanol (8%) had been previously utilized as co-solvent for nitrosoarenes for yeast TK reactions.[224] However, the reaction did not yield satisfactory results, leading to an increased proportion of byproducts and complicating the isolation of the pure HA. This was probably because aqueous alcoholic solutions promote substrate decomposition.[235]

Co-solvent screening

In order to investigate the optimal co-solvent and best conditions leading to the highest solubility of these hydrophobic aromatic compounds in aqueous solution, and therefore to the highest reaction rates, different co-solvents were examined on analytical scale (250 µL). For this co-solvent screen, a collection of completely water-miscible solvents were selected, which had been shown to be compatible with TK,[222] or were similar to those reported. Among this selection, some polar protic alcohols such as methanol, isopropanol, and 2-methyl-2-butanol; together with polar-aprotic DMSO, dimethylformamide (DMF), tetrahydrofuran (THF), acetonitrile (MeCN), and acetone; and non-polar solvents cyclohexane and toluene were investigated. Also, ethanol and DCM were included again to have a complete comparison of different co-solvents. All solvents tested were able to dissolve **5b** to some extent (Figure 4.14).

Figure 4.14. The substrate **5b** dissolved in various solvents, from left to right: DMSO, DMF, THF, acetone, acetonitrile, isopropanol, 2-methyl-2-butanol, ethanol, cyclohexane, methanol, toluene, and DCM.

The nitroso compound **5b** was very well soluble in DMSO, DMF, THF, acetone, acetonitrile, toluene, and DCM, being the solute and the solvent completely miscible and giving a green clear solution. Expectedly, **5b** was not well soluble in the various alcohols, forming a suspension, which precipitated fairly fast. Moreover, cyclohexane was capable to dissolve **5b** slightly better than the alcohols yet also forming a suspension. Some organic reactions have been proven to work with suspensions instead of clear solutions.[236-237] Therefore, all the solvents were tested as co-solvent for the aqueous TK reactions and the incubation temperatures were varied (25-50 ºC) (Figure 4.15).

Regarding the consumption rate of the nitrosoarenes and selectivity for HA generation minimizing the side product formation, the best results from this screen were offered at RT with acetonitrile, DMF, DMSO and acetone. Although THF, toluene, and DCM were very good solvents for the dissolution of **5b**, they gave very poor results with respect to formation of the corresponding HA, having 2-methyl-2-butanol a much bigger conversion rate to product despite its worse solubility.

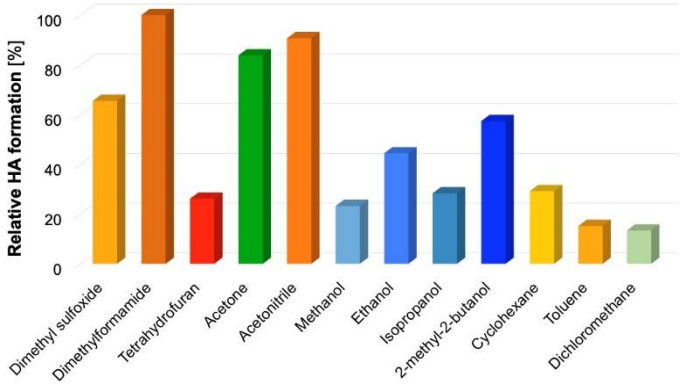

Figure 4.15. Co-solvent screen (10%) for conversion of **5b** (50 mM) at RT. Assay solution (250 µL): HPA (50 mM), ThDP (2.4 mM), $MgCl_2$ (9 mM), TEA buffer (50 mM, pH 7.45) and TK_{gst} N/S (0.1 mg).

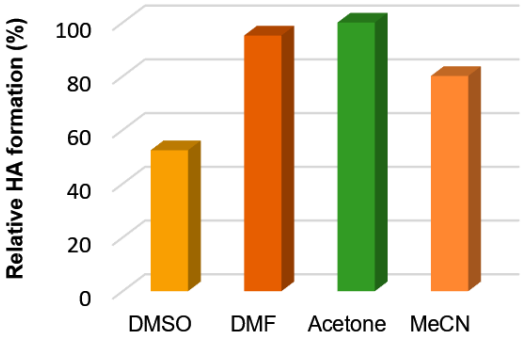

Figure 4.16. Co-solvent screen (20%) for conversion of **5b** (50 mM) at RT. Assay solution (250 µL): HPA (50 mM), ThDP (2.4 mM), $MgCl_2$ (9 mM), TEA buffer (50 mM, pH 7.45) and TK_{gst} N/S (0.1 mg).

This proves that the solubility of the substrate is not the only limiting factor for the reaction. In order to take advantage from the high tolerance towards organic solvents of the thermostable TK_{gst},[222] the four best co-solvents (DMSO, DMF, acetone and acetonitrile) were tested with **5b** (50 mM), varying the temperature (25-50 ºC), and modifying the co-solvent final concentration from 10% to 20%. The best conditions were obtained for acetone with the highest concentration of co-solvent (20%) at RT, followed closely by DMF (Figure 4.16). In addition, acetone offered the possibility for

simplified work-up of the reaction as the purification step by column chromatography was no longer necessary. This confirmed acetone as the co-solvent with the best overall results.

The optimized protocol was applied to the enzymatic reactions with **5a** and **5b** and indeed the yields were enhanced in both cases. Comparing the results, it is observed that the yield improvement with the new protocol for **5b** (28 to 54%) almost doubled that of **5a** (41 to 50%). This is probably due to the fact that the solubility of **5a** in aqueous solution is much higher than that of **5b**. Hence, although this new protocol was not tested on the entire set of nitroso substrates, the yield increment in the optimized reactions compared to the initially developed reaction conditions supports the premise that the optimized protocol would likely offer enhanced HA yields for all less soluble nitrosoarenes. However, although the yields could be significantly improved by the new protocol, the solubility of the nitrosoarenes does not appear to be the only limiting factor for the yields obtained in the enzymatic reaction. Possibly, reducing the nitrosoarene concentration in the reaction to improve solubility, augmenting the enzyme concentration added and/or screening for a different TK_{gst} variant with better tolerance towards nitrosoarenes with a more accurate library towards nitrosoarenes specifically, could further improve the reaction yields.

4.2.9. Chemical side product formation from continuous substrate addition

During the reaction engineering experiments, the continuous addition of **5b** to the enzymatic reaction *via* syringe pump was tested. However, this resulted to be not only detrimental for the production of the corresponding HA, but also a significant raise of side products was observed. Closer NMR and mass-spectrometric analysis revealed the unanticipated generation of *N*-(4-bromophenyl)formamide (**19b**), which was isolated with a ca. 3% yield after column chromatography with silica gel and CH/EA 10:1. The non-enzymatic synthesis of *N*-(4-(dimethylamino)phenyl)formamide (**19p**) had been previously detected by reductive formylation of **5p** with glyoxylic acid (GA),[238] which apparently happens *via* the corresponding HA intermediate **18** (Scheme 4.10).[239]

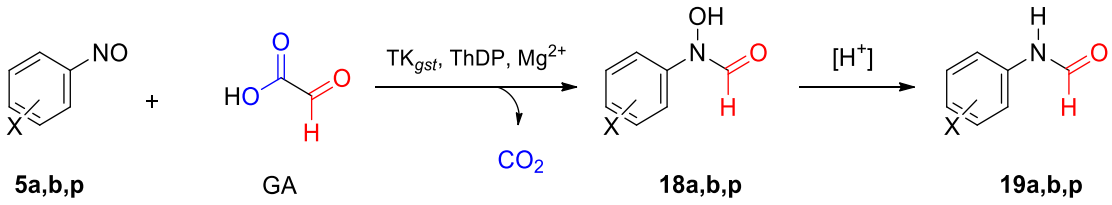

Scheme 4.10. Spontaneous chemical condensation of nitrosoarenes (**5a,b,p**) with GA with presumed subsequent generation of corresponding formanilides (**19**) under acidic conditions.

Apparently, the conversion of the HA **18** to the formanilide **19** is a reductive process, giving the best overall conversion rate at pH 4. At pH neutral (7), the conversion was rather slow, and above that pH other unknown side reactions are a competence.[238]

In an attempt to better understand the mechanism of this new reaction that yielded the formanilide **19b**, the nitrosoarenes **5a** and **5b** were mixed separately with GA in TEA buffer

(50 mM, pH 7.45) in the absence of enzyme and left to react at RT. Thereupon, it was observed that both reactions only produced the expected HAs **18a** and **18b**, which were isolated with a yield of 79% and 70% respectively after an extractive acid-base work-up followed by removal of the solvent. Expectedly, the generated HA **18a** and **18b** also turned red upon contact with ferric chloride stain as usual.

However, the mechanism of production of the formanilide 1**9b**, which seemed to only be formed in the presence of TK_{gst} and HPA during the enzymatic reaction, is still enigmatic, because up to date the potential generation of GA from HPA is unknown.

In summary, GA was found to react spontaneously with nitrosoarenes without the need of a catalyst; PA was discovered to slowly produce small amounts of HA in the absence of enzyme; whereas HPA did not form any detectable HA when the enzyme was not present even upon longer incubation times. Moreover, control reactions confirmed that no HA was formed when the donor substrate was missing. These results verify that the formation of the corresponding HA depends strongly not only on the structure of the nitrosoarene but also on that of the ketoacid component, and that TK_{gst}-catalysis of HA is an exclusive conversion opportunity of HPA.

5. Summary and outlook

Considering the high electronic and structural resemblance between nitrosobenzene (**5a**) and benzaldehyde (**7**), engineered variants of TK_{gst} were successfully employed to convert the former as alternative electrophilic substrates to generate the corresponding *N*-aryl HAs **6** (Scheme 5.1).

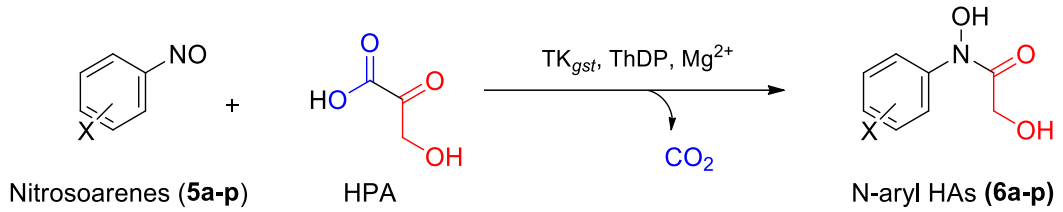

Scheme 5.1. General TK_{gst}-catalyzed formation of *N*-aryl HA by ketol addition to nitrosoarenes.

The corresponding TK_{gst} N/S variant, which had been engineered for enhanced acceptance of benzaldehyde with HPA as donor substrate, offered ca. 7-fold higher initial rates in reactions with nitrosoarenes and HPA as compared to the WT-TK_{gst}.

An array of variously *para*-, *meta*- and *ortho*-mono- and disubstituted nitrosoarenes (**5a-p**) was tested in this chapter. Regarding the reaction rates and yields, electron withdrawing substitution appeared to accelerate the reactivity, whereas strong electron donating groups were found to significantly retard the rate of the reaction. For instance, no HA was generated from the TK_{gst}-catalyzed reaction with *N*,*N*-dimethyl-4-nitrosoaniline (**5p)**. Moreover, by using PA as the ketoacid donor component, structural modifications in the HA structure were introduced. The acceptance of PA as donor by the engineered TK_{gst} L/S variant in this type of biocatalytic process further widens the scope of this enzyme towards a combination of non-hydroxylated-2-oxoacids and aromatic electrophiles, yet at the cost of reduced rates and product yields. However, to truly extend the reaction scope towards the simultaneous application of two non-native components, novel engineered TK variants would be required. Nevertheless, sixteen different *N*-aryl HA could be prepared by this method.

From a co-solvent screen during reaction engineering with **5b**, acetone proved to be especially beneficial regarding the significantly simplified work-up and higher yields. Also, *via* the deeply colored iron(III)-HA complexation (Scheme 5.2), the unequivocal and sensitive detection of the HA could be performed.

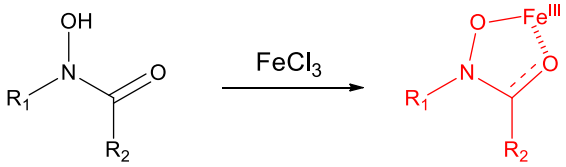

Scheme 5.2. Iron (III) complexation by a general HA.

Furthermore, formation of the corresponding HAs seemed to depend strongly in both the structure of the nitrosoarene employed and that of the ketoacid component. For instance, iron(III) was found to catalyze the reaction with PA to form the corresponding HA (**15**), whereas no HA (**6**) was formed by iron(III) catalysis when employing HPA as donor substrate.

Chapter II

Development of a Novel High-Throughput Assay for Evaluation of Relative Transketolase Activity

6. Theoretical background

The identification of enzymes with novel properties requires generally the screening of large libraries comprising several thousands to hundred thousand clones, containing each DNA fragments derived from genomes of living microorganisms or DNA isolated by metagenomics approaches.[240] Independently of the technique used to generate mutations from a wild-type gene in an enzyme (reviewed in Section 1.2), it is crucial to have an efficient, robust, specific, and rapid method to demonstrate that the mutated enzymes exhibit the desired properties within the library of variants, which may be of larger or less large size. Numerous technologies are accessible to isolate variants of interest, which can be divided into selection techniques and the so-called screening assays, as well as into *in vivo* and *in vitro* approaches.[241]

6.1. Selection techniques

A selection technique is an *in vivo* test that pose a direct link between cell growth/survival and improved/novel enzyme function. In these techniques, cells are transformed with the library and subsequently plated on selective medium. Selections are thus restricted to engineering enzymes that have been developed in such a way that they ensure the cell survival by metabolizing toxic elements; or engineering enzymes able to synthesize essential nutrients for the cells, which are auxotrophic for those elements.[241] These selection methods are efficient, rapid, and allow for the fast screening of large libraries (up to 10^{10} mutants). However, the existence of secondary metabolic pathways which can lead to cell survival without the assistance of the desired enzyme has to be taken into account when developing these type of selection tests.[242] The group of Hecquet has developed the only *in vivo* selection test for TK activity described in the literature to date.[243] This type of metabolic assay employ specially modified synthetic compounds that combine a ketose group, potentially recognized by TK, and the side chain of an amino acid, such as L-methionine or L-leucine.[244] Furthermore, the authors investigated successfully the extension of the *in vivo* selection assay principle by using the side chain of various amino acids, including alanine, valine, and threonine.[245-246]

6.2. Screening assays

A screening assay is an *in vitro* test in which each enzyme is individually tested for a determined property. Screening assays make it possible to connect the conversion of a substrate into a product with a detectable signal.[247] The enzyme activity might cause various measurable modifications: change of physical properties, such as molecular weight, color and/or turbidity by precipitation of the product; change of physicochemical properties, as for example pH and/or adsorption; and spectral changes that can occur directly, because of structural differences between the substrate and the generated product, or indirectly, through for example a chemical indicator system. These signals can be detected with conventional analytical methods, such as chromatography, MS, UV/VIS spectroscopy, fluorimetry, polarimetry, infrared spectroscopy and/or NMR.[247] Accordingly, when designing an efficient screening assay, the selected parameter is of outmost importance.

Depending on the effort and time invested for the screening of a single variant, screening assays can be classified into low-, medium- and high-throughput assays. Low-throughput assays, as for example exhaustive investigation of each single variant *via* standard analytical methods,[248] including gas chromatography-mass spectrometry (GC-MS) or high performance liquid chromatography (HPLC), is very laborious, time consuming, and expensive, due to the high demand on HPLC and GC laboratory equipment. For this reason, medium- or preferably high-throughput assays (usually defined at 10^4 to 10^6 tests per day[62]) have been developed; this being particularly important when applying directed evolution techniques where the library sizes increase exponentially.[249] Due to this fact, the most common enzyme assays are those that produce recordable changes in light absorbance or fluorescence in the reaction medium.[247]

The specific requirements for screening method design normally differ from reaction to reaction. Nevertheless, all methods must comply with some common principles: they must be sensitive enough to allow the identification of the target characteristic with high signal-to-noise ratio; reproducible; stable; must accurately differentiate between positive and negative hits (molecules that show the desired type of activity in a screening assay); and last but not least, they must be economically feasible for frequent measurements.[62] Moreover, the library screening methods may be also categorized into two main types: liquid-phase and solid-phase screening assays.[250]

Liquid-phase assays

The microtiter plate-based method is the most widely used screening format for identification of desirable enzyme variants, because it resembles a miniature cuvette system, allowing the detection of comparatively low improvements in the desired enzyme function or property compared to other assays like colony screening assays. The majority of the microtiter plates use chromogenic or fluorogenic substrates, which react to form spectroscopically different colored products that can be then detected.[56] For this type of screening method, single transformed colonies are individually grown in 96-well microtiter plates, induced to express the corresponding mutated enzymes, and lysed. The extracted enzyme variants may be subsequently evaluated in a second plate, allowing the screening performance of this liquid-phase assay to more than 10^3 enzyme variants per single researcher per week, even without the aid of a robotic support.[241, 251] The microtiter plate screening capacity can be expanded by using smaller wells to increase their number on a plate, existing not only 96-well plates but also 384-, 1,536- and 3,456-well plates. The company Diversa has even created 1,000,000-well plates, achieving the absolute record to date.[241]

Solid-phase supported assays

The agar plate-based screening strategy, also known as colony screening assay, includes the direct correlation of the host organism growth on selective agar plates with the enzyme function to be screened. The key factor in this screening technique is that substrate conversion or product formation create a visual signal, such as change of color or appearance of fluorescence, that allows the identification of colonies expressing the enzyme with the desirable properties.[241]

The halo formation by extracellular secretion of enzymes into the agar plate solid media in contact with a particular substrate or mixture of substrates, also permits the fast screening of improved enzyme variants when compared to the WT-enzyme.[252] This solid-phase supported assay can serve to reduce the screening effort by differentiating *in situ* promising variants from the less active or inactive variants. To perform this agar plate-based method, colonies are directly subjected to enzyme expression and screened on adsorbent and microporous membranes. Afterwards, the most active colonies are picked for further screening or for sequencing. In this way, the colony screening assay can be referred to as a high-throughput preliminary screening method, as it has been successfully used to screen 10,000-20,000 enzyme variants per researcher and per week, respectively.[251] Thus, the application of agar plate-based tests to screen enzyme libraries can increment significantly the throughput compared to the microtiter plate-based assay, by at least one order of magnitude, which implies the decrease of the screening effort and cost. In general, agar plate-based assays are easy to operate, robust, and excellent in identifying active variants, however, they are weaker in detecting differences in catalytic rates of enzyme variants.[241]A comparison between selection techniques and screening assays is shown in Figure 6.1.

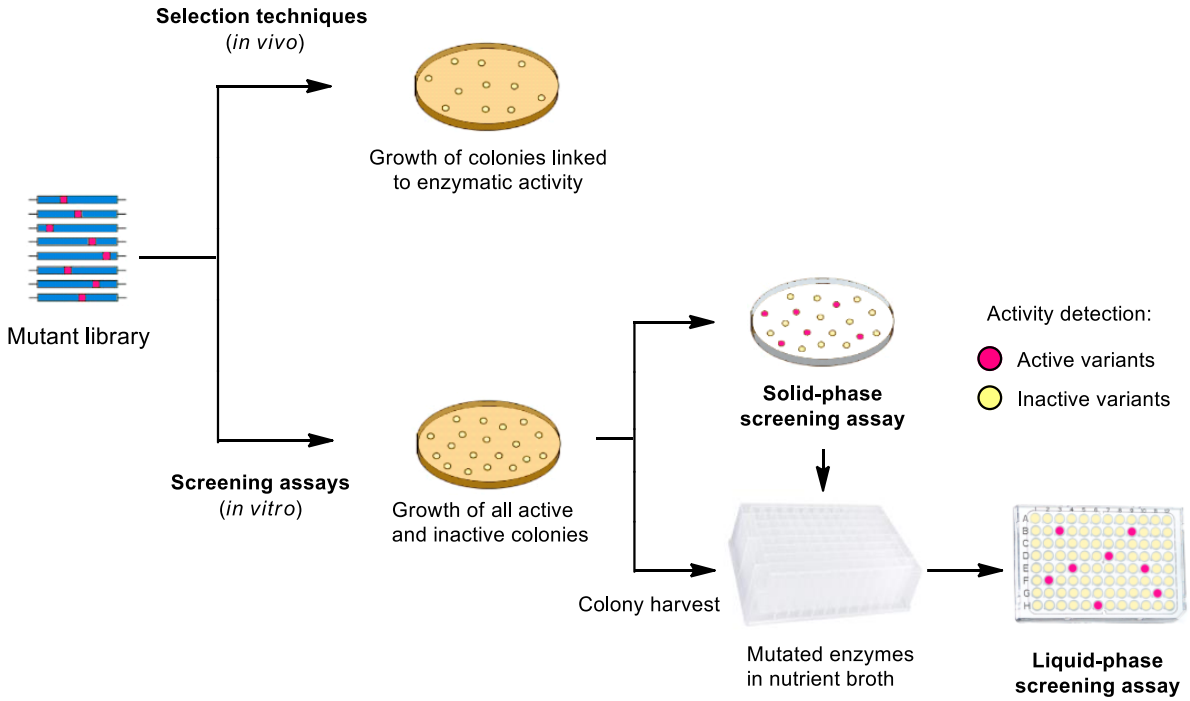

Figure 6.1. General classification of the most utilized technologies accessible to isolate variants of interest.

Further screening methods include the use of pico and femtoliter reactors. In this process, substrates, enzymes, cells and products are held together inside tiny droplets in water-oil mixtures. The droplets in which reactions proceed positively can then be sorted by means of fluorescence (*fluorescence-activated cell sorting system*, FACS). Also, individual cells can be observed and selected in microreactors with help of the FACS system. *In vitro* selection enables the selection of gene libraries (simple linear PCR products).[241]

Aside from the cell-based screening methods, a cell-free technology has been created for ultra-high-throughput (>10^7 variants per day) screening for enzyme activities, known as *in vitro*

compartmentalization. This type of *in vitro* selection enables the selection of gene libraries with suitable transcription/translation mixture in an oil emulsion where water-in-oil droplets are formed (*fluorescence-activated droplet sorting system*, FADS). The encoded proteins within the droplets can be then selected by additional methods.[241]

Over the past decades, many studies have led to the development of more and more innovative screening assays to demonstrate the modification or improvement of the desired properties in a target enzyme within an enzyme library. The properties to be modified may be the enantioselectivity, stereoselectivity, catalytic activity, resistance to organic solvents and thermostability.[253-254] Depending on the property to be modified, diverse screening methods have been developed for the screening of enzyme variants with novel properties.

The enzymatic properties of bacterial TKs, particularly the substrate specificity towards phosphorylated and non-phosphorylated acceptor aldehydes, has been widely investigated in several studies.[1, 79] The traditional assay for TK activity measurement uses D-R5P and either D-ribulose-5-P or L-erythrulose,[223] due to their exceptional substrate qualities as donor and acceptor, respectively (Scheme 6.1).[255] The reaction is monitored spectrophotometrically by the quantity of reduced nicotinamide adenine dinucleotide (NADH) consumed by reactions catalyzed by auxiliary enzymes.[204, 256]

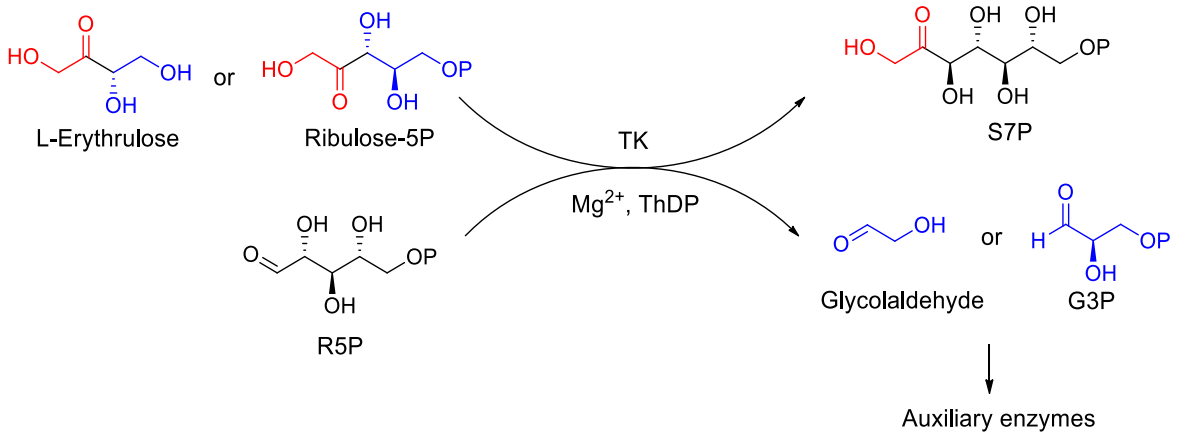

Scheme 6.1. Traditional assay principle for TK activity determination.

Comparable multi-enzyme assays have been reported, including the use of L-erythrulose, 4-deoxy-L-erythrulose, and 4-deoxy-D,L-erythrulose as alternative donor substrates;[109] the coupling of the original assay for the production of X5P from xylulose;[255] and the application of F6P and G3P for the *in situ* generation of E4P.[257] Furthermore, an umbelliferone-based fluorescent assay has been designed for the determination of TK activity and stereoselectivity.[258-260] Although there are various methods to measure TK activity, most of the aforementioned methods require auxiliary enzymes, which increases the cost and the time of the enzymatic assays.

There are also other types of assays to determine the enzyme activity that do not require auxiliary enzymes and can be performed in continuous mode: high-throughput, colorimetric, pH-based assays. The pH-assay principle has been successfully applied to the monitoring of

enzymatic reactions involving ester hydrolysis,[261] nucleotidyl transfer,[262] phosphoryl transfer,[263] glycosyl transfer,[264] and decarboxylation reactions.[265] This principle has also been used to measure TK activity with *p*-nitrophenol as the pH indicator,[266] albeit the low sensitivity of the latter does not allow kinetic determinations of low enzyme activities typical for non-natural acceptors. Moreover, recently during a collaboration between the groups of Hecquet and Fessner a new pH-based high-throughput screening assay method was reported, where HPA is used as the donor and phenol red is used as a sensitive pH indicator.[205]

During the TK catalytic reaction with HPA as donor, one equivalent of bicarbonate is generated upon HPA decarboxylation, which causes a rise on the pH value of the reaction system (Scheme 6.2). The pH changes must be *in situ* monitored by a pH indicator.

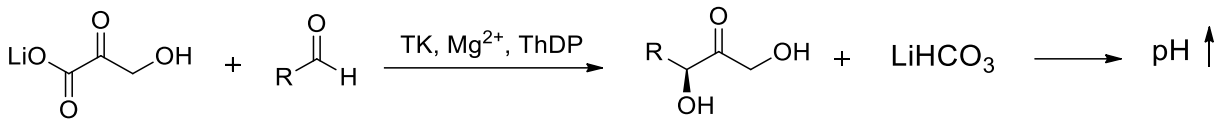

Scheme 6.2. Principle of the pH-based assay for TK activity measurement.

In addition to the TK activity assays aforementioned, several assay formats have been devised to examine the substrate tolerance of TK by direct measurement of remaining substrate or product generated, such as measurement of product generation by optical activity[267] or ellipsometry, which is highly dependent on substrate structure and nature.[268] Measurement of HPA depletion by near-UV spectroscopic monitoring,[269] enzymatic assay[270] or HPLC analysis,[271-272] is hindered by low throughput or low sensitivity. Tetrazolium red-based oxidation assays are limited to non-hydroxylated aldehyde acceptors, since the hydroxylated substrates react directly with the tetrazolium red;[273] whereas colorimetric determination assays of ketose production by heterocyclic condensation reactions are hampered by low specificity.[274] Also, both latter methods demand multiple reagent handling steps and therefore, are laborious and time consuming. Moreover, the methods based on product formation are very specific and are usually limited to a single product at a time, *i.e.* for every different product to be investigated a new assay format has to be developed. Additionally, a notable disadvantage of all the methods involving substrate or product determination is that they are usually discontinuous and therefore, they are not applicable in a high through-put manner.

7. Results and discussion

7.1. Iron (III) assay principle

An assay based on colorimetric determinations is a direct analysis of the enzyme of interest, allowing both for fast qualitative and, under appropriately controlled conditions and proper calculations, also for quantitative measurements.[275] The pH-based assay methodology developed by our group, in collaboration with the group of Hecquet, and used to screen TK_{gst} libraries,[205] relies on the detection of pH shifts. Because most nitrosoarenes (**5**) are easily evaporated due to their high volatility, the pH-based methodology is not reliable for the screening of these type of volatile compounds. Moreover, this general assay is not able to fully differentiate between variants producing the desired product and the ones that have hydrolytic activity where decarboxylation is followed by hydrolysis of the intermediate. Consequently, together with the active variants, it can also give false positive hits where there is, in fact, no product formation. With that in mind, the establishment of an easy to handle TK screening method specifically for the use of **5** as TK acceptor substrates has been one of the goals of this work.

Taking advantage of the chelating ability of HA towards metals, a novel colorimetric assay has been developed for the qualitative or semi-quantitative evaluation of TK_{gst} activity. The method is based on the determination of the HA product (**6**) generated during the TK catalysis with nitrosobenzene derivatives (**5**) as acceptors, HPA as donor, TK cofactors ThDP and $MgCl_2$. After the TK-catalyzed reaction, ferric chloride is added to the mixture *in situ*. The generated *N*-aryl-HAs (**6**) react with iron(III) and form deeply red colored iron(III)-HA complexes, which are not only visible by the naked eye, but also measurable due to the change in the spectroscopic properties.

The iron(III) assay was first developed, optimized and applied in liquid-phase. Subsequently, the strategy was transferred to solid-phase to directly identify the colonies expressing active TK_{gst} variants against **5** with the naked eye.

7.2. Iron (III) assay for liquid-phase

7.2.1. Iron (III) method in continuous mode

Theoretically, this assay principle could be applied in a continuous fashion, where all the reagents would be added at the same time in a one-pot reaction, which would make possible the real-life monitoring of the TK reactions due to their changes in absorbance. For that reason, the development of a continuous one-pot one-step colorimetric assay with iron (III) chloride and **5** using HPA as donor was pursued. The principle of the continuous assay is depicted in Scheme 7.1.

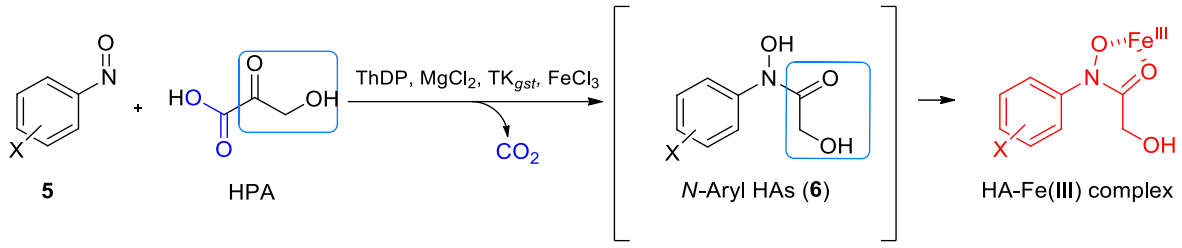

Scheme 7.1. Principle of the continuous colorimetric iron (III) assay for TK activity measurement.

First of all, 1-bromo-4-nitrosobenzene (**5b**) was generally employed as acceptor for the development and optimization of this liquid-phase method, for the same reasons as it was utilized for the optimization of the preparative scale method: its lower volatility compared to nitrosobenzene yet a very similar reactivity.

For the first tests, the same conditions as for the preparative scale reactions were used, with exception of the concentration of TEA buffer which was reduced to 2 mM, and DMSO was used as co-solvent. Microtiter plates are usually made of polystyrene. Acetone is able to solvate polystyrene, and thus can etch the microtiter plate's surface and give unreliable results. To explore the suitability of the co-solvent (20%) for the assay, a set of experiments was carried out utilizing DMSO or acetone as co-solvents to improve **5b** solubility in the TK$_{gst}$ reactions. The concentration of **5b** varied from 0.2 to 50 mM. Iron(III) was not added prior to incubation. The kinetic measurements are shown in Figure 7.1.

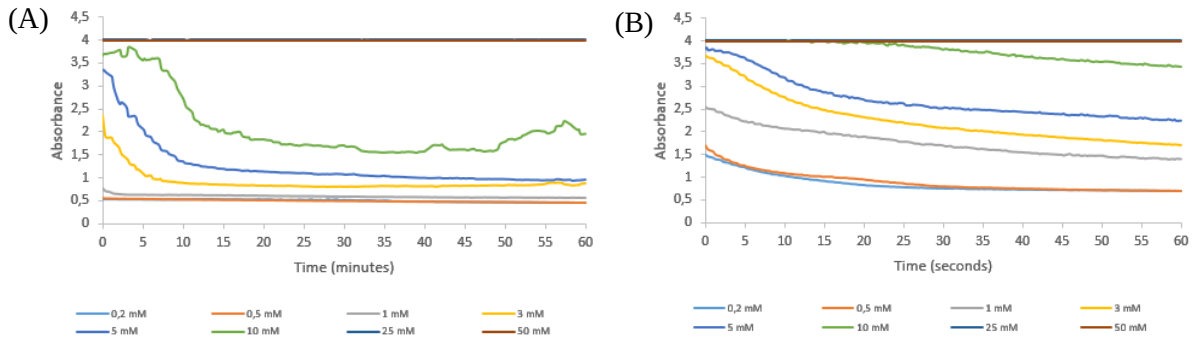

Figure 7.1. Kinetics of the TK$_{gst}$ reaction with **5b** using A) acetone or B) DMSO as co-solvents.

Looking at graphic A, the curves seem to decrease much faster for the acetone than for the DMSO reactions. However, for the reactions with the lowest amounts of **5b** and for the reactions with concentrations higher than 25 mM the curves are basically horizontal. At 10 mM the curve decreases only to slightly increase again with acetone, making the shape of the curves not consistent altogether. This can be due to the higher solubility of **5b** in acetone and maybe even to volatility issues but also to the partial degradation of the microtiter plate in this solvent. For graphic B, the curves decrease slower but in a consistent mode, leading also to horizontal curves with concentrations higher than 10 mM. Moreover, concentrations higher than 3 mM led to no improvement of the kinetics but only to higher OD, making them unacceptable for the assay.

Additionally, the generation of **6b** by both co-solvents in this preliminary assay test was confirmed by performing the usual discontinuous iron(III) test where equal amounts of reaction mixture were mixed with ferric chloride 1% (w/m) (Figure 7.2).

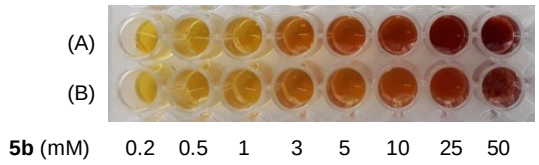

Figure 7.2. 96-microwell plate color comparison between A) acetone and B) DMSO as co-solvents, after discontinuous test with $FeCl_3$.

Although acetone provided the best solubility of the nitroso compound and accordingly a faster TK reaction, both co-solvents were suitable for the generation of the corresponding HA (**6b**), which was generated with no significant color difference. Considering the potential partial degradation of the microwell plate with acetone and hence the possible lack of reliability, DMSO was chosen as reaction co-solvent for the liquid-phase assay.

Moreover, the higher the concentration of **5b** added the slower the kinetics, and in consequence, the flatter the kinetic curve and the higher the OD. Because of the high volatility of the nitrosoarenes and their high reactivity, and thus, lack of accuracy of the measurements, kinetic data was not collected in the next experiments. Even though the red color became more intense the higher the concentration, a precipitate was formed at 50 mM signaling that the solutions were saturated. Consequently, the concentration of the reagents had to be optimized. Also, for the discontinuous iron(III) test, double amount of $FeCl_3$ was added (2%), in order to try to intensify the red coloration.

Experiments with different concentrations of acceptor, donor, and ferric chloride were performed in order to find the optimum conditions where the red coloration would be clearly distinguishable and developed *in situ* without any additional step. A set of experiments with great excess of HPA compared to **5b** were performed (50 /1 mM), and the concentration of ferric chloride added prior to incubation was varied from 0.3 mM to 10 mM. Control reactions were also carried in parallel in the absence of enzyme. No red color formation was observed at all even when performing afterwards the discontinuous iron(III) test.

The concentration of HPA was then reduced in another series of experiments to 10 mM, yet still in excess, since the complete conversion of the nitrosoarene was desired in order to achieve the strongest color. The amount of TK_{gst} N/S mutant was also decreased to 0.125 mg/mL. Yet, again no red color formation was observed after the incubation with $FeCl_3$, only a turbid white to yellowish solution as the concentration of iron increased. HPLC analysis of the reactions proved that **6b** was produced in a high amount in the reaction where no iron was present during incubation. For the rest of reactions which contained enzyme and iron during the TK reaction, a very small peak of HA product was produced. As the iron concentration increased, the concentration of byproducts drastically reduced, yet the HA peak did not augment. The only explanations plausible could be that iron(III) is able to either inhibit the enzyme to some extent, or to interact with HPA. Considering that no reactions turned red upon contact with ferric chloride in the discontinuous iron(III) test, the latter is the most probable explanation.

For the next batch of experiments, HPA was further reduced to 1 mM. We reasoned that with an equal ratio between acceptor and donor, **5b** would be still fully converted to **6b**, leaving no HPA to react with iron(III). The results of these experiments are shown in Figure 7.3.

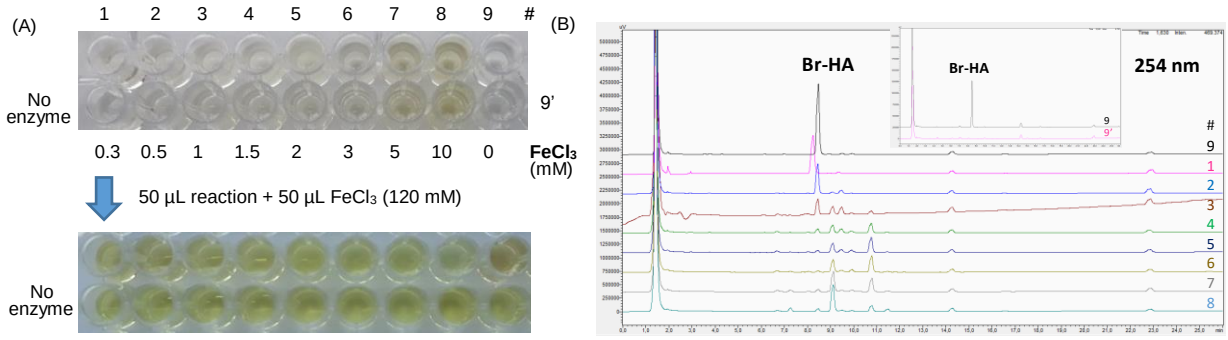

Figure 7.3. A) Reactions in 96-microwell plates with **5b**. Top plate: reactions before discontinuous iron(III) test with $FeCl_3$ (2%); bottom plate: reactions after discontinuous monitoring with $FeCl_3$; upper row: reactions in the presence of enzyme; bottom row: reactions in its absence. B) HPLC profile (254 nm) from the TK reactions from upper plate $FeCl_3$: 1) 0.3 mM, 2) 0.5 mM, 3) 1 mM, 4) 1.5 mM, 5) 2 mM, 6) 3 mM, 7) 5 mM, 8) 10 mM, and 9) 0 mM. Small profile: reaction without iron in the presence (9) or in the absence (9') of enzyme.

Once again, the results were unsatisfactory since no red color formation was produced after the incubation with ferric chloride. However, the reactions were less turbid than before, and as the concentration of iron increased the solutions turned more orange than before, despite having the same amount of iron in both sets of experiments. The discontinuous iron(III) test gave similar results than in the former experiments. All the reactions turned yellow except for experiment #9 (reaction in the absence of iron(III)), which acquired a darker orange color. HPLC analysis (Figure 7.3, B) showed that **6b** was formed in high amount for the reaction where no iron was present during incubation (lane #9). For the reactions performed in the absence of enzyme (Figure 7.3, A, bottom row) no product was detected in any case. For the reactions what contained both enzyme and iron(III) during incubation, a small peak of HA product was produced, in a bigger ratio than before. In this case, as the iron concentration increased, the amount of desired product decreased until there was almost no conversion, and the byproducts ratio increased. This fact supports the hypothesis that the presence of iron(III) during incubation probably hinders the HPA availability for the TK reaction. Still, it was mysterious why for the reactions containing **6b**, no red color formation was developed upon contact with iron(III) after reaction.

In order to address this issue and impede the possible interaction of HPA with iron(III), the ratio of HPA/**5b** was further reduced, first to 1/3 and subsequently to 1/5. Also, a lower range of ferric chloride concentration was utilized in this case varying from 0.1 to 3 mM, since apparently very high quantities of iron(III) were detrimental for the reaction. In both sets of experiments, the solutions had a much higher turbidity than before, probably partly due to the saturation of the solution with the nitroso compound, as the latter is only partially soluble in water even with aid of high amounts of co-solvent (20%). Unfortunately, the results obtained were similar to the previous experiments. HPLC analysis confirmed a high amount of **6b** in the reaction in the absence of iron during incubation again, and also a significant amount in

reactions containing the enzyme and low amounts of ferric chloride. Moreover, the generation of **6b** decreased as the iron(III) increased, augmenting also the byproducts ratio, as previously observed. Although **6b** was clearly present in some reactions, none of the reactions turned red or even orange upon contact with ferric chloride in the discontinuous iron(III) test.

To investigate the effect of HPA in the iron(III)-HA complexation during the assay, a set of experiments were carried out. HPA (varying concentration from 0 to 10 mM), and **6b** (2 mM) solved in methanol were mixed, together with ferric chloride (2 mM) and TEA buffer. A positive control where no HPA was added, and a negative control where no **6b** was present were likewise employed (Figure 7.4).

A)

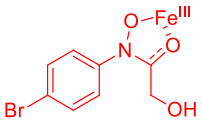

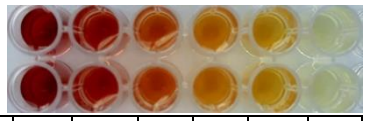

HPA (mM)	0	1.25	2.5	5	10	10
5b (mM)	2	2	2	2	2	0

B)

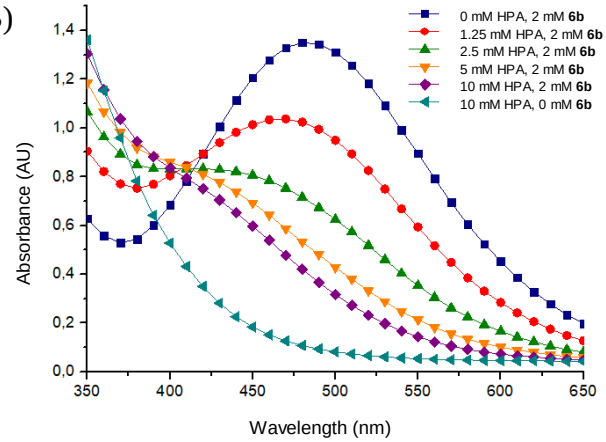

Figure 7.4. Effect of HPA in iron(III)-HA complex formation. Fixed conditions: $FeCl_3$ (2 mM), TEA buffer (2 mM, pH 7.45) and **6b** (2 mM) solved in MeOH in every well except for the negative control which contains no **6b**. The concentration of HPA was gradually varied from 0 mM to 2 mM. Total volume: 200 µL. Experiment performed in duplicates. A) Color comparison, B) spectrum of absorbance comparison.

The difference in coloration when increasing the concentration of HPA added to the **6b** solution could be observed with the naked eye (Figure 7.4, A) and the absorbance was measured with a plate reader by performing a spectrum measurement with a wavelength range from 250 nm to 700 nm. The spectrum is shown only from 350 to 650 nm for a more understandable vision. The free iron(III) can be seen in all wells around 290 nm, and the maximum absorbance for the iron(III)-HPA complex appears at 490 nm. For the next experiments, ferric chloride and TEA buffer were considered for the blanks for a more accurate examination of results. The experiment was carried out in duplicates and the result proved to be reproducible. The results of this experiment showed that as the HPA concentration was gradually increasing, the red color of the solution, and therefore the iron(III)-HA complex already formed, was disappearing. And the maximum absorbance of the latter (blue curve, Figure 7.4, B) was decreasing the more HPA was added. This proved that a continuous assay with iron could not be implemented, since independently from the amount of HA present, the HPA was hindering the red color formation or even its permanence.

The only reasonable explanation for this would be some kind of interaction between HPA and iron. HPA bears three chelating motifs in its structure (Scheme 7.2, A), which compete for the

iron(III) with the singular chelating point of HA (Scheme 7.2, B), making the interaction of iron(III) with HPA stronger and more stable than the one with HA. This could explain why no matter how much iron(III)-HA was formed, the red color was not stable when adding HPA.

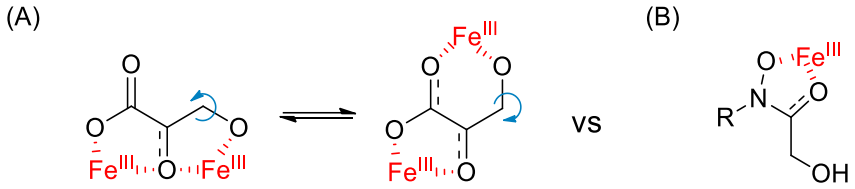

Scheme 7.2. (A) Three possible chelating points in HPA structure for the iron (III) vs (B) only one in the HA molecule.

The absorbance spectrum of a solution containing HPA, TEA buffer and ferric chloride was measured (Figure 7.5), and the last two were subtracted to obtain the spectrum of the iron(III)-HPA complex (Figure 7.5., small graph). The free iron(III) (blue curve) had its maximum absorbance at 300 nm, whereas the HPA-Fe (III) complex (yellow) achieved its maximum at 390 nm.

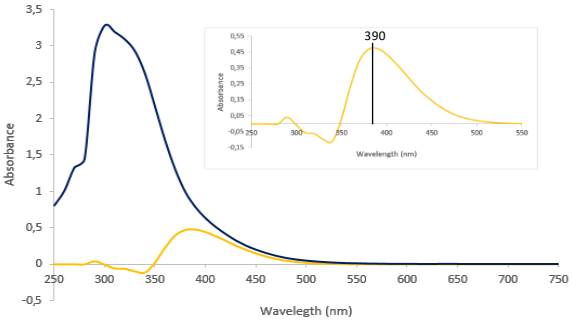

Figure 7.5. Spectrum measurement of the iron(III)-HPA complex. Conditions: HPA (2 mM), TEA buffer (5 mM, pH 7.45), $FeCl_3$ (2 mM). Total volume: 200 µL. The blue curve was recorded utilizing TEA buffer as blank, and for the yellow curve TEA buffer and $FeCl_3$ were used as blank. The maximum wavelength of the iron(III)-HPA complex was 390 nm.

Since HPA reacts with iron(III) in such a vigorous manner, two important consequences can happen: on the one hand, there is barely free HPA available for the TK reaction, and therefore, very small amounts of HA can be formed, if any; while on the other hand, even if some HA is formed and complexed with iron(III), the red color from the iron(III)-HA complex cannot be maintained, as the colorless iron(III)-HPA complex is much more strong and robust. Also, modifying the ratio of reagents did not seem to help for the purpose, because even if there is some free HA left in the solution, if HPA is in excess, the free iron(III) will be chelated by HPA and therefore less to no red color will be formed.

7.2.2. Iron (III) method in discontinuous mode

After all the failed attempts to perform the assay in continuous mode in a one-pot one-step fashion, another strategy was sought where the assay could be implemented in telescopic mode (one-pot two-step) as an endpoint detection assay. For this method, the reagents were added first and the reaction was incubated until the HA product was formed. Then, ferric chloride was added *in situ* to the reaction without previous treatment, forming the corresponding iron(III)-HA complex. The discontinuous principle is shown in Scheme 7.3.

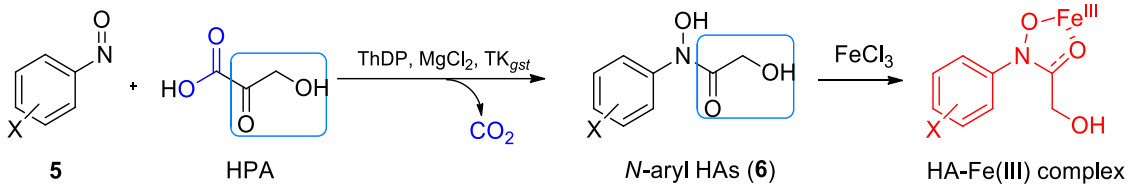

Scheme 7.3. Principle of the discontinuous colorimetric iron (III) assay for TK activity evaluation *via in situ* formation of iron(III)-HA complex for assay validation.

Since the iron(III)-HA complex has its maximum absorbance at around 490 nm and the iron(III)-HPA complex at 390 nm, the formation of the iron(III)-HPA complex to a small extent would not significantly modify the results of the assay. Anyhow, for the results to be unambiguous there must be a compromise between the concentrations of HPA, nitrosoarene, and ferric chloride, being an excess of the acceptor nitrosoarene favored.

The feasibility of the endpoint assay was proven by a quick set of experiments with TK_{gst} N/S performed in the total absence of iron(III) (row A), in its presence (6 mM) during the incubation of the reaction (row B), and only adding it (6 mM) to the reactions after 1 hour of incubation (row C) (Figure 7.6).

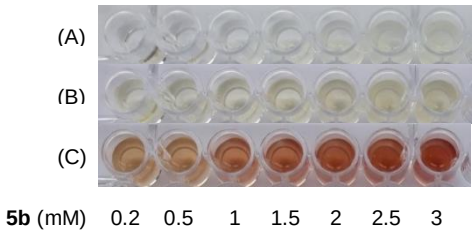

Figure 7.6. Reactions after 1 h incubation. A) in the absence of $FeCl_3$, B) in the presence of $FeCl_3$ (6 mM), C) adding $FeCl_3$ (6 mM) after incubation.

The concentration of HPA was fixed at 3 mM and the concentration of **5b** was varied from 0.2 to 3 mM. The three rows were clearly distinguishable by the naked eye. The red color in the last row that formed immediately upon contact with iron(III) was gradually becoming more intense as the concentration of the acceptor raised. The presence of the corresponding HA in all the reactions was proven by analysis *via* HPLC. The HPLC profile of the smallest concentration (0.2 mM, lane #1), a middle concentration (1.5 mM, #2), and the highest concentration (3 mM, #3) of **5b** are depicted in Figure 7.7.

For the reactions incubated in the presence of ferric chloride (pink), the product peak observed was very small, if any, compared to the reactions incubated in its absence (black) but to which iron had been added afterwards. Moreover, no Br-HA could be seen for reactions in the presence of iron(III) when the HPA was in excess (#1, #2), as expected. Also, in the complete absence of iron(III) the product peak was even bigger (lane A, blue peak). In view of the results, this new strategy seemed to be a good basis for the further development of a high-throughput assay for screening of TK_{gst} variants towards nitrosoarenes.

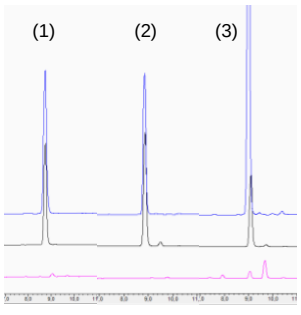

Figure 7.7. HPLC profile (254 nm) from the TK reactions in the presence $FeCl_3$ during incubation (pink), after incubation (black), or its absence (blue).

Prior to assay performance, the general assay conditions were optimized. Aspects such as pH-value of the solution, buffer component and buffer concentration were investigated. In addition, quality detection parameters like standard curve, limits of detection (LOD) and quantification (LOQ) were assessed. These first optimizations were achieved with purified substrates.

pH-value of the solution

In the first place, the effect of the pH in the assay was investigated (Figure 7.8). For this, **6b** solved in methanol was utilized, together with TEA buffer and ferric chloride (2 mM).

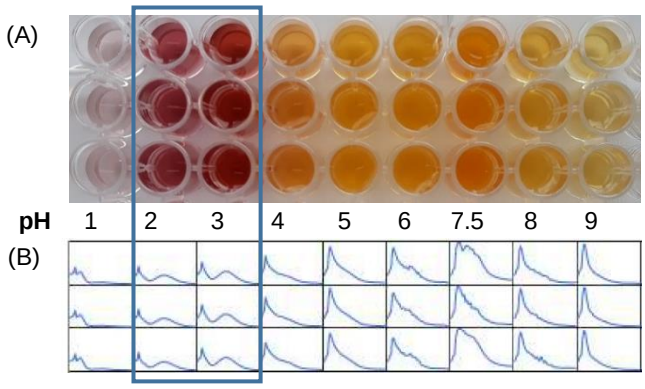

Figure 7.8. Effect of TEA buffer (2 mM, pH 7.45) at different pHs in iron(III)-HA-complex formation. Conditions: $FeCl_3$ (2 mM) and **6b** (2 mM). Total volume: 200 µL. Experiments performed in triplicates. (A) Color comparison, (B) spectrum of absorbance comparison.

At pH one, the solutions were colorless/faint purple, indicating that at such an acidic pH, the complexation of iron(III) by the HA was lost and the HA was dissociated, giving a very small signal in the spectrum graphs (Figure 7.8, B). When the pH was too alkaline, raised above 8, the color of the solutions was again vanished yielding a very faint yellow solution. This was probably because at such alkaline pH the ferric chloride dissociates and cannot be chelated neither by the HA nor by the buffer component. Between pH 4 and pH 8, the color of the solutions was very dark yellow-orange, and a distorted mix of signals was observed in the spectrum graphs. This indicated that probably other complexes are formed, being apparently the iron(III)-HA complex with 3:1 structure among them. Additionally, the buffer component plausibly reacts with the abundant leftover iron(III) at alkaline pH to form a iron(III)-TEA complex, giving a distinctive dark orange color which acquires its maximum intensity at pH 7.5. Between pH 2 and pH 3, the red-purple coloration was optimal. Moreover, two clearly differentiable signals were observed in the spectrum graphs, a very small free $FeCl_3$ signal and a new peak probably corresponding to the iron(III)-HA 1:1 complex signal. These experimental observations are in agreement with the literature,[194] which postulated that the generated *N*-aryl-HA reacts with iron(III) in a pH-dependent manner. In alkaline media (pH $\geq$ 7.5) the complex acquires a 3:1 structure, and when the pH becomes acidic, the ferric trihydroxamate cannot withstand the competition from the medium protons and consequently degrades to a 1:1 complex. The 1:1 structure is characterized by a deep red-purple color, complying what it was observed experimentally. At pH lower than 2 it is ultimately dissociated entirely losing its color. Unfortunately, to the best of our knowledge, no dissociation constants have been measured.

Buffer component

It is known that all pH buffers can interact with metals in a stronger or weaker manner.[276] To examine the scope of the assay, five different buffers, including glycylglycine (Gly-Gly) buffer, tris(hydroxymethyl)-aminomethane (TRIS) buffer, phosphate buffer, 4-(2-hydroxyethyl)-1-piperazine-ethanesulfonic acid (HEPES) buffer, and TEA buffer, were tested in the next experiments at various concentrations (2 mM, 5 mM, 10 mM, 25 mM, and 50 mM) (Figure 7.9). The initial pH of all solutions before adding ferric chloride was 7.45. The experiments were duplicated.

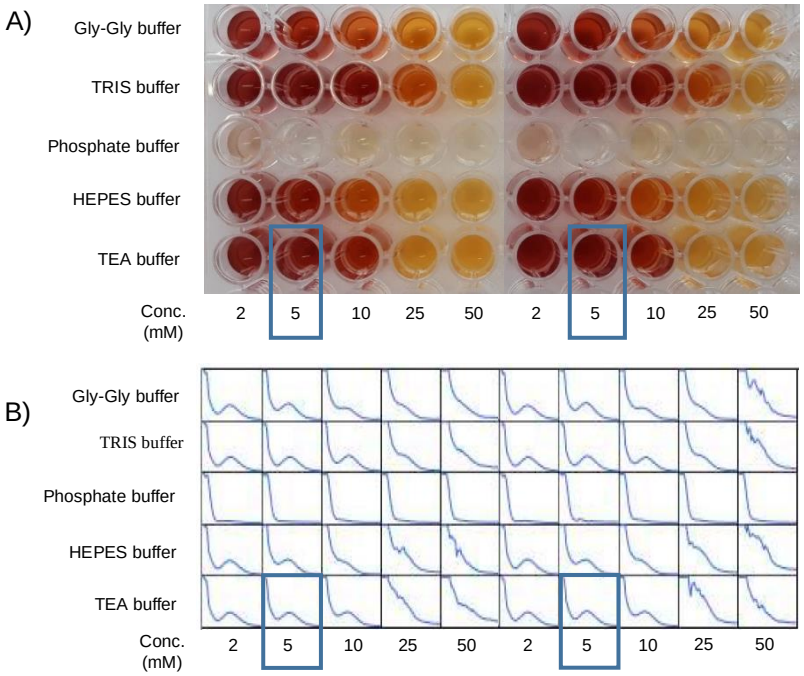

Figure 7.9. Effect of various buffers (initial pH 7.45) at different concentrations in iron(III)-HA complex formation: Gly-Gly buffer, TRIS buffer, phosphate buffer, HEPES buffer, and TEA buffer. Fixed conditions: $FeCl_3$ (2 mM), and **6b** (2 mM). Total volume: 200 µL. Experiment performed in duplicates. (A) Color comparison, (B) spectrum of absorbance comparison.

Phosphate interacts with polyvalent cations such as iron(III) very strongly,[276] impeding the chelation of iron(III) by the HA, and thus preventing the red color formation at any buffer concentration. Therefore, phosphate buffer is inadequate for the assay purpose. This can also be corroborated by the lack of any HA-Fe signal in the spectrums. At high concentrations, such as 25 and 50 mM, the solutions were completely yellow for all of the buffer types, probably due to the complexation of iron(III) by the different buffer components at pH above 4. This can be confirmed by the spectrum graphs, as from 25 mM the iron(III)-HA complex signal detected between 2 and 10 mM had vanished, losing thus its characteristic red coloration. Since at 10 mM Gly-Gly and HEPES buffers were visibly less red (the iron(III)-HA complex signal was significantly smaller), the signal for TEA and TRIS buffers was also slightly smaller, and at 2 mM the iron(III)-HA signal was very similar but then the solution is too less buffered, 5 mM was found optimal for the iron(III) assay. Between TRIS and TEA buffer at 5 mM no

appreciable difference was observed, and because for all other experiments TEA had been used, TEA (5 mM) was chosen as the optimal buffer for the assay.

Detection parameters

To generate a calibration curve for the ferric chloride assay, stock solutions of HPA (20 mM) in TEA buffer (5 mM, pH 7.45), nitroso **5b** (20 mM), DMSO (20%) and HA **6b** (20 mM) were prepared and applied gradually varying the conversion to HA product from 0 to 100% (Figure 7.10. B, C, D). To create blanks for absorbance measurements, wells containing TEA buffer (5 mM, pH 7.45), $FeCl_3$ (6 mM), and methanol were prepared (Figure 7.10, A). The utilized components for the standard curve were selected because all these reagents, when tested separately, were able to modify the color of the assay solution and thus, the absorbance value.

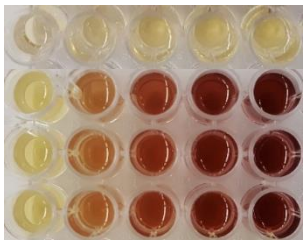

HPA (mM)	2	1.5	1	0.5	0
5b (mM)	2	1.5	1	0.5	0
6b (mM)	0	0.5	1	1.5	2
Conv. (%)	0	25	50	75	100

Figure 7.10. Standard curve for **6b**. Conditions: nitroso **5b** (2-0 mM), HPA (2-0 mM), Br-HA **6b** (0-2 mM), TEA buffer (5 mM, pH 7.45), $FeCl_3$ (6 mM). A) Blanks, B, C, D) Experiments performed in triplicates.

The color gradually went from yellow at 0% of conversion, where no **6b** was present, to dark red at 100%, where no HPA nor **5b** were to be found. At 0% only the substrates are present, and HPA makes a colorless to yellow complex with iron(III) (absorbing around 390 nm). As the conversion to HA raised, the complex iron(III)-HPA weakened and eventually broke, and a new complex formed, the desired iron(III)-HA complex, thus acquiring every step a darker red color. Until there was no reagents left (100%), where only the complex between the HA and the iron(III) was present and therefore, the color was very dark red. This color difference can be well observable by the naked eye. However, the absorbance spectrum for all the experiments was recorded with a plate reader, and the blanks were subtracted prior to representing all curves in a graphic (Figure 7.11.).

Analyzing the graphic, the results of the curves corresponded to the microplate observations. When no **6b** was present, the maximum absorbance was reached at 390 nm, where the iron(III)-HPA complex absorbs. Also, the absorbance of **5b** lies in the same interval. As the concentration of substrates decreased and the amount of the HA product increased, the iron(III)-HPA complex formed weakened and **6b** competed for the iron(III). Thus, the absorbance in the range from 360 to the false isosbestic point (430 nm) decreased and at the same time the absorbance at wavelengths larger than 430 nm increased, reaching the maximum

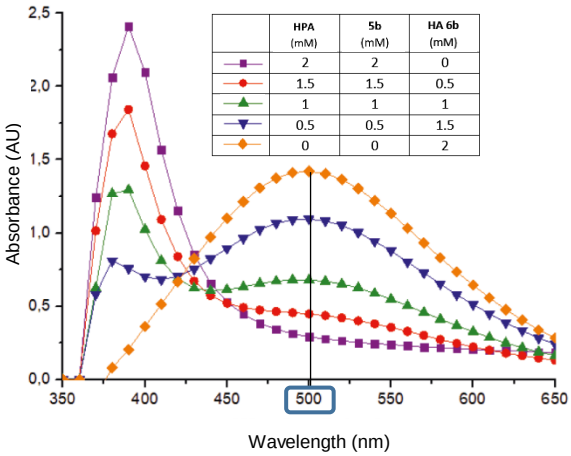

Figure 7.11. Standard curve spectrum for HA **6b**.

absorbance at 500 nm where no reagents were added (orange curve). This means that the complex iron(III)-HA has its λ_{max} at that wavelength under the applied conditions. The results could be expected, since the visible color of the solutions containing mainly HA turn red upon contact with ferric chloride, and the red color transmits at absorbances from around 490 to 560 nm, where its complementary green color absorbs (Figure 7.12.).[277] For instance, the iron(III)-HPA) complex absorbs at 390 nm, from the color wheel it can be supposed that the color of this solution will be yellow to the eye, and that is exactly what can be observed in the experiments.

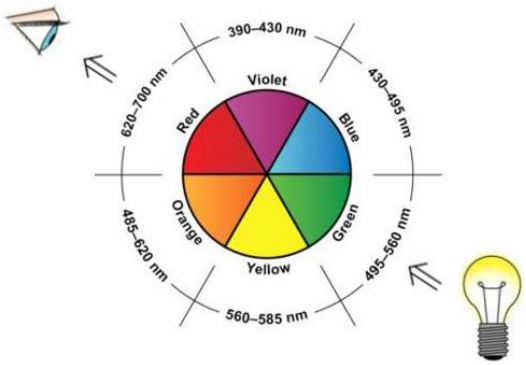

Figure 7.12. Color wheel showing the approximate relationship between the wavelength of light or color absorbed and the color transmitted or observed. The figure shows that the solution that appears red to the eye absorbs green light as its complementary color. The light bulb and eye are rotated synchronously around the wheel. Figure modified from the literature.[277]

A calibration curve for the assay was recorded at 500 nm (λ_{max}) with variation of **6b** concentration from 0 to 2 mM (Figure 7.13.). The mean values were calculated from the triplicates and the absorbance of the corresponding blanks was subtracted. The results were plotted as scatter in the graphic and a linear regression was calculated. The absorbance obtained at 0 mM concentration was considerably high although no product **6b** was present. This was due to the presence of the unreacted reagents HPA and **5b** (purple line in Figure 7.11). Because of that reason, even after subtracting the blank absorbance, the linear regression line did not cross zero. Nevertheless, from the linear regression of the calibration curve showed good linearity over the entire range, the limits of detection (LOD) and limits of quantification (LOQ) being 0.0154 mM and 0.0466 mM respectively.

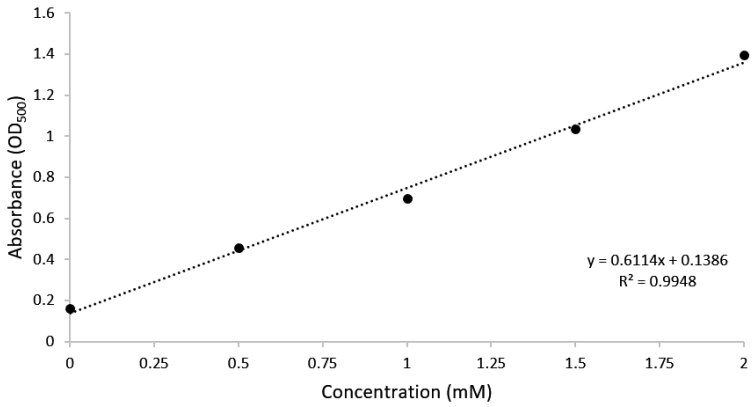

Figure 7.13. Standard curve for **6b**. The linear range of the colorimetric assay was found to be up to 2 mM of **6b** per 200 µL well.

In order for the endpoint assay not only to be able to distinguish active candidates by the naked eye as qualitative analysis but also to measure the absorbance and gather enough data for semi-

quantitative studies, the enzymatic reaction conditions of the assay were determined. Aspects such as substrates concentration, cofactors concentration and enzyme amount were examined.

Concentration of HPA

For the first optimization experiments, purified and lyophilized TK_{gst} N/S was utilized. Some preliminary experiments were performed in order to test the conditions of the assay. For that, **5b** (1 mM), TK_{gst} N/S (0.25 mg/mL), ThDP (2.4 mM), $MgCl_2$ (9 mM), and TEA buffer (5 mM, pH 7.45) were employed, together with varying concentrations of HPA from 0 to 2 mM (Figure 7.14. A, B, C). Control reactions without enzyme were also run under the same conditions (Figure 7.14, D)

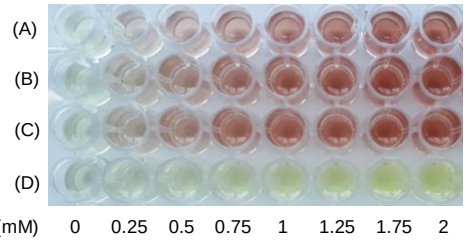

Figure 7.14. Influence of HPA concentration in TK_{gst} reaction for the iron(III)-HA complex formation. Experiment performed in triplicates. A,B,C) Reactions in the presence of enzyme, D) reactions in the absence of enzyme.

Already after reaching a concentration of 1 mM of HPA, the color and spectrum did not improve. However, color intensity did also not decrease due to the chelation of iron (III) by free HPA. In the tests with purified **6b** this was a major problem. Nonetheless, when adding ferric chloride after the TK reaction it does not appear to have such a big influence. As aforementioned, this is probably because the iron(III)-HA complex has its λ_{max} at around 500 nm and the iron(III)-HPA at 390 nm, and therefore, the formation of small amounts of the HPA-Fe (III) complex should not modify the results of the assay significantly.

Concentration of thiamine diphosphate and magnesium chloride

To explore if the presence of ThDP had any effect on the iron(III)-HA complex formation, a few quick tests were performed in duplicates in the presence of **6b** (Figure 7.15.). First no ThDP was added, and then 2.4 mM, and 4.8 mM in TEA (2 mM) buffer pH 7.5 were added respectively. It can be observed that at the usual concentration of ThDP (2.4 mM) added to the reaction, the red coloration had already been lost. The same concentrations of ThDP were added in a smaller amount of buffer, to test if the addition of buffer had some kind of effect on the pH and thus the coloration was lost, however, the same result happened.

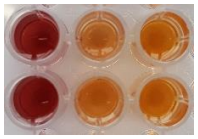

Figure 7.15. Effect of ThDP concentration (mM) in the iron(III)-HA complex stability

When performing a similar experiment to investigate the effect of Mg^{2+} in the desired complex formation, no change of color was observed when adding the same volume of $MgCl_2$ in buffer or using even higher concentrations (Figure 7.16).

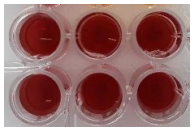

Figure 7.16. Effect of Mg^{2+} concentration (mM) in the iron(III)-HA complex stability

Due to the strong influence of free ThDP on the color stability of the assay, it was important to investigate if ThDP supplement was necessary for the generation of **6b**, and if so, which would be the lowest concentration needed. For that reason, the effect of supplemental ThDP in the TK_{gst} reaction and subsequently in the red color formation was examined. For that, several experiments where ThDP was modified were performed. In Figure 7.17, the final and conclusive experiment where the color was most intense is shown. For this, **5b** (1 mM), HPA (1.5 mM), TK_{gst} N/S (0.25 mg/mL), $MgCl_2$ (9 mM), TEA buffer (5 mM, pH 7.45) were employed, together with varying concentrations of ThDP from 0 to 2.4 mM. The experiments were performed in triplicates.

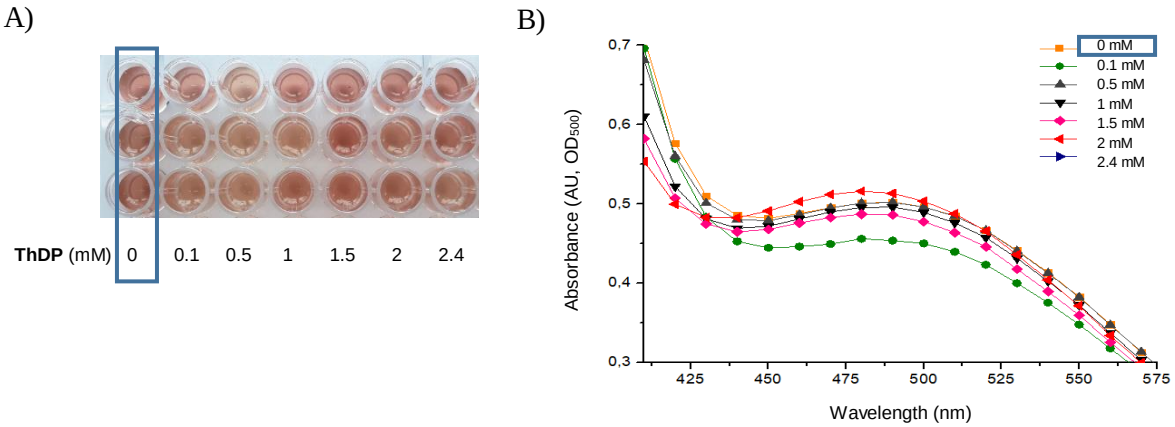

Figure 7.17. Effect of ThDP concentration in TK_{gst} reaction for the iron(III)-HA complex formation. Experiment performed in triplicates and average values are represented. A) Color comparison, B) spectrum of absorbance comparison. The 0 mM concentration is highlighted in a blue rectangle.

In view of the results, all the experiments showed product formation. This was confirmed by comparing all the spectrum measurements for all the experiments (Figure 7.17, B). No considerable change in the shape of the curve or in the absorbance maximum was observed when there was no ThDP added (0 mM). It appeared that the addition of ThDP to the TK reactions before the assay was not necessary, probably due to small amounts of ThDP that possibly were purified and lyophilized together with the TK mutant, leaving the holoenzyme ready for the catalysis. Because the extra addition of ThDP seemed not to be important and the aim of this assay was to apply it for the screening of TK libraries using lysates, where in principle sufficient amounts of ThDP should be also present since no purification step is carried out, no ThDP was added for the following experiments to optimize the assay conditions.

Amount of enzyme

The amount of holoenzyme added also had to be optimized, since the color of the reactions were up to date not very intense in order to distinguish between active candidates or non-active ones. Also, the concentrations of the substrates were raised to 2 mM for both **5b** and HPA, and the rest remained the same, with exception of ThDP which addition was avoided. In Figure 7.18, the color screening (A), and the spectrum measurements for all the experiments from 400 to 650 nm are shown (B). For the new concentrations of substrates (2 mM), addition of TK_{gst}

N/S (0.25 mg/mL) proved to be optimum, since there was no visual difference after that concentration and it had the maximum absorbance.

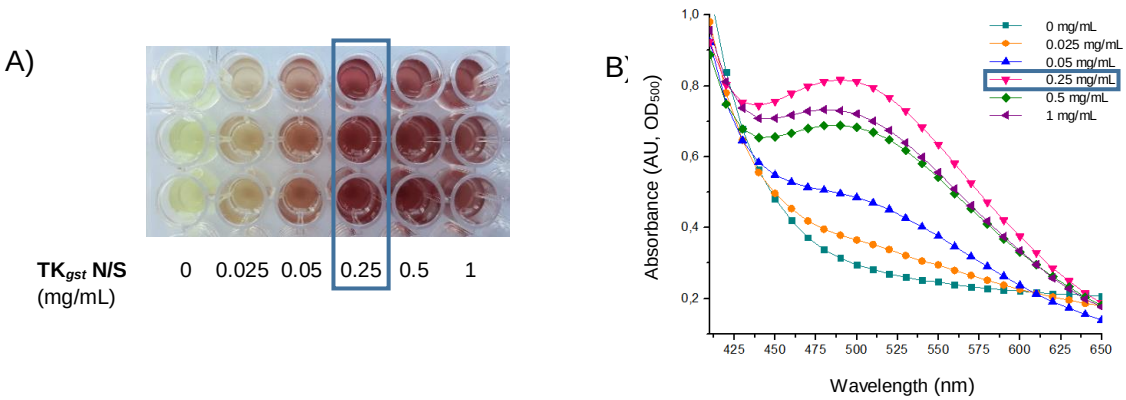

Figure 7.18. Effect of purified TK$_{gst}$ N/S concentration in TK$_{gst}$ reaction. Experiment performed in triplicates.A) Color comparison, B) spectrum of absorbance comparison. 0.25 mg/mL is highlighted in a blue rectangle.

Concentration of magnesium chloride

To investigate the optimal concentration of Mg^{2+} for the assay, several experiments in the absence and in the presence of various concentrations of $MgCl_2$ (0, 0.25, 0,5, 1, 2.5, 5, 7.5 and 9 mM) were performed. In Figure 7.19, the color screening (A) and the spectrum measurements for all the experiments from 400 to 650 nm are shown (B).

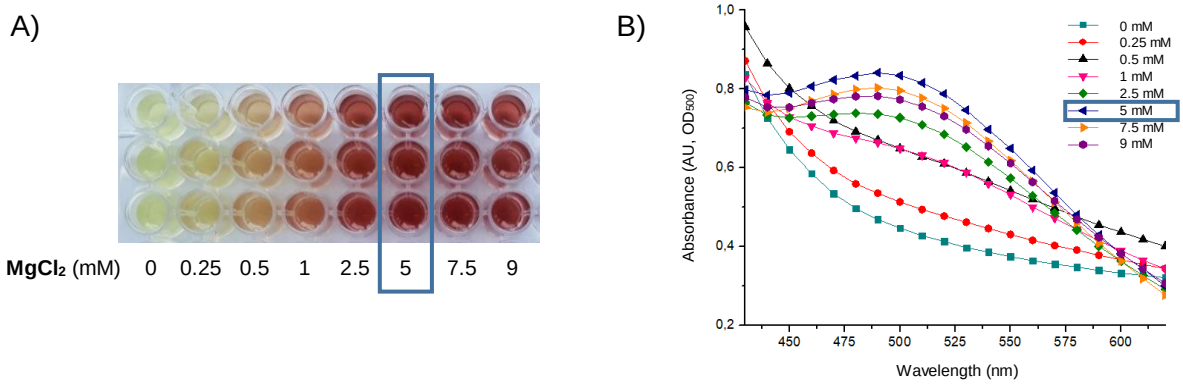

Figure 7.19. Effect of Mg^{2+} concentration in TK$_{gst}$ reaction. Experiment performed in triplicates. A) Color comparison, B) spectrum of absorbance comparison. The best concentration (5 mM) is highlighted in a blue rectangle.

The addition of the $MgCl_2$ was found to be necessary for the reaction, as in its absence or in the presence of very low amounts of this cofactor, no **6b** was produced and thus, no red color was observed. However, beyond 5 mM there was no visual difference in the color of the solutions. Analyzing the graphic, in excess of 5 mM the absorbance starts to decrease and the curve starts to flatten again. The best results for the assay are thus obtained when employing 5 mM of $MgCl_2$ for the TK reaction.

7.2.3. Iron (III) method implementation with cell free extract

Once the conditions were optimized with purified enzyme, the assay was implemented first by extrapolating the optimized assay conditions to the use of cell free extract (CFE), to explore a more real scenario as when using purified enzyme. To calculate how much amount of enzyme was to be added, the concentration of the total soluble protein in the CFE was measured *via* BCA test, giving 485.66 µg/mL. Considering that usually the TK protein expressed inside the CFE should correspond to around 65% of total soluble protein, 300 µg/mL (62%) were taken as the total amount of TK inside of the CFE for further calculations.

Applying the conditions optimized for the assay with purified TK, no color was observed at all for any reaction. After some failed attempts modifying diverse conditions, the amount of CFE added was varied from 0 to 2 mg/mL for the next set of experiments, and a little excess of **5b** was used relative to HPA (2 /1.5) to make sure that no HPA was left after reaction.

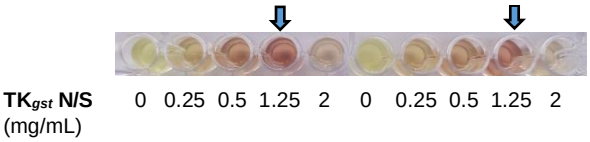

Figure 7.20. Color screening of **5b** with endpoint assay, varying CFE TK$_{gst}$ N/S from 0 to 2 mg/mL. Incubation for 60 minutes at RT. Best result pointed with blue arrow.

Moreover, the amount of ferric chloride added after incubation was increased to 12 mM for a better color generation. The assay was performed adding iron(III) after 30 and after 60 minutes. The best coloration was achieved after 60 minutes (Figure 7.20). The experiments were duplicated.

The best results were obtained when adding 1.25 mg/mL of CFE. Moreover, the absorbance of the wells was measured and a comparison between the absorbance of the solutions with different quantities of CFE at various wavelengths is shown in Figure 7.21.

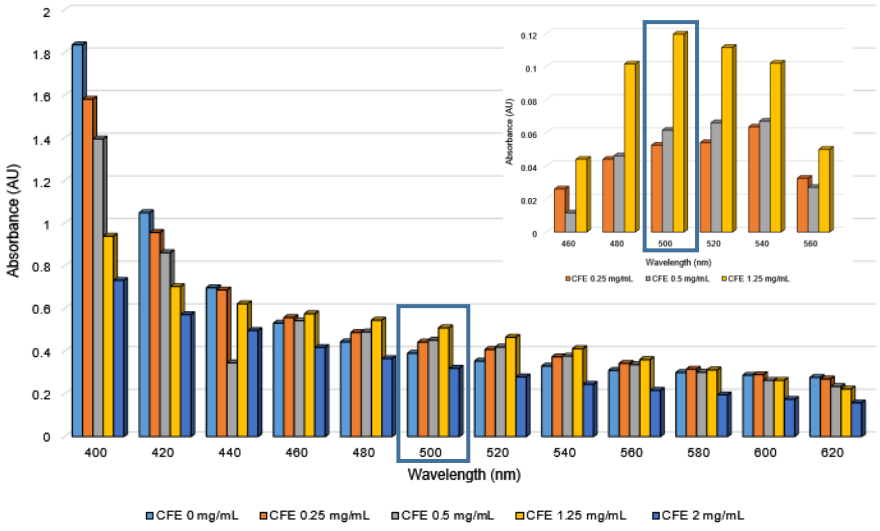

Figure 7.21. Absorbance of the solutions with different quantities of CFE at various wavelengths. The average of the absorbance values of the duplicates is represented in the graphic. In the small graphic, the absorbance values of the best wavelengths are represented after subtracting the background (light blue) where no CFE was present (0 mg/mL).

The background noise (reactions in the absence of CFE) was rather high. However, by subtracting the signals containing no CFE from the rest of the experiments, a clear distinction between relative activities can be observed (Figure 7.21, small graphic). Equal to the assay with purified TK_{gst} N/S, the highest absorbance was obtained at λ=500 nm. In an attempt to reduce the background noise by reducing the HPA concentration added, HPA was varied from 0 to 2.5 mM. The assay was performed again adding $FeCl_3$ after 30 and after 60 minutes, reaching once more the best results after 60 minutes. In Figure 7.22, the color screening after 60 minutes (A) and the absorbance values of the solutions giving the best results at 500 nm 60 minutes are shown (B). The experiments were triplicated.

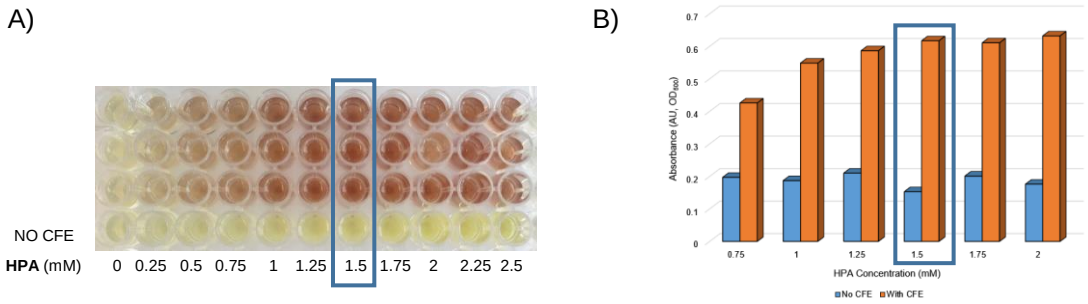

Figure 7.22. Screening of **5b** with endpoint assay, varying HPA from 0 to 2.5 mM. A) Plate incubated 60 minutes at RT (bottom row: negative control without CFE), B) Absorbance values from 0.75 to 2 mM HPA after 30 min (figure left) and after 60 min (figure right) at 500 nm. Average values from triplicates represented in the graphic. The best HPA concentration (1.5 mM) appears highlighted in a blue rectangle.

In Figure 7.22, A there is a nice gradual scale of colors, when no HPA was added at all, the solutions are very pale yellow-colorless, and upon increasing HPA content, the color becomes redder and more intense, until 1.25 mM, after which concentration there is no more appreciable difference in the color intensity. Considering the negative controls in the absence of CFE, none of them formed any HA even adding the highest amount of HPA. However, the yellow color becomes increasingly intense the more amount of HPA added. This is apparently due to the iron(III)-HPA complex formed. Moreover, after 60 minutes a much better difference between the reaction and the background (without CFE) was observed compared to after only 30 minutes. This was presumably because after 30 minutes of reaction, the HA product generated was at a lower concentration and there were many more interfering reagents increasing the background absorbance.

To implement the conditions optimized for the use of CFE TK_{gst} N/S and to prove that they were generally applicable to any nitroso compound, two of the nitrosoarenes produced in the library described in Chapter I, 1-nitroso-3-(trifluoromethyl)benzene (**5l**) and 2-chloro-1-methyl-4-nitrosobenzene (**5j**) were employed together with **5b** in a set of experiments varying the quantity of CFE added again, to confirm that this was also the best concentration for the other two nitrosoarenes. The latter compounds were selected among the whole library because the electronic properties of the three compounds differ considerably since they all possess very different substituent types at diverse positions of the benzene ring, and therefore, it is a good comparison to prove the applicability of the assay to different types of nitrosoarenes. The experiments were incubated at RT and measured after 30 and 60 minutes. In Figure 7.23, the

color screening after 60 minutes (A), and the absorbance values of the solutions giving the best results at 500 nm after 60 minutes (B) are depicted.

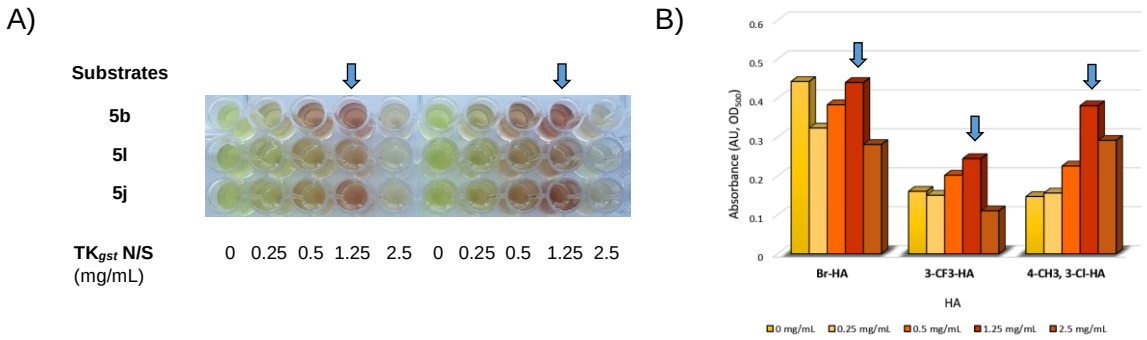

Figure 7.23. Screening of three different substrates with endpoint assay. A) Color comparison, B) Absorbance values at different concentrations of CFE for the three substrates. The best CFE concentration (1.25 mg/mL) appears pointed with an arrow.

From the screening, the color among wells can be very well distinguished by the naked eye. For the third row with substrate **5j**, the color varied in a very similar fashion as for the first substrate **5b**, giving 1.25 mg/mL the most red and intense color, slightly worse than the former compound. For the second row with **5l**, 1.25 mg/mL gave also the best results, however, the color of the solution was not red yet orange. The reaction seemed to be much slower, which was expected since this compound is one of the worst tolerated by TK_{gst}. To confirm the observed results, analysis of the absorbance values after 60 minutes is shown in Figure 7.23 B). As observed in the color screening, the absorbance values were much higher for the first substrate than for the second, and only slightly higher than for the third one. The background noise (in the absence of CFE) was still high and also the absorbance of the reaction with 2.5 mg/mL of CFE presumably due to the reaction turbidity. Nevertheless, with the best CFE amounts (0.5 to 1.25 mg/mL) the absorbance values agree with the visual results from the color screening, where the reddest color was achieved with the CFE (1.25 mg/mL).

7.2.4. Iron(III) method application with hits from a L382X/D470X library

The ultimate goal of this work was to prove the applicability of the assay with libraries of lysates directly to simulate the real conditions after creating a mutagenesis library. In order to first optimize the assay in a medium scale, the 16 best candidates active with benzaldehyde (**7**)[6] from the L382X/D470X mutagenesis library created by D. Yi for screening of TK_{gst} variants towards propanal, were screened.[210] For that, the lysate samples were prepared adapting a common literature protocol.[212] The cells from the glycerol stocks were first cultured in LB medium containing kanamycin as antibiotic or no antibiotic for the negative controls containing untransformed BL21(DE3) strain. After incubation, the bacteria were induced by addition of IPTG to the LB medium. After overnight shaking, the cells were then harvested and washed with TEA buffer, and the supernatant was removed. The pellets were lysed by addition of TEA buffer containing lysozyme and cyanase, and incubated at 37 ºC for 30 min for cell lysis. The

lysates were incubated at 50 ºC for heat purification of TK_{gst}, centrifuged, and the resultant supernatant was utilized directly for the assay screening.

For the first reaction engineering experiments, **5b** was employed again. Also, the assay conditions were used as previously optimized with CFE, except the quantity of the lysate added which had to be examined to achieve optimum conditions. First, 50 µL of TK_{gst} lysate samples were added to reactions containing **5b** (2 mM) solved in DMSO (20%), HPA (1.5 mM), $MgCl_2$ (5 mM), and TEA buffer (5 mM, pH 7.45), and $FeCl_3$ (12 mM) was added after the incubation with the lysates. Also, two negative controls were added to the experiments, reactions with untransformed BL21(DE3) (#9) and in the absence of enzyme (#18). Unexpectedly, very few rows turned red upon contact with iron(III), and most surprisingly, the TK_{gst} N/S variant did not show any color. Due to the strange results, the solutions were analyzed *via* HPLC, which confirmed that the principle of the assay was working properly, as only the rows that had red coloration showed a large product peak in the HPLC profiles. The screening results with **5b** are shown in Figure 7.24.

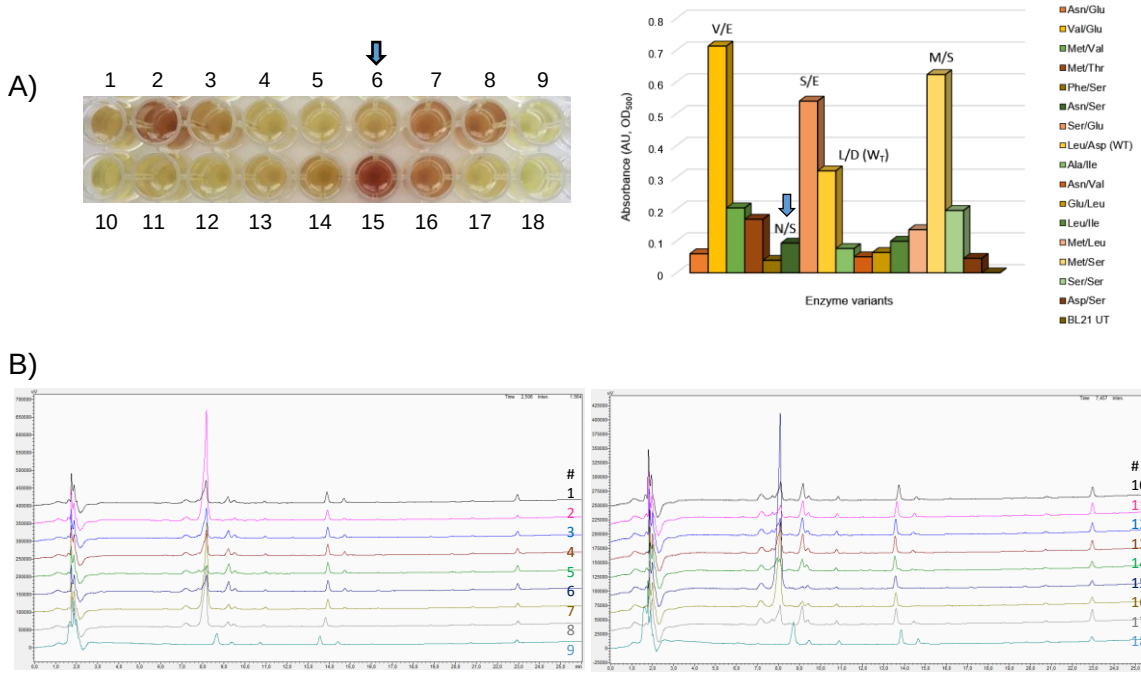

Figure 7.24. Screening assay with **5b** and 16 hits from TK_{gst} L382X/D470X library with optimized conditions. Total assay volume: 200 µL. Plate was incubated 30 minutes at RT. Sequences: 1: N/E; 2: V/E; 3: M/V; 4: M/T; 5: F/S; 6: N/S; 7: S/E; 8: L/D (WT-TK); 9: negative control untransformed BL21(DE3); 10: A/I; 11: N/V; 12: E/L; 13: L/I; 14: M/L; 15: M/S; 16: S/S; 17: D/S; 18: negative control no lysate. A) Color screening (left), graphic with absorbance values (right). The variant TK_{gst} N/S is pointed with a blue arrow. B) HPLC profiles of first row (left) and second row experiments (right panel).

In order to discard experimental errors, the experiments were repeated. TK amount was reduced to 40 µL and incubated for 1 hour instead of 30 minutes. However, the results were comparable again.

Although the assay principle proved successful, it was very mysterious why the anticipatedly most active variant N/S that had even been used for the preparative scale synthesis of HA was giving such a low conversion under the assay conditions. In order to explore this further,

different approaches were regarded. The mutant was sequenced to discard any possible mistake. Also, to discard the possible degradation of the glycerol stock, the N/S mutant was transformed again. However, the freshly prepared variant also did not show any color. Although the extra addition of ThDP had been proved unnecessary for the assay during the optimization with pure TK_{gst} and with CFE TK_{gst}, it was thought that maybe there wasn't sufficient ThDP cofactor in the lysates for the TK reactions to happen. To investigate this, the assay was carried in the absence (A) and in the presence (B) of ThDP (2.4 mM) (Figure 7.25).

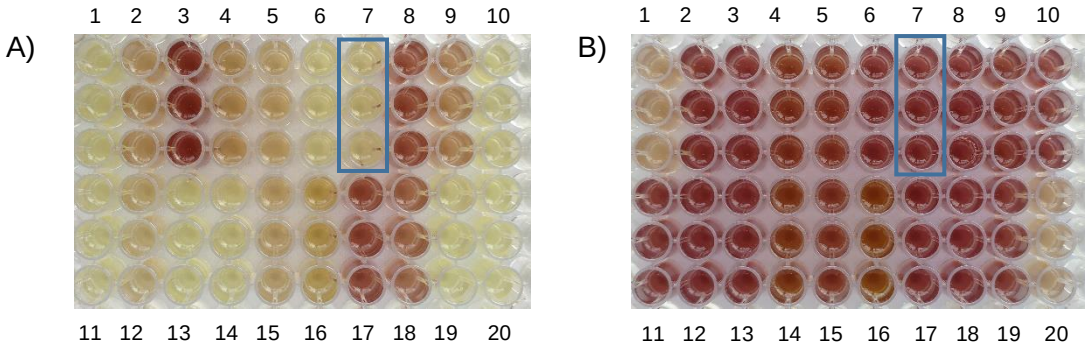

Figure 7.25. Color screening with **5b** in the absence (A) or presence (B) of supplemental ThDP (2.4 mM). Total assay volume: 200 µL. Plate was incubated 45 minutes at RT. The experiments were performed in triplicates. 1, 20: Control negative untransformed BL21(DE3); 2: N/E; 3: V/E; 4: M/V; 5: M/T; 6: F/S; 7: N/S; 8: S/E; 9: L/D (WT); 10, 11: Control positive TK_{gst} N/S from fresh stock; 12: A/I; 13: N/V; 14: E/L; 15: L/I; 16: M/L, 17: M/S; 18: S/S, 19: D/S, The variant TK_{gst} N/S is marked with a blue rectangle.

When no supplemental ThDP was added (Figure 7.25, A), very few variants were producing the desired HA which turned red upon contact with ferric chloride after the reaction, 3 (V/E), 8 (S/E), 17 (M/S) and 18 (S/S). This fact could indicate that these variants are so active that very small amounts of residual ThDP are enough for catalysis, *i.e.* these variants would be still quite active even with partial apoprotein unlike the rest. However, it could also indicate that not the same amount of residual ThDP was present in every well since all the bacteria solutions were cultivated, expressed and lysed separately. When suppling the reactions with ThDP (Figure 7.25, B), all of the solutions became very red upon contact with iron(III), except for the reactions with untransformed BL21(DE3), which turned pale pink at such high concentration of ThDP due to their inherent TK. The strong color development proved that the addition of ThDP was indeed necessary for the assay when utilizing directly lysates for the TK reactions, because not all the variants were expressed with enough ThDP to be used as cofactor for the enzymatic reactions. Therefore, it was a requirement to convert the apoenzyme into a holoenzyme (active enzyme with cofactor bound) ready for catalysis.

To further analyze the results obtained with the colorimetric screening, the solutions containing supplemental ThDP were analyzed with a spectrophotometer (Figure 7.26). TEA buffer and ferric chloride were used as plate blanks. For the negative controls with untransformed BL21(DE3) (1, 20), only the leftover iron(III)-HPA complex and/or nitrosoarene peak (around 390 nm) was observed, and no signal for Br-HA could be detected as expected, since the color was very pale.

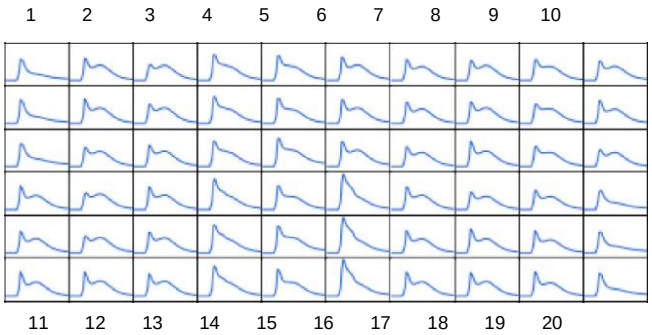

Figure 7.26. Spectrum comparison from assay with supplemental ThDP (2.4 mM).

However, for the rest of the solutions, except for 14 and 16, together with the iron(III)-HPA peak, another peak around 500 nm was also generated, which corresponded to the iron(III)-HA complex. This further verified the generation of **6b**.

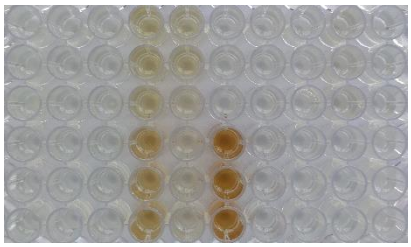

Figure 7.27. Reactions with **5b** directly after incubation with the lysates prior to adding $FeCl_3$.

For the variants 14 (E/L) and 16 (M/L), a small amount of HA product was presumably produced because of the orange-red coloration, yet those solutions had already a dark orange color after incubation, probably due to the concurrent synthesis of a colored byproduct (Figure 7.27). In wells 4 (M/V) and 5 (M/T) this is also observed, yet not strong enough to interfere in the TK reaction. Nevertheless, there seems to be a pattern for the orange coloration of the solutions. The strongest color was L382 position combined with a leucine in the D470 position (16). Analysis of the only other variant containing leucine in the D470 position, showed that these variant (14), also produced the colored byproduct in a considerable amount. Furthermore, with exception of the variant 17 (M/S), the other variants producing a low quantity of the byproduct also bear a methionine mutation in the L382 position, variants 4 (M/V) and 5 (M/T). When combining the L382M with a very good tolerated mutation such as D470S in 17 (M/S), no byproduct was formed. This was probably because in that case the HA production was preferred. However, when L382M was combined with low accepted mutations such as D470L (16), the byproduct formation was favored.

Obviously, the quantity of lysate added was too high in order to be able to distinguish relative reaction rates. According to the results obtained, the parameters were modified in various rounds of experiments. Less quantity of lysates (20, 30 µL) was used for the screening of the positive hits with **5b**, **5l**, and **5j**. Also, the concentration of ThDP was halved to 1.2 mM and subsequently to 0.6 mM. Moreover, the concentration of ferric chloride was decreased to 6 mM. The final screening results of **5b**, **5l**, and **5j** with the optimized conditions are shown in Figure 7.28, figure 7.29 and Figure 7.30, respectively. The corresponding microtiter plates are shown together with a display of the relative HA generation in every well normalized to 100.

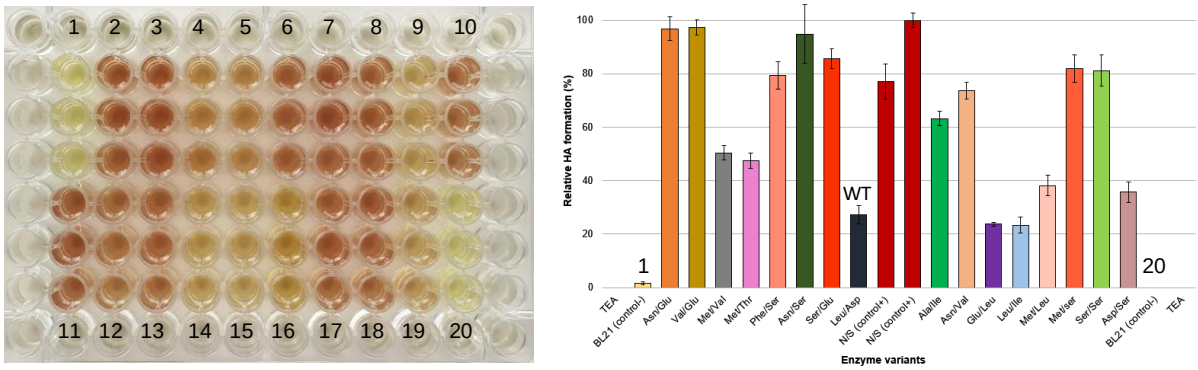

Figure 7.28. Screening results of hits plate with **5b**. The experiments were performed in triplicates, being the average of absorbance values represented in the graphic. 1, 20: Control negative untransformed BL21(DE3); 2: N/E; 3: V/E; 4: M/V; 5: M/T; 6: F/S; 7: N/S; 8: S/E; 9: L/D (WT); 10, 11: Control positive TK_{gst} N/S from fresh stock; 12: A/I; 13: N/V; 14: E/L; 15: L/I; 16: M/L, 17: M/S; 18: S/S, 19: D/S. The lysate was diluted 1:2 prior to use.

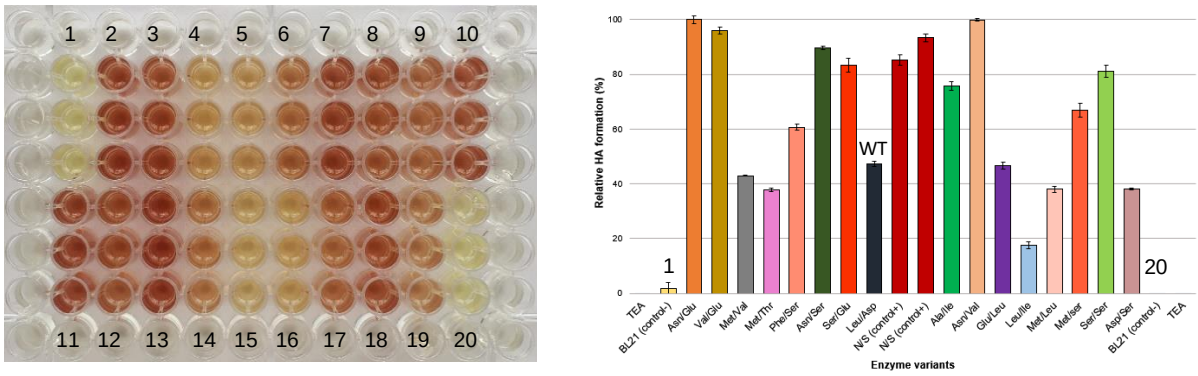

Figure 7.29. Screening results of hits plate with **5l**. The experiments were performed in triplicates, being the average of absorbance values represented in the graphic. 1, 20: Control negative untransformed BL21(DE3); 2: N/E; 3: V/E; 4: M/V; 5: M/T; 6: F/S; 7: N/S; 8: S/E; 9: L/D (WT); 10, 11: Control positive TK_{gst} N/S from fresh stock; 12: A/I; 13: N/V; 14: E/L; 15: L/I; 16: M/L, 17: M/S; 18: S/S, 19: D/S.

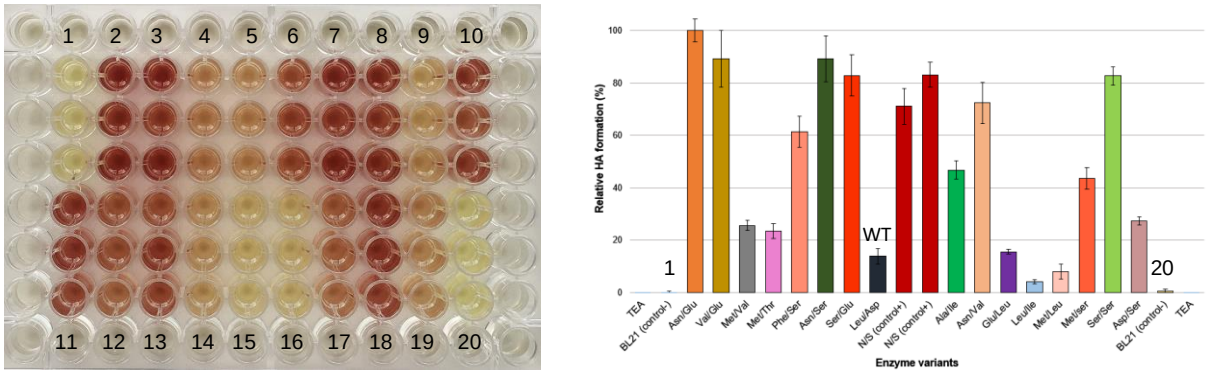

Figure 7.30. Screening results of hits plate **5j**. The experiments were performed in triplicates, being the average of absorbance values represented in the graphic. 1, 20: Control negative untransformed BL21(DE3); 2: N/E; 3: V/E; 4: M/V; 5: M/T; 6: F/S; 7: N/S; 8: S/E; 9: L/D (WT); 10, 11: Control positive TK_{gst} N/S from fresh stock; 12: A/I; 13: N/V; 14: E/L; 15: L/I; 16: M/L, 17: M/S; 18: S/S, 19: D/S. The lysate was diluted 1:1 prior to use.

For all of them 20 µL of lysate was added yet in order to differentiate very active candidates from the rest, for the **5b** screening the lysates were diluted 1:2 prior to use, and for the **5j** 1:1. For **5l**, the relative rates of the different variants were well distinguished already without dilution of lysates. All plates were incubated 30 minutes at RT. The experiments were performed in triplicates. However, even if the reactions with the first and third substrate were diluted due to their fast reaction rates, very small pipetting and/or handling errors translate already in a visible color difference, making it very difficult to make exact triplicates. However, since the absorbance values represented are the average of the triplicate measurements, this is not very significant for the assay output.

The negative controls containing untransformed BL21(DE3) (1, 20) show no coloration, and their background absorbance was very low, unlike in the experiments with CFE, allowing for a very good differentiation relative to the active variants. The positive control containing TK_{gst} N/S from freshly prepared stock (10, 11) gave strong red coloration and absorbance as expected. Although at different rates, all of the substrates, no matter the substitution on the benzene ring, show the same pattern. The most intense colored variants, *i.e.* the most active candidates (2 (N/E), 3 (V/E), 7 (N/S), 8 (S/E), 13 (N/V) and 18 (S/S)), are common to the three substrate screenings. Apparently, the asparagine mutation in the L382 position was one of the best tolerated variations for the TK_{gst}, as all variants carrying this mutation are very active. When combining this mutation with well tolerated ones such as glutamic acid (2) or serine (7) in the D470 position, very active variants are obtained. In the same way, all candidates carrying a glutamic acid or serine instead of aspartic acid in the D470 position seem to be favored also when combined with other mutations such as valine (3) or serine (18) in the L382 position. Also, the variant 15 (L/I) is inactive with all the substrates. As aforementioned, 14 (E/L) and 16 (M/L) did yield a colored byproduct and therefore, they did not produce a high quantity of HA. Thus, the color did not turn red in contact with $FeCl_3$ for **5b** and **5j**. However, the variant 14, which was producing less amount of byproduct, did produce some HA with **5l** that can be visible in the microtiter plate and also in the absorbance value. Furthermore, WT-TK (9) is also able to convert nitrosoarenes albeit at much lower reaction rates; for the first and third substrates, the lysate was diluted 1:2 and 1:1 respectively, and the measurable quantity of HA produced was too low to color upon contact with iron(III) or to measure absorbance; for the second substrate, which lysates were not diluted prior to addition, the WT-TK (9) shows acceptable conversion. Expectedly, three of the most active variants, 3 (V/E), 8 (S/E), and 18 (S/S), had shown very good activity even with partial apoprotein. The effect of the different mutations in the toleration of the nitrosoarene substrates by TK_{gst} will be further explored later in this chapter.

The results prove that the assay can be generally applied to any type of nitrosoarenes to identify active hits. For evaluation and validation of high-throughput screening methods, Zhang *et al.* defined a statistical parameter called "Z-factor" as a dimensionless screening window coefficient[278] which considers both the assay signal dynamic range and the data variation associated with the signal measurements, and thus provides a useful tool for assay quality assessment and for comparison among assays in different formats. The larger the *Z*-factor value of an assay, the higher the suitability of the assay for high-throughput screening. The assay method is judged to be ideal when Z-factor equals 1, and excellent when $1.0 > Z \geq 0.5$. If $0.5 >$

$Z \geq 0.0$, the assay cannot be performed in high-throughput format, and if $Z < 0$, screening is essentially impossible. To evaluate the suitability of the optimized assay for high-throughput setup, the *Z*-factor of the screening assays performed with the three nitrosoarenes was calculated. For the **5b** assay, the *Z*-factor value was 0.84; for that of **5l** *Z*-factor was equal to 0.90, and for that of **5j**, *Z*-factor was 0.73. In all cases the *Z*-factor values were around 0.8, verifying that the ferric chloride assay developed offers excellent quality for its use with high-throughput purposes.

7.2.5. Final application of the iron (III) method with a L382X/D470X library

In order to demonstrate the efficiency of this novel assay as a preliminary and/or primary screening method for the screening of TK_{gst} libraries with nitrosoarenes, the assay scale was upgraded. For that, one plate from the original L382X/D470X library towards propanal[210] previously screened towards benzaldehyde by T. Saravanan,[6] was screened with the iron(III) method, and the results were compared to those obtained for benzaldehyde.

First, the cell lysates were prepared again from the glycerol stocks as described in the experimental part, and the corresponding lysate supernatant (20 µL) was added to the 96-well microtiter plates for the assay. Some preliminary tests were carried out where the lysate sample added and/or the incubation time of the reactions were varied. For **5b** and **5j**, the lysates were diluted 1:1 prior to use. For **5l**, the rate of the different variants was well differentiable already without diluting the lysates. Reactions with **5b** were incubated for 15 minutes at RT, and with **5l** and **5j** for 30 minutes. The experiments were performed in duplicates. The final colorimetric screening results of the chosen 96 candidates with the optimized conditions are shown in Figure 7.31. A, B and C respectively. In Figure 7.32, the normalized screening results, together with the results for benzaldehyde (**7**, D) screening with the pH assay, are displayed graphically for better comparison of relative activities. The raw data can be found in the experimental part (pages 228-221).

The purpose of the TK_{gst} L382X/D470X library was to target the aspartic acid residue at position 470 because it appeared to control the enantioselective binding of 2-hydroxyaldehydes by specific hydrogen bonding to the OH group. Also, the leucine at position 382, because it is located at the opposite side to D470 and was thought to probably contribute to substrate binding, served to complement the residue exchange consequences from D470.

When considering propanal for the protein engineering experiments, it was found that the replacement of D470 by isoleucine (I) or leucine (L) contributed to a non-polar lining of the substrate channel, which benefited the binding of the aliphatic aldehydes.[210] Expectedly, with benzaldehyde and the nitroso compounds, no active mutations contained either of the two nonpolar residues in the 470 position. Apparently, an exchange of the native negatively charged D470 with a polar but uncharged serine or threonine residue seemed to improve the productive binding of benzaldehyde and the nitroso compounds for the carboligation step. Indeed, some activity could be observed in wells H7 and E12 (both L/T) with benzaldehyde, although the L382 remains unchanged. For the nitroso compounds in general, very little activity was observed when leucine was present at position 382, *e.g.* for the wildtype (C10, (L/D)).

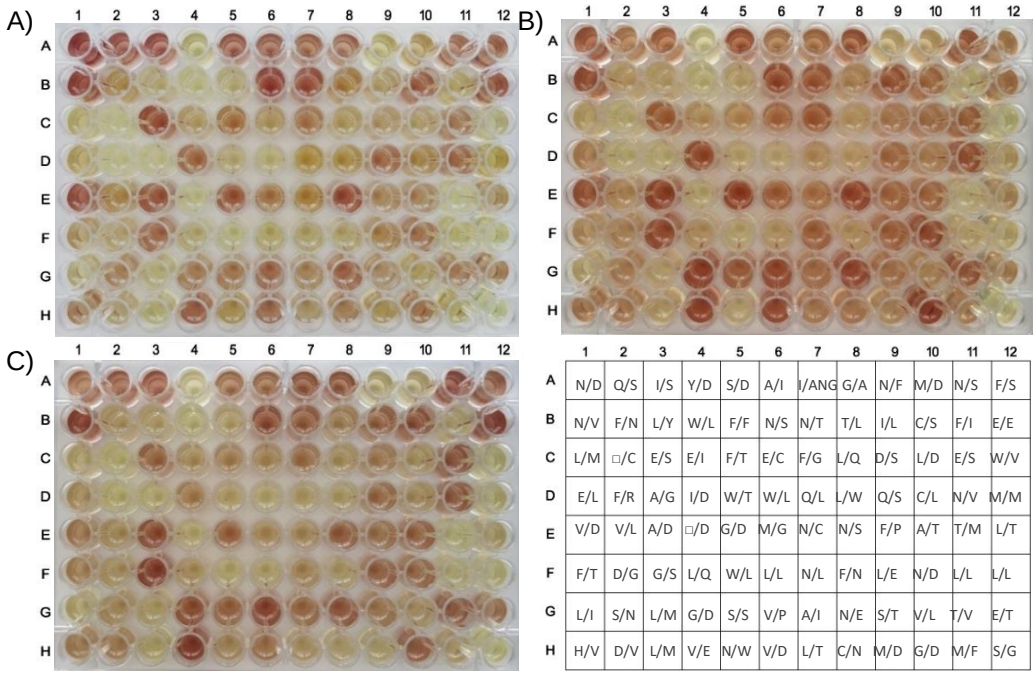

	1	2	3	4	5	6	7	8	9	10	11	12
A	N/D	Q/S	I/S	Y/D	S/D	A/I	I/ANG	G/A	N/F	M/D	N/S	F/S
B	N/V	F/N	L/Y	W/L	F/F	N/S	N/T	T/L	I/L	C/S	F/I	E/E
C	L/M	□/C	E/S	E/I	F/T	E/C	F/G	L/Q	D/S	L/D	E/S	W/V
D	E/L	F/R	A/G	I/D	W/T	W/L	Q/L	L/W	Q/S	C/L	N/V	M/M
E	V/D	V/L	A/D	□/D	G/D	M/G	N/C	N/S	F/P	A/T	T/M	L/T
F	F/T	D/G	G/S	L/Q	W/L	L/L	N/L	F/N	L/E	N/D	L/L	L/L
G	L/I	S/N	L/M	G/D	S/S	V/P	A/I	N/E	S/T	V/L	T/V	E/T
H	H/V	D/V	L/M	V/E	N/W	V/D	L/T	C/N	M/D	G/D	M/F	S/G

Figure 7.31. Color screening results with the three nitrosoarenes. A) **5b**; B) **5l**; C) **5j**. For A and C, the lysates were diluted 1:1 prior to use. Plate A was incubated for 15 minutes at RT, and plate B and C for 30 minutes. The experiments were performed in duplicates, yet only one plate for each set of experiments is shown. Corresponding mutations from the L382X/D470X library are shown in template in a one letter code fashion. □: Stop codon; ANG: A+overlapped peaks (ATGC)+G.

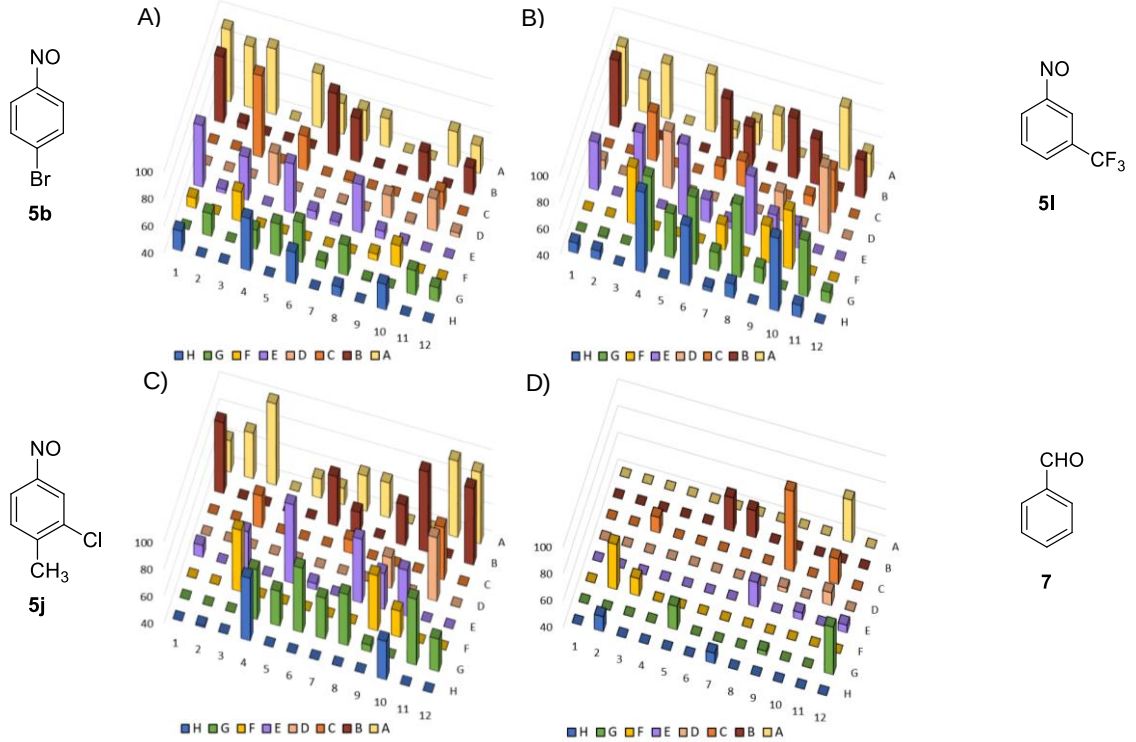

Figure 7.32. Absorbance screening results with the three nitrosoarenes and comparison to benzaldehyde (**7**) screening results with pH assay. A) **5b**; B) **5l**; C) **5j**; D) **7**. The experiments were performed in duplicates, being the average of absorbance values represented in the graphic.

Yet, when combining the L382 residue with a very well tolerated mutation such as glutamic acid (E), the activity increased compared to the wildtype (F9, (L/E)).Unexpectedly, all hits for benzaldehyde included an exchange of the hydrophobic L382 by a polar or even anionic residue, which by its location should be positioned in direct contact with the large hydrophobic aromatic system.[6] The most active candidate of the benzaldehyde screening (C9, (D/S)) contained the both best tolerated mutations, the D382 and the S470. All variants carrying the D382 mutation were active with benzaldehyde, including F2 (D/G) and H2 (D/V). Whereas, for none of the nitrosoarenes mutations at D382 seemed to be good. On the contrary, it appeared to be detrimental for the enzyme activity, as the variant in C9 (D/S), although containing a very well tolerated mutation (S470) showed very low activity with nitrosoarenes, and no other variant containing the D382 mutation was active. This finding was very interesting because when prolonging the polar chain by only one carbon (to glutamic acid), a rather active variant was generated (C3, C11 (E/S)). Moreover, all candidates carrying a serine or glutamic acid modification in the D470 position seemed to be favored also when combined with other mutations such as valine, serine or glutamic acid in the 382 position (H4, (V/E), (C3, C11 (E/S)), B12 (E/E), G6 (S/S). As mentioned above, an exchange of the native negatively charged D470 with a polar but uncharged serine or threonine residue seemed to be beneficial for enzyme activity, probably because these hydroxyl-containing residues can activate the aldehyde by allowing the protonation of the carbonyl- or nitroso-oxygen necessary when nucleophilic addition occurs. Moreover, it seems that the exchange of aspartic acid for glutamic acid in the D470 position yields very active variants although both residues are only differentiated by a methylene group. This could plausibly be because glutamic acid has a larger size and thus it may require a different orientation in the active-site pocket than aspartic acid, being able to potentially interact with both the oxygen and the nitrogen of the nitroso compounds and promote some kind of additional activation of the enzyme.

Considering the most active candidates with **7** and nitrosoarenes, an asparagine mutation in the L382 position appeared to be one of the best tolerated variations for TK_{gst}, and when combined with a well-tolerated serine, a very active candidate is produced (A11, B6, E8, (N/S)). The N/S mutation was the most active candidate for **7** when screening all the positive hit plates from the L382X/D470X library,[6] and was therefore chosen for the preparative scale synthesis and used as positive control. Here, only one plate containing positive hits was used for the screening.

Comparing the different substitution patterns of the nitrosoarenes, they can be differentiated into *para*-substituted (**5b**), *meta*-substituted (**5l**), and doubly *para*- and *meta*-substituted (**5j**). The substituents are in each case electronically different, however, the steric requirements are relatively similar. Noteworthy, although most of the active variants were consistently active with all of the nitrosoarenes, the relative activities were very different in some cases. For example, A1 (N/D) and E1 (V/D) were very active with *p*-Br (**5b**), quite active with *m*-CF_3 (**5l**), yet not very active with the combination *p*-Cl, *m*-CH_3 (**5j**). And the opposite was observed for B9 (I/L) and F9 (L/E), these variants being highly active with *p*-Cl, *m*-CH_3, still active with *m*-CF_3, but not (or barely) active with *p*-Br. In the absence of obvious direct binding interactions such as hydrogen bonds to substituents, these catalytic rate differences among the various nitrosoarenes could be due to differences in polarity, together with the electronic behavior of the different nitroso compounds.

In order to get an insight on the potential effect of the polarity of the different compounds in the TK activities, the partition coefficient (*P*) was used. *P* describes the ratio of concentrations of a substrate in a mixture of two immiscible solvents at equilibrium, assessing the propensity of a neutral compound to dissolve in an immiscible biphasic system of lipid (fats, oils, organic solvents) and water. Usually, one of the solvents is hydrophobic, such as 1-octanol, while the second is water. When the logarithm of *P* (log*P*) = 0, the compound is equally partitioned between the lipid and the aqueous phase; if log < 0, the compound has a higher affinity for the aqueous phase (it is more hydrophilic); and when log*P* > 0, a higher concentration of compound is in the lipid phase (it is is more lipophilic). Using ChemDraw software, log*P* for the different compounds was calculated, being 1.78 (98.37% in octanol and 1.63% in water) for **7** and 2 (99.01% in octanol and 0.99% in water) for **5a**. To prove the reliability of this computer-generated data, both compounds were compared in a TLC run in a mixture of CH/EA 4:1. Indeed, $R_{f(\text{benzaldehyde})}$ was 0.71 whereas $R_{f(\text{nitrosobenzene})}$ was 0.80, confirming that **7** is slightly more polar than **5a**, as indicated by the log*P*. By means of ChemDraw, Log*P* for **5l** and **5j** were also calculated, being 2.91 (99.88% in octanol and 0.12% in water) and 3.03 (99.91% in octanol and 0.09% in water) respectively, which was also coherent since both compounds are very apolar. To investigate the effect of the polarity more in depth, the log *P* of propanal was also calculated (0.08 (54.59% in octanol and 45.41% in water)). Since the library had been created and screened for this compound, it seemed appropriate to compare the polarity and behavior also for propanal. Because **7** is the less tolerated substrate and the most polar, and the nitroso compounds are highly non-polar in contrast to propanal, no clear relationship between polarity and enzyme activity could be extracted. Therefore, the catalytic rate differences between nitrosoarenes (**5**) and benzaldehyde (**7**) must be due to electronic and steric factors of the different nitroso compounds, yet also to the different interactions in the second step of the TK catalysis. Because **5a** and **7** are extremely similar, the only clear difference between them is the replacement of the carbonyl group for a nitroso group. This could give the opportunity to **5a** to form not only polar interactions through its oxygen, as with **7**, but also potentially through its nitrogen atom, what would rise the tolerance of TK towards nitrosoarenes in comparison to benzaldehyde. However, it is difficult to draw a conclusive argument without a more accurate library for either benzaldehyde (**7**) or nitrosoarenes (**5**).

Addressing the hypothesis previously presented, the positive hits plate showed many more active candidates with nitrosoarenes than with benzaldehyde, demonstrating that the nitrosoarenes are in general much better tolerated than benzaldehyde. Also, most of the active variants with nitrosoarenes were not the most active with benzaldehyde and *vice versa*. Unfortunately, this does not verify our hypothesis that benzaldehyde could be replaced by nitrosobenzene in screenings of large libraries of variants, as by choosing the most potent candidates from the nitrosoarenes screening, active candidates with benzaldehyde would be unnoticed. However, the direct comparison between nitrosobenzene and benzaldehyde is not available to date, and the TK_{gst} L382X/D470X library was created for the aliphatic propanal substrate, and not for the aromatic benzaldehyde. In order to have accurate results to accept or reject the presented hypothesis, new mutagenesis would have to be performed to construct

libraries where the targeted mutations would plausibly be different from the sites L382 and D470, and then investigate this further.

A good start could be considering the work performed with TK_{eco} for improved acceptance of benzaldehyde (**7**).[132] In that study, four promising variants were selected, D469E, D469K, D469T, and F434A, the latter giving the overall highest yield (10%). As **7** has few features that allow the enzyme to form interactions to enhance its specificity, it is poorly accepted, and therefore, its benzoic derivatives 3-FBA (**20**) and 4-FBA (**21**) were selected for further investigations.[133] The variant D469T reached a final yield of 65% within 2 hours, compared to the low 2% yield achieved after 17 hours with **7**. Interestingly, the variant F434A, which had shown the best result with benzaldehyde, did not accept either of its substituted analogues **20** and **21**, possibly due to steric hindrance. To investigate the influence of the interactions between the phosphate binding residues (R358, H461, and R520) and the carboxyl groups of **20** and **21** on the enhancement of the rates, mutations of these residues were made together with the D469T mutation which had shown the best results.[134] The variant D469T/R520Q was found to give the best results towards **20** and **21**. Thus, a triple variant library starting from the D469T/R520Q mutations was created with the S385X mutation, showing up to 13-fold greater activity than D469T towards aromatic aldehydes. H461 and R358 were excluded from further mutations because the former was found previously to lead to stability issues, and the latter forms charge-charge interactions with the substrate that seem important to retain.[133]

In view of these results, to investigate our hypothesis more accurately, new mutagenesis targets for TK_{gst} could be therefore a combination of the phosphate binding residues R521 and S385 with D470 mutations already created, which interact with the substrate *via* a mixture of charge–charge interactions and hydrogen bonds, similar to those found in the yeast TK structure complexed with E4P (Figure 7.33).[102]

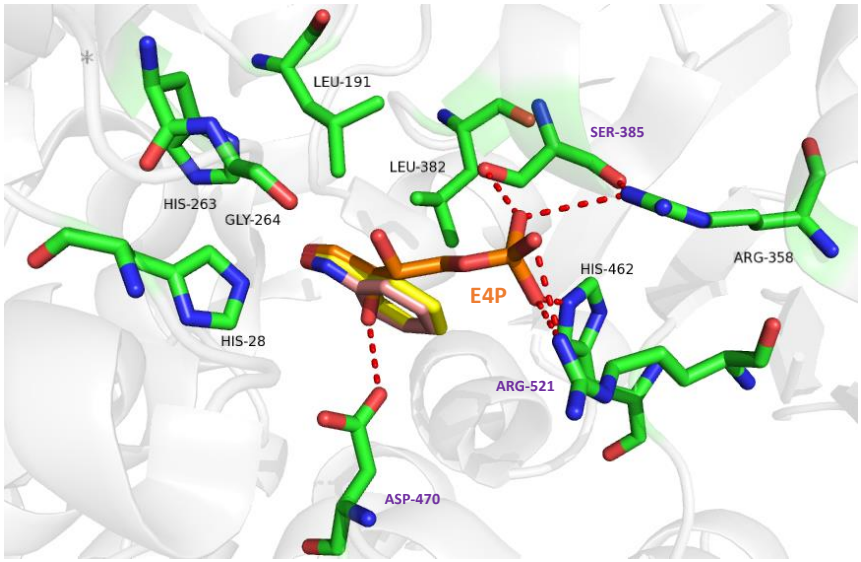

Figure 7.33. A) Model of the acceptor binding pocket employing the X-ray crystal structure of TK_{ban} (PDB entry 3M49) with substrate conformation of E4P from the TK_{yst} crystal structure (PDB entry 1NGS). The dotted red lines correspond to hydrogen bonds interactions. Benzaldehyde (**7**, yellow) and nitrosobenzene (**5a**, light pink) are superimposed over E4P (orange). Residue numbering corresponds to TK_{gst}, being R521, S385 and D470 colored purple. Image was generated with PyMOL.[214]

Nevertheless, the iron(III) colorimetric assays proved to offer consistent results. For instance, some variants were presented in duplicates or even triplicates in the plate. For example, the candidates N/S (A11, B6, E8), E/S (C3, C11), G/D (7, E4, H10), and N/V (B1, D11) were all active although the activity pattern was different among them. The plausible reason for this was because the bacteria containing the corresponding variants were cultivated and expressed separately in different wells, therefore the triplicates do not come from the same cultivation solutions. And the inactive variants L/L (F6, F11, F12), L/M (G3, H3) showed no activity in all corresponding wells. Also, to confirm the veracity of the results, plasmids of a few random candidates were extracted for sequencing, matching the sequences already analyzed by D. Yi.[210] Furthermore, the presence of similar amount of protein in each well was confirmed by quantitative analysis of the protein samples with the Bicinchoninic acid (BCA) method, being the average of the total soluble protein in the lysate around 1740 µg/mL. Additionally, 8 candidates among the active and inactive variants (A3: I/S; A11: N/S; B1: N/V; C1: L/M; C9: D/S; F2: D/G; H2: D/V; H7: L/T) were selected according the assay results, and compared with the purified TK_{gst} N/S variant (1 mg/mL) for SDS page gel quantification with ImageJ software. As gathered from the calculations in the presence and absence of lysozyme, around 84% of the lysate consisted of the desired TK, which was equal to ca. 95% of total protein after expression before lysis (in the absence of lysozyme). The photos of the BCA analysis and SDS gel, together with the images for SDS gel quantification are supplied in the Appendix (pages 226-227).

Additionally, to evaluate and demonstrate the suitability of the presented assay with the final conditions as a library screening method for high-throughput setup, the *Z*-factor of the colorimetric method with the three nitrosoarenes was calculated. For the assay with **5b**, Z=0.76; for **5l**, Z=0.88, and for **5j**, Z=0.82. In all cases, the *Z*-factor values were around 0.8, verifying that the ferric chloride assay has excellent suitability to be used in high-throughput format for the screening of TK_{gst} libraries with nitroso-containing compounds.

To further exemplify the applicability of the ferric chloride as semi-quantitative method, the standard curve can be used to extrapolate the concentration of the final product in the different reaction mixtures. The approximate concentration values of the **5b** assay were calculated by plotting the values in the standard curve with equation ***y= 0.6114x+0.1386*** (Table 7.1).

Table 7.1. Concentration values of **6b** produced in the iron(III) method with **5b**.

	1	2	3	4	5	6	7	8	9	10	11	12
A	0.814	0.755	0.779	0.245	0.711	0.579	0.577	0.566	0.251	0.392	0.603	0.561
B	0.781	0.436	0.219	0.146	0.204	0.757	0.652	0.406	0.305	0.569	0.223	0.556
C	0.347	0.200	0.893	0.346	0.598	0.328	0.417	0.290	0.351	0.336	0.504	0.251
D	0.387	0.147	0.163	0.583	0.203	0.148	0.409	0.362	0.531	0.415	0.586	0.427
E	0.756	0.426	0.649	0.103	0.685	0.451	0.426	0.679	0.448	0.417	0.115	0.395
F	0.461	0.272	0.572	0.194	0.121	0.188	0.226	0.197	0.440	0.526	0.217	0.191
G	0.344	0.532	0.194	0.513	0.586	0.632	0.446	0.575	0.410	0.277	0.543	0.482
H	0.517	0.373	0.238	0.702	0.396	0.583	0.360	0.458	0.354	0.549	0.288	0.067

The maximum concentration of product **6b** achieved by TK_{gst} (0.893 mM) was obtained by variant E/S in well C3. The very active variants offer HA yields between 0.5 and 1, which is in accordance with the visual color results from the standard curve. Because some variants

produce a yellow to orange byproduct that raises the absorbance values and therefore the apparent yield of the final HA, the combination of both the colorimetric screening and the absorbance measurements should help to discard non-red solutions and thus, avoid selecting inactive or weakly active variants.

7.3. Iron (III) assay for solid-phase

In vitro solid-phase supported assays performed on agar plates have found successful applications in the directed evolution of diverse enzymes, such as esterases,[279] oxidases[280-284], racemases,[285] and transaminases[286-288], with the aim of increasing the screening throughput by directly evaluating colonies that express gene variants of the enzymes of interest.[288]

While preparing this Ph.D. thesis, L. Hecquet and co-workers published the application of the pH-based assay principle to solid-phase supported assays for the screening of TK_{gst} libraries in directed evolution.[289] As previously mentioned, the TK-catalyzed reaction generates one equivalent of bicarbonate upon decarboxylation of the ketoacid donor, causing the pH to rise. Because the pH-assay is based on the detection of pH shifts, it is potentially less suitable to screen TK libraries towards volatile nitrosobenzene and related compounds. Hence, this methodology is not a reliable method for the purpose of this study.

However, a high-throughput solid-phase screening assay specifically designed for the screening of TK variants towards nitrosoarenes for the generation of valuable HA was unexplored to date. In this work, it was studied whether the ferric chloride assay strategy could be successfully applied to solid-phase screening assays in agar plates.

7.3.1. Iron (III) method development with TK_{gst} N/S and BL21(DE3)

To test the applicability of a ferric chloride-based solid-phase supported assay, a protocol was first developed with positive and negative controls used previously in the microtiter plate-based assay: *E. coli* BL21(DE3) cells containing the TK_{gst} N/S mutations as positive control and untransformed BL21(DE3) as negative control. The former cells were grown in LB plates supplemented with kanamycin (100 µg/mL) as antibiotic, whereas the latter were grown in LB plates containing no antibiotic, as the untransformed cells carry no antibiotic resistance inside. After growth of recombinant *E. coli* cells in agar plates until the colonies had reasonable and homogeneous size, the bacteria were first transferred to a nylon Hybond-*N*-membrane. Subsequently, the membrane was removed from the agar with the colonies stuck to it, and the proteins were then expressed by placing the membrane, colonies facing up, on an induction plate containing IPTG as inducer and kanamycin or no antibiotic for the untransformed BL21(DE3) colonies, as described in the experimental part.

In order to investigate the best assay conditions, the colonies were also grown directly over the Hybond-*N*-membrane placed on top of an LB agar plate supplemented with kanamycin (100 µg/mL) or no antibiotic for the negative control. However, the colonies turned out to be quite

smaller and requiring much longer growth time than when growing them first directly on the agar and then transferring them to the membrane. The original agar plate (master plate) from which the colonies had been removed was incubated again at 37 ºC usually for 5 h until the colonies had regrown again and thus could be easily sequenced or picked for further rounds of screening.

To favor the transport of the substrates and products in and out of the cells, cell permeabilization was done by immersing the membrane in liquid nitrogen for 5 to 10 seconds. Afterwards, filter paper was soaked in the reagent's solution containing the acceptor, the donor, the cofactors and TEA buffer, and the membrane was placed on top of the filter paper, with the colonies still facing up. For the negative controls without substrates, the membrane was placed on top of the filter paper soaked only in TEA buffer. Both membranes were incubated at 37 ºC for 30 minutes. After the incubation time, membranes were dipped into or sprayed with an aqueous ferric chloride solution. The colonies expressing variants of the gene of interest turned red upon contact with $FeCl_3$ and the signal-to-noise ratio allowed the differentiation of active *vs* inactive colonies. The general procedure for the ferric chloride solid-phase supported assay is depicted in Scheme 7.4.

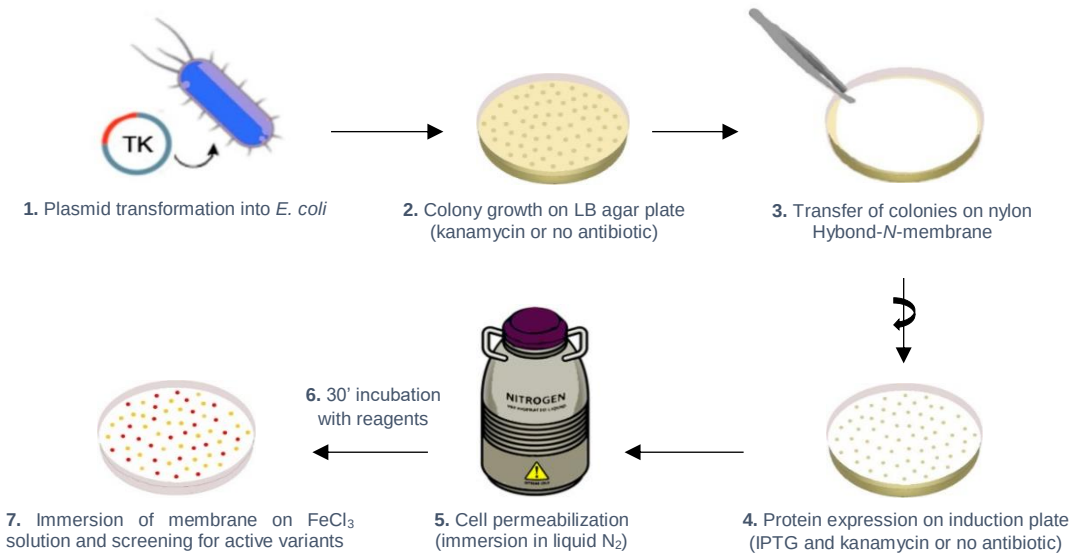

Scheme 7.4. General procedure of agar plate-based screening assay with iron (III). 1) *E. coli* BL21 (DE3) cells were transformed with plasmid coding TK_{gst} variants, or used untransformed as negative control. 2) Colonies were grown on LB agar plates (containing kanamycin for transformed BL21(DE3) cells and no antibiotic for untransformed cells) at 37 ºC for 16 to 18 h. 3) Transfer of the colonies onto a nylon Hybond-*N*-membrane. 4) Proteins were expressed by placing the membrane, colonies facing up, on an induction plate containing IPTG at 37 ºC for 5-6 h. 5) Cell permeabilization by membrane immersion in liquid nitrogen for 5-10 sec. 6) The membrane was placed on top of a filter paper soaked in the reagents solution and incubated at 37 ºC for 30 minutes. 7) The membrane was dipped into an aqueous $FeCl_3$ solution for differential display of active variants.

The conditions from the ferric chloride liquid-phase assay were transferred and further optimized to offer a rapid, reliable and sensitive solid-phase supported assay.

Nitrosobenzene solubility

At first, **5a** was employed as acceptor for the development and optimization of this solid-phase supported method instead of **5b**, because the former can be purchased commercially at a fairly low price, making it readily available with an acceptable purity (≥ 97%), and also because the solubility of **5a** in water is significantly better than that of **5b**. To further rise the solubility of **5a** in water, DMSO (20%) was used as co-solvent. 2,6-Dimethyl-β-cyclodextrin has been previously reported to dissolve nitrosobenzene in water without the aid of any co-solvent.[290] For that reason, hydroxypropyl-β-cyclodextrin (HP-β-CD) has also been tested during the optimization of the conditions for the same purpose. Direct dissolution of **5a** and HP-β-CD in deionized water, and ultra-sonication of the mixture at RT for 30 minutes, yielded a blue homogeneous solution similar to when solving the acceptor directly in DMSO. When mixing both **5a** solutions, with DMSO or with HP-β-CD, separately with the HPA-buffer solution, both mixtures remained clear green/blueish. DMSO was used as co-solvent for the reaction. However, if a rise in the solubility of other nitrosoarenes that are less soluble in the mixture DMSO/water would be required, HP-β-CD could be probably be useful as well.

At the beginning, similar conditions as in the optimized liquid-phase method were used: acceptor **5a** (10 mM), DMSO (20%), donor HPA (7.5 mM), and TEA buffer (5 mM, pH 7.45), so that the acceptor/donor ratio remained the same as in the liquid-phase assay (4/3). Since the bacterial colonies usually already contain the cofactors in some proportion, the addition of cofactors was avoided at first.

Iron (III) chloride optimal concentration

Furthermore, different concentrations of ferric chloride were evaluated (2 mM, 6 mM, and 12 mM, as in the liquid-phase assay) yet no colonies turned red upon contact with the low concentrations of ferric chloride (2 mM and 6 mM). When employing the higher concentration (12 mM), colonies acquired an orange color. Thus, it was obvious that a considerably higher concentration of iron (III) was required. For the assay final conditions, ferric chloride (252 mM) gave good results. Moreover, two different ways of applying the ferric chloride solution to the colonies were investigated, spraying the solution over the colonies, or dipping the membrane into the solution. For homogeneity reasons, the latter was chosen for the further development of the method (see Figure 7.36, B, left, in the "concentration of reagents" Section below).

Cell permeabilization

To explore if the cell permeabilization step was essential, two membranes were simultaneously treated in two different ways, without prior cell permeabilization and with cell permeabilization by means of liquid nitrogen treatment. Controls were performed in the absence of reagents (Figure 7.34).

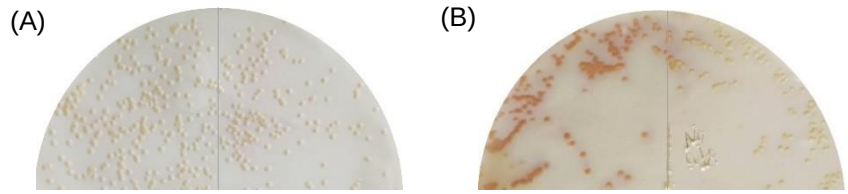

Figure 7.34. Membranes with *E. coli* colonies containing TK_{gst} N/S mutations after spraying with $FeCl_3$ (252 mM) solution in the presence of the reagents (left half of circumference) or their absence (right half). Conditions: commercial **5a** (10 mM), DMSO (20%), HPA (7.5 mM), TEA buffer (5 mM, pH 7.45), and $FeCl_3$ (252 mM). A) No cell permeabilization, B) cell permeabilization by immersing the membranes in liquid nitrogen.

The dividing line in both membranes A and B is not completely accurate as it was difficult to dip only a quarter of the membrane in the solution containing the reagents and the other quarter only in TEA buffer solution, so there was some diffusion and, therefore, the colonies close to the dividing line have a faint orange color similar to the dark orange color from the colonies in the left of the membrane. However, the colonies at the opposite side where there was absence of reagents are not colored. Hence, the cell permeabilization step proved to be crucial for the assay, since the avoidance of this step led to no color development (Figure 7.34, A).

Presence of cofactors

To investigate if added cofactors were necessary for the solid-phase supported assay albeit whole colonies were employed, experiments in the presence or absence of cofactors were performed (Figure 7.35). Although in the absence of cofactors some colonies turned light orange and, in some cases, a faint violet halo appeared, it is clear that the addition of enzyme cofactors is essential for the colorimetric assay.

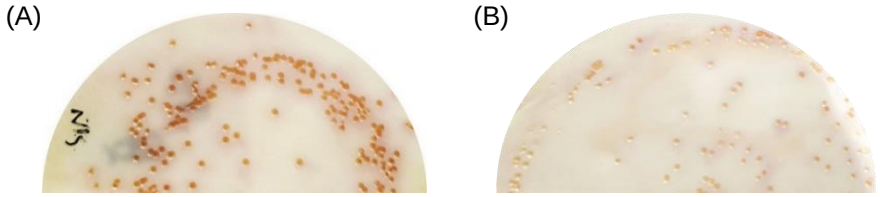

Figure 7.35. Membranes with *E. coli* colonies containing TK_{gst} N/S mutations after spraying with $FeCl_3$ (252 mM) solution. Conditions: A) **5a** (5 mM), DMSO (20%), HPA (5 mM), ThDP (0.2 mM), $MgCl_2$ (1 mM), TEA buffer (5 mM, pH 7.45); B) equal treatment of membrane yet in the absence of cofactors.

Concentration of reagents

The optimum concentration of the reagents was also examined for the colonies expressing the N/S variant and compared to the negative control untransformed BL21 (DE3) as depicted in Figure 7.36. Leaving all other parameters constant, the concentrations of acceptor and donor were first tested at 5 mM and 10 mM: Control experiments in the absence of substrates were also performed in parallel.

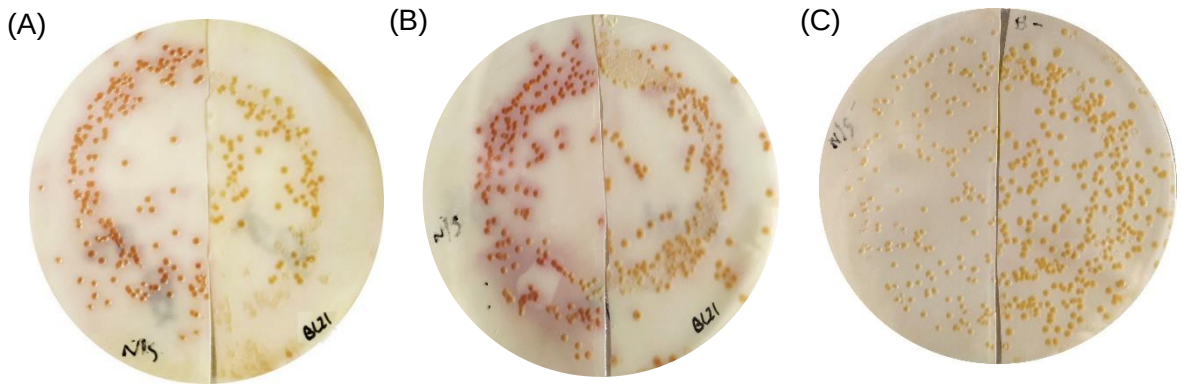

Figure 7.36. Membranes with *E. coli* colonies containing TK_{gst} N/S mutations (left half) or untransformed BL21(DE3) (right half) after spraying with $FeCl_3$ (252 mM) solution. Common conditions for A and B: ThDP (0.2 mM), $MgCl_2$ (1 mM), DMSO (20%), TEA buffer (5 mM, pH 7.45). A) **5a** (5 mM), HPA (5 mM); B) **5a** (10 mM), HPA (10 mM); C) Absence of substrates.

In the absence of substrates as negative control, no red color formation nor violet halo were observed neither for the colonies expressing the variant nor for the untransformed BL21 (DE3). For the untransformed BL21 (DE3), no red color development was observed even at higher concentrations of substrates. Whereas for the variant, the highest concentration proved to be better for the differentiation among active and non-active colonies, as the red color became more intense the higher the concentration. However, the red color was yet not very intense for a clear distinction between active colonies and inactive colonies in the same membrane, being that the goal of this assay. Also, it could be seen that the homogeneity of the color in the colonies when spraying the ferric chloride solution had to be improved (Figure 7.36, B, left). Thus, the membranes were rather dipped instead of sprayed for the next experiments.

To explore if an unambiguous color distinction among active and non-active colonies was possible, the concentration of the substrates was further raised in another set of experiments (Figure 7.37). The concentrations of the cofactors ThDP and $MgCl_2$ were raised to 0.6 mM and 2.5 mM respectively, and both concentrations of acceptor and donor were increased to 15 mM. In parallel, it was also investigated if dipping the membranes in the aqueous ferric chloride solution, instead of spraying it, would give complete homogeneity of the color among the colonies. Control experiments in the absence of substrates were also performed in parallel.

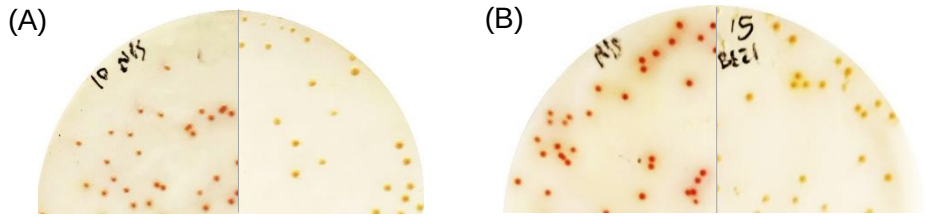

Figure 7.37. Membranes with *E. coli* colonies containing TK_{gst} N/S mutations (left half) or untransformed BL21(DE3) (right half) with A) 10 mM or B) 15 mM of both substrates, after dipping the membrane in aqueous $FeCl_3$ (252 mM) solution. Common conditions for A and B: ThDP (0.6 mM), $MgCl_2$ (2.5 mM), DMSO (20%), TEA buffer (5 mM, pH 7.45).

The highest concentration of substrates (15 mM) gave the best contrast between active and non-active colonies (Figure 7.37, B). Also, dipping the membrane in the aqueous ferric chloride solution proved the reproducibility of the assay and the homogeneity of the color among the colonies. Again, for the negative controls with BL21 (DE3) untransformed colonies no red color was developed even at the highest concentration (right half), and also not in the absence of substrates.

7.3.2. Iron (III) method implementation with TK_{gst} N/S and TK empty vector

Since the untransformed BL21 (DE3) has no antibiotic resistance, it cannot be grown together with the TK_{gst} variant on the same agar plate. Therefore, for the implementation of the assay on the same membrane, TK_{gst} N/S variant was used as the positive control and *E. coli* cells transformed with the corresponding empty plasmid not expressing TK_{gst} were utilized as the negative control, because they also contain kanamycin resistance (Figure 7.38). The experiments were performed in duplicates. Control experiments in the absence of substrates were also performed in parallel.

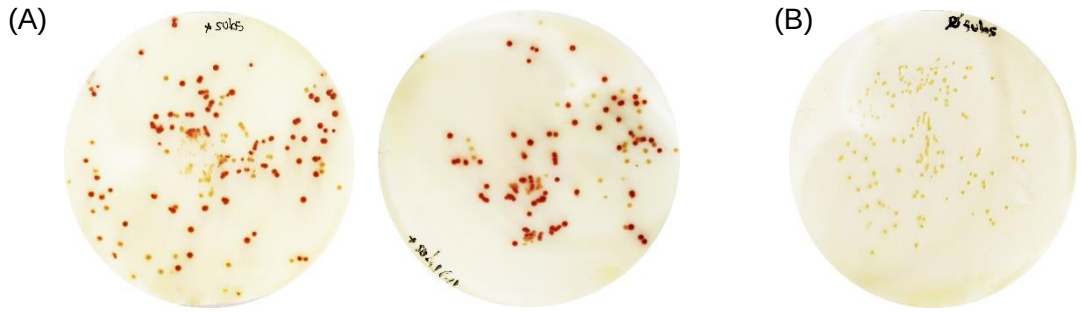

Figure 7.38. Membranes with *E. coli* colonies containing TK_{gst} N/S mutations and the empty vector in A) the presence or B) absence of substrates after dipping the membrane in aqueous $FeCl_3$ (252 mM) solution. Conditions for the reactions with substrates: **5a** (15 mM), DMSO (20%), HPA (15 mM), ThDP (0.6 mM), $MgCl_2$ (2.5 mM), TEA buffer (5 mM, pH 7.45). The experiments were performed in duplicates with similar result.

The conditions used were the ones optimized before, and no further optimization had to be made, as the difference between the colors among the various colonies was clearly visible with the naked eye. As expected, no red coloration was observed for *E. coli* cells transformed with empty plasmid acting as negative control, as well as in the absence of substrates. These tests were ideal to check the sensitivity and specificity of the solid-phase supported assay.

7.3.3. Iron (III) method application with a TK_{gst} L382X/D470X library

To demonstrate the efficiency of this assay as a preliminary screening and/or primary screening method for TK_{gst} variant libraries, the same plate containing the positive hits of the TK_{gst} L382X/D470X library produced previously by D. Yi.[210] (96 candidates), screened towards **7** by T. Saravanan,[6] and screened with the iron(III) liquid-phase assay, was also re-screened here with the new developed and optimized ferric chloride solid-phase supported assay. For that purpose, the 96-well microtiter plate containing the positive hits of the TK_{gst} L382X/D470X

library were picked with a sterilized replica plater from the corresponding glycerol stocks and transferred into a 96-well microtiter plate containing LB medium. The bacteria containing solutions were covered with an acetate foil and a small hole was drilled over each well for aeration, followed by incubation at 30 ºC for 16 to 18 h.

In order to prepare a mixed library from the selected plate containing the positive hits of the TK_{gst} L382X/D470X library to be able to analyze the mixture in the agar plate with the iron(III) assay and identify the unknown colonies containing the active variants, the different strains from the plate had to be combined. To do so, equal amounts of the bacteria containing solutions in each well were then mixed together. To find out the optimal colony growth in agar plates, various tests were performed until an acceptable and homogeneous growth of colonies on the agar plate was achieved. Considering the knowledge acquired from the former experiments, colonies were diluted $1/10^{-6}$ and three different volumes of the bacteria solutions were applied to the agar plates, 50, 75 and 100 µL. The latter gave the best results, enough to prove the application of the assay without yielding a too overfilled plate. No additional optimization of the assay conditions was made because the contrast between colonies was evidently visible with the naked eye (Figure 7.39).

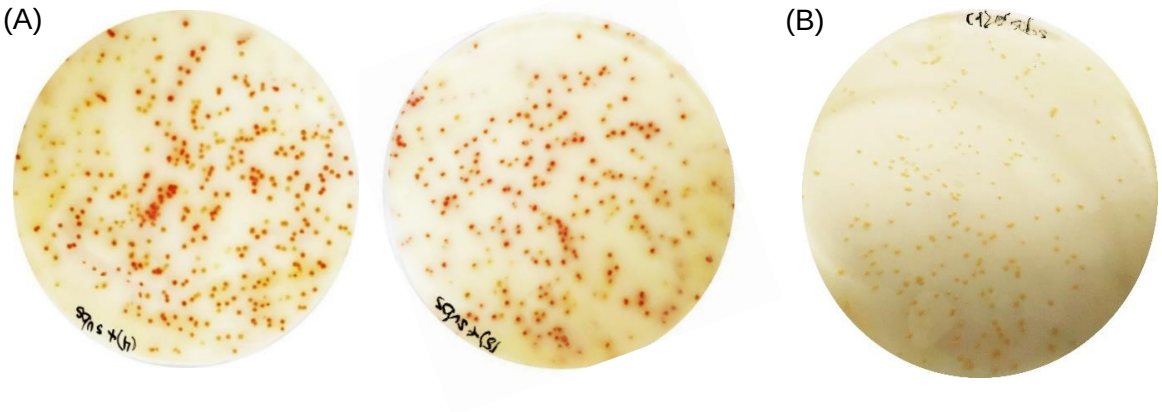

Figure 7.39. Membranes with *E. coli* colonies containing positive hits of the TK_{gst} L382X/D470X library in A) the presence or B) absence of substrates after dipping the membrane in aqueous $FeCl_3$ (252 mM) solution. Conditions for the reactions with substrates: **5a** (15 mM), DMSO (20%), HPA (15 mM), ThDP (0.6 mM), $MgCl_2$ (2.5 mM), TEA buffer (5 mM, pH 7.45). The experiments were performed in duplicates with similar result.

Because one of the plates containing only positive hits (96) from the TK_{gst} L382X/D470X library was screened, there is a considerably higher ratio of highly active (red-colored) colonies than when screening a whole original mutagenesis library of at least 4000 clones. However, the screening still resulted in diverse patterns of coloring as expected, ranging from dark red to yellow depending on how active were the colonies carrying specific mutations. The most active colonies could be easily discriminated as they turned very red upon contact with the ferric chloride solution, whereas the inactive colonies acquired only a faint yellow or orange coloration. These experiments were also carried out in the absence of substrates as negative control. As expected, no red coloration was observed for the colonies that had not been subjected to the presence of the substrates.

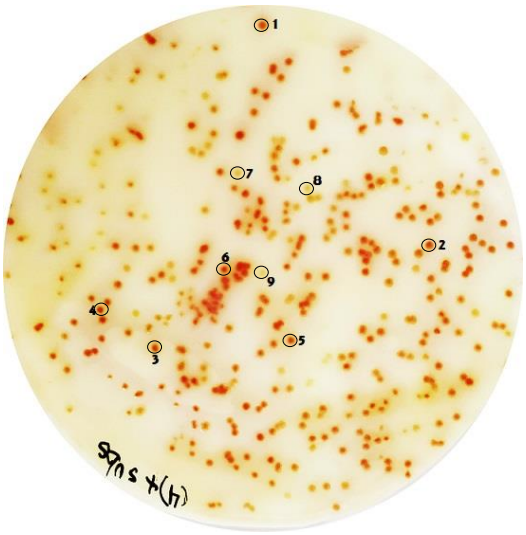

Figure 7.40. Membranes with *E. coli* colonies containing positive hits of the TK_{gst} L382X/D470X library after dipping the membrane in aqueous $FeCl_3$ (252 mM) solution. Picked colonies are numbered from 1 to 9 and circled in black.

To confirm the assay functionality, a range of colored colonies were picked from the master plate containing 472 colonies (from the first membrane in Figure 7.39). Red colored colonies were picked as proof of positive candidates (1-6), and yellow or orange colonies as negative or inactive variants (7-9) (Figure 7.40). The putative hits could be easily identified on the master plates by comparison with the membrane. It should be noted that due to the transfer of the colonies from the agar plate to the membrane and subsequent flipping of the same, the colonies will be positioned as a mirror image of the master agar plate. For the identification of the pick colonies, the samples were sequenced.

Although the nitrosoarene used for the solid-phase supported assay (nitrosobenzene **5a**), lacks a substitution in the benzene ring as compared to the nitrosoarenes employed for the liquid assay, the generated product, and thus, the TK_{gst} activity should be comparable. Indeed, the results obtained with the solid-phase supported assay were in line with those of the liquid-phase screenings. The positive hits had shown activity with the microplate assay with all of the substrates (1: S/D; 2: E/S; 3,4: Q/S; 5,6: N/S), while the negative ones did not have any detectable activity (7: S/G; 8: Y/D; 9: STOP codon/C). In Figure 7.41, the screening results of 1-bromo-4-nitrosobenzene (**5b**) are depicted again for better comparison between both screening methodologies, and the variants with the same sequence as the picked colonies from the membrane are marked, proving good consistency between the solid- and liquid- phase assays.

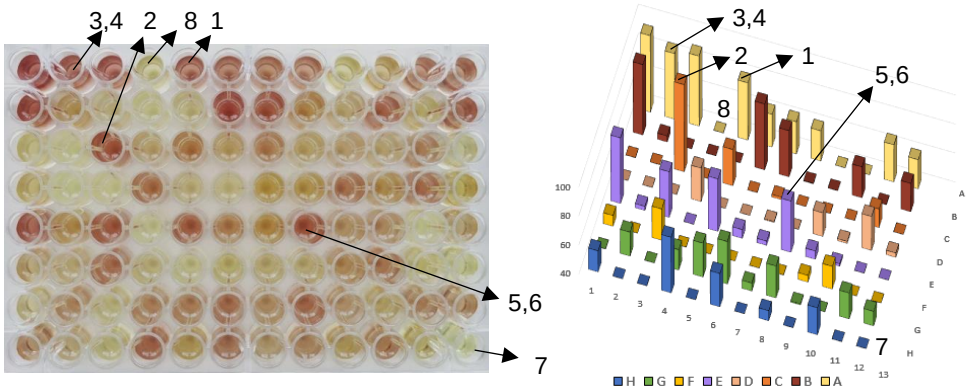

Figure 7.41. Results of screening of positive hits of the TK_{gst} L382X/D470X library towards **5b** with liquid-phase assay. Variants with equivalent sequence to the picked colonies are pointed with an arrow and numbered. 1: S/D; 2: E/S; 3,4: Q/S; 5,6: N/S; 7: S/G; 8: Y/D.

This colorimetric solid-phase supported assay has two drawbacks: (1) because the membranes were immersed in liquid nitrogen prior to screening, and they were also dipped in a concentrated ferric chloride aqueous solution, the colonies were no longer alive after the assay. This was even confirmed by trying to sequence some colored colonies straight from the screened membrane with no success, as the colonies did not re-grow at all. Therefore, colonies cannot be picked directly from the assayed membrane to confirm the method applicability. (2) Moreover, the color of the colonies vanished fairly fast and a purplish halo appeared around them which further spread to the membrane. This effect did not allow the identification of hits directly from the membrane within 5-10 minutes. This is presumably due to the chemical diffusion of the -ron(III)-HA complex out of the cells into the environment (Figure 7.42).

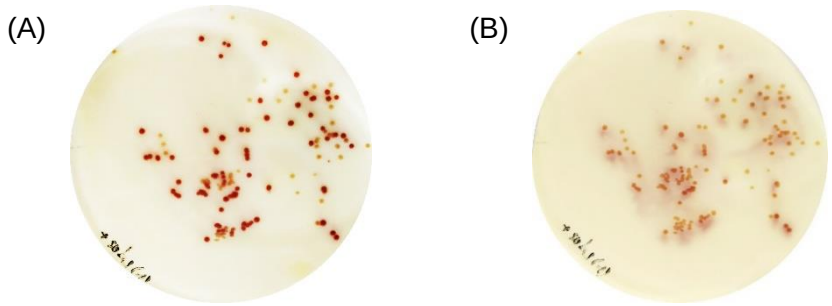

Figure 7.42. Membranes with *E. coli* colonies containing TK_{gst} N/S mutations and the empty vector A) immediately after dipping the membrane in aqueous $FeCl_3$ solution and B) after 20 minutes.

Nevertheless, these limitations can be solved by taking a high-quality picture of the colored membrane immediately after color development and then comparing it to the master plate as a mirror image exactly the same as if it was the membrane itself. The advantages of taking a picture of the membranes for screening is that the colonies do not have to be picked immediately, as the master plates can be stored at 4 ºC several weeks, and thus, many membranes can be assayed at the same time; and that the pictures can be modified with a computer program to show the mirror image of the membrane and this can be directly compared to the master plate very easily. Furthermore, by adjusting the contrast and brightness of the picture, the difference among the colonies can even be more noticeable in order to really pick only the strongest colored cells for further screening. In this thesis, the membranes were screened by utilizing the pictures presented giving good and reliable results.

Further optimization of the assay could be done to avoid the diffusion of materials from the cells. Maybe the membrane was still slightly wet before dipping it into the aqueous ferric chloride solution and thus, facilitate the diffusion of materials out of the cells. To prevent that, the membranes could be dried or shortly frozen with liquid nitrogen and thawed again prior to the last step, so that the only liquid remaining in the colonies is the ferric chloride solution, which excess could be removed from the membrane. In addition, other solvents could be used for the ferric chloride solution instead of water, as the latter is also soluble in some water miscible organic solvents, such as ethanol or methanol. Alternatively, other organic solvents could be tested. Also, instead of dipping the membrane in a ferric chloride solution, iron(III) could be added to an agar plate and the membrane could be momentarily placed on top of this plate to avoid excess of liquid when staining the colonies and thus, promotion of material

diffusion out of the colonies. Furthermore, the membrane could also be dried or frozen immediately after color development, which might help retaining the iron(III)-HA complex inside the colonies and therefore, their red coloration. If following any of these suggestions would not lead to a better retention of the iron(III)-HA complex inside the colonies, a reduction in the ferric chloride concentration used could also be explored. Being the concentration smaller, the iron(III) accumulation in inactive cells would be reduced and therefore, the orange background color would be reduced, giving an even lower background noise. Nevertheless, for the presented assay as it is, the background noise was still low enough to allow a good differentiation between active and inactive colonies. This allowed the avoidance of a dialysis step to remove unspecific background noise used in other solid-phase supported assays.[288-289]

The application of solid surface color assay to screen enzyme libraries prepared on agar plates serves to accelerate the search of potent candidates by incrementing the throughput compared to the microtiter plate-based method by at least one order of magnitude, which implies as well the decrease of the screening effort and cost. In fact, for example, if 1,000 colonies were to be screened from an agar plate after mutagenesis by means of these two assays, the requirements and the necessary time vary considerably (Scheme 7.5).

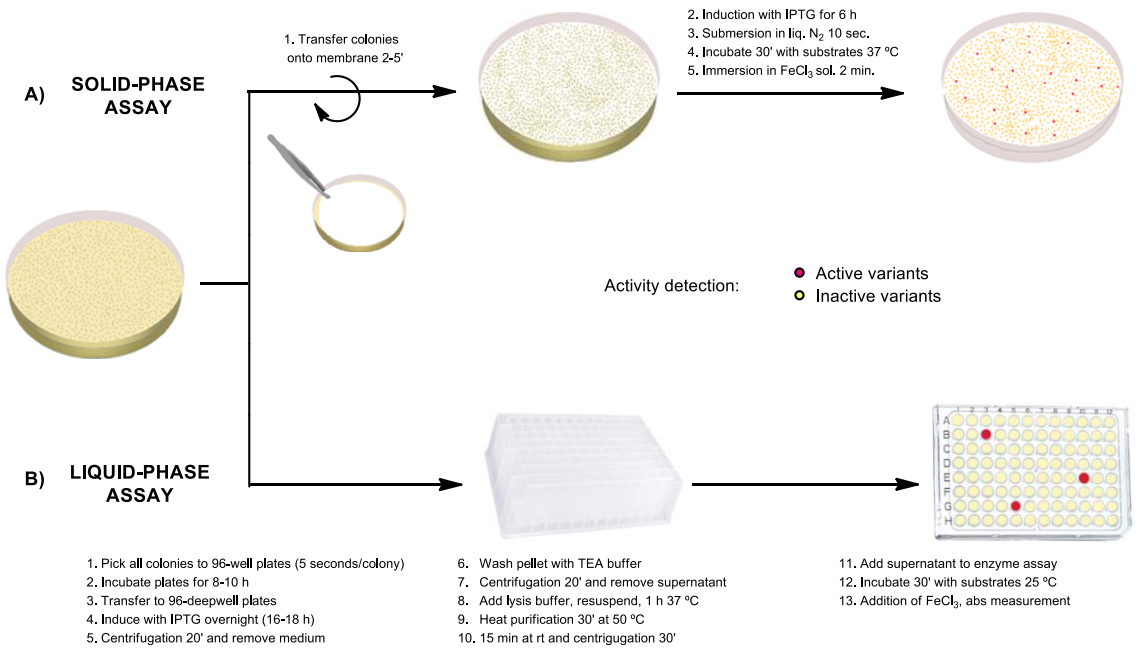

Scheme 7.5. Procedure steps for solid surface screening assay (A) *versus* liquid-phase assay (B) with iron (III) starting from the same agar plate after mutagenesis.

By utilizing the solid-phase supported assay the entire screening could be done within 1 hour, without considering the induction time (around 6 h), if using 2 membranes (500 colonies per membrane) in regular 100 mm petri dishes. Considering the time needed for the whole process with the solid-phase supported assay starting from the agar plate after mutagenesis: transfer of the colonies to the membranes (2-5 minutes per membrane depending on the size of the agar plate), together with the induction time (around 6 h for all membranes together), immersion in liquid nitrogen (10 seconds per membrane plus a buffer time (up to 1 minutes for both)), incubation with reagents (30 minutes for both membranes together), and immersion in a ferric

chloride solution (up to 2 minutes per membrane), 2 membranes in standard 100 mm petri dishes could be screened in ca. 6.6 h. As a general observation, up to 4 membranes could be certainly prepared and screened per researcher per hour. Therefore, in a normal working day (8 h) a minimum of 4 membranes containing 2,000 colonies (500 each) in standard 100 mm petri dishes (58 cm^2) could be screened per researcher with the solid surface assay.

When using the microtiter plate-based assay, the time needed for the screening of the same number of colonies (2,000) is significantly longer, as already for the process of manually picking every colony and transferring it to the microtiter plates, ca. 3 hours would be necessary (considering 5 seconds for each colony, and without taking necessary pauses into account). The microtiter plates must be then incubated with the LB medium and kanamycin for 8-10 hours, and then the pre-culture has to be transferred to 96-deepwell plates and induced with IPTG overnight (16-18 h). Then a series of centrifugation, washing with TEA buffer and supernatant removal steps are followed (ca. 1 h total) prior to lysis of the cells during 1 h at 37 ºC and heat purification of the thermostable TK_{gst} for 30 minutes at 50 ºC. Then, the cells should cool down for at least 15-20 minutes at RT, and subsequently, the plates need to be centrifuged for 30 minutes to make sure that the debris has precipitated completely. The supernatant can be now added to the enzymatic assay, and the reactions are incubated with the substrates for 30 minutes at RT. For screening 2,000 colonies, ca. 21 96-well plates would be needed. From experience, 4 microtiter plates can be handled at the same time. Thus, 12 hours of common steps (without considering the overnight incubation) should be multiplied by 6, and then at least 4 hours in total for reaction incubations, addition of the ferric chloride solution and absorbance measurements. Considering the time needed for the whole process with the liquid-phase assay starting from the agar plate after mutagenesis as in the calculations with the solid-phase supported assay, at least 79 h would be necessary to screen 2,000 colonies in 21 96-well plates. Considering that a regular working day consists of 8 h, 10 working days would be necessary to screen 2,000 colonies per researcher with the liquid-phase assay without the aid of a robot.

To conclude, to assay 2,000 colonies with the solid-phase supported assay 1 day would be enough, while for the liquid-phase assay to screen the same number of colonies without the aid of a robot at least 9 days would be necessary. If the number of the instantly screened colonies is increased, the throughput of the solid-phase supported assay relative to the liquid-phase assay considerably augments. Indeed, if 5,000 colonies were to be screened with both assays, with the solid-phase supported assay on commercially available round 150 mm petri dishes (145 cm^2), this could be done in also 1 day (8 hours) using 4 membranes (ca. 1,250 colonies each), as the time for each handling step does not rise significantly. Whereas for the liquid-phase assay, 52 96-well plates would have to be assayed in a minimum of 21 days (168 hours), which accounts already for a difference of 2 orders of magnitude. Moreover, for the solid-phase supported assay, square petri dishes up to 245 mm (500 cm^2) are commercially available, with which at least 8,620 colonies in 2 conventional membranes (ca. 4,310 each) could be screened in 8 hours (1 working day). If this would be done with the liquid-phase assay, 90 plates in a minimum of 37 days would have to be screened. Therefore, the higher number of the colonies to be screened, the bigger the difference in orders of magnitude between the solid- and the liquid-phase assay, and also the reduced screening effort from the solid compared to the liquid assay.

Furthermore, this solid-phase supported assay is more economic since the working time is drastically reduced, decreasing significantly the expenses related to employee salary, easy to handle and to screen. In addition, the solid surface assay is much more environmentally friendly than the liquid-phase assay. For instance, considering an estimation of ecological factors, the liquid-phase consumes a significantly higher amount of plastic than the solid-phase surface assay (Table 7.2).

Table 7.2. Comparison between plastic consumed in both liquid-phase and the solid-phase surface assays.

2,000 colonies	Liquid-phase	Solid-phase
Disposable tips (total)	18.144	
10 µL tips	2016	
200 µL tips	12096	
1 mL tips	4.032	
96-well microtiter plates	21	
Acetate foils	84	
100 mm Petri dishes		4
Nylon membranes 10x10cm		4
Total plastic (kg)	11	0.67

In view of the presented calculations, the solid surface assay is around 2 order of magnitude more ecologically friendly as the liquid-phase assay. Indeed, if 5,000 colonies were to be screened, only 4 150 mm petri dishes (145 cm^2) and 4 nylon membranes 20x20cm would be employed, accounting for approximately 0.71 kg of plastic; while the amount of plastic consumed in the liquid-phase assay rises exponentially. The plastic material could be recycled and then less material would be needed, yet that would augment also working time, energy efficiency, costs and pollution for the environment.

The ferric chloride colorimetric assay principle applied to agar plates allows the *in situ* detection of active TK_{gst} variants with the naked eye from a large enzyme library, removing intermediate steps from the liquid-phase method such as colony picking, growth of bacterial populations, lysis, removal of cell debris, and enzyme extraction. Thus, the screening effort in directed evolution is drastically reduced, and the throughput of the assay is acutely increased as only active colonies are picked for further screening. This is noteworthy because in a normal situation after mutagenesis only 2-5% of total variants are active. After a first or even second round of screening with the solid-phase supported assay, further screening with the liquid-phase assay in order to differentiate catalytic rates would be optimal. The ideal screening method would be the combination of these two newly developed assay types.

8. Summary and outlook

In this chapter, a novel colorimetric endpoint assay for the screening of TK_{gst} variants against nitrosoarene substrates has been developed to be applicable in high-throughput fashion. This method is based on the ability of HA products to chelate metals such as iron(III). By determining the HA product generated during enzymatic catalysis, a qualitative or even semi-quantitative assessment of enzyme activity can be performed. In Scheme 8.1 the steps of the discontinuous iron(III) assay are shown.

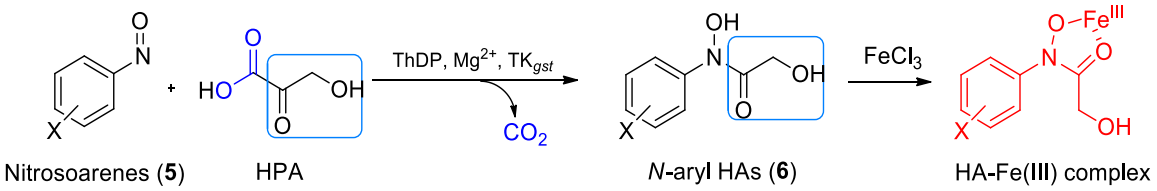

Scheme 8.1. Principle of the discontinuous iron(III) assay for TK relative activity evaluation with nitrosoarenes with subsequent *in situ* formation of iron(III)-HA complex for assay validation.

Firstly, the TK_{gst} catalysis with **5** as acceptor substrates and HPA as donor substrate, in the presence of ThDP and Mg^{2+} takes place. Then, ferric chloride is added *in situ* to generate the corresponding iron(III)-HA complex. This chelate acquires a 3:1 structure at low pH, producing a red-purple color which is not only visible by the naked eye but also measurable at 500 nm with a plate reader. This assay was first developed, optimized and successfully applied in liquid-phase, and one plate with positive hits from the TK_{gst} L382X/D470X library[210] was screened to prove its broad applicability. Secondly, the strategy was transferred to solid-phase to allow directly recognizing with the naked eye those colonies that express active TK_{gst} variants against a variety of nitrosoarenes. A schematic comparison between both liquid assays and solid-phase supported assays is depicted in Figure 8.1.

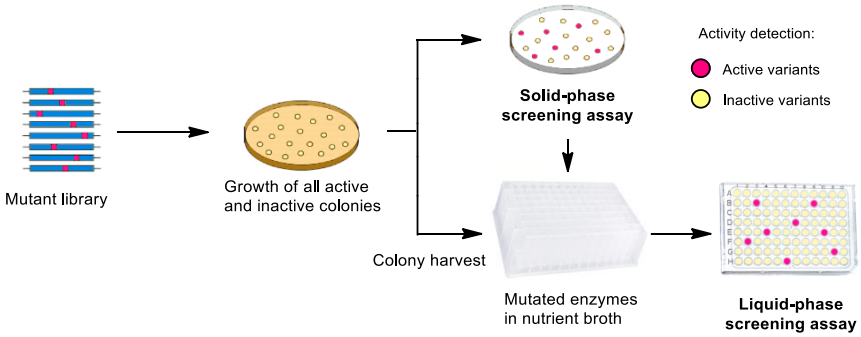

Figure 8.1. General representation of the iron(III) colorimetric assay on solid surface *vs* in liquid-phase starting from the same agar plate after mutagenesis.

The results obtained with both assay formats were consistent. These sensitive screening methods should be suitable for estimating the substrate tolerance of TKs from different sources with a wide collection of nitroso-containing compounds. Because these colorimetric screening methods are uncomplicated, they should also prove relevant for the reliable screening of broad TK libraries indispensable in the directed evolution of novel enzymes.

Chapter III

N-Aryl Hydroxamates as Potential Anti-Cancer Molecules

9. Theoretical background

9.1. What is cancer?

In order to understand how anticancer molecules act, *i.e.* how the treatment of tumors takes place and how such a treatment can be optimized, it is appropriate to clarify how cancer develops in the first place.

Cancer is a genetic disease that can appear almost anywhere in the human body, which is composed of billions of cell types. In a normal case scenario, these cells have the ability to divide when old or when defective cells need to be replaced. This process usually takes place in a controlled manner, where the information is copied from one cell to the newly formed one. During this process errors can occur, generating mutations in the cell's DNA. The new mutated cell contains different information about its function and division as the healthy cell, and thus, they can keep dividing and multiplying producing an overexpression of cells. The immune system cannot differentiate between the normal and abnormal cells, and therefore, the mutated cells remain in the body forming an excessive amount of tissue (Figure 9.1.). This produces the so-called tumors, which can be divided into malignant or benign tumors. The first type, the cancerous tumors, can invade nearby tissues and spread *via* the blood vessels (metastasize), being able in this way to form new tumors in other parts of the body and possibly destroy various organs. The second type, the benign tumors, grow more slowly and do not spread throughout the body, so that other areas of the body remain unaffected and metastasis is excluded. When removed, benign tumors unlikely re-grow again. Moreover, cancer cells have the ability to camouflage themselves by adopting the characteristics and properties of healthy cells and are therefore indistinguishable. These special properties make it particularly difficult to identify and treat tumors at an early stage. In addition, mutated cancer cells do not have a normal aging process and cell death is postponed indefinitely. The main cause of death from cancer is the attack on healthy organs, so that a functional disorder occurs and the corresponding organs can no longer carry out their original life-sustaining function.[291-292]

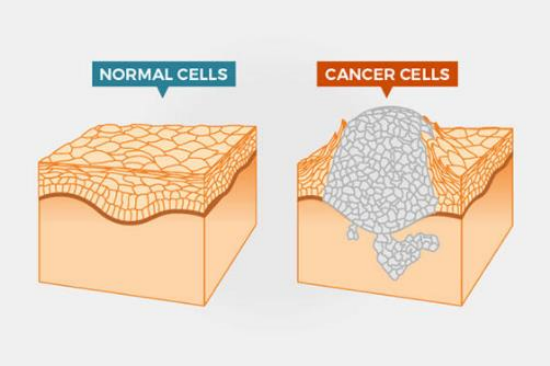

Figure 9.1. Healthy (left) vs cancerous (right) cells. The latter divide uncontrollably and spread into surrounding tissues. Extracted from literature [290]

Although several anti-cancer therapies are known up to date, the interest in this work relies on the inhibition of zinc-dependent enzymes as antitumor therapy.

9.2. Zinc-dependent enzymes

Following iron, zinc is the second most abundant trace metal found in the human body. It is involved in a broad range of functions that are essential to humans for both physical and mental health. This is due to its crucial role for the catalytic function and structural stability of more

than 300 diverse enzymes, and thus, it is essential to all forms of life.[293] Usually, zinc is an essential cofactor for the biological function of these enzymes. In zinc-requiring proteins, the zinc ion can have an either catalytic, co-catalytic or structural role. In the first one, the zinc ion directly engages in the bond-making or bond-breaking step. In a co-catalytic zinc site, there are other metal ions bound in proximity to one another, one playing a catalytic role and the other metal ions boost the catalytic activity of the site. When playing a structural role, the zinc ion mainly stabilizes the tertiary structure of a protein in an analogous manner to the disulfide bonds. Independently from its role, removal of the bound zinc from its site can lead to a loss of enzymatic activity.[294]

A unique characteristic of the catalytic zinc site is that the zinc-binding structure has at least one water molecule which is key for the catalytic site because it can be polarized by a general base, ionized to zinc-bound hydroxide, or displaced by the substrate. In particular, catalytic zinc sites supply accessible targets for drugs due to the ability of a wide range of functional groups (*e.g.*, hydroxamates or sulfonamides) to coordinate directly to the metal ion, displacing the zinc-water in the active site and inhibiting the enzyme.[294] Among the many enzymes that use zinc with a catalytic role, histone deacetylases (HDACs) are very relevant for current anti-cancer therapies.

Histone deacetylases (HDACs)

HDACs are zinc-containing enzymes that catalyze the removal of acetyl groups from acetylated lysine residues in the *N*-terminal extreme of histone proteins. There are approximately 20 human HDACs, which can be classified in four classes: class I, II and class IV are zinc-dependent metalloenzymes, while class III are NAD^+-dependent enzymes.[295] The overexpression of HDACs is closely connected to a large variety of cancers, inflammatory diseases, metabolic disorders and neurological diseases. Whereas the inhibition of HDAC activity induces histone hyperacetylation and reactivation of suppressed genes, it also hinders angiogenesis, and consequently combats tumor cell survival and proliferation leading to cell growth arrest and apoptosis (programmed cell death).[296-297]

As a result, the development of HDAC inhibitors (HDACi) has become a promising therapeutic strategy to combat these diseases and more in particular, cancer.[156, 298]

Inhibitors of histone deacetylases (HDACi)

HDACi are able to chelate the zinc ion located in the catalytic pocket of the HDAC, inhibiting in this way the deacetylation processes. This leads to an accumulation of hyperacetylated histones and transcription factors, and consequently to tumor cell death.[299]

Looking at X-ray crystallographic and structure-activity relationship (SAR) studies of numerous HDACi, it was proposed that the HDACi pharmacophore comprises of three main parts: (1) a strong metal-binding domain, which resides in the protein interior and complexes with the catalytic metal ion; (2) a long aliphatic or aromatic chain, which operates as a carbon linker; and (3) a capping group, which is solvent-exposed and interacts with the amino acids

close to the entrance of the active site.[199, 295] For instance, trichostatin A (TSA), a natural HA produced by the organism *Streptomyces hygroscopicus* that possesses anti-fungal, antibiotic and anti-tumor activity, and is a very powerful HDACi, bears all these parts. According to X-ray crystallographic studies of the TSA inhibitor bound to a histone deacetylase homologue (histone deacetylase-like protein, HDLP) from *Aquifex aeolicus*, the Zn^{2+} cation is coordinated by Asp 168, Asp 258, His 170 and by the hydroxamic acid in a chelating manner.[300] The observation of the bidentate chelate formation between the inhibitor and the Zn^{2+} ion is in agreement with inhibition studies with HA from other zinc-dependent enzymes, such class II aldolases.[301] Moreover, TSA forms hydrogen bonds with His 131 and His 132 with its two available protons.[300] An approximate representation of a general HA pharmacophore HDLP is shown in Figure 9.2.

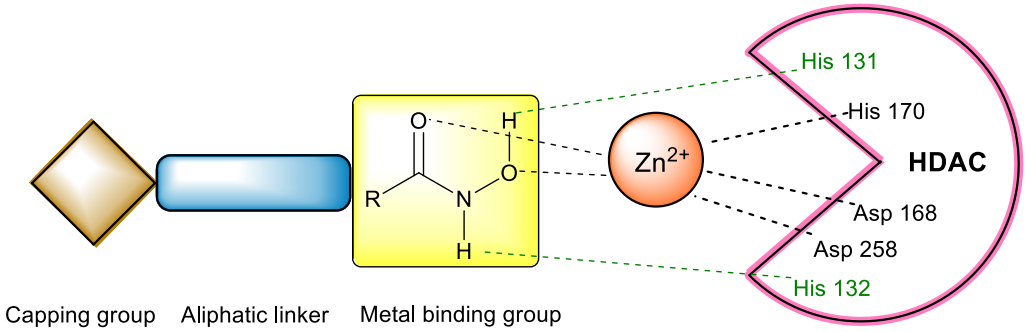

Figure 9.2. Interaction of a general HA pharmacophore with a HDAC homologue (HDLP).

Following this premise, many compounds have been developed for the treatment of various types of cancer. Among them, a large variety of HAs are included.[302] TSA has been used as a model to design powerful synthetic analogues, such as suberoylanilide hydroxamic acid (SAHA), also known as *Vorinostat*. A structure comparison between TSA and SAHA is shown in Scheme 9.1.

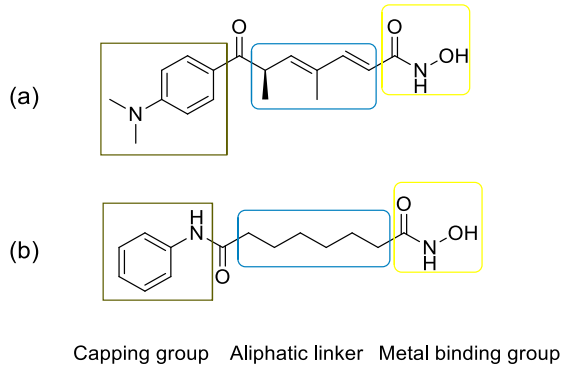

Scheme 9.1. Structure of natural HA TSA (a) and synthetic HA SAHA (*Vorinostat*) (b). The parts comprising an HDACi pharmacophore are highlighted.

Vorinostat was the first member of the HA class to enter into human clinical trials and was approved in 2006 by the U. S. Food and Drug Administration (FDA). This pharmaceutical was the first HDACi to reach the market and is currently marketed by Merck under the name Zolinza® for the treatment of cutaneous T-cell lymphomas (CTCL).[303-305] Further studies have been performed with *Vorinostat* for the treatment of other cancer types; it has shown encouraging results for the treatment of breast cancer, cervical cancer, and lung cancer.[299, 306]

Considering the versatility and potency of the synthetic drug *Vorinostat*, other HAs with a similar pharmacophore were developed and are currently in clinical trials. In those molecules the carbon linker does not consist exclusively of an aliphatic chain but also includes an aromatic moiety. Some of these compounds are: *Belinostat*, *Abexinostat*, *Pracinostat*, *Reminostat*, *Givinostat*, and *Panobinostat* (Scheme 9.2).

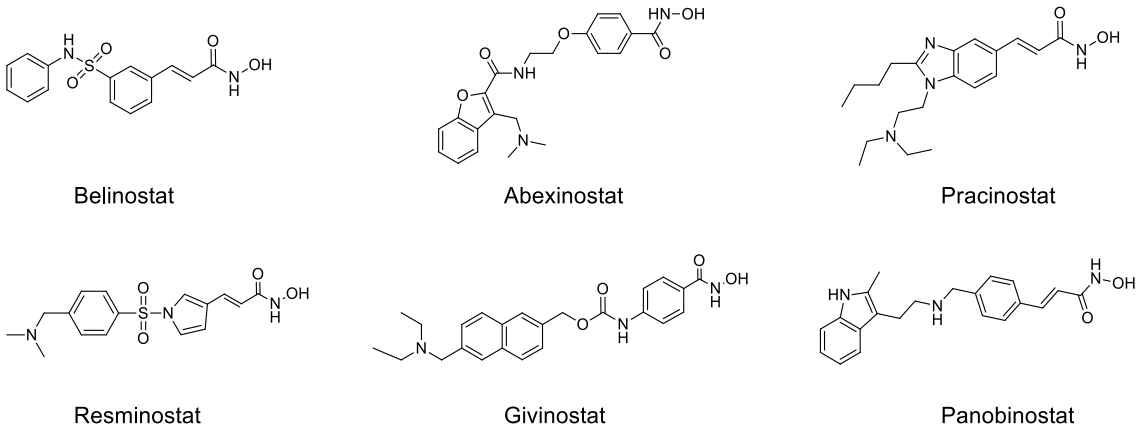

Scheme 9.2. Structure of various hydroxamate-based HDACi.

The HDACi mentioned, except for *Abexinostat*, have shown *in vitro* potency at micromolar concentrations only and are still in clinical trials. Howlever, *Abexinostat* has been shown to have activity at nanomolar concentrations against a broad collection of cancers, including hematopoietic cancers, or bone and soft-tissue sarcomas.[307] Besides the strong anti-tumor effect of *Abexinostat* when administered alone, combination of this drug with other compounds, such as bortezomib,[308] with conventional chemotherapy agents,[309] or even with radiotherapy,[310] extends the application of this versatile pharmaceutical. In July 2019, *Abexinostat* received fast-track designation by the FDA for the treatment of relapsed or refractory follicular lymphoma.[311] Because it bears its hydroxamate functionality directly attached to the aromatic ring, it serves as a good structural target related to the enzymatically synthesized *N*-aryl HA compounds presented in this doctoral thesis (Scheme 9.3).

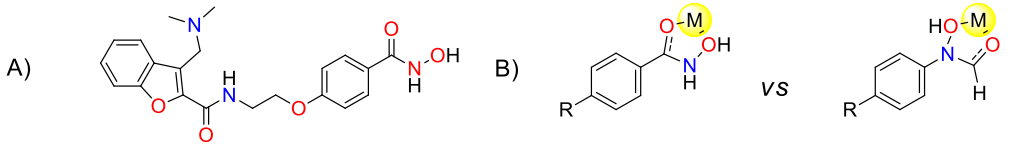

Scheme 9.3. Structure of arylated hydroxamate-based *Abexinostat* (A), and comparison of metal chelating structure of *C*-aryl vs *N*-aryl hydroxamates (B).

Interestingly, it appears that retro-HA with an inverse constitution (**3**) are much less common and seem to not have been studied yet for biomedical applications. This could be due to the speculation that the genotoxicity of nitrosoarenes and their potential for cancer generation are linked to their metabolic conversion by TK,[224, 312] rat liver preparations[313] or heart mitochondria.[231]

10. Results and discussion

10.1. Synthesis of *N*-hydroxy-4-(4-phenylbutyrylamino)benzamide

The biological properties of HA are closely associated to their capacity to chelate metals, such as iron(III) and zinc(II) among others. Because retro-HA have a similar structure and metal binding ability, it is coherent to hypothesize that they should also offer comparable biological properties. In order to investigate this premise, various HA were synthesized and tested for inhibitory activity towards HDAC.

N-Hydroxy-4-(4-phenylbutyrylamino)benzamide (HTPB) is a hydroxamate-tethered phenylbutyrate derivative that was created relatively recently.[10] HTPB has been patented for its capacity to inhibit HDAC activity with sub-micromolar potency for the treatment of diverse types of tumors, including prostate-, or lung cancer, and leukemia.[206] After comparing molecular docking studies of HTPB and TSA, Lu *et al.*[314] reasoned that the high potency for both HDACi was attributable to the three constitutional features already discussed above: the hydroxamate group, the cap group, and the linker. The hydroxamate builds a salt bridge with the zinc cation, being this the driving force for ligand binding, whereas the cap group and linker anchor the ligand inside the pocket through hydrophobic and/or π-π stacking interactions. Importantly, these crucial structural features are also present in the proposed retro-HA, supporting the feasibility of the presented conjecture.

Due to its relatively uncomplicated structure, reasonably straightforward synthesis and biological feasibility, HTPB is an excellent molecule to study this hypothesis empirically. Accordingly, structurally akin *N*-aryl HA with inverse constitution were designed and synthesized. In addition, HTPB was synthesized and used as reference for *in vitro* HDAC inhibition tests to investigate the relative inhibitory activity of reverse HA. A comparison between the structure of the HTPB drug and that of the analogous retro-HAs is presented in Figure 10.1.

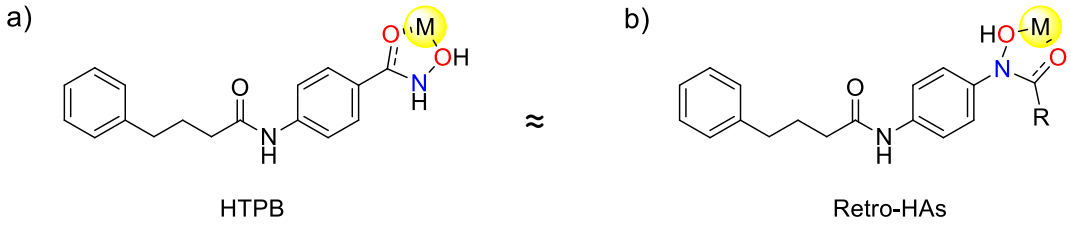

Figure 10.1. Structural comparison between HTPB and the retro-HA. R= H, CH_3, CH_2OH. Although these reverse HA have an inverse constitution, the metal binding capacity remains the same.

The synthesis of HTPB was conducted following a protocol reported by Shieh *et al*,[315] shown in Scheme 10.1.

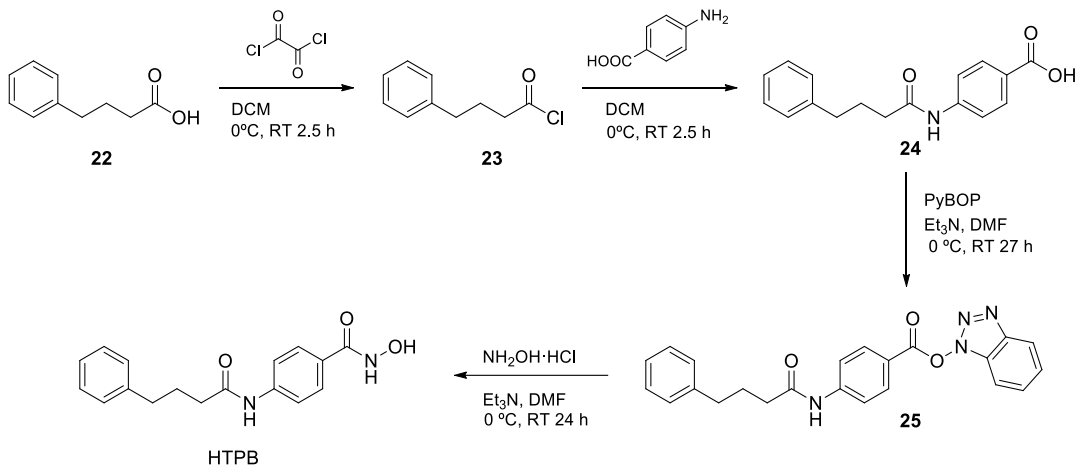

Scheme 10.1. Synthesis of HTPB.

Carboxylic amides are generally generated from activated carboxylic acid derivatives and amines through a nucleophilic acyl substitution reaction. The most common way to activate carboxylic acids is to convert them to acid chlorides. The chlorination of carboxylic acids can be achieved by means of several chlorinating reagents, such as oxalyl chloride, phthaloyl dichloride, and thionyl chloride.[316] The amidation of the carboxylic acid (**22**) into the acyl chloride (**23**) was performed by using oxalyl chloride in order to mimic the literature synthesis route.

The acid chloride (**23**) was obtained with a very high yield of 92% and used without purification. The second step, which constituted the coupling of the acyl chloride with the amine, led to the carboxylic acid (**24**) with a 63% isolated yield. Distinct to the literature protocol, a white solid precipitated after overnight incubation of the reaction at RT, which was filtered from the reaction mixture and separated. The liquid phase was quenched with water and extracted with DCM as in the literature protocol. Both isolated fractions were combined and stirred 15 min with 1 N HCl to remove triethylamine (Et_3N) traces. Also discordant with the literature, no column chromatography was necessary to remove impurities from the product since the NMR spectrum confirmed a very high purity of the compound.

The last two steps comprised of the activation of the carboxylic acid with the coupling reagent benzotriazol-1-yloxytripyrrolidinophosphonium hexafluorophosphate (PyBOP), and a standard amide coupling to yield HTPB. Since the reaction scale had been considerably augmented with respect to the literature protocol, 2 equivalents of Et_3N were used instead of 1.2, and the reaction mixture was left to stir 24 hours with PyBOP. Because by TLC analysis the educt spot was still visible, more Et_3N (0.8 eq.) and PyBOP (0.1 eq.) were added to the mixture. Considering that no more **24** was converted to product after 3 hours, the reaction was cooled to 0 ºC and hydroxylamine hydrochloride was added to the intermediate **25**. Different from the literature protocol, after 2.5 h of incubation at RT, a white solid precipitated, which was filtered off and washed with water. The reaction was quenched with water, and both solid and liquid phase

were treated separately. First, the solid was purified by column chromatography in a mixture of DCM/MeOH 10:1, giving a pink solid with a 21% isolated yield. Then, the liquid-phase was extracted with ethyl acetate, dried, and likewise purified by column chromatography in a mixture of DCM/MeOH 9:1. The product was obtained as a pink solid also with a 21% yield. Thus, HTPB was isolated with a total moderate yield of 42%. The loss of yield compared to the literature (87%) could be due to an incomplete conversion in the third step, and also because the crude mixture of step 4 in both the solid- and liquid-phases had appreciable solubility issues occurring during the extraction process.

The identity of the HTPB for both fractions was confirmed by NMR and HPLC. Although no impurity signals were observed, to remove the colored contamination for the cell viability tests, activated charcoal was added to the pink HTPB (54 mg), stirred at 40 ºC for 15 min, and filtered. A colorless powder (31 mg) was obtained with a moderate purification yield of 58%.

10.2. Design and synthesis of the *N*-aryl retro-HA analogues

To synthesize the desired retro-HAs, a retrosynthetic analysis of the molecule was first considered. For that, the target molecule is fragmented (Scheme 10.2).

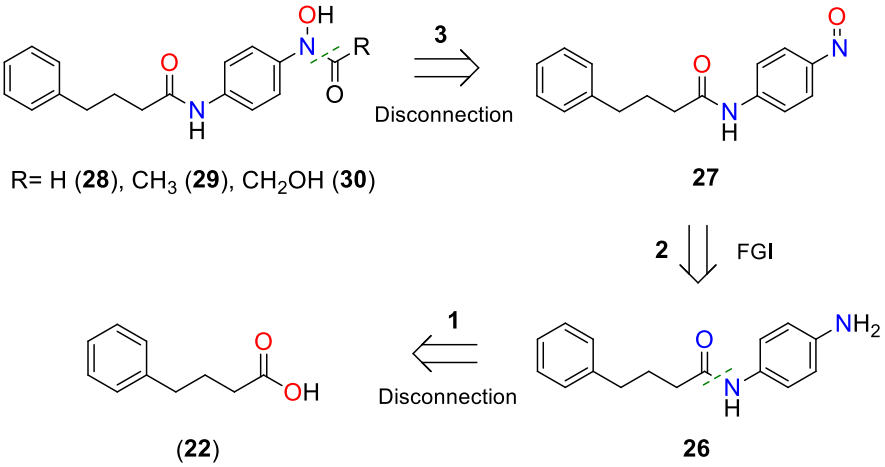

Scheme 10.2. Basic retrosynthetic analysis of *N*-aryl-HAs. R= H (**28**), CH_3 (**29**), CH_2OH (**30**).

The third step comprises a standard amide synthesis which could be achieved by chemical approach by utilizing either glacial acetic acid (AcOH) and α-oxoacids to synthesize compounds **29** and **30**, or by spontaneous reaction with glyoxylic acid (GA) to generate the formamide analogous **28**. Theoretically, these compounds could also be produced by means of an enzymatic approach with TK_{gst}. First, the chemical synthesis of the three compounds was performed, and then the enzymatic synthesis of **30** was undertaken. For the second step, a functional group interconversion from an amine to a nitroso group is required. This can be accomplished by oxidation of the generated amine **26** with oxone to produce the corresponding nitroso compound **27**. For the first step, the amine **26** has to be synthesized from the corresponding carboxylic acid **22**, which should be previously activated as the equivalent acid chloride (Scheme 10.3).

10.2.1. Synthesis of *N*-(4-aminophenyl)-4-phenylbutanamide

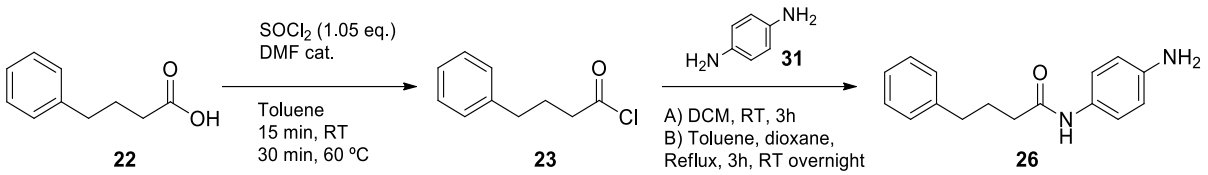

Scheme 10.3. Synthesis of *N*-(4-aminophenyl)-4-phenylbutanamide **26.**

Herein, phenylbutanoyl chloride **23** was generated by reaction of phenylbutanoic acid **22** with thionyl chloride. The latter is the most utilized reagent because of its low price and volatility, leading to an easy treatment of the product by distillation.[316] The reaction was performed in toluene and DMF was employed as the reaction catalyst, forming the active *Vilsmeier-Haack-reagent*,[317] which then reacts with the carboxylic acid **22** to build the acid chloride. It is to be noted that only 5% excess of thionyl chloride was needed for the reaction, granting its efficient removal *via* distillation. In addition, employing toluene as the reaction solvent provides the benefit of co-distilling the DMF together, which is crucial as the DMF could interfere in the following step. TLC is not appropriate to follow the progress of the reaction, as acid chlorides react with silica to form back the carboxylic acids. However, during this reaction sulfur dioxide is formed. That allows for the monitorization of the reaction with a gas bubbler instead, the stop of bubbling indicating the reaction end. After distillation of the solvent and the reagents *in situ*, product **23** was obtained with a 91% yield. The identity and purity of the acid chloride **23** was confirmed by NMR, and the product was used for the next step without further purification.

The generated acid chloride **23** was mixed with a two-fold excess of the diamine to suppress the production of undesired disubstituted product **32**. To carry out the reaction, two different conditions were used. Reaction A was performed solely in DCM at RT for three hours, adapting a protocol from *Tan et al.*,[318] while reaction B was done in a 1:1 mixture of toluene and dioxane, refluxed for three hours, and left at RT overnight, following a protocol from *Böhm et al*.[319] In both cases the acid chloride **23** was slowly dropped into a solution of the diamine **31** to prevent high local concentration of **23** and thus reduce formation of the disubstituted product **32**. However, soon after the addition of **23** was started, the undesirable **32** started to precipitate, as confirmed by TLC. The precipitate was separated from the solution by filtration, but TLC showed that besides the desired monosubstituted product **26** there was some amount of **32** remaining in the reaction solution in both systems. Before column chromatography, the mass of the crude product obtained after reaction B was 1.5 times that of reaction A, however, after column chromatography only 2.0 g (57% yield) of pure product **26** were collected from reaction B, whereas reaction A afforded 2.8 g (81% yield). This implies that the selectivity towards the desired product **26** was better in reaction A. As the interest relies on the highest selectivity, *i.e.* isolated yield, the conditions of reaction A were considered optimal for this synthetic step.

Furthermore, **31** was commercially available at a fairly low price and the reaction gave good yield with fairly good selectivity towards the desired product **26**. Therefore, although the side product formation **32** could not be completely avoided and thus, some yield was lost, this

simplified synthesis was still much faster, less tedious, and more economic than the usual application of protecting and deprotecting groups for the free amine group in **31**.

10.2.2. Synthesis of *N*-(4-nitrosophenyl)-4-phenylbutanamide

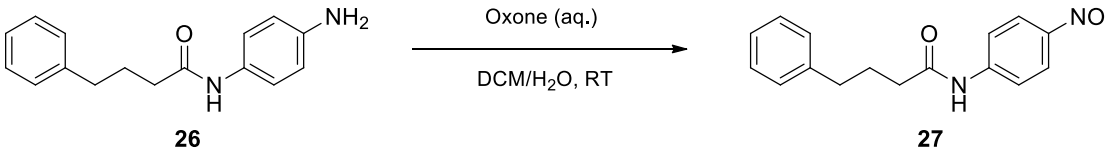

26 **27**

Scheme 10.4. Synthesis of *N*-(4-nitrosophenyl)-4-phenylbutanamide **27**.

For conversion to the nitrosoarene, the amide **26** was dissolved in DCM under inert atmosphere, and an aqueous solution of oxone was added dropwise into the aniline solution. At the beginning, only the minimum amount of solvent necessary to dissolve the educt was used to facilitate a fast reaction by direct contact of the reagents. However, as the oxone solution was being added, the solution turned turbid and formed a precipitate. Therefore, more solvent had to be added to keep the reaction stirring and to dissolve the precipitated SM. The reaction was left to react overnight, and after TLC showed still presence of SM, another half equivalent of oxone was added. After confirming that no educt was left on the reaction by TLC (3 h), the reaction was diluted again for better homogeneity, quenched, worked-up with a standard laboratory protocol, and the solvent was removed under reduced pressure. The product **27** was isolated with a 63% yield. Analysis of the product *via* HPLC, NMR, and MS confirmed that the desired nitrosoarene **27** had been clearly produced, yet the nitro product **33** was also present as a side product, together with traces of azoxybenzene derivative **34** (Figure 10.2).

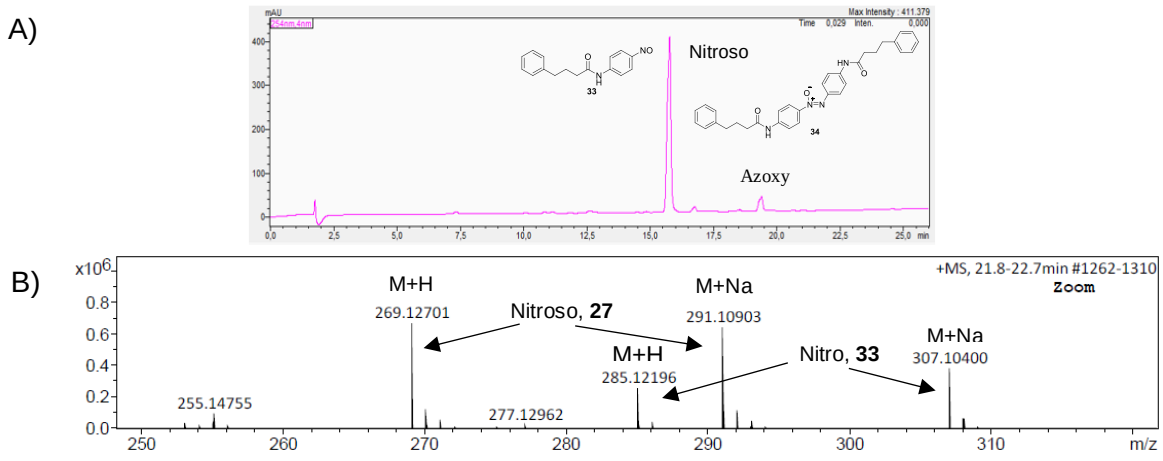

Figure 10.2. (A) HPLC profile of isolated *N*-(4-nitrosophenyl)-4-phenylbutanamide **27** at 254 nm, where traces of azoxy byproduct **34** were detected; (B) Zoom from mass spectrum of **27**, where the presence of the nitro side product **33** was observed.

Most of the signals from **27** overlay with **33** in NMR and HPLC and therefore, it was not possible to calculate the exact purity of the nitroso compound. Anyway, as previously discussed in Chapter I, the nitroso product **27** was utilized in the next steps without further purification

since the nitroso compounds are very reactive and easily decomposed, and the side products do not interfere greatly in the enzymatic reaction or in the acid catalyzed reactions. In the TLC analysis directly after the reaction was finished, mostly only the desired nitroso compound **27** was detectable. Since the nitroso compounds are very reactive, it is possible that the most part of the nitro compound **33** did not only originate from the reaction but eventually also from oxidation of the nitroso compound with air during the work-up process or during the removal of the solvent. With the nitroso compound SM at hand, the synthesis of the retro-HAs was carried out.

10.2.3. Synthesis of *N*-(4-(*N*-hydroxyformamido)phenyl)-4-phenylbutanamide

First, the direct formyl analog **28** was synthesized by taking advantage of the fact that GA is able to spontaneously condensate with nitrosoarenes in a non-enzymatic way, as discussed in Chapter I (Scheme 10.5).[239]

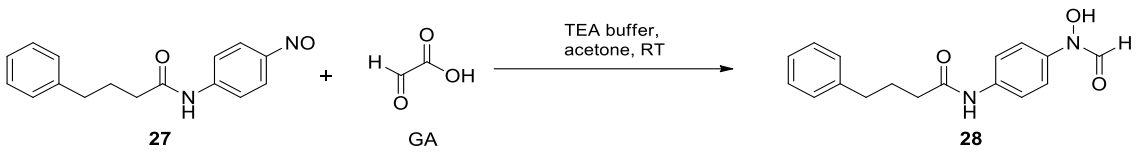

Scheme 10.5. Synthesis of *N*-(4-(*N*-hydroxyformamido)phenyl)-4-phenylbutanamide **28** with GA.

An excess of GA (5 eq.) was utilized for the reaction to avoid the dimerization of the nitroso compound, and to favor the GA-reaction over any possible competing oxidation reaction of **27**.

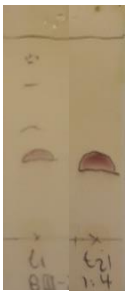

Figure 10.3. TLC plate of oxidation reaction with **27** after 1 h and 21 h. TLC: CH/EA 1:4.

The desired product spot could be immediately identified in the TLC monitoring as it turned dark red upon contact with the $FeCl_3$ staining reagent (Figure 10.3). Corbett *et al.* [239] reported that this reaction type was almost totally restricted to aqueous solvents, having the addition of small amounts of organic solvents an inhibitory effect on the reaction rate. However, since in the preparative part the HA library was successfully synthesized using up to 20% of acetone as co-solvent, the same amount was used at first for this reaction. Yet, the reaction was still turbid after 4 hours probably due to incomplete dissolution of SM in the reaction mixture. To further improve the solubility, another 5 mL of acetone were added. After 21 h, the solution was clear and only a small amount of turbidity remained on the top layer. Thought to be probably due to undissolved SM, 5 mL more of acetone were added to the reaction. The total volume of the reaction was 60 mL with 34% of acetone as co-solvent, proving that this reaction tolerates very high amounts of organic co-solvents without having major detrimental effects.

After a total conversion time of 25 h, the reaction was stopped and treated with a common acid-basic work-up. Evaporation of the solvent furnished the crude product, which was purified by preparative TLC with CH/EA 1:1 as mobile phase. Alternatively, a microcolumn could be used

for the same purpose. Analysis of the product by NMR and MS verified the successful obtention of *N*-(4-(*N*-hydroxyformamido)phenyl)-4-phenylbutanamide (**28**) as a pale pink solid with high purity (>90%) and a yield of 115 mg (61%).

Because the color of the HA product was pale pink and the compound should have been colorless, apparently some small color impurities were present. Since the HA compounds were synthesized to be analyzed as possible anticancer drugs in biological tests, colored impurities were thought to be undesirable. Attempts to further purify the compound by standard use of activated charcoal, as previously done successfully with HPTB, resulted in the loss of material, possibly due to a strong adherence of the **28** to the charcoal.

Plausibly, starting the reaction with already more acetone as co-solvent would yield a higher reaction rate, as seemingly the speed of the reaction was limited by the solubility of the SM. To probe this, the reaction was performed again with 34% acetone from the start. Indeed, after only 3.5 h almost no more SM was observed by HPLC or TLC analysis. In order to try to optimize the conditions of the reaction and remove the color impurities, a different protocol was used for the work-up of the reaction. Simultaneous removal of miscible solvents acetone/water and filtration of formed precipitate by standard laboratory protocols furnished the crude product. Then, purification by recrystallization by diffusion with a mixture of acetone/pentane was performed. The principle behind the recrystallization by diffusion of a more volatile solvent into a sample of lower volatility is depicted in Figure 10.4.

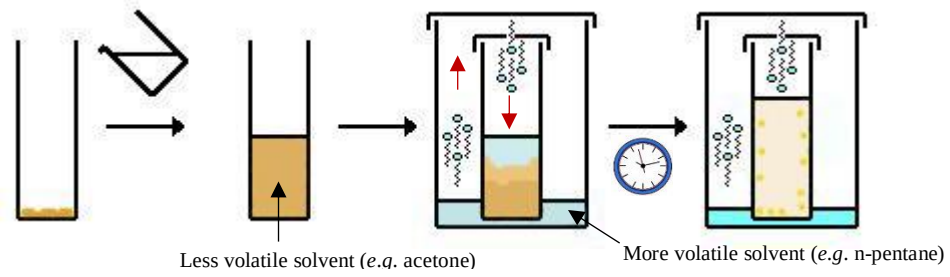

Figure 10.4. Principle of slow gas diffusion as recrystallization method. The more volatile solvent (*e.g.* n-pentane) bearing the less dissolving power, is poured inside the big beaker, and should diffuse into the small vial containing a saturated solution of the product in the lower volatile solvent (*e.g.* acetone) with the highest dissolution power. This should decrease the total dissolution power, forming the pure product crystals.

The n-pentane, which was the most volatile solvent having the less dissolving power, evaporated from the big vial and diffused into the acetone, which had the better product dissolution. Because the polarity of the solution was decreased and therefore, the total dissolution power was reduced, a yellow precipitate was formed. However, acetone slightly evaporated afterwards as well and thus, the crystals were mostly collected from the walls of the small vial. Product **28** was obtained as white-yellow crystals (61 mg, 33%) with 98% purity, as confirmed by HPLC and NMR.

The yield of the reaction using the second work-up/purification protocol including the recrystallization step was almost half compared to that of the first reaction work-up including the preparative TLC/microcolumn. Although after the first protocol some colored impurities

were present, the purity evident from NMR, TLC and HPLC analysis was good, confirming that the first protocol would be sufficient for this reaction, giving the highest yield with an acceptable purity (>90%).

10.2.4. Synthesis of *N*-(4-(*N*-hydroxyacetamido)phenyl)-4-phenylbutanamide and *N*-(4-(*N*,2-dihydroxyacetamido)phenyl)-4-phenylbutanamide

A) By a standard protocol via chemical

The acid conditions reported by Sakamoto *et al*.[229] and already successfully employed in the chemical synthesis of **15a** with PA, were adapted to synthesize compounds **29** and **30**. For that, PA or HPA were utilized respectively, together with glacial acetic acid (Scheme 10.6).

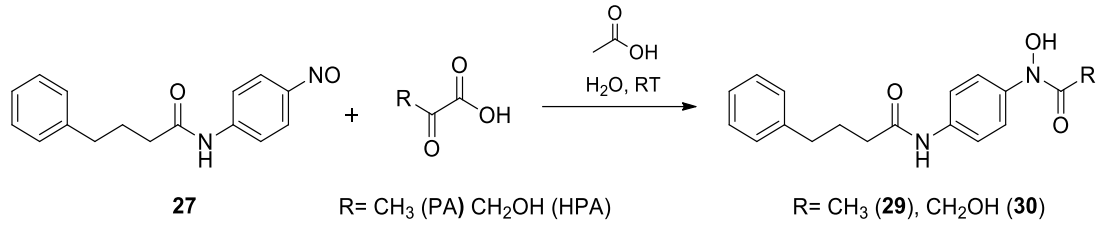

Scheme 10.6. Synthesis of *N*-(4-(*N*-hydroxyacetamido)phenyl)-4-phenylbutanamide (**29**) and *N*-(4-(*N*,2-dihydroxyacetamido)phenyl)-4-phenylbutanamide (**30**) *via* acid catalyzed mechanism.

Both reactions were performed successfully and furnished the corresponding crude products, which were then purified *via* short column chromatography starting with CH/EA 10:1, to remove the azoxy compounds and related impurities, and then changing the gradient fast to 1:1 until no more byproducts got released from the column. Once the product was eluting, the polarity of the mobile phase was increased to CH/EA 1:4. Both short columns took long time and for the second one mostly (**30**), part of the product seemed to stick to the silica even when using pure ethyl acetate for the elution. This could partially explain the loss of yield. Nevertheless, *N*-(4-(*N*-hydroxyacetamido)phenyl)-4-phenylbutanamide (**29**) and *N*-(4-(*N*,2-dihydroxyacetamido)phenyl)-4-phenylbutanamide (**30**) were obtained in high purity, as confirmed by NMR and MS analysis, with moderate yields of 66% and 48%, respectively. In the HPLC analysis, a byproduct signal was clearly visible yet the purity was about 90%. Attempts to further purify the compound *via* preparative TLC with EtOAc/EtOH (100:1) produced considerable loss of yield and improved the purity only to 93%. The byproduct could not be removed completely.

B) Application of TK_{gst} to generate N-(4-(N,2-dihydroxyacetamido)phenyl)-4-phenylbutanamide

To investigate the possibility of using green enzymatic synthesis to generate complex *N*-aryl-HA molecules with potential anticancer activity, TK_{gst} was employed in an enzymatic reaction with **27** and HPA to produce **30** (Scheme 10.7).

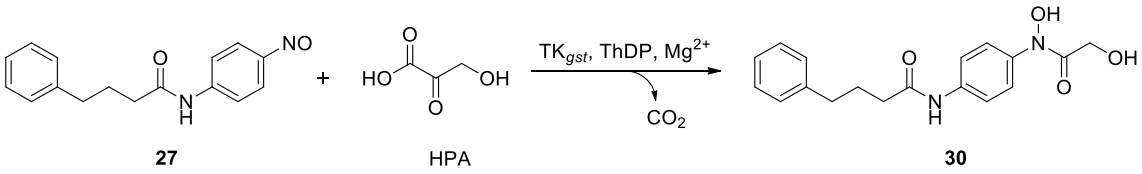

Scheme 10.7. Synthesis of **30** *via* enzymatic synthesis with TK$_{gst}$ in the presence of cofactors ThDP and Mg^{2+}.

Analytical scale reactions (500 µL) were conducted in TEA buffer (50 mM, pH 7.45) at RT with changing parameters, including the enzyme amount (0.2 and 0.6 mg) and the concentration of **27** (10 mM, 25 mM and 50 mM), with all other parameters constant, such as HPA (50 mM), co-solvent concentration (20% acetone), and cofactor concentrations ThDP (2.4 mM) and $MgCl_2$ (9 mM). Control reactions in the absence of either the enzyme or any of the substrates did not lead to any detectable product formation. There was no appreciable difference between the highest concentrations **27** (25 and 50 mM). From these initial tests, the highest concentration of enzyme (0.6 mg/0.5 mL) together with the intermediate concentration of nitroso compound (25 mM) gave the best results. Comparing the reaction mixture with the chemically synthesized reference compound allowed the identification of the desired product peak from the enzymatic reaction among the wide range of byproducts.

The reaction scale was then increased to 25 mL with a high concentration of enzyme (50 mg/25 mL). After 18 hours, HPLC confirmed the formation of the desired product **30** (Figure 10.5, A) together with diverse byproducts typical from this reaction, such as the amine **26** and the azoxybenzene **34** compounds, due to the high reactivity of nitroso compounds. At this stage, the reaction was not finished, as the presence of considerable amounts of SM **27** was visualized at a wavelength of 320 nm (Figure 10.5, B).

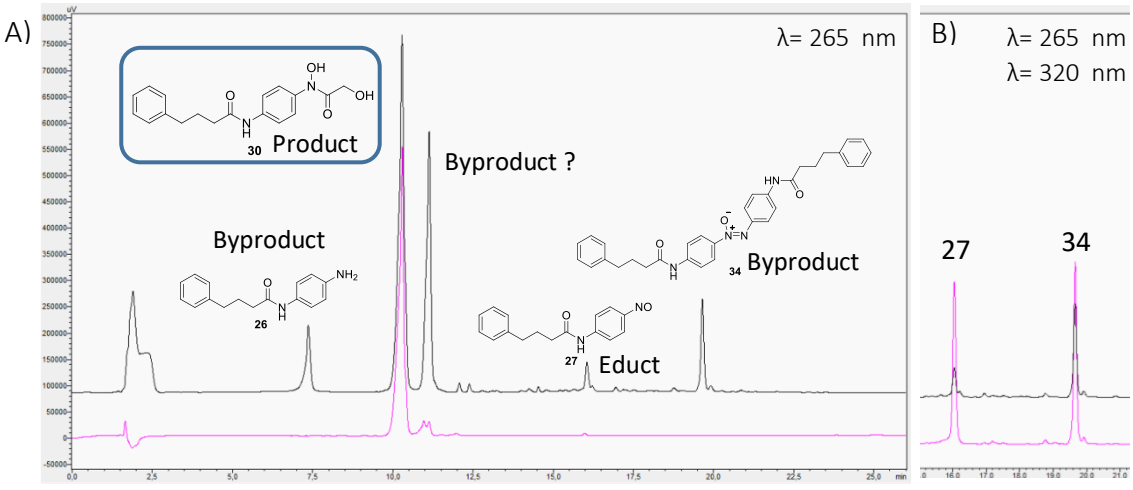

Figure 10.5. A) HPLC profile (λ= 265 nm) from TK$_{gst}$ reaction (black), and comparison to **30** isolated *via* chemical (93% purity) (pink). The desired product was generated in the enzymatic reaction among various byproducts, all confirmed by LC-MS. B) Comparison between leftover **27** and formed azoxy compound **34** at 265 nm (black) and 320 nm (pink).

With a retention time very similar to the peak of the desired product (10 min), a new byproduct peak (11.5 min) was observed. LC-MS confirmed that this compound was **29**, also confirmed by comparing the HPLC profile of the enzymatic reaction to the chemically synthesized

compound **29** (Figure 10.6). The desired product **30** was only generated by the action of the enzyme, however, this byproduct (**29**) had to be generated during the incubation time *via* some chemical pathway.

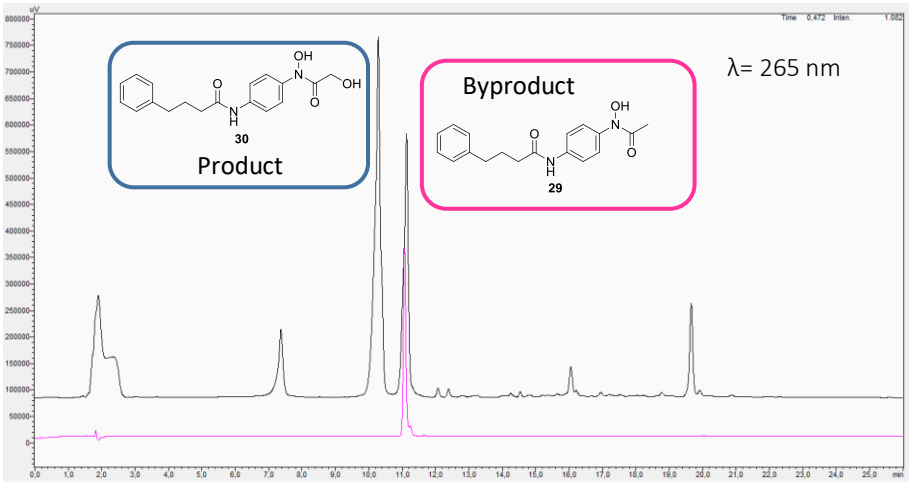

Figure 10.6. HPLC profile (λ= 265 nm) from TK_{gst} reaction (black), and comparison to **29** isolated *via* chemical (pink). Byproduct **29** confirmed by comparison of HPLC profiles and by LC-MS.

To discard the unlikely involvement of acetone (co-solvent) in the chemical synthesis of **29**, a series of experiments changing the reaction conditions were tested at an analytical scale (500 µL). In the various experiments, acetone and DMSO were separately tested as co-solvents for the reactions in the presence and absence of enzyme, and in the presence and absence of HPA. The results for the reactions with both co-solvents were very similar. In the absence of HPA neither of the compounds were formed; in the absence of enzyme, the byproduct **29** was favored and for the desired product **30** only a very small signal produced from a chemical background reaction was observed. Only when both the enzyme and the donor substrate HPA were present, both products **29** and **30** were generated in a significant amount. Up to date the exact mechanism for the chemical production of compound **29** is still unknown. However, the concentration of **30** was higher than that of **29** in the presence of enzyme. Presumably, after careful optimization of the reaction conditions, including the amount of enzyme to be added, the desired product **30** could be more strongly favored against the byproduct **29**.

The reaction was not further purified. Nevertheless, it was verified that the desired byproduct **30** could be synthesized *via* enzymatic coupling by utilizing TK_{gst}, and both compounds could be isolated and purified in one step to recover both valuable *N*-aryl-HA with potential medicinal properties. This proves that TK_{gst} could be used to synthesize a relevant *N*-aryl-HA.

10.2.5. Synthesis of *N*,2-dihydroxy-*N*-(naphthalen-2-yl)acetamide

In order to widen the scope of HA used in the cell viability assays and to have *N*-aryl-HAs with a different structure, yet small enough to fit in the active pocket of the HDAC enzyme, the synthesis of **38-40** was pursued (Scheme 10.8). The naphthalene structure was chosen because

of its theoretical synthetic simplicity and because, due to its intrinsic rigidity. it could serve to simulate the cinnamic structure present in various HDACi, such as *Pracinostat* or *Panobinostat*,

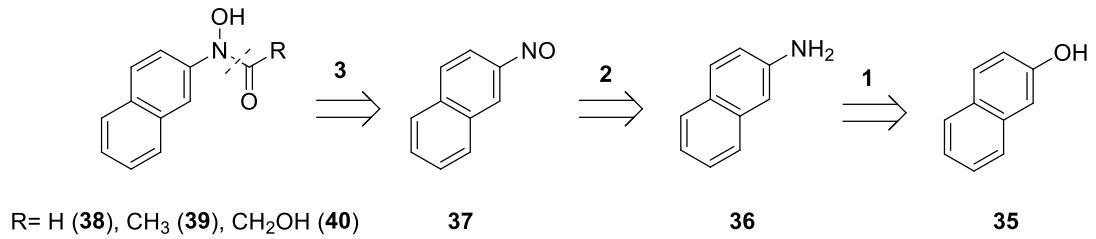

Scheme 10.8. Basic retrosynthetic analysis of *N*-naphthyl-HAs. R= H (**38**), CH_3 (**39**), CH_2OH (**40**).

Because commercial 2-naphtylamine at a price of 498 €/g was very costly, it was synthesized in the laboratory *via* direct amination of naphthol under metal-free conditions according to Yu *et al*.[320] The reaction is shown in Scheme 10.9.

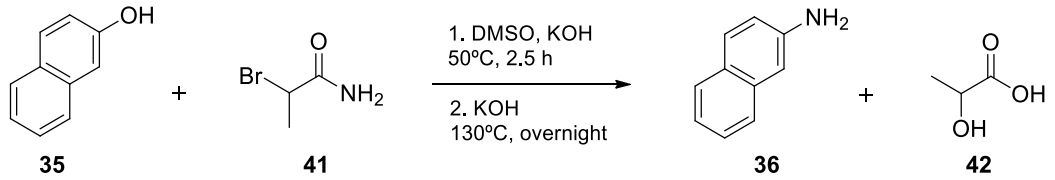

Scheme 10.9. Synthesis of 2-naphtylamine **36**.

This reaction was carried out in a three-step one-pot synthesis starting from the *O*-alkylation of naphthol **35**, followed by a Smiles rearrangement using 2-bromopropanamide (**41**) as the aminating agent, and finishing with the hydrolysis of the intermediate to release the aminated product **36** and 2-hydroxypropanoic acid (**42**). In an attempt to obtain complete conversion, the reaction conditions were slightly modified, adding instead of 1.05 eq. aminating reagent **41** and 2.15 total eq. KOH, 2 equivalents of **41** and 5.5 total eq. KOH. Furthermore, instead of incubating the last step only for 2 hours, the reaction was left to stir overnight. In addition, the treatment of the reaction proceeded in a different manner as in the reported protocol. The combined organic layers were not dried over $MgSO_4$ and filtered prior to evaporating the solvent under reduced pressure and drying the product by lyophilization. Moreover, no further purification was necessary since the compound was obtained with high purity as confirmed by NMR, where only a very small amount of DMSO (1%) was still present. The reaction was successfully performed with a very high yield of 97%. The obtained yield was considerably higher as the one reported (78%), proving that the optimization of the reaction conditions and treatment improved the performance of the reaction significantly.

The second step consisted in the oxidation of the generated amine **36** to produce the corresponding nitroso compound **37**. The reaction was performed with oxone, as with all the previously synthesized nitroso compounds, adapting the protocol from Priewisch and Rück-Braun[203] (Scheme 10.10).

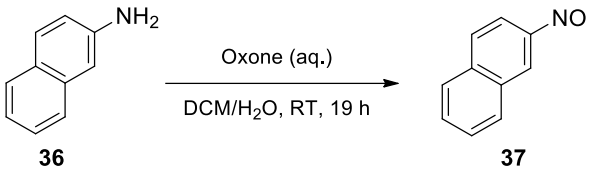

Scheme 10.10. Synthesis of 2-nitrosonapththalene (**37**) *via* oxidation of 2-napththylamine (**36**).

To avoid over oxidation of the product **37**, the reaction was started with 1.50 eq. of oxone, and after 3 h another 0.5 eq. was added. The monitoring of the reaction was done by means of TLC and HPLC analysis until complete conversion of the SM. A new peak was arising with an expected retention time similar to the typical retention time of nitroso compounds, with the usual peak corresponding to the nitro compound **43** eluting immediately before. LC-MS analysis of the reaction mixture corroborated this, as a mass of 158.05 g [$M+H^+$] was found for that the presumed product peak. The starting amine **36** and the nitro compound **43** were also identified by LC-MS. In Figure 10.7, the comparison of the HPLC profiles of the reaction is displayed at various reaction times (0, 30 min, 2.5 h and 19 h).

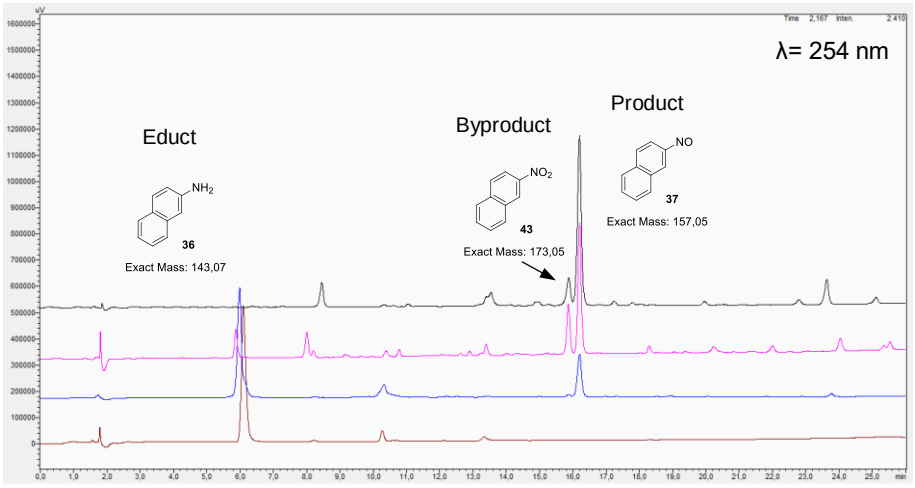

Figure 10.7. HPLC profile from the oxidation reaction after 0 min (brown), 30 min (blue), 2.5 h (pink), and 19 h (black). As the reaction proceeds, the peak of the amine **36** decreases until its complete disappearance, and the supposed nitroso product **37** peak appears, together with the less favored nitro byproduct among other small byproduct peaks.

Because **36** had been completely consumed, the work-up of the reaction was followed and carried out as habitual. An HPLC probe was taken from the crude product after concentrating the treated organic phase to a minimum amount of volume (Figure 10.8, black), confirming that **37** was still the main component after treatment of reaction. However, after total evaporation of the solvent until dryness the peak of the **37** had almost vanished compared to the rest of the byproducts, which had increased significantly (Figure 10.8, pink).

This led to the conclusion that the nitroso product **37** obtained was not stable. Associating the loss of product to the oxidation of the solid material in short contact with the air after evaporation of the solvent, the reaction and work-up were repeated and monitored *via* HPLC.

However, the organic layer was divided in two batches. The first batch was distilled under argon atmosphere until dryness and an NMR sample was directly submitted.

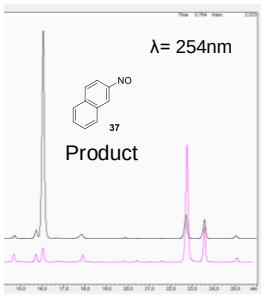

Figure 10.8. HPLC profile from the crude product after work-up yet still solved in a minimum amount of solvent (black) vs crude product after total dryness (pink).

The second batch was concentrated to a small volume using the rotary evaporator, flushed with argon, and measured directly *via* NMR. Both NMR analyses were unsuccessful in identifying the presence of **37** as there seemed to be a mixture of different compounds inside. The nitroso group is a very reactive moiety, and therefore small amounts of byproducts are usually obtained in the oxidation reactions from the corresponding amines, yet in the case of 2-nitrosonaphthalene **37** the reactivity is significantly increased. This is probably due to the additional electron density that the naphthalene ring contributes to the nitroso group. In order to bypass these complications, the next approach to generate the corresponding *N*-aryl HA **39** was directly undertaken without previously isolating **37**. The procedure is shown in Scheme 10.11.

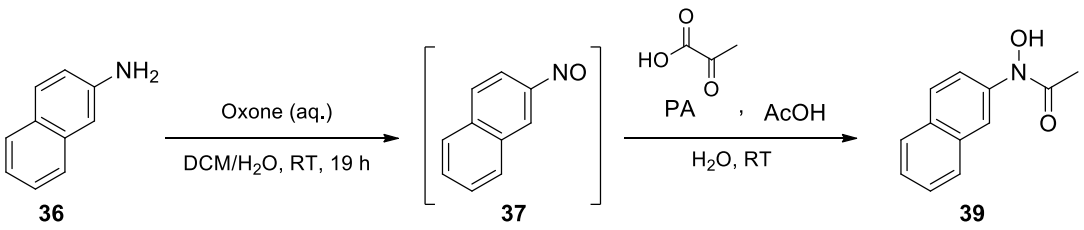

Scheme 10.11. Synthesis of **39** from **36** without previous isolation of **37**.

First, the oxidation of **36** and following work-up was repeated. Then, the crude mixture containing **37** as majoritary product, as confirmed by HPLC, was distilled under argon until only around 2 mL of solvent were left in the flask. Adapting the chemical protocol used for the synthesis of *N*-aryl HA,[229] PA dissolved in glacial AcOH was slowly added to **37**. The mixture was stirred at RT and monitored by HPLC and TLC. In Figure 10.9, the comparison of the HPLC profiles of the reaction at various reaction times (0, 15 min and 16 h) is displayed. Evident from the HPLC analysis, **37** had already decomposed partly to generate a wide range of byproducts prior to starting the second reaction. Nevertheless, a considerable quantity of **37** was still present when the reaction with PA was initiated (Figure 10.9, blue). A new peak with retention time of ca. 11.5 min was formed among the many byproducts, presumably corresponding to the desired *N*-aryl HA **39**. However, this assumption could not be confirmed, as no spot colored red upon contact with the $FeCl_3$ stain. This could be because the quantity of the product was too small in the mixture to be able to be detected, or because the peak did not correspond to *N*-hydroxy-*N*-(naphthalen-2-yl)acetamide **39**. Moreover, it could also not be identified *via* LC-MS given the high proximity and quantity of byproducts.

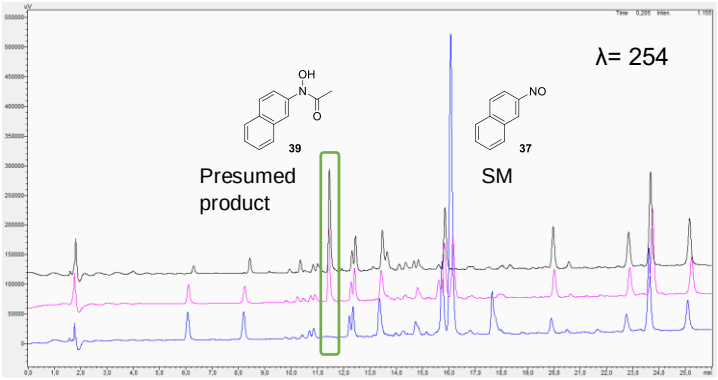

Figure 10.9. HPLC profile (λ= 254 nm) from the crude product after 0 min (blue), 15 min (pink) and 16 h (black). The single new peak generated is marked with a green rectangle.

In an effort to isolate and characterize the newly formed compound, purification *via* column chromatography was attempted with CH/EA (10:1). However, **39** could not be isolated from the byproducts to verify the identity of the peak formed and confirm if it could be synthesized from the crude mixture containing **37** in solution. Although plausibly after scaling up the reaction significantly and adjusting the conditions, enough quantity of product, **39** could possibly be isolated for characterization, a very low yield was to be expected due to the great number of byproducts produced during oxidation of **37**. This demonstrates that the use of isolated **37** (purity ≥ 80%) is a requirement for the final reaction to succeed.

In an attempt to circumvent this problem, another nitrosation protocol was tested for the synthesis of **37**.[321] Potassium naphthalene-2-trifluoroborate (**44**) was employed as the organoboron species and nitrosonium tetrafluoroborate as the nitrosation agent for the reaction shown in Scheme 10.12.

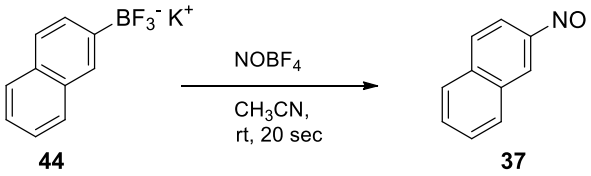

Scheme 10.12. Synthesis of **37** *via* nitrosation of potassium naphthalene-2-trifluoroborate **44**.

The nitrosation of the arylboron species **44** most likely occurs by an *ipso*-substitution, by which the attachment of the entering group is performed in a position where another substituent is already located. During the reaction, the tricoordinate boron species bearing a Lewis acidic boron moiety with an empty p-orbital would undergo attack of sodium nitrite. This would form an ate-complex **46** where the boron would have a negative formal charge and the nitroso group would become more electrophilic, being able to be then attacked by the aromatic ring *via* an *ipso*-substitution to afford the nitroso product **37** (Scheme 10.13).[322]

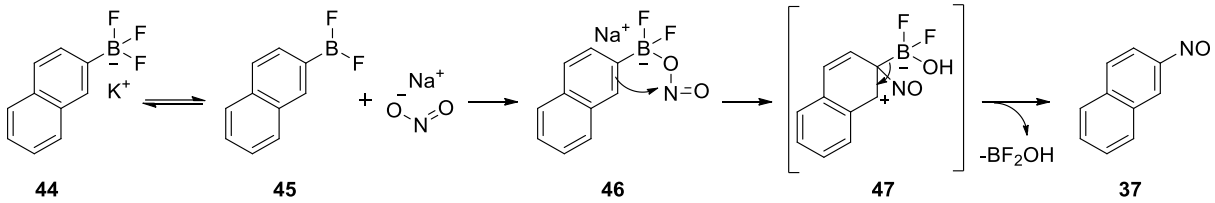

Scheme 10.13. Mechanistic pathway of the *ipso*-nitrosation of **44**. Scheme adapted from Molander *et al.*[322]

In order to reproduce the reported results, the reaction was performed on the same scale and followed exactly as in the literature.[321] The reaction mixture was analyzed by means of HPLC and TLC analysis, which indicated a mixture of different compounds. LC-MS could not identify the peak corresponding to the nitroso compound **37**. Therefore, a comparison between the HPLC profile from the previous oxone oxidation after 19 h (black) and the reaction mixture from the *ipso*-nitrosation (pink) was pursued (Figure 10.10).

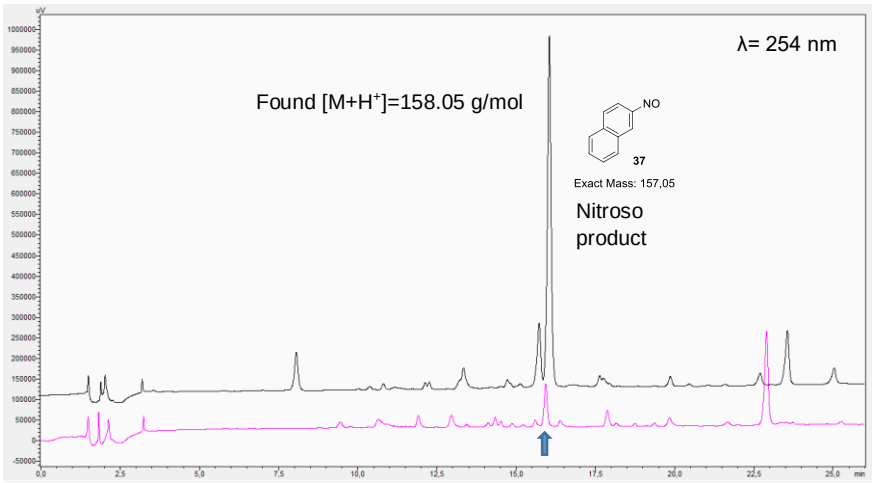

Figure 10.10. HPLC profile (λ= 254 nm) from oxidation reaction after 19h (black) compared to reaction *via ipso*-nitrosation (pink). The new peak (signalized with a blue arrow) from the latter is in a retention time that is not conclusive for its identity.

The peak formed in the *ipso*-nitrosation that should correspond to **37** (signalized with a blue arrow in Figure 10.10) appeared at an average retention time between **37** and nitro compound **43**, making its identity difficult to assign. In an effort to isolate and characterize the new compound, work-up and purification of the reaction were followed *via* standard protocols. After column chromatography of the crude mixture with CH/EA in a gradient starting with 10:1 until 4:1 and monitored *via* TLC analysis, five different fractions were isolated as reddish or tan solids, as described in the literature, and characterized *via* NMR and HPLC. Inexplicably, no desired product **37** was observed in any of these fractions upon comparing the NMRs to the reference.[321] The reported literature yield was already very low (15%) proving the extreme instability and difficulty of isolation of **37**, compared all the previous nitroso compounds successfully generated and isolated. Because all efforts to isolate **37** as SM or directly the final *N*-aryl HA **39** proved unsuccessful, the synthesis was abandoned.

10.3. *In vitro* HDAC inhibition assays

10.3.1. Assay principle and functionality

To investigate the hypothesis that retro-HA should offer comparable pharmacological versatility because of their similar structure and metal binding competence to common HA, the group of *N*-aryl HAs **28**, **29** and **30**, together with HTPB as reference, were sent for *in vitro* testing of HDAC inhibition activity to the chemical epigenetics research group of M. Jung (Institute of pharmaceutical sciences, Albert-Ludwigs-University, Freiburg).

In the same way that HDAC enzymes generally catalyze the removal of acetyl groups from acetylated lysine residues in the *N*-terminal extreme of histone proteins, they have also the ability to remove acetyl groups from compounds containing lysine residues. Considering this, non-isotopic assays have been developed for the measurement of HDAC activity.[323-325] Non-isotopic assays are systems that use a non-radioactive isotope signal. The principle of this type of assays is depicted in Scheme 10.14. Depending on the HDAC class used for the assays in this work, two different fluorogenic substrates have been employed: (S)-[5-acetylamino-1-(4-methyl-2-oxo-2H-chromen-7-ylcarbamoyl)-pentyl]-carbamic acid benzyl ester, also termed ZMAL, for the enzymes HDAC6 and HDAC1; and (S)-[1-(4-methyl-2-oxo-2H-chromen-7-ylcarbamoyl)-pentyl-5-(trifluoroacetamido)]-carbamic acid benzyl ester, also named ZMFTAL, for the enzymes *sm*HDAC8, *h*HDAC8 and *tc*DAC2.

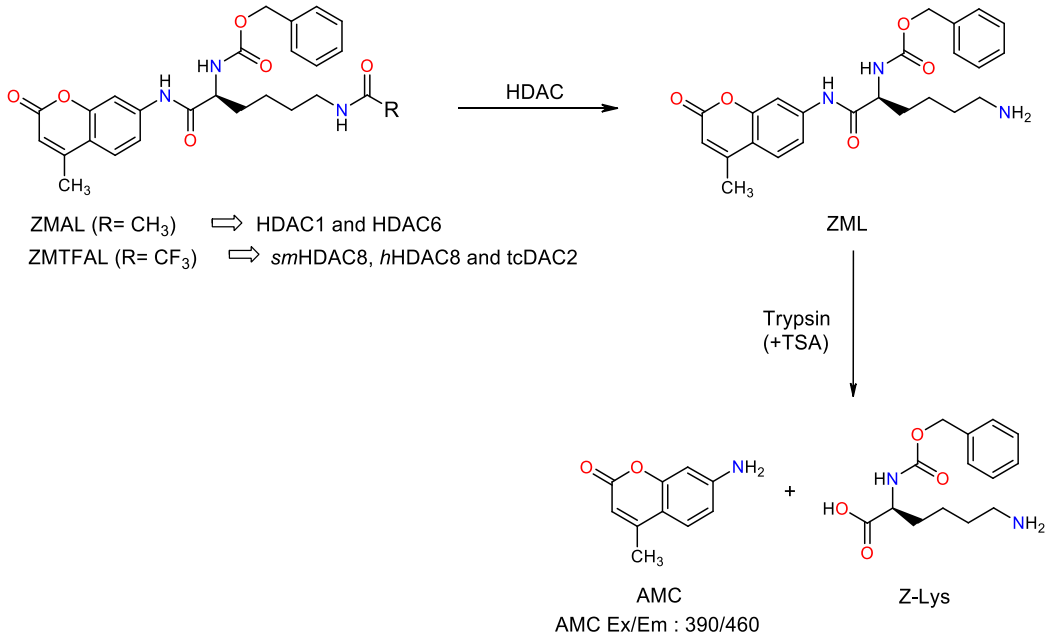

Scheme 10.14. HDAC assay principle with ZMAL (R= CH_3) or ZMTFAL (R=CF_3) as substrates.

In order to measure the activity of HDACs, the amides ZMAL or ZMFTAL can be utilized in a two-step enzymatic fluorogenic assay. In the first step, the removal of the acetyl group or trifluoroacetyl group takes place, catalyzed by the HDAC, releasing acetic acid or trifluoroacetic acid, and the deacetylated metabolite of ZMAL, (S)-[5-amino-1-(4-methyl-2-oxo-2H-chromen-7-yl)carbamoyl)-pentyl]-carbamic acid benzyl ester, also referred to as ZML. In a subsequent step, the deacetylated peptide serves as a substrate of trypsin, which cleaves the

peptide bond between the carboxyl- and the amino group of the lysine residue. This can only happen once the molecule has been deacetylated. Trypsin breaks the molecule in two parts yielding *N*-α-benzyloxycarbonyl-lysine, also termed Z-Lys, and the fluorescent compound 7-amino-4-methylcoumarin, also known as AMC. The fluorescence of the latter can then be measured with an excitation wavelength of 390 nm and an emission wavelength of 460 nm.[325]

Following the same principle, if a potent inhibitor for HDAC (HDACi) would be added simultaneously together with the substrates ZMAL or ZMFTAL, the first step consisting in the deacetylation of the lysine residues would be directly affected. Because trypsin can only cleave molecules that have been previously deacetylated, less to none AMC would be produced, generating accordingly a smaller fluorescence signal, which could be measured in a high-throughput fashion with a plate reader. The inhibition of the HDACi can be calculated by subtracting the fluorescence signal detected in the presence of the HDACi to the signal in its absence, usually taken as 100%. Ideally, if a HDACi has full inhibition power (100%) no fluorescence would be detectable. With this in mind, *in vitro* HDAC inhibition assays were performed with the corresponding reverse HA acting as potential HDACi.

In the experimental assays, a solution of trypsin with a relatively high concentration of the natural HDACi Trichostatin A (TSA), was added to the assay solutions containing the HDACi after exactly 90 minutes of incubation to stop any remaining HDAC activity. Hence, only the incubation time with the HDACi was responsible for the turnover of the ZML substrate, and thus, the fluoresce signal. This is because trypsin can only convert the amount of substrate that was deacetylated at that point in time.

10.3.2. Empirical effect of hydroxamic acids on histone deacetylation

The inhibition potential of *N*-aryl HAs on the deacetylation activity of diverse HDAC enzymes, including those from human recombinants (HDAC6, HDAC1, and *h*HDAC8) and from *Schisosoma mansoni* (*sm*HDAC8) and *Trypanosoma cruci* (*tc*DAC2), has been measured by K. Schmidtkunz in the group of M. Jung. For the *in vitro* HDAC inhibition assays serial concentrations of *N*-aryl HAs as HDACi were applied (100 µM, 10 µM, 1 µM, 0.1 µM). The enzyme incubated with DMSO and substrates ZMAL or ZMFTAL in the absence of HA was used as control reaction. As blank, reactions in the absence of enzyme were also measured. The experiments were performed in duplicates and the fluorescence values were averaged. The experimental procedures as well as the calculated data collected in a table are included in the Experimental part and Appendix for informative reasons (Page 177 and 247, respectively). The results are graphically displayed in Figure 10.11.

Although the assay methodology, HDAC class, and cell type utilized for this work differ from the ones employed in the original literature,[10] HTPB was used as positive control and reference material for the *in vitro* HDAC assays, as its inhibitory activity towards HDACs should remain high independently from the organism containing the HDAC or the assay type. The results obtained from the assays verify this premise, because HTPB displayed a high inhibitory potential for all the HDAC types and sources.

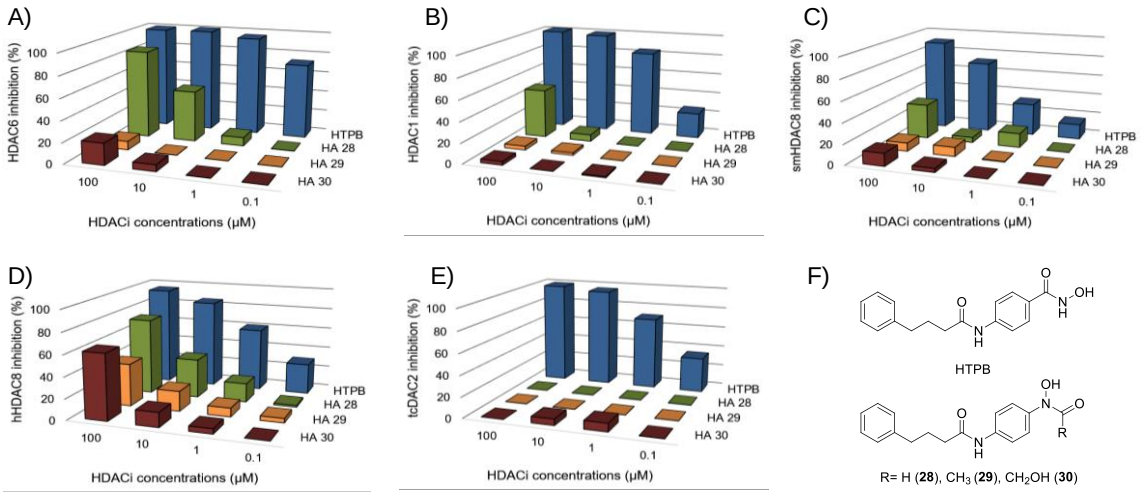

Figure 10.11. Graphical representation of the results from the *in vitro* HDAC inhibition assays with HDAC6 (A), HDAC1 (B), smHDAC8 (C), hHDAC8 (D), and tcDAC2 (D). Structures of HTPB (blue) and analogous retro *N*-aryl HA **28** (green), **29** (yellow) and **30** (burgundy) employed as HDACi are shown in F.

In particular, HTPB showed very high inhibitory activity for HDAC6 even at 1 µM. In the case of the *N*-aryl HAs, some HDACi activity was detected for all enzymes tested except for the HDAC from *Trypanosoma cruci*, *tc*DAC2, which deacetylase activity was basically unaffected by the retro-HA. Only a very small inhibition was observed with **30** at middle concentrations 10 µM and 1 µM. Next, the results displayed in the graphics are thoroughly analyzed.

In regard to the direct analogue of HTPB, **28** (green), more than 30% of inhibition was shown for all HDACs at a concentration of 100 µM. Remarkably, around 80% of inhibition of both HDAC6 and *h*HDAC8 was reached. Even when lowering the concentration to 10 µM still around 50% of inhibition of the former and 40% of the latter was detected. At 1 µM, **28** still retained a small activity against HDAC6, *sm*HDAC8 and *h*HDAC8, almost reaching 20% for the latter. At concentrations below 1 µM no activity was noticed for any enzyme. Concerning **29** (yellow), noteworthy is to remark that for *h*HDAC8 some inhibition was shown at even the lowest concentration, having 40% of inhibition at 100 µM, and still almost 20% at 10 µM. For the same enzyme class, *sm*HDAC8, some activity was also observed at 100 µM and 10 µM, displaying around 10% of inhibition for both concentrations. Moreover, around 8% of inhibition was detected for HDAC6 at the highest concentration. For HDAC1, basically no inhibitory activity was observed even at high concentrations. **30** showed slightly more inhibitory power than **39**, reaching more than 60% of inhibition with *h*HDAC8 at 100 µM. At such concentration, also with HDAC6 and smHDAC8 **30** showed approximately 20% and 12% of inhibition potential. When decreasing the concentration to 10 µM, **30** was still able to inhibit 15% of *h*HDAC8 activity.

As the concentration of HDACi applied decreased 10-fold or more, the inhibition potential reduced drastically. Accordingly, for these compounds to have a good inhibition they would have to be applied in relatively high concentrations (≥100 µM). Conventionally, pharmaceuticals with nanomolar potency are highly sought after by researchers based on the estimation that such large potency anticipates high clinical efficacy. However, *in vitro* potency

is not the only factor determining the potential clinical efficacy of a compound. Other factors such as pharmacokinetic (including its absorption, distribution, metabolism and excretion), physiochemical, and toxicological factors are equally or even more influential.[11] The importance of having a molecule with nanomolar potency is therefore limited, being more important the availability of sufficient levels of the agent able to reach its target while not causing dose-limiting side effects. Holbeck *et al*. summarized all FDA-approved anticancer drugs from the NCI-60 panel in a comprehensive manner.[326] This collected data reveal that *in vitro* nanomolar cytotoxicity provide only limited relevance to clinical efficacy in humans. Moreover, *in vitro* activity did not foresee clinical efficacy for several of these compounds. For instance, anastrazole (GI_{50} 2500 µM) showed considerably better clinical efficacy than tamoxifen (GI_{50} 4.6 µM) in the ATAC (Arimidex, Tamoxifen, Alone or in Combination) trial of 9366 postmenopausal women with estrogen receptor-positive breast cancer.[327] Another example of this is valproic acid (VPA). VPA is a branched short-chain fatty acid currently marketed as an antiepileptic drug which has been also recently discovered as a HDACi.[328] *In vitro*, VPA inhibits HDAC activity in high micromolar to low millimolar range (0.4-2 mM), having also low cytotoxic activity against cancer cell lines with IC_{50} values comprised between 0.5 and 6 mM. Conversely, VPA has shown potent anticancer activity in animal models, strongly suppressing the growth of tumor xenografts.[11] The latter example is very relevant to this work because VPA has the ability to inhibit the same type of enzymes as HAs, causing hyperacetylation of histones most probably by binding to the catalytic center of HDACs in a comparable manner as the HA molecules. In fact, from a study performed with radiolabeled VPA, Göttlicher *et al*. concluded that VPA and TSA not only have akin effects on HDAC activity but also share identical binding sites as they appear to compete for the active site.[328] Therefore, despite the fact that nanomolar potency is desirable, it has no absolute predictive value when developing therapeutics to treat complex diseases such as cancer.[11]

In summary, HTPB having the conventional HA structure displayed considerably higher inhibition potential with all the enzymes than the corresponding retro-HAs. All the latter offered rather satisfactory HDAC inhibition at the highest concentration assayed (100 µM) for *h*HDAC8. Furthermore, the corresponding HTPB-analog **28** presented acceptable inhibitory activity at 100 µM for all the HDACs tested except for the one from *Trypanosoma cruci* (*tc*DAC2). Thus, even when having to apply substantially higher amounts of **28** than of HTPB, the inhibitory potential of the former is confirmed. Apparently, the formyl moiety (**28**) is tolerated best among the retro-HA motifs tested. This compound is different from the latter group because it has a smaller size and lacks the potential binding interactions that could take place with the more enlarged retro-HA containing other functional groups. Hence, the results obtained might be attributable to steric factors in the HDAC active-site.

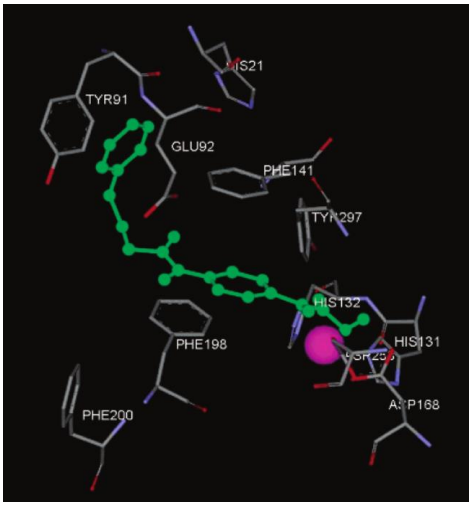

Figure 10.12. Modeled docking of HTPB (green) in the active-site pocket of HDLP. Zn^{2+} cation represented as a magenta ball. Figure extracted from Lu *et al.*[312]

The HDAC catalytic domain consists of a narrow, tube like pocket comprising the length equivalent of four- to six-carbon straight chains. The deacetylation catalysis is facilitated by the cooperation between a Zn^{2+} cation, positioned near the polar bottom of the enzyme pocket, and two His-Asp charge relay systems.[10] In Figure 10.12, the orientation of HTPB in the active-site pocket of HDLP is shown.[314] Conceivably, if the hydroxamate group is enlarged the molecule would have to find a different orientation, thereby possibly breaking some important π-π and/or hydrophobic interactions with the Phe 141/Phe 198 and Tyr 91/Glu 92 subdomains. However, in light of the importance of these interactions for optimal ligand anchoring of the hydroxamate functionality to the Zn^{2+} cation, disruption of any of these interactions might lead to a decrease in the inhibitory potency. To test this premise, an analog to HTPB with an additional ethylene moiety in the amide linkage of HTPB, and thus with an enlarged hydroxamate group, was prepared and analyzed in the literature (Figure 10.13, A).[314] Indeed, the inhibitory potency of **48** resulted to cause more than one order of magnitude increase in IC50 values in comparison to HTPB (1.2 ± 0.2 µM and 44 ± 6 nM, respectively).

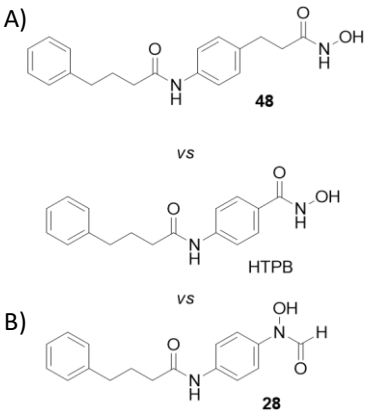

Figure 10.13. Structural comparison between HTPB and A) its enlarged analog **48**, B) its retro-HA analog **28**.

Moreover, retro-HA **28** (Figure 10.13, B) lacks one polar interaction from the replacement of N-**H**(OH) for N-(OH). The absence of this NH-proton appears to be detrimental for HDAC inhibition, probably because it precludes the polar interactions between HTPB and His 132. Moreover, the reverse hydroxamic acid structure could also be preventing the polar interaction between HTPB and His 131, which would decrease the inhibition potency as well. However, in view of the results, the hypothesis that retro-HAs should have similar biological properties than their homologous HA has been validated. Possibly, analyzing these in detailed molecular docking studies and improving their structure accordingly could lead to compounds with higher inhibitory potential. Hence, our studies could serve to open a new research opportunity for anticancer drugs where this novel class of *N*-aryl HA compounds could be investigated for their broader pharmacological properties.

Interestingly, **30** exhibited more than 60% of inhibition of *h*HDAC8 at 100 µM. As presented earlier in this chapter, **30** could also be generated from the reaction of the nitroso compound **27** with HPA by means of the enzyme TK_{gst}. Because enzymes require milder reaction conditions and offer a broad variety of advantages,[12] this research highlights the attractive possibility of generating reverse HA with HDAC inhibitory potential *via* enzymatic catalysis.

11. Summary and outlook

In this chapter, it was hypothesized that *N*-aryl HAs (**3**), also named retro-HAs, presumably grant alike pharmacological properties as the well-known *C*-aryl HA (**2**), based on the fact that both type of molecules have the ability to chelate metal ions, such as iron (III) and zinc(II), in a similar manner (Scheme 11.1).

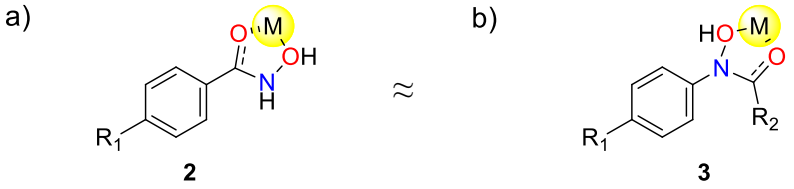

Scheme 11.1. Metal chelation by *C*-arylated HA *vs* isomeric *N*-arylated HA. M= metal ion, R_2= H, CH_3, CH_2OH.

To investigate this hypothesis, the easily-accessible and potent HDACi HTPB[10] and akin *N*-aryl HAs (**28**, **29** and **30**) were synthesized chemically and were investigated by K. Schmidtkunz (group of M. Jung) for their potential activity in *in vitro* HDAC inhibition tests.

The results from the HDAC inhibition assays validated the proposed premise, as all retro-HAs tested produced acceptable to good HDAC inhibition at the highest concentration analyzed (100 µM) for human *h*HDAC8. Additionally, the direct HTPB-analogue HA **28** (H) offered acceptable inhibitory activity at 100 µM for all the HDAC tested from humans, including HDAC1, HDAC6 and *h*HDAC8, or even from *Schisosoma mansoni*, like *sm*HDAC8. The HDAC from *Trypanosoma cruci*, *tc*DAC2, was not influenced by the retro-HAs. Although the most effective concentration (100 µM) was higher as the conventional nanomolar scale, it was concluded that this has no anticipating value for its biological effect when targeting therapeutics to combat cancer.[11] Conceivably, modifying the structure of the retro-HAs by means of molecular docking studies could yield molecules with greater HDAC inhibitory ability. To the best of our knowledge, retro-HAs seem to not have been tested to date for biomedical applications. Therefore, this valuable new information could be considered when researching for novel anticancer pharmaceuticals.

Moreover, compound **30**, which inhibited *h*HDAC8 more than 60% at 100 µM, was shown to be also produced via TK_{gst}-mediated catalysis in a laboratory proof of concept experiment. Because enzymes provide a vast variety of advantages,[12] this opens the enticing application of biocatalysts for the generation of retro-HAs with biomedical properties.

12. Experimental part

12.1. Reagents and devices

12.1.1. Generalities

Unless otherwise stated, reactions were stirred with a magnetic stirring bar at RT, which stands for room temperature and corresponds to 22-25 ºC. For reactions above 25 ºC, a polyethylene glycol oil bad was used, and when cooling down to 0 ºC was required, an ice-bad was used. When the solvent was removed "under reduced pressure", it was done at a rotary evaporator with a membrane pump for vacuum and a water bath at 40 ºC. After removal of the solvent, most compounds were frozen with liquid nitrogen and the remaining water was evaporated using a lyophilizer (freeze dryer). In some cases, the drying of the substances was done in high vacuum with an oil pump. Reactions under inert gas were performed applying argon gas from *Linde*. The devices and media used to work with microorganisms and DNA was previously autoclaved.

12.1.2. Chemicals

Commercial reagents were purchased commercially and used without further purification, except for 3-chloroaniline, 3-methylaniline, 3- chloro-4-methylaniline, 2-chloroaniline and 3-(trifluoromethyl)aniline which were distilled prior to use. The majority of the chemicals were purchased from *Sigma-Aldrich*, *Acros Organics*, *Alfa Aesar* and *TCI*. Other sources of supply of reagents: 4-nitroaniline and *N',N*-diisopropylcarbodiimide were obtained from *Fluka AG*, thiamine diphosphate and triethanolamine were provided by *AppliChem*, 4-(trifluoromethyl)aniline was given by *Riedel-de-Häen*, and lithium hydroxide was bought from *Grüssing*.

12.1.3. Solvents

Except as otherwise indicated, all solvents, including deuterated solvents, were commercially available and were used as received. When absolute DCM was required, it was dried over calcium chloride as drying agent and afterwards distilled over calcium hydride following a standard procedure.[329]

12.1.4. Mass spectrometry (MS)

Electrospray ionization **(**ESI) mass spectra were recorded with an *Impact II ESI-Q-TOF* spectrometer from *Bruker*, and electron ionization (EI) mass spectra were registered with a *Finnigan MAT 95* spectrometer.

12.1.5. Nuclear magnetic resonance (NMR) spectrometry

All samples were solved in deuterated solvents and measured in one of the following devices:

- *Bruker* 300 MHz Avance II: 300 MHz ^{1}H-NMR and 75.5 MHz ^{13}C-NMR
- *Bruker* 300 MHz Avance III: 300 MHz ^{1}H-NMR and 75.5 MHz ^{13}C-NMR, DEPT, ^{1}H-^{1}H-COSY, ^{1}H-^{13}C-HSQC, ^{1}H-^{13}C-HMBC
- *Bruker* 500 MHz DRX 500: 500 MHz ^{1}H-NMR, 125.8 MHz ^{13}C-NMR, DEPT, ^{1}H-^{1}H-COSY, ^{1}H-^{13}C-HSQC, ^{1}H-^{13}C-HMBC

All chemical shifts were normalized to the corresponding deuterated solvent peaks, relative to the tetramethylsilane standard (δ= 0 ppm), and are reported in ppm:

- D_2O: δ (^{1}H)= 4.79 ppm
- Acetone-d_6: δ (^{1}H)= 2.05 ppm, δ (^{13}C)= 29.84 ppm, 206.26 ppm
- DMSO-d_6: δ (^{1}H)= 2.50 ppm, δ (^{13}C)= 39.52 ppm
- Metanol-d_4: δ (^{1}H)= 3.31 ppm, δ (^{13}C)= 49.00 ppm
- $CDCl_3$: δ (^{1}H)= 7.26 ppm, δ (^{13}C)= 77.16 ppm

All coupling constants (*J*) are given in Hertz (Hz). For the assignment, s stands for singlet, d for doublet, t for triplet, q for quartet and m for multiplet. To evaluate the NMR spectra the software *MestReNova* was used.

12.1.6. Melting point range

The melting points were recorded on a SMP10 device from *Stuart* and have not been corrected.

12.1.7. UV/Vis-Spectra- Microplate reader

The UV/Vis measurements of 96-well-microplates were carried out in a *SPECTRAMAX 190* plate reader from *Molecular Devices*. The data evaluation was executed with the *SoftMax Pro 6.5.1* program. Except otherwise stated, the measurements were performed at a wavelength of λ= 562 nm for protein quantification with the bicinchoninic acid (BCA) method and λ= 500 nm for assay screening.

12.1.8. Other devices and materials

Instrument or material	**Manufacturer**
Centrifuges 5415D, 5804, 5810R	*Eppendorf*
Pipettes and multipipettes	*Eppendorf*
Vortexer, MS1 Minishaker	*IKA*
96-well microtiter plates flat-bottom	*Sarstedt*
96-well microtiter plates deep-bottom	*Sarstedt*
96-well microtiter plates round-bottom	*Sarstedt*
Acetate film for 96-well plates	*Sarstedt*
Thermomixer for incubation	*Eppendorf*
HPTLC applicator: TCL sampler ATS4	*CAMAG*
Microplates incubator 1000	*Heidolph*
Nickel column: HisTrap	*GE Healthcare*, Bio-Sciences AB

SDS-Gel electrophoresis	*Bio-Rad*, Mini Protean II
Ultrafiltration cell, Vivacell 250	*Stedim* Biotech AG Sartorius
Ultrasound bath RK52H	Sonorex
Autoclave	*Systec*, VX 150
Heating oven	*Heraeus*
Magnetic stirrer with heating function RCT basic	*IKA*
Thermometer ETS-D4 fuzzy	*IKA*
Heating gun HL 1810 S	*Steinel* Vertrieb GmbH
Preparative flash-system/with UV and ELS detector	*Teledyne* ISCO, CombiFlash EZ Prep
Rotary evaporator R-114	*Büchi*
Water bath rotary evaporator B-480	*Büchi*
Balance AS60/220.R2	*Radwag*
Titrator TitroLine® 7000	*SI Analytics*
Hybond-N-membrane 0.45 µm RPN.303N	*Amersham*
Filter paper (90 mm) (solid-phase supported assay)	*Macherey-Nagel*
Replica plater	TU Darmstadt

12.1.9. Cells, culture media, buffers and other molecular biology materials

***E. coli* BL21 (DE3) cells** from *New England BioLabs*

The *E. coli* BL21 (DE3) strain was utilized for protein expression. Genotype: fhuA2 [lon] ompT gal (λ DE3) [dcm] ΔhsdS λ DE3 = λ sBamHIo ΔEcoRIB int::(lacI::PlacUV5::T7 gene1) i21 Δnin5

Auto-induction (AI)-Medium

The AI-medium is employed for protein expression cultures. The following substances are dissolved in deionized (DI)-water:

Tryptone	10 g/L
Yeast extract	5 g/L
NH_4Cl	2.68 g/L
Na_2SO_4	0.71 g/L
Glycerol (85%)	5.88 g/L
Glucose	0.50 g/L
Lactose	2 g/L

The solution is autoclaved. After cooling to room temperature and prior to use, the following sterile and filtered solutions have to be added:

$MgSO_4$ (2 M)	1 mL/L
K_2HPO_4 (1 M)	40 mL/L
KH_2PO_4 (1 M)	10 mL/L
Trace metal solution	1 mL/L

Trace metal solution (in 0.1 M HCl)

It contains a combination of metal salts for preparing the AI-Medium.

$FeCl_3$	50 mM
$CaCl_2$	20 mM
$MnCl_2$	20 mM
$ZnSO_4$	10 mM
$CoCl_2$	2 mM
$CuCl_2$	2 mM
$NiCl_2$	2 mM

Luria-Bertani (LB)-Medium

Rich medium extensively utilized for culturing *E. coli* cells. The following substances are dissolved in DI-water:

Yeast extract	5 g/L
Peptone	10 g/L
NaCl	5 g/L

The pH value is adjusted to 7.4 and the solution is autoclaved.

* For the cell culture media AI and LB, antibiotics were added prior to bacteria cultivation. For TK_{gst} cultivations, kanamycin was added to give a final concentration of 30 µg/mL.

Phosphate wash-buffer 20 mM, pH 7.4

Buffer solution used in protein purification

$NaPO_4$	20 mM
NaCl	0.5 M

Imidazol IMAC buffer, pH 7.4

Buffer solution employed in protein purification

$NaPO_4$	20 mM
NaCl	0.5 M
Imidazole	30 mM

SDS-PAGE loading buffer

Buffer solution utilized for sample preparation for SDS electrophoresis

Tris/HCl (1 M stock, pH 6.8)	0.5 M
Glycerol	20%
SDS	10%
Bromophenol blue (2% in EtOH)	0.005%

EDTA (from 0.5 M solution)	50 mM

SDS-PAGE buffer

Buffer solution utilized for SDS electrophoresis

TRIS	3 g/L
Glycine	14 g/L
SDS	1 g/L

SDS-PAGE-gel (polyacrylamide gel) composition

TRIS (760 mM, pH 7.4)	1 mL
Serine (1 M, pH 7.4)	1 mL
Glycine (1 M, pH 7.4)	1 mL
Asparagine	132 mg
Acrylamide (30%)	2.75 mL
Bis-acrylamide (2%)	APS (10%)
TEMED	10 µL
DI-Water	3 mL

TEA buffer 50 mM, pH 7.45

Buffer action between pH 7.0-8.3. Used also for dilutions (2 mM, 5 mM, 10 mM and 25 mM)

TEA	7.5 g/L

Glycylglycine buffer 50 mM, pH 7.45

Buffer action between pH 7.5-8.9. Used also for dilutions (2 mM, 5 mM, 10 mM and 25 mM)

Glycylglycine	6.6 g/L

Phosphate assay-buffer 50 mM, pH 7.45

Buffer action between pH 5.8-8.2. Used also for dilutions (2 mM, 5 mM, 10 mM and 25 mM)

KH_2PO_4 (1 M solution)	9.4 mL/L
K_2HPO_4 (1 M solution)	40.6 mL/L

HEPES buffer 50 mM, pH 7.45

Buffer action between pH 6.8-8.2. Used also for dilutions (2 mM, 5 mM, 10 mM and 25 mM)

HEPES	11.9 g/L

TRIS buffer 50 mM, pH 7.45

Buffer action between pH 7.0-9.0. Used also for dilutions (2 mM, 5 mM, 10 mM and 25 mM)

TRIS	6 g/L

12.2. Standard operating procedures (SOPs)

12.2.1. Laboratory techniques

SOP 1: Thin layer chromatography (TLC)

For the analysis of the reaction progress by TLC, silica gel coated aluminium plates from *Merck KGaA*, Darmstadt, were used (silica gel 60 with Fluorescence indicator UV_{254}). The detection was done under UV-light (λ= 254 nm), and by dipping the TLC-plates in the corresponding staining solutions. If there was no coloration appearing, the TLC-plates were heated by means of a heating gun. The specified solvent mixtures correspond to volume ratios. If not otherwise noted, the following staining reagents were used:

- Anisaldehyde: 200 mL EtOH (abs.), 7.5 mL H_2SO_4 (conc.), 2.2 mL AcOH, 5.5 mL 4-anisaldehyde (4-methoxybenzaldehyde).
- Ninhydrin: 0.6 g ninhydrin, 200 mL *n*-Butanol, 6.0 mL AcOH.
- Potassium permanganate: 1.0 g $KMnO_4$, 5 g K_2CO_3, 1.75 mL NaOH 1 M, 100 mL H_2O
- Ferric chloride: 1 g of $FeCl_3$ in a 50% aqueous methanol mixture (100 mL total volume)

TLC can also be utilized on a small semi-preparative scale to separate mixtures up to 100 mg. In this case, the mixture is applied to the plate as an even thin layer horizontally about 1.2 cm from the bottom of the plate. Once developed with the solvent, the compounds separate in horizontal bands that can be scratched from the TLC plate. The general protocol is represented in Figure 12.1.

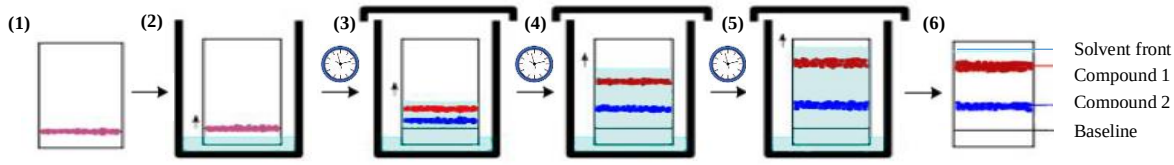

Figure 12.1. General protocol for preparative TLC. (1) The sample is applied evenly to the TLC plate as a very thin layer (pink). (2) The TLC plate is introduced in a chamber containing the mobile phase (mixture of solvents), and it is left until the solvent almost reached the top of the plate (3-4). (5) The TLC plate is removed from the chamber and the front of the solvent is marked with pencil for later calculation of the *Rf*. (6) The separated bands are observed under UV or by staining a small part of the plate, and the desired product is scratched off the plate.

For preparative TLC, the sample was dissolved in around 200 µL of an appropriate solvent (acetone or ethyl acetate) and carefully added to the baseline of the TLC plate (20x15 cm) by means of a 200 µL pipette. The TLC was placed inside a chamber containing the mobile phase and left to run for usually 30-45 minutes. The front of the solvent is marked with pencil for later calculation of the R_f. Once dried, the product band (visualized by UV or by staining a small part of the plate) was scratched from the TLC plate by means of a spatula and isolated. To the resulting silica gel mixture EtOAc or acetone were added while shaking for 30 minutes to extract the product from the silica. The solid was filtered and washed with EtOAc until no more product came out (monitored by spot TLC), followed by a short centrifugation in 1 mL Eppendorf tubes. The solution from the tubes was transferred to a round-bottom flask without

surpassing half of its capacity, and the precipitate was discarded. The solvent was removed under reduced pressure to afford the desired product.

SOP 2: Gravity column chromatography

The purification by column chromatography was carried out over silica gel with a particle size of 0.060-0.200 mm from *Acros Organics*. The solvent mixtures noted correspond to volume ratios. Unless otherwise indicated, the column was packed by dissolving the silica gel in cyclohexane or dichloromethane and stirring until homogeneous and gas-free. In most cases, the product was dissolved in EtOAc, silica was added and the solvent was removed under vacuum, leaving the product bound to silica which was then added to the column in a dry-load fashion. In some exceptional cases, in which the product was soluble in the less polar solvent, a "wet-load" column was performed, where the product was dissolved in a small amount of apolar solvent and added directly to the packed column. A solvent gradient starting from non-polar to polar was applied until the complete elution of substances.

SOP 3: Flash column chromatography

The purification by flash column chromatography was performed over silica gel 60 with a particle size of 0.04-0.063 mm from *Roth*. The column was manually packed by subsequently adding small portions of dry silica upon bouncing the column after each addition to assure a dense packing. The apolar solvent was added to condition the column and then the product was subjected onto the precolumn as dry load on silica. Then, the elution was started and monitored by means of the CombiFlash software. The fractions containing the product were detected via UV and automatically collected.

SOP 5: Column chromatography with microcolumn

A Pasteur pipette with a short tip is provided with a piece of cotton wool and filled with dry silica gel of particle size 0.04-0.063 mm. The sample to be purified is absorbed on silica gel and added to the silica gel in the Pasteur pipette as a horizontal layer. Finally, the top layer is covered with a small layer of sea sand. The solvent is then added directly to the dry column using a glass funnel as the solvent reservoir.

SOP 6: High performance liquid chromatography (HPLC)

HPLC data were recorded using a HPLC system from *Shimadzu* LC-20AT with an SPD-M20A UV diode array detector. The mobile phase consisted on a mixture of acetonitrile-water with 0.1% of formic acid. A XBridge C18 from *Waters* was used as the HPLC column (pore size: 3.5 µm, length: 150 mm, diameter: 3.0 mm). Unless mentioned otherwise, the method most commonly used was a gradient starting from 10% of acetonitrile until 95% with a flow rate of 0.5 $mL \cdot min^{-1}$ in 26 min. Reaction samples were directly analyzed after dilution in EtOAc, DCM or MeOH (25-50 µL of sample in 1 mL of solvent), and removal of precipitates via filtration or

centrifugation. Detection was performed in general at 215 nm, and particularly at 254 nm for HAs and 320 nm for nitrosoarene compounds.

SOP 7: Lyophilization

The lyophilization from samples was carried out in a lyophilizer of the *LyoQuest* type from *Telstar*. Residual water was removed from products, as well as from enzymes by a freeze-drying procedure utilizing a lyophilizer. For this, the sample containing rests of water was immersed into liquid nitrogen upon continuous movement. Once the sample was uniformly frozen, it was placed onto the lyophilizer for a minimum of 48 h.

SOP 8: Purification with activated charcoal

The crude product was dissolved in methanol and activated charcoal was added. The solution was stirred at 40 ºC for 30 minutes. Afterwards, the activated charcoal was filtered off, washed with more methanol, and the product was collected after solvent evaporation under reduced pressure.

12.2.2. Molecular biology techniques

SOP 9: Melting temperature (T_m) measurement with nanoDSF

To measure the stability of the TK_{gst} variants against thermal unfolding, the Prometheus NT.48 instrument from *NanoTemper Technologies* was employed. The protein solutions were prepared by dissolving 1 mg of enzyme in 1 mL of TEA buffer (5 mM or 50 mM). 10 µL of samples were introduced in the glass capillaries, which were then placed in the sample holder. A melting scan method with a temperature gradient of 1 ºC/min ranging from 20 ºC to 110 ºC was chosen, and the change in the protein fluorescence was monitored at 330 and 350 nm.

SOP 10: SDS-PAGE GEL (Sodium dodecyl sulfate-polyacrylamide gel electrophoresis)

For the qualitative analysis of protein samples SDS-PAGE can be utilized. This method is based on the separation of the proteins by their molecular weight on a polymer gel. For this purpose, acylamide/bis-acrylamide gels (10%) were employed. The preparation of the samples was carried out by homogenizing the protein suspensions (20 µL) in SDS-PAGE loading buffer (20 µL, 5% dithiothreitol (2M)) in an Eppendorf tube. Subsequently, the proteins were placed inside a heat block at 95 ºC for 5 min for denaturation via heat shock treatment. Then, the denatured protein mixtures (10 µL) were applied into the wells of the polyacrylamide gel together with a protein marker as weight reference (Blue Prestained Protein Standard, Broad Range, *NEB*). SDS-PAGE-buffer was utilized to fill the electrophoresis chamber, which was then subjected to an electric field of 200 V for 30-45 min until the bromophenol blue band had reached the bottom of the gel. After the appropriate time, the gel was submerged in a solution of *Coomasie Brilliant Blue* dye (75 mg *Coomasie G250 Brilliant Blue* in 1 L of H_2O) for visualization of the

protein bands, and it was microwaved for 30 sec. Finally, the gel was placed on a shaker at room temperature until a sufficient staining of the protein bands was observable. The staining solution was removed, the gel was covered with water and heated for 30 sec again. The gel was allowed to shake at room temperature in the water bath until the background color had diminished and well appreciable bands were observed. To quantify the gels from the assay the computer software ImageJ was used.

SOP 11: Qualitative protein analysis with the Bradford-test

During protein purification by IMAC, the Bradford-test was employed as quick analytical proof of residual protein in eluted fractions. When the dye Coomassie Brilliant Blue G-250 binds to the protein, an absorbance shift is generated which can be observed by the blue color achieved. For this analytical assessment, the eluting fraction (1-10 µL) was pipetted to a solution of Bradford-reagent (50 µL, 1:4 diluted in DI-water, *Bio-Rad*) on a ceramic spot plate. If blue color appears, protein is still present.

SOP 12: Quantitative protein analysis with Bicinchoninic acid (BCA) assay

The Bicinchoninic acid (BCA) assay is a colorimetric biochemical assay used for the accurate analysis of total protein concentration in a solution. This analytical procedure relies on two reactions. First, copper(II)sulfate is reduced by the peptide bonds in the protein releasing Cu^{+1}, which is then chelated by two molecules of BCA forming a purple-colored complex. The concentration of protein present can be quantified by its absorbance at 562 nm.

The BCA assay was operated by using and following the instructions of a commercial kit from *Thermo Scientific*: A standard curve of BSA protein in TEA (2 mM) buffer was prepared by performing a dilution series in triplicate with aqueous bovine serum albumin (BSA) (1 mg BSA/mL, 0.15 M NaCl, 0.05% sodium azide) as represented in Table 12.1. To a flat-bottom 96-well microtiter plate 25 µL of the dilution series previously prepared are added.

Table 12.1. Dilution series of BSA stock

Concentration (µg/mL)	0	200	400	600	800	1000
Volume (BSA) (µL)	0	20	40	60	80	100
Volume (buffer) (µL)	100	80	60	40	20	0

Then, the protein samples were obtained by dissolving 1 mg/mL of proteins in TEA (2 mM) buffer, and adding 25 µL of each to the empty wells from the 96-well plate in triplicate. The BCA working reagent was prepared by mixing the BCA solution with copper(II) sulfate solution in a ratio 50:1. Finally, the latter (200 µL per well) was added to the 96-well plate, which was sealed with acetate foil and shaken at 37 ºC for 30 min. After the incubation time, foil was removed and absorbance was measured at 562 nm by means of a plate reader.

SOP 13: Miniprep for isolation and purification of plasmid DNA for sequencing

For extraction of plasmid DNA, the commercial GenElute Plasmid Miniprep Kit from *Sigma-Aldrich* was utilized following the instructions from the manufacturer. The protocol is based on alkaline lysis. An overnight culture of *E. coli* (3 mL) was centrifuged at 12000 x g for 1 min and the supernatant was removed. After resuspending the pellet in the residual medium, lysis buffer (200 µL) was added and the vessel was inverted 6-8 times for good mixing. Afterwards, the mixture was incubated at room temperature for 3-5 minutes until the solution became clear. Then, neutralizing buffer (350 µL) was added and the tube was gently inverted 3-4 times. The mixture was centrifuged at 12000 x g for 10 min to remove cell debris. The supernatant (500 µL) was subsequently loaded onto a miniprep binding column, which was placed inside a microcentrifuge tube, and was centrifuged again at 12000 x g for 1 minute. The flow-through of the mini column was discarded and two washing steps followed (500 µL and 750 µL of wash solution, respectively), with in between two corresponding centrifugations (12000x g for 1 min, each). Afterwards, the binding column was transferred to a clean collection tube. The elution buffer (30 µL) was then applied and the mixture was centrifuged at 12000 x g for 1 min. The attained plasmid was directly used for DNA sequencing.

Expression and purification of TK_{gst} variants

SOP 14: Protein expression (large scale)

To a sterile Erlenmeyer baffled flask filled with AI-medium kanamycin (1 mL/L) and antifoam emulsion (1 mL/L) were added. Subsequently, inoculation of the mixture with cells by means of a sterilized toothpick was performed, and the flask was loosely closed with lids made out of aluminium foil for aeration. Then, the flask was left to incubate in a shaker at 37 ºC/30 ºC and 210 rpm for 16-18 hours. Afterwards, the mixture was centrifuged at 12000 g for 30 min, followed by removal of the supernatant. Finally, the cell pellets were stored at -20 ºC prior to lysis.

SOP 15: Cell lysis (large scale)

The cell pellets were thawed and resuspended in phosphate buffer (20 mM, pH 7.5, 200 mL/L culture), followed by addition of lysozyme (0.5 mg/mL pellet suspension) and DNAse (1 µL/mL pellet suspension from DNAse stock solution of 1 mg/mL). The suspension was stirred at 37 ºC for 1 h. Afterwards, a NaCl solution (5 M, 200 µL/mL) and subsequently phosphate wash-buffer (800 µL/mL) were added. Finally, the resulting cell suspension was centrifuged at 4000 g for 45 min and the supernatant was collected and purified by affinity chromatography or heat shock treatment.

SOP 16: Protein purification by immobilized metal affinity chromatography (IMAC)

IMAC can be used to purify recombinant proteins carrying a terminal sequence of polyhystidines (His-tag). This is possible due to the ability of histidine to strongly chelate metal ions such as nickel. First, the nickel-affinity column was equilibrated with phosphate wash-buffer. Then, to the cell supernatant a solution of imidazole (5 M) was added until a final concentration of 30 mM prior to column loading. The column was washed with 10 column volumes of first imidazole IMAC buffer and afterwards phosphate wash-buffer. The target protein was eluted with phosphate wash-buffer containing chelating agent EDTA (50 mM) until no more protein eluted (verified via Bradford-test). Finally, the buffer was exchanged to TEA buffer (2 mM, pH 7.5), concentrated by ultrafiltration, and the solution containing the desired enzyme was freeze-dried to yield the pure protein powder. After washing the column with 10 column volumes of phosphate wash-buffer containing NaCl (0.5 M) to remove EDTA, it was charged with 1 column volume of $NiSO_4$-solution (100 mM) for regeneration and then with 5 column volumes of phosphate wash-buffer.

12.3. Experiments Chapter I

SOP 17 for the HPTLC Experiments

For visualizing all isolated *N*-aryl HA in the same TLC plate under exactly the same conditions, the retro-HA were dissolved in EtOAc (3 mg/mL) and were submitted to an HPTLC auto-sampler. The device was programmed for spraying 7 mm bands with 5 µL of samples on two HPTLC silica plates (20 x 7 cm). The plates were developed in a solution of CH/EtOAc 1:4, carefully dried by an air flow, and stained by dipping either into the staining agent ferric chloride or anisaldehyde. The same HA-solutions were used for the ferric chloride discontinuous assay.

12.3.1. Qualitative discontinuous assay with ferric chloride

The discontinuous ferric chloride liquid-method for the HA product verification directly after reaction or with pure products, was performed by mixing equal quantities of the reaction mixture or the pure product solutions in MeOH (50 µL) with aqueous $FeCl_3$ (50 µL, 0.5% w/v).

12.3.2. Analytical scale reactions

Reactions were carried out in an analytical volume of 500 or 1000 µL in Eppendorf vessels with acceptor (nitrosoarene) and donor (HPA or PA) concentrations of 50 mM, TK_{gst} N/S (0.2 mg/mL) for HPA reactions or TK_{gst} L/S (0.6 mg/mL) for PA reactions, cofactors ThDP (2.4 mM) and Mg^{2+} (9 mM), DMSO (20%), and TEA buffer (50 mM, pH 7.45). Control reactions each in the absence of acceptor, donor, or the TK_{gst} variant were incubated in parallel. The reactions were left to shake at RT and samples were extracted and analyzed by HPLC, *via* discontinuous ferric chloride liquid-method or by TLC staining with $FeCl_3$.

12.3.3. Synthesis protocols and characterization of compounds

12.3.3.1. Synthesis of hydroxypyruvate

Synthesis of bromopyruvate.

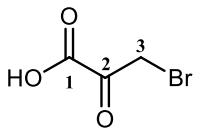

Yield: 266.60 g (1.60 mol, 93%).

In a 500 mL flat flange reactor, pyruvic acid (95%, 151 g, 121 mL, 1.72 mol, 1 eq.) were dissolved at ambient temperature in 150 mL of previously dried DCM. Twelve drops of sulfuric acid were added and the solution is heated to 70 °C by means of an oil bath whilst stirring with a KPG-stirrer. Then, bromine (265.2 g, 85 mL, 1.66 mol, 1 eq.) was added through a dropping funnel over a time span of 2 h. The NaOH in the connected gas washing bottles must be changed at least once. After the bromine addition was completed, the solution was left stirring for

another 30 min and then cooled in an ice bath overnight to precipitate the product. Afterwards, 14 mL of cyclohexene and 70 mL of dried petroleum ether were added to the reaction mixture at room temperature, after which the reactor was cooled again in an ice bath. The solvent was removed by filtration. Hereafter, the sand-colored solid was washed with 100 mL of cold, dried petroleum ether. The product was dried in a desiccator over NaOH pellets under vacuum for 5 days. The drying agent has to be exchanged several times. 3-Bromopyruvic acid was obtained as a yellowish-white powder and was stored at -18 ºC. ^{1}H-NMR (300 MHz, D_2O, 300 K): δ = 3.58 (s, 2 H, 3-H); ^{13}C-NMR (75 MHz, D_2O, 300 K): δ = 172.21 (C-2), 92.76 (C-1), 35.44 (C-3).

Synthesis of hydroxypyruvate (HPA).

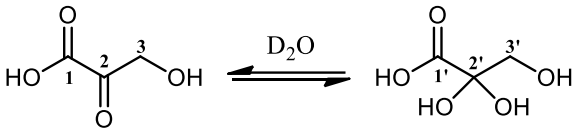

HPA was synthesized as its lithium salt based on *Dickens and Williamson*.[112] **Yield:** 10.80 g (98.18 mmol, 55%).

In a 1L 2-neck flask attached to a dropping funnel, bromopyruvate (30 g, 0.18 mol; 1 eq.) was dissolved in 300 mL of deionized H_2O and 3 drops phenolphthalein (0.5% in ethanol) were added. LiOH-hydrate (56%, 21.38 g, 0.50 mol) was also dissolved in 500 mL of deionized H_2O and 360 mL were dropped slowly over the former solution at RT. The pH value was controlled with a pH-Stat device, and the addition was stopped when the pH-value stayed 10 min constant at pH 8, being fundamental that the pH does not rise above 8.9. Then, 2 g of activated charcoal were added to the reaction mixture and filtrated. The pH of the filtrate was adjusted to 5 by the addition of acetic acid. Afterwards, the volume of the filtrate was reduced under vacuum to a volume of 60-65 mL until the solution became turbid and light-yellow crystals appeared. The mixture was left under inert atmosphere at 4 ºC overnight to complete crystallization. The crystals were collected by filtration, washed with cold ethanol, and then suspended in ethanol at 40 ºC for 30 min. Furthermore, the product was filtrated and washed with cold ethanol again, affording a white powder which was dried over $CaCl_2$ or P_2O_5 in a desiccator under vacuum overnight. Finally, HPA-lithium salt was obtained as a colorless powder. ^{1}H-NMR (500 MHz, D_2O): δ = 4.73 (s, 2H, 3-H), 3.68 (s, 2H, 3'-H); ^{13}C-NMR (126 MHz, D_2O): δ = 202.63 (C-2), 176.62 (C-1'), 167.52 (C-1), 94.37 (C-2'), 66.13 (C-3), 65.42 (C-3').

12.3.3.2. Synthesis of nitrosoarenes

Compounds **5b**, **5n** and **5o** have been synthesized according to the procedure described by Priewisch *et al.*[203] and they are in agreement with the literature spectroscopic properties; compound **5m** was prepared following another similar literature protocol[330] and the properties are in accordance with the literature as well. The rest of the compounds were achieved by adapting the procedure from Priewisch *et al.*[203] to each case and the spectroscopic properties of the substances **5c**[331], **5d**[332], 5**g**[331], **5h**[332], **5i**[331], **5j**[321], and **5k**[333] and **5e**[334] are in agreement with the properties already reported in the literature. To the best of our knowledge,

compounds **5f** and **5l** were previously not described. All compounds were synthesized with a purity of 80-90% and were used without further purification.

SOP 18 for the synthesis of nitrosoarenes

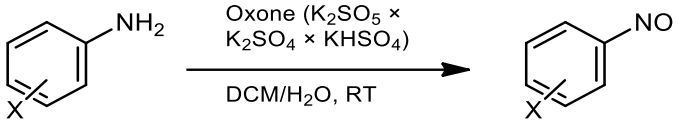

The corresponding aniline (1.0 eq.) was dissolved in DCM. To this solution, Oxone (K_2SO_5 × K_2SO_4 × $KHSO_4$) (2.0-4.5 eq.) dissolved in deionized H_2O was added dropwise. The solution was stirred under argon atmosphere at RT until complete consumption of starting material. Once the reaction was finished, saturated $NaHCO_3$ solution (80 mL) was added slowly and the mixture was extracted three times with DCM. The combined organic layers were washed first with 1M HCl (40 mL), then with brine solution (50 mL) and afterwards dried over $MgSO_4$. The solvent was removed under reduced pressure at 30 ºC. Exact quantities of reagents and solvents are specified in each compound description separately.

1-Bromo-4-nitrosobenzene (5b).

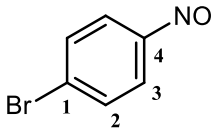

Yield: 130 mg (0.53 mmol, 54%).

Melting point: 86-88 ºC (lit.[335] 95 ºC).

TLC (4:1 CH/EA): R_f: 0.84

According to the general procedure, 2.5 g (14.53 mmol, 1 eq.) of 4-bromoaniline in 45 mL of DCM were mixed with 20.0 g (65.06 mmol, 4.5 eq.) of Oxone dissolved in 200 mL of deionized H_2O. Compound **5b** was isolated as a yellow solid. ^{1}H-NMR (300 MHz, $CDCl_3$): δ 7.77 (s, 4H, H-2, H-3); ^{13}C-NMR (75 MHz, $CDCl_3$): δ 163.83 (C-4), 132.69 (C-2), 131.67 (C-1), 122.10 (C-3).

1-Chloro-4-nitrosobenzene (5c).

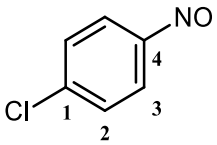

Yield: 2.80 g (19.78 mmol, 94% yield).

Melting point: 82-84 ºC (lit.[335] 92-93 ºC).

TLC (10:1 CH/EA): R_f: 0.60

According to the general procedure, 3.0 g (21.19 mmol, 1 eq.) of 4-chloroaniline in 75 mL of DCM were mixed with 15 g (48.80 mmol, 2.3 eq.) of Oxone dissolved in 296 mL of deionized H_2O. Compound **5c** was isolated as a dark yellow solid. Column chromatography on silica gel (CH/EA 50:1) resulted in partial decomposition of the product. ^{1}H-NMR (300 MHz, $CDCl_3$): δ 7.88 – 7.82 (m, 1H, H-3), 7.63 – 7.56 (m, 1H, H-2). ^{13}C-NMR (75 MHz, $CDCl_3$): δ 163.75 (C-4), 142.46 (C-1), 129.67 (C-2), 122.14 (C-3).

1-Chloro-3-nitrosobenzene (5d).

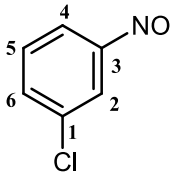

Yield: 3.28 g (23.17 mmol, 80% yield).

Melting point: 66-68 ºC (lit.[336] 72 ºC).

TLC (6:1 CH/EA): R_f: 0.55

According to the general procedure, 3.7 g (3.0 mL, 28.69 mmol, 1 eq.) of 3-chloroaniline in 180 mL of DCM were mixed with 26.4 g (85.04 mmol, 3 eq.) of Oxone dissolved in 120 mL of deionized H_2O. Compound **5d** was isolated as a dark yellow solid. ^{1}H-NMR (500 MHz, $CDCl_3$): δ 8.05 (ddd, ^3J = 7.8, ^4J = 1.8, ^4J =1.2 Hz, 1H, H-4), 7.69 (ddd, ^3J = 7.9, ^4J = 2.1, ^4J = 1.2 Hz, 1H, H-6), 7.65 – 7.59 (m, 2H, H-2, H-5); ^{13}C-NMR (126 MHz, $CDCl_3$): δ 165.06 (C-3), 136.03 (C-1), 134.93 (C-6), 130.70 (C-5), 121.36 (C-4), 118.75 (C-2).

1-Chloro-2-nitrosobenzene (5e).

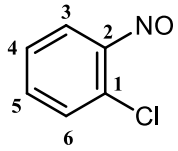

Yield: 3.61 g (25.50 mmol, 89%).

Melting point: 63-65 ºC (lit.[334] 64.5-65.5).

TLC (4:1 CH/EA): R_f: 0.70

According to the general procedure, 3.6 g (3.0 mL, 28.52 mmol, 1 eq.) of 2-chloroaniline in 230 mL of DCM were mixed with 26.1 g (85.04 mmol, 3 eq.) of Oxone dissolved in 120 mL of deionized H_2O. Compound **5e** was isolated as a dark green solid. ^{1}H-NMR (300 MHz, $CDCl_3$): δ 7.80 (dd, ^3J = 8.0, ^4J =1.2 Hz, 1H, H-3), 7.69 – 7.60 (m, 1H, H-4), 7.31 – 7.20 (m, 1H, H-5), 6.25 (dd, ^3J = 8.1, ^4J =1.7 Hz, 1H, H-6); ^{13}C-NMR (75 MHz, $CDCl_3$): δ 161.36 (C-2), 143.16 (C-1), 137.14 (C-5), 132.68 (C-6), 127.16 (C-4), 109.21 (C-3); MS (APCI): m/z calculated for $[C_6H_4ClNO]+H^+$ = 142.004, found 142.005.

1-Methyl-4-nitrosobenzene (5g).

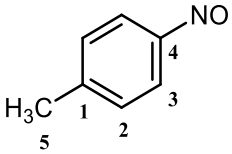

Yield: 2.65 g (21.87 mmol, 78% yield).

TLC (5:1 CH/EA): R_f: 0.48

According to the general procedure, 3.0 g (28.00 mmol, 1 eq.) of 4-methylaniline in 180 mL of DCM were mixed with 26.14 g (85.04 mmol, 3 eq.) of Oxone dissolved in 120 mL of deionized H_2O. Compound **5g** was isolated as a as a pale brown solid. ^{1}H-NMR (500 MHz, $CDCl_3$): δ 7.80 (d, ^3J = 8.2 Hz, 2H, H-2), 7.38 (d, ^3J = 8.0 Hz, 2H, H-3), 2.44 (s, 3H, H-5); ^{13}C-NMR (126 MHz, $CDCl_3$): δ 165.60 (C-4), 147.20 (C-1), 129.73 (C-2), 121.24 (C-3), 21.92 (C-5).

1-Methyl-3-nitrosobenzene (5h).

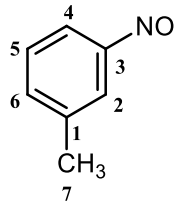

Yield: 3.32 g (27.41 mmol, 98% yield).

TLC (6:1 CH/EA): R_f: 0.56

According to the general procedure, 3.0 g (3.0 mL, 28.00 mmol, 1 eq.) of 3-methylaniline in 180 mL of DCM were mixed with 26.1 g (85.04 mmol, 3 eq.) of Oxone dissolved in 120 mL of deionized H_2O. Compound **5h** was isolated as a dark yellow solid. ^{1}H-NMR (300 MHz, $CDCl_3$): δ 7.77 (dt, ^3J = 6.7, ^4J = 2.1 Hz, 1H, H-4), 7.63 (s, 1H, H-2), 7.57–7.46 (m, 2H, H-5, H-6), 2.50 (s, 3H, H-7); ^{13}C-NMR (75 MHz, $CDCl_3$): δ 166.26 (C-3), 139.44 (C-1), 136.21 (C-6), 129.08 (C-5), 120.84 (C-2), 119.00 (C-4), 21.14 (C-7).

1,2-Dichloro-4-nitrosobenzene (5f).

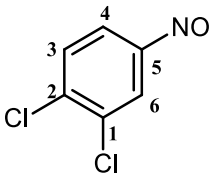

Yield: 2.97 g (16.87 mmol, 91% yield).

Melting point: 84-87 ºC (lit.[337] 88 ºC).

TLC (5:1 CH/EA): R_f: 0.64

According to the general procedure, 3.0 g (18.52 mmol, 1 eq.) of 3,4-dichloroaniline in 285 mL of DCM were mixed with 40.0 g (130.13 mmol, 7 eq.) of Oxone dissolved in 190 mL of deionized H_2O. Compound **5f** was isolated as an ochre solid. ^{1}H-NMR (500 MHz, $CDCl_3$): δ 7.88 (dd, ^3J = 8.4, ^4J = 2.2 Hz, 1H, H-5), 7.85 (d, ^4J = 2.1 Hz, 1H, H-3), 7.75 (d, ^3J = 8.4 Hz, 1H, H-6); ^{13}C-NMR (126 MHz, $CDCl_3$): δ 161.86 (C-4), 139.49 (C-1), 133.54 (C-2), 130.45 (C-6), 120.60 (C-3), 119.66 (C-5); HRMS (EI): m/z calculated for $[C_6H_3Cl_2NO]^+$ = 174.9586, found 174.9585.

1-Chloro-2-methyl-4-nitrosobenzene (5i).

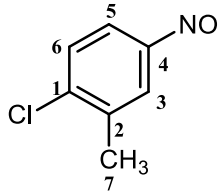

Yield: 3.01 g (19.35 mmol, 91% yield).

Melting point: 66-69 ºC (lit.[338] 73-74 ºC).

TLC (4:1 CH/EA): R_f: 0.84

According to the general procedure, 3.0 g (21.21 mmol, 1 eq.) of 4-chloro-3-methylaniline in 300 mL of DCM were mixed with 50.0 g (162.70 mmol, 7.7 eq.) of Oxone dissolved in 300 mL of deionized H_2O. Compound **5i** was isolated as a dark yellow solid. ^{1}H-NMR (500 MHz, $CDCl_3$): δ 7.78 (d, ^4J = 1.8 Hz, 1H, H-3), 7.67 (dd, ^3J = 8.4, ^4J = 2.3 Hz, 1H, H-5), 7.58 (d, ^3J = 8.4 Hz, 1H, H-6), 2.53 (s, 3H, H-7); ^{13}C-NMR (126 MHz, $CDCl_3$): δ 164.13 (C-4), 142.60 (C-1), 137.68 (C-2), 130.01 (C-6), 123.36 (C-5), 119.32 (C-3), 20.16 (C-7).

2-Chloro-1-methyl-4-nitrosobenzene (5j).

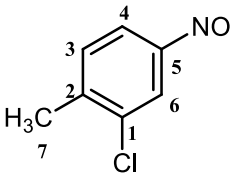

Yield: 2.67 g (17.16 mmol, quantitative yield).

Melting point: 57-59 ºC (lit.[321] 66-68 ºC).

TLC (4:1 CH/EA): R_f: 0.80

According to the general procedure, 3.0 g (2.60 mL, 21.40 mmol, 1 eq.) of 3-chloro-4-methylaniline in 260 mL of DCM were mixed with 56.6 g (184.1 mmol, 8.6 eq.) of Oxone dissolved in 312 mL of deionized H_2O. Compound **5j** was isolated as a dark yellow solid. ^{1}H-NMR (300 MHz, $CDCl_3$): δ 7.89 (dd, ^3J = 8.0, ^4J = 2.0 Hz, 1H, H-5), 7.69 (d, ^4J = 1.9 Hz, 1H, H-3), 7.50 (d, ^3J = 8.0 Hz, 1H, H-6), 2.46 (s, 3H, H-7); ^{13}C-NMR (75 MHz, $CDCl_3$): δ 164.93 (C-4), 144.56 (C-2), 135.84 (C-1), 131.55 (C-6), 120.80 (C-3), 120.01 (C-5), 20.70 (C-7).

1-Nitroso-3-(trifluoromethyl)benzene (5l).

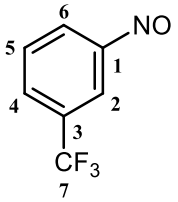

Reaction yield: 2.44 g (13.93 mmol, 70%).

Melting point: 65-67 ºC.

TLC (4:1 CH/EA): R_f: 0.78

According to the general procedure, 3.2 g (20.02 mmol, 1 eq.) of 3-(trifluoromethyl)aniline in 33 mL of DCM were mixed with 30.0 g (97.60 mmol, 4.9 eq.) of Oxone dissolved in 158 mL of deionized H_2O. Compound **5l** was isolated as an ochre powder. For further purification, sublimation of the crude product (1.2 g) was performed in a cooling finger, which was heated in an oil bath at 60 ºC. A blue powder was obtained with a purity of 90% (450 mg, 46% yield). ^{1}H-NMR (500 MHz, $CDCl_3$): δ 8.08 – 8.01 (m, 2H, H-2, H-6), 7.90 (d, ^3J = 7.8 Hz, 1H, H-4), 7.72 (t, ^3J = 8.1 Hz, 1H, H-5); ^{13}C-NMR (126 MHz, $CDCl_3$): δ 163.85 (C-1), 131.32 (C-3), 130.28 (C4, C-5), 123.81 (C-6, C-7), 117.49 (C-2); HRMS (EI): m/z calculated for $[C_7H_4F_3NO]^+$ = 175.0240, found 175.0239.

4-Nitroso-1-(trifluoromethyl)benzene (5k).

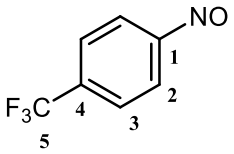

Yield: 0.57 g (3.25 mmol, 74%).

Melting point: 43-45 ºC.

TLC (4:1 CH/EA): R_f: 0.87

According to the general procedure, 0.70 g (0.55 ml, 4.34 mmol, 1 eq.) of 4-(trifluoromethyl)aniline in 11 mL of DCM were mixed with 10.0 g (32.53 mmol, 4.87 eq.) of Oxone dissolved in 53 mL of deionized H_2O. Compound X was isolated as an orange solid. ^{1}H-NMR (300 MHz, $CDCl_3$): δ 8.00 (d, ^3J = 8.3 Hz, 2H, H-2), 7.92 (d, ^3J = 8.6 Hz, 2H); ^{13}C-NMR (75 MHz, $CDCl_3$): δ 164.06 (C-1), 126.91 (C-3), 125.69 (C-4), 123.04 (C-5), 120.80 (C-2).

1-Nitro-4-nitrosobenzene (5m).

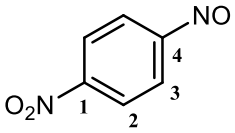

Yield: 5.54 g (3.25 mmol, 70%).

Melting point: 117-120 ºC (lit.[335] 116 ºC).

TLC (10:1 DCM/MeOH): R_f: 0.86

According to the literature protocol,[330] to an aqueous solution of oxone (48.1 g, 156.53 mmol, 3 eq.) in 300 mL of deionized H_2O, 4-nitroaniline (7.2 g, 52.1 mmol, 1 eq.) was added at 0 ºC and the suspension was vigorously stirred at RT under inert atmosphere. Once the end of the reaction was confirmed by TLC, it was filtered and washed with deionized H_2O. After recrystallization from methanol, **5m** was isolated as yellow plates. ^{1}H-NMR (300 MHz, $CDCl_3$): δ 8.54 – 8.47 (m, 2H, H-2), 8.08 – 8.01 (m, 2H, H-3); ^{13}C-NMR (75 MHz, $CDCl_3$): δ 162.49 (C-4), 150.48 (C-1), 125.45 (C-3), 121.29 (C2).

4-Nitrosobenzoic acid (5n).

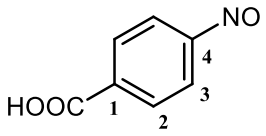

Yield: 2.87 g (3.25 mmol, 87%).

Melting point: 211 ºC (dec.) (lit.[330] 227-230 ºC dec.).

TLC (3:1 CH/EA): R_f: 0.32

According to the general procedure, 3.0 g (21.87 mmol, 1 eq.) of 4-aminobenzoic acid in 50 mL of DCM were mixed with 27.0 g (87.84 mmol, 4 eq.) of Oxone dissolved in 136 mL of deionized H_2O. Since the product precipitated in this case, it was filtered instead of extracted, washed with deionized H_2O and dried in a desiccator over $CaCl_2$. Column purification resulted in partial decomposition and recrystallization did not improve the purity significantly. Compound **5n** was isolated as a yellow solid. ^{1}H-NMR (500 MHz, DMSO-d^6): δ 8.28 – 8.23 (m, 2H, H-2), 8.05 – 7.99 (m, 2H, H-3); ^{13}C-NMR (126 MHz, DMSO-d^6): δ 166.14 (C-5), 165.00 (C-4), 136.51 (C-1), 130.97 (C-3), 120.56 (C-2).

3-Nitrosobenzoic acid (5o).

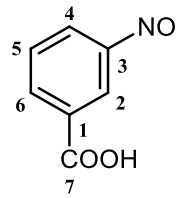

Yield: 4.60 g (30.44 mmol, 84%).

Melting point: 188 ºC (dec.).

TLC (10:1 DCM/MeOH): R_f: 0.48

According to the general procedure, 5.0 g (36.40 mmol, 1 eq.) of 3-aminobenzoic acid in 100 mL of DCM were mixed with 22.40 g (72.87 mmol, 2 eq.) of Oxone dissolved in 160 mL of deionized H_2O. Since the product precipitated in this case, it was filtered instead of extracted, washed with deionized H_2O and dried in a desiccator over $CaCl_2$. Compound **5o** was isolated as a yellow solid. ^{1}H-NMR (300 MHz, DMSO-d^6): δ 8.38 (dt, J = 7.7, 1.5 Hz, 1H, H-6), 8.34 (t, J = 1.8 Hz, 1H, H-2), 8.16 (ddd, J = 7.9, 2.1, 1.2 Hz, 1H, H-4), 7.87 (t, J = 7.8 Hz, 1H, H-5); ^{13}C-NMR (75 MHz, DMSO-d^6): δ 166.09 (C-7), 165.22 (C-3), 136.25 (C-6), 132.50 (C-1),

130.48 (C-5), 124.25 (C-4), 120.95 (C-2); MS (EI): m/z calculated for $[C_7H_5NO_3]$-H^+ = 150.02, found 150.02.

12.3.3.3. Synthesis of N-aryl hydroxamic acids

SOP 19 for the enzymatic synthesis of hydroxamic acids (optimized protocol with acetone)

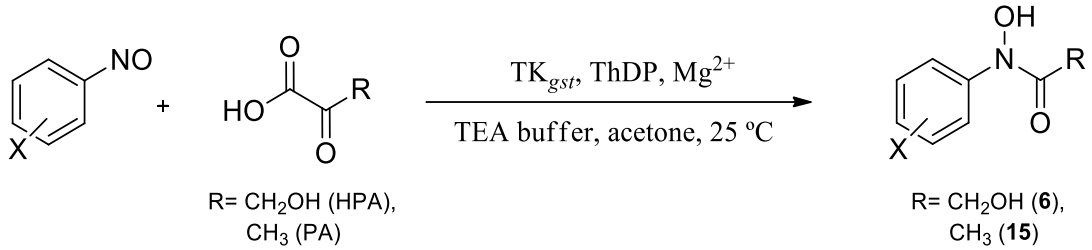

ThDP (28 mg, 0.06 mmol, 2.4 mM) and $MgCl_2 \cdot 6H_2O$ (48 mg, 0.24 mmol, 9.4 mM) were dissolved in TEA buffer (17 mL, 50 mM) and the pH was carefully adjusted to 7.45. To the solution, lyophilized TK_{gst} enzyme (10 mg of the variant L382N/D470S for HPA reactions and 50 mg of H102L/H474S for PA reactions) was added and the mixture was incubated at RT for 30 min. Afterwards, HPA or sodium-PA (152 mg, 1.38 mmol, 50 mM) dissolved in TEA buffer (3 mL, 50 mM, pH 7.45) was added, followed by first, 3 mL of acetone, and then a solution of the corresponding nitroso compound (50 mM) in 2 mL of acetone. The total volume was adjusted to 25 mL with 20% of acetone as co-solvent. Reactions were stirred at RT and the conversion monitored by TLC and HPLC. After consumption of starting material, the pH of the reaction was basified (pH 10-12) by addition of 6M NaOH, and the reaction mixture was extracted three times with ethyl acetate. The aqueous phase was then acidified to pH 4-5 by means of 6M HCl, and it was extracted again with ethyl acetate. The combined organic layers were washed with brine solution, dried over $MgSO_4$, and the solvent was removed under reduced pressure. No further purification was performed.

In exploratory preparative reactions with ethanol and DMSO as co-solvents, the total volume used was also 25 mL but adding 8% of ethanol or DMSO (2 mL) instead of acetone. Reactions were performed at 50 ºC. Following extractive work-up, the crude materials were dry loaded on a silica column and purified using CH/EA (1:1) as eluent.

_N_-Phenyl-_N_,2-dihydroxyacetamide (6a).

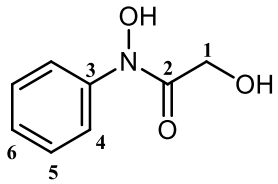

Yield: 104 mg (0.62 mmol, 50%).

Melting point: 65-66 ºC (lit.[224] 64.5-65.5 ºC).

TLC (1:4 CH/EA): R_f: 0.61

N-Phenyl-*N*,2-dihydroxyacetamide (**6a**) was isolated as a colorless solid. ^{1}H-NMR (500 MHz, CD_3OD): δ 7.67 (d, ^3J = 8.4 Hz, 2H, H-4), 7.38 (t, ^3J = 8.0 Hz, 2H, H-5), 7.19 (t, ^3J = 7.5 Hz, 1H, H-6), 4.46 (s, 2H, H-1); ^{13}C-NMR (126 MHz, CD_3OD): δ 173.28 (C-2), 142.53 (C-3), 129.63 (C-4), 126.61 (C-5), 121.43 (C-6), 61.57 (C-1); MS (EI): m/z calculated for $[C_8H_9NO_3]^+$

= 167, found 167, 151, 149, 119, and 109 (base peak). The spectroscopic properties are in accordance with the literature data.[339]

N-(4-Bromophenyl)-*N*,2-dihydroxyacetamide (6b).

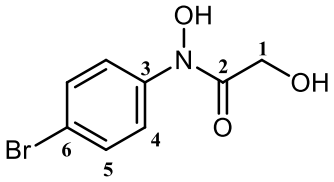

Yield: 130 mg (0.53 mmol, 54%).

Melting point: 128-129 ºC.

TLC (1:4 CH/EA): R_f: 0.57

N-(4-Bromophenyl)-*N*,2-dihydroxyacetamide (**6b**) was isolated as a slightly tan solid. ^{1}H-NMR (300 MHz, CD_3OD): δ 7.66 (dt, ^3J = 9.1 Hz, 2H, H-4), 7.52 (dt, ^3J = 9.1 Hz, 2H, H-5), 4.47 (s, 2H, H-1); ^{13}C-NMR (75 MHz, CD_3OD): δ 173.53 (C-2), 141.86 (C-3), 132.59 (C-4), 122.66 (C-6), 61.65 (C-1); HRMS (ESI): m/z calculated for $[C_8H_8BrNO_3]^+$ = 245.97603, found 245.97598.

N-(4-Chlorophenyl)-*N*,2-dihydroxyacetamide (5c).

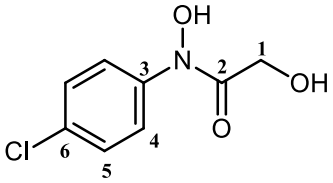

Yield: 102 mg (0.51 mmol, 41%).

Melting point: 123-124 ºC (lit.[224] 124-125 ºC).

TLC (1:4 CH/EA): R_f: 0.59

N-(4-Chlorophenyl)-*N*,2-dihydroxyacetamide (**5c**) was isolated as a slightly tan solid. ^{1}H-NMR (300 MHz, CD_3OD): δ 7.71 (dt, ^3J = 9.1 Hz, 2H, H-4), 7.38 (dt, ^3J = 9.1 Hz, 2H, H-5), 4.48 (s, 2H, H-1); ^{13}C-NMR (75 MHz, CD_3OD): δ 173.52 (C-2), 141.37 (C-3), 131.41 (C-4), 129.58 (C-5), 122.45 (C-6), 61.62 (C-1); MS (EI): m/z calculated for $[C_8H_8ClNO_3]^+$ = 201, found 201.

N-(3-Chlorophenyl)-*N*,2-dihydroxyacetamide (5d).

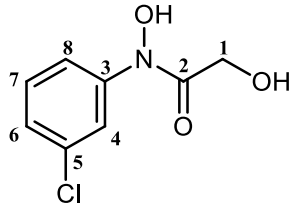

Yield: 48 mg (0.24 mmol, 20%).

Melting point: 110-111 ºC.

TLC (1:4 CH/EA): R_f: 0.65

N-(4-Chlorophenyl)-*N*,2-dihydroxyacetamide (**5d**) was isolated as a slightly tan solid. ^{1}H-NMR (300 MHz, CD_3OD): δ 7.81 (t, ^4J = 2.1 Hz, 1H, H-4), 7.67 (dd, ^3J = 8.5, ^4J = 2.1 Hz, 1H, H-8), 7.35 (t, ^3J = 8.2 Hz, 1H, H-7), 7.17 (dd, ^3J = 8.1, ^4J= 2.1 Hz, 1H, H-6), 4.49 (s, 2H, H-1); ^{13}C-NMR (75 MHz, CD_3OD): δ 173.77 (C-2), 143.83 (C-3), 135.25 (C-5), 130.91 (C-7), 125.98 (C-6), 120.59 (C-4), 118.76 (C-8), 61.75 (C-1); MS (EI): m/z calculated for $[C_8H_8ClNO_3]+H^+$ = 202, found 202.

_N_-(3,4-Dichlorophenyl)-_N_,2-dihydroxyacetamide (5f).

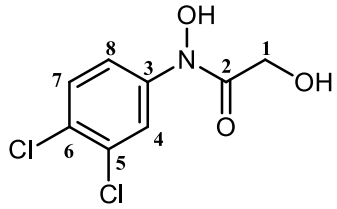

Yield: 30 mg (0.13 mmol, 10%).

Melting point: 126-127 ºC.

TLC (1:4 CH/EA): R_f: 0.61

_N_-(3,4-Dichlorophenyl)-_N_,2-dihydroxyacetamide (**5f**) was isolated as an amber solid. ^{1}H-NMR (500 MHz, CD_3OD): δ 7.87 (d, ^{4}J = 2.5 Hz, 1H, H-4), 7.58 (dd, ^{3}J = 8.9, ^{4}J =2.5 Hz, 1H, H-8), 7.40 (d, ^{3}J = 8.9 Hz, 1H, H-7), 4.37 (s, 2H, H-1); ^{13}C-NMR (126 MHz, CD_3OD): δ 173.92 (C-2), 142.35 (C-3), 133.19 (C-5), 131.37 (C-7), 128.87 (C-6), 121.92 (C-4), 119.84 (C-8), 61.76 (C-1); MS (EI): m/z calculated for $[C_9H_{10}ClNO_3]+H^+$ = 235, found 235.

_N_-(_p_-Tolyl)-_N_,2-dihydroxyacetamide (5g).

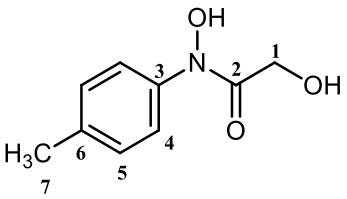

Yield: 110 mg (0.61 mmol, 49%).

Melting point: 120-121 ºC (lit.[224] 119-119.5 ºC).

TLC (1:4 CH/EA): R_f: 0.61

_N_-(_p_-Tolyl)-_N_,2-dihydroxyacetamide (**5g**) was isolated as a colorless solid. ^{1}H-NMR (300 MHz, CD_3OD): δ 7.52 (d, ^{3}J = 8.0 Hz, 2H, H-4), 7.21 (d, ^{3}J = 8.0 Hz, 2H, H-5), 4.45 (s, 2H, H-1), 2.34 (s, 3H, H-7); ^{13}C-NMR (75 MHz, CD_3OD): δ 173.09 (C-2), 140.00 (C-3), 130.16 (C-4, C-5), 121.87 (C-6), 61.47 (C-1), 20.96 (C-7); HRMS (ESI): m/z calculated for $[C_9H_{11}NO_3]^+$ = 181.08117, found 181.08121.

_N_-(_m_-Tolyl)-_N_,2-dihydroxyacetamide (5h).

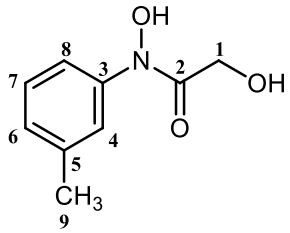

Yield: 66 mg (0.36 mmol, 29%).

Melting point: 92-93 ºC.

TLC (1:4 CH/EA): R_f: 0.63

_N_-(_m_-Tolyl)-_N_,2-dihydroxyacetamide (**5h**) was isolated as a slightly tan solid. ^{1}H-NMR (300 MHz, CD_3OD): δ 7.57 – 7.39 (m, 2H, H-4, H-8), 7.25 (t, ^{3}J = 7.9 Hz, 1H, H-7), 7.03 (d, ^{3}J = 7.6 Hz, 1H, H-6), 4.44 (s, 2H, H-1), 2.35 (s, 3H, H-9); ^{13}C-NMR (75 MHz, CD_3OD): δ 173.21 (C-2), 142.41 (C-5), 139.70 (C-3), 129.50 (C-7), 127.47 (C-6), 122.36 (C-4), 119.00 (C-8), 61.55 (C-1), 21.53 (C-9); MS (EI): m/z calculated for $[C_9H_{11}NO_3]^+$ = 181, found 181.

***N*-(4-Chloro-3-methylphenyl)-*N*,2-dihydroxyacetamide (5i).**

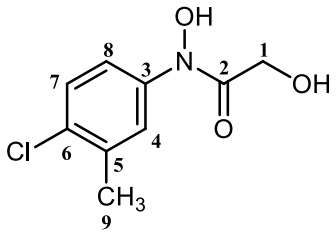

Yield: 100 mg (0.46 mmol, 37%).

Melting point: 143-144 ºC.

TLC (1:4 CH/EA): R_f: 0.63

N-(4-Chloro-3-methylphenyl)-*N*,2-dihydroxyacetamide (**5i**) was isolated as a colorless solid. ^{1}H-NMR (300 MHz, CD_3OD): δ 7.77 (d, ^{4}J = 2.2 Hz, 1H, H-4), 7.55 (dd, ^{3}J = 8.4, ^{4}J = 2.3 Hz, 1H, H-8), 7.29 (d, ^{3}J = 8.4 Hz, 1H, H-7), 4.47 (s, 2H, H-1), 2.36 (s, 3H, H-9); ^{13}C-NMR (75 MHz, CD_3OD): δ 173.48 (C-2), 141.56 (C-3), 134.99 (C-5), 133.88 (C-6), 131.85 (C-4), 121.36 (C-7), 119.35 (C-8), 61.61 (C-1), 19.48 (C-9); HRMS (ESI): m/z calculated for $[C_9H_{10}ClNO_3]+H^+$ = 216.04220, found 216.04237.

***N*-(3-Chloro-4-methylphenyl)-*N*,2-dihydroxyacetamide (5j).**

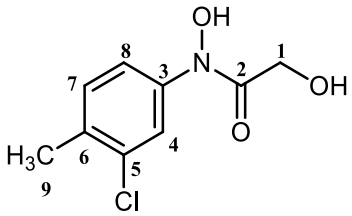

Yield: 87 mg (0.40 mmol, 32%).

Melting point: 125-126 ºC.

TLC (1:4 CH/EA): R_f: 0.59

N-(3-Chloro-4-methylphenyl)-*N*,2-dihydroxyacetamide (**5j**) was isolated as a slightly tan solid. ^{1}H-NMR (500 MHz, CD_3OD): δ 7.64 (d, ^{4}J = 2.7 Hz, 1H, H-4), 7.51 (dd, ^{3}J = 8.8, ^{4}J = 2.7 Hz, 1H, H-8), 7.34 (d, ^{3}J = 8.8 Hz, 1H, H-7), 4.45 (s, 2H, H-1), 2.37 (s, 3H, H-9); ^{13}C-NMR (126 MHz, CD_3OD): δ 173.77 (C-2), 141.61 (C-3), 137.68 (C-5), 130.33 (C-4), 123.84 (C-7), 120.52 (C-8), 61.94 (C-1), 20.60 (C-9); MS (EI): m/z calculated for $[C_9H_{10}ClNO_3]^+$ = 215, found 215

***N*-(4-(Trifluoromethyl)phenyl)-*N*,2-dihydroxyacetamide (5k).**

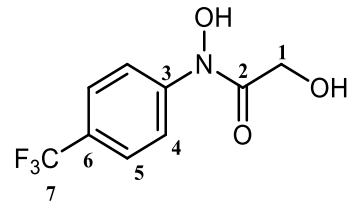

Yield: 27 mg (0.11 mmol, 9%).

Melting point: 110-112 ºC (lit.[224] 112-114 ºC).

TLC (1:4 CH/EA): R_f: 0.65

N-(4-(Trifluoromethyl)phenyl)-*N*,2-dihydroxyacetamide (**5k**) was isolated as a pale pink solid. ^{1}H-NMR (300 MHz, CD_3OD): δ 7.85 (d, ^{3}J = 8.6 Hz, 2H, H-5), 7.56 (d, ^{3}J = 8.7 Hz, 2H, H-4), 4.41 (s, 2H, H-1); ^{13}C-NMR (75 MHz, CD_3OD): δ 174.08 (C-2), 145.75 (C-3), 126.77 (C-4), 123.83 (C-6), 120.05 (C-5), 114.34 (C-7), 61.85 (C-1); MS (EI): m/z calculated for $[C_9H_8F_3NO_3]+H^+$ = 236, found 236.

_N_-(3-(Trifluoromethyl)phenyl)-_N_,2-dihydroxyacetamide (5l).

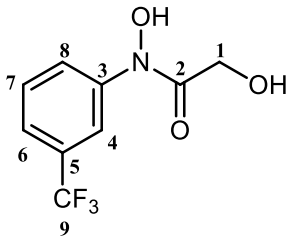

Yield: 50 mg (0.21 mmol, 17%).

Melting point: 90-91 ºC (lit.[224] 90.5-91.5 ºC).

TLC (1:4 CH/EA): R_f: 0.67

N-(3-(Trifluoromethyl)phenyl)-*N*,2-dihydroxyacetamide (**5l**) was isolated as a colorless solid. ^{1}H-NMR (300 MHz, CD_3OD): δ 7.98 (s, 1H, H-4), 7.89 (d, ^3J = 8.3 Hz, 1H, H-8), 7.46 (t, ^3J = 8.0 Hz, 1H, H-7), 7.34 (d, ^3J = 7.8 Hz, 1H, H-6), 4.40 (s, 2H, H-1); ^{13}C-NMR (75 MHz, CD_3OD): δ 174.01 (C-2), 143.33 (C-3), 132.16 (C-5), 130.55 (C-9), 127.25 (C-7), 123.63 (C-8), 122.37 (C-6), 116.97 (C-4), 61.76 (C-1); MS (ESI): m/z calculated for $[C_9H_8F_3NO_3]+H^+$ = 236.05, found 236.05.

_N_-Phenyl-_N_-hydroxyacetamide (15a)

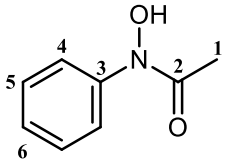

Yield: 10 mg (0.06 mmol, 5%).

Melting point: 65-66 ºC (lit.[229] 66-67 ºC)

TLC (10:1 DCM/MeOH): R_f: 0.65

N-Phenyl-*N*-hydroxyacetamide (**15a**) was isolated as a slightly tan solid. ^{1}H-NMR (300 MHz, CD_3OD): δ 7.46 (d, ^3J=7.8 Hz, 2H, *o,o'*-H-4), 7.28 (t, ^3J= 7.8 Hz, 2H, *m,m'*-H-5), 7.19–7.03 (m, 1H, *p*-H-6), 2.15 (s, 3H, H-1); ^{13}C-NMR (75 MHz, CD_3OD): δ 174.89 (C-2), 142.63 (C-3), 129.66 (C-5), 127.26 (C-6), 122.94 (C-4), 22.05 (C-1). All properties are in consonance with the literature data and with those of an authentic sample prepared by chemical synthesis.[229]

SOP 20 for the chemical synthesis of hydroxamic acids with glyoxylic acid

Glyoxylic acid monohydrate (115 mg, 1.25 mmol, 50 mM) was dissolved in TEA buffer (20 mL, 50 mM) and the pH was adjusted to 7.45. Then, 3 mL of acetone were added and the mixture was shortly stirred. Subsequently, the corresponding nitroso compound (50 mM) dissolved in 2 mL of acetone was added. The total volume was adjusted to 25 mL with 20% of acetone as co-solvent. Reactions were stirred at RT and monitored by HPLC and TLC. After consumption of the starting material, the pH was basified (pH 10-12) by addition of 6M NaOH and the reaction mixture was extracted twice with ethyl acetate. The water phase was then acidified to pH 4-5 by means of 6M HCl, and it was extracted again with ethyl acetate. The combined organic layers were washed with brine solution, dried over $MgSO_4$ and the solvent was removed under reduced pressure. No further purification was performed.

_N_-Phenyl-_N_-hydroxyformamide (18a).

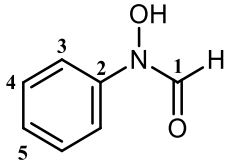

Yield: 136 mg (0.99 mmol, 79%).

Melting point: 66-68 ºC (lit. 67-69 ºC)

TLC (1:1 CH/EA): R_f: 0.63

_N_-Phenyl-_N_-hydroxyformamide (**18a**) was isolated as a cream color solid. ^{1}H-NMR (300 MHz, CD_3OD): δ 9.38 (br s, 1H, N-OH), 8.37 (s, 1H, H-1), 7.34 – 7.09 (m, 5H, H-3, H-4, H-5); ^{13}C-NMR (75 MHz, CD_3OD): δ 155.54 (C-1), 138.07 (C-2), 129.49 (C-4), 127.06 (C-5), 118.92 (C-3).; HR-MS (EI): m/z calculated for $[C_7H_7NO_2]+H^+$ = 138.0549, found 138.0548. All properties are in agreement with the literature.[229]

_N_-(4-Bromophenyl)-_N_-hydroxyformamide (18b).

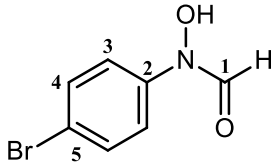

Yield: 190 mg (0.88 mmol, 70%).

Melting point: 123-124 (lit.[340] 126 ºC).

TLC (1:1 CH/EA): R_f: 0.63

_N_-(4-Bromophenyl)-_N_-hydroxyformamide (**18b**). was isolated as a cream color solid. Mixture of rotamers Z/E, ratio 1.1:0.9. ^{1}H-NMR (500 MHz, CD_3OD): δ 8.64 (s, 2H (H-1-Z, H-1'-E), 7.78–7.23 (m, 8H (H-3-Z, H-3'-E; H-4-Z, H-4'-E)); ^{13}C-NMR (126 MHz, CD_3OD): δ 163.16 (H1'-_E_), 158.65 (H1-_Z_), 140.84 (H2, H2'), 133.47 (H3'-_E_), 132.70 (H3-_Z_), 121.33 (H4, H4'); HR-MS (EI): m/z calculated for $[C_7H_6BrNO_2]^+$ = 215, found 215, 199, 187, 171 (base peak).

Accidental isolation of _N_-(4-bromophenyl)formamide (19b).

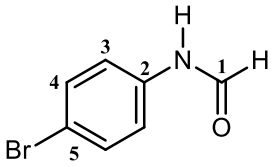

Yield: 7 mg (0.034 mmol, 3%).

Compound **19b** was isolated as a side product from the enzymatic reaction from **5b** to **6b** via slow addition of **5b** with a syringe pump. _N_-(4-Bromophenyl)formamide (**19b**) was isolated as pale orange solid. Mixture of rotamers Z/E, ratio 4.2:1.0. ^{1}H-NMR (500 MHz, CD_3OD): δ=8.71 (s, 0.3H, H1'-_E_), 8.28 (s, 1.2H, H1-_Z_), 7.60–7.39 (m, 6.0H, H3-, H4-_Z_, H3'-_E_), 7.14–7.08 (m, 0.6H, H4-_E_); ^{13}C-NMR (126 MHz, CD_3OD): δ 164.55 (H1'-_E_), 161.58 (H1-_Z_), 138.28 (H2-_Z_), 133.61 (H3'-_E_), 132.94 (H3-_Z_), 122.70 (H4-_Z_), 121.20 (H4'-_E_), 117.82 (H5-_Z_); MS (EI): m/z calculated for $[C_7H_6BrNO]^+$ = 199, found 199, 171, 143. The spectroscopic properties were in agreement with literature data.[341]

Chemical synthesis of *N*-phenyl-*N*,2 dihydroxyacetamide (6a).

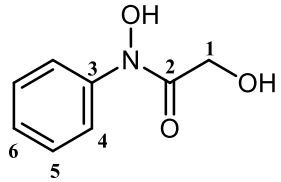

Yield: 80 mg (0.48 mmol, 35%).

Adapting a literature procedure,[224] a suspension of phenylhydroxylamine (150 mg, 1.37 mmol, 1 eq.) in 3 mL of anhydrous ether in a 10 mL round bottomed flask was stirred and cooled with an ice-water bath. To this stirred suspension, *N,N'*-diisopropylcarbodiimide (0.20 g, 0.25 mL, 1.56 mmol. 1.1 eq.) in 0.5 mL of anhydrous ether was added, followed by the addition of glycolic acid (0.12 g, 1.14 eq., 1.56 mmol) in 0.4 mL of anhydrous DMF over a 10 minutes period. The ice bath was removed and stirring was continued for 80 minutes until complete conversion of the starting material. Then 3 mL of n-butanol were added and the mixture was stirred for 15 additional minutes. The reaction mixture was extracted twice with 1 mL of 1 N NaOH solution, followed by 1.2 mL of water. The combined aqueous extract was washed with 1.2 mL of ether and the pH was adjusted to 6 with a 4 N HCl solution. The suspension was extracted with 5 mL of ethyl acetate, and the organic portion washed with 0.6 mL of water and 0.6 mL of brine. After drying the organic layer over $MgSO_4$ and evaporating the solvent under reduced pressure, compound **6a** was obtained as yellow needles. ^{1}H-NMR (500 MHz, CD_3OD): δ 7.72 – 7.62 (m, 2H, H-4), 7.44 – 7.31 (m, 2H, H-5), 7.25–7.13 (m, 1H, H-6), 4.47 (s, 2H, H-1); ^{13}C-NMR (126 MHz, CD_3OD): δ 173.2697 (C-2), 142.50 (C-3), 129.65 (C-4), 126.70 (C-5), 121.66 (C-6), 61.59 (C-1).

Chemical synthesis of *N*-phenyl-*N*-hydroxyacetamide (15a).

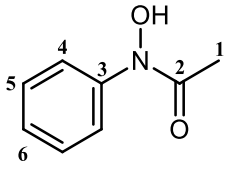

Yield: 405 mg (2.70 mmol, 41%).

Melting point: 66-67 ºC (lit.[229] 66-67 ºC)

TLC (10:1 DCM/MeOH): R_f: 0.65

Following a literature procedure,[229] to glacial acetic acid (20 mL) containing nitrosobenzene (0.72 g, 6.67 mmol) was added slowly 10 mL of an aqueous solution of sodium pyruvate (1.83 g, 16.67 mmol) with neutral pH. The mixture was stirred at RT until complete consumption of the nitrosobenzene. Afterwards 1 mL of ammonium bicarbonate (16.67 mmol) was added and the solvent was removed under reduced pressure. The residue was dissolved in 1 M NaOH (80 mL) and the resulting solution was extracted three times with Et_2O. The pH of the aqueous layer was adjusted with 5M H_3PO_4 to 5.5, followed by extraction with Et_2O (3x 40 mL). The combined organic layers were dried over $MgSO_4$ and the solvent was evaporated under reduced pressure. The crude product was recrystallized from a mixture of benzene: hexane 1:1. *N*-Phenyl-*N*-hydroxyacetamide (**15a**) was obtained as colorless crystals. ^{1}H-NMR (300 MHz, CD_3OD): δ 7.57 (d, ^3J=7.9 Hz, 2H, *o,o'*-H-4), 7.37 (t, ^3J= 7.7 Hz, 2H, *m,m'*-H-5), 7.21 (t, ^3J = 7.6 H, 1H, *p*-H-6), 2.25 (s, 3H, H-1); ^{13}C-NMR (75 MHz, CD_3OD): δ 175.52 (C-2), 142.28 (C-3), 129.33 (C-5), 126.69 (C-6), 122.62 (C-4), 21.76 (C-1); HR-MS (EI): m/z calculated for [$C_8H_9NO_2$] = 151.0628, found 151.0629. The spectroscopic properties were in agreement with the previously published ones.[229]

12.4. Experiments Chapter II

12.4.1. Development of *liquid-phase iron(III) assay*

12.4.1.1. Assay final conditions with cell free extract (CFE)

During the method optimization, the substrates **5b**, **5l**, and **5j** were screened with the endpoint assay using CFE from TK_{gst} N/S as the reaction catalyst. To the 96-well plates, $MgCl_2$ (5 mM), TEA buffer (5 mM, pH 7.45), varying concentrations of CFE from 0 to 2.5 mg/mL, and HPA (1.5 mM) were added. The reactions were initiated by the addition of the corresponding nitrosoarene (2 mM) dissolved in DMSO (20%). The total volume in each well was 200 µL. The reactions were incubated at RT and 900 rpm for 60 min. After the corresponding incubation time, $FeCl_3$ (12 mM) was added and the solutions were shortly mixed. The absorbance values were read by a plate-reader at 500 nm.

SOP for protein expression for library screening in 96 well-microtiter plates

To a round bottom microtiter plate, LB medium (130 µL) containing kanamycin (50 mg/mL) was added. The plate was covered with a sealing foil and a hole was perforated in each well for aeration. Meanwhile, the glycerol stocks from the library plate were thawed at room temperature. The foil was shortly removed to inoculate the prepared plate with 5 µL of each clone, the plate was sealed again and incubated at 37 ºC and 900 rpm for 8 hours. The resulting precultures (100 µL) were transferred to a 96-deepwell plate filled with LB medium (containing 50 mg/mL of kanamycin and 0.1 mM IPTG), and the plate was sealed, perforated and incubated at 30 ºC and 1200 rpm overnight (OD_{600} < 0.6). After incubation, the deepwell-plate was centrifuged at 4000 g for 20 min at 4 ºC. The culture medium was removed, the pellet was resuspended with TEA buffer (200 µL, 5 mM, pH 7.45), and the plate was centrifuged at 4000 g for 20 min at 4 ºC. The supernatant was discarded again and the pellets were frozen at -80 ºC. For screening, the cell lysis was carried out. For this purpose, the frozen pellets were thawed and resuspended in lysis buffer (200 µL, TEA buffer (5 mM, pH 7.45), 0.5 mg/mL lysozyme and 4 U/mL cyanase). The deep-well-plate was sealed and incubated at 37 ºC for 1 hour, followed by 30 min at 50 ºC for heat purification. The plate was allowed to stand at room temperature for 15 min for the settlement of the precipitated proteins, and then centrifuged at 4000 g for 30 min. The resulting supernatants were transferred to 96-well flat bottom plates.

12.4.1.2. Assay final conditions with 16 best candidates from TK_{gst} L382X/D470X library

The substrates **5b**, **5l**, and **5j** were screened with the endpoint assay using freshly produced cell lysates directly as the reaction catalyst. From the L382X/D470X mutagenesis library created by D. Yi for screening of TK_{gst} variants towards propanal,[210] the 16 best candidates screened towards benzaldehyde from T. Saravanan[6] were screened with the ferric chloride assay. Immediately after lysis, the resulting supernatants (20 µL) were transferred to 96-well flat bottom plates. For the substrates **5b** and **5j** the lysates were diluted 1:2 and 1:1 respectively prior to use. To the 96-well plates, $MgCl_2$ (5 mM), ThDP (0.6 mM), TEA buffer (5 mM, pH

7.45) and HPA (1.5 mM) were added. The reactions were initiated by the addition of the corresponding nitrosoarene (2 mM) dissolved in DMSO (20%). The total volume in each well was 200 µL. The reactions were incubated at RT and 900 rpm for 30 min. After the corresponding incubation time, $FeCl_3$ (6 mM) was added and the solutions were shortly mixed. The absorbance values were read by the plate-reader at 500 nm.

12.4.1.3. Optimized reaction system for the final assay with TK_{gst} L382X/D470X library

The substrates **5b**, **5l**, and **5j** were screened with the endpoint assay using cell lysates as the reaction catalyst. Directly after lysis, the resulting supernatants (20 µL) were transferred to 96-well flat bottom plates. For the substrates **5b** and **5j** the lysates were diluted 1:1 prior to use. To the 96-well plates, $MgCl_2$ (5 mM), ThDP (0.6 mM), TEA buffer (5 mM, pH 7.45) and HPA (1.5 mM) were added. The reactions were initiated by the addition of the corresponding nitrosoarene (2 mM) dissolved in DMSO (20%). The total volume in each well was 200 µL. The reactions were incubated at RT and 900 rpm for 30 min in the case of the substrates **5l** and **5j**, and for 15 min for **5b**. After the corresponding incubation time, $FeCl_3$ (6 mM) was added and the solutions were shortly mixed. The absorbance values were read by the plate-reader at 500 nm. The absorbance results were treated, normalized and presented as graphical representations. The raw and treated values are below in this chapter.

12.4.1.4. Calibration curve, limit of detection and limit of quantification

To generate a calibration curve for the ferric chloride assay, a series of gradually increasing final concentrations of **6b** solved in methanol from 0 mM to 2 mM in a 96-microwell flat plate were utilized. Simultaneously, gradually decreasing final concentrations of HPA and **5b**, solved in TEA buffer (5 mM, pH 7.45) and methanol respectively, both from 2 mM to 0 mM were applied. The reactions also contained extra added volume of TEA buffer (5 mM, pH 7.45) and $FeCl_3$ (6 mM). The total volume was 200 µL. Experiments containing the same amount of TEA buffer (5 mM, pH 7.45), $FeCl_3$ (6 mM), and methanol where corresponding, yet no substrates or HA product, were prepared as controls. The absorbance of the solutions was measured at 500 nm by means of a plate reader and a standard curve $\boldsymbol{y = ax + b}$ was obtained. LOD was calculated as $\boldsymbol{LOD = 3.3Sb / \bar{a}}$, and LOQ was defined as $\boldsymbol{LOD = 10Sb / \bar{a}}$, where *Sb* is the standard deviation of the control.

12.4.1.5. *Z*-Factor calculation

For the evaluation and validation of the liquid-assay method, the *Z*-factor was calculated separately using the data of the assays with the three substrates **5b**, **5l** and **5j** according to the formula $Z = 1 - [(3\cdot(\sigma s + \sigma c))/ |\mu s + \mu c|]$, where σs is the standard deviation of the sample, σc is the standard deviation of the control, μs is the sample average, and μc is the control average. The assay method is judged to be ideal when $Z=1$, and excellent when $1.0 > Z \geq 0.5$. If $0.5 > Z$

≥ 0.0, the assay cannot be employed in high-throughput format, and if $Z < 0$, screening is impossible.

12.4.2. Development of solid-phase supported iron(III) assay

SOP for agar plate preparation

Agar plates were prepared by addition of LB medium (250 mL) to 5 g agar. The resulting suspension was stirred and autoclaved. Then, the solution was cooled down to 50 °C while stirring. Afterwards, kanamycin (250 µL) was added to the solution. The solution was shortly stirred and finally added to the petri dishes.

12.4.2.1. Growth of colonies in agar plates for TK_{gst} L382X/D470X library screening

To a round bottom microtiter plate, LB medium (130 µL) containing kanamycin (50 mg/mL) of was added. The plate was covered with a sealing foil and a hole was perforated in each well for aeration. Meanwhile, the glycerol stocks from the L382X/D470X library plate were thawed at room temperature. The foil was shortly removed and the plate was inoculated with *E. coli* BL21(DE3) cells (5 µL) carrying the transketolase of interest gene coding plasmids. The plate was sealed again and incubated at 30 ºC and 900 rpm for 16-18 hours. When performing assays with BL21 (DE3) untransformed cells or empty plasmid as controls, the inoculation was done with sterilized toothpicks from the glycerol stocks. For the assays with BL21 (DE3) untransformed, no antibiotic was added to the LB medium. After incubation, 20 µL from each well were combined and mixed for the whole library plate screening. Either the mixture cells were then diluted 1 to 10^{-6} with LB medium supplemented with kanamycin (50 mg/mL), or the single clones as in the experiments with BL21 (DE3) untransformed cells or the TK_{gst} N/S variant. The dilutions were vortexed to ensure a good mix and 100 µL were plated out on LB agar plates supplemented with kanamycin (100 µg/mL) as antibiotic. For assays containing BL21 (DE3) untransformed cells, LB plates without antibiotic were used, as they have no antibiotic resistance inside. The plates were incubated at 37 °C for 17-18 h to gain homogeneous colonies of a reasonable size.

12.4.2.2. Membrane transfer, expression, masterplate preparation and permeabilization

Afterwards, the colonies were first transferred to a labelled nylon Hybond-*N*-membrane by gently pressing the membrane against the agar plate until it was completely absorbed to the agar. Then the membrane was taken off from the agar with the colonies stuck to it, and the membrane was placed, with the colonies facing up, on an induction plate containing IPTG (2 mM) as inducer and kanamycin (100 µg/mL). Again, for the BL21 (DE3) untransformed colonies the plates were missing the antibiotic. The induction plate carrying the membrane was incubated for 4 to 6 hours at 37 ºC. The original agar plate from which the colonies had been removed (master plate) was incubated again at 37 ºC for around 5 h until the colonies have regrown again and thus can be easily sequenced or picked for further rounds of screening. Finally, the master plate was secured with parafilm and stored at 4º C until needed. Cell

permeabilization was performed by immersing the membranes in liquid nitrogen for 5 to 10 seconds.

12.4.2.3. Solid-phase supported assay procedure

Filter paper was soaked in the reagent's solution containing **5a** (15 mM), HPA (15 mM), ThDP (0.6 mM), $MgCl_2$ (2.5 mM) and TEA buffer (5 mM, pH 7.45). For the negative controls without substrates, the filter paper was soaked only in TEA buffer (5 mM, pH 7.45). Then, the membranes were placed on top of the filter papers, with the colonies facing up, and incubated at 37 ºC for 30 minutes. Afterwards, the membranes were dipped into an aqueous $FeCl_3$ (252 mM) solution for color development. Photos of the colored membranes were immediately taken upon ferric chloride staining and manually reversed with photoshop in order to obtain their mirror image and thus, facilitate colony picking.

12.5. Experiments Chapter III

12.5.1. Synthesis protocols and characterization of compounds

12.5.1.1. Synthesis of 4-(4-phenylbutanamido)benzoic acid (24)

Synthesis adapted from *Shieh et al.* [315]

Step 1: Synthesis of acid chloride with oxalyl chloride

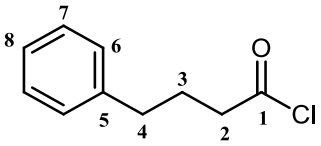

Yield: 5.10 g (27.92 mmol, 92%)

In a 250 mL round bottom flask, 4-phenylbutanoic acid (**22**) (5.0 g, 30.45 mmol, 1 eq.) was dissolved in anhydrous DCM (76 mL) under inert atmosphere. To this solution, oxalyl chloride (5.2 mL, 30.45 mmol, 1 eq.) was added at 0 ºC. The mixture was warmed to room temperature and was stirred for 2.5 h. The solvent, together with the reagents, was distilled *in situ*, and the crude product was co-evaporated with anhydrous DCM (76 mL) under reduced pressure. 4-Phenylbutanoyl chloride (**23**) was obtained as a clear yellow oily liquid and used in the next step without further purification. ^{1}H-NMR (300 MHz, $CDCl_3$): δ 7.45 – 7.09 (m, 5H, H-6, H-7, H-8), 2.96 (t, ^{3}J = 7.3 Hz, 7.3 Hz, 7.3 Hz, 2H, H-2), 2.74 (t, ^{3}J = 7.6 Hz, 7.6 Hz, 2H, H-4), 2.10 (p, J = 7.4 Hz, 7.4 Hz, 7.4 Hz, 7.4 Hz, 2H, H-3); ^{13}C-NMR (75 MHz, $CDCl_3$): δ 173.55 (C-1), 140.40 (C-5), 128.62 (C-6), 128.45 (C-7), 126.37 (C-8), 46.24 (C-4), 34.20 (C-2), 26.56 (C-3).

Step 2: Synthesis of final product (24)

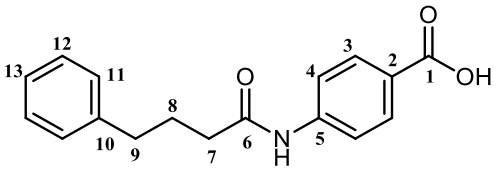

Yield: 5.40 g (19.05 mmol, 70%)

Melting point: 244-245 ºC (dec.).

The acid chloride **23** (5.0 g, 27.37 mmol, 1 eq.) was dissolved in anhydrous DCM (76) at 0 ºC and 4-amino benzoic acid (5.0 g, 36.45 mmol, 1.3 eq.) was added followed by triethylamine (6.3 mL, 45.7 mmol, 1.67 eq.) under inert atmosphere. The reaction was left to stir at RT overnight (17 h). Then, the reaction was terminated with water (150 mL). The reaction mixture was separated and treated in two different ways: the first one consisted in the filtration and subsequent drying of the white formed precipitate. The second part was then extracted with DCM (1 L). The combined organic layers were dried over $MgSO_4$, filtered, and the solvent was evaporated under reduced pressure. The product was stirred with 1 N HCl (100 mL) for 15 min and filtered, to give 4-(4-phenylbutanamido)benzoic acid (**24**) as a white solid. No further purification was performed.

^{1}H-NMR (300 MHz, DMSO-d^{6}): δ 10.18 (s, 1H, H-1), 7.88 (d, ^{3}J = 8.3 Hz, 2H, H-3), 7.71 (d, ^{3}J = 8.3 Hz, 2H, H-4), 7.28 (t, ^{3}J = 7.4 Hz, 2H, H-12), 7.23–7.11 (m, 3H, H-11, H-13), 2.62 (t, ^{3}J = 7.7 Hz, 2H, H-7), 2.36 (t, ^{3}J = 7.5 Hz, 2H, H-9), 1.90 (p, ^{3}J = 7.5, 7.7 Hz, 2H, H-8); ^{13}C-NMR (75 MHz, DMSO-d^{6}): δ 171.61 (C-6), 167.02 (C-1), 143.37 (C-5), 141.65 (C-10), 130.40 (C-3), 128.39 (C-11), 128.37 (C-12), 125.86 (C-13), 124.96 (C-2), 118.37 (C-4), 35.91 (C-9), 34.64 (C-7), 26.65 (C-8); HRMS (EI): m/z calculated for $[C_{17}H_{17}NO_3]+ H^+$ = 284.12814, found 284.12812.

12.5.1.2. Synthesis of *N*-hydroxy-4-(4-phenylbutanamido)benzamide (HTPB)

Synthesis adapted from *Shieh et al*.[315]

Step 1: Synthesis of intermediate (25) with PyBOP

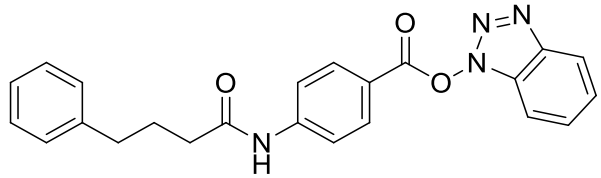

TLC (4:1 EA/CH): R_f: 0.20

To a stirred solution of the resulting acid **24** (4.00 g, 14.12 mmol, 1.0 eq.) in DMF (14 mL) at 0 ºC, triethylamine (3.90 mL, 28.2 mmol, 2 eq.) was added followed by PyBOP (10.20 g, 19.7 mmol, 1.4 eq.). Then, the reaction was warmed to RT and allowed to stir for 27 h.

Step 2: Synthesis of HTPB

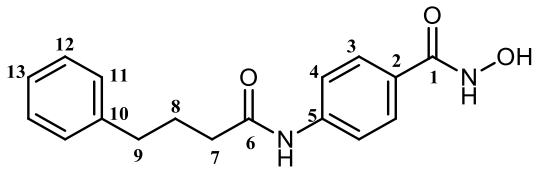

Total yield from both synthesis: 1.74 g pink product (14.11 mmol, 41%); **Yield purification with activated charcoal:** 116 mg white product (39%)

Melting point: 180-181 ºC (dec.).

TLC (4:1 MeOH/CHA): R_f: 0.50

To the reaction mixture from step 1 containing **25**, hydroxylamine hydrochloride (1.9 g, 28.23 mmol, 2 eq.) was added at 0 ºC followed by triethylamine (2.9 mL, 21.18 mmol, 1.5 eq.), and the reaction was left to stir at RT for 24 h. The reaction was quenched by the addition of deionized water (70 mL) and was treated separately: the formed precipitate was filtered and washed with more water, prior to purification via column chromatography with DCM/MeOH 10:1 as mobile phase. The filtrate was extracted with EtOAc, and the combined organic phases were washed with brine and dried over $MgSO_4$. The drying agent was filtered and the solvent was removed under reduced pressure. The crude product was purified by column chromatography with DCM/MeOH 9:1 as mobile phase. *N*-Hydroxy-4-(4-phenylbutanamido)benzamide (HTPB) was obtained as a dark pink solid. A small amount of HTPB (300 mg) was further purified with activated charcoal to afford a white solid.

^{1}H-NMR (500 MHz, DMSO-d^{6}): δ 11.10 (s, 1H, OH), 10.10 (s, 1H, N*H*OH), 8.94 (s, 1H, N*H*CO), 7.73–7.66 (dd, ^{3}J= 8.2 Hz, 4H, H-3, H-4), 7.32–7.18 (m, 5H, H-12, H-11, H-13), 2.64 (t, ^{3}J = 7.6 Hz, 2H, H-7)), 2.37 (t, ^{3}J = 7.5 Hz, 2H, H-9), 1.92 (p, ^{3}J = 7.5 Hz, 2H, H-8); ^{13}C-NMR (126 MHz, DMSO-d^{6}): δ 171.29 (C-6), 163.95 (C-1), 141.80 (C-5), 141.59 (C-10), 128.30 (C-11), 128.28 (C-12), 127.61 (C-3), 126.95 (C-2), 125.77 (C-13), 118.29 (C-4), 35.79 (C-9), 34.57 (C-7), 26.59 (C-8); HRMS (EI): m/z calculated for $[C_{17}H_{18}N_2O_3]$+ H^+ = 299.13896, found 299.13902.

12.5.1.3. Synthesis of *N*-(4-aminophenyl)-4-phenylbutanamide (26)

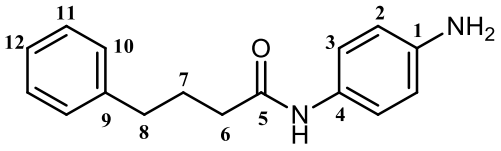

Yield (A): 2.83 g (11.13 mmol, 81%)

Yield (B): 2.00 g (7.86 mmol, 57%)

TLC (1:2 CH/EA): R_f: 0.26

Reaction A: Synthesis adapted from *Tan et al*.[318] In a 500 mL round bottom flask *p*-phenylendiamine (**31**) (2.96 g, 27-37 mmol, 2 eq.) was dissolved in 150 mL of DCM. Then, 4-phenylbutanoyl chloride (**23**) (2.50 g, 13.68 mmol, 1 eq.) was dissolved in 50 mL of DCM. The solution was dropped slowly over 2 h to the amine solution by means of a dropping funnel. The reaction was left to stir at RT 1 h after the dropping was concluded. Common work-up below.

Reaction B: Synthesis adapted from *Böhm et al*.[319] In a 500 mL round bottom flask *p*-phenylendiamine (**31**) (3.0 g, 27.37 mmol, 2 eq.) was dissolved in 100 mL of toluene. Then, 4-phenylbutanoyl chloride (**23**) (2.5 g, 13.68 mmol, 1 eq.) was dissolved in 100 mL of dioxane. The solution is dropped over 2 h to the to the amine solution. Once the dropping concluded, the reaction was left stirring overnight at RT. Common work-up below.

Then, the solution is filtered and washed with cold DCM. The filtrate was left in the fridge overnight and the generated precipitate is filtered again. The filtrate was then concentrated under reduced pressure, and the crude product was purified by column chromatography (using 50 g silica per gram of crude product in a gradient starting from DCM/EA 2:1 to DCM/EA 2:3). *N*-(4-Aminophenyl)-4-phenylbutanamide (**26**) was isolated as a white solid.

^{1}H-NMR (300 MHz, DMSO): δ 7.13-7.34 (m, 7H, H-10, H-11, H-12, H-3), 6.50 (d, ^{3}J= 8.7, 2H, H-2), 4.85 (s, 2H, H-8, NH_2), 2.60 (t, ^{3}J = 7.6 Hz, 7.6 Hz, 2H, H-8), 2.24 (t, ^{3}J = 7.5 Hz, 7.5 Hz, 2H, H-6), 1.87 (p, ^{3}J= 7.5, 7.5, 7.5, 7.5, 2H, H-7); ^{13}C-NMR (75 MHz, DMSO): δ 169.90 (C-5), 144.40 (C-1), 141.70 (C-9), 128.60 (C-4), 128.30 (C-11), 128.20 (C-10), 125.70 (C-12), 120.09 (C-3), 119.80 (C-2), 35.60 (C-8), 34.70 (C-6), 27.00 (C-7); MS (EI): m/z calculated for $[C_{16}H_{18}N_2O]^+$= 254, found 254.

12.5.1.4. Synthesis of *N*-(4-nitrosophenyl)-4-phenylbutanamide (27)

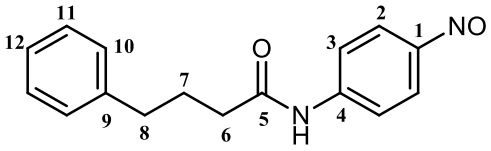

Yield: 1.89 g (7.04 mmol, 63%).

TLC (1:2 CH/EA): R_f: 0.77

According to the general procedure SOP 18, 2.8 g (11.11 mmol, 1 eq.) of N-(4-aminophenyl)-4-phenylbutanamide (**26**) in 125 mL of DCM were mixed with 8.7 g (17.22 mmol, 2 eq.) of oxone dissolved in 70 mL of deionized H_2O. Prior to common work up, the solution was diluted with 500 mL of DCM and 300 mL of deionized water. *N*-(4-Nitrosophenyl)-4-phenylbutanamide (**27**) was isolated as a dark green solid. ^{1}H-NMR (300 MHz, $CDCl_3$): δ 7.66-7.99 (m, 4H, H-2, H-3), 7.17-7.42 (m, 5H, H-10, H-11, H-12), 2.78 (t, ^3J = 7.4 Hz, 7.4 Hz, 2H, H-8), 2.48 (t, ^3J = 7.4 Hz, 7.4 Hz, 2H, H-6), 2.15 (p, ^3J= 7.4, 7.4, 7.3, 7.3, 2H, H-7); ^{13}C-NMR (75 MHz, $CDCl_3$): δ 171.45 (C-5), 163.88 (C-1), 144.59 (C-4), 140.97 (C-9), 128.52 (C-10), 128.49 (C-11), 126.20 (C-12), 118.74 (C-3), 118.76 (C-2), 36.85 (C-8), 34.93 (C-6), 26.46 (C-7); MS (EI): m/z calculated for $[C_{16}H_{16}N_2O_2]^+$= 268, found 268.

12.5.1.5. Synthesis of *N*-aryl hydroxamic acids

Synthesis of *N*-(4-(N-hydroxyformamido)phenyl)-4-phenylbutanamide (28)

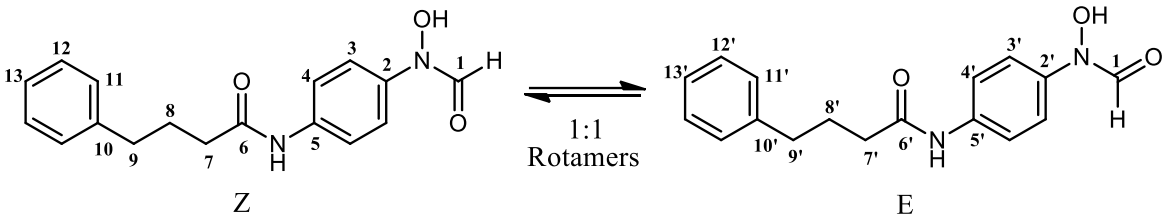

Yield (synthesis 1): 115 mg (0.38 mmol, 61%)

Yield (synthesis 2): 61 mg (0.20 mmol, 33%)

Melting point: 119-120 ºC.

TLC (1:4 CH/EA): R_f: 0.55

Synthesis 1: According to the general procedure SOP 20, *N*-(4-(N-Hydroxyformamido)-phenyl)-4-phenylbutanamide (**28**) was isolated as pale pink solid.

Synthesis 2: Same reaction procedure but with 34% of acetone from the start (20 mL). For the work-up, the miscible solvents acetone/water were removed concomitantly under reduced pressure, leaving a white precipitate that was filtered off, washed with distilled water, and dried over calcium chloride in the desiccator under vacuum overnight. Then, the crude product was purified by recrystallization by diffusion with a mixture of acetone/pentane. For that, the product **28** was dissolved in a minimum amount of acetone in a 10 mL snap cap vial, which was placed inside a 50 mL beaker with lid containing 0.5-1 cm of n-pentane, and it was kept at room temperature until precipitation of the product. Then, the supernatant was carefully removed from the yellow precipitate with a syringe, and the solid was washed with n-pentane.

After evaporation of the solvent under reduced pressure, *N*-(4-(N-Hydroxyformamido)phenyl)-4-phenylbutanamide (**28**) was isolated as cream crystals.

^{1}H-NMR (500 MHz, acetone-d^{6}): δ 9.67 (s, 2H, 2N-OH), 9.19 (s, 2H, 2NH), 8.59 (d, ^{4}J = 15.6 Hz, 2H, 2CHO), 7.70 (s, 6H, H-3, H-4, H-3'), 7.37 (s, 2H, H-4'), 7.06-7.31 (m, 10H, H-11, H-12, H-13, H-11', H-12', H-13'), 2.67 (q, ^{3}J= 9.7 Hz, 8.6 Hz, 4H, H-7, H-7') , 2.38 (q, ^{3}J= 9.8 Hz, 8.5 Hz, 4H, H-9, H-9'), 1.99 (m, 4H, H-8, H-8'); ^{13}C-NMR (126 MHz, acetone-d^{6}): δ 172.08 (C-6, C-6'), 161.81 (C-1), 156.69 (C-1'), 143.13 (C-10, C-10'), 129.59 (C-11, C-12), 129.46 (C-11', C-12'), 126.95 (C-13, C-13'), 121.01 (C-4), 120.83 (C-3), 120.39 (C-4'), 120.02 (C-3'), 37.24 (C-9, C-9'), 36.17 (C-7, C-7'), 28.20 (C-8, C-8'); HRMS (ESI): m/z calculated for $[C_{17}H_{18}N_2O_3]+H^+$= 299.13910, found 299.13902.

SOP 21 for the chemical synthesis of hydroxamic acid-drugs with pyruvate

Adapting a literature procedure,[229] to glacial acetic acid (20 mL) containing the corresponding nitroso compound (1.25 mmol, 1 eq.) was added slowly 5 mL of an aqueous solution of sodium pyruvate (344 mg, 3.13 mmol, 2.5 eq) with neutral pH (6-7). Reactions were stirred at RT until complete consumption of the nitrosoarene. Afterwards, the leftover starting material (the nitro component mostly) was filtered off the reaction mixture under reduced pressure, and the reaction solvent was evaporated. The minimum amount of deionized water was added and the flask was immersed in liquid nitrogen prior to lyophilization. The product was purified in a short silica column utilizing a gradient from CH:EA 10:1 to CH:EA 1:4.

N-(4-(N-Hydroxyacetamido)phenyl)-4-phenylbutanamide (29)

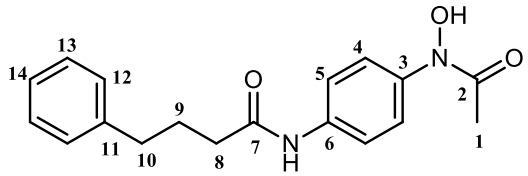

Yield: 258 mg (0.83 mmol, 66%)

Melting point: 97-98 ºC.

TLC (1:4 CH/EA): R_f: 0.47

N-(4-(N-Hydroxyacetamido)phenyl)-4-phenylbutanamide (**29**) was isolated as a dark amber solid. ^{1}H-NMR (500 MHz, CD_3OD): δ 7.72-7.39 (m, 4H, H-4, H-5), 7.26 (t, ^{3}J = 7.5 Hz, 2H, H-13), 7.23-7.18 (m, 2H, H-12), 7.18-7.13 (m, 1H, H-14), 2.69 (t, ^{3}J = 7.6 Hz, 2H, H-8), 2.38 (t, ^{3}J = 7.5 Hz, 2H, H-10), 2.34-2.05 (m, 3H, H-1). 2.00 (p, ^{3}J = 7.5, 7.6 Hz, 2H, H-9); ^{13}C-NMR (126 MHz, CD_3OD): δ 173.92 (C-7, C-2), 142.57 (C-3, C-6), 138.04 (C-11), 129.16 (C-12), 129.07 (C-13), 126.63 (C-14), 123.04 (C-5), 120.79 (C-4), 36.94 (C-10), 35.95 (C-8), 28.20 (C-9), 21.57 (C-1); HRMS (ESI): m/z calculated for $[C_{18}H_{20}N_2O_3]+ H^+$ = 313.15493, found 313.15467.

***N*-(4-(N,2-Dihydroxyacetamido)phenyl)-4-phenylbutanamide (30)**

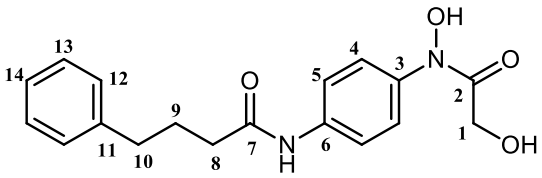

Yield: 180 mg (0.55 mmol, 48%)

Melting point: 110-111 ºC.

TLC (1:10 CH/EA): R_f: 0.37

N-(4-(N,2-Dihydroxyacetamido)phenyl)-4-phenylbutanamide (**30**) was isolated as an amber solid. ^{1}H-NMR (500 MHz, CD_3OD): δ 7.58 (m, 4H, H-4, H-5), 7.26 (t, ^3J = 7.5 Hz, 2H, H-13), 7.23 – 7.18 (m, 2H, H-12), 7.18 – 7.12 (m, 1H, H-14), 4.45 (s, 2H, H-1), 2.68 (t, ^3J = 7.6 Hz, 2H, H-8), 2.38 (t, ^3J = 7.5 Hz, 2H, H-10), 2.00 (m, ^3J = 7.5, 6.4 Hz, 2H, H-9); ^{13}C-NMR (126 MHz, CD_3OD): δ 172.77 (C-2, C-7), 141.43 (C-3, C-6), 136.91 (C-11), 128.03 (C-12), 127.93 (C-13), 125.49 (C-14), 120.64 (C-5), 119.73 (C-4), 59.99 (C-1), 35.79 (C-10), 34.82 (C-8), 27.07 (C-9); HRMS (ESI): m/z calculated for $[C_{18}H_{20}N_2O_4]+ H^+$ = 329.14960, found 329.14958.

12.5.1.6. Synthesis of 2-naphtylamine (36)

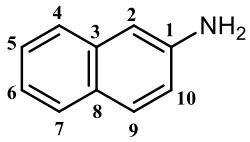

Yield: 4.57 g (3.19 mmol, 97%)

TLC (1:1 CH/EA): R_f: 0.52

According to a literature protocol,[320] 2-naphtol (**35**) (4.7 g, 32.91 mmol, 1 eq.) was dissolved in 100 mL of DMSO under argon atmosphere. Next, pulverized KOH (3.7 g, 66.36 mmol, 2 eq.) was added followed by 2-bromopropanamide (**41**) (10.0 g, 65.83 mmol, 2 eq.). The mixture was stirred at 50 ºC for 2.5 h. Pulverized KOH (3.7 g, 66.36 mmol, 2 eq) was added again, and the mixture was heated to 130 ºC. The reaction was monitored via TLC and allowed to stir overnight. After 17 h, more KOH (2.8 g, 49.79 mmol, 1.5 eq.) was added in three portions of 0.93 g each and the reaction was left to react for 2 hours extra. The solution was slowly cooled to room temperature and brine (90 mL) was added. The organic phase was separated and the aqueous phase was extracted four times with DCM (120 mL). The combined organic phases were washed with brine and evaporated under reduced pressure. The minimum amount of deionized water was added and the flask was immersed in liquid nitrogen prior to lyophilization. 2-Naphtylamine (**36**) was isolated as an amber solid. ^{1}H-NMR (300 MHz, $CDCl_3$): δ 7.67–7.39 (m, 3H, H-4, H-7, H-9), 7.34–7.19 (m, 1H, H-5), 7.12 (m, 1H, H-6), 6.93–6.71 (m, 2H, H-2, H-10), 3.66 (s, 2H, NH_2); ^{13}C-NMR (75 MHz, $CDCl_3$): δ 144.15 (C-1), 134.96 (C-3), 129.22 (C-9), 128.00 (C-8), 127.75 (C-7), 126.37 (C-5), 125.83 (C-4), 122.49 (C-6), 118.27 (C-10), 108.61 (C-2).

12.5.2. Tests with hydroxamic acids for inhibition of HDAC activity

As mentioned in Chapter 3, the tests to measure the inhibitory HDAC activity of the *N*-aryl HA **28**, **29** and **30** in comparison to the positive HA reference HTPB were performed by K. Schmidtkunz (group of M. Jung, Freiburg). Thus, the experimental procedures written here play a mere informative role.

For HDAC1 and HDAC6:

Human recombinant HDAC1 (BPS Bioscience, Catalog #: 50051) or human recombinant HDAC6 (BPS Bioscience, Catalog #: 50006) were diluted in incubation buffer containing Tris-HCl (50 mM) pH 8.0, NaCl (137 mM), KCl (2.7 mM), $MgCl_2$ (1 mM) and BSA (1 mg/mL). A total of 52 µL of this dilution were incubated with 3 µL of different concentrations of inhibitors in DMSO and 5 µL of the fluorogenic substrate ZMAL (126 µM) at 37 °C in OptiPlate-96 black microplates (PerkinElmer). Total volume 60 µL. After 90 min incubation time, 60 µL of the stop solution containing Trichostatin A (33 µM) and trypsin (6 mg/mL) dissolved in trypsin buffer (Tris-HCl 50 mM, pH 8.0, NaCl 100 mM) were added. The mixture was incubated at 37 °C for 30 min, and the fluorescence was measured on a BMG LABTECH POLARstar OPTIMA plate reader (BMG Labtechnologies, Germany) with an excitation wavelength of 390 nm and an emission wavelength of 460 nm.[342]

For TcDAC2; smHDAC8, hHDAC8:

The enzymes for these tests (human hHDAC8, *sm*HDAC8 from *Schisosoma mansoni*, and *tc*DAC2 from *Trypanosoma cruci*) were obtained from Christophe Romier (Institute of Genetics and of Molecular and Cellular Biology (IGBMC), Strasbourg). Activity assays were performed in ½ AreaPlate-96 F microplates (PerkinElmer). Total assay volume of 30 µL contained 12.5 µL assay buffer [Tris buffer (15 mM), pH 7.5, KH_2PO_4 (50 mM), $MgSO_4 \cdot 7\ H_2O$ (3 mM) and KCl (10 mM)], 10 µL of enzyme solution in assay buffer, 2.5 µL of different concentrations of inhibitors in DMSO and 5 µL of the fluorogenic substrate ZMTFAL (25 µM) in assay buffer. The microplates were incubated at 37 ºC for 90 min. After incubation, 30 µL of stop solution, containing 2.5 µL Trichostatin A (TSA) (33 µM) and 5 µL trypsin (6 mg/mL) in trypsin buffer [Tris-HCl (50 mM), pH 8.0, NaCl (100 mM)], were added. After further incubation at 37 ºC for 30 min, the fluorescence signal was measured on a BMG LABTECH POLARstar OPTIMA plate reader (BMG Labtechnologies, Germany) with an excitation wavelength of 390 nm and an emission wavelength of 460 nm.

13. References

[1] G. Schenk, R. G. Duggleby, P. F. Nixon, *Int. J. Biochem. Cell. Biol.* **1998**, *30*, 1297-1318.
[2] F. T. Zimmermann, A. Schneider, U. Schorken, G. A. Sprenger, W.-D. Fessner, *Tetrahedron Asymmetry* **1999**, *10*, 1643-1646.
[3] N. J. Turner, *Curr. Opin. Biotechnol.* **2000**, *11*, 527-531.
[4] S. R. Marsden, L. Gjonaj, S. J. Eustace, U. Hanefeld, *ChemCatChem* **2017**, *9*, 1808-1814.
[5] J. Abdoul-Zabar, I. Sorel, V. Helaine, F. Charmantray, T. Devamani, D. Yi, V. d. Berardinis, D. Louis, P. Marliere, W.-D. Fessner, L. Hecquet, *Adv. Synth. Catal.* **2013**, *355*, 116-128.
[6] T. Saravanan, M.-L. Reif, D. Yi, M. Lorillière, F. Charmantray, L. Hecquet, W.-D. Fessner, *Green Chem.* **2017**, *19*, 481.
[7] E. M. F. Muri, M. J. Nieto, R. D. Sindelar, J. S. Williamson, *Curr. Med. Chem.* **2002**, *9*, 1631-1653.
[8] R. Codd, *Coord. Chem. Rev.* **2008**, *252*, 1387-1408.
[9] V. M. Richon, Y. Webb, R. Merger, T. Sheppard, B. Jursic, L. Ngo, F. Civoli, R. Breslow, R. A. Rifkind, P. A. Marks, *Proc. Natl. Acad. Sci. U.S.A.* **1996**, *93*, 5705.
[10] Q. Lu, Y.-T. Yang, C.-S. Chen, M. Davis, J. C. Byrd, M. R. Etherton, A. Umar, C.-S. Chen, *J. Med. Chem.* **2004**, *47*, 467-474.
[11] C. C. Wong, K.-W. Cheng, B. Rigas, *J. Pharmacol. Exp. Ther.* **2012**, *341*, 572-578.
[12] K. Faber, *Biotransformations in Organic Chemistry*, Seventh ed., Springer International Publishing AG, Switzerland, **2018**.
[13] K. J. Laidler, *Pure Appl. Chem.* **1996**, *68*, 149-192.
[14] H. Heinemann, in *Catalysis science and technology, Vol. 1* (Eds.: J. R. Anderson, M. Boudart), Springer, New York, **1981**.
[15] B. Lindström, L. J. Pettersson, *CatTech* **2003**, *7*, 130-138.
[16] J. N. Armor, *Catal. Today* **2011**, *163*, 3–9.
[17] W. H. D. Camp, in *Chiral Liquid Chromatography* (Ed.: W. J. Lough), Springer, Dordrecht, **1989**, pp. 14-22.
[18] G. E. Ehrlich, *Am. J. Hosp. Pharm.* **1992**, *49(9 Suppl 1)*, S15-18.
[19] R. L. Brent, *Pediatrics* **2004**, *113*, 957-968.
[20] S. W. Smith, *Toxicol. Sci.* **2009**, *110*, 4–30.
[21] M. T. Miller, *Trans. Am. Ophthalmol. Soc.* **1991**, *89*, 623–674.
[22] F. G. Adly, A. Ghanem, *Catalysts* **2019**, *9*.
[23] R. A. Sheldon, J. M. Woodley, *Chem. Rev.* **2018**, *118*, 801−838.
[24] Z. Karagölge, B. Gür, *Iğdır Univ. J. Inst. Sci. & Tech.* **2016**, *6*, 89-96.
[25] W. M. Adams, *The Future of Sustainability: Re-thinking Environment and Development in the Twenty-first Century. Report of the IUCN Renowned Thinkers Meeting, 29–31 January 2006*, **2006**.
[26] K. B. Buchholz, P. B. Poulsen, in *Applied biocatalysis* (Eds.: A. J. J. Straathof, P. Adlercreutz), Harwood Academic Publishers, Taylor & Francis e-Library, **2005**, pp. 1-17.
[27] C. Walsh, *Nature* **2001**, *409*, 226–231.
[28] S. M. Roberts, *J. Chem. Soc., Perkin Trans. 1* **1998**.
[29] P. T. Anastas, J. C. Warner, *Green Chemistry: Theory and Practice*, Oxford University Press, Oxford, U.K., **1998**.
[30] J. Albarrán-Velo, D. González-Martínez, V. Gotor-Fernández, *Biocatal. Biotransformation.* **2017**, *36*, 102-130.
[31] T. Anthonsen, in *Applied biocatalysis*, Second ed. (Eds.: A. J. J. Straathof, P. Adlercreutz), Hardwood Academic Publishers, Taylor & Francis e-Library, **2005**, pp. 18-61.
[32] A. J. Straathof, S. Panke, A. Schmid, *Curr. Opin. Biotechnol.* **2002**, *13*, 548-556.
[33] Grand View Research, Enzymes Market Size, Share & Trends Analysis Report By Application, (Industrial Enzymes, Specialty Enzymes), By Product (Carbohydrase, Proteases, Lipases), By Source, By Region, And Segment Forecasts, 2020-2027, **2020**.
[34] Mordor Intelligence, Global Industrial Enzymes Market Report, Growth, Trends, Covid-19 Impact, And, Forecasts, (2021-2026), **2020**.

[35] Grand View Research, Healthcare Specialty Enzymes Market Size, Share & Trends Analysis Report By Application, By, Source, (Carbohydrases, Proteases), By Product, By Technique, By Application, By Usage, By End Use, By Region, And Segment Forecasts, 2020-2027, **2020**.
[36] S. Luetz, L. Giver, J. Lalonde, *Biotechnol. Bioeng.* **2008**, *101*, 647-653.
[37] T. Akkoyun, A. Arslan, I. Turhan, M. Karhan, *Curr. Opin. Biotechnol.* **2011**, *22*, S61.
[38] L. P. Wackett, *Microb. Biotechnol.* **2010**, *3* 729–730.
[39] A. Schmid, J. S. Dordick, B. Hauer, A. Kiener, M. Wubbolts, B. Witholt, *Nature* **2001**, *409*, 258-268.
[40] F. Tao, Y. Liu, Q. Luo, F. Su, Y. Xu, F. Li, B. Yu, C. Ma, P. Xu, *Bioresour. Technol.* **2011**, *102*, 9380-9387.
[41] X. Y. Tang, H. L. Sun, B. F. He, *Prog. Chem.* **2009**, *21*, 2726-2733.
[42] *Organic synthesis with enzymes in non-aqueous media*, Willey-VCH, Weinheim, **2008**.
[43] J. M. Bolivar, B. Nidetzky, *Green Process. Synth.* **2013**, *2*, 541–559.
[44] R. Karande, A. Schmid, K. Buehler, *Org. Process Res. Dev.* **2016**, *20*, 361-370.
[45] U. T. Bornscheuer, G. W. Huisman, R. J. Kazlauskas, S. Lutz, J. C. Moore, K. Robins, *Nature* **2012**, *485*, 185-194.
[46] J. M. Blamey, F. Fischer, H.-P. Meyer, F. Sarmiento, M. Zinn, in *Biotechnology of Microbial Enzymes*. (Ed.: G. Brahmachari), Academic Press, **2017**, pp. 347-403.
[47] N. J. Turner, *Trends Biotechnol.* **2003**, *21*, 474-478.
[48] C. Li, R. Zhang, J. Wang, L. M. Wilson, Y. Yan, *Trends Biotechnol.* **2020**, *38*, 729-744.
[49] A. Currin, N. Swainston, P. J. Dayace, D. B. Kell, *Chem. Soc. Rev.* **2015**, *44*.
[50] B. Turanli-Yildiz, C. Alkim, Z. P. Cakar, in *Protein Engineering* (Ed.: P. Kaumaya), IntechOpen, Rijeka, Croatia, **2012**.
[51] O. Kuchner, F. H. Arnold, *Trends Biotechnol.* **1997**, *15*, 523-530.
[52] F. H. Arnold, *FASEB J.* **1993**, *7*, 744-749.
[53] J. E. Ness, M. Welch, L. Giver, M. Bueno, J. R. Cherry, T. V. Borchert, W. P. C. Stemmer, J. Minshull, *Nat. Biotechnol.* **1999**, *17*, 893-896.
[54] S. Raillard, A. Krebber, Y. Chen, J. E. Ness, E. Bermudez, R. Trinidad, R. Fullem, C. Davis, M. Welch, J. Seffernick, L. P. Wackett, W. P. C. Stemmer, J. Minshull, *Chem. Biol.* **2001**, *8*, 891-898.
[55] N. E. Labrou, *Curr. Protein Pept. Sci.* **2010**, *11*, 91-100.
[56] M. S. Packer, D. R. Liu, *Nat. Rev. Genet.* **2015**, *16*, 379-394.
[57] R. C. Cadwell, G. F. Joyce, *PCR Methods Appl.* **1992**, *2*, 28-33.
[58] F. K. Tamaki, *Emerging Top. Life Sci.* **2020**, *4*, 119-127.
[59] J. D. Sutherland, *Curr. Opin. Chem. Biol.* **2000**, *4*, 263–269.
[60] www.evoenzyme.com/technology, 15.11.2021.
[61] R. A. Chica, N. Doucet, J. N. Pelletier, *Curr. Opin. Biotechnol.* **2005**, *16*, 378–384.
[62] L. Ye, C. Yang, H. Yu, *Appl. Microbiol. Biotechnol.* **2018**, *102*, 559-567.
[63] I. V. Korendovych, *Methods Mol. Bio.* **2018**, *1685*.
[64] *Enzyme Catalysis in Organic Synthesis, a Comprehensive Handbook, 3 Volume Set, 3rd,*, Second ed., Wiley-VCH, Weinheim, **2012**.
[65] K. Buchholz, V. Kasche, U. T. Bornscheuer, *Biocatalysts and Enzyme Technology*, Second ed., Wiley-VCH, Weinheim, **2012**.
[66] G. A. Strohmeier, H. Pichler, O. May, M. Gruber-Khadjawi, *Chem. Rev.* **2011**, *7*, 4141–4164.
[67] A. Liese, K. Seelbach, C. Wandrey, *Industrial Biotransformations*, Wiley-VCH, Weinheim, **2006**.
[68] R. N. Patel, *Stereoselective Biocatalysis*, New York-Basel, **2000**.
[69] C. Eijkman, *Arch. Pathol. Anat. Physiol. Klin. Med.* **1897**, *148*, 523-532.
[70] B. Jansen, W. Donath, *Geneeskundig Tijdschrift voor Nederlandsch-Indie* **1926**, *66*, 1-2.
[71] M. A. Crook, in *Laboratory Assessment of Vitamin Status* (Ed.: D. Harrington), Academic Press, **2019**, pp. 149-164.
[72] B. Harrow, *Casimir Funk. Pioneer in Vitamins and Hormones*, Dodd, Mead and Company, New York, **1955**.
[73] C. T. Jurgenson, T. P. Begley, S. E. Ealick, *Annu. Rev. Biochem.* **2009**, *78*, 569-603.
[74] F. Jordan, *Nat. Prod. Rep.* **2003**, *20*, 184-201.

[75] G. Malandrinos, M. Louloudi, N. Hadjiliadis, *Chem. Soc. Rev.* **2006**, *35*, 84-692.
[76] G. L. Barletta, Y. Zou, W. P. Huskey, F. Jordan, *J. Am. Chem. Soc.* **1997**, *119*, 2356-2362.
[77] H. Iding, P. Siegert, K. Mesch, M. Pohl, *Biochim. Biophys. Acta, Protein Struct. Mol. Enzymol.* **1998**, *1385*, 307-322.
[78] M. Mueller, D. Gocke, M. Pohl, *FEBS J.* **2009**, *276*, 2894-2904.
[79] G. A. Sprenger, M. Pohl, *J. Mol. Catal. B Enzym.* **1999**, *6*, 145-159.
[80] H. C. Hailes, D. Rother, M. Mueller, R. Westphal, J. M. Ward, J. Pleiss, C. Vogel, M. Pohl, *FEBS J.* **2013**, *280*, 6374-6394.
[81] M. Widmann, R. Radloff, J. Pleiss, *BMC Biochem.* **2010**, *11*, 9.
[82] G. de la Haba, I. G. Leder, E. Racker, *J. Biol. Chem.* **1955**, *214*, 409-426.
[83] G. A. Kochetov, O. N. Solovjeva, *Biochim. Biophys. Acta* **2014**, *1844*, 1608-1618.
[84] G. Sprenger, *Arch. Microbiol.* **1995**, *164*, 324-330.
[85] U. Schörken, G. A. Sprenger, *Biochim. Biophys. Acta, Protein Struct. Mol. Enzymol.* **1998**, *1385*, 229-243.
[86] Y. Kobori, D. C. Myles, G. M. Whitesides, *J. Org. Chem.* **1992**, *57*, 5899-5907.
[87] Y. Lindqvist, G. Schneider, U. Ermler, M. Sundström, *EMBO J.* **1992**, *11*, 2373-2379.
[88] M. Nikkola, Y. Lindqvist, G. Schneider, *J. Mol. Biol.* **1994**, *238*, 387-404.
[89] J. Littlechild, N. Turner, G. Hobbs, M. Lilly, A. Rawas, H. Watson, *Acta Cryst.* **1995**, *D51*, 1074-1076.
[90] P. Asztalos, C. Parthier, R. Golbik, M. Kleinschmidt, G. Huebner, M. S. Weiss, R. Friedemann, G. Wille, K. Tittmann, *Biochemistry* **2007**, *46*, 12037-12052.
[91] P. E. Affaticati, S.-B. Dai, P. Payongsri, H. C. Hailes, K. Tittmann, P. A. Dalby, *Sci. Rep.* **2016**, *6*, 35716.
[92] N. J. Veitch, D. A. Maugeri, J. J. Cazzulo, Y. Lindqvist, M. P. Barrett, *Biochem. J.* **2004**, *382*, 759-767.
[93] M. Pasquini, S. Fermani, D. Tedesco, Chiara Sciabolini, P. Crozet, M. Naldi, J. Henri, U. Vothknecht, Carlo Bertucci, S. D. Lemaire, M. Zaffagnini, F. Francia, *Biochim. Biophys. Acta BBA - Gen. Subj* **2017**, *1861*, 2132-2145.
[94] P. C. Heinrich, H. Steffen, P. Janser, O. Wiss, *Eur. J. Biochem.* **1972**, *30*, 533-541.
[95] V. A. Selivanov, M. V. Kovina, N. V. Kochevova, L. E., Meshalkina, G. A. Kochetov, *J. Mol. Catal. B Enzym.* **2003**, *26*, 33-40.
[96] S. J. Costelloe, J. M. Ward, P. A. Dalby, *J. Mol. Evol.* **2008**, *66*, 36-49.
[97] G. A. Kochetov, *Biochem. (Mosc.)* **2001**, *66*, 1077-1085.
[98] A. Ranoux, U. Hanefeld, *Top. Catal.* **2013**, *56*, 750-764.
[99] G. Schneider, Y. Lindqvist, *Biochim. Biophys. Acta, Protein Struct. Mol. Enzymol.* **1998**, *1385*, 387-398.
[100] G. A. Kochetov, I. A. Sevostyanova, *Life* **2005**, *57*, 491 – 497.
[101] M. Gyamerah, A. J. Willetts, *Enzyme Microb. Technol.* **1997**, *20*, 127-134.
[102] U. Nilsson, L. Meshalkina, Y. Lindqvist, G. Schneider, *J. Biol. Chem.* **1997**, *272*, 1864-1869.
[103] C. Wikner, U. Nilsson, L. Meshalkina, C. Udekwu, Y. Lindqvist, G. Schneider, *Biochemistry* **1997**, *36*, 15643-15649.
[104] Y. A. Muller, Y. Lindqvist, W. Furey, G. E. Schulz, F. Jordan, G. Schneider, *Structure* **1993**, *1*, 95-103.
[105] X. Sheng, Y. Liu, C. Liu, *J. Mol. Graph. Model.* **2013**, *39*, 23-28.
[106] A. Ranoux, S. K. Karmee, J. Jin, A. Bhaduri, A. Caiazzo, I. W. C. E. Arends, U. Hanefeld, *ChemBioChem* **2012**, *13*, 1921-1931.
[107] G. A. Sprenger, U. Schörken, G. Sprenger, H. Sahm, *Eur. J. Biochem.* **1995**, *230*, 525-532.
[108] O. A. Esakova, L. E. Meshalkina, G. A. Kochetov, R. Golbik, *Biochem. (Mosc.)* **2009**, *74*, 1234-1238.
[109] L. Hecquet, J. Bolte, C. Demuynck, *Biosci. Biotechnol. Biochem.* **1993**, *57*, 2174-2176.
[110] J. J. Villafranca, B. Axelrod, *J. Biol. Chem.* **1971**, *246*, 3126-3131.
[111] P. Srere, J. R. Cooper, M. Tabachnick, E. Racker, *Arch. Biochem. Biophys.* **1958**, *74*, 295-305.
[112] F. Dickens, D. H. Williamson, *Biochem. J.* **1958**, *68*, 74-81.
[113] R. Wohlgemuth, *J. Mol. Catal. B Enzym.* **2009**, *61*, 23-29.

[114] J. Bolte, C. Demuynck, O. Constant, L. Hecquet, in *Microbial Reagents in Organic Synthesis* (Ed.: S. Servi), Kluwer Academy, Dordrecht, **1992**, pp. 57-66.
[115] J. Bolte, C. Demuynck, H. Samaki, *Tetrahedron Lett.* **1987**, *28*, 5525-5528.
[116] G. R. Hobbs, M. D. Lilly, N. J. Turner, J. M. Ward, A. J. Willets, J. M. Woodley, *J. Chem. Soc., Perkin Trans. 1* **1993**, 165-166.
[117] C. Demuynck, J. Bolte, L. Hecquet, V. Dalmas, *Tetrahedron Lett.* **1991**, *32*, 5085-5088.
[118] L. Hecquet, C. Demuynck, G. Schneider, J. Bolte, *J. Mol. Catal. B Enzym.* **2001**, *11*, 771-776.
[119] D. Crestia, C. Guerard, H. Veschambre, L. Hecquet, C. Demuynck, J. Bolte, *Tetrahedron Asymmetry* **2001**, *12*, 869-876.
[120] K. G. Morris, M. E. B. Smith, N. J. Turner, M. D. Lilly, R. K. Mitra, J. M. Woodley, *Tetrahedron Asymmetry* **1996**, *7*, 2185-2188.
[121] F. Effenberger, V. Null, T. Ziegler, *Tetrahedron Lett* **1992**, *33*, 5157-5160.
[122] C. Andre, C. Guerard, L. Hecquet, C. Demuynck, J. Bolte, *J. Mol. Catal. B Enzym.* **1998**, *5*, 459-466.
[123] I. A. Bykova, O. N. Solovjeva, L. E. Meshalkina, M. V. Kovina, G. A. Kochetov, *Biochem. Biophys. Res. Commun.* **2001**, *280*, 845-847.
[124] E. Fiedler, R. Golbik, G. Schneider, K. Tittmann, H. Neef, S. Konig, G. Hubner, *J. Biol. Chem.* **2001**, *276*, 16051-16058.
[125] O. N. Solovjeva, M. V. Kovina, M. G. Zavialova, V. G. Zgoda, D. S. Shcherbinin, G. A. Kochetov, *Biosci. Rep.* **2020**, *40*.
[126] O. N. Solovjeva, *Anal. Biochem.* **2021**, *613*, 1-14.
[127] I. A. Sevostyanova, O. N. Solovjeva, G. A. Kochetov, *Biochem. Biophys. Res. Commun.* **2004**, *313*, 771-774.
[128] H. C. Wilkinson, P. A. Dalby, *FEBS J.* **2020**, *288*, 1935-1955.
[129] E. G. Hibbert, T. Senussi, S. J. Costelloe, W. Lei, M. E. B. Smith, J. M. Ward, H. C. Hailes, P. A. Dalby, *J. Biotechnol.* **2007**, *131*, 425-432.
[130] E. G. Hibbert, T. Senussi, M. E. B. Smith, S. J. Costelloe, J. M. Ward, H. C. Hailes, P. A. Dalby, *J. Biotechnol.* **2008**, *134*, 240-245.
[131] A. Cazares, J. L. Galman, L. G. Crago, M. E. B. Smith, J. Strafford, L. Rios-Solis, G. J. Lye, P. A. Dalby, H. C. Hailes, *Org. Biomol. Chem.* **2010**, *8*, 1301-1309.
[132] J. L. Galman, D. Steadman, S. Bacon, P. Morris, M. E. B. Smith, J. M. Ward, P. A. Dalby, H. C. Hailes, *Chem. Commun. (Camb.)* **2010**, *46*, 7608-7610.
[133] P. Payongsri, D. Steadman, J. Strafford, A. MacMurray, H. C. Hailes, P. A. Dalby, *Org. Biomol. Chem.* **2012**, *10*, 9021-9029.
[134] P. Payongsri, D. Steadman, H. C. Hailes, P. A. Dalby, *Enzyme Microb. Technol.* **2015**, *71*.
[135] M. T. Reetz, M. Bocola, J. D. Carballeira, D. Zha, A. Vogel, *Angew. Chem. Int. Ed.* **2005**, *44*, 4192-4196.
[136] M. Board, A. Colquhoun, E. A. Newsholme, *Cancer Res.* **1995**, *55*, 3278-3285.
[137] F. Subrizi, M. Cárdenas-Fernández, G. J. Lye, J. M. Ward, P. A. Dalby, T. D. Sheppard, H. C. Hailes, *Green Chem.* **2016**, *18*.
[138] H. Yu, R. I. H. Lopez, D. Steadman, D. Mendez-Sanchez, S. Higson, A. Cazares-Korner, T. D. Sheppard, J. M. Ward, H. C. Hailes, P. A. Dalby, *FEBS J.* **2020**, *287*, 1758–1776.
[139] M. E. B. Smith, E. G. Hibbert, A. B. Jones, P. A. Dalby, H. C. Hailes, *Adv. Synth. Catal.* **2008**, *350*, 2631-2638.
[140] P. A. Dalby, J. P. Aucamp, R. George, R. J. Martinez-torres, *Biochem. Soc. Trans.* **2007**, *35*, 1606-1609.
[141] M. J.Danson, D. W.Hough, Rupert J.M.Russell, G. L.Taylor, L. Pearl, *Protein Eng. Des. Sel.* **1996**, *9*, 629-630.
[142] P. Morris, L. Rios-Solis, R. García-Arrazola, G. J. Lye, P. A. Dalby, *Enzyme Microb. Technol.* **2016**, *89*, 85-91.
[143] H. Yu, Y. Yan, C. Zhang, P. A. Dalby, *Sci. Rep.* **2017**, *7*.
[144] J. Damnjanovic, H. Nakano, Y. Iwasaki, *Biotechnol. Bioeng.* **2014**, *111*, 674–682.
[145] H. C. Hailes, P. A. Dalby, G. J. Lye, F. Baganz, M. Micheletti, N. Szita, J. M. Ward, *Curr. Org. Chem.* **2010**, *14*, 1883-1893.
[146] T. Ziegler, A. Straub, F. Effenberger, *Angew. Chem. Int. Ed. Engl.* **1988**, *27*, 716-717.

[147] F. Charmantray, P. Dellis, V. Helaine, S. Samreth, L. Hecquet, *Eur. J. Org. Chem.* **2006**, 5526-5532.
[148] L. Hecquet, M. Lemaire, J. Bolte, C. Demuynck, *Tetrahedron Lett.* **1994**, *35*, 8791-8794.
[149] L. Hecquet, J. Bolte, C. Demuynck, *Tetrahedron* **1996**, *52*, 8223-8232.
[150] L. Hecquet, J. Bolte, C. Demuynck, *Tetrahedron* **1994**, *50*, 8677-8684.
[151] F. Charmantray, V. Helaine, B. Legeret, L. Hecquet, *J. Mol. Catal. B: Enzym.* **2009**, *57*, 6-9.
[152] D. C. Myles, P. J. Andrulis, III, G. M. Whitesides, *Tetrahedron Lett.* **1991**, *32*, 4835-4838.
[153] K. M. Draths, D. L. Pompliano, D. L. Conley, J. W. Frost, A. Berry, G. L. Disbrow, R. J. Staversky, J. C. Lievense, *J. Am. Chem. Soc.* **1992**, *114*, 3956-3962.
[154] H. Lossen, *Liebigs Ann. Chem.* **1869**, *150*, 314-322.
[155] C. J. Marmion, D. Griffith, K. B. Nolan, *Eur. J. Inorg. Chem.* **2004**, 3003-3016.
[156] S. P. Gupta, A. Sharma, in *Hydroxamic Acids: A Unique Family of Chemicals with Multiple Biological Activities* (Ed.: S. P. Gupta), Springer, **2013**, pp. 1-17.
[157] L. Bauer, O. Exner, *Angew. Chem. Int. Ed.* **1974**, *13*, 376-384.
[158] K. K. Ghosh, *Indian J. Chem., Sect. B: Org. Chem. Incl. Med. Chem.* **1997**, *36B*, 1089-1102.
[159] D. A. Brown, R. A. Coogan, N. J. Fitzpatrick, W. K. Glass, D. E. Abukshima, L. Shiels, M. Ahlgrén, K. Smolander, T. T. Pakkanen, T. A. Pakkanen, M. Perakyla, *J. Chem. Soc., Perkin Trans. 2* **1996**, *2*, 2673-2679.
[160] M. Birus, R. v. Eldik, M. Gabricevic, A. Zahl, *Eur. J. Inorg. Chem.* **2002**, 819-825.
[161] O. Exner, B. Kakac, *Collect. Czech. Chem. Commun.* **1963**, *28*, 1656-1663.
[162] B. García, F. Secco, S. Ibeas, A. Muñoz, F. J. Hoyuelos, J. M. Leal, M. L. Senent, M. Venturini, *J. Org. Chem.* **2007**, *72*, 7832–7840.
[163] B. Monzyk, A. L. Crumbliss, *J. Am. Chem. Soc.* **1979**, *101*, 6203-6213.
[164] O. Exner, M. Hradil, J. Mollin, *Collect. Czech. Chem. Commun.* **1993**, *58*, 1109-1121.
[165] B. García, S. Ibeas, F. J. Hoyuelos, J. M. Leal, *J. Org. Chem.* **2001**, *66*, 7986-7993.
[166] K. Yang, B. Lou, *Mini. Rev. Med. Chem.* **2003**, *3*, 349-360.
[167] F. M. Martin, R. P. Beckett, C. L. Bellamy, P. F. Courtney, S. J. Davies, A. H. Drummond, R. Dodd, L. M. Pratt, S. R. Patel, M. L. Ricketts, R. S. Todd, A. R. Tuffnell, J. W. S. Ward, M. Whittaker, *Bioorg. Med. Chem. Lett.* **1999**, *9*, 2887-2892.
[168] C. B. Xue, X. He, R. L. Corbett, J. Roderick, Z. R. Wasserman, R. Q. Liu, B. D. Jaffee, M. B. Covington, M. Qian, J. M. Trzaskos, R. C. Newton, R. L. Magolda, R. R. Wexler, C. P. Decicco, *J. Med. Chem.* **2001**, *44*, 3351-3354.
[169] A. D. Baxter, R. Bhogal, J. Bird, J. F. Keily, D. T. Manallack, J. G. Montana, D. A. Owen, W. R. Pitt, R. J. Watson, R. E. Wills, *Bioorg. Med. Chem. Lett.* **2001**, *11*, 1465-1468.
[170] B. Barlaam, PatriceKoza, J. Berriot, *Tetrahedron lett.* **1999**, *55*, 7221-7232.
[171] M. A. Alam, *Curr. Org. Synth.* **2019**, *23*, 978-993.
[172] M.-H. Chen, M. G. Steiner, S. E. d. Laszlo, A. A. Patchett, M. S. Anderson, S. A. Hyland, H. R. Onishi, L. L. Silver, C. R. H. Raetz, *Bioorg. Med. Chem. Lett.* **1999**, *9*, 313-318.
[173] W. B. Renfrow, C. R. Hauser, *J. Am. Chem. Soc.* **1937**, *59*.
[174] D. G. Hoare, A. Olson, D. E. Koshland, *J. Am. Chem. Soc.* **1968**, *90*, 1638-1643.
[175] E. Bamberger, *Ber. Dtsch. Chem. Ges.* **1900**, *33*.
[176] N. S. Nandurkar, R. Petersen, K. Qvortrup, V. V. Komnatnyy, K. M. Taveras, S. T. L. Quementa, R. Frauenlob, M. Givskov, T. E. Nielsen, *Tetrahedron lett.* **2011**, *52*, 7121-7124.
[177] G. Giacomelli, A. Porcheddu, M. Salaris, *Org. Lett.* **2003**, *5*, 2715-2717.
[178] A. Porcheddu, G. Giacomelli, *J. Org. Chem.* **2006**, *71*, 7057-7059.
[179] A. Porcheddu, G. Giacomelli, in *The chemistry of Hydroxylamines, Oximes and Hydroxamic Acids* (Eds.: Z. Rappoport, J. F. Liebman), John Wiley & Sons, Ltd., **2009**, pp. 163-231.
[180] G. N. Papadopoulos, C. G. Kokotos, *Chem. Eur. J.* **2016**, *22*, 6964-6967.
[181] B. R. Kant, B. S. Kant, B. T. Chand, B. A. Kumar, in *Microbial Applications, Vol. 2* (Ed.: V. C. Kalia), Springer, Cham, **2017**, pp. 169-184.
[182] A. Volonterio, S. Bellosta, P. Bravo, M. Canavesi, E. Corradi, S. V. Meille, M. Monetti, N. Moussier, M. Zanda, *Eur. J. Org. Chem.* **2002**, *2002*, 428-438.
[183] S. Price, S. E. Osbourn, *Org. Lett.* **2005**, *7*, 3761-3763.
[184] L. R. Scolnick, A. M. Clements, J. Liao, L. Crenshaw, M. Hellberg, J. May, T. R. Dean, D. W. Christianson, *J. Am. Chem. Soc.* **1997**, *119*, 850-851.

[185] E. Farkas, A. Enyedy, G. Micera, E. Garribba, *Polyhedron* **2000**, *19*, 1727–1736.
[186] T. W. Failes, M. D. Hall, T. W. Hambley, *Dalton Trans.* **2003**, 1596-1600.
[187] C. Mulcahy, F. M. Dolgushin, K. A. Krot, D. Griffith, C. J. Marmion, *Dalton Trans.* **2005**, 1993-1998.
[188] B. Kurzak, E. Farkas, T. Glowiak, H. Kozlowski, *J. Chem. Soc. Dalton Trans.* **1991**, 163-167.
[189] C. J. Milios, E. Manessi-Zoupa, S. P. Perlepes, *Transit. Met. Chem.* **2002**, *27*, 864–873.
[190] H. J. Lindner, S. Göttlicher, *Acta Cryst.* **1969**, *25*, 832-842.
[191] E. Farkas, E. Kozma, M. Pethö, K. M. Herlihy, G. Micera, *Polyhedron* **1998**, *17*, 2220-2231.
[192] A. Dessì, G. Micera, D. Sanna, L. S. Erre, *J. Inorg. Biochem.* **1992**, *48*, 279–287.
[193] E. Adiguzel, F. Yilmaz, M. Emirik, M. Ozil, *J. Mol. Struct.* **2017**, *1127*, 403-412.
[194] J. B. Neilands, *Science* **1967**, *156*, 1443-1447.
[195] J. B. Neilands, *J. Biol. Chem.* **1995**, *270*, 26723–26726.
[196] R. C. Hider, X. Kong, *Nat. Prod. Rep.* **2010**, *27*, 637-657.
[197] A. L. Crumbliss, *Coord. Chem. Rev.* **1990**, *105*, 155-179.
[198] S. Bertrand, J.-J. Hélesbeux, G. Larcher, O. Duval, *Mini-Rev. Med. Chem.* **2013**, *13*, 1311-1326.
[199] D. K. Jain, A. Singh, V. K. Patel, P. C. Sharma, A. K. Gupta, A. K. Sharma, H. Rajak, *Int. J. Pharm. Pharm. Sci.* **2014**, *6*, 648-650.
[200] E. M. F. Muri, M. J. Nieto, J. S. Williamson, *Med. Chem. Rev.* **2004**, *1*, 385-394.
[201] G. Klein, J.-L. Reymond, *Angew. Chem. Int. Ed.* **2001**, *40*.
[202] G. Klein, D. Kaufmann, S. Schurch, J.-L. Reymond, *Chem. Commun.* **2001**.
[203] B. Priewisch, K. Rück-Braun, *J. Org. Chem.* **2005**, *70*, 2350-2352.
[204] B. L. Horecker, P. Z. Smyrniotis, *Methods Enzymol.* **1955**, *1*, 371-375.
[205] D. Yi, T. Devamani, J. Abdoul-Zabar, F. Charmantray, V. Helaine, L. Hecquet, W.-D. Fessner, *ChemBioChem* **2012**, *13*, 2290-2300.
[206] C.-S. Chen, L. Qiang, in *PCT Int. Appl., Vol. WO 2005/055928 A2*, A61K ed., The Ohio State University Research Foundation, USA, USA, **2005**, p. 90.
[207] P. J. Donk, *J. Bacteriol.* **1920**, *5*, 373-374.
[208] P. Kotzekidou, in *Encyclopedia of Food Microbiology, Vol. vol*, second ed. (Eds.: C. A. Batt, M. L. Tortorello), Elsevier, **2014**, pp. 129-134.
[209] R. R. F. Jahromi, P. Morris, R. J. Martinez-Torres, P. A. Dalby, *J. Biotechnol.* **2011**, *155*, 209-216.
[210] D. Yi, T. Saravanan, T. Devamani, F. Charmantray, L. Hecquet, W.-D. Fessner, *Chem. Commun. (Camb.)* **2015**, *51*, 480-483.
[211] J. Abdoul-Zabar, M. Lorilliere, D. Yi, T. Saravanan, T. Devamani, L. Nauton, F. Charmantray, V. Helaine, W.-D. Fessner, L. Hecquet, *Adv. Synth. Catal.* **2015**, *357*.
[212] C. Zhou, T. Saravanan, M. Lorilliere, D. Wei, F. Charmantray, L. Hecquet, W.-D. Fessner, D. Yi, *ChemBioChem* **2017**, *18*.
[213] N. Maltseva, Y. Kim, K. Kwon, A. Joachimiak, W. F. Anderson, *RCSB protein data bank* **2010**, *3M49*.
[214] W. L. DeLano, *The PyMOL Molecular Graphics System, Version 1.3* **2002**, Schrödinger LLC, http://www.pymol.org.
[215] M. Lorilliere, R. Dumoulin, M. L'enfant, A. Rambourdin, V. Thery, L. Nauton, W.-D. Fessner, F. Charmantray, L. Hecquet, *ACS Catal.* **2019**, *9*, 4754−4763.
[216] T. B. Granström, G. Takata, M. Tokuda, K. Izumori, *J. Biosci. Bioeng* **2004**, *97*, 89-94.
[217] Z. Ahmed, *Electron J. Biotechn.* **2001**, *4*, 1-9.
[218] Z. Li, Y. Gao, H. Nakanishi, X. Gao, L. Cai, *Beilstein J. Org. Chem.* **2013**, *9*, 2434–2445.
[219] B. Li, S. Varanasi, P. Relue, *Green Chem.* **2013**, *15*, 2149-2157.
[220] T. Saravanan, S. Junker, M. Kickstein, S. Hein, M.-K. Link, J. Ranglack, S. Witt, M. Lorilliere, L. Hecquet, W.-D. Fessner, *Angew. Chem. Int. Ed.* **2017**, *56*, 5358-5362.
[221] H. Casajus, L. Nauton, A. Lagarde, V. Thery, F. Charmantray, M. Leremboure, W.-D. Fessner, L. Hecquet, *ChemCatChem* **2020**, *12*, 5772–5779
[222] A. O. Magnusson, A. Szekrenyi, H.-J. Joosten, J. Finnigan, S. Charnock, W.-D. Fessner, *FEBS J.* **2019**, *286*, 184-204.
[223] M. Lorillière, M. D. Sousa, F. Bruna, E. Heuson, T. Gefflaut, V. d. Berardinis, T. Saravanan, D. Yi, W.-D. Fessner, F. Charmantray, L. Hecquet, *Green Chem.* **2017**, *19*, 425-435.

[224] M. D. Corbett, B. R. Corbett, *Biochem. Pharmacol.* **1986**, *35*, 3613-3621.
[225] B. G. Gowenlock, G. B. Richter-Addo, *Chem. Rev.* **2004**, *104*, 3315-3340.
[226] L. V. Desai, H. A. Malik, M. S. Sanford, *Org. lett.* **2006**, *8*, 1141-1144.
[227] J. Hutton, W. A. Waters, *J. Chem. Soc. B* **1968**, 191-195.
[228] O. Exner, in *Advances in Linear Free Energy Relationships* (Eds.: N. B. Chapman, J. Shorter), Springer, Boston, MA, **1972**, pp. 1-69.
[229] Y. Sakamoto, T. Yoshioka, T. Uematsu, *J. Org. Chem.* **1989**, *54*, 4449-4453.
[230] P. Zuman, B. Shah, *Chem. Rev.* **1994**, *94*, 1621.
[231] T. Yoshioka, T. Uematsu, *Biochem. J.* **1993**, *290*, 783-790.
[232] R. A. Usmanov, G. A. Kochetov, *Biokhimiya* **1983**, *48*, 772-781.
[233] S. Ursic, B. Nigovic, V. Vrcek, V. Pilepie, *Tetrahedron Letters* **1995**, *36*, 9547-9550.
[234] D. Radivoj, V. Pilepić, S. Uršić, *Croat. Chem. Acta* **1996**, *69*, 1633 - 1638.
[235] M. D. Corbett, *Bioorg. Chem.* **1974**, *3*, 361-365.
[236] A. J. J. Straathof, M. J. J. Litjens, J. J. Heijnen, in *Enzymes in Nonaqueous Solvents* (Eds.: E. N. Vulfson, P. J. Halling, H. L. Holland), Humana Press, **2001**, pp. 603-610.
[237] S. Narayan, J. Muldoon, M. G. Finn, V. V. Fokin, H. C. Kolb, K. B. Sharpless, *Angew. Chem. Int. Ed.* **2005**, *44*, 3275 –3279.
[238] M. D. Corbett, B. R. Corbett, *J. Org. Chem.* **1981**, *46*, 466-468.
[239] M. D. Corbett, B. R. Corbett, *J. Am. Chem. Soc.* **1980** *45*, 1980-2835.
[240] W. Liebl, A. Angelov, J. Juergensen, J. Chow, A. Loeschcke, T. Drepper, T. Classen, J. Pietruzska, A. Ehrenreich, W. R. Streit, K.-E. Jaeger, *Appl. Microbiol. Biotechnol.* **2014**, *98*, 8099–8109.
[241] H. Leemhuis, R. M. Kelly, L. Dijkhuizen, *IUBMB Life* **2009**, *61*, 222-228.
[242] S. V. Taylor, P. Kast, D. Hilvert, *Angew. Chem. Int. Ed.* **2001**, *40*, 3310-3335.
[243] G. Simon, M. Bouzon, F. Charmantray, V. Helaine, B. Legeret, P. Marliere, L. Hecquet, *Bioorg. Med. Chem. Lett.* **2009**, *19*, 3767-3770.
[244] L. Hecquet, W.-D. Fessner, V. Helaine, F. Charmantray, in *Cascade Biocatalysis: Integrating Stereoselective and Environmentally Friendly Reactions* (Eds.: S. Riva, W.-D. Fessner), Wiley-VCH, Weinheim, **2014**, pp. 315-337.
[245] G. Simon, T. Eljezi, B. Legeret, F. Charmantray, J. Castillo, C. Guerard-Helaine, M. Lemaire, M. Bouzon-Bloch, P. Marliere, V. Helaine, L. Hecquet, *ChemCatChem* **2013**, *5*, 784-795.
[246] L. Hecquet, V. Helaine, F. Charmantray, M. Lemaire, in *Modern Biocatalysis* (Eds.: W.-D. Fessner, T. Anthonsen), Wiley-VCH Verlag GmbH & Co. KGaA, Weinheim, **2009**, pp. 287-298.
[247] J.-L. Reymond, *Enzyme Assays. High-throughput Screening, Genetic Selection and Fingerprinting*, Wiley-VCH, Weinheim, **2006**.
[248] C. K. Savile, J. M. Janey, E. C. Mundorff, J. C. Moore, S. Tam, W. R. Jarvis, J. C. Colbeck, A. Krebber, F. J. Fleitz, J. Brands, P. N. Devine, G. W. Huisman, G. J. Hughes, *Science* **2010**, *329*, 305-309.
[249] K. L. Tee, T. S. Wong, *Biotechnol. Adv.* **2013**, *31*, 1707–1721.
[250] A. Madhavan, R. Sindhu, P. Binod, R. K. Sukumaran, A. Pandey, *Bioresour. Technol.* **2017**, *245*, 1304–1313.
[251] M. S. Weiß, U. T. Bornscheuer, M. Höhne, in *Protein Engineering: Methods and Protocols, Vol. 1685* (Eds.: U. T. Bornscheuer, M. Höhne), Humana Press, New York, NY, **2018**, pp. 283-296.
[252] J. H. Shim, Y. W. Kim, T. J. Kim, H. Y. Chae, J. H. Park, H. Cha, J. W. Kim, Y. R. Kim, T. Schaefer, T. Spendler, T. W. Moon, K. H. Park, *Protein Eng. Des. Sel.* **2004**, *17*, 205-211.
[253] D. Wahler, J.-L. Reymond, *Curr. Opin. Chem. Biol.* **2001**, *5*, 152–158.
[254] S. Brakmann, *Chembiochem* **2001**, *2*, 865–871.
[255] J.-Y. Lee, D.-E. Cheong, G.-J. Kim, *Biotechnol. Lett.* **2008**, *30*, 899-904.
[256] M. X. Du, J. Sim, L. Fang, Y. Zheng, S. Koh, J. Stratton, J. Pons, J. J.-X. Wang, B. Carte, *J. Biomol. Screen.* **2004**, *9*, 427-433.
[257] C. Naula, V. P. Alibu, J. M. Brock, N. J. Veitch, R. J. S. Burchmore, M. P. Barrett, *J. Biochem. Biophys. Methods* **2008**, *70*, 1185-1187.
[258] A. Sevestre, V. Helaine, G. Guyot, C. Martin, L. Hecquet, *Tetrahedron Lett.* **2003**, *44*, 827-830.

[259] A. Sevestre, F. Charmantray, V. Helaine, A. Lasikova, L. Hecquet, *Tetrahedron* **2006**, *62*, 3969-3976.
[260] F. Charmantray, B. Legeret, V. Helaine, L. Hecquet, *J. Biotechnol.* **2010**, *145*, 359-366.
[261] L. E. Janes, A. Cimpoia, R. J. Kazlauskas, *J. Org. Chem.* **1999**, *64*, 9019-9029.
[262] N. He, D. Yi, W.-D. Fessner, *Adv. Synth. Catal.* **2011**, *353*, 2384-2398.
[263] E. Chapman, C.-H. Wong, *Bioorg. Med. Chem.* **2002**, *10*, 551-555.
[264] C. Deng, R. R. Chen, *Anal. Biochem.* **2004**, *330*, 219-226.
[265] R. M. Rosenberg, R. M. Herreid, G. J. Piazza, M. H. O'Leary, *Anal. Biochem.* **1989**, *181*, 59-65.
[266] G. Hübner, R. Golbik, *Biochem. Int.* **1992**, *26*, 545-550.
[267] G. A. Kochetov, R. A. Usmanov, A. T. Mevkh, *Anal. Biochem.* **1978**, *88*, 296-301.
[268] I. A. Sevostyanova, O. N. Solovjeva, G. A. Kochetov, *Biochem. (Mosc.)* **2006**, *71*, 560-562.
[269] G. A. Kochetov, P. P. Filippov, *Anal. Biochem.* **1972**, *48*, 286-291.
[270] A. W. Holldorf, *Methods Enzym. Anal. (3rd Ed.)* **1984**, *6*, 578-582.
[271] R. K. Mitra, J. M. Woodley, *Biotechnol. Tech.* **1996**, *10*, 167-172.
[272] O. J. Miller, E. G. Hibbert, C. U. Ingram, G. J. Lye, P. A. Dalby, *Biotechnol. Lett.* **2007**, *29*, 1759-1770.
[273] M. E. B. Smith, U. Kaulmann, J. M. Ward, H. C. Hailes, *Bioorg. Med. Chem.* **2006**, *14*, 7062-7065.
[274] Z. Dische, A. Devi, *Biochim Biophys Acta* **1960**, *39*, 140-144.
[275] R. J. Kazlauskas, in *Enzyme Assays. High-throughput Screening, Genetic Selection and Fingerprinting* (Ed.: J.-L. Reymond), Wiley-VCH, Weinheim, **2006**, pp. 17-39.
[276] C. M. H. Ferreira, I. S. S. Pinto, E. V. Soares, H. M. V. M. Soares, *RSC Adv.* **2015**, *5*, 30989-31003.
[277] W. R. Algar, C. A. G. D. Jong, E. J. Maxwell, C. G. Atkins, *J. Chem. Educ.* **2016**, *93*, 162–165.
[278] J.-H. Zhang, T. D. Y. Chung, K. R. Oldenburg, *J Biomol Screen* **1999**, *4*, 67-73.
[279] U. T. Bornscheuer, J. Altenbuchner, H. H. Meyer, *Biotechnol. Bioeng.* **1998**, *58*.
[280] S. Delagrave, D. J. Murphy, J. L. R. Pruss, A. M. Maffia, B. L. Marrs, E. J. Bylina, W. J. Coleman, C. L. Grek, M. R. Dilworth, M. M. Yang, D. C. Youvan, *Protein Eng.* **2001**, *14*, 261–267.
[281] S. Gerstenbruch, H. Wulf, N. Mußmann, T. O'Connell, K.-H. Maurer, U. T. Bornscheuer, *Appl. Microbiol. Biotechnol.* **2012**, *96*, 1243–1252.
[282] M. Alexeeva, A. Enright, M. J. Dawson, M. Mahmoudian, N. J. Turner, *Angew. Chem. Int. Ed.* **2002**, *41*, 3177-3180.
[283] F. Escalettes, N. J. Turner, *ChemBioChem* **2008**, *9*, 857 – 860.
[284] S. V. Khoronenkova, V. I. Tishkov, *Anal. Biochem.* **2008**, *374*, 405–410.
[285] S. C. Willies, J. L. White, N. J. Turner, *Tetrahedron* **2012**, *68*, 7564-7567.
[286] D. Baud, N. Ladkau, T. S. Moody, J. M. Ward, H. C. Hailes, *Chem. Commun.* **2015**, *51*.
[287] A. P. Green, N. J. Turner, E. O'Reilly, *Angew. Chem. Int. Ed.* **2014**, *53*, 10714-10717.
[288] M. S. Weiß, I. V. Pavlidis, C. Vickers, M. Höhne, U. T. Bornscheuer, *Anal. Chem.* **2014**, *86*, 11847-11853.
[289] N. Ocal, A. Lagarde, L. Hecquet, *ChemBioChem* **2021**, *22*, 11-18.
[290] F. Tao, Q. Wang, *RSC Adv.* **2015**, *5*, 46007–46010.
[291] National Cancer Institute, What Is Cancer?, (https://www.cancer.gov/about-cancer/understanding/what-is-cancer), 03.02.2022.
[292] G. Heise, Wie entsteht Krebs in der Zelle und im Körper?, **2019**, (https://www.dw.com/de/wie-entsteht-krebs-in-der-zelle-und-im-k%C3%B6rper/a-19024789), 03.02.2022.
[293] D. W. Christianson, *Adv. Protein Chem.* **1991**, *42*, 281-355.
[294] K. A. McCall, C.-c. Huang, C. A. Fierke, *J. Nutr.* **2000**, *130*, 1437S-1446S.
[295] C. Salmi-Smail, A. Fabre, F. Dequiedt, A. Restouin, R. Castellano, S. Garbit, P. Roche, X. Morelli, J. M. Brunel, Y. Collette, *J. Med. Chem.* **2010**, *53*, 3038–3047.
[296] C. Zhao, H. Dong, Q. Xu, Y. Zhang, *Expert Opin. Ther. Pat.* **2020**, *30*, 263-274.
[297] H. Weinmann, E. Ottow, in *Comprehensive Medicinal Chemistry II*, Elsevier Ltd., Schering AG, Berlin, Germany, **2007**, pp. 221–251.
[298] M. Whittaker, C. D. Floyd, Peter Brown, A. J. H. Gearing, *Chem. Rev.* **1999**, *99*, 2735−2776.

[299] Z. Syed, K. Sonu, A. Dongre, G. Sharma, M. Sogani, *Int. J. Biol. Biomed.* **2020**, *14*, 75-88.
[300] M. S. Finnin, J. R. Donigian, A. Cohen, V. M. Richon, R. A. Rifkind, P. A. Marks, R. Breslow, N. P. Pavletich, *Nature* **1999**, *401*, 188-193.
[301] W.-D. Fessner, A. Schneider, H. Held, G. Sinerius, C. Walter, M. Hixon, J. V. Schloss, *Angew. Chem. Int. Ed.* **1996**, *35*, 2219-2221.
[302] S. Movafagh, A. Munson, in *Epigenetics of Cancer Prevention*, Elsevier Inc., **2019**, pp. 75-105.
[303] V. M. Richon, X. Zhou, R. A. Rifkind, P. A. Marks, *Blood Cells Mol. Dis.* **2001**, *27*, 260-264.
[304] B. S. Mann, J. R. Johnson, M. H. Cohen, R. Justice, R. Pazdur, *The Oncologist* **2007**, *12*, 1247–1252.
[305] C. Avendaño, J. C. Menéndez, in *Medicinal Chemistry of Anticancer Drugs*, Elsevier B. V., **2008**, pp. 307-349.
[306] V. M. Richon, *Br. J. Cancer* **2006**, *95*, S2-S6.
[307] S. Bhalla, S. Balasubramanian, K. David, M. Sirisawad, J. Buggy, L. Mauro, S. Prachand, R. Miller, L. I. Gordon, A. M. Evens, *Clin. Cancer Res.* **2009**, *15*, 3354-3365.
[308] G. S. Sholler, S. S. Roberts, E. A. Currier, J. P. Bond, *J. Cancer Ther. Res.* **2013**, *2*, 1-21.
[309] G. Lopez, J. Liu, W. Ren, W. Wei, S. Wang, G. Lahat, Q.-S. Zhu, W. G. Bornmann, D. J. McConkey, R. E. Pollock, D. C. Lev, *Clin. Cancer Res.* **2009**, *15*, 3472-3483.
[310] E. Deutsch, E. C.-J. Moyal, V. Gregorc, P. A. Zucali, J. Menard, J.-C. Soria, I. Kloos, J. Hsu, Y. Luan, E. Liu, R. Vezan, T. Graef, S. Rivera, *Oncotarget* **2017**, *8*, 56199-56209.
[311] L. Astor, FDA Grants Fast Track Designation to Abexinostat for Fourth-Line Follicular Lymphoma, **2019**, (https://www.targetedonc.com/view/fda-grants-fast-track-designation-to-abexinostat-for-fourthline-follicular-lymphoma), 15.03.2022.
[312] M. D. Corbett, B. R. Corbett, *Chem. Res. Toxicol.* **1988**, *1*, 222-227.
[313] T. Yoshioka, T. Uematsu, *Drug Metab. Dispos.* **1998**, *26*, 705-710.
[314] Q. Lu, D.-S. Wang, C.-S. Chen, Y.-D. Hu, C.-S. Chen, *J. Med. Chem.* **2005**, *48*, 5530-5535.
[315] J.-M. Shieh, T.-T. Wei, Y.-A. Tang, S.-M. Huang, W.-L. Wen, M.-Y. Chen, H.-C. Cheng, S. B. Salunke, C.-S. Chen, P. Lin, C.-T. Chen, Y.-C. Wang, *PLoS One* **2012**, *7*, 1-11.
[316] A. Leggio, E. L. Belsito, G. D. Luca, M. L. D. Gioia, V. Leotta, E. Romio, C. Siciliano, A. Liguori, *RSC Adv.* **2016**, *6*, 34468-34475.
[317] K. Kikugawa, T. Kawashima, *Chem. Pharm. Bull.* **1971**, *19*, 2629-2630.
[318] B. Tan, D. P. Hickey, R. D. Milton, F. Giroud, S. D. Minteer, *J. Electrochem. Soc.* **2015**, *162*, H102-H107.
[319] M. Böhm, A. Mitsch, P. Wissner, I. Sattler, M. Schlitzer, *J. Med. Chem.* **2001**, *44*, 3117-3124.
[320] J. Yu, Y. Wang, P. Zhang, J. Wu, *Synlett* **2013**, *24*, 1448-1454.
[321] K. D. Otley, J. A. Ellman, *J. Org. Chem.* **2014**, *79*, 8296-8303.
[322] G. A. Molander, L. N. Cavalcanti, *J. Org. Chem.* **2012**, *77*, 4402–4413.
[323] K. Hoffmann, G. Brosch, P. Loidl, M. Jung, *Nucleic Acids Res.* **1999**, *27*, 2057-2058.
[324] B. Heltweg, J. Trapp, M. Jung, *Methods* **2005**, *36*, 332–337.
[325] D. Wegener, F. Wirsching, D. Riester, A. Schwienhorst, *Chem. Biol.* **2003**, *10*, 61-68.
[326] S. L. Holbeck, J. M. Collins, J. H. Doroshow, *Mol. Cancer Ther.* **2010**, *9*, 1451-1460.
[327] A. Howell, J. Cuzick, M. Baum, A. Buzdar, M. Dowsett, J. F. Forbes, G. Hoctin-Boes, J. Houghton, G. Y. Locker, J. S. Tobias, A. T. Group, *Lancet* **2005**, *365*, 60-62.
[328] M. Göttlicher, S. Minucci, P. Zhu, O. H. Krämer, A. Schimpf, S. Giavara, J. P. Sleeman, F. L. Coco, C. Nervi, P. G. Pelicci, T. Heinzel, *EMBO J.* **2001**, *20*.
[329] W. L. F. Armarego, C. L. L. Chai, *Purification of Laboratory Chemicals*, Sixth ed., Elsevier, **2009**.
[330] F. Tibiletti, M. Simonetti, K. M. Nicholas, G. Palmisano, M. Parravicini, F. Imbesi, S. Tollari, A. Penoni, *Tetrahedron* **2010**, *66*, 1280-1288.
[331] A. Defoin, *Synthesis* **2004**, *5*, 706-710.
[332] D. Zhu, M. Lu, P. J. Chua, B. Tan, F. Wang, X. Yang, G. Zhong, *Org. Lett.* **2008**, *10*, 4585-4588.
[333] S. Krakert, A. Terfort, *Aust. J. Chem.* **2010**, *63*, 303-314.
[334] A. Jankowiak, E. Obijalska, P. Kaszynski, A. Pieczonka, J. Victor G. Young, *Tetrahedron* **2011**, *67*, 3317-3327.
[335] C. K. Ingold, *J. Chem. Soc.* **1925**, 513-518.

[336] E. H. Bartlett, C. Eaborn, D. R. M. Walton, *J. Chem. Soc. C* **1970**, 1717-1718.
[337] G. M. Kraay, Diss. Amsterdam **1926**.
[338] A. Defoin, G. Geffroy, D. L. Nouen, D. Spileers, J. Streith, *Helv. Chim. Acta* **1989**, *72*, 1199-1215.
[339] R. Tatsunami, T. Yoshioka, *J. Agric. Food Chem.* **2006**, *54*, 590-596.
[340] N. Ayyangar, *Indian J. Chem. B* **1989**, *28B*, 961-963.
[341] C. Zhang, Z. Xu, T. Shen, G. Wu, L. Zhang, N. Jia, *Org. Lett.* **2012**, *14*, 2362–2365.
[342] A. P. Saraswati, N. Relitti, M. Brindisi, J. D. Osko, G. Chemi, S. Federico, A. Grillo, S. Brogi, N. H. McCabe, R. C. Turkington, O. Ibrahim, J. O'Sullivan, S. Lamponi, M. Ghanim, V. P. Kelly, D. Zisterer, R. Amet, P. Hannon, F. Vanni, C. Ulivieri, Daniel Herp, F. Sarno, A. D. Costanzo, F. Saccoccia, G. Ruberti, M. Jung, L. Altucci, S. Gemma, S. Butini, D. W. Christianson, G. Campiani, *ACS Med. Chem. Lett.* **2020**, *11*, 2268-2276.
[343] in *Pure Appl. Chem., Vol. 56, Joint commission on biochemical nomenclature*, **1984**, pp. 595-624.

14. Appendix

14.1. List of frequently used abbreviations

Amino acids are abbreviated according to the one or three letter code.[343]

AHA	Acetohydroxamic acid
AMC	7-amino-4-methylcoumarin
AcOH	Acetic acid
BCA	Bicinchoninic acid
BSA	Bovine serum albumin
CFE	Cell free extract
CH	Cyclohexane
δ	Chemical shift
DCM	Dichloromethane
DHAP	Dihydroxyacetone phosphate
DHE-ThDP	Dihydroxyethyl-ThDP
DI	Deionized
DIC	*N,N'*-Diisopropylcarbodiimide
DMF	Dimethylformamide
DMSO	Dimethylsulfoxide
DTT	Dithiothreitol
d	Doublet (NMR)
EA	Ethyl acetate
EI	Electron ionization
ee	Enantiomeric excess
ESI	Electrospray ionization
E4P	D-Erythrose 4-phosphate
E. coli	*Escherichia coli*
eq.	Equivalent
Et_3N	Triethylamine
et al.	(lat.) *et alii* oder *et aliae*
e.g.	(lat.) *exempli gratia*
FBA	Formylbenzoic acid
F6P	D-Fructose 6-phosphate
FDA	United States Food and Drug Administration
GA	Glyoxylic acid
G3P	Glyceraldehyde 3-phosphate
Gly-Gly	Glycylglycine
HA	Hydroxamic acid
HDAC	Histone deacetylase
HDACi	HDAC inhibitor
HDLP	Histone deacetylase-like protein
HPA	Hydroxypyruvic acid
HPLC	High performance liquid chromatography
HP-β-CD	Hydroxypropyl-β-cyclodextrin
HPTLC	High performance thin layer chromatography
HTPB	*N*-hydroxy-4-(4-phenyl-butyryl-amino)-benzamide
HTS	High-Throughput Screening
Hz	Hertz
IPTG	Isopropyl β-D-thiogalactoside
J	Coupling constant (Hz, NMR)
KDa	Kilodalton
Lit.	Literature
LB	Lysogeny broth
LOD	Limit of detection
LOQ	Limit of quantification
MeCN	Acetonitrile

MeOH	Methanol
min.	Minute
MS	Mass spectrometry
m	Multiplet (NMR)
NADH	Nicotinamide adenine dinucleotide
nanoDSF	Nanoscale differential scanning Fluorimetry
NMR	Nuclear magnetic resonance
SSM	Site saturation mutagenesis
P	Partition coefficient
PA	Pyruvate
PEG	Polyethylene glycol
ppm	Parts per million
PPP	Pentose phosphate pathway
PyBOP	Benzotriazol-1-yloxy-tripyrrolidinophosphonium hexafluorophosphate
q	Quartet (NMR)
R_f	Retention factor
rpm	Revolutions per minute
R5P	D-Ribose 5-phosphate
RT	Room temperature
SAR	Structure-activity relationship
SAHA	Suberoylanilidehydroxamic acid
S7P	D-Sedulose 7-phosphate
SDS-PAGE	Sodium dodecyl sulfate polyacrylamide gel electrophoresis
s	Singlet (NMR)
SM	Starting material
SOP	Standard operating procedure
TEA	Triethanolamine
ThDP	Thiamine diphosphate
THF	Tetrahydrofurane
TK	Transketolase
TK_{ban}	TK from *Bacillus anthracis*
TK_{eco}	TK from *E. coli*
TK_{yst}	TK from baker's yeast
TK_{gst}	TK from *Geobacillus stearothermophilus*
TLC	Thin layer chromatography
TSA	Trichostatin A
T_m	Melting temperature
t	Triplet (NMR)
UV	Ultra violet
via	(lat.) by means of
WT	Wild-type
X5P	D-Xylulose 5-phosphate
ZMAL	(S)-benzyl (6-acetamido-1-((4-methyl-2-oxo-2H-chromen-7-yl)amino)-1-oxohexan-2-yl)carbamate
ZMF-TAL	(S)-benzyl (1-((4-methyl-2-oxo-2H-chromen-7-yl)amino)-1-oxo-6-(2,2,2-trifluoroacetamido)hexan-2-yl)-carbamate
Z-Lys	(S)-[5-amino-1-(4-methyl-2-oxo-2H-chromen-7-yl)carbamoyl)-pentyl]-carbamic acid benzyl ester

14.2. Data from CHAPTER I

NMR Spectra

Bromopyruvate

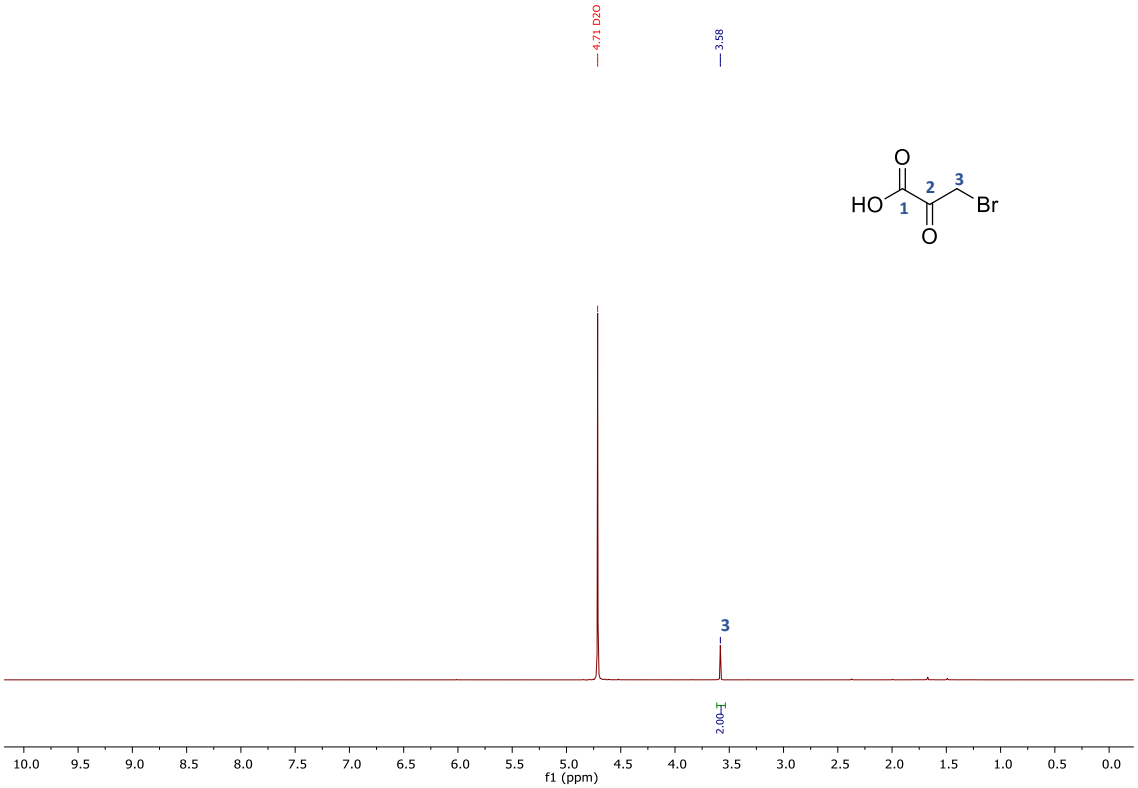

^{1}H-NMR spectrum of bromopyruvate (300 MHz, D_2O)

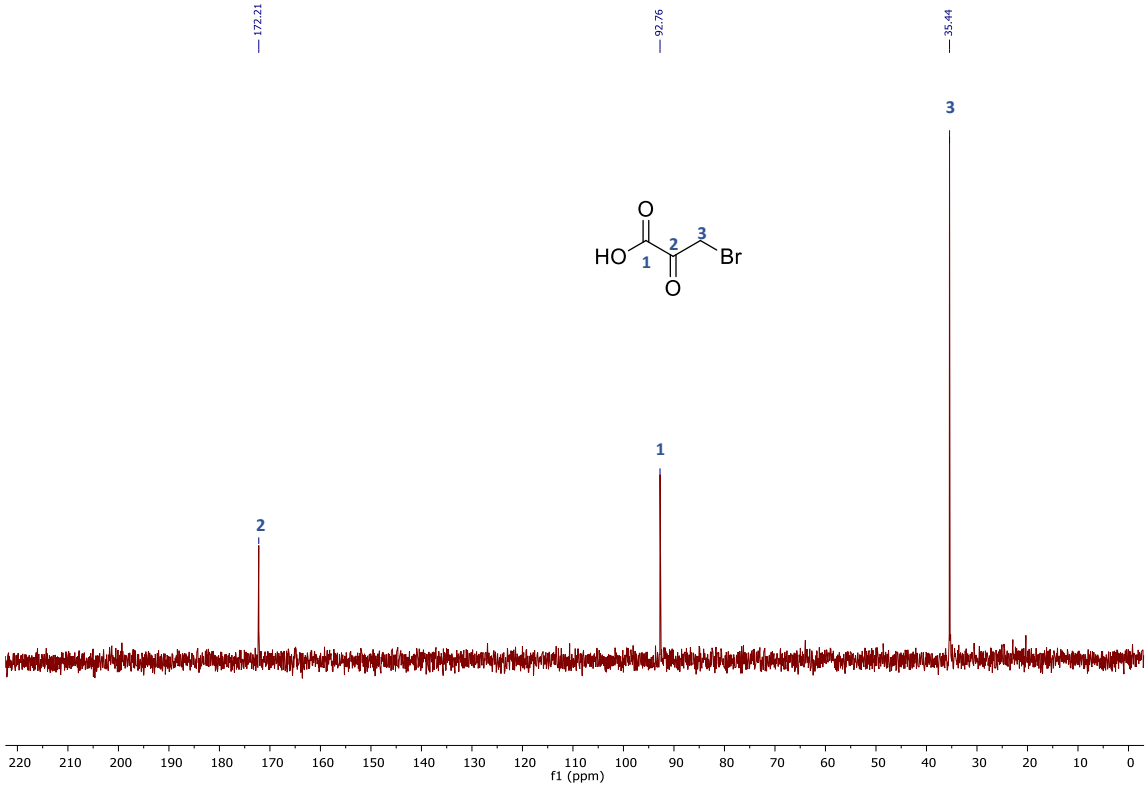

^{13}C-NMR spectrum of bromopyruvate (75 MHz, D_2O)

Hydroxypyruvate

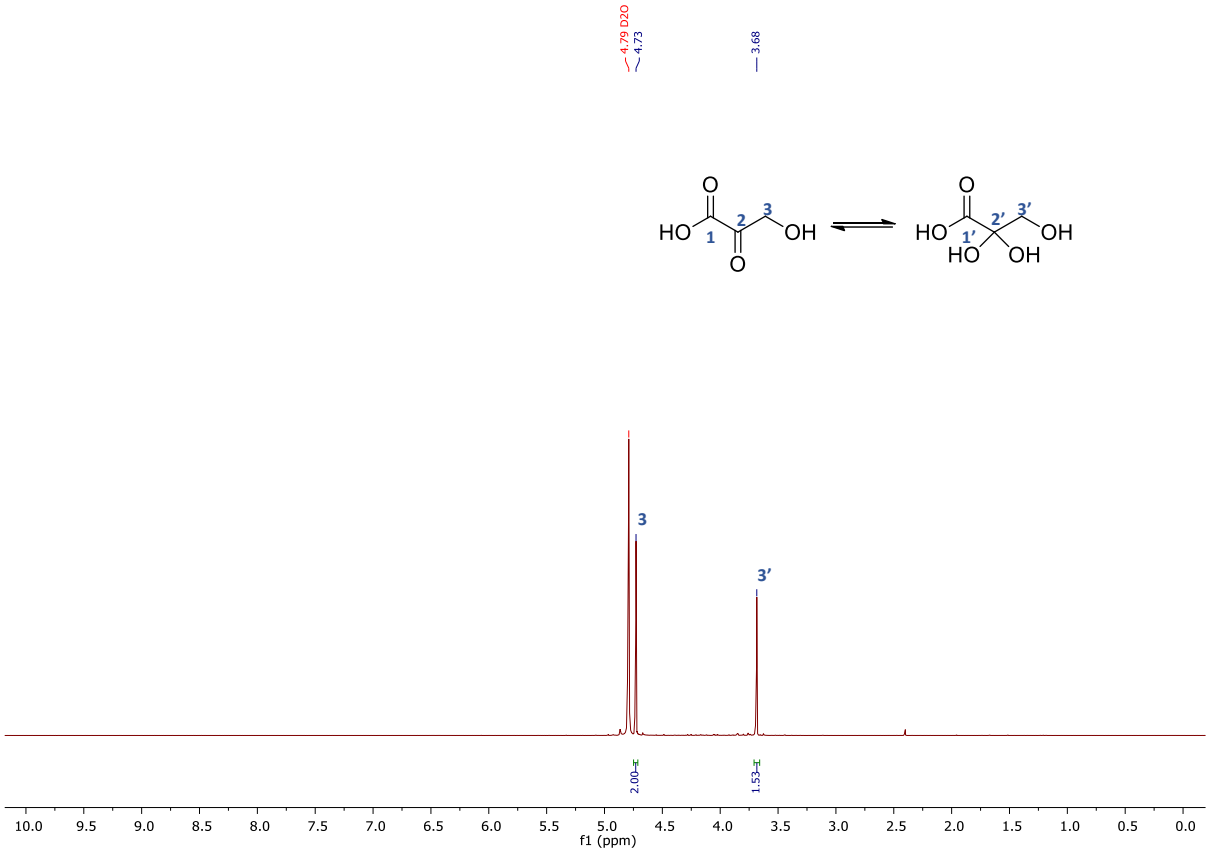

^{1}H-NMR spectrum of hydroxypyruvate (300 MHz, D_2O)

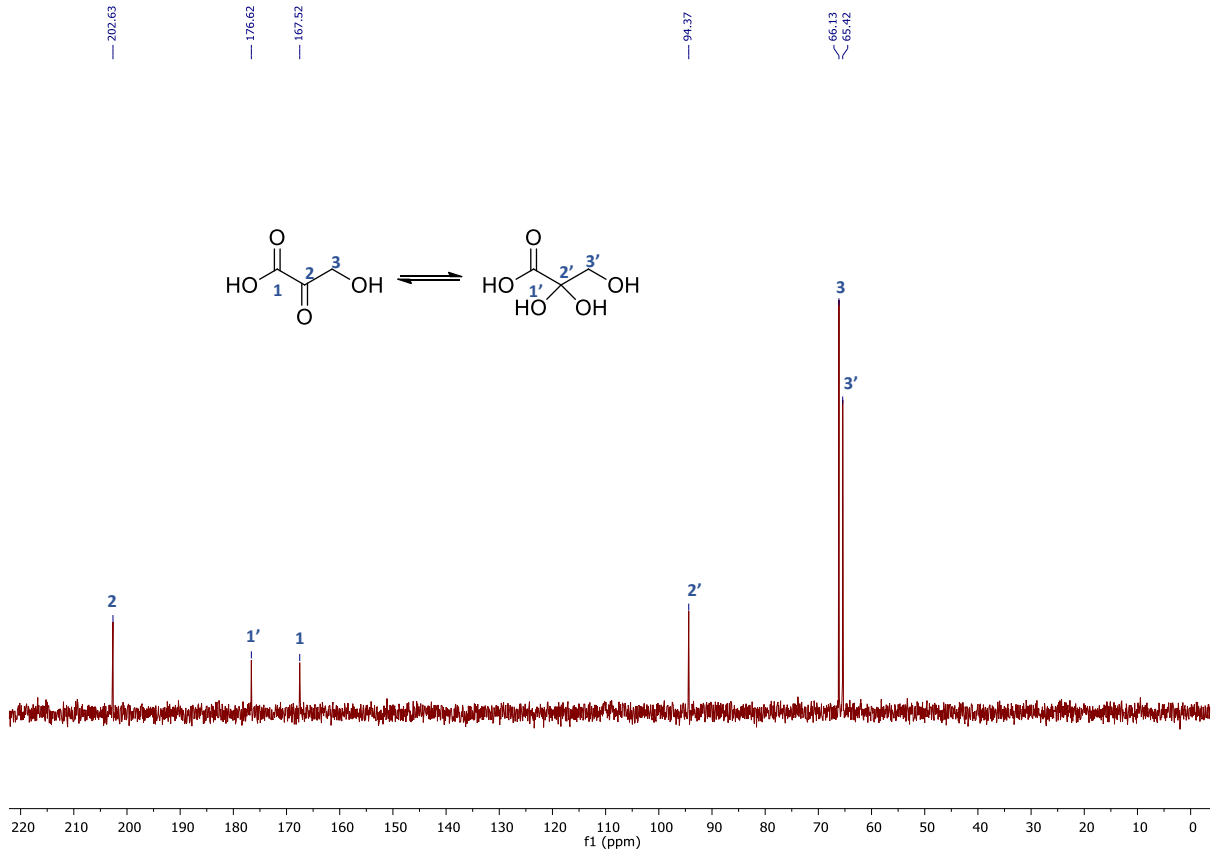

^{13}C-NMR spectrum of hydroxypyruvate (75 MHz, D_2O)

1-Bromo-4-nitrosobenzene (5b)

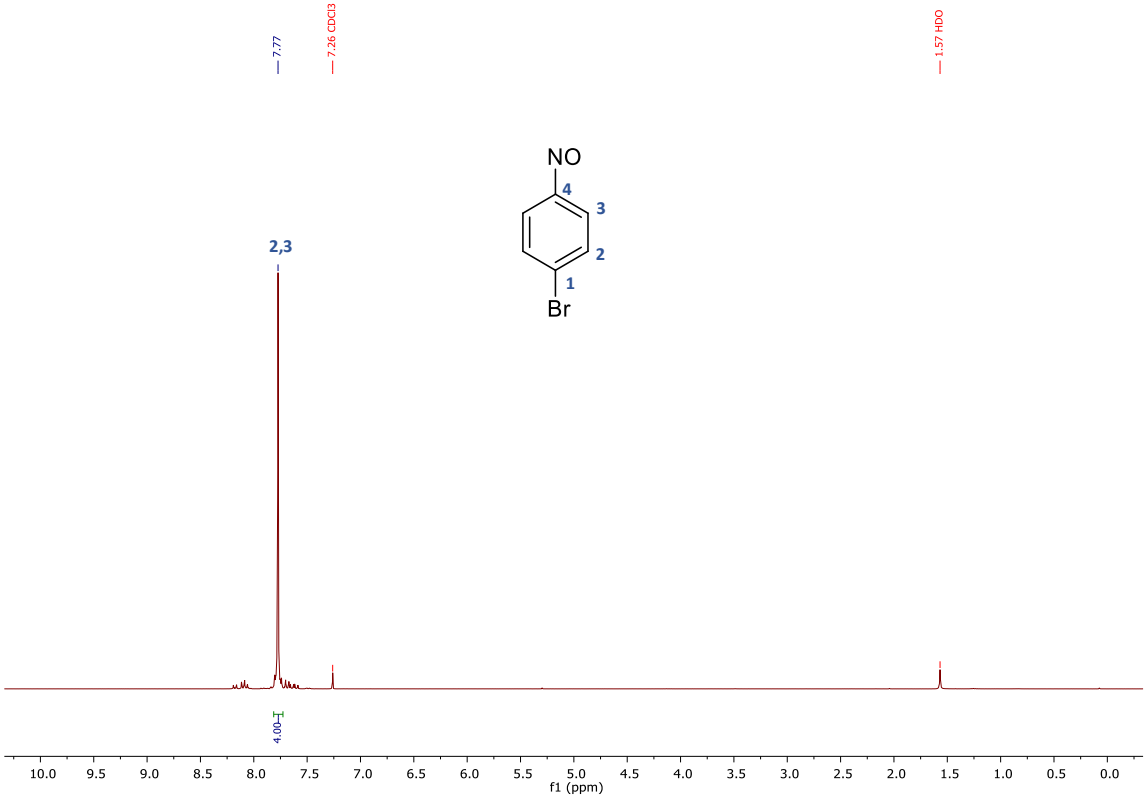

^{1}H-NMR spectrum of 1-bromo-4-nitrosobenzene **(5b)** (300 MHz, $CDCl_3$)

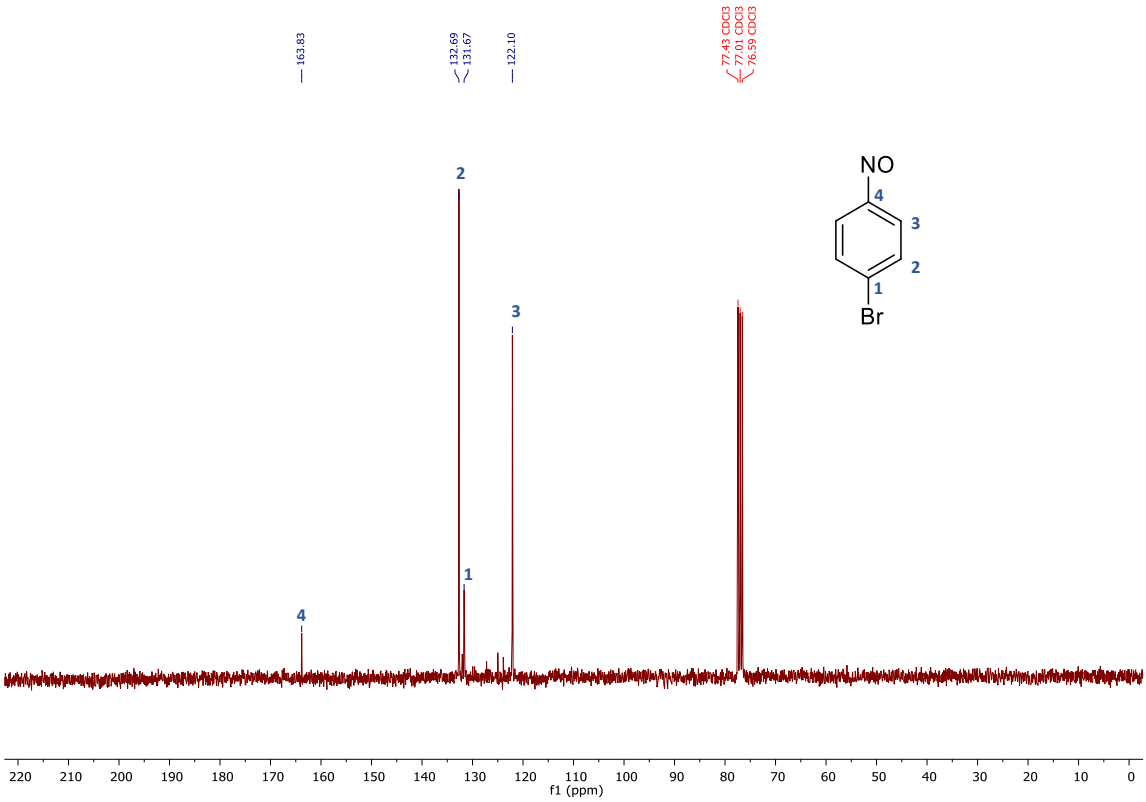

^{13}C-NMR spectrum of 1-bromo-4-nitrosobenzene **(5b)** (75 MHz, $CDCl_3$)

1-Chloro-4-nitrosobenzene (5c)

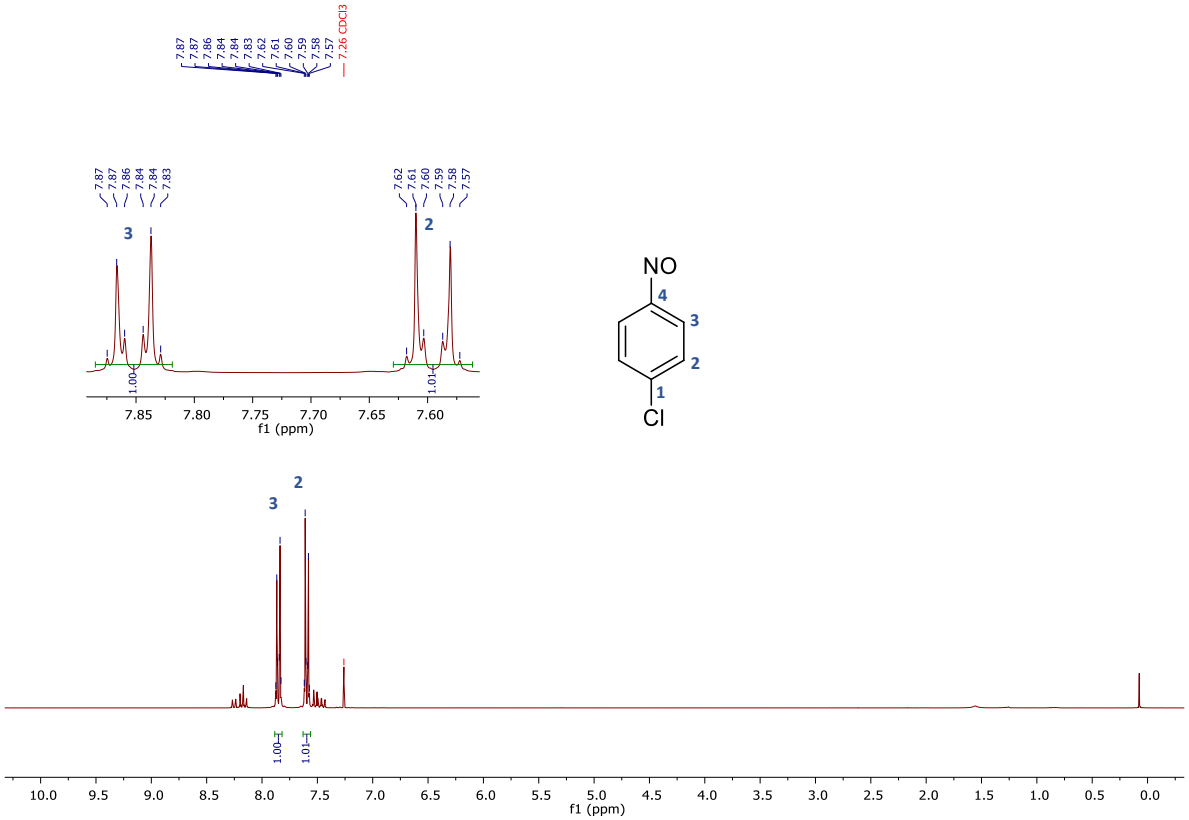

^{1}H-NMR spectrum of 1-chloro-4-nitrosobenzene **(5c)** (300 MHz, $CDCl_3$)

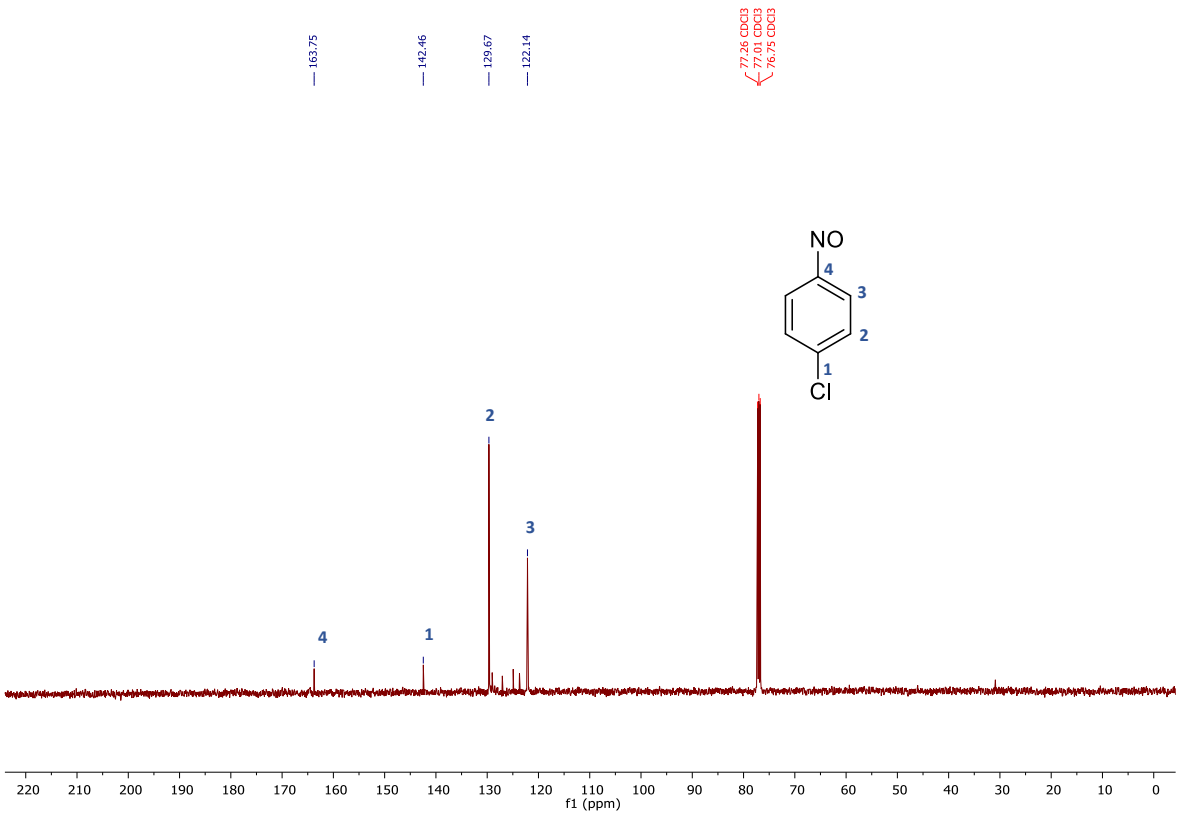

^{13}C-NMR spectrum of 1-chloro-4-nitrosobenzene **(5c)** (75 MHz, $CDCl_3$)

1-Chloro-3-nitrosobenzene (5d)

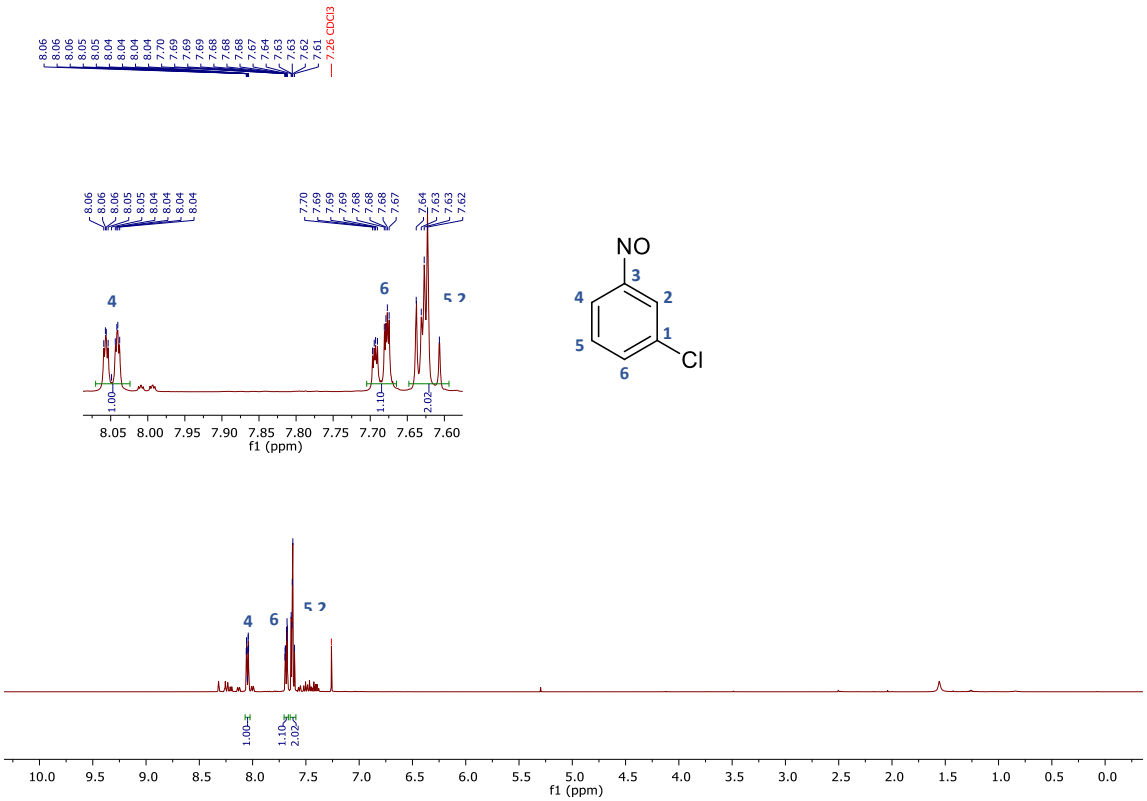

^{1}H-NMR spectrum of 1-chloro-3-nitrosobenzene **(5d)** (500 MHz, $CDCl_3$)

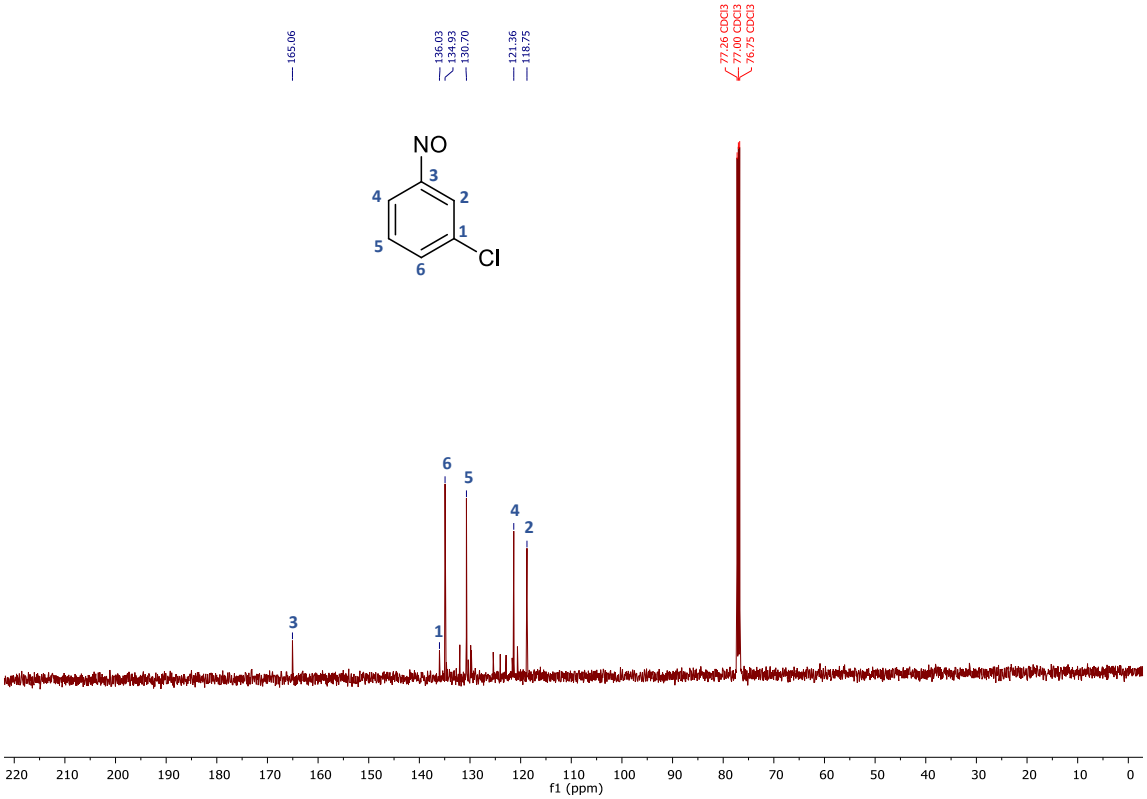

^{13}C-NMR spectrum of 1-chloro-3-nitrosobenzene **(5d)** (126 MHz, $CDCl_3$)

1-Chloro-2-nitrosobenzene (5e)

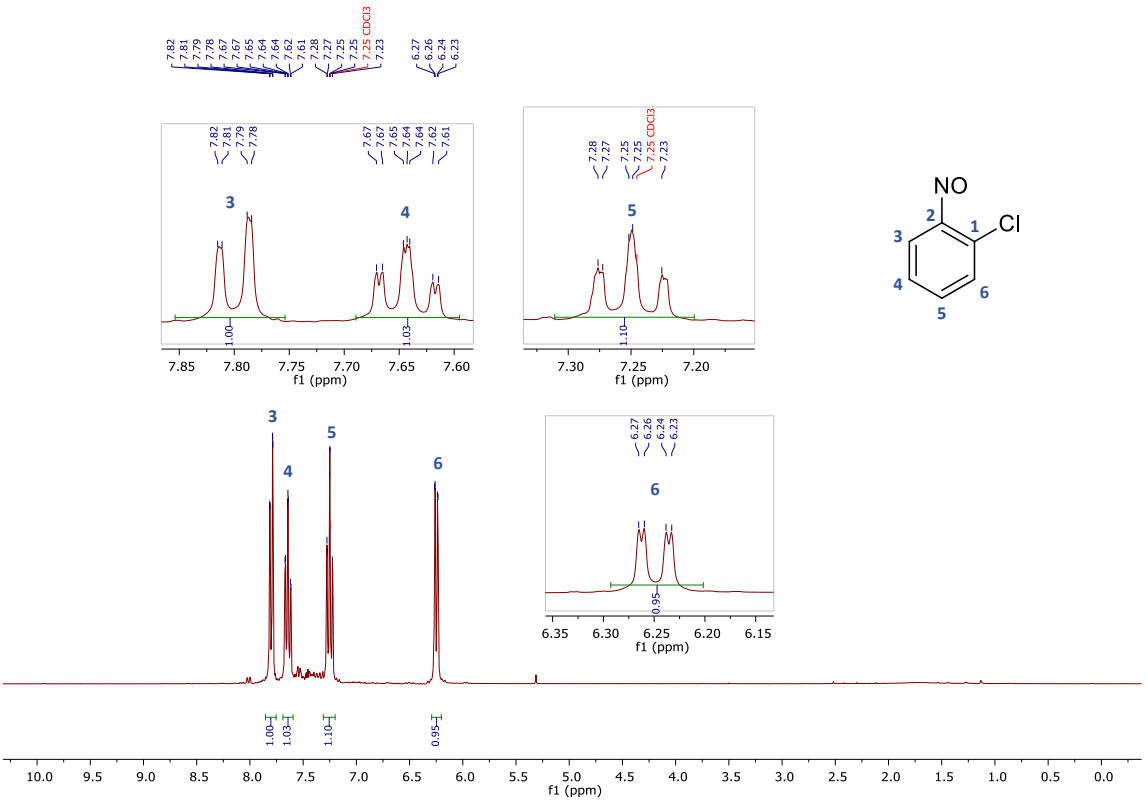

^{1}H-NMR spectrum of 1-chloro-2-nitrosobenzene **(5e)** (300 MHz, $CDCl_3$)

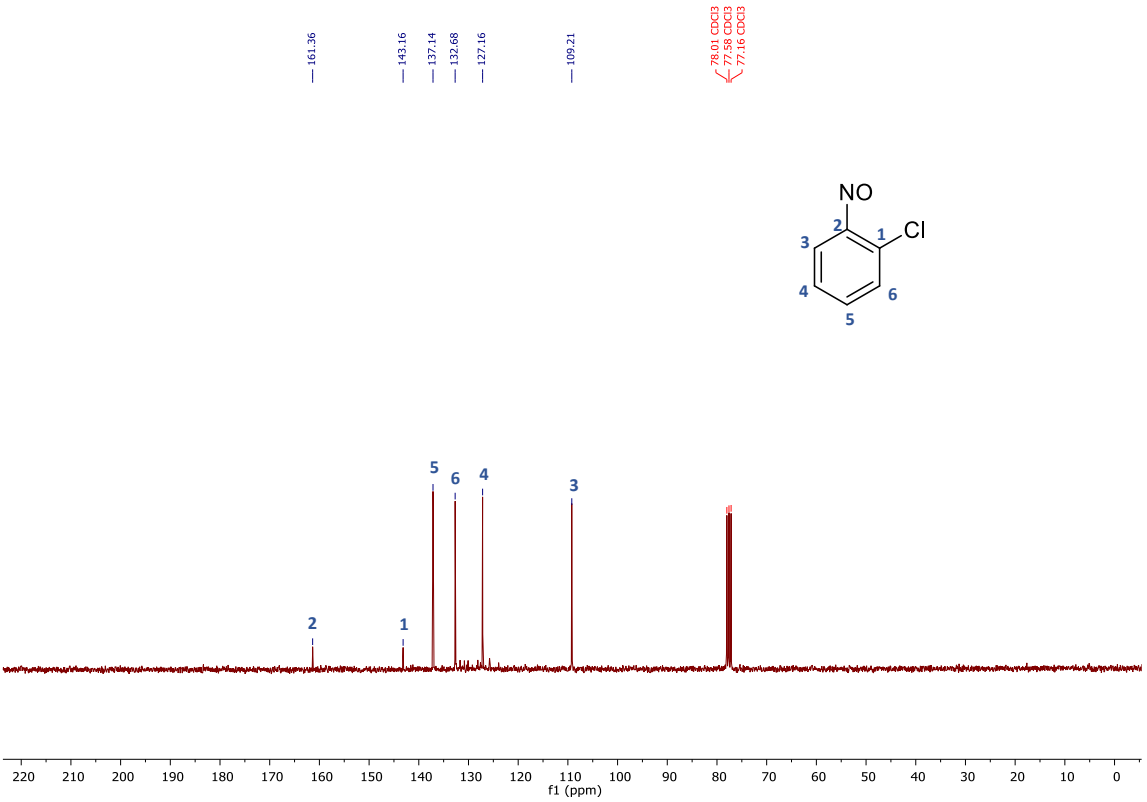

^{13}C-NMR spectrum of 1-chloro-2-nitrosobenzene **(5e)** (75 MHz, $CDCl_3$)

1,2-Dichloro-4-nitrosobenzene (5f)

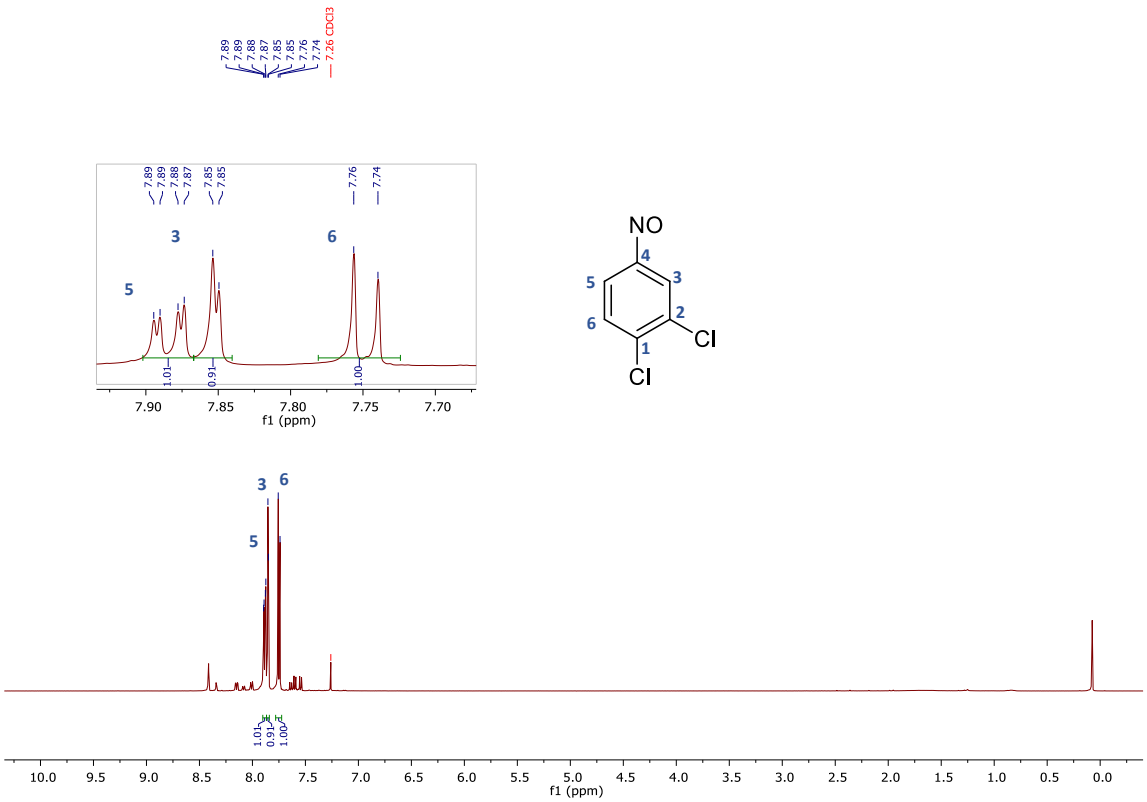

^{1}H-NMR spectrum of 1,2-dichloro-4-nitrosobenzene **(5f)** (500 MHz, $CDCl_3$)

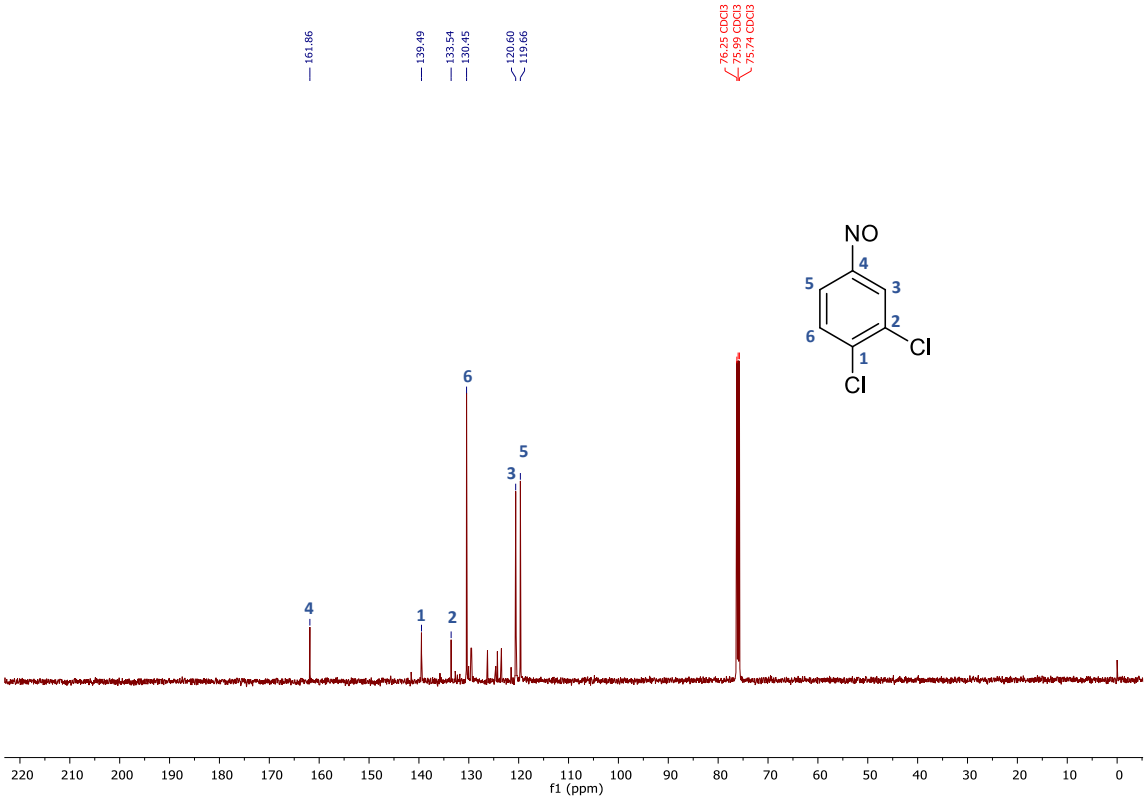

^{13}C-NMR spectrum of 1,2-dichloro-4-nitrosobenzene **(5f)** (126 MHz, $CDCl_3$)

1-Methyl-4-nitrosobenzene (5g)

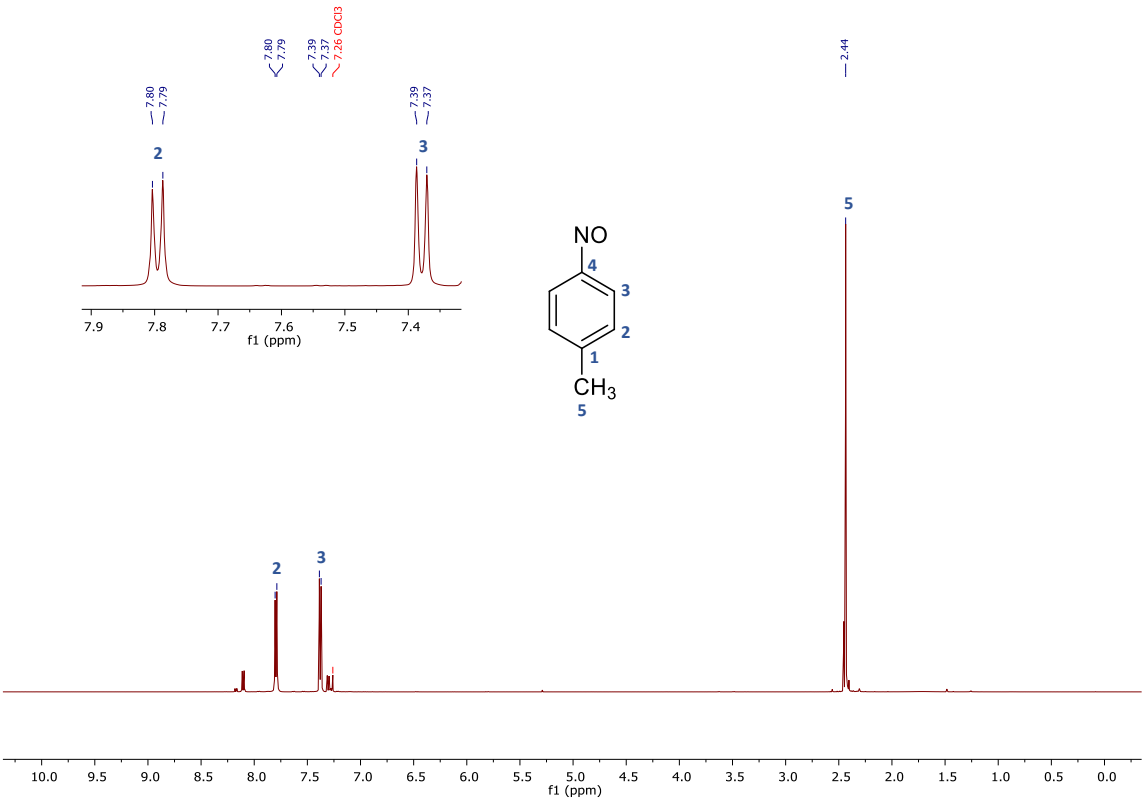

^{1}H-NMR spectrum of 1-methyl-4-nitrosobenzene **(5g)** (500 MHz, $CDCl_3$)

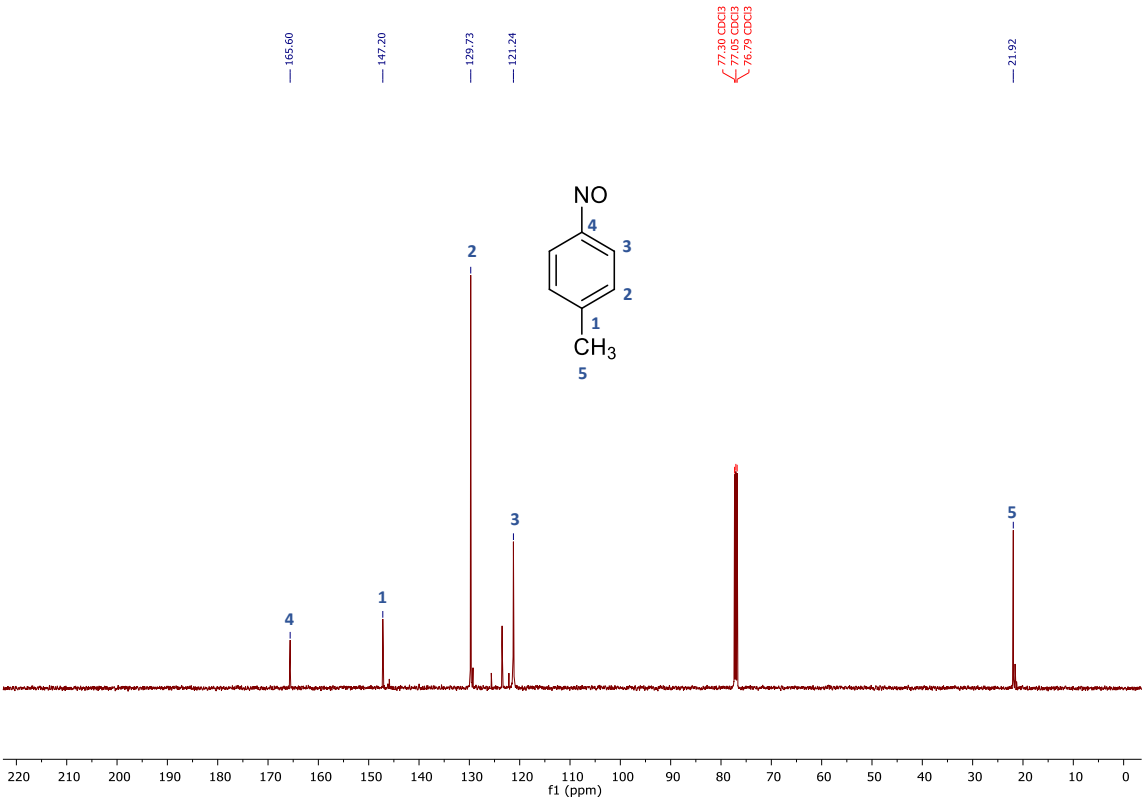

^{13}C-NMR spectrum of 1-methyl-4-nitrosobenzene **(5g)** (126 MHz, $CDCl_3$)

1-Methyl-3-nitrosobenzene (5h)

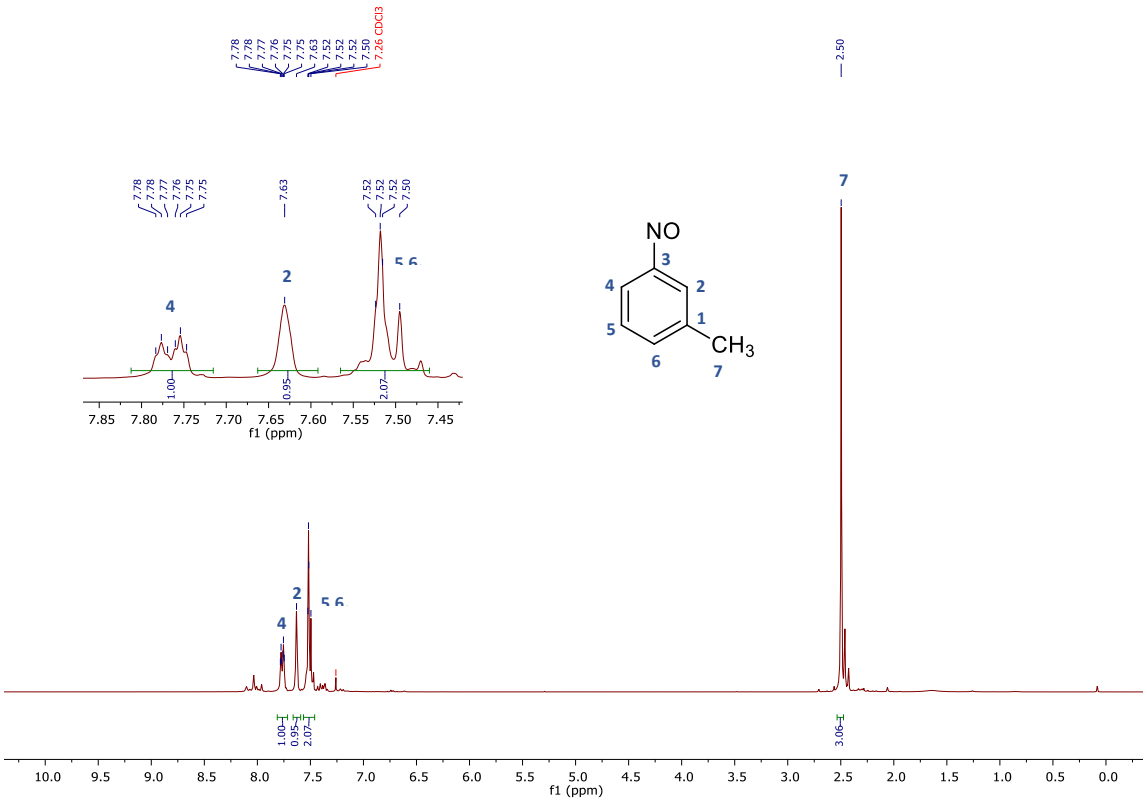

^{1}H-NMR spectrum of 1-methyl-3-nitrosobenzene **(5h)** (300 MHz, $CDCl_3$)

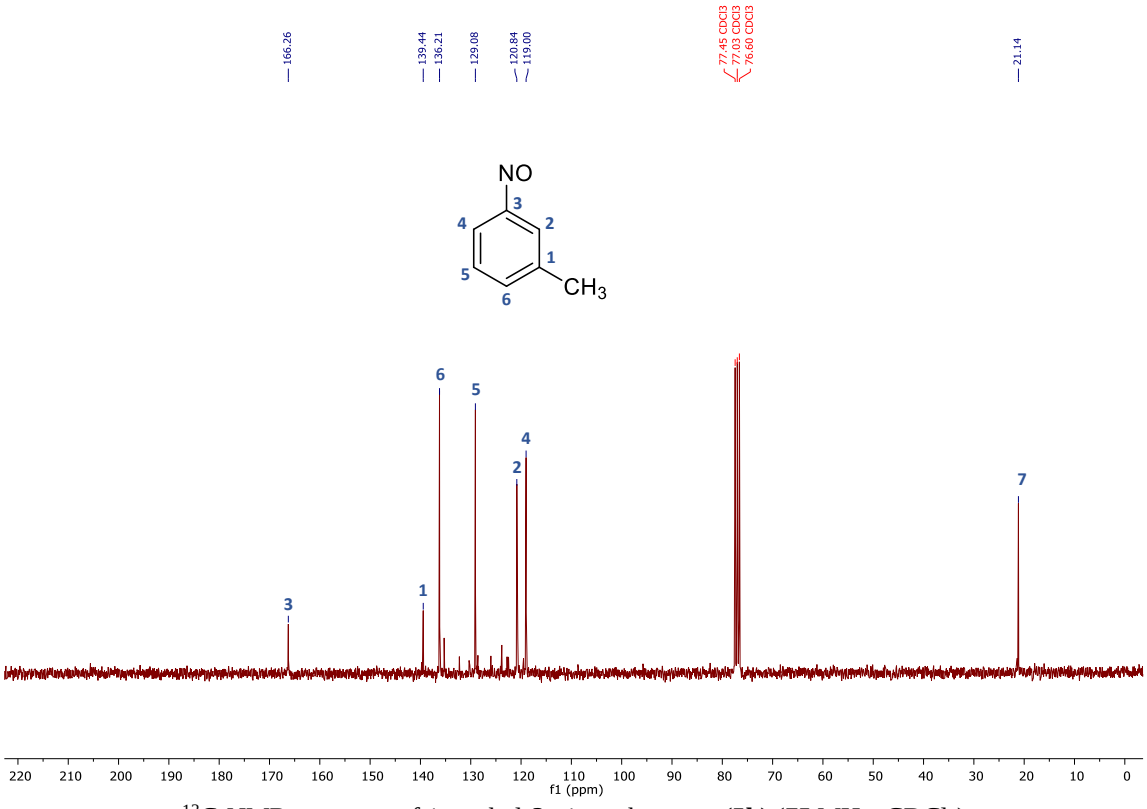

^{13}C-NMR spectrum of 1-methyl-3-nitrosobenzene **(5h)** (75 MHz, $CDCl_3$)

1-Chloro-2-methyl-4-nitrosobenzene (5i)

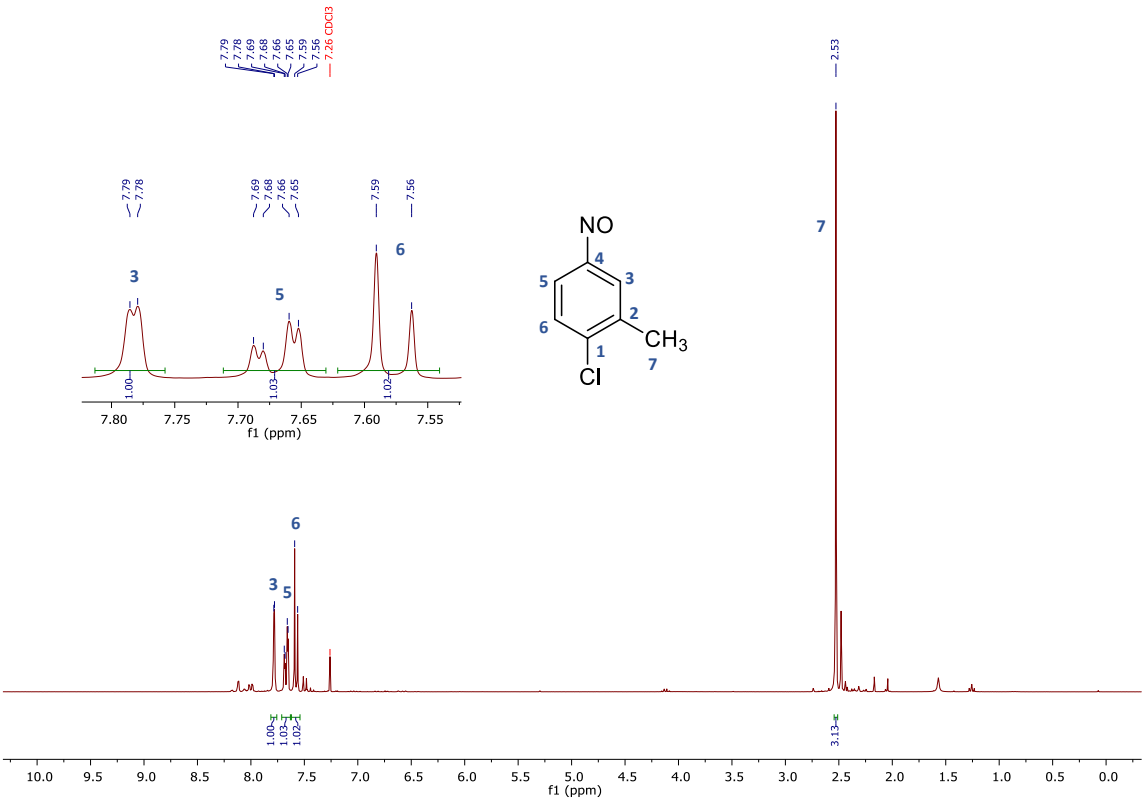

^{1}H-NMR spectrum of 1-chloro-2-methyl-4-nitrosobenzene **(5i)** (300 MHz, $CDCl_3$)

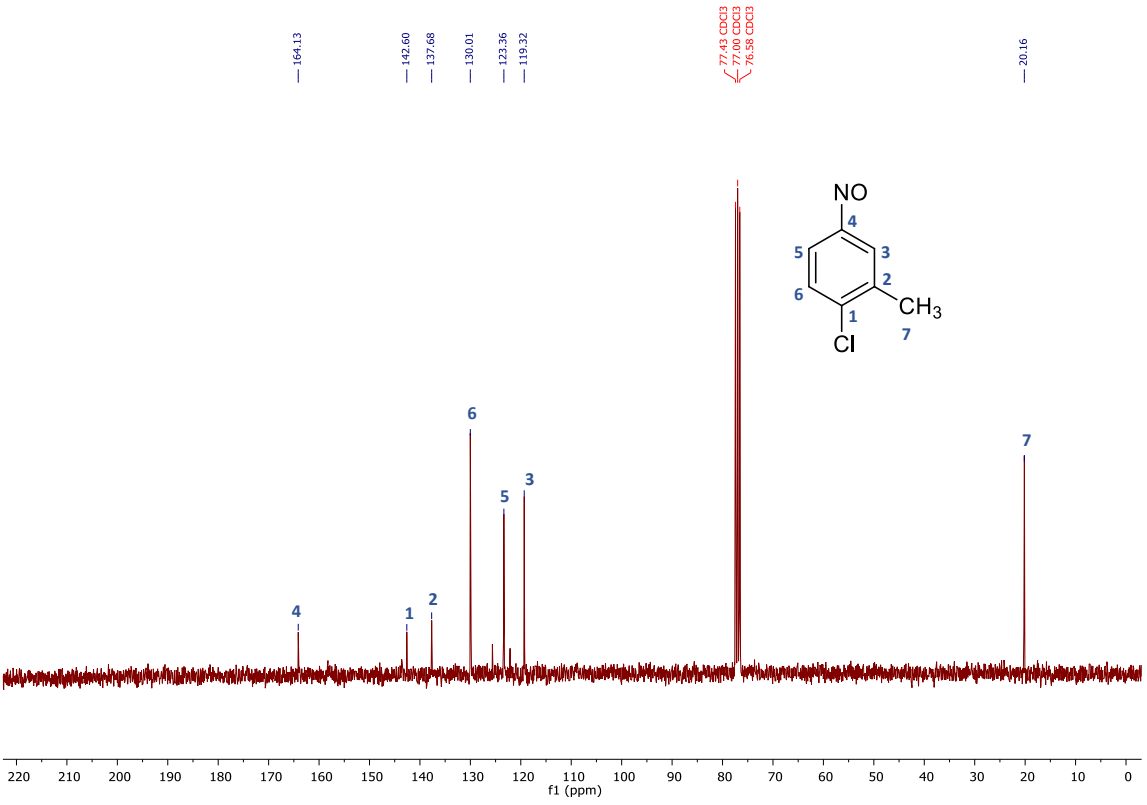

^{13}C-NMR spectrum of 1-chloro-2-methyl-4-nitrosobenzene **(5i)** (75 MHz, $CDCl_3$)

2-Chloro-1-methyl-4-nitrosobenzene (5j)

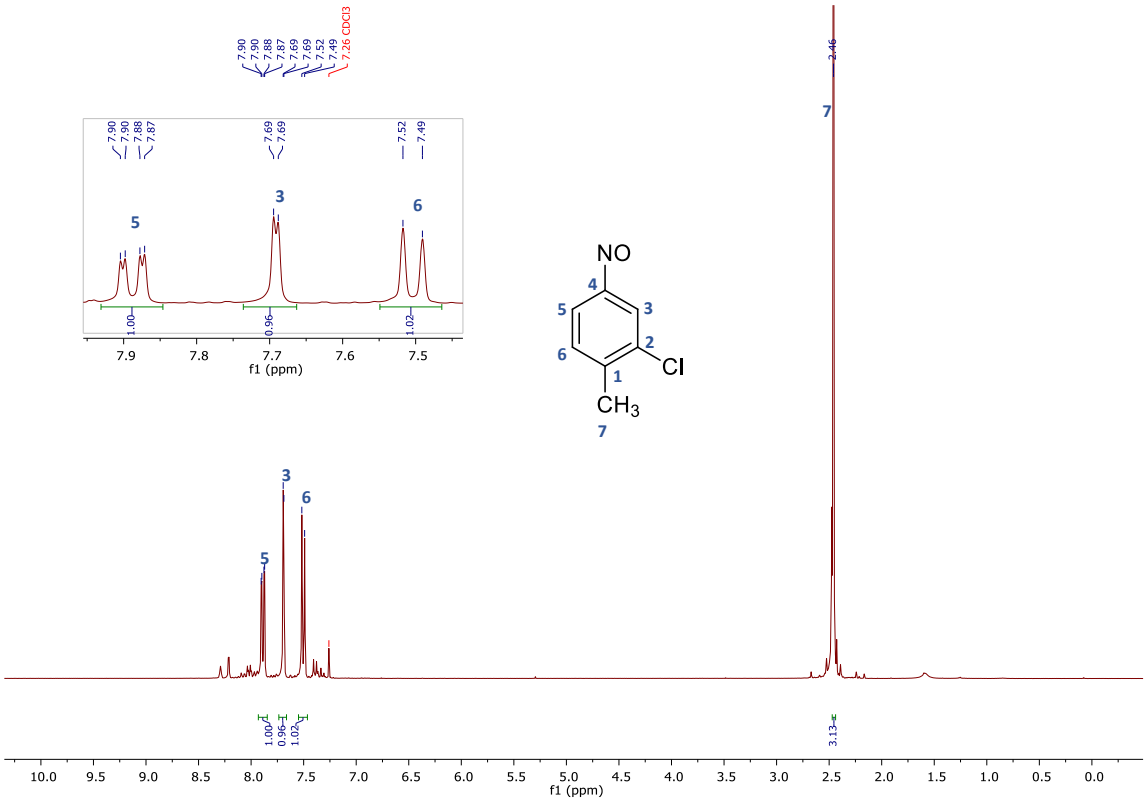

^{1}H-NMR spectrum of 2-chloro-1-methyl-4-nitrosobenzene **(5j)** (300 MHz, $CDCl_3$)

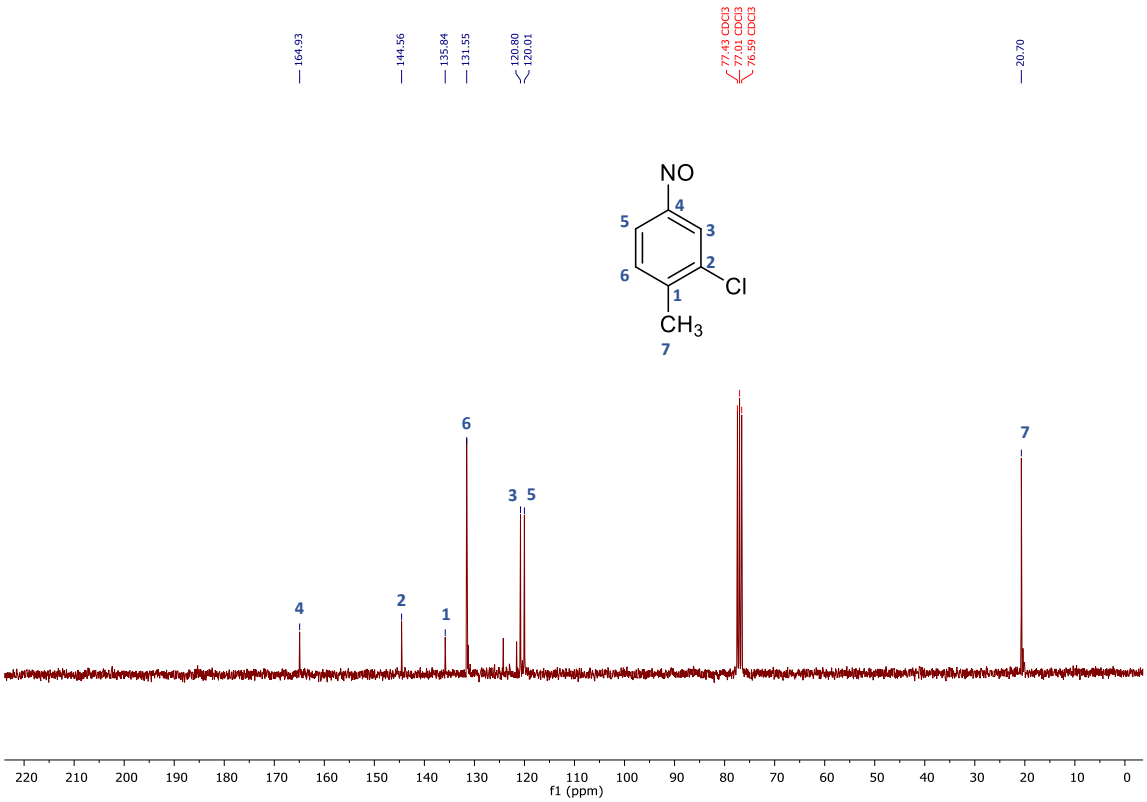

^{13}C-NMR spectrum of 2-chloro-1-methyl-4-nitrosobenzene **(5j)** (75 MHz, $CDCl_3$)

4-Nitroso-1-(trifluoromethyl)benzene (5k)

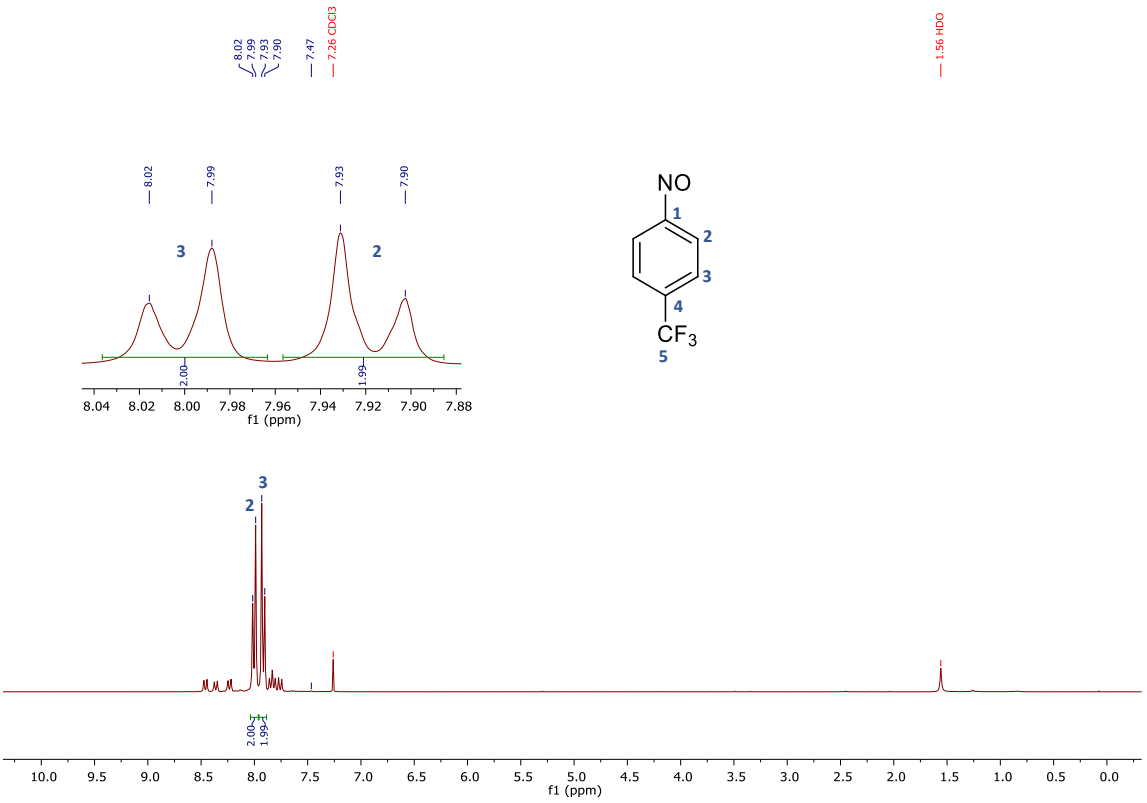

^{1}H-NMR spectrum of 4-nitroso-1-(trifluoromethyl)benzene **(5k)** (300 MHz, $CDCl_3$)

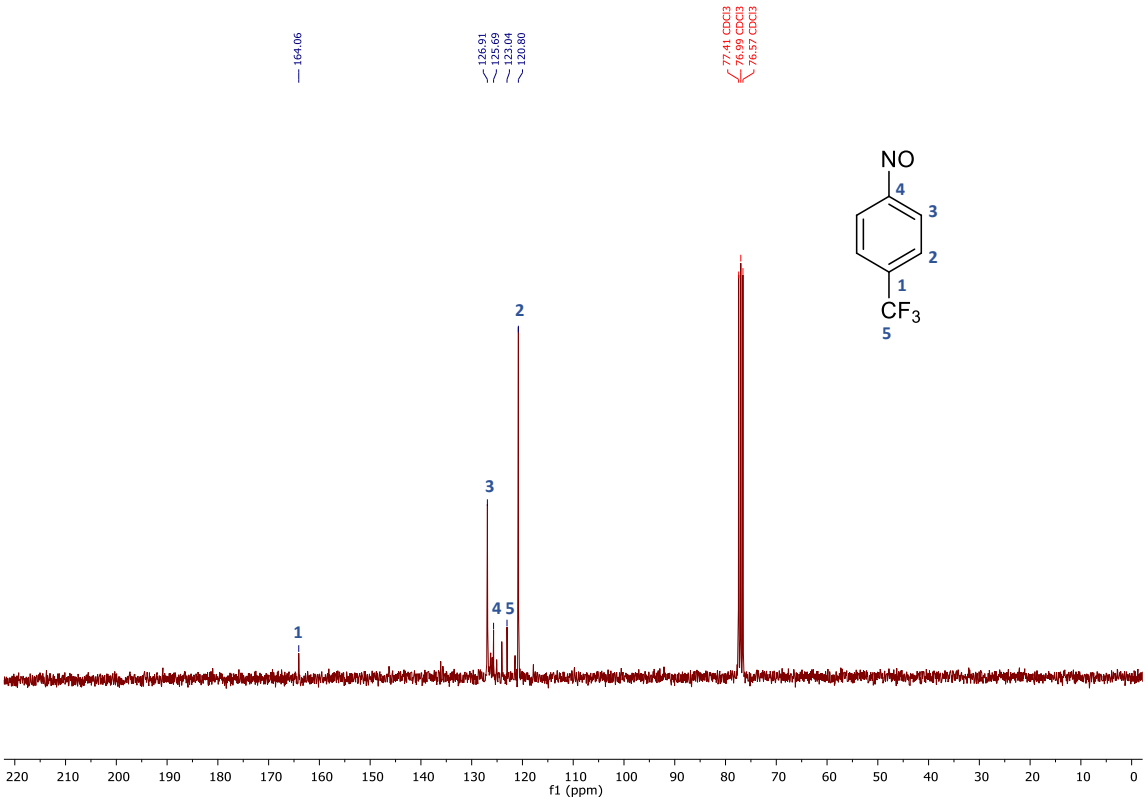

^{13}C-NMR spectrum of 4-nitroso-1-(trifluoromethyl)benzene **(5k)** (75 MHz, $CDCl_3$)

3-Nitroso-1-(trifluoromethyl)benzene (5l)

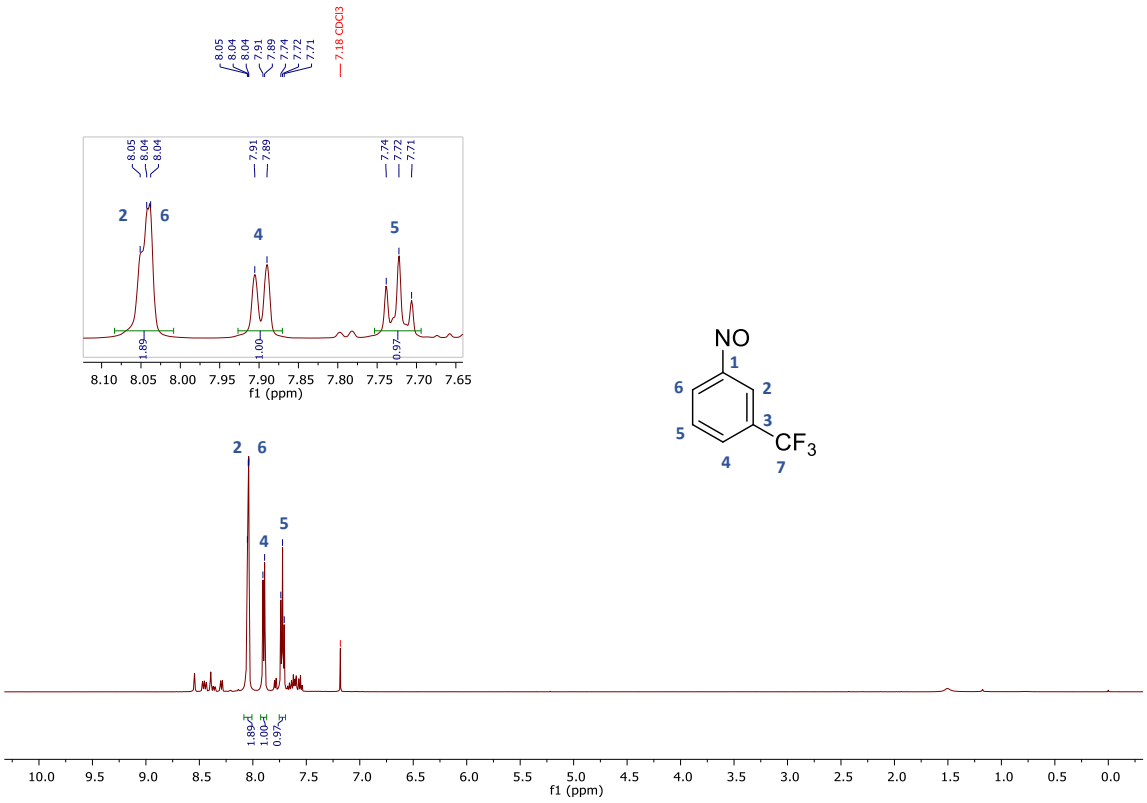

^{1}H-NMR spectrum of 3-nitroso-1-(trifluoromethyl)benzene **(5l)** (500 MHz, $CDCl_3$)

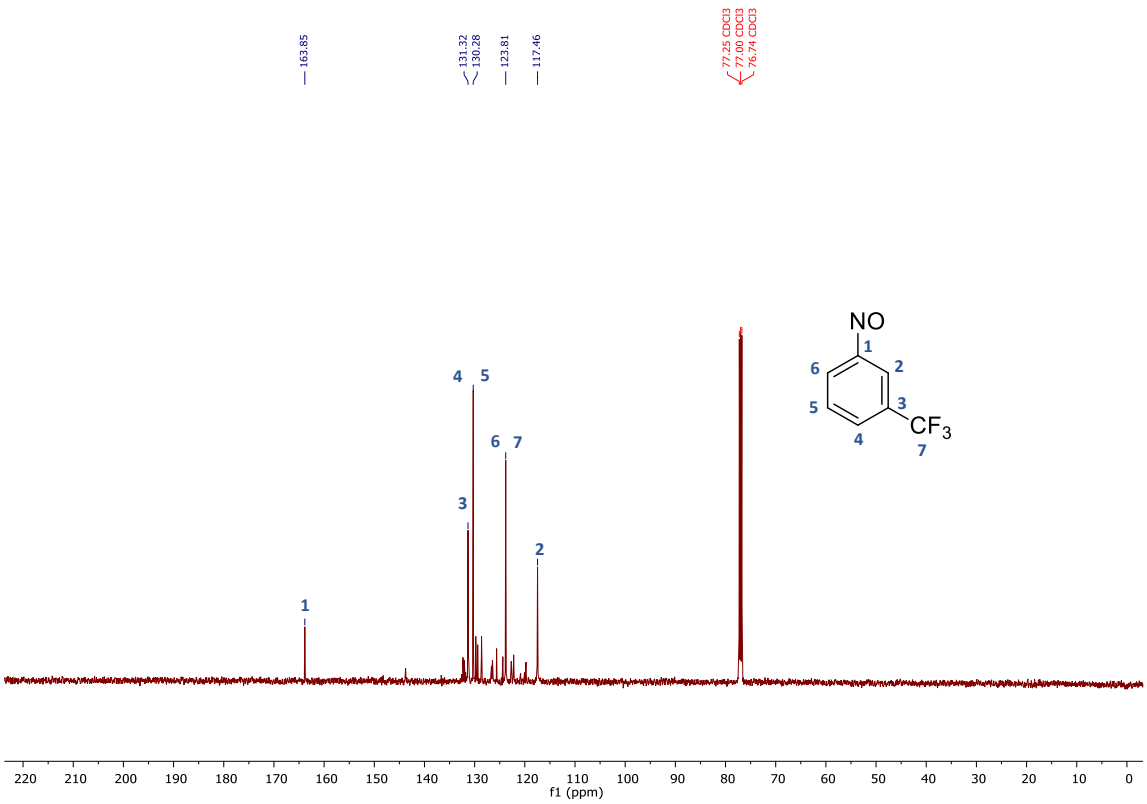

^{13}C-NMR spectrum of 3-nitroso-1-(trifluoromethyl)benzene **(5l)** (126 MHz, $CDCl_3$)

1-Nitro-4-nitrosobenzene (5m)

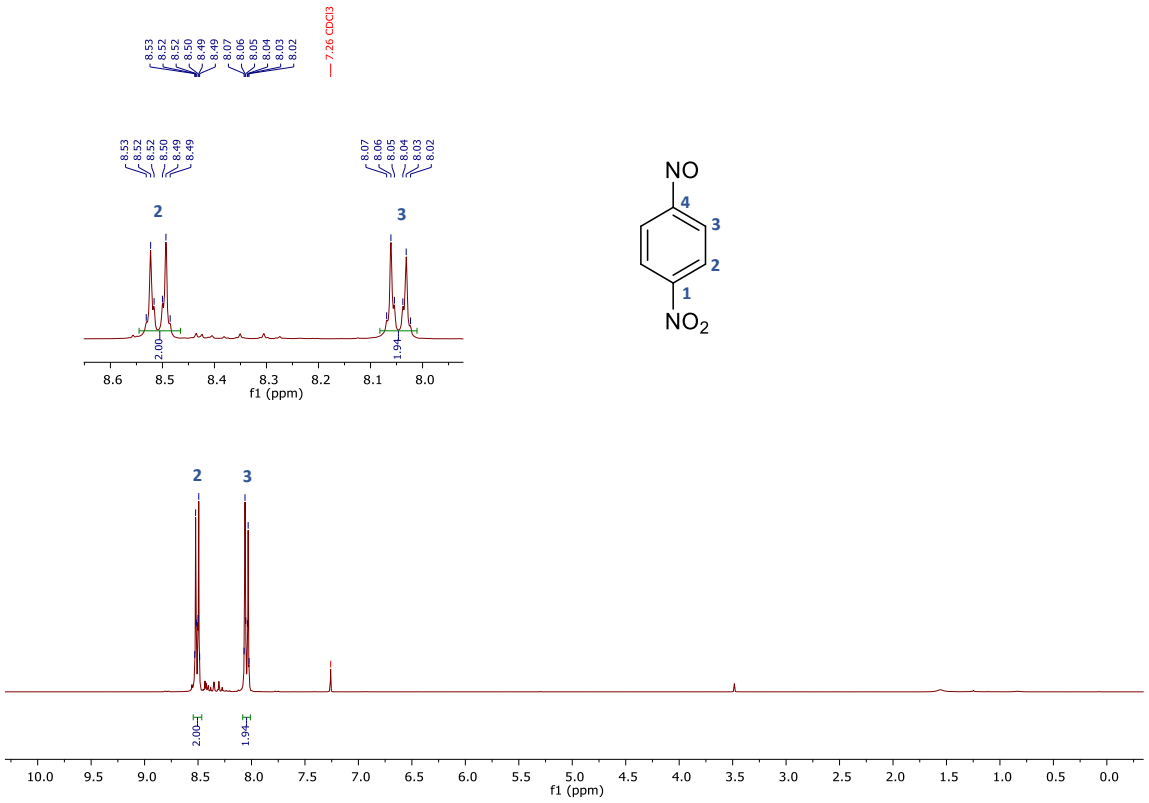

^{1}H-NMR spectrum of 1-nitro-4-nitrosobenzene **(5m)** (300 MHz, $CDCl_3$)

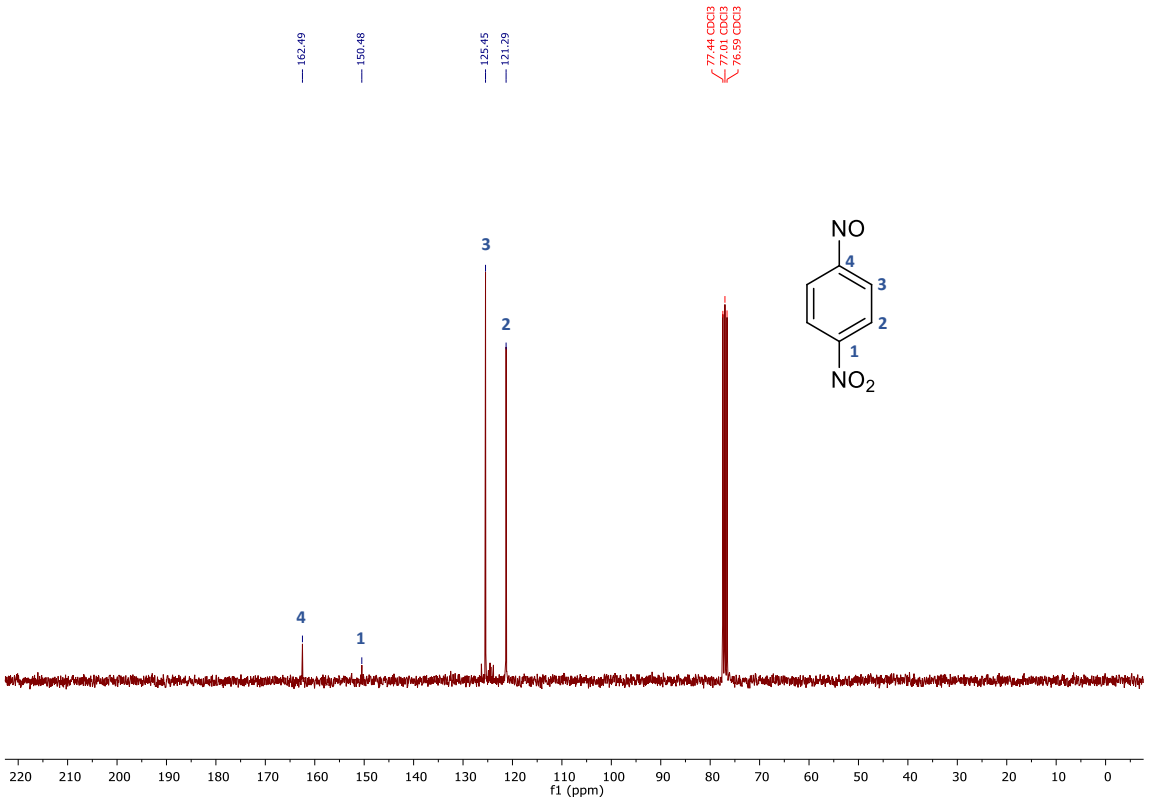

^{13}C-NMR spectrum of 1-nitro-4-nitrosobenzene **(5m)** (75 MHz, $CDCl_3$)

4-Nitrosobenzoic acid (5n)

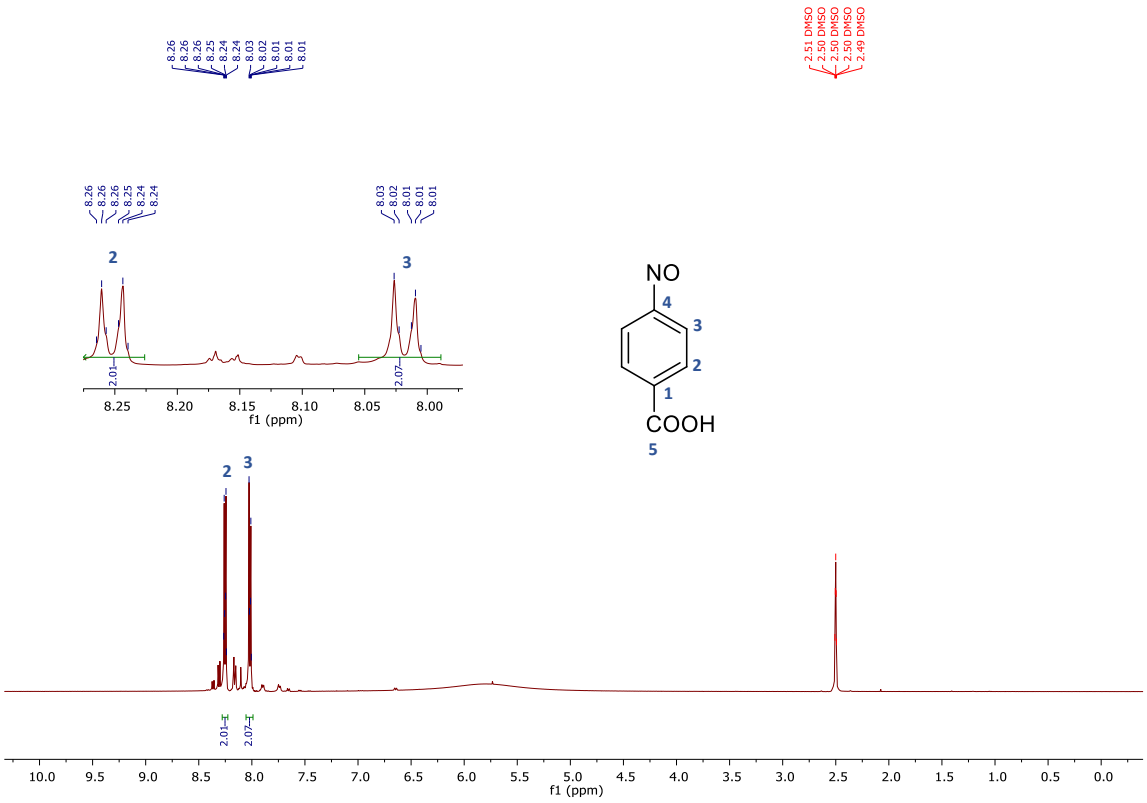

^{1}H-NMR spectrum of 4-nitrosobenzoic acid **(5n)** (500 MHz, DMSO-d^{6})

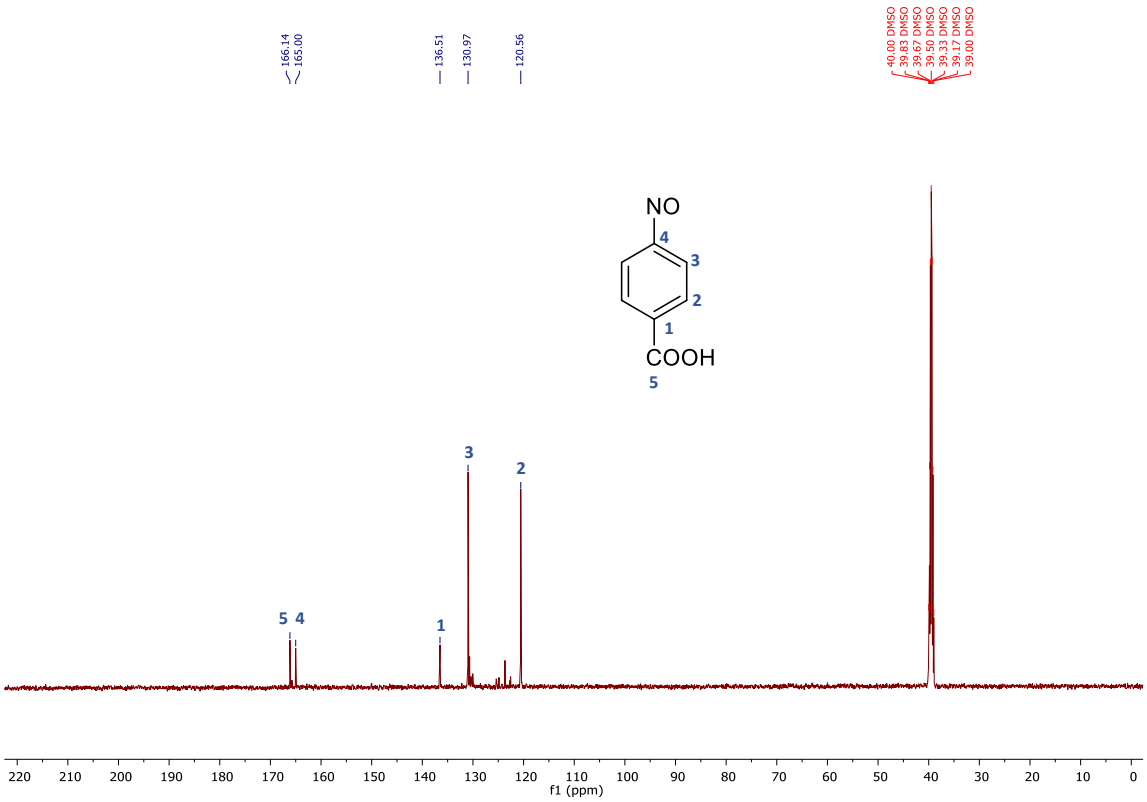

^{13}C-NMR spectrum of 4-nitrosobenzoic acid **(5n)** (126 MHz, DMSO-d^{6})

3-Nitrosobenzoic acid (5o)

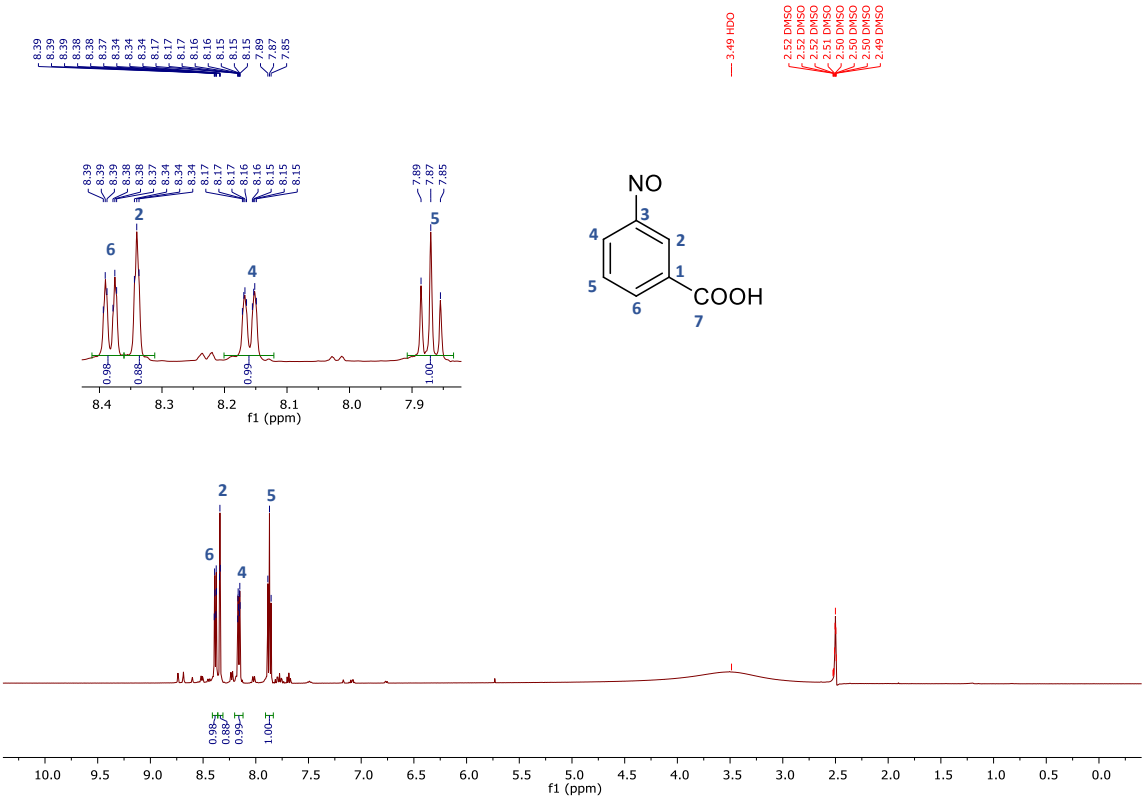

^{1}H-NMR spectrum of 3-nitrosobenzoic acid **(5o)** (500 MHz, DMSO-d^{6})

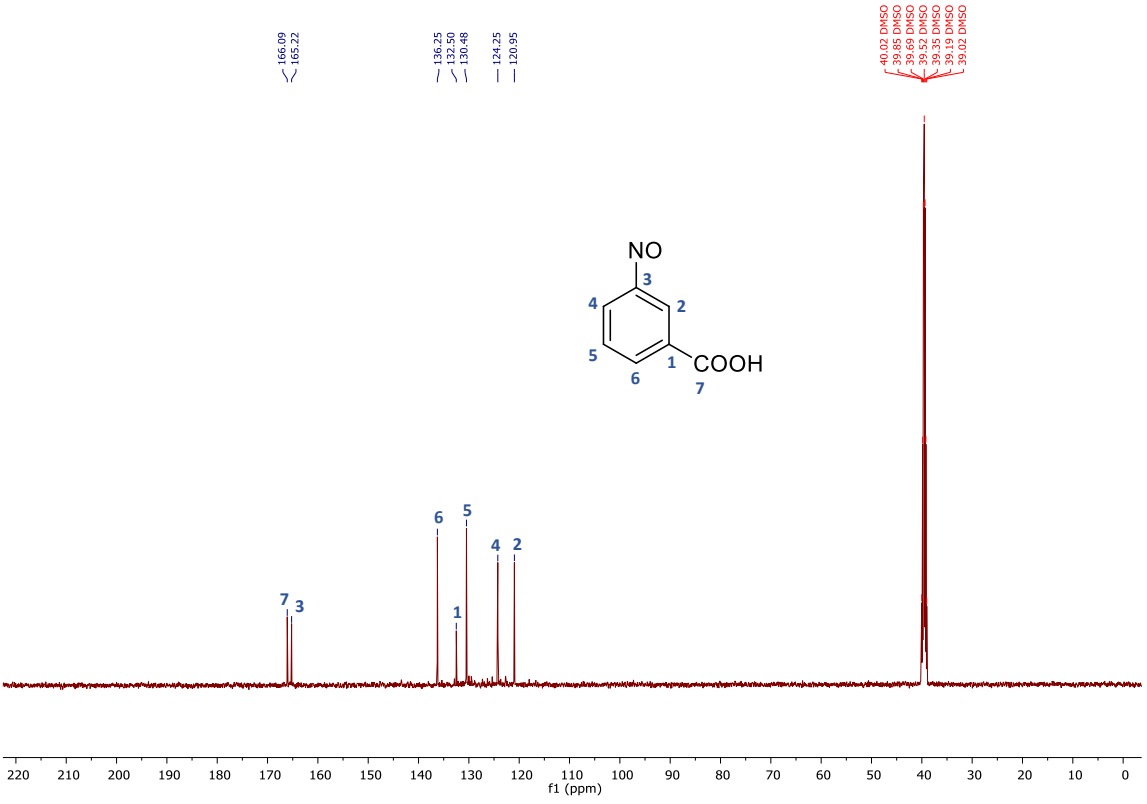

^{13}C-NMR spectrum of 3-nitrosobenzoic acid **(5o)** (126 MHz, DMSO-d^{6})

N-Phenyl-*N*,2-dihydroxyacetamide (6a)

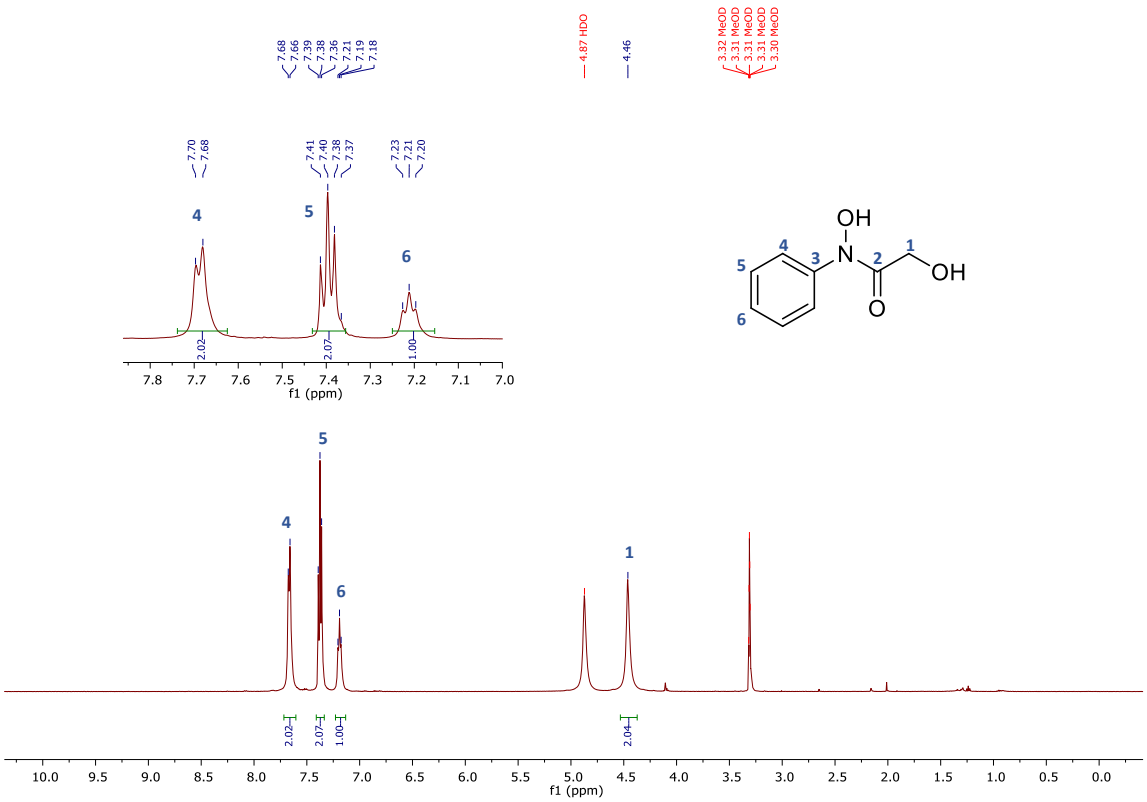

^{1}H-NMR spectrum of *N*-phenyl-*N*,2-dihydroxyacetamide **(6a)** (500 MHz, CD_3OD)

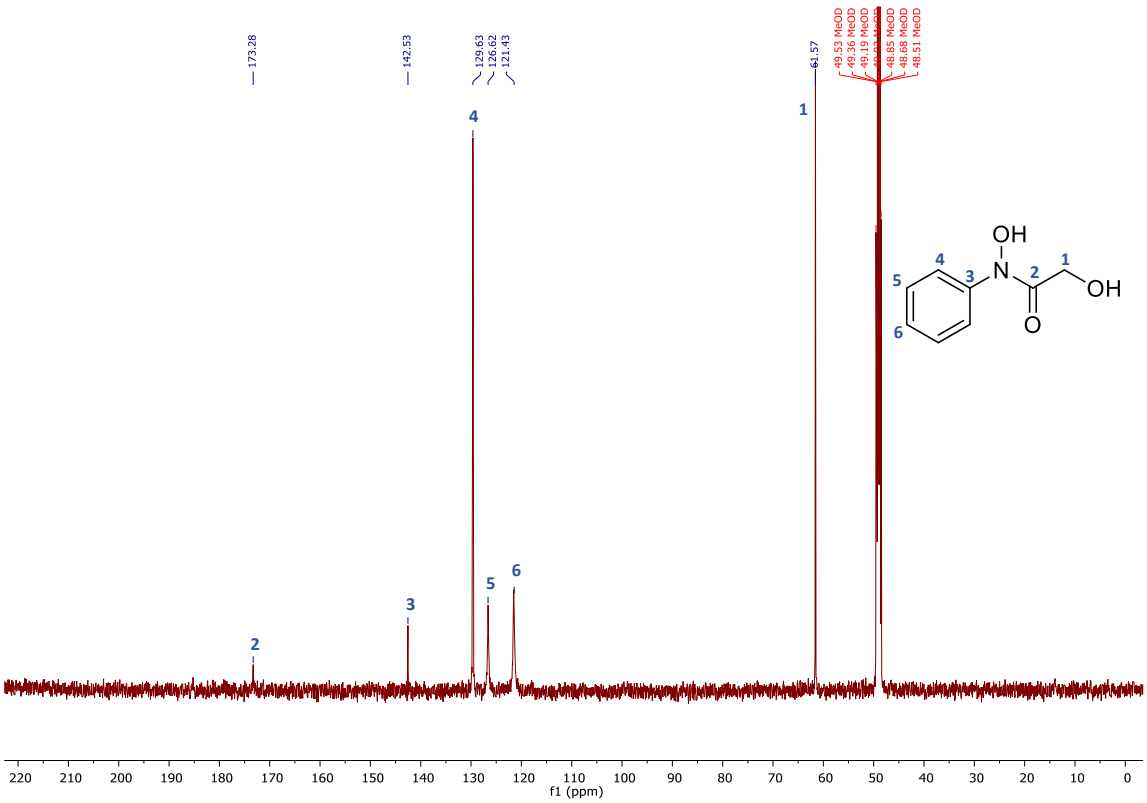

^{13}C-NMR spectrum of *N*-phenyl-*N*,2-dihydroxyacetamide **(6a)** (126 MHz, CD_3OD)

N-(4-Bromophenyl)-*N*,2-dihydroxyacetamide (6b)

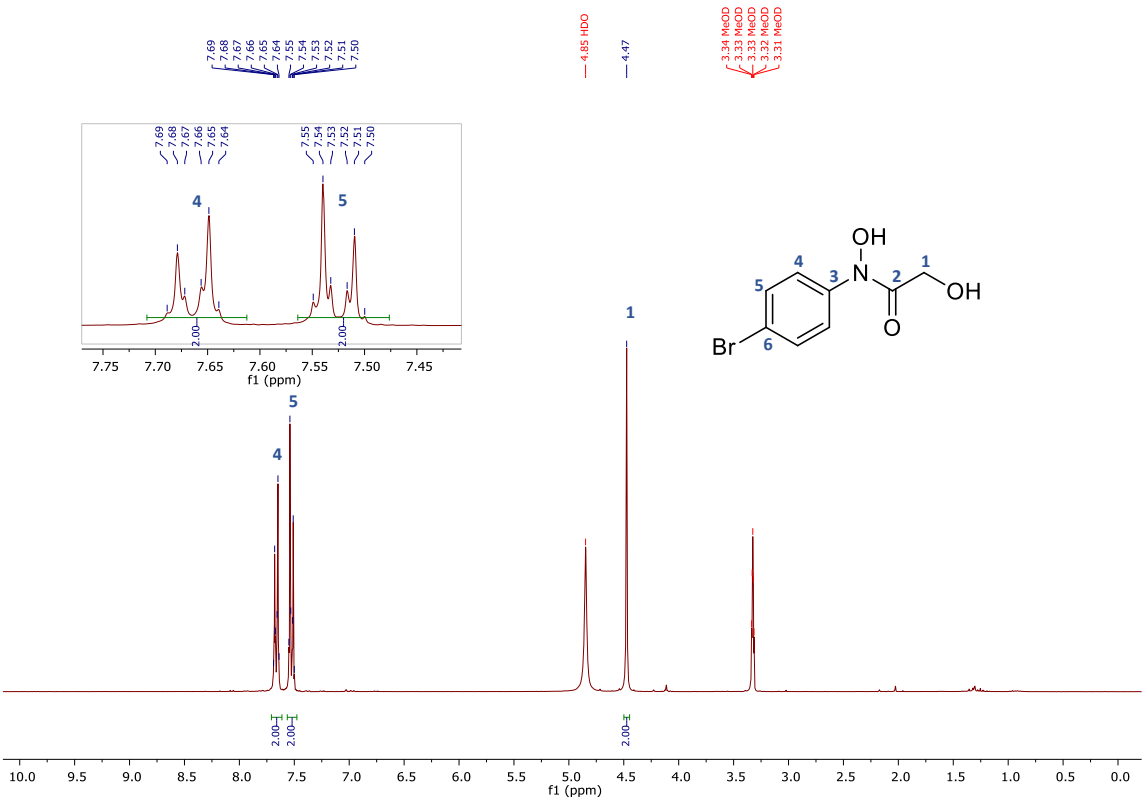

^{1}H-NMR spectrum of *N*-(4-bromophenyl)-*N*,2-dihydroxyacetamide **(6b)** (300 MHz, CD_3OD)

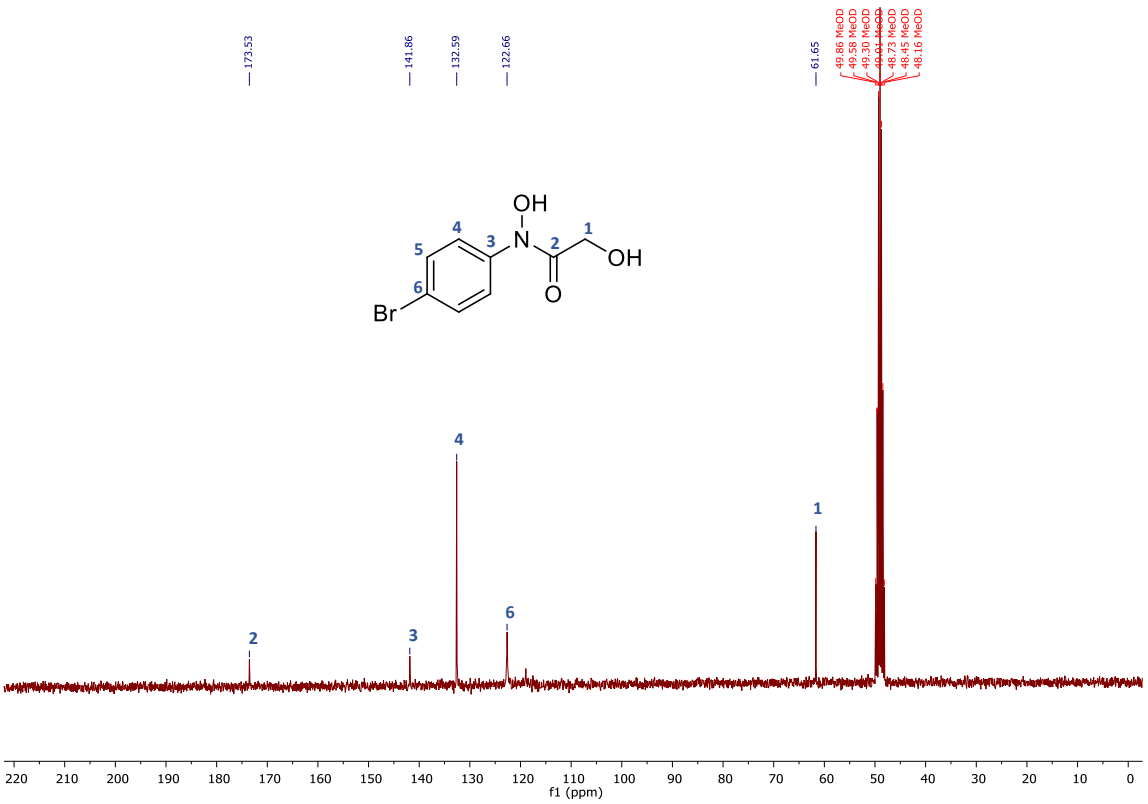

^{13}C-NMR spectrum of *N*-(4-bromophenyl)-*N*,2-dihydroxyacetamide **(6b)** (75 MHz, CD_3OD)

N-(4-Chlorophenyl)-*N*,2-dihydroxyacetamide (6c)

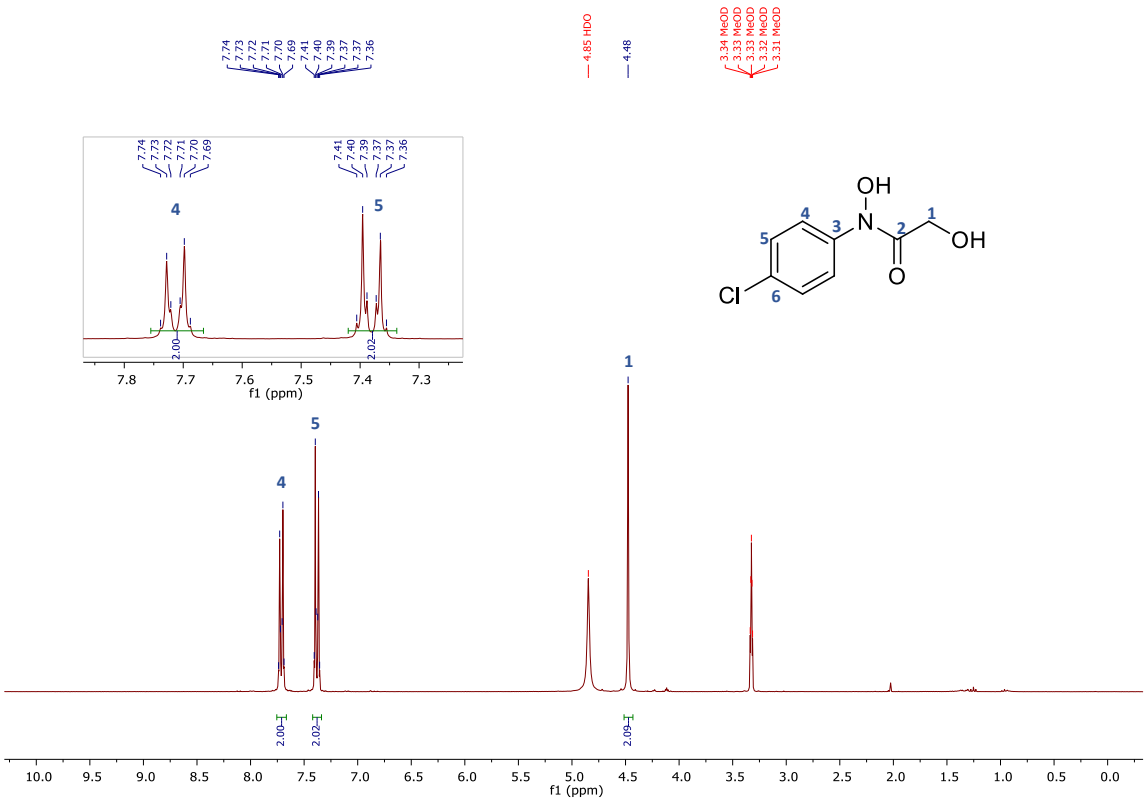

^{1}H-NMR spectrum of *N*-(4-chlorophenyl)-*N*,2-dihydroxyacetamide **(6c)** (300 MHz, CD_3OD)

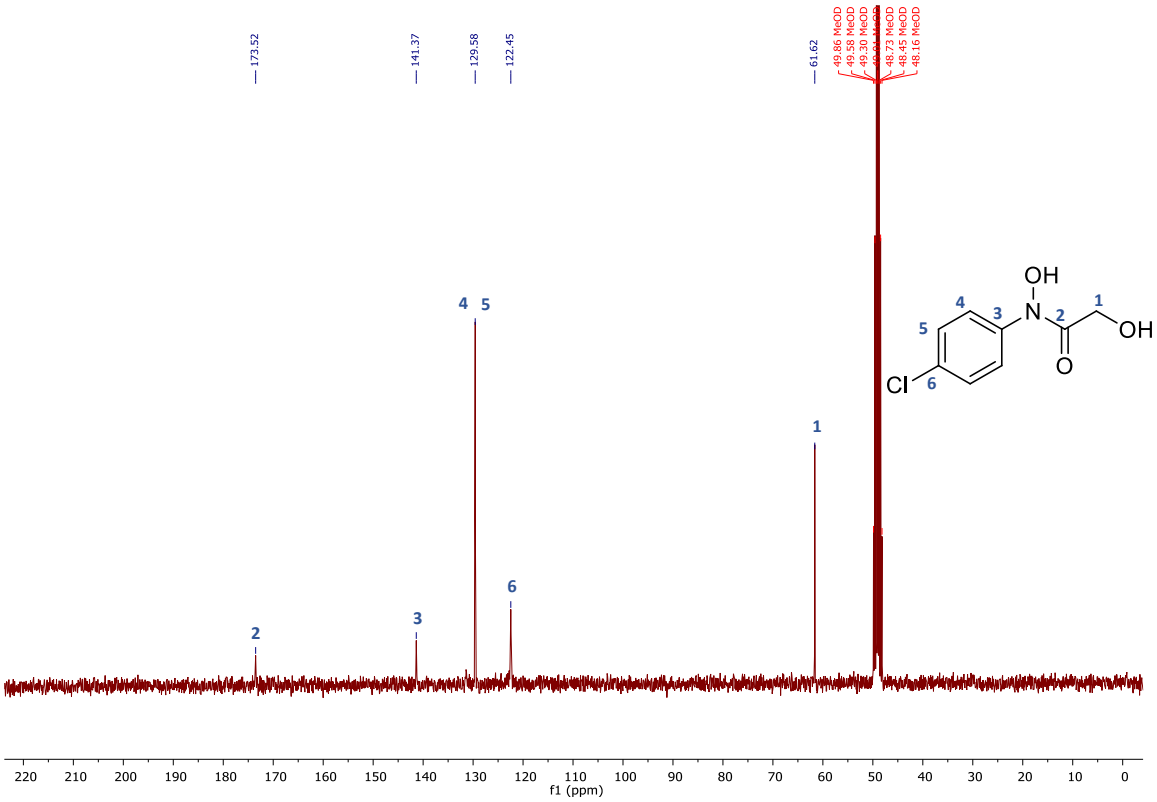

^{13}C-NMR spectrum of *N*-(4-chlorophenyl)-*N*,2-dihydroxyacetamide **(6c)** (75 MHz, CD_3OD)

N-(3-Chlorophenyl)-*N*,2-dihydroxyacetamide (6d)

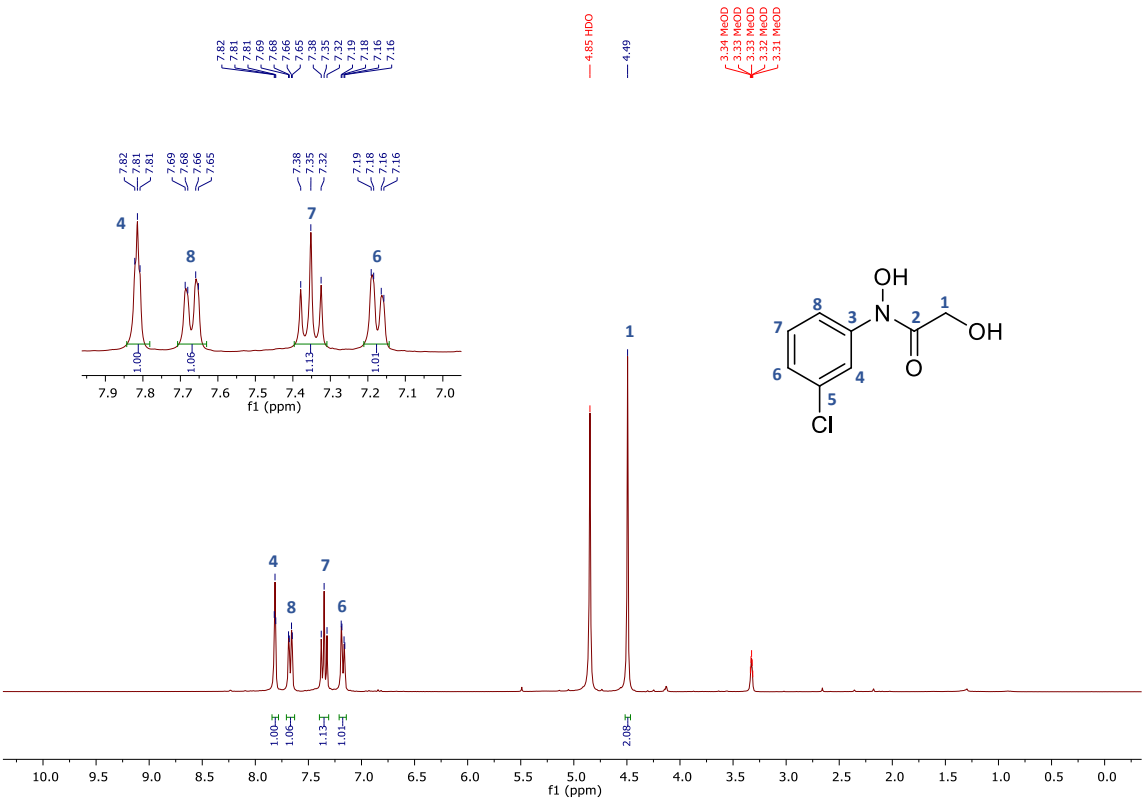

^{1}H-NMR spectrum of *N*-(3-chlorophenyl)-*N*-2-dihydroxyacetamide **(6d)** (300 MHz, CD_3OD)

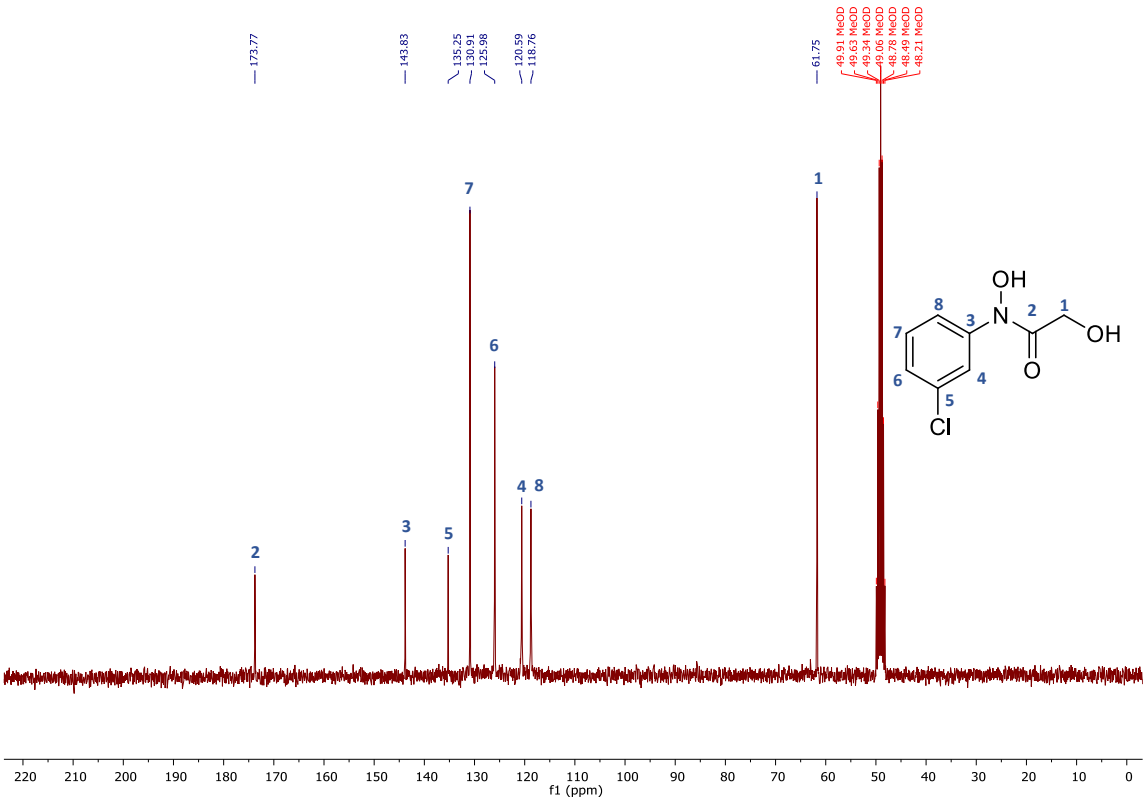

^{13}C-NMR spectrum of *N*-(3-chlorophenyl)-*N*,2-dihydroxyacetamide **(6d)** (75 MHz, CD_3OD)

N-(3,4-Dichlorophenyl)-*N*,2-dihydroxyacetamide (6f)

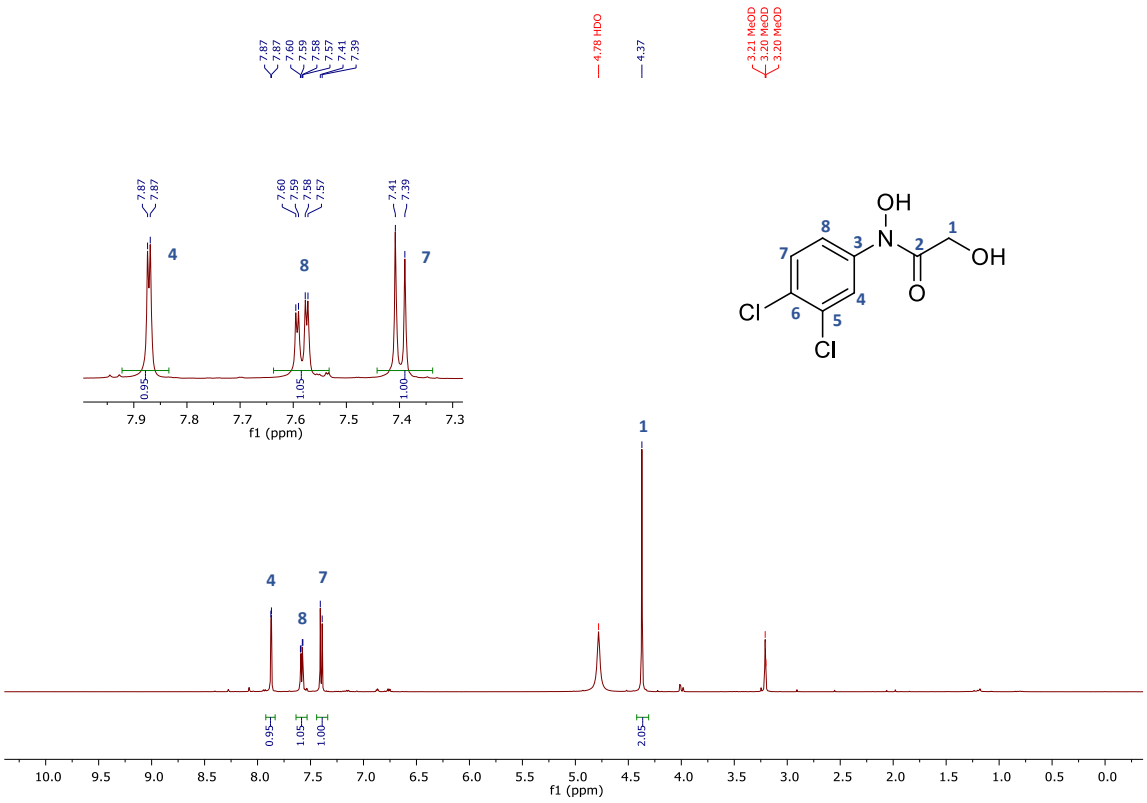

^{1}H-NMR spectrum of *N*-(3,4-dichlorophenyl)-*N*,2-dihydroxyacetamide **(6f)** (500 MHz, CD_3OD)

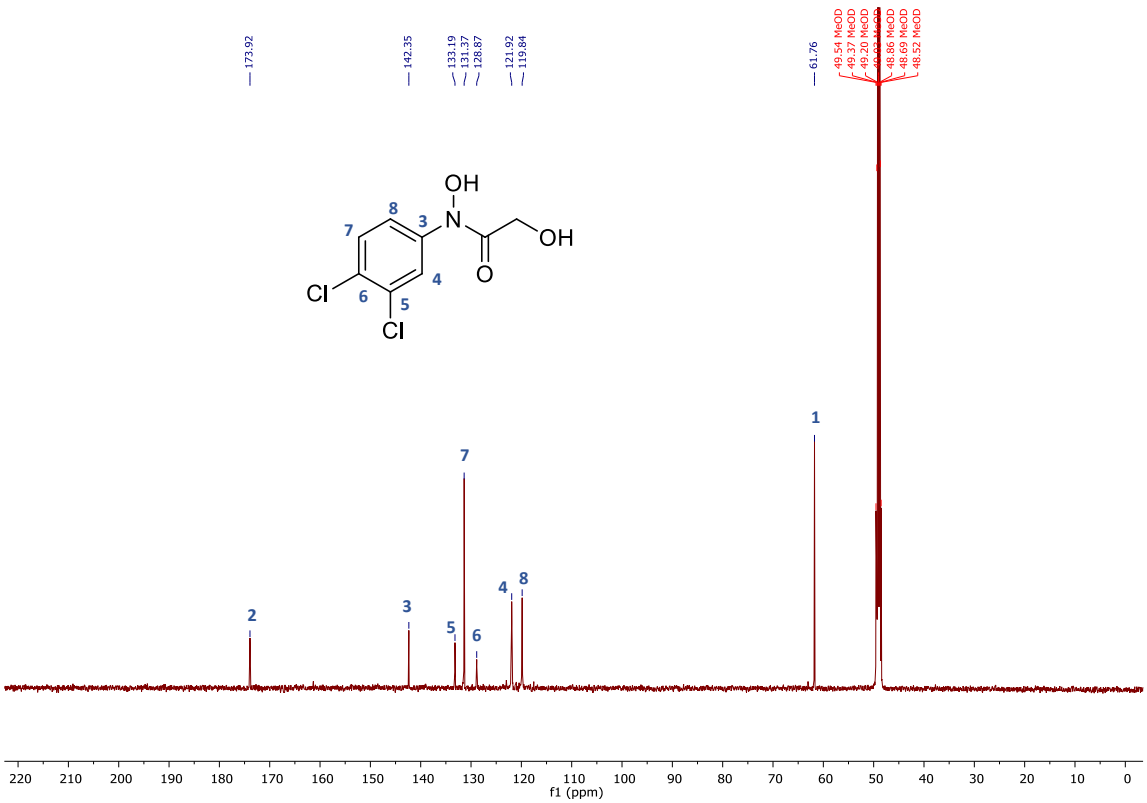

^{13}C-NMR spectrum of *N*-(3,4-dichlorophenyl)-*N*,2-dihydroxyacetamide **(6f)** (126 MHz, CD_3OD)

N-(*p*-Tolyl)-*N*,2-dihydroxyacetamide (6g)

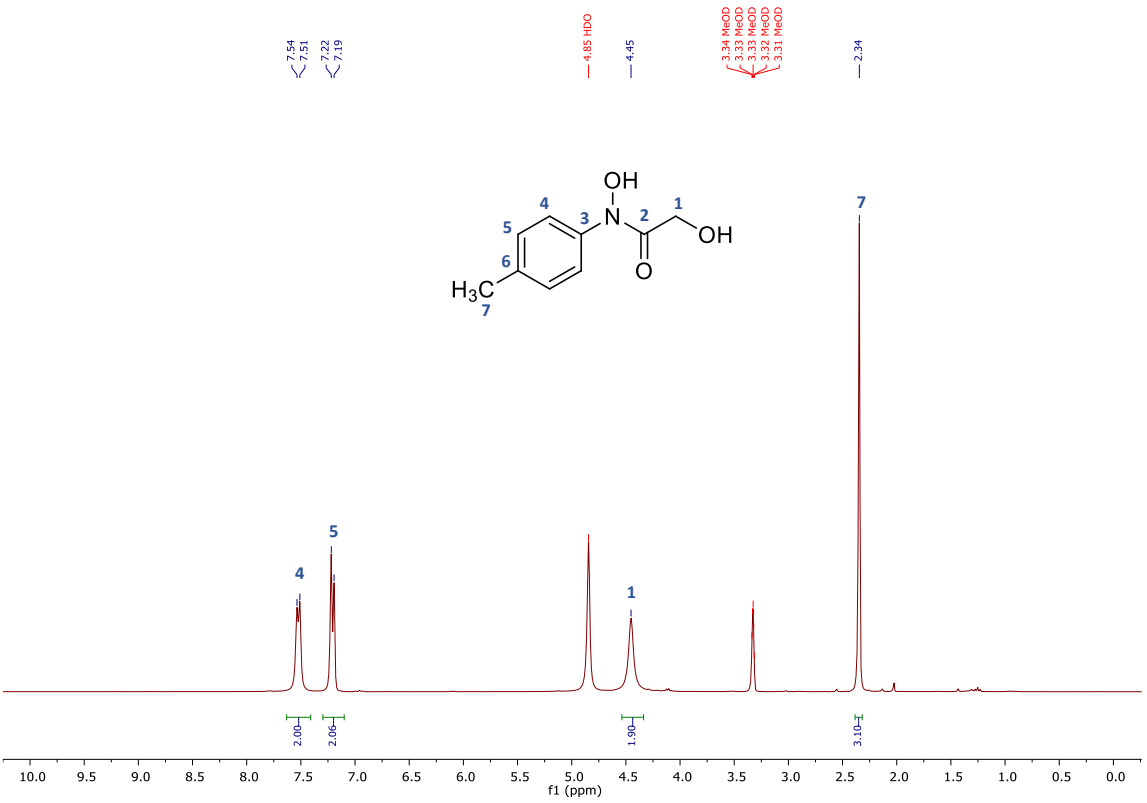

^{1}H-NMR spectrum of *N*-(*p*-tolyl)-*N*,2-dihydroxyacetamide **(6g)** (300 MHz, CD_3OD)

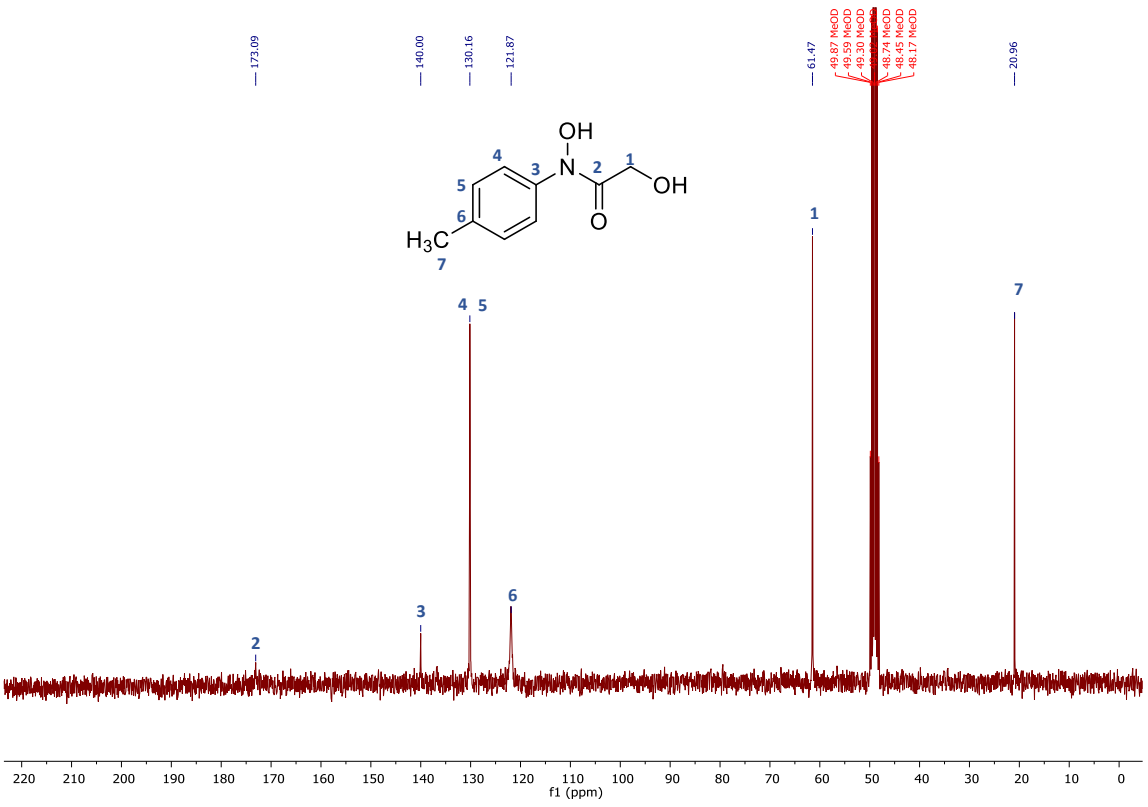

^{13}C-NMR spectrum of *N*-(*p*-tolyl)-*N*,2-dihydroxyacetamide **(6g)** (75 MHz, CD_3OD)

N-(*m*-Tolyl)-*N*,2-dihydroxyacetamide (6h)

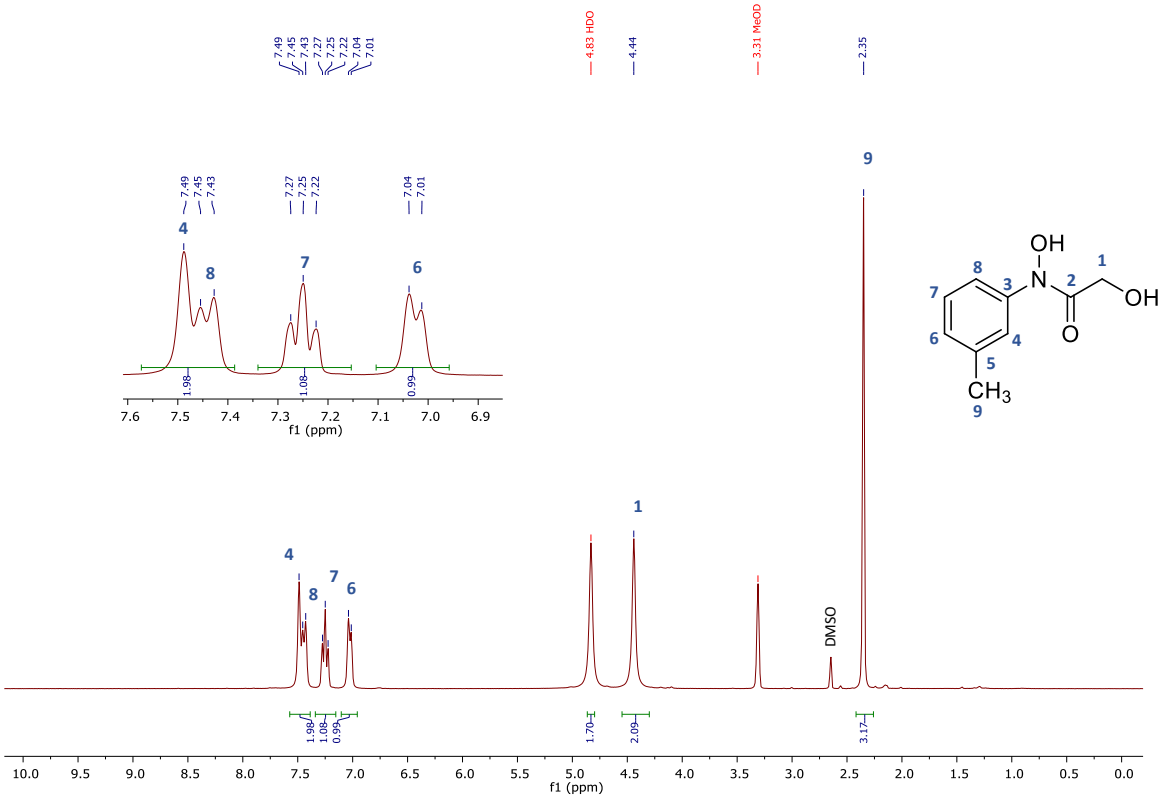

^{1}H-NMR spectrum of *N*-(*m*-tolyl)-*N*,2-dihydroxyacetamide **(6h)** (300 MHz, CD_3OD)

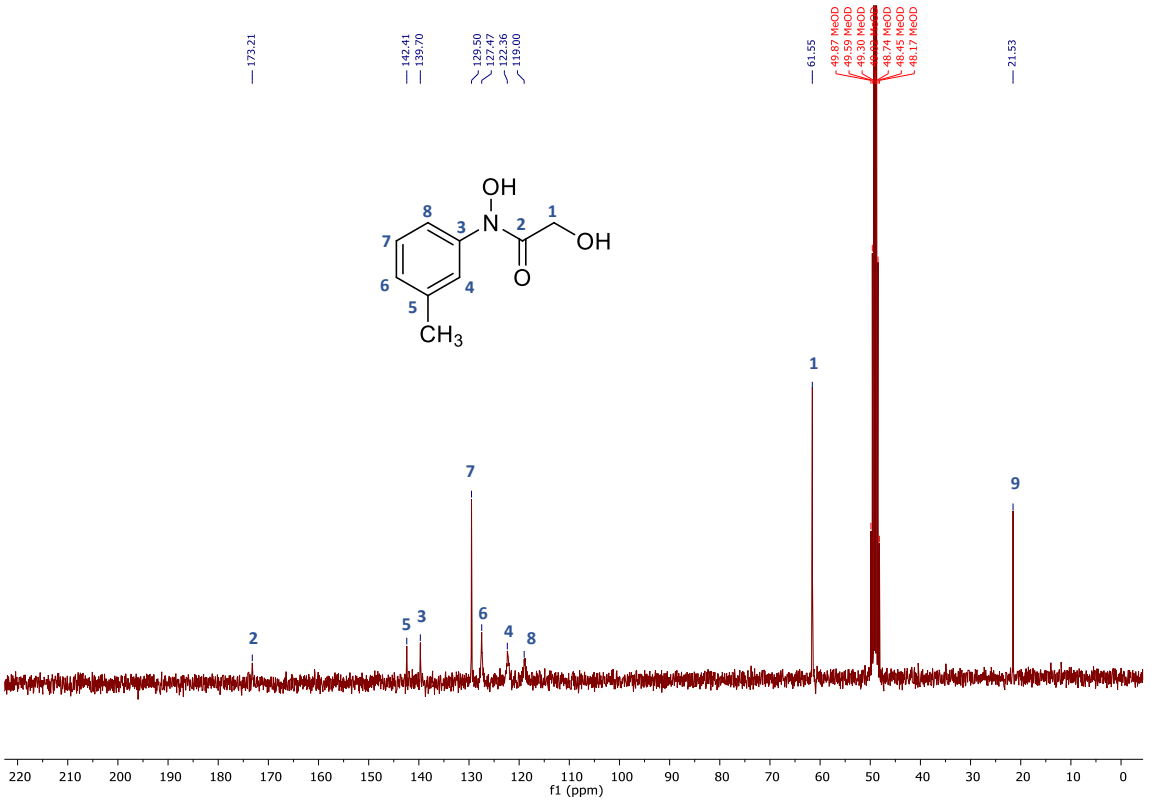

^{13}C-NMR spectrum of *N*-(*m*-tolyl)-*N*,2-dihydroxyacetamide **(6h)** (75 MHz, CD_3OD)

N-(4-Chloro-3-methylphenyl)-*N*,2-dihydroxyacetamide (6i)

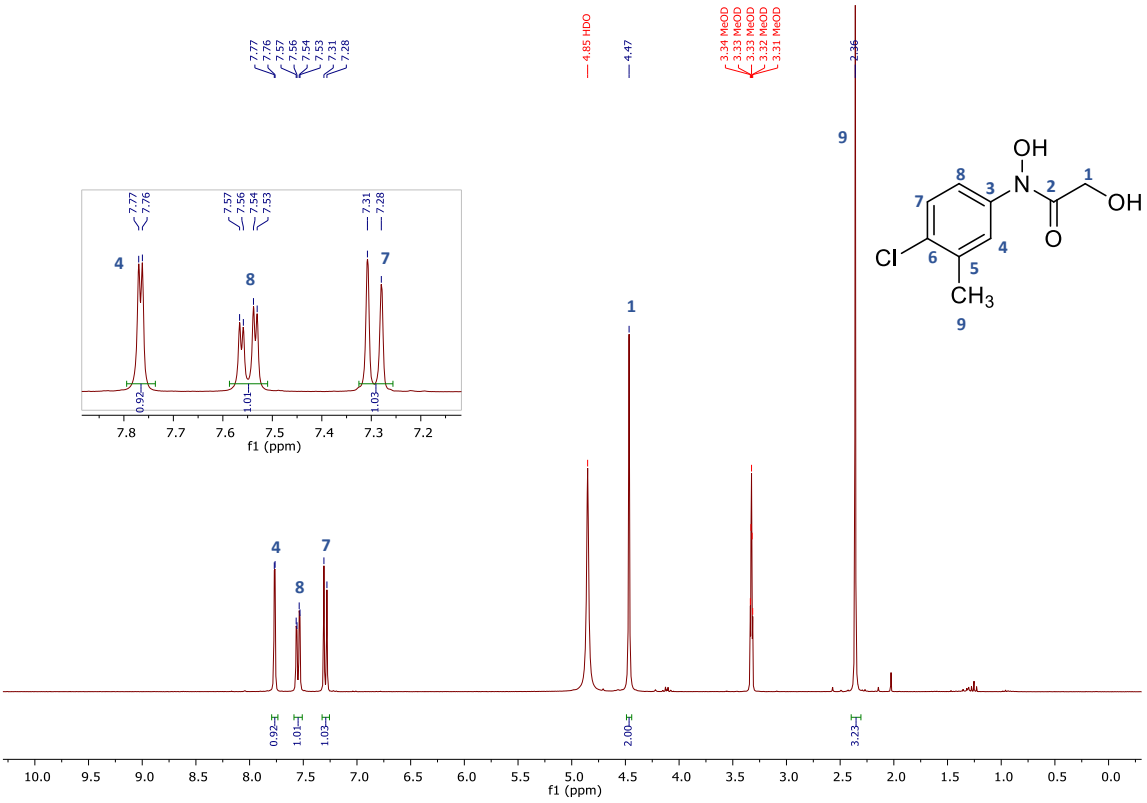

^{1}H-NMR spectrum of *N*-(4-chloro-3-methylphenyl)-*N*,2-dihydroxyacetamide **(6i)** (300 MHz, CD_3OD)

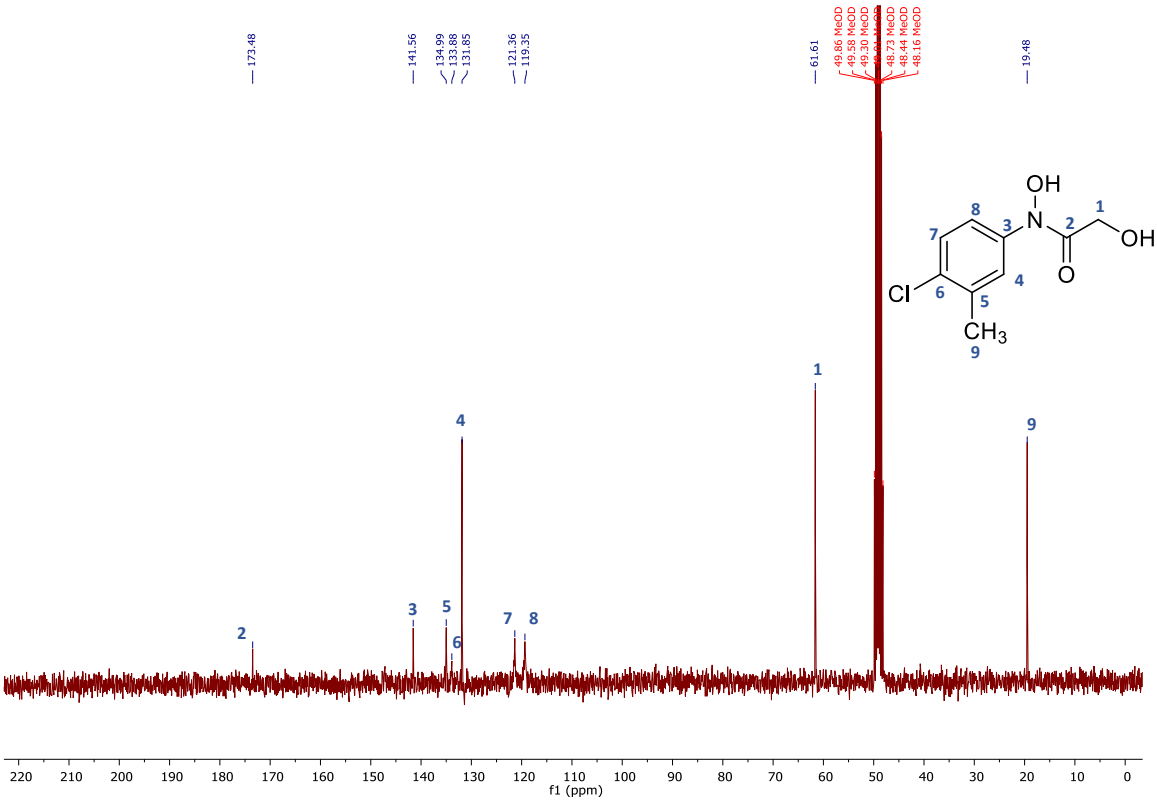

^{13}C-NMR spectrum of *N*-(4-chloro-3-methylphenyl)-*N*,2-dihydroxyacetamide **(6i)** (75 MHz, CD_3OD)

N-(3-Chloro-4-methylphenyl)-*N*,2-dihydroxyacetamide (6j)

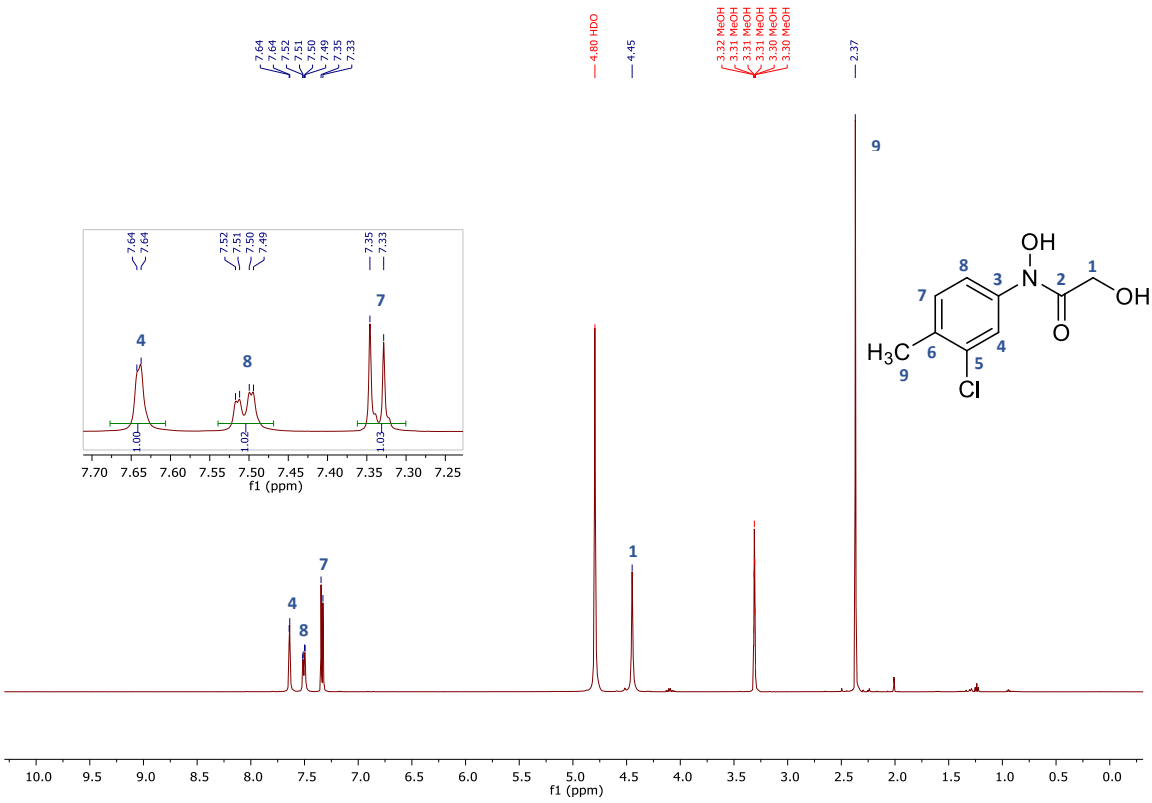

^{1}H-NMR spectrum of *N*-(3-chloro-4-methylphenyl)-*N*,2-dihydroxyacetamide **(6j)** (500 MHz, CD_3OD)

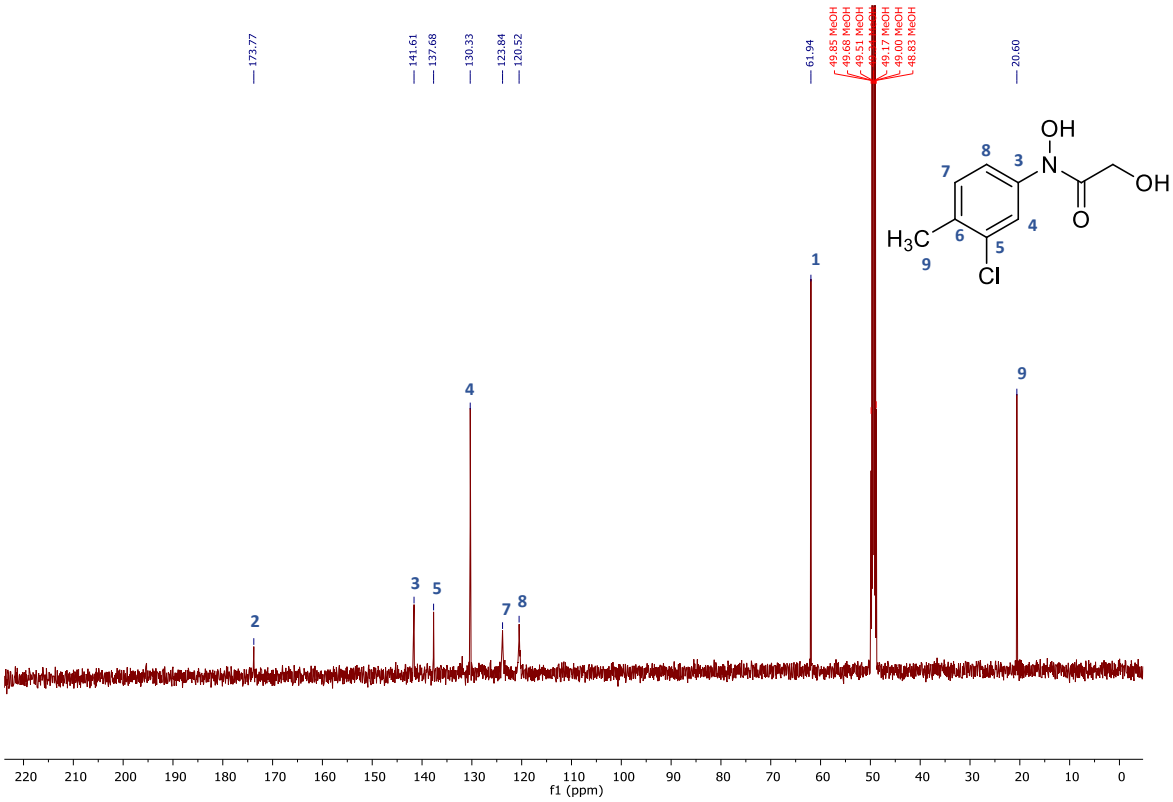

^{13}C-NMR spectrum of *N*-(3-chloro-4-methylphenyl)-*N*,2-dihydroxyacetamide **(6j) (**126 MHz, CD_3OD)

N-(4-(Trifluoromethyl)phenyl)-*N*,2-dihydroxyacetamide (6k)

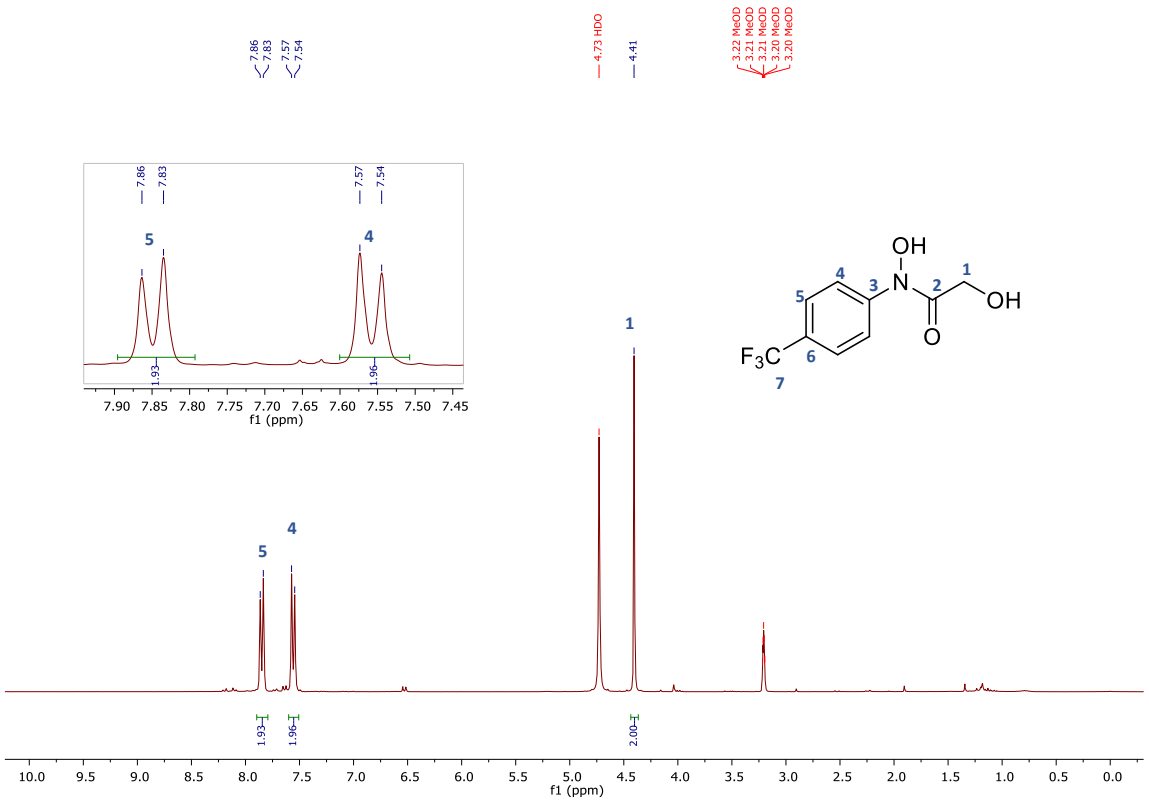

^{1}H-NMR spectrum of *N*-(4-(trifluoromethyl)phenyl)-*N*,2-dihydroxyacetamide **(6k)** (300 MHz, CD_3OD)

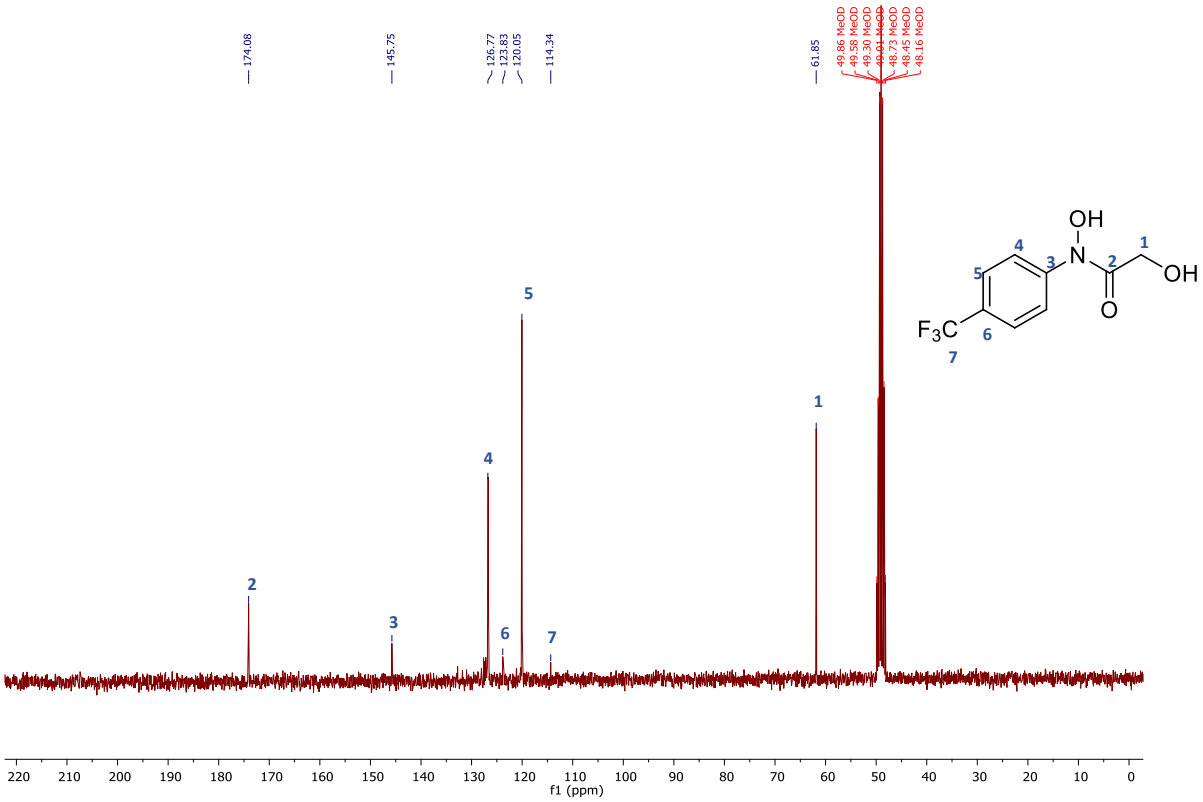

^{13}C-NMR spectrum of *N*-(4-(trifluoromethyl)phenyl)-*N*,2-dihydroxyacetamide **(6k)** (75 MHz, CD_3OD)

N-(3-(Trifluoromethyl)phenyl)-*N*,2-dihydroxyacetamide (6l)

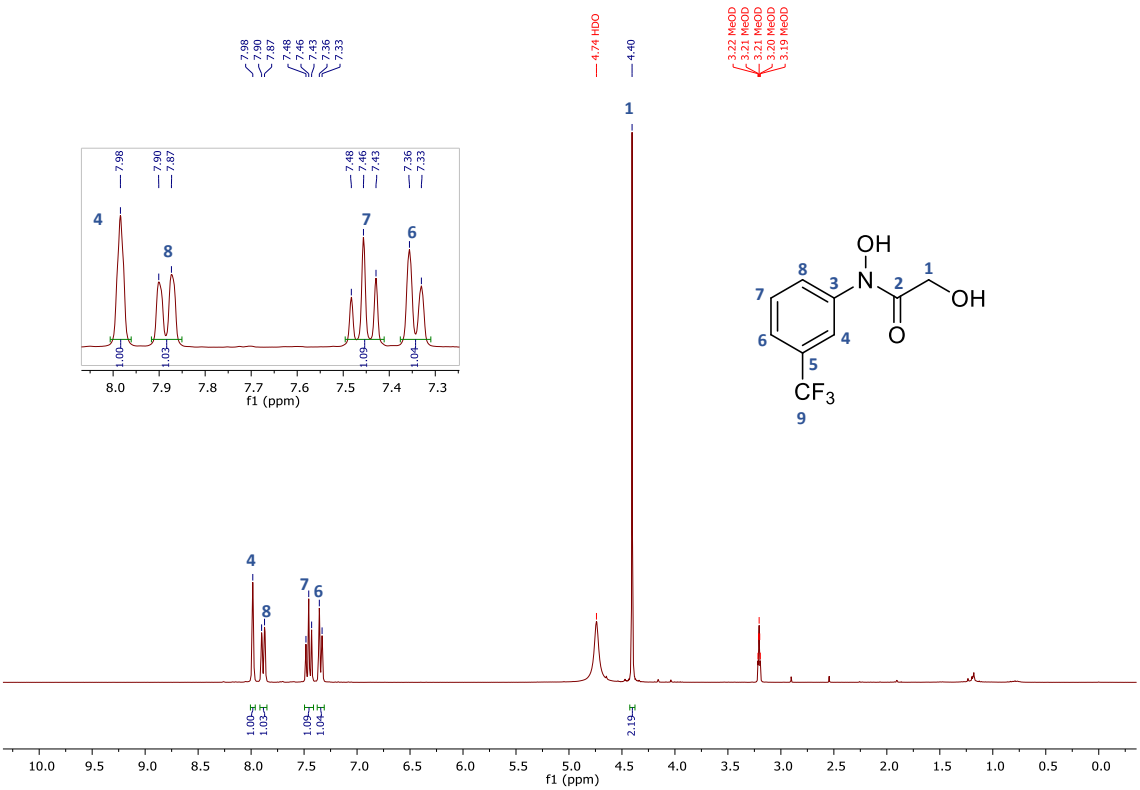

^{1}H-NMR spectrum of *N*-(3-(trifluoromethyl)phenyl)-*N*,2-dihydroxyacetamide **(6l)** (300 MHz, CD_3OD)

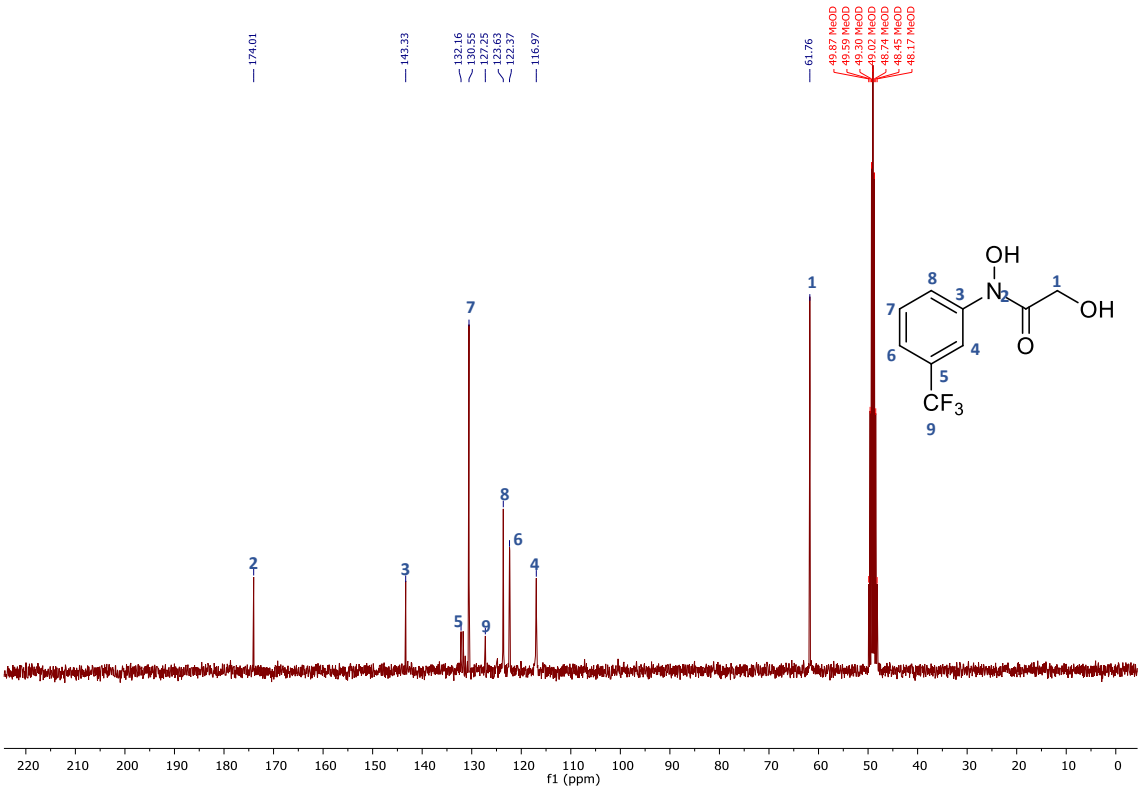

^{13}C-NMR spectrum of *N*-(3-(trifluoromethyl)phenyl)-*N*,2-dihydroxyacetamide **(6l)** (75 MHz, CD_3OD)

4-(*N*,2-Dihydroxyacetamido)benzoic acid (6n) (after column chromatography)

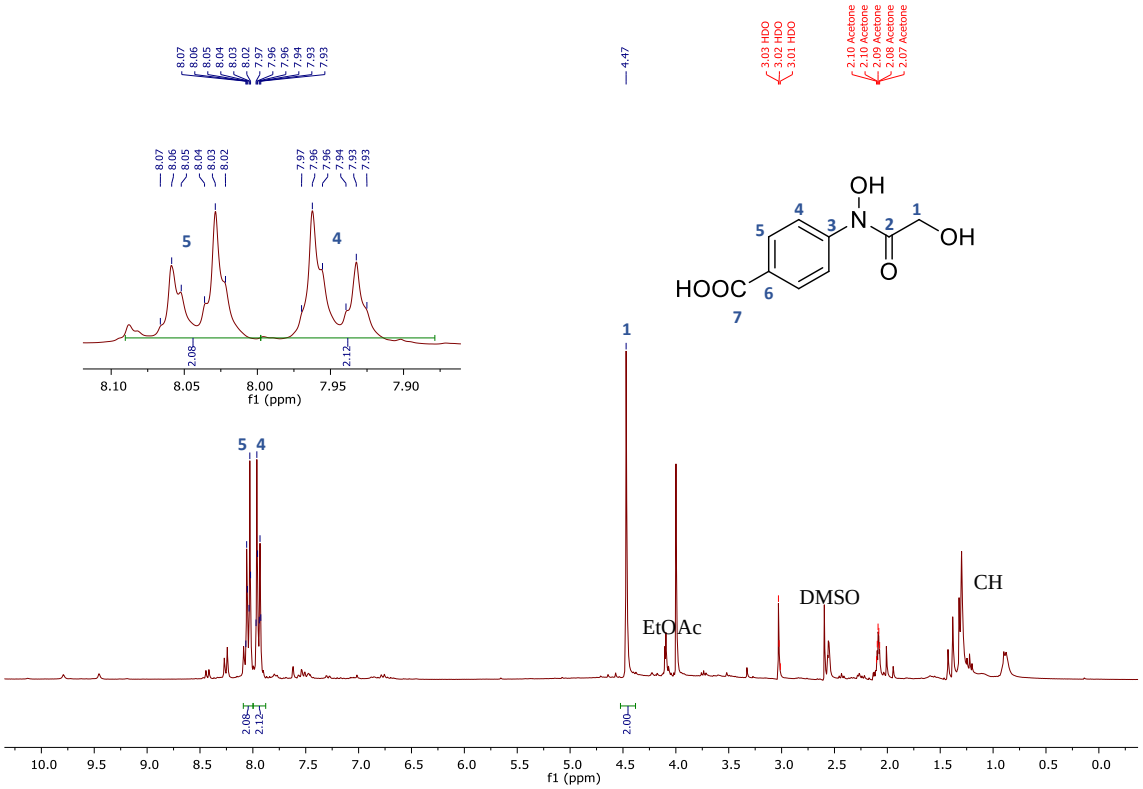

^{1}H-NMR spectrum of 4-(*N*,2-dihydroxyacetamido)benzoic acid **(6n)** (300 MHz, acetone-d^{6})

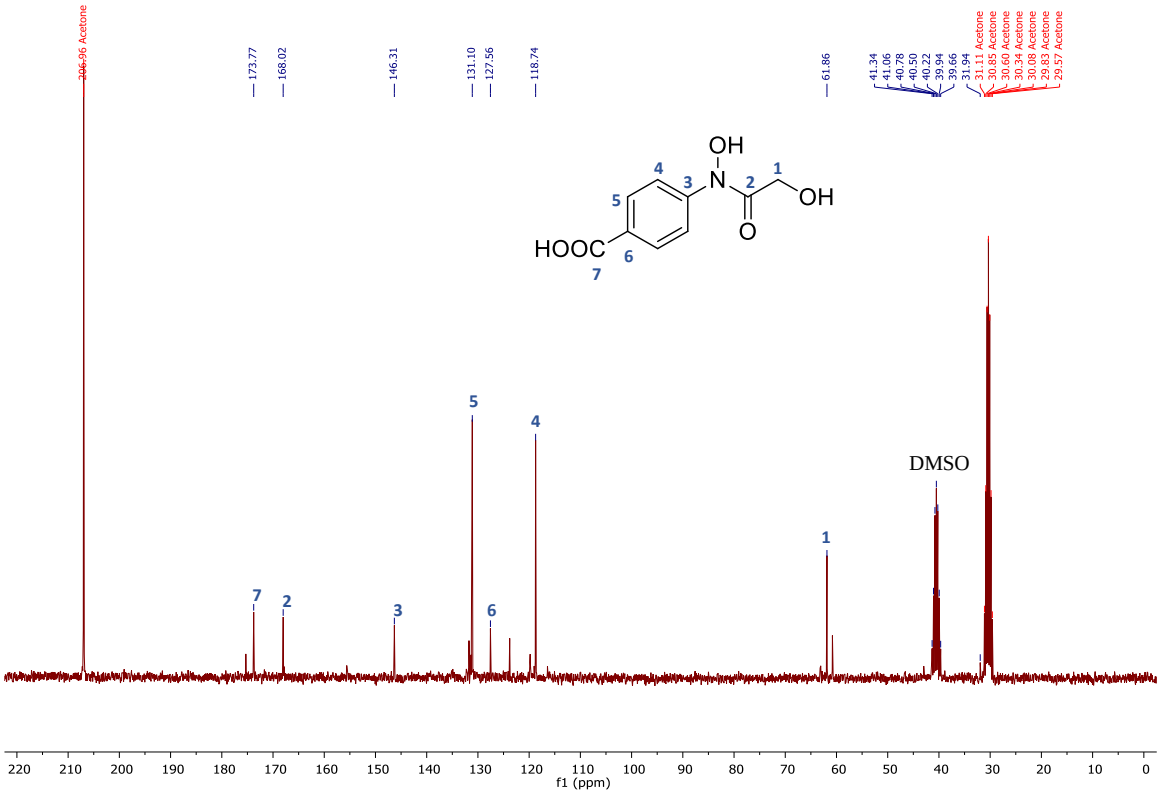

^{13}C-NMR spectrum of 4-(*N*,2-dihydroxyacetamido)benzoic acid **(6n)** (75 MHz, acetone-d^{6})

N-Phenyl-*N*-hydroxyacetamide (15a)

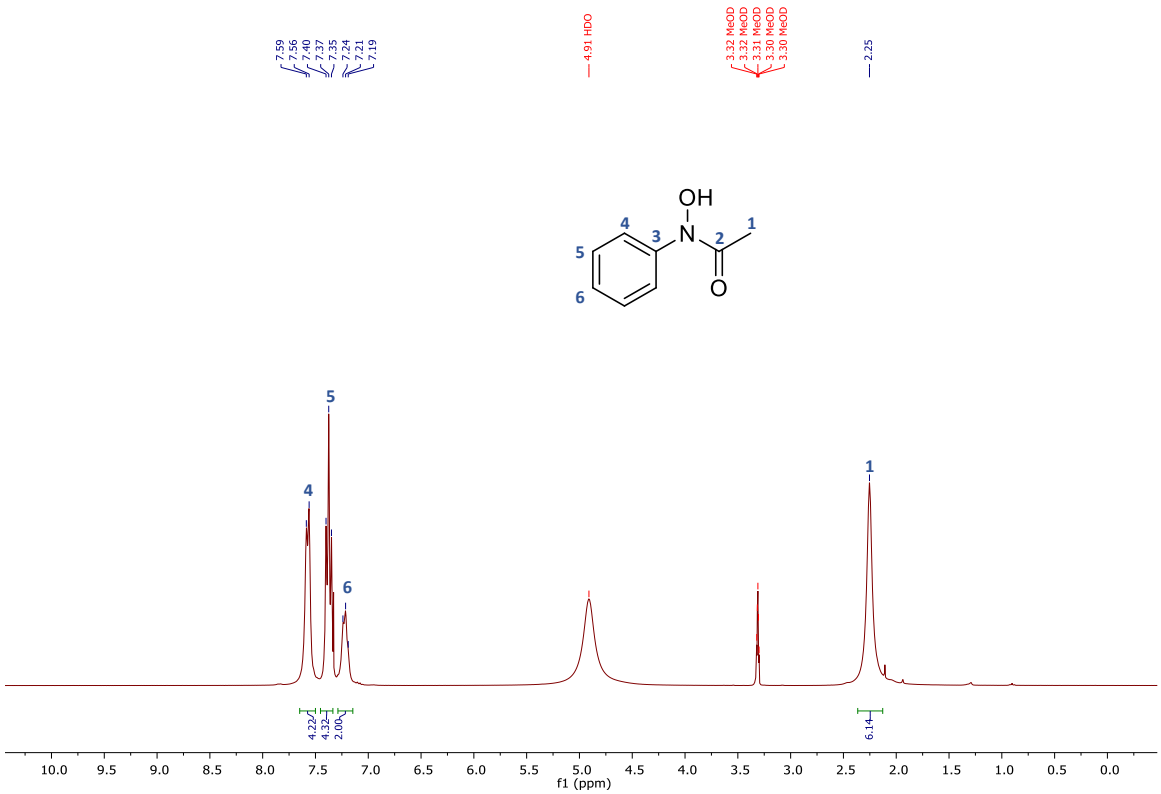

^{1}H-NMR spectrum of *N*-phenyl-*N*-hydroxyacetamide **(15a)** (300 MHz, CD_3OD)

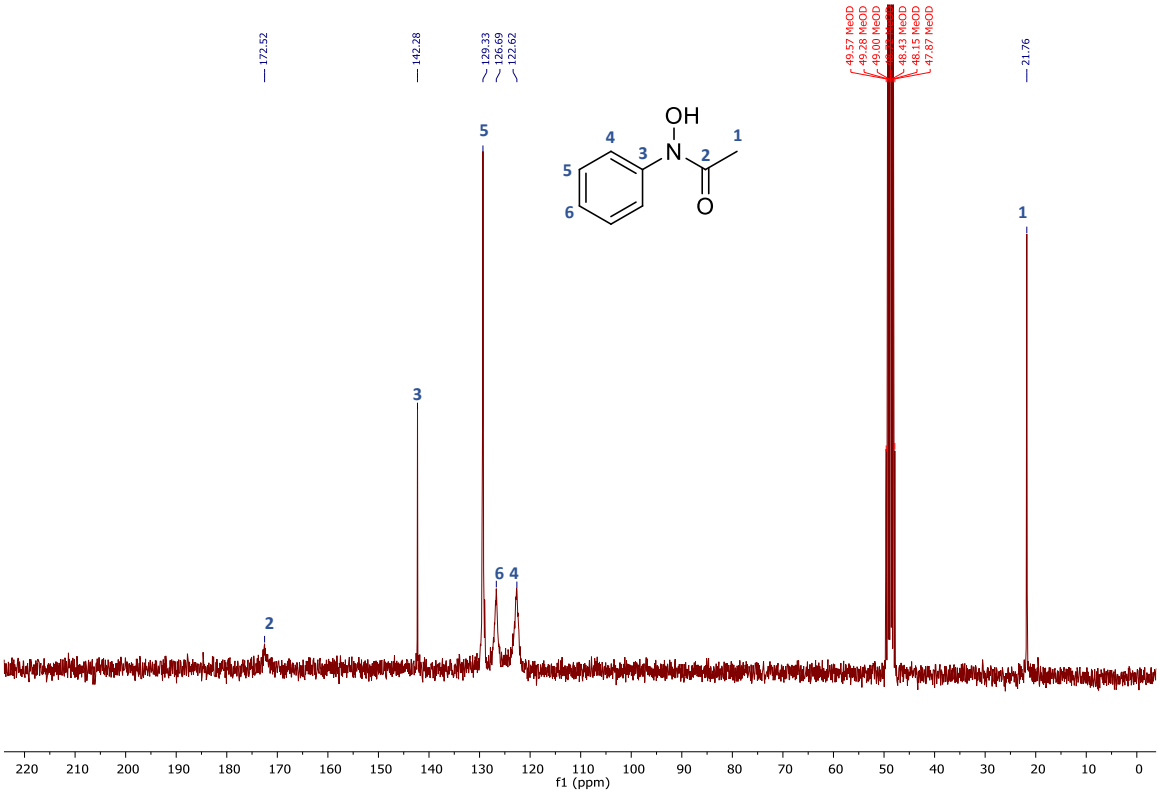

^{13}C-NMR spectrum of *N*-phenyl-*N*-hydroxyacetamide **(15a)** (75 MHz, CD_3OD)

4-(*N*-Hydroxyacetamido)benzoic acid (15n) (after column chromatography)

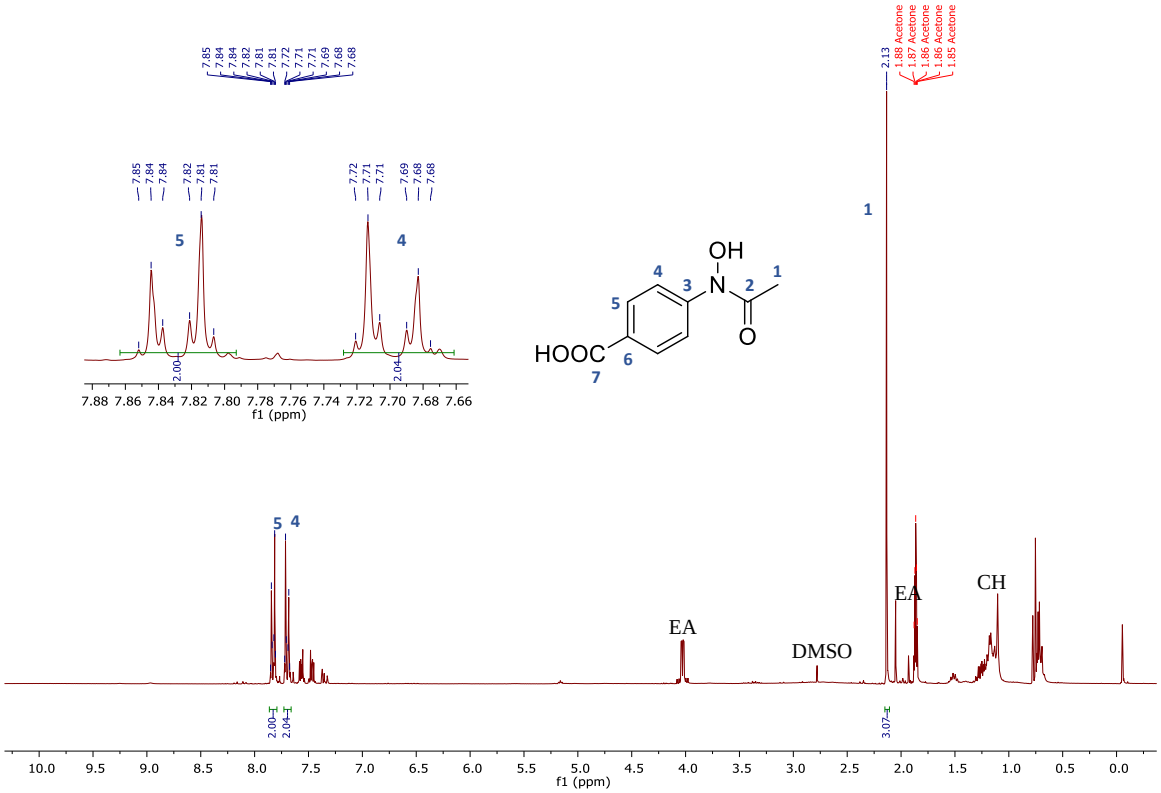

^{1}H-NMR spectrum of 4-(*N*-hydroxyacetamido)benzoic acid **(15n)** (300 MHz, acetone-d^{6})

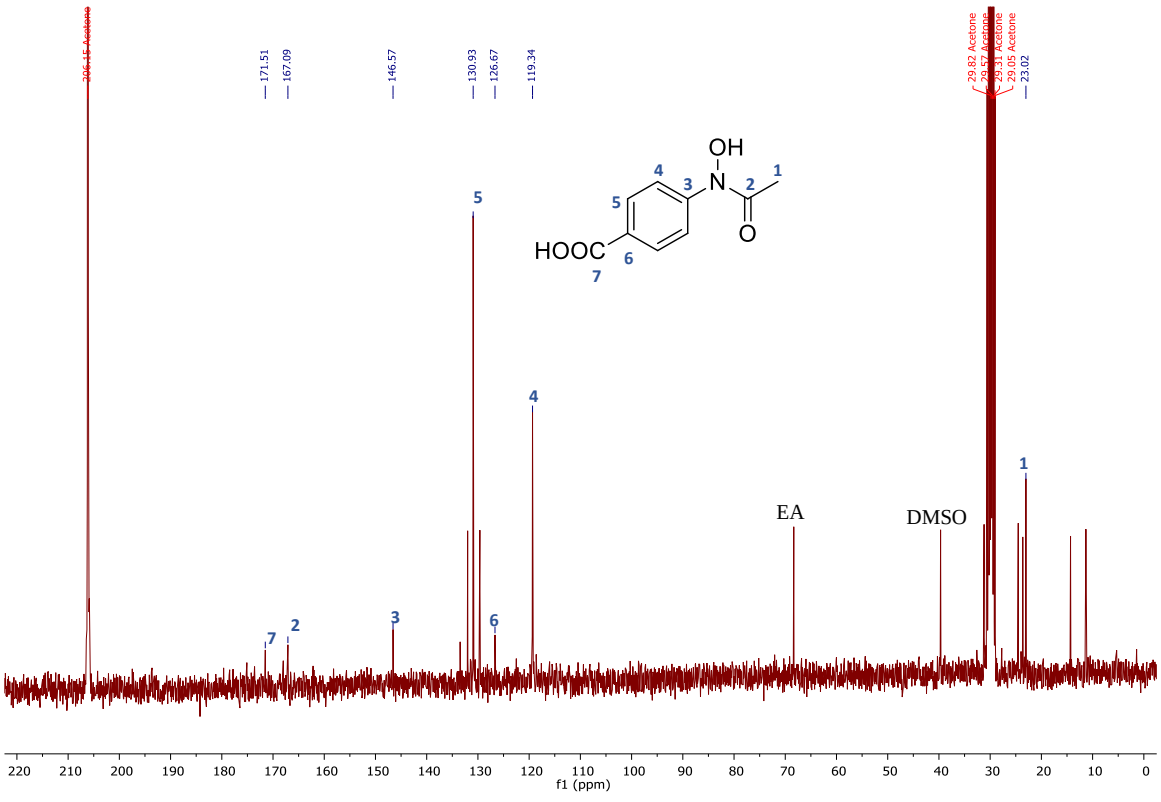

^{13}C-NMR spectrum of 4-(*N*-hydroxyacetamido)benzoic acid **(15n)** (75 MHz, acetone-d^{6})

N-Phenyl-*N*-hydroxyformamide (18a)

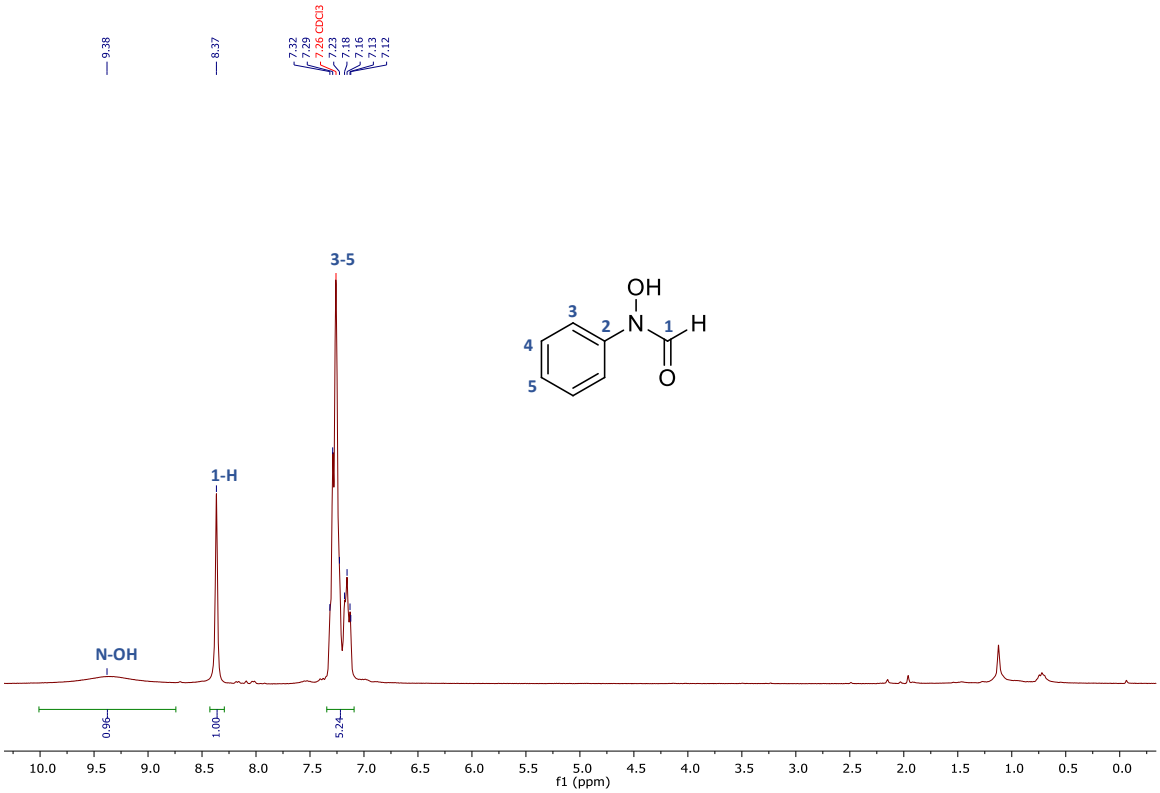

^{1}H-NMR spectrum of *N*-phenyl-*N*-hydroxyformamide **(18a)** (300 MHz, $CDCl_3$)

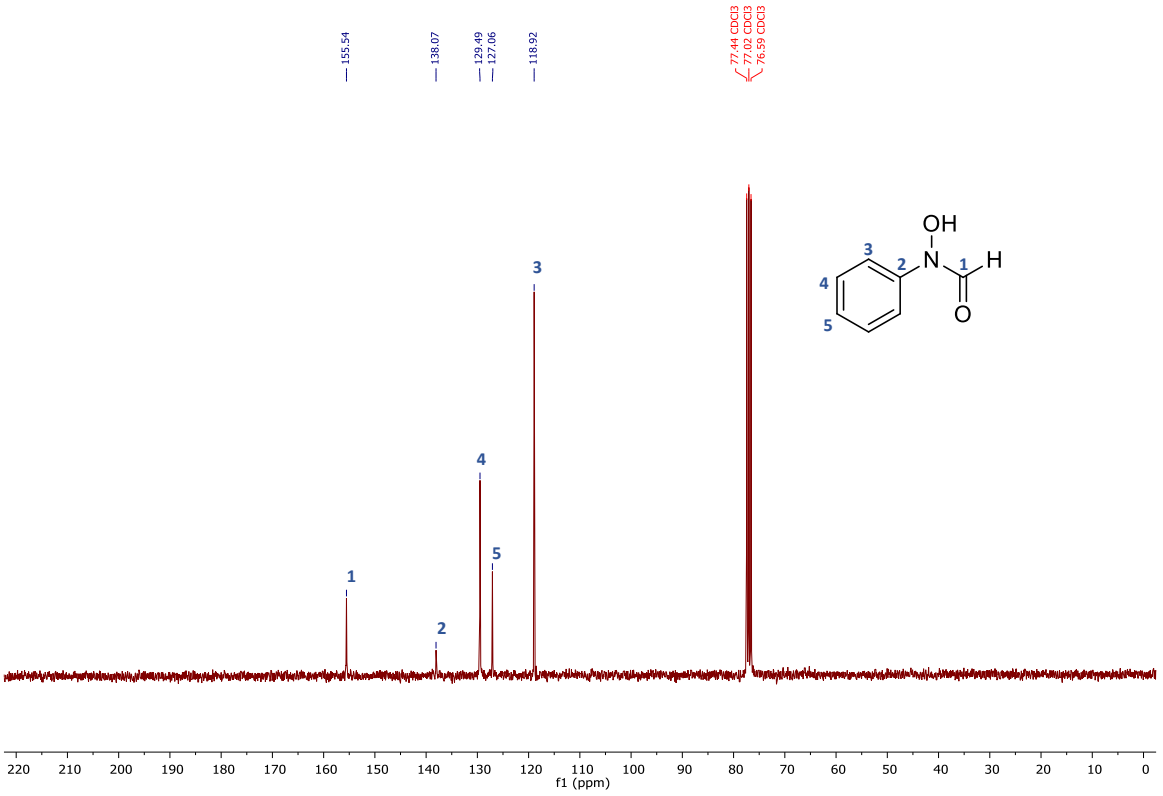

^{1}3C-NMR spectrum of *N*-phenyl-*N*-hydroxyformamide **(18a)** (75 MHz, $CDCl_3$)

N-(4-Bromophenyl)-*N*-hydroxyformamide (18b)

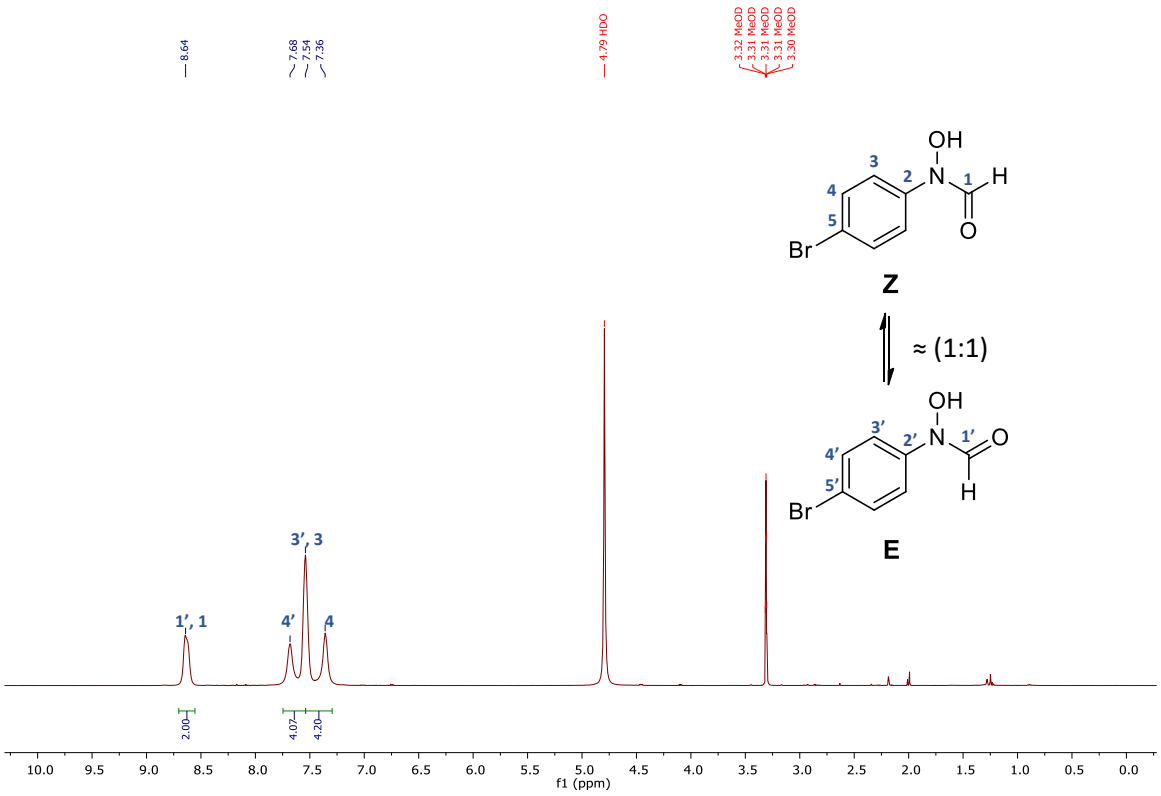

^{1}H-NMR spectrum of *N*-(4-bromophenyl)-*N*-hydroxyformamide **(18b)** (500 MHz, CD_3OD)

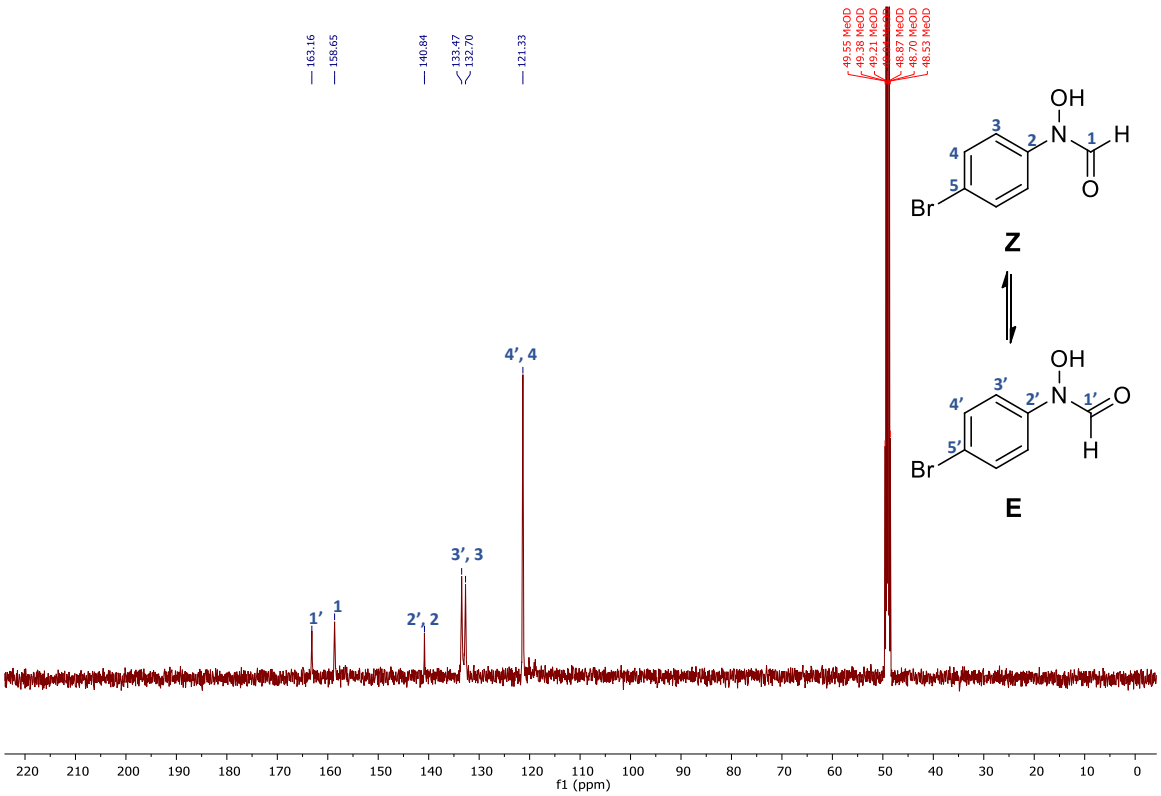

^{13}C-NMR spectrum of *N*-(4-bromophenyl)-*N*-hydroxyformamide **(18b)** (125 MHz, CD_3OD)

N-(4-Bromophenyl)formamide (19b)

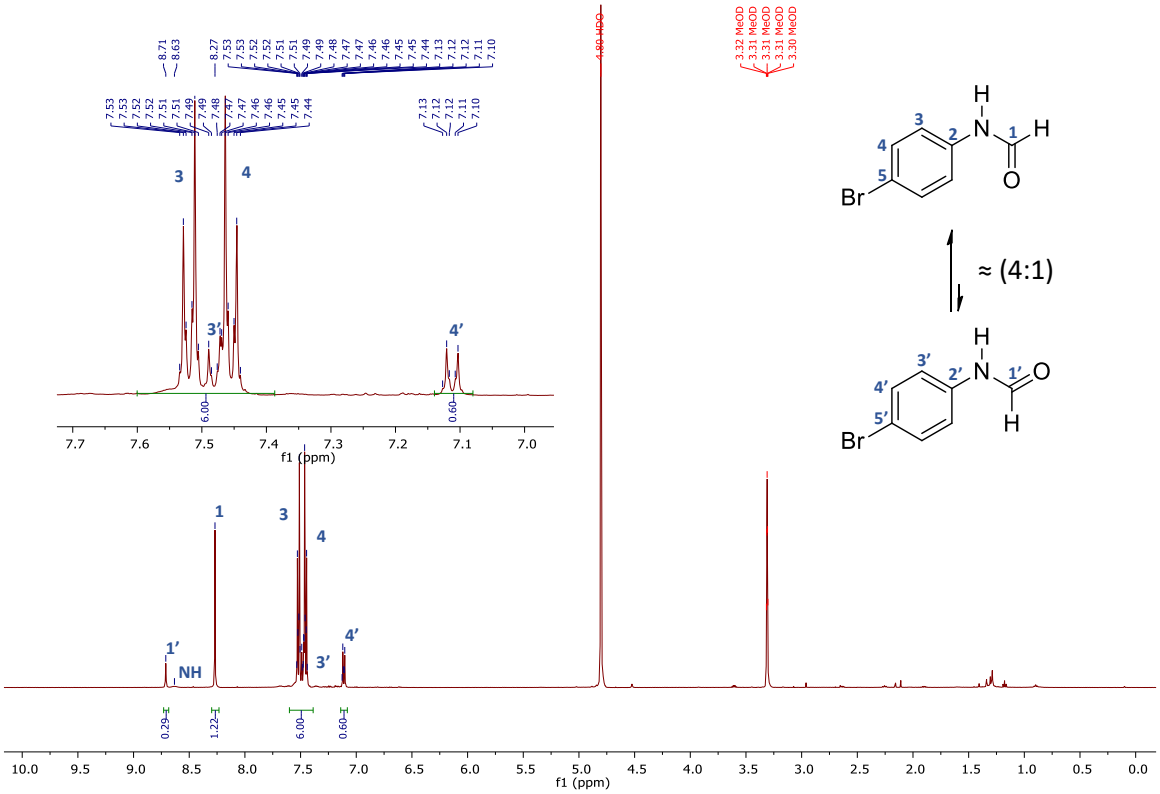

^{1}H-NMR spectrum of *N*-(4-bromophenyl)formamide **(19b)** (500 MHz, CD_3OD)

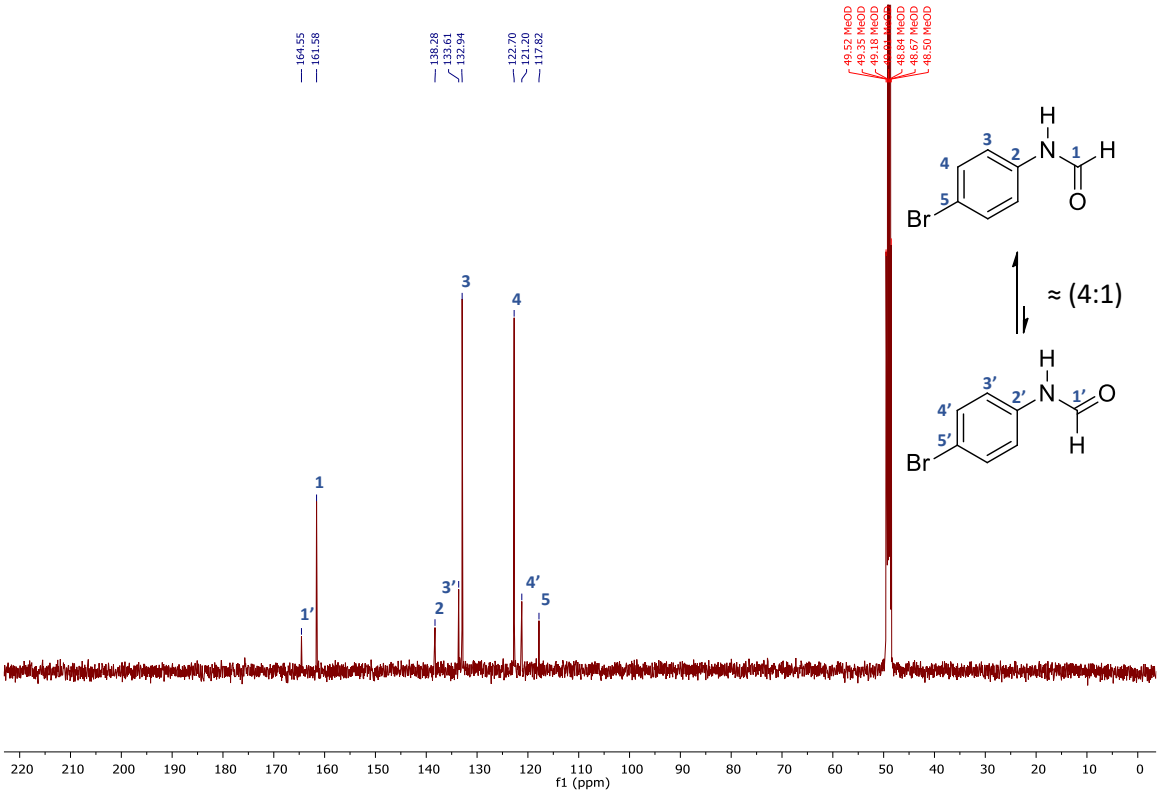

^{13}C-NMR spectrum of *N*-(4-bromophenyl)formamide **(19b)** (126 MHz, CD_3OD)

HPLC chromatograms of the HA 6e, 6m 6n, 6o and 15n

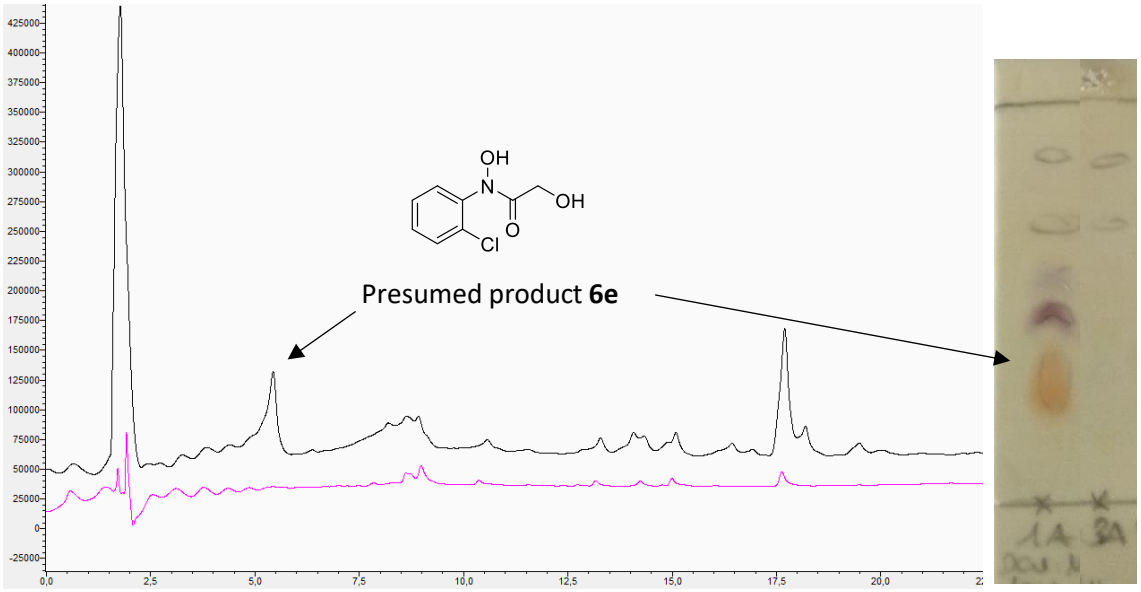

HPLC chromatogram of enzymatic reaction from **5e** and HPA to yield **6e**, and TLC developed with DCM/MeOH (10:1) and stained with $FeCl_3$. Black: reaction in the presence of enzyme (1A), pink: reaction in the absence of enzyme (3A

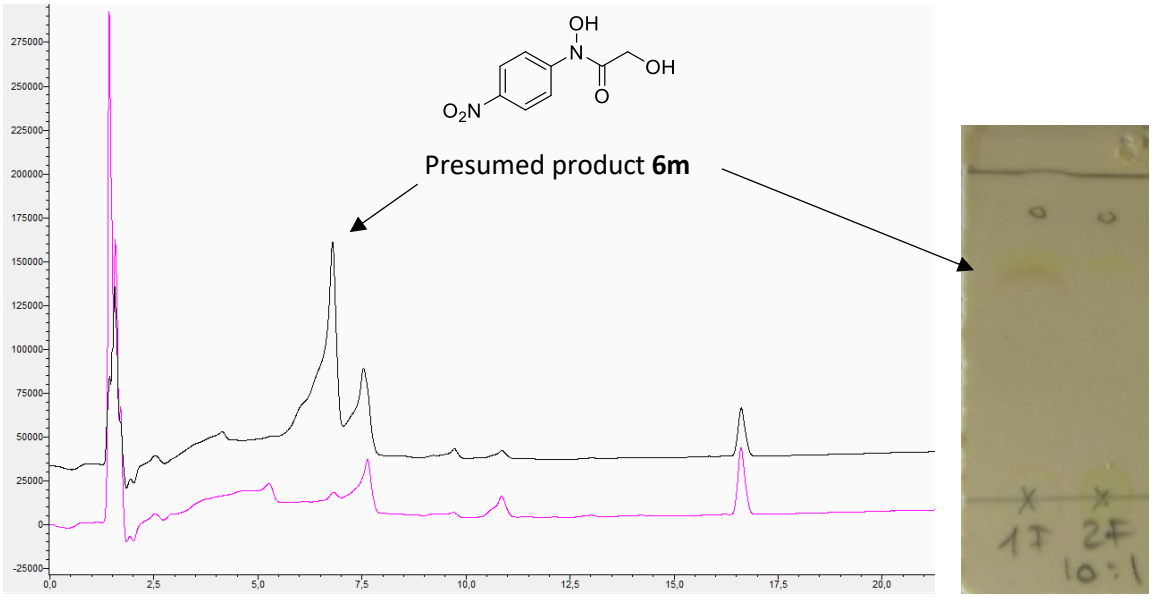

HPLC chromatogram of enzymatic reaction from **5m** and HPA to yield **6m**, and TLC developed with DCM/MeOH (10:1) and stained with $FeCl_3$. Black: reaction in the presence of enzyme (1F), pink: reaction in the absence of enzyme (2F).

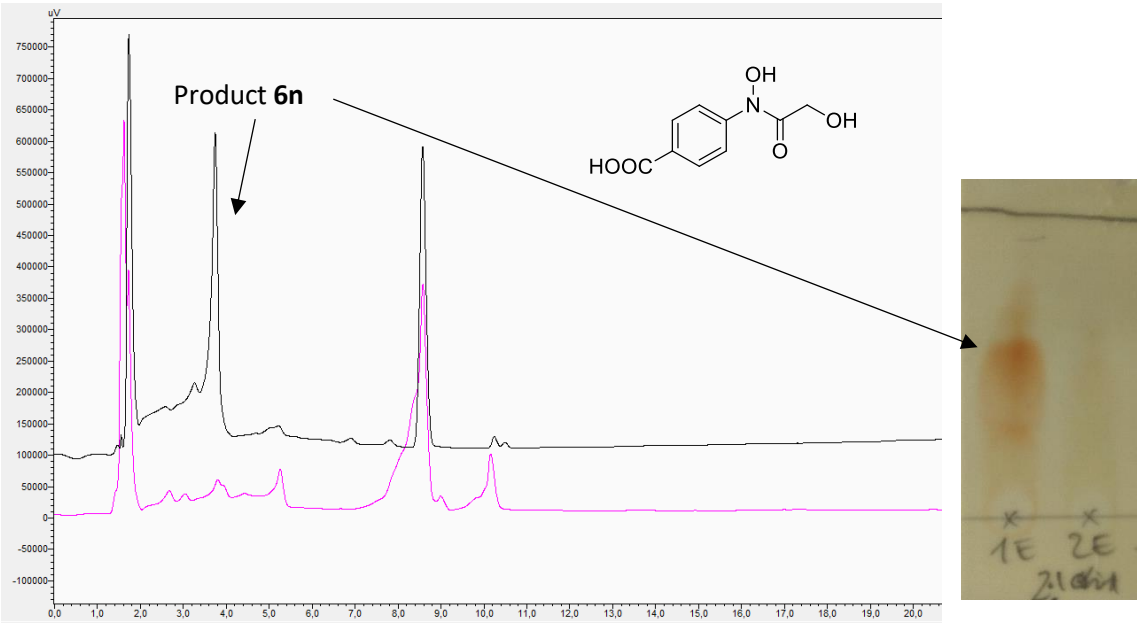

HPLC chromatogram of enzymatic reaction from **5n** and HPA to yield **6n**, and TLC developed with DCM/MeOH (2:1) and stained with $FeCl_3$. Black: reaction in the presence of enzyme (1E), pink: reaction in the absence of enzyme (2E).

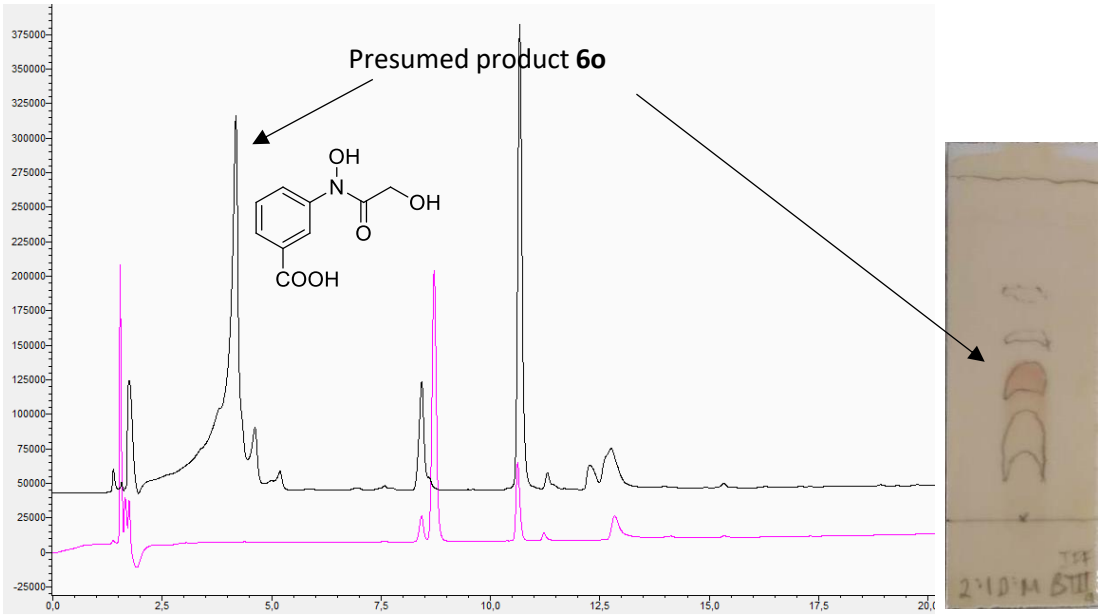

HPLC chromatogram of enzymatic reaction from **5o** and HPA to yield **6o**, and TLC developed with DCM/MeOH (2:1) and stained with $FeCl_3$. Black: reaction in the presence of enzyme, pink: starting material before reaction. In the chromatogram there is a new peak that appears in the presence of enzyme, and in the TLC a spot colors red with $FeCl_3$.

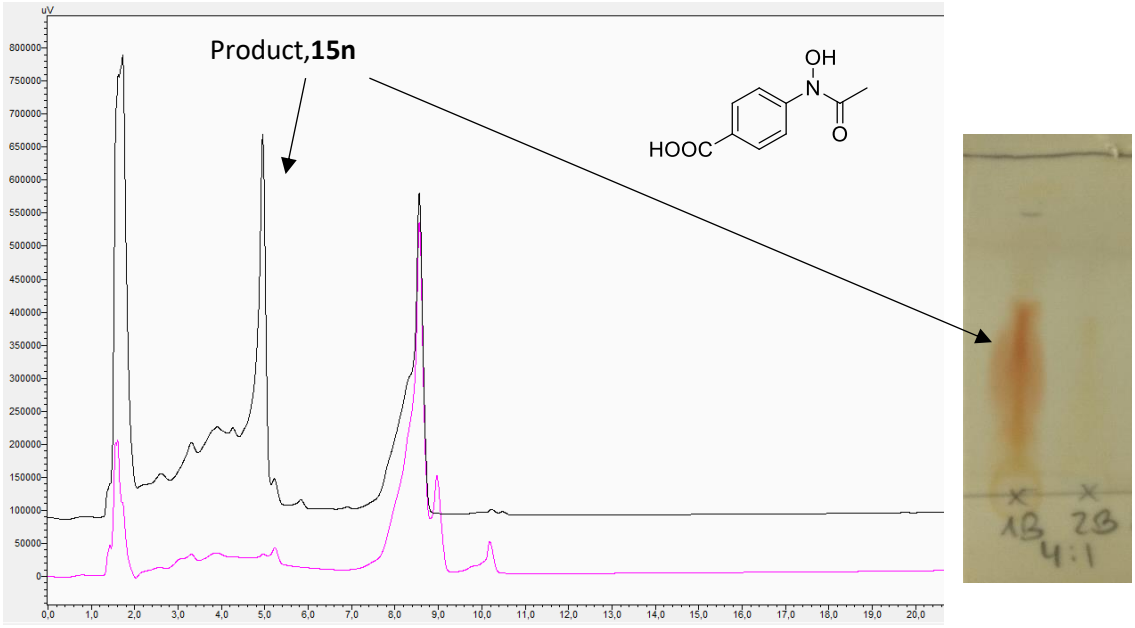

HPLC chromatogram of enzymatic reaction from **5n** and PA to yield **15n**, and TLC developed with DCM/MeOH (4:1) and stained with $FeCl_3$. Black: reaction in the presence of enzyme (1B), pink: reaction in the absence of enzyme (2B).

14.3. Data from CHAPTER II

BCA assay (A) and SDS-PAGE gel (B) from the liquid-phase assay

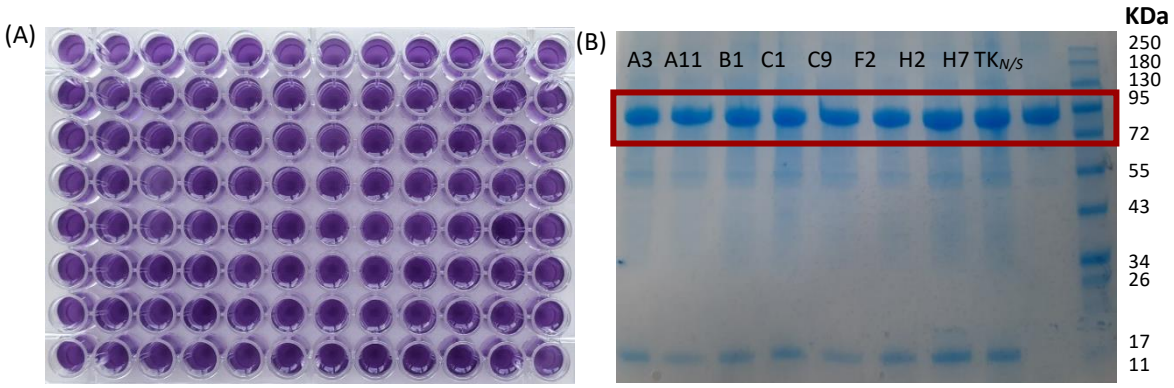

A) 96-well microtiter plate with BCA method. B) SDS gels of 8 random active and inactive variants from the liquid-phase assay: A3: I/S; A11: N/S; B1: N/V; C1: L/M; C9: D/S; F2: D/G; H2: D/V; H7: L/T; $TK_{N/S}$: TK_{gst} variant (N/S) (1 mg/mL) purified as positive control for quantification and comparison. The last column shows the ladder, and with the red square the corresponding TK_{gst} bands are highlighted. The last bands that can be seen in the gel at the bottom correspond to the lysozyme (14.3 KDa) from cell lysis. 10 µL of samples were mixed with 10 µL of protein loading buffer and 7.5 µL were added to the gel.

SDS-PAGE gel ImageJ results from the liquid-phase assay

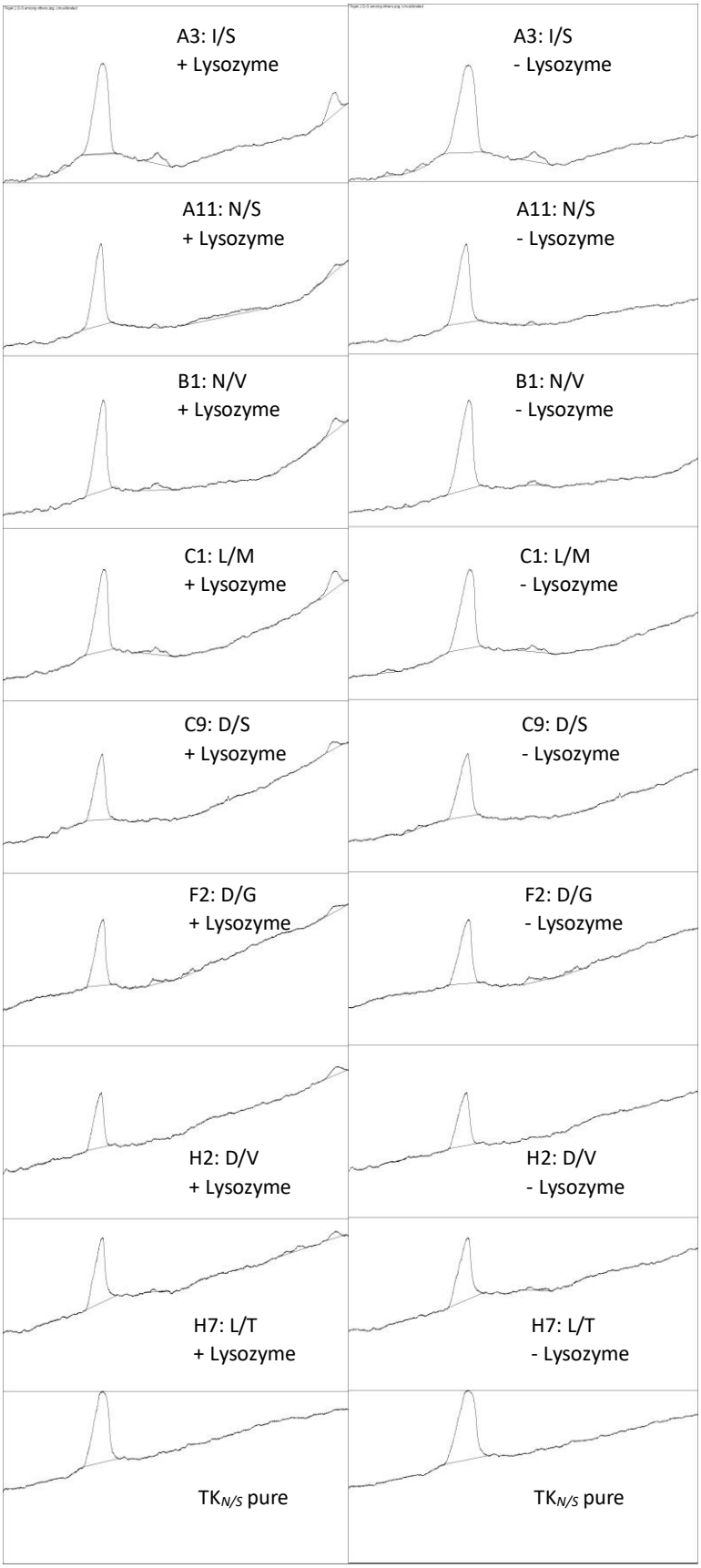

Raw and treated results from liquid-phase assay

- ***N-(4-Bromophenyl)-N,2-dihydroxyacetamide (6b)***

Plate 1:

0.505	0.576	0.600	0.289	0.573	0.446	0.461	0.461	0.294	0.372	0.503	0.453
0.507	0.412	0.290	0.254	0.299	0.539	0.503	0.372	0.345	0.414	0.273	0.409
0.403	0.300	0.697	0.382	0.526	0.362	0.374	0.337	0.406	0.413	0.465	0.340
0.405	0.246	0.258	0.497	0.270	0.236	0.410	0.383	0.476	0.416	0.484	0.491
0.556	0.390	0.500	0.215	0.564	0.396	0.399	0.532	0.507	0.420	0.247	0.421
0.502	0.336	0.478	0.270	0.241	0.285	0.308	0.285	0.454	0.463	0.311	0.326
0.425	0.514	0.281	0.503	0.583	0.583	0.471	0.486	0.447	0.321	0.509	0.453
0.483	0.388	0.320	0.605	0.410	0.520	0.397	0.441	0.372	0.512	0.347	0.195

Plate 2:

0.767	0.625	0.631	0.288	0.574	0.539	0.521	0.508	0.290	0.385	0.512	0.510
0.726	0.399	0.255	0.202	0.228	0.664	0.571	0.402	0.306	0.560	0.277	0.548
0.299	0.221	0.671	0.319	0.483	0.317	0.413	0.296	0.301	0.275	0.428	0.244
0.346	0.211	0.218	0.494	0.256	0.223	0.367	0.338	0.450	0.369	0.511	0.308
0.646	0.408	0.571	0.187	0.551	0.433	0.400	0.575	0.318	0.367	0.171	0.340
0.339	0.274	0.498	0.245	0.184	0.222	0.246	0.232	0.361	0.457	0.232	0.185
0.273	0.414	0.233	0.402	0.410	0.467	0.352	0.495	0.331	0.295	0.433	0.414
0.426	0.346	0.248	0.531	0.351	0.470	0.320	0.397	0.338	0.436	0.283	0.164

Average plate minus the smallest value (not normalized):

0.457	0.421	0.436	0.109	0.394	0.313	0.312	0.305	0.113	0.199	0.328	0.302
0.437	0.226	0.093	0.049	0.084	0.422	0.358	0.208	0.146	0.307	0.096	0.299
0.171	0.081	0.505	0.171	0.325	0.160	0.214	0.137	0.174	0.164	0.267	0.113
0.196	0.049	0.059	0.316	0.083	0.050	0.209	0.181	0.284	0.213	0.318	0.220
0.421	0.219	0.356	0.022	0.378	0.235	0.220	0.374	0.233	0.214	0.030	0.201
0.241	0.126	0.309	0.078	0.033	0.074	0.097	0.079	0.228	0.281	0.092	0.076
0.169	0.285	0.078	0.273	0.317	0.346	0.232	0.311	0.210	0.128	0.291	0.254
0.275	0.187	0.104	0.389	0.201	0.316	0.179	0.239	0.175	0.295	0.135	0.000

Final average plate normalized and used for the graphical results:

90.483	83.362	86.294	21.575	78.014	62.050	61.763	60.426	22.298	39.361	64.952	59.792
86.541	44.699	18.445	9.611	16.583	83.640	70.815	41.124	28.864	60.872	18.950	59.218
33.924	16.098	100.000	33.795	64.348	31.627	42.402	27.071	34.439	32.548	52.939	22.367
38.807	9.730	11.602	62.565	16.524	9.879	41.391	35.806	56.187	42.114	62.931	43.620
83.461	43.471	70.498	4.343	74.924	46.492	43.531	74.122	46.175	42.362	5.868	39.797
47.789	24.902	61.139	15.415	6.601	14.692	19.267	15.722	45.165	55.583	18.178	15.068
33.558	56.375	15.375	54.068	62.822	68.448	45.967	61.594	41.510	25.417	57.702	50.295
54.504	37.123	20.683	76.974	39.827	62.496	35.469	47.393	34.756	58.376	26.804	0.000

To exemplify the applicability of the ferric chloride semi-quantitative method. The approximate concentration values of the **6b** plate were calculated considering the average values before the smallest value was subtracted, and by plotting the values in the standard curve with equation ***y= 0.6114x+0.1386***.

Average plate (not normalized):

0.636	0.600	0.615	0.288	0.573	0.493	0.491	0.485	0.292	0.378	0.507	0.481
0.616	0.405	0.273	0.228	0.263	0.602	0.537	0.387	0.325	0.487	0.275	0.478
0.351	0.261	0.684	0.350	0.504	0.339	0.394	0.316	0.353	0.344	0.447	0.292
0.375	0.229	0.238	0.495	0.263	0.229	0.388	0.360	0.463	0.392	0.497	0.400
0.601	0.399	0.535	0.201	0.558	0.414	0.399	0.554	0.413	0.393	0.209	0.380
0.421	0.305	0.488	0.257	0.213	0.254	0.277	0.259	0.407	0.460	0.271	0.256
0.349	0.464	0.257	0.452	0.497	0.525	0.412	0.490	0.389	0.308	0.471	0.433
0.455	0.367	0.284	0.568	0.381	0.495	0.359	0.419	0.355	0.474	0.315	0.179

Final concentration values:

0.814	0.755	0.779	0.245	0.711	0.579	0.577	0.566	0.251	0.392	0.603	0.561
0.781	0.436	0.219	0.146	0.204	0.757	0.652	0.406	0.305	0.569	0.223	0.556
0.347	0.200	0.893	0.346	0.598	0.328	0.417	0.290	0.351	0.336	0.504	0.251
0.387	0.147	0.163	0.583	0.203	0.148	0.409	0.362	0.531	0.415	0.586	0.427
0.756	0.426	0.649	0.103	0.685	0.451	0.426	0.679	0.448	0.417	0.115	0.395
0.461	0.272	0.572	0.194	0.121	0.188	0.226	0.197	0.440	0.526	0.217	0.191
0.344	0.532	0.194	0.513	0.586	0.632	0.446	0.575	0.410	0.277	0.543	0.482
0.517	0.373	0.238	0.702	0.396	0.583	0.360	0.458	0.354	0.549	0.288	0.067

- ***N-(3-(Trifluoromethyl)phenyl)-N,2-dihydroxyacetamide (5l)***

Plate 1:

0.685	0.590	0.674	0.278	0.666	0.460	0.502	0.528	0.402	0.411	0.709	0.565
0.709	0.374	0.308	0.251	0.304	0.694	0.609	0.459	0.747	0.666	0.271	0.657
0.358	0.242	0.624	0.383	0.421	0.515	0.493	0.370	0.427	0.502	0.586	0.256
0.476	0.244	0.240	0.667	0.254	0.247	0.409	0.346	0.578	0.457	0.728	0.452
0.634	0.434	0.718	0.251	0.721	0.497	0.463	0.648	0.543	0.503	0.290	0.405
0.426	0.390	0.659	0.362	0.225	0.332	0.562	0.355	0.597	0.698	0.335	0.337
0.315	0.442	0.345	0.735	0.631	0.730	0.519	0.770	0.491	0.454	0.676	0.521
0.479	0.462	0.349	0.765	0.314	0.685	0.456	0.519	0.414	0.709	0.495	0.234

Plate 2:

0.697	0.575	0.672	0.277	0.701	0.504	0.574	0.660	0.396	0.441	0.703	0.520
0.736	0.372	0.307	0.256	0.287	0.698	0.606	0.407	0.645	0.603	0.273	0.547
0.377	0.232	0.668	0.370	0.427	0.489	0.608	0.362	0.430	0.471	0.658	0.231
0.488	0.220	0.223	0.695	0.232	0.232	0.385	0.337	0.548	0.438	0.710	0.418
0.656	0.424	0.758	0.218	0.765	0.579	0.487	0.733	0.568	0.579	0.245	0.417
0.400	0.381	0.702	0.350	0.223	0.337	0.535	0.365	0.599	0.678	0.330	0.331
0.314	0.464	0.355	0.779	0.627	0.721	0.522	0.727	0.530	0.431	0.682	0.458
0.496	0.500	0.364	0.794	0.302	0.702	0.469	0.489	0.439	0.789	0.496	0.224

Average plate minus the smallest value (not normalized):

0.467	0.359	0.449	0.054	0.460	0.258	0.314	0.370	0.175	0.202	0.482	0.319
0.499	0.149	0.084	0.030	0.072	0.473	0.384	0.209	0.472	0.411	0.048	0.378
0.144	0.013	0.423	0.153	0.200	0.278	0.327	0.142	0.205	0.263	0.399	0.020
0.258	0.008	0.008	0.458	0.019	0.016	0.174	0.118	0.340	0.224	0.495	0.211
0.421	0.206	0.514	0.011	0.520	0.314	0.251	0.467	0.332	0.318	0.044	0.187
0.189	0.162	0.457	0.132	0.000	0.111	0.325	0.137	0.374	0.465	0.109	0.110
0.091	0.229	0.127	0.533	0.406	0.502	0.297	0.525	0.287	0.219	0.455	0.266
0.264	0.258	0.133	0.556	0.085	0.470	0.239	0.281	0.203	0.526	0.272	0.006

Final average plate normalized and used for the graphical results:

84.048	64.527	80.739	9.684	82.717	46.417	56.524	66.541	31.544	36.364	86.737	57.279
89.749	26.877	15.125	5.395	12.886	84.983	69.005	37.667	84.911	73.905	8.704	68.060
25.942	2.410	76.000	27.426	35.995	50.040	58.844	25.555	36.912	47.253	71.666	3.588
46.426	1.457	1.385	82.304	3.489	2.913	31.265	21.266	61.056	40.284	89.048	37.982
75.776	36.966	92.429	1.888	93.427	56.542	45.158	83.958	59.671	57.099	7.877	33.702
34.071	29.098	82.178	23.793	0.000	19.926	58.475	24.602	67.296	83.554	19.630	19.836
16.392	41.255	22.786	95.909	72.961	90.226	53.394	94.371	51.605	39.376	81.827	47.765
47.406	46.309	23.955	100.000	15.196	84.498	42.955	50.445	36.436	94.506	48.934	1.016

- ***N-(3-Chloro-4-methylphenyl)-N,2-dihydroxyacetamide (6j)***

Plate 1:

0.443	0.489	0.672	0.239	0.430	0.424	0.486	0.476	0.264	0.289	0.645	0.615
0.524	0.292	0.297	0.235	0.254	0.551	0.436	0.339	0.593	0.763	0.248	0.620
0.266	0.240	0.465	0.314	0.341	0.350	0.388	0.275	0.345	0.264	0.546	0.253
0.292	0.215	0.214	0.365	0.234	0.214	0.264	0.261	0.539	0.343	0.678	0.239
0.422	0.332	0.457	0.206	0.784	0.429	0.385	0.679	0.571	0.605	0.223	0.332
0.340	0.306	0.522	0.311	0.197	0.231	0.368	0.282	0.672	0.492	0.235	0.249
0.266	0.330	0.305	0.550	0.507	0.593	0.576	0.571	0.415	0.373	0.657	0.509
0.306	0.342	0.244	0.497	0.336	0.337	0.296	0.290	0.242	0.499	0.272	0.195

Plate 2:

0.525	0.575	0.653	0.248	0.456	0.443	0.509	0.515	0.294	0.278	0.627	0.623
0.711	0.279	0.263	0.217	0.222	0.538	0.455	0.321	0.437	0.535	0.219	0.654
0.275	0.206	0.506	0.336	0.365	0.351	0.458	0.288	0.385	0.300	0.564	0.258
0.349	0.193	0.208	0.353	0.270	0.246	0.263	0.253	0.422	0.290	0.508	0.242
0.414	0.295	0.559	0.192	0.504	0.369	0.333	0.508	0.427	0.460	0.217	0.305
0.380	0.298	0.649	0.301	0.278	0.203	0.320	0.288	0.457	0.440	0.218	0.227
0.262	0.350	0.264	0.543	0.483	0.598	0.457	0.531	0.386	0.320	0.546	0.467
0.438	0.425	0.250	0.683	0.325	0.419	0.293	0.246	0.255	0.517	0.295	0.174

Average plate minus the smallest value (not normalized):

0.299	0.348	0.478	0.059	0.259	0.249	0.313	0.311	0.094	0.099	0.451	0.435
0.433	0.101	0.095	0.042	0.053	0.360	0.261	0.145	0.330	0.464	0.049	0.452
0.086	0.038	0.301	0.140	0.168	0.166	0.239	0.097	0.180	0.098	0.371	0.071
0.136	0.019	0.026	0.174	0.067	0.046	0.079	0.073	0.296	0.132	0.408	0.056
0.233	0.129	0.324	0.014	0.460	0.214	0.175	0.409	0.315	0.348	0.036	0.134
0.175	0.118	0.401	0.122	0.053	0.032	0.160	0.101	0.380	0.282	0.042	0.054
0.080	0.156	0.101	0.362	0.311	0.411	0.332	0.366	0.216	0.162	0.417	0.304
0.188	0.199	0.062	0.405	0.146	0.194	0.110	0.084	0.064	0.324	0.099	0.000

Final average plate normalized and used for the graphical results:

62.599	72.665	100.000	12.350	54.048	51.999	65.400	65.034	19.730	20.734	94.355	90.874
90.509	21.131	19.929	8.734	11.148	75.320	54.665	30.372	69.090	97.084	10.218	94.596
17.932	8.033	62.996	29.337	35.211	34.710	49.877	20.305	37.699	20.462	77.536	14.765
28.386	4.030	5.514	36.445	14.096	9.570	16.563	15.225	61.856	27.602	85.366	11.660
48.811	27.016	67.731	2.995	96.101	44.839	36.518	85.575	65.808	72.759	7.427	28.020
36.664	24.622	83.902	25.500	11.075	6.768	33.393	21.016	79.470	58.909	8.796	11.190
16.688	32.567	21.016	75.728	64.982	86.014	69.362	76.564	45.194	33.967	87.184	63.456
39.215	41.556	13.061	84.759	30.591	40.469	23.054	17.472	13.427	67.689	20.755	0.000

Sequences from the solid-phase supported assay

WILD-TYPE: L382/D470, TTG (Leu)/GAC (Asp)

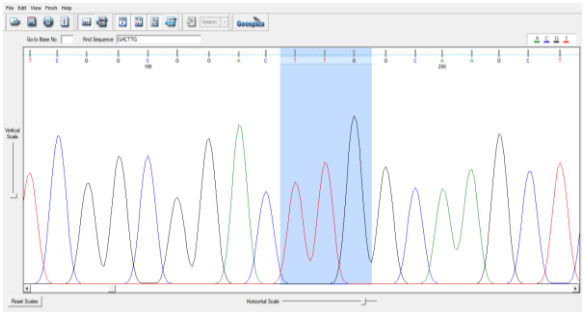

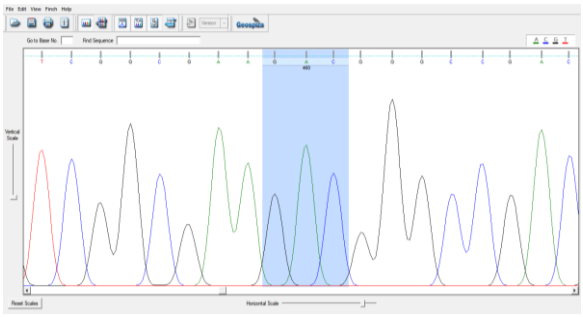

1: L382S/D470D, TCC (Ser)/GAC (Asp)

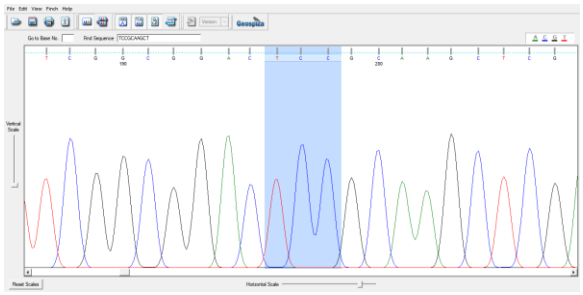

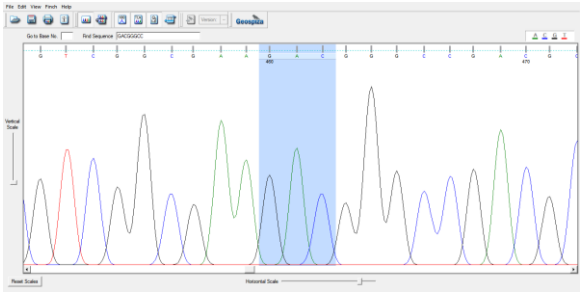

2: L382E/D470S, GAG (Glu)/TCC (Ser)

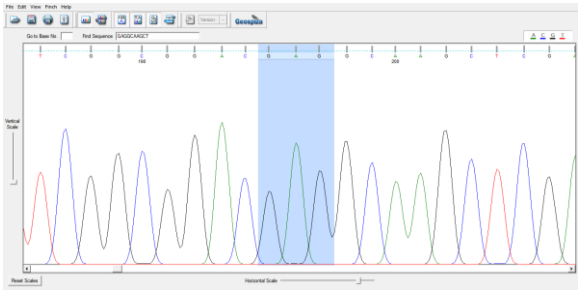

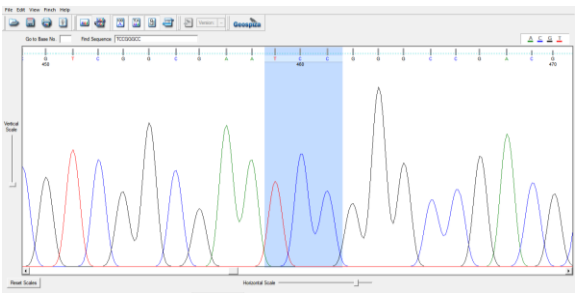

3: L382Q/D470S, CAG (Gln)/AGC (Ser)

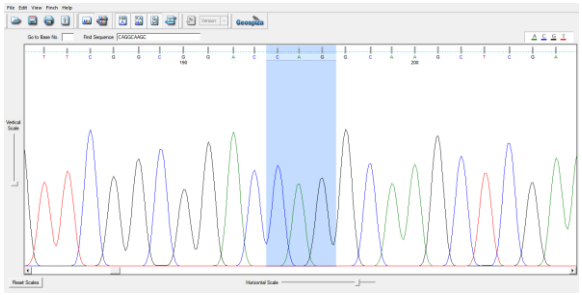

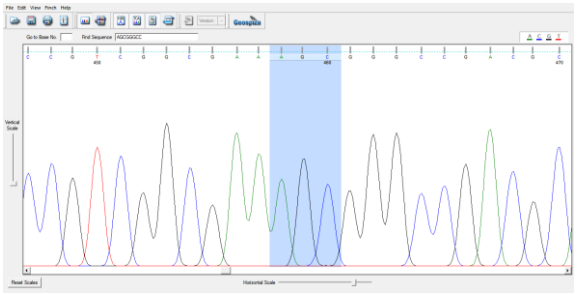

4: L382Q/D470S, CAG (Gln)/AGC (Ser)

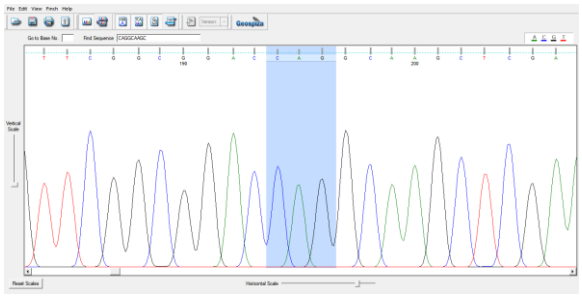

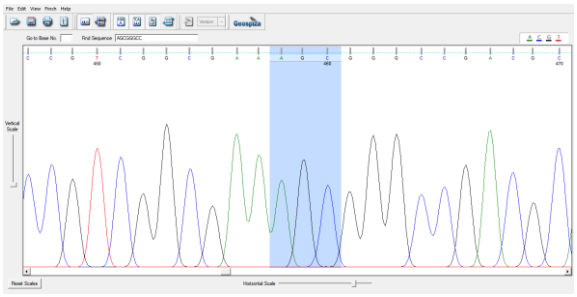

5: L382N/D470S, AAC (Asn)/AGC (Ser)

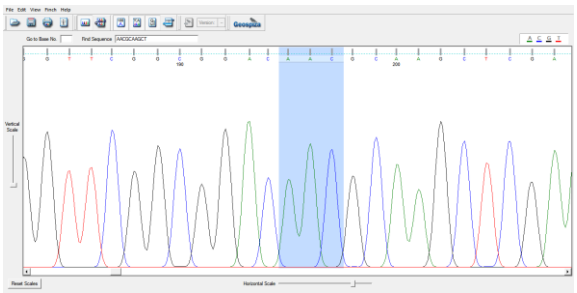

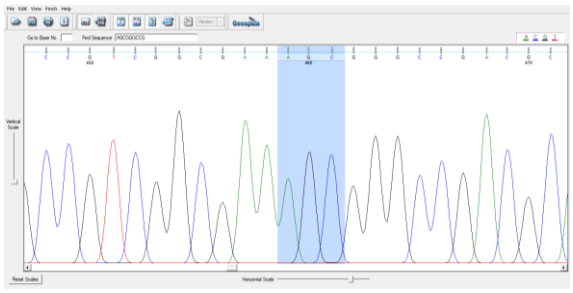

6: L382N/D470S, AAC (Asn)/TCC (Ser)

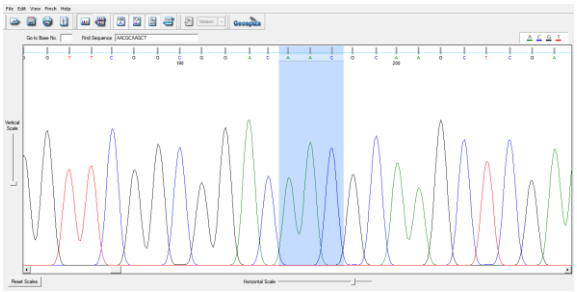

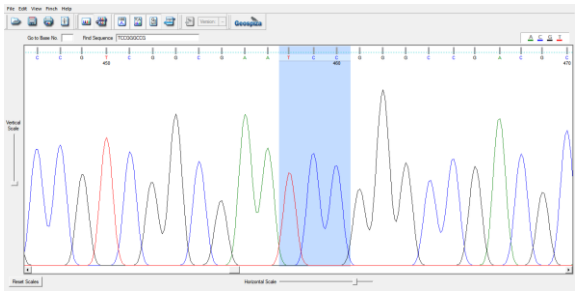

7: L382S/D470G, AGC (Ser)/GGG (Gly)

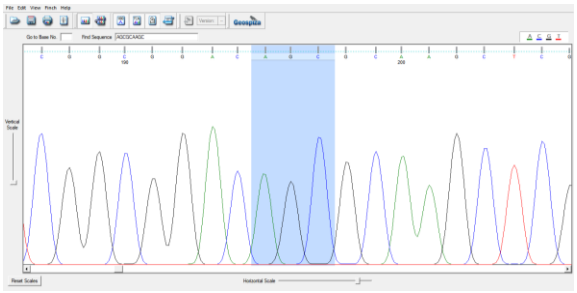

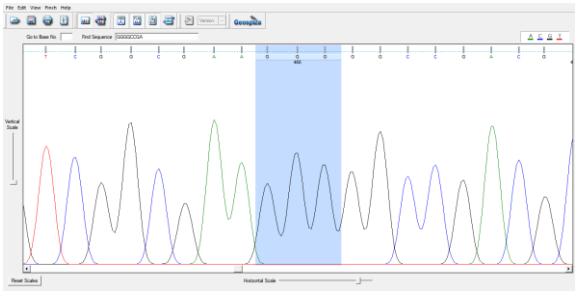

8: L382Y/D470D, TAC (Tyr)/GAC (Asp)

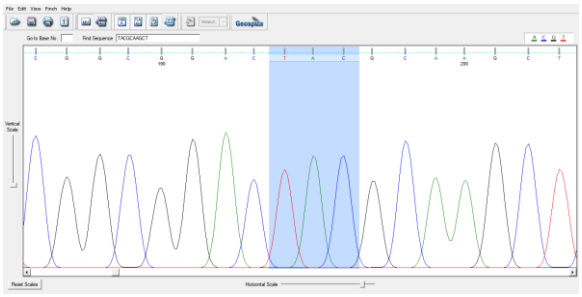

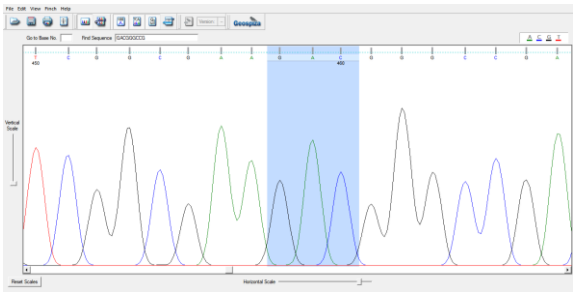

9: L382□/D470C, TAG (STOP)/TGC (Cys)

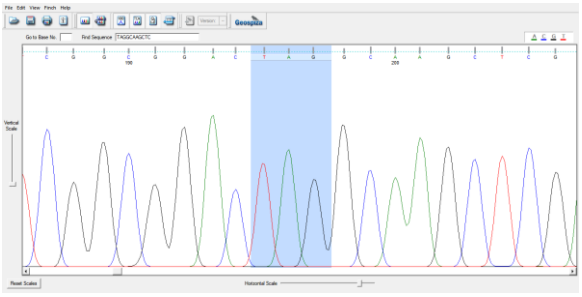

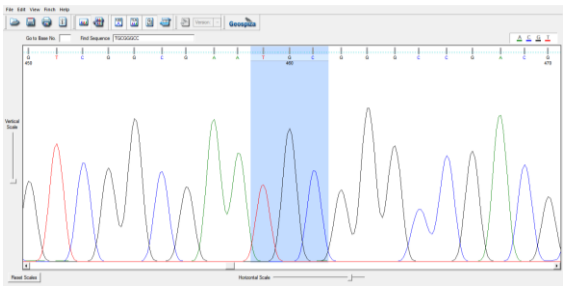

14.4. Data from CHAPTER III
NMR Spectra

4-Phenylbutanoic acid chloride (23)

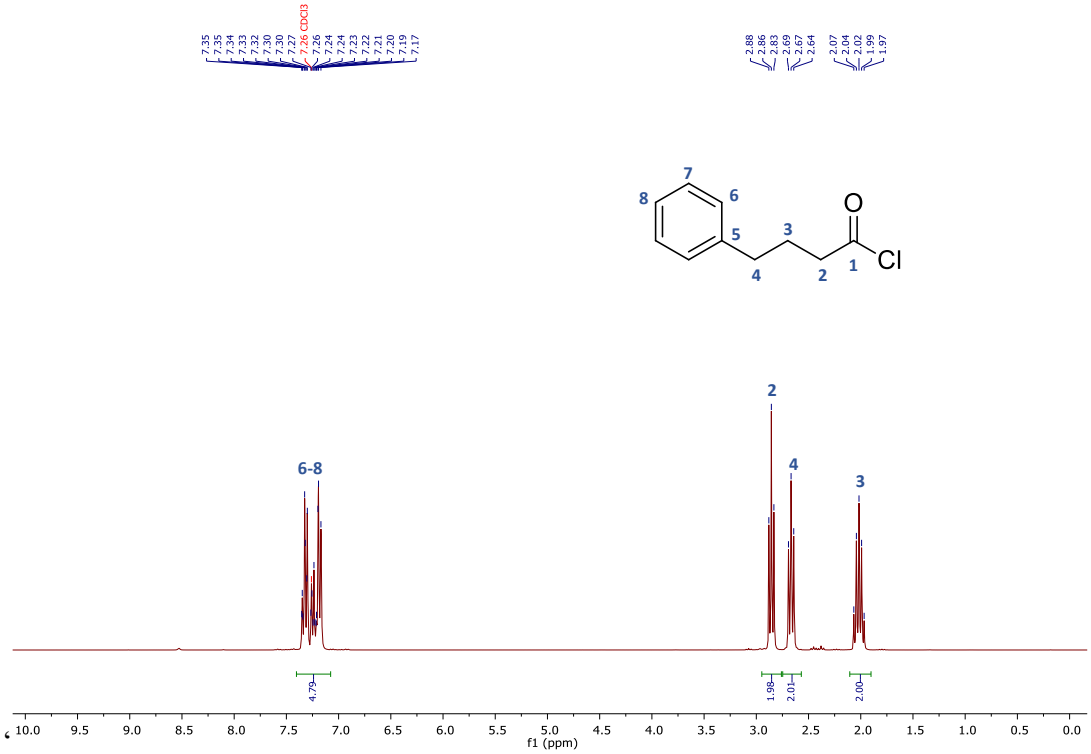

^{1}H-NMR spectrum of 4-phenylbutanoic acid chloride **(23)** (300 MHz, $CDCl_3$)

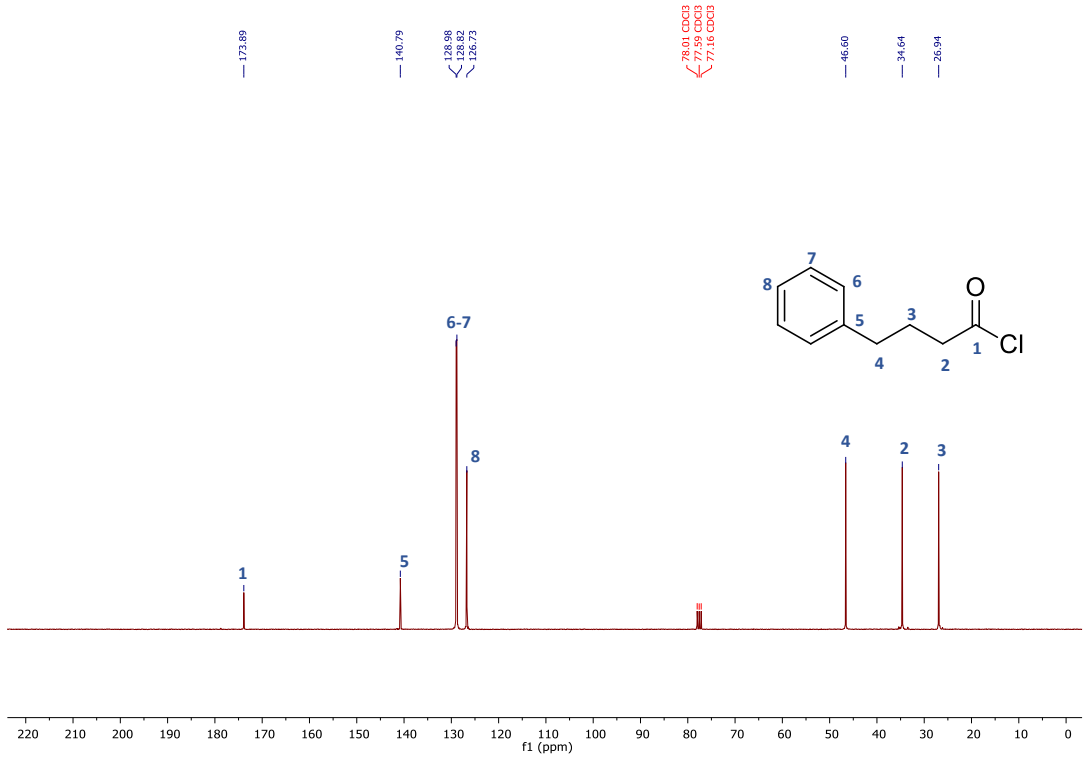

^{13}C-NMR spectrum of 4-phenylbutanoic acid chloride **(23)** (75 MHz, $CDCl_3$)

4-(4-Phenylbutanamido)benzoic acid (24)

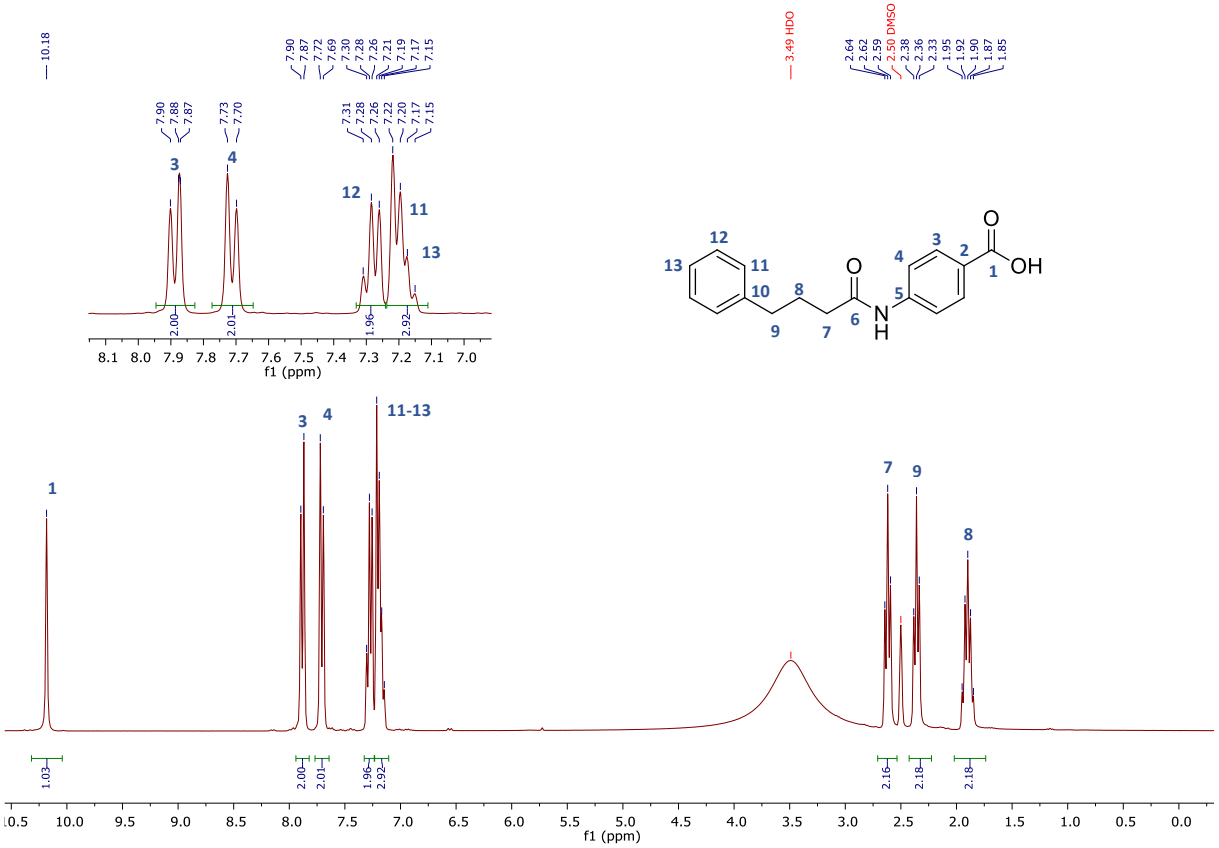

^{1}H-NMR spectrum of 4-(4-phenylbutanamido)benzoic acid **(24)** (300 MHz, DMSO-d^{6})

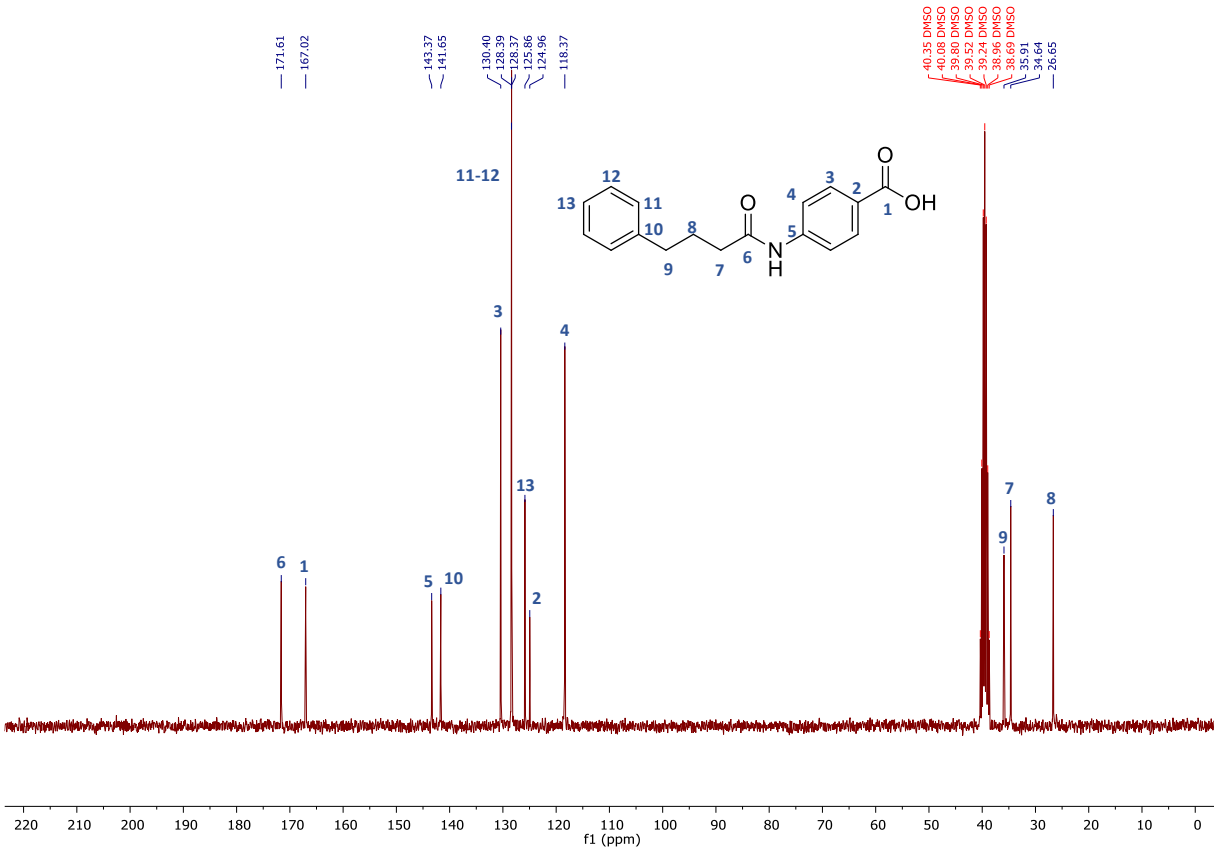

^{13}C-NMR spectrum of 4-(4-phenylbutanamido)benzoic acid **(24)** (75 MHz, DMSO-d^{6})

N-Hydroxy-4-(4-phenylbutanamido)benzamide (HTPB)

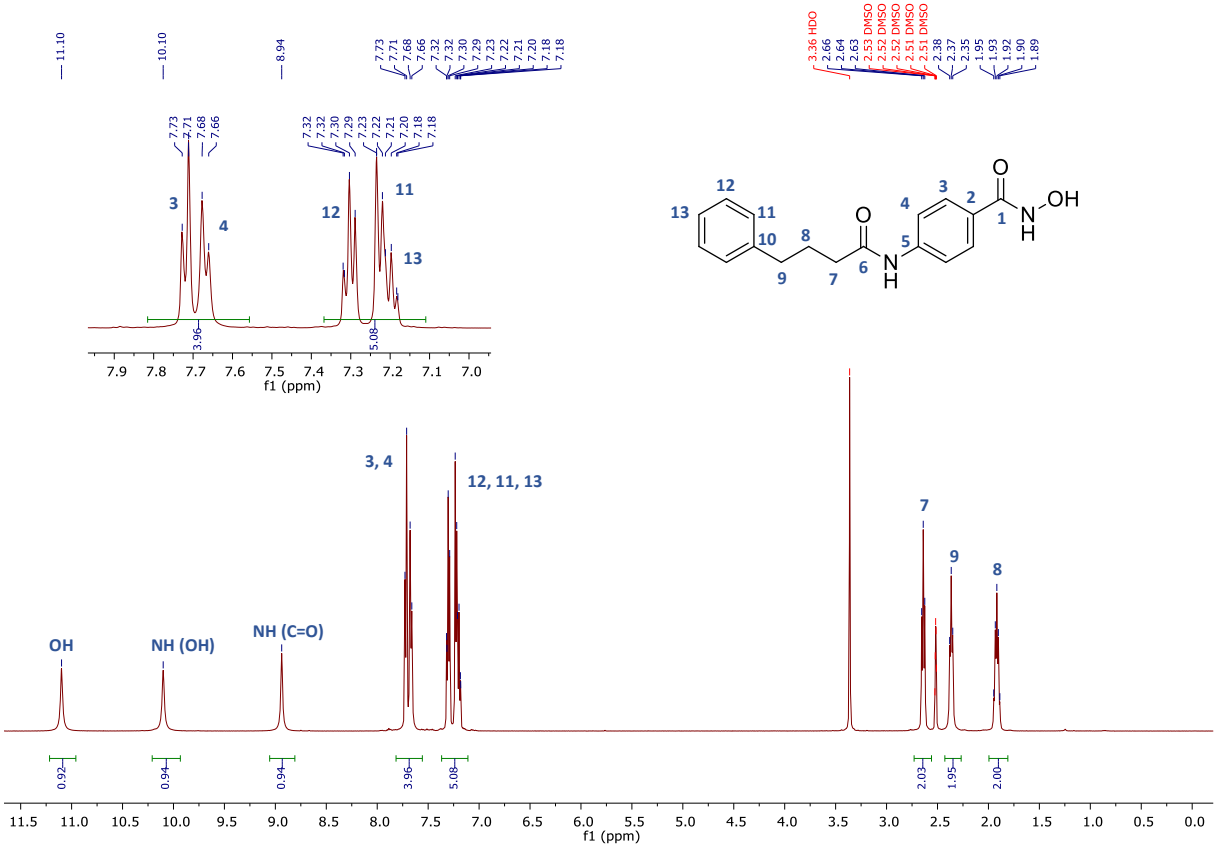

^{1}H-NMR spectrum of *N*-hydroxy-4-(4-phenylbutanamido)benzamide (HTPB) (500 MHz, DMSO-d^{6})

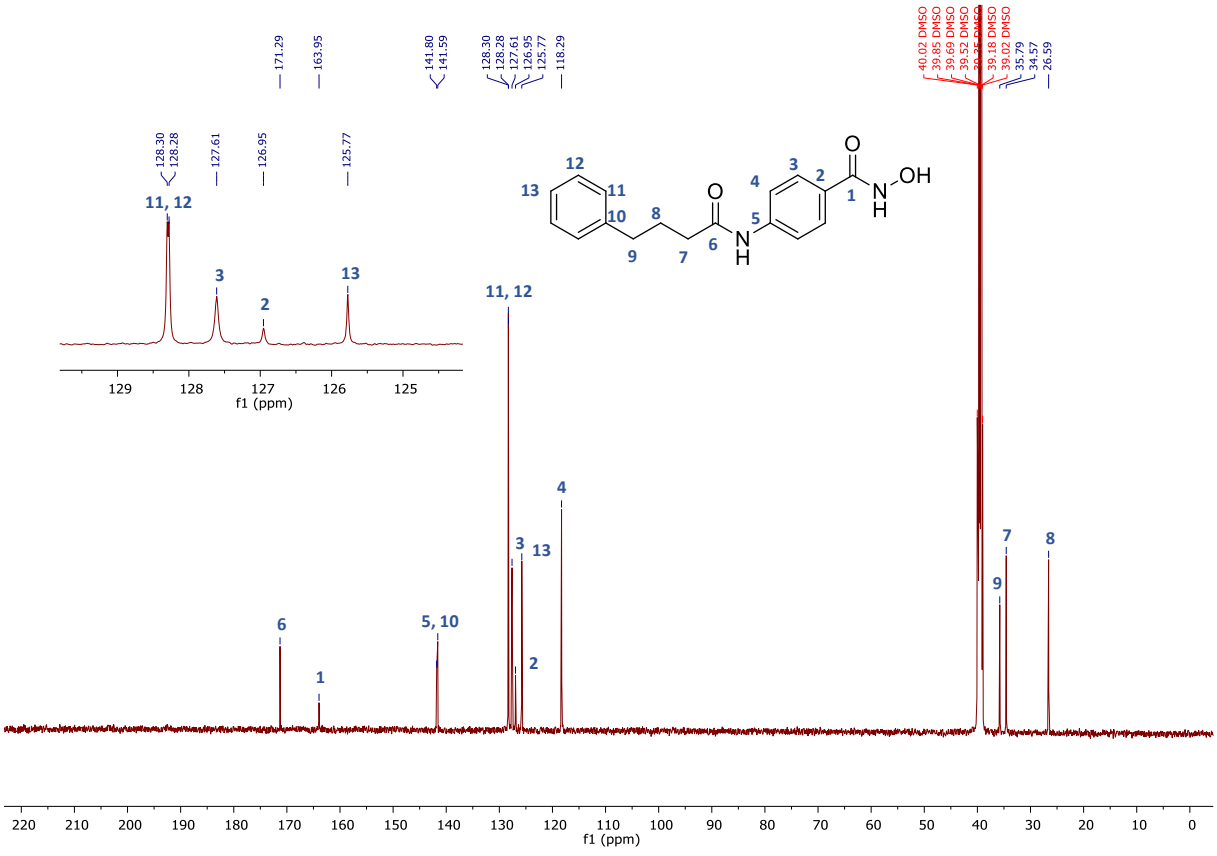

^{13}C-NMR spectrum of *N*-hydroxy-4-(4-phenylbutanamido)benzamide (HTPB) (126 MHz, DMSO-d^{6})

N-(4-Aminophenyl)-4-phenylbutanamide (26)

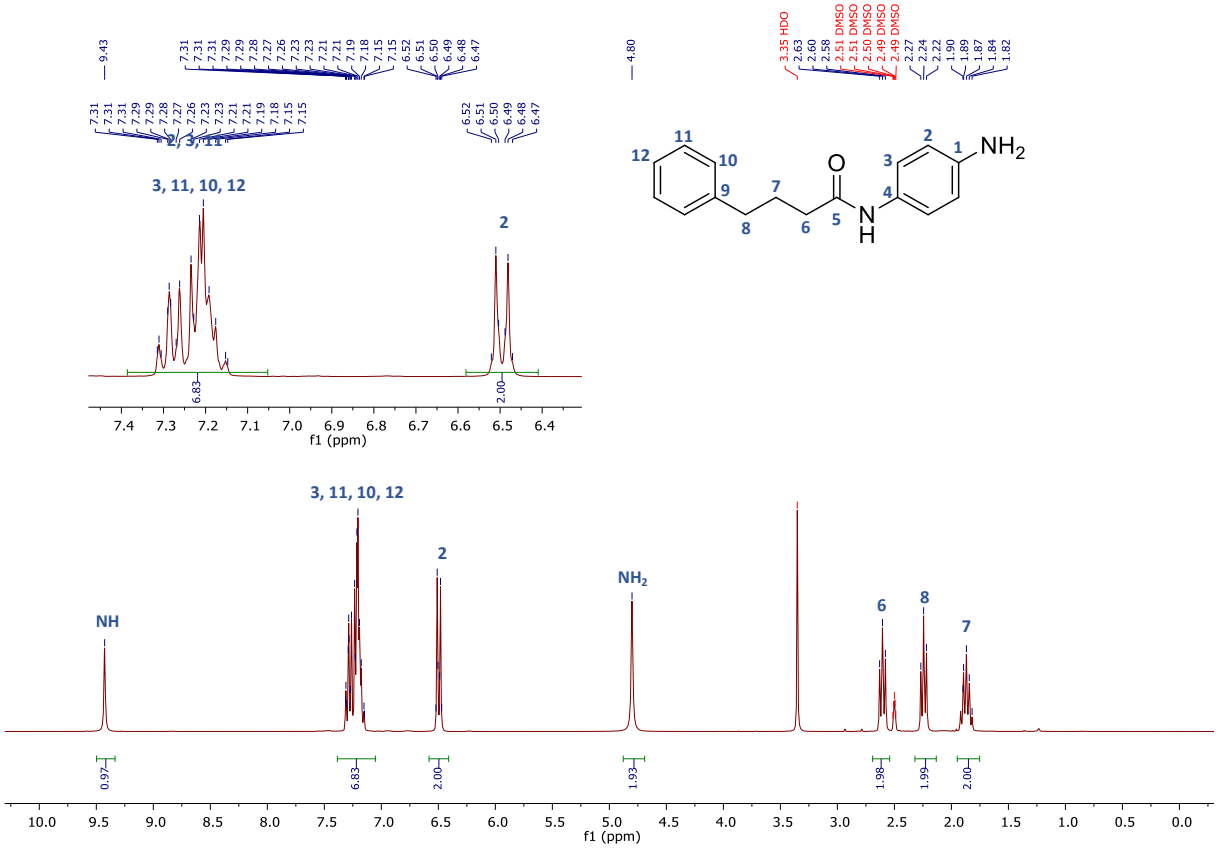

^{1}H-NMR spectrum of *N*-(4-aminophenyl)-4-phenylbutanamide **(26)** (300 MHz, DMSO-d^{6})

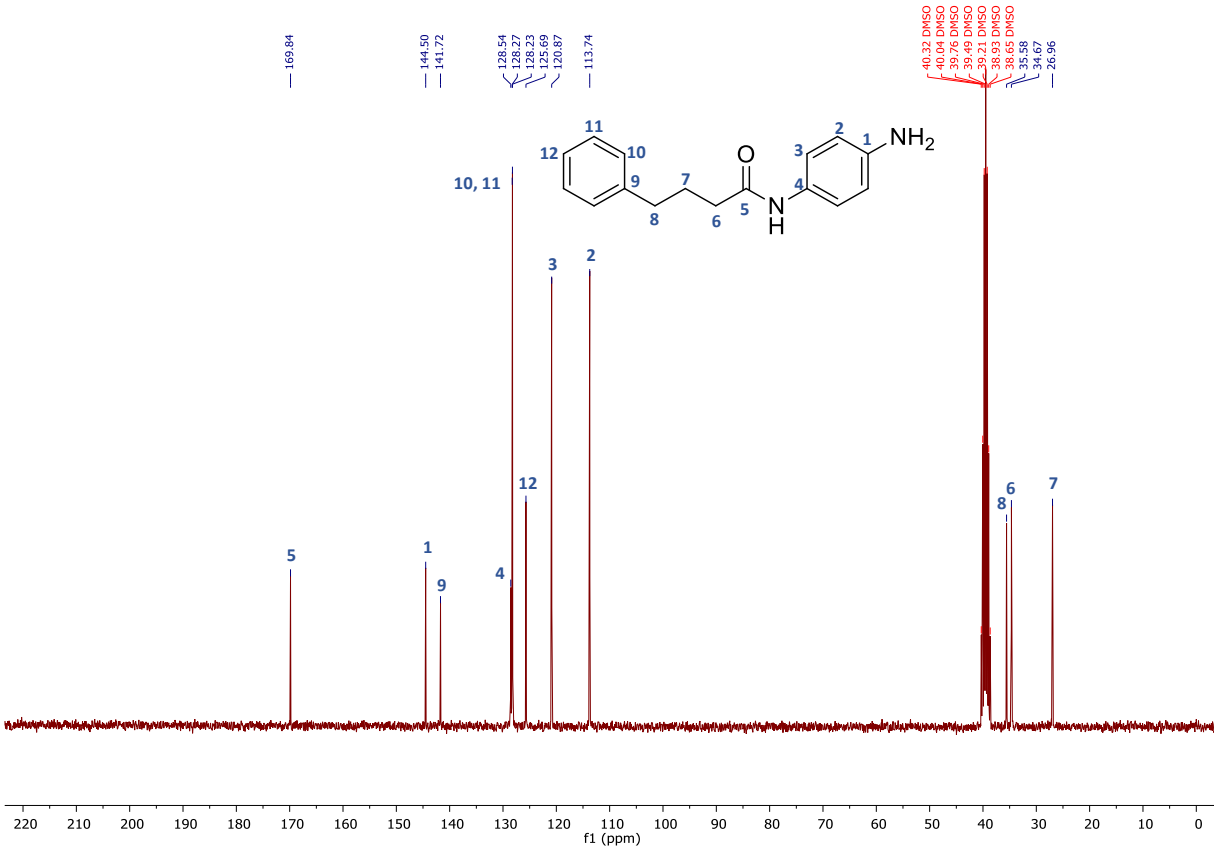

^{13}C-NMR spectrum of *N*-(4-aminophenyl)-4-phenylbutanamide **(26)** (75 MHz, DMSO-d^{6})

N-(4-Nitrosophenyl)-4-phenylbutanamide (27)

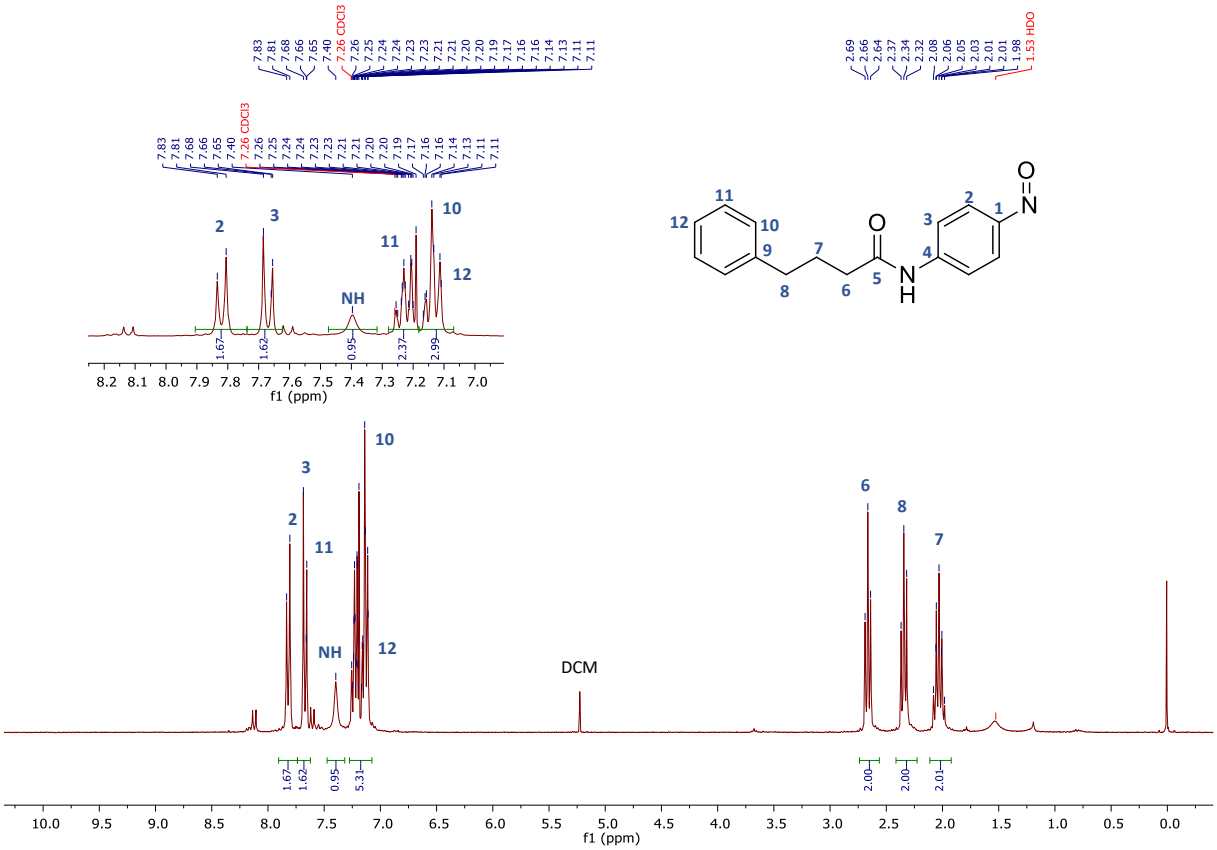

^{1}H-NMR spectrum of *N*-(4-nitrosophenyl)-4-phenylbutanamide **(27)** (300 MHz, $CDCl_3$)

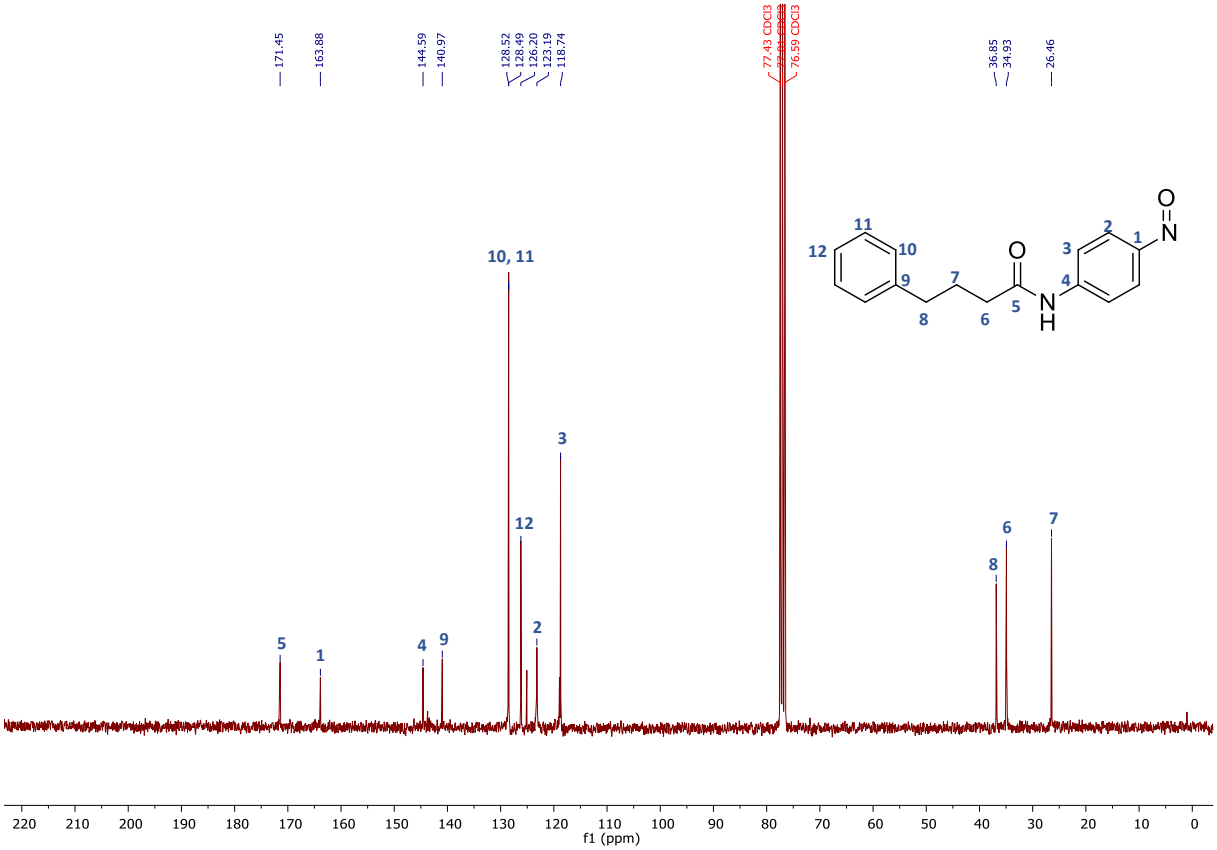

^{13}C-NMR spectrum of *N*-(4-nitrosophenyl)-4-phenylbutanamide **(27)** (75 MHz, $CDCl_3$)

N-(4-(*N*-Hydroxyformamido)phenyl)-4-phenylbutanamide (28)

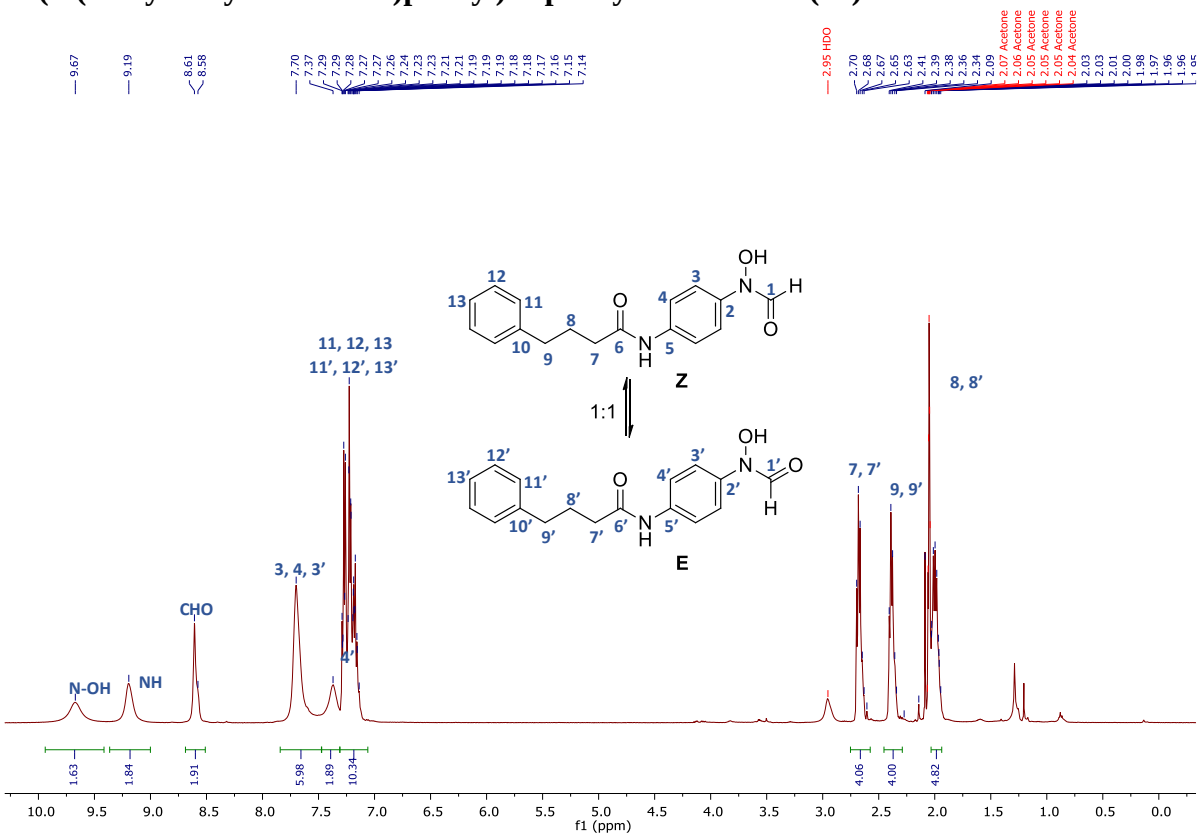

^{1}H-NMR spectrum of *N*-(4-(*N*-hydroxyformamido)phenyl)-4-phenylbutanamide **(28)** (500 MHz, acetone-d^{6})

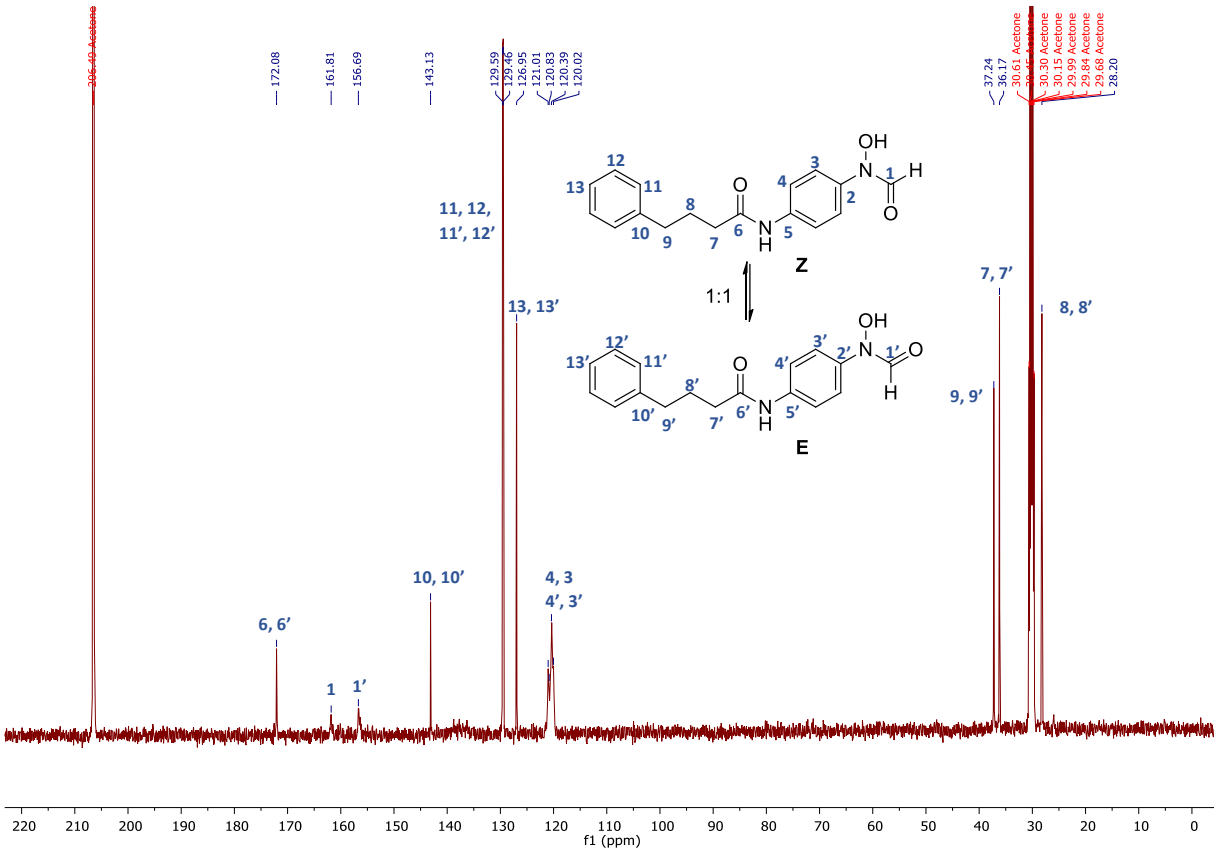

^{13}C-NMR spectrum of *N*-(4-(*N*-hydroxyformamido)phenyl)-4-phenylbutanamide **(28)** (126 MHz, acetone-d^{6})

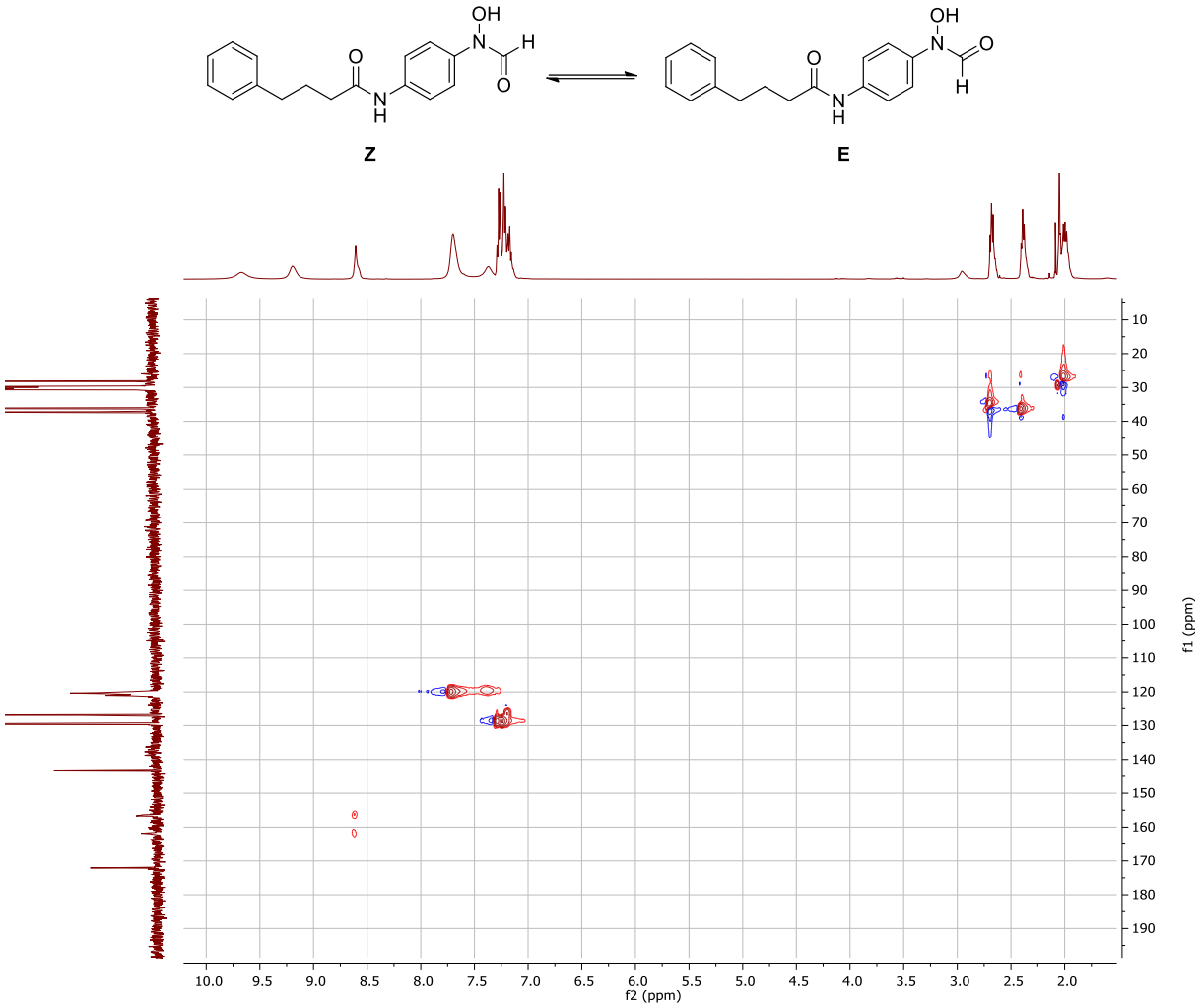

HSQC spectrum of *N*-(4-(*N*-hydroxyformamido)phenyl)-4-phenylbutanamide **(28)** (500, 126 MHz, acetone-d^6)

N-(4-(*N*-Hydroxyacetamido)phenyl)-4-phenylbutanamide (29)

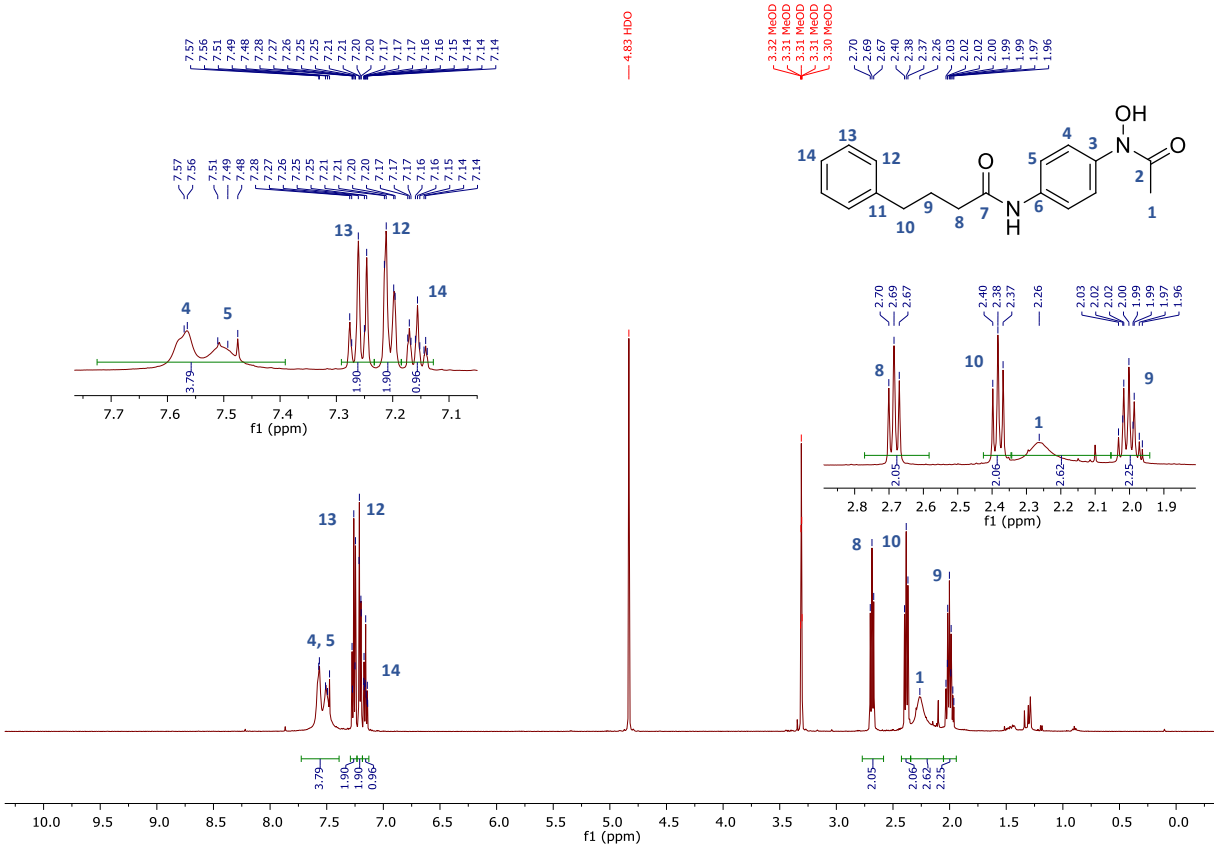

^{1}H-NMR spectrum of *N*-(4-(*N*-hydroxyacetamido)phenyl)-4-phenylbutanamide **(29)** (500 MHz, CD_3OD)

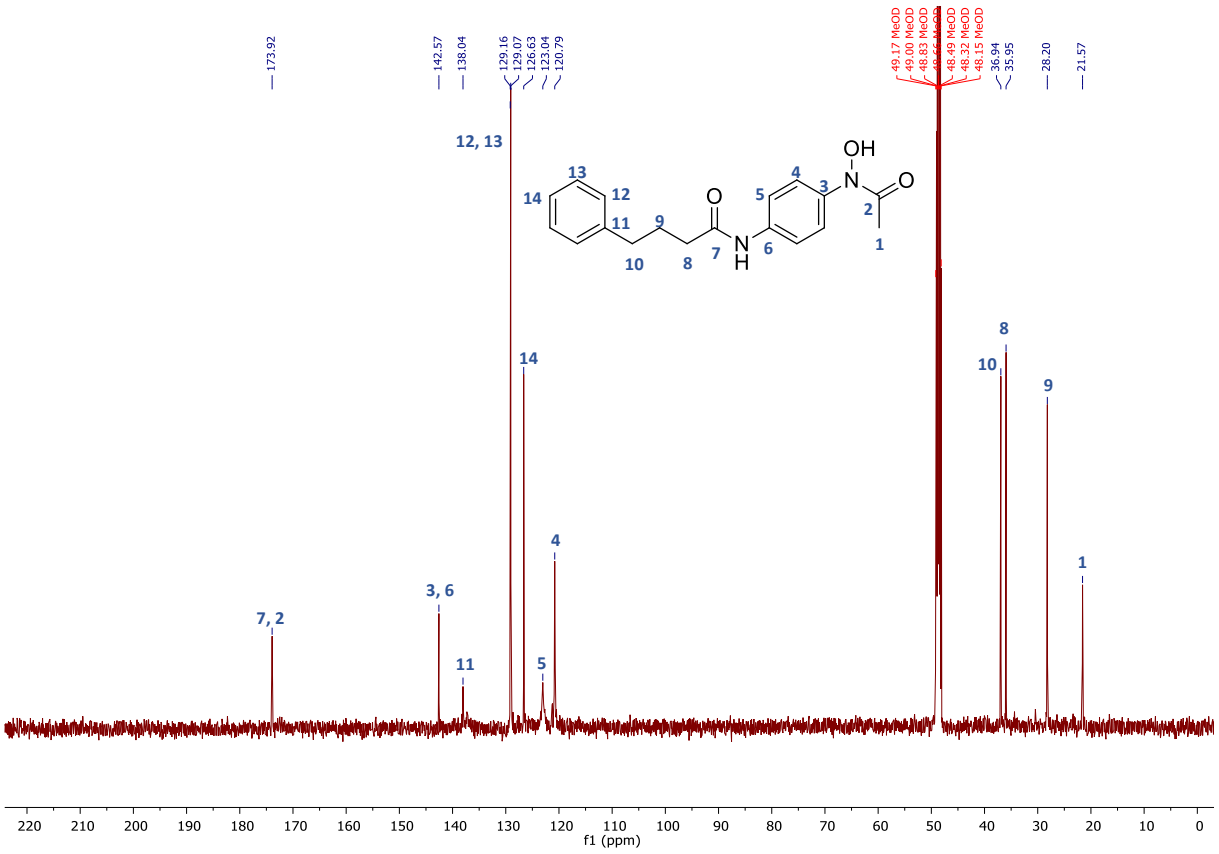

^{13}C-NMR spectrum of *N*-(4-(*N*-hydroxyacetamido)phenyl)-4-phenylbutanamide **(29)** (126 MHz, CD_3OD)

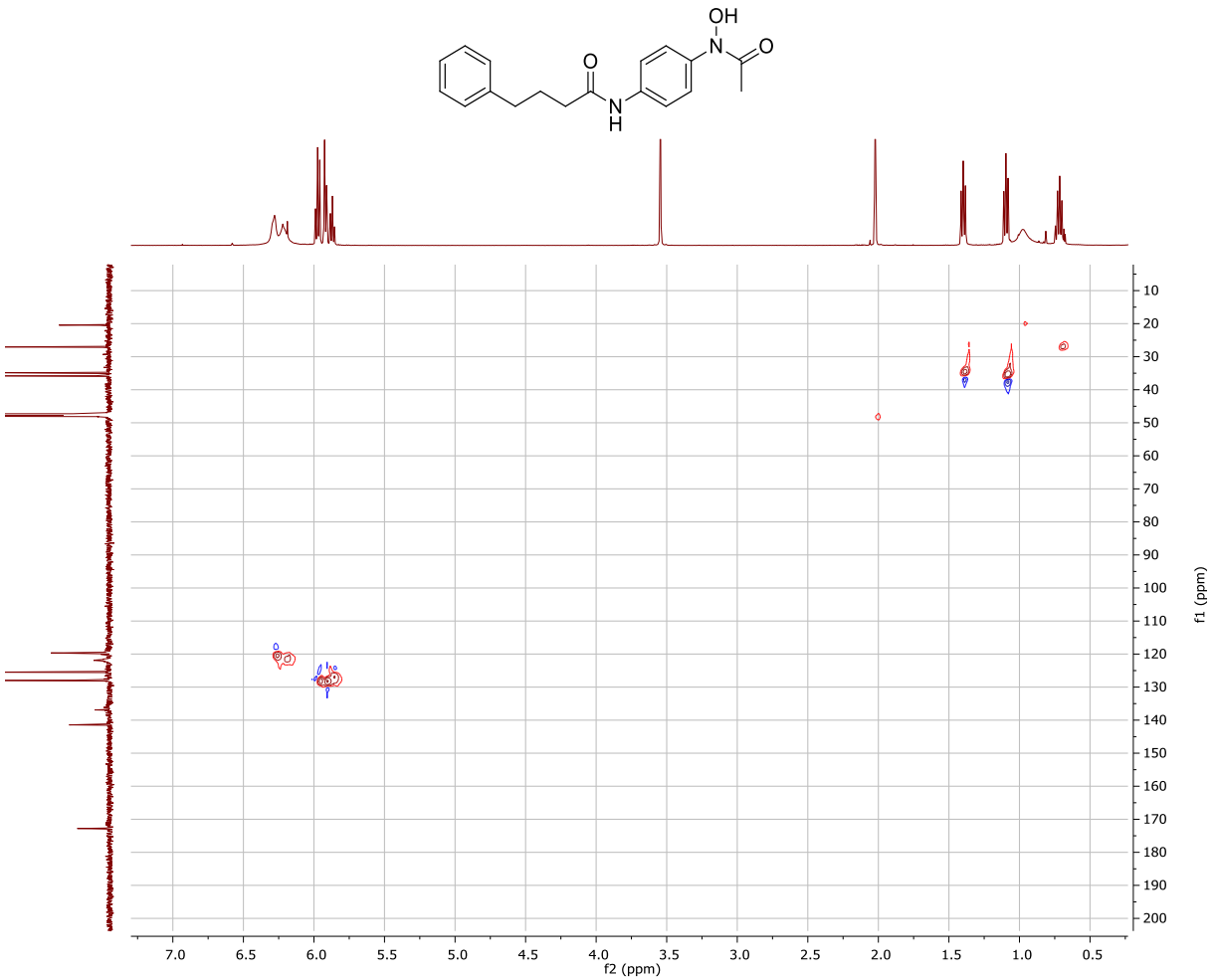

HSQC spectrum of *N*-(4-(*N*-hydroxyacetamido)phenyl)-4-phenylbutanamide **(29)** (500, 126 MHz, CD_3OD)

N-(4-(*N*,2-Dihydroxyacetamido)phenyl)-4-phenylbutanamide (30)

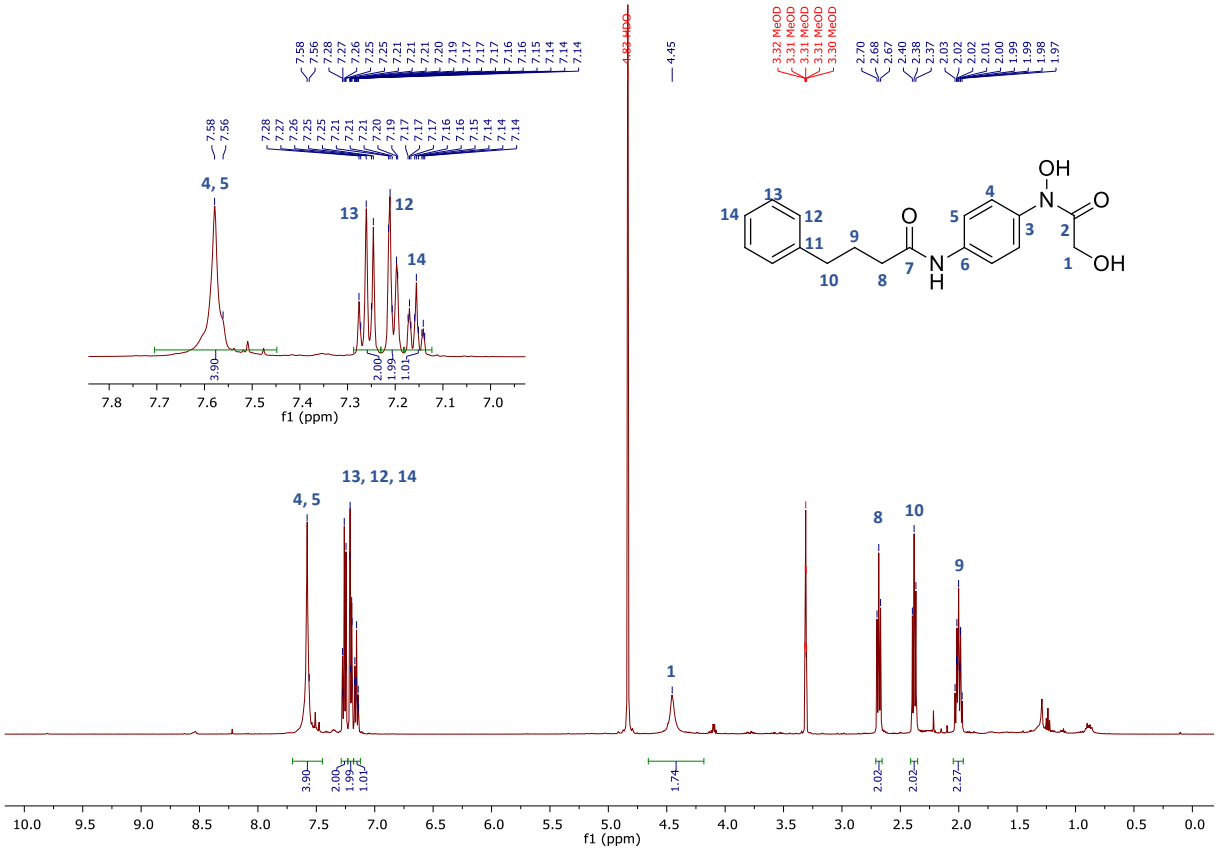

^{1}H-NMR spectrum of *N*-(4-(*N*,2-dihydroxyacetamido)phenyl)-4-phenylbutanamide **(30)** (500 MHz, CD_3OD)

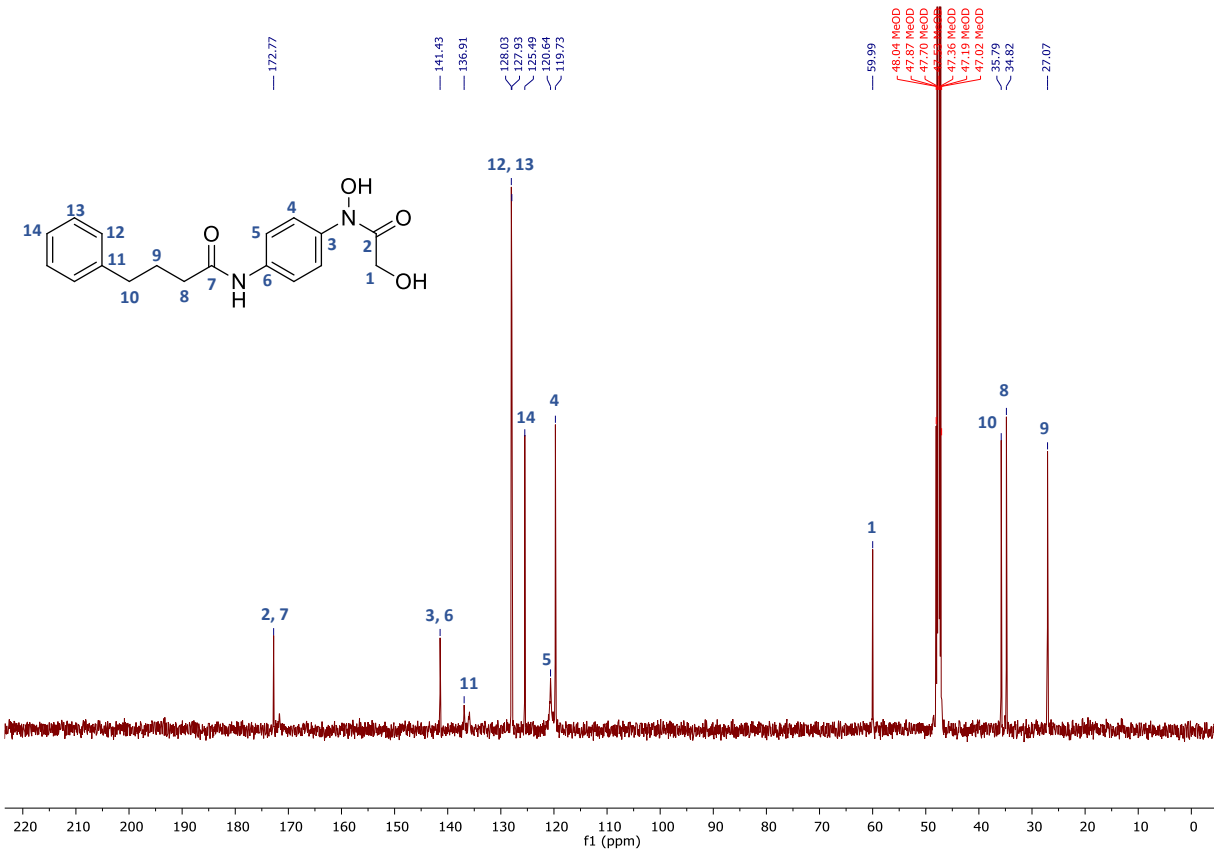

^{13}C-NMR spectrum of *N*-(4-(*N*,2-dihydroxyacetamido)phenyl)-4-phenylbutanamide **(30)** (126 MHz, CD_3OD)

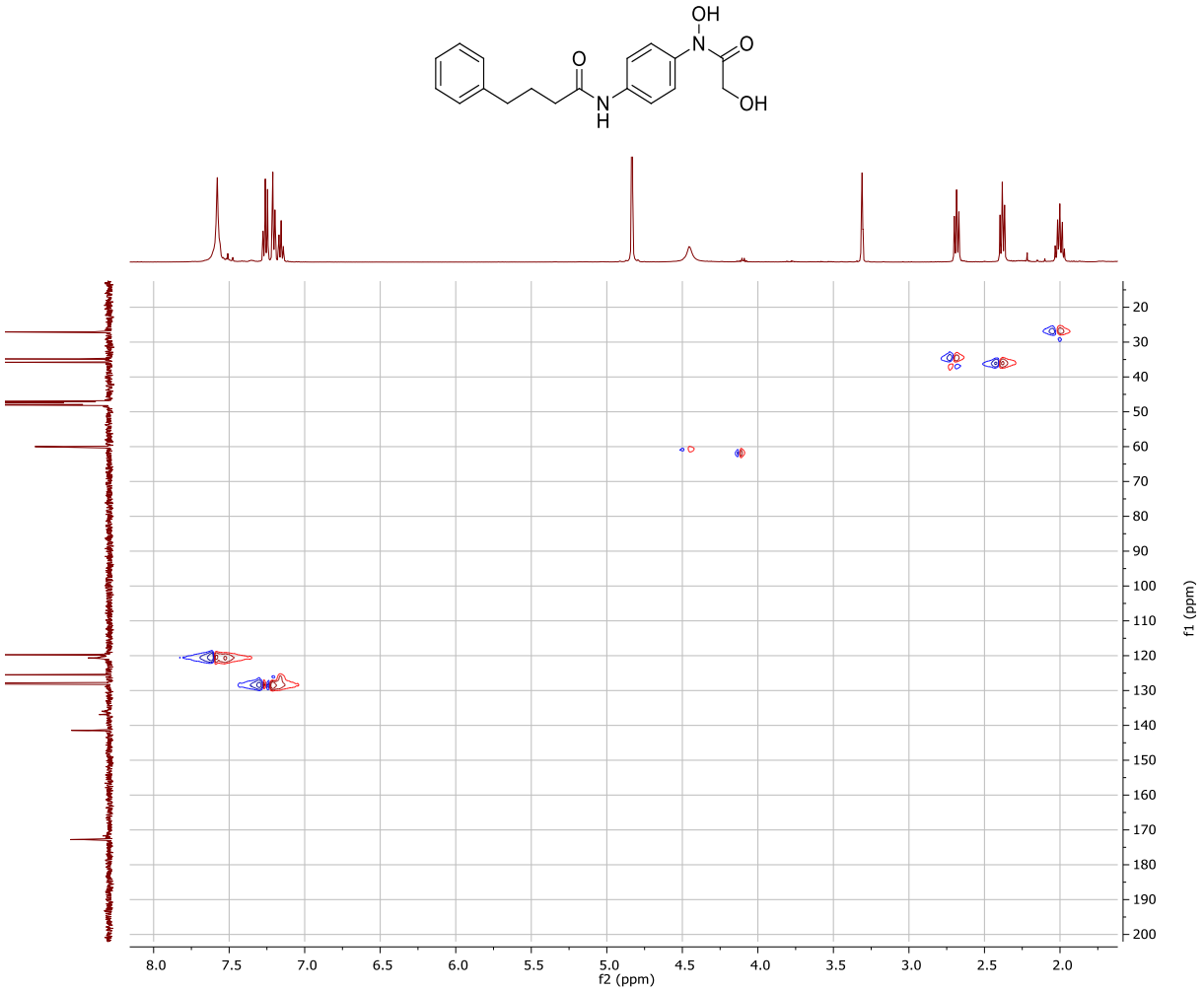

HSQC spectrum of *N*-(4-(*N*,2-dihydroxyacetamido)phenyl)-4-phenylbutanamide **(30)** (500, 126 MHz, CD_3OD)

2-Naphtylamine (36)

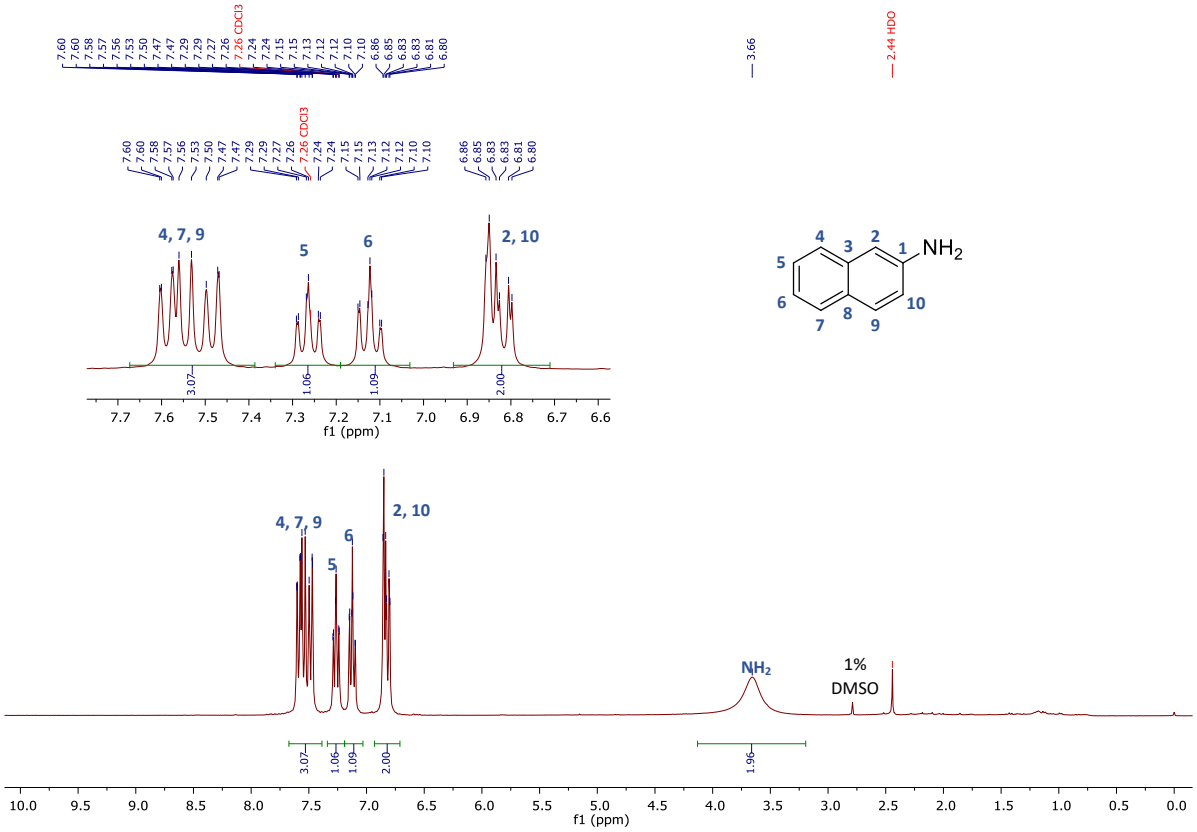

^{1}H-NMR spectrum of 2-naphtylamine **(36)** (300 MHz, $CDCl_3$)

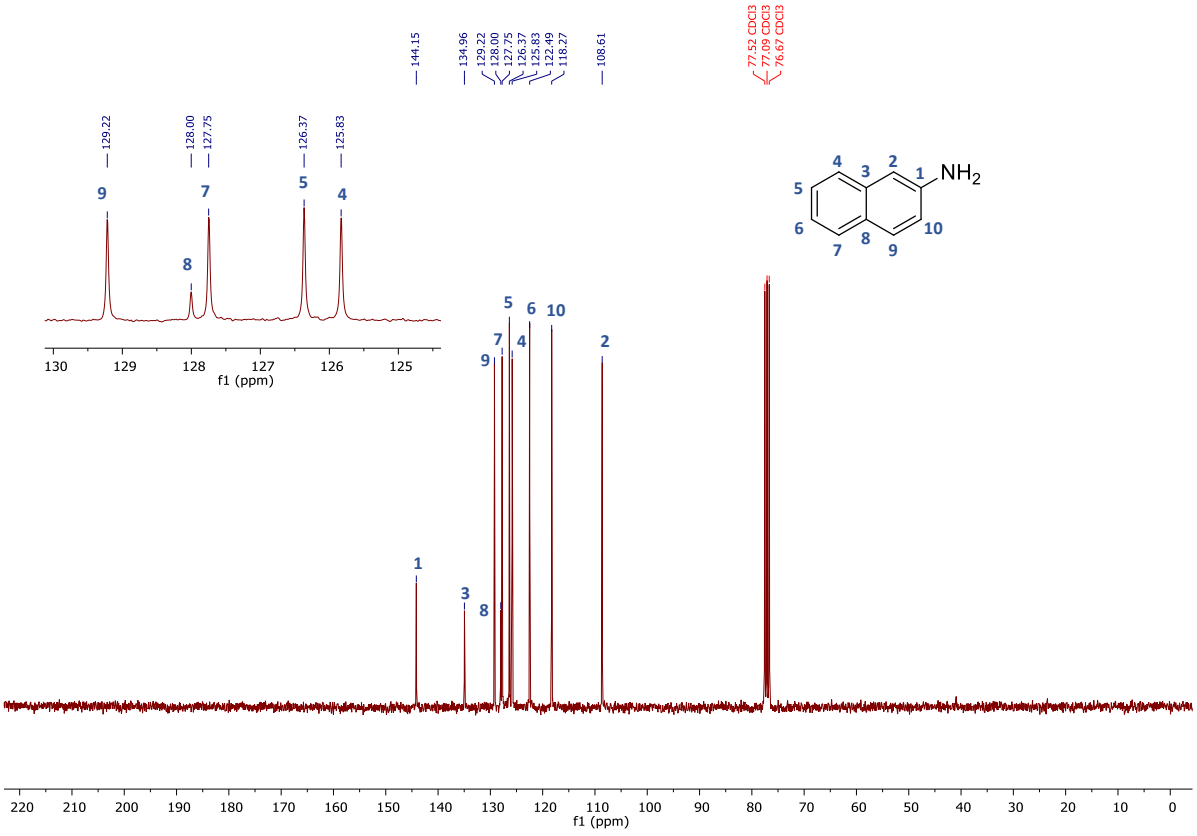

^{13}C-NMR spectrum of 2-naphtylamine **(36)** (75 MHz, $CDCl_3$

Experimental and treated data from *in vitro* HDAC inhibition tests

Treated and calculated data from duplicate measurements (>20 highlighted in pink)

		HDAC6 Substrate: ZMAL		**HDAC1** Substrate: ZMAL		**smHDAC8** Substrate: ZMTFAL		**hHDAC8** Substrate: ZMTFAL		**tcDAC2** Substrate: ZMTFAL	
Type of inhibitor	c [µM]	average inhibition [%]	± deviation	average inhibition [%]	± deviation	average inhibition [%]	± deviation	average inhibition [%]	± deviation	average inhibition [%]	± deviation
HTPB	100	99.32	2.69	100.73	0.05	90.29	0.24	94.82	0.51	98.75	0.08
	10	100.12	2.64	99.01	0.25	71.31	3.08	84.75	0.48	95.46	0.46
	1	95.45	1.15	83.23	0.00	31.66	4.00	60.10	2.06	70.07	0.48
	0.1	72.16	0.83	24.82	2.19	14.89	22.28	29.13	5.60	33.83	0.64
HA 28 (R=H)	100	84.61	2.99	47.98	0.15	34.26	6.69	72.77	4.08	-12.34	0.25
	10	48.80	6.92	6.49	2.00	5.11	9.67	37.11	3.63	-5.19	4.72
	1	8.14	17.89	-2.96	0.00	13.84	15.73	18.00	4.45	-5.72	2.01
	0.1	-3.23	8.38	-4.69	0.08	-0.48	16.05	1.62	1.06	-6.18	1.47
HA 29 ($R=CH_3$)	100	8.17	8.91	3.75	0.07	8.15	5.87	40.28	5.11	-23.06	3.97
	10	-7.67	7.64	2.36	2.45	9.03	3.19	18.98	3.26	-6.82	3.60
	1	-10.13	10.26	-0.46	0.85	0.39	0.44	8.30	0.64	-4.17	1.11
	0.1	-8.88	2.75	-0.82	1.99	-1.98	5.00	4.07	2.04	-0.47	5.54
HA 30 ($R=CH_2OH$)	100	20.49	0.01	3.46	3.20	12.48	2.59	62.05	0.97	-15.76	3.75
	10	6.22	0.90	-5.12	0.19	3.77	0.44	13.77	2.63	5.98	1.24
	1	-0.21	1.49	1.00	0.77	-6.76	2.09	4.81	2.06	.94	1.12
	0.1	-2.40	1.53	-3.13	3.33	-2.13	3.56	-13.38	4.34	-0.82	0.48

14.5. Extra material

The 20 Amino acids

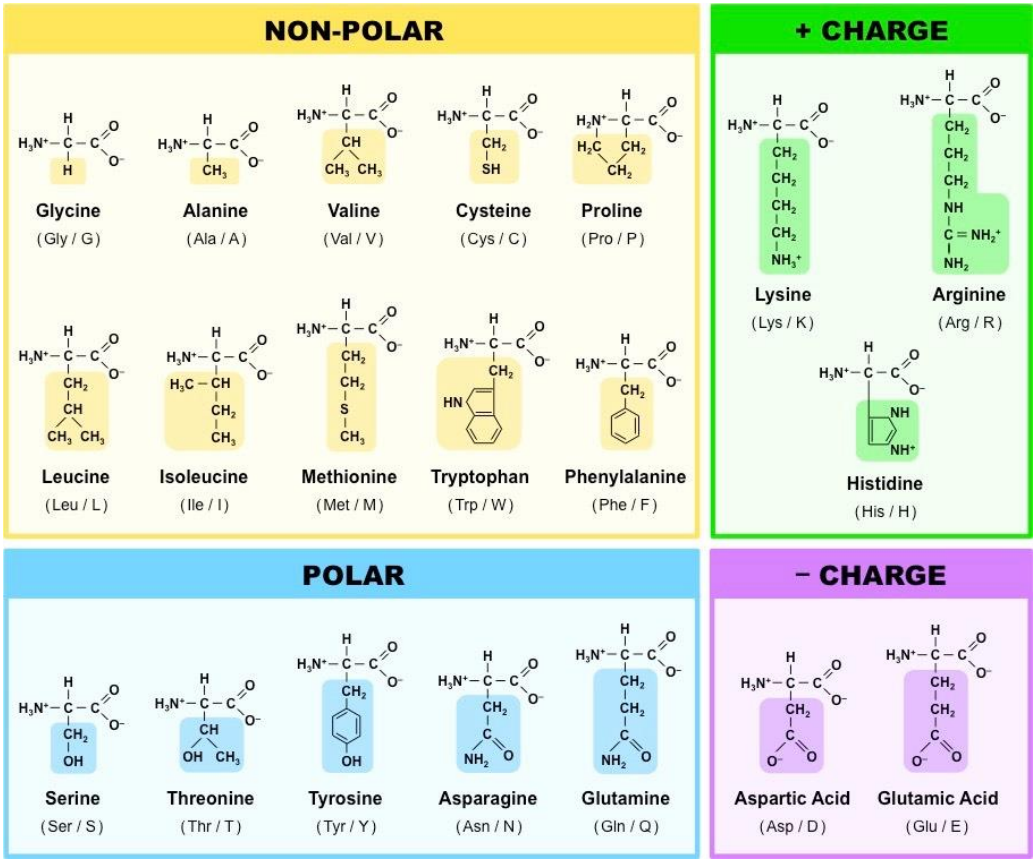

(https://ib.bioninja.com.au/standard-level/topic-2-molecular-biology/24-proteins/amino-acids.html, 29.03.2022)

Equivalences of key amino acids in different TK sources

TK_{gst}	TK_{ban}	TK_{yst}	TK_{eco}
H28	H28	H30	H26
H263	H263	H263	H261
H474	H474	H481	H473
S385	S385	S386	S385
R358	R358	R359	R358
H462	H462	H469	H461
R521	R521	R528	R520
D470	D470	D477	D469
H102	H102	H103	H100

The standard RNA codon table organized in a wheel

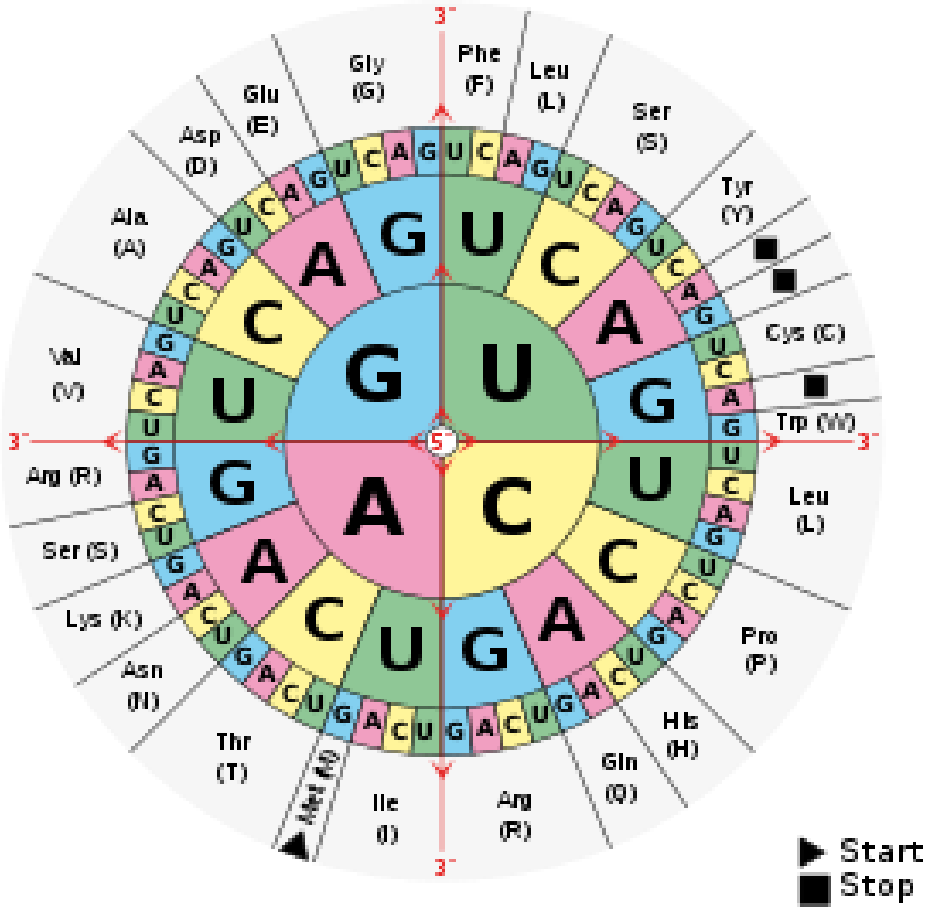

(Wikipedia, DNA and RNA codon tables, https://en.wikipedia.org/wiki/DNA_and_RNA_codon_tables, 29.03.2022)